

5 December 2008 | \$10

Science

Organ
Development

AAAS



COVER

A mouse embryo at 9 days of gestation, stained for α -fetoprotein in the liver bud and yolk sac (upper left and right green domains) and for the transcription factor Pdx-1 in the ventral and dorsal pancreas buds (upper and lower red domains). Understanding the basis for organ development can provide insights into disease and stem cell programming. See the special section beginning on page 1489.

Image: Ewa Wandzioch and Ken Zaret

DEPARTMENTS

- 1429 Science Online
- 1431 This Week in *Science*
- 1437 Editors' Choice
- 1440 Contact *Science*
- 1443 Random Samples
- 1445 Newsmakers
- 1567 New Products
- 1571 Science Careers

EDITORIAL

- 1435 A Scientific Approach to Policy
by Bruce Alberts

SPECIAL SECTION

Organ Development

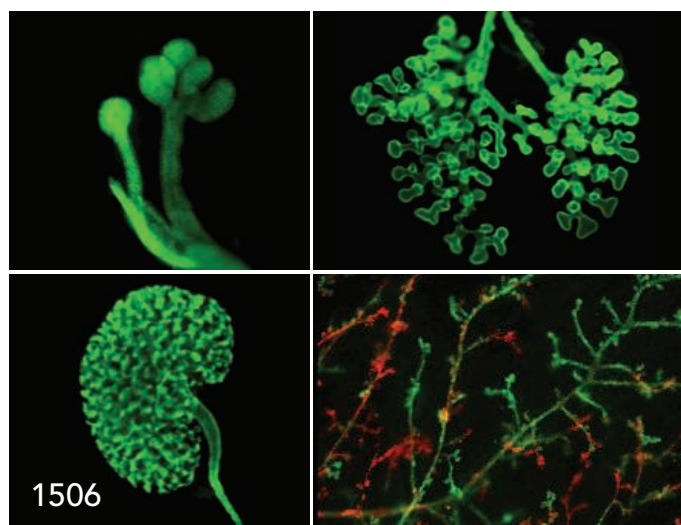
INTRODUCTION

- New Release: *The Complete Guide to Organ Repair* 1489

REVIEWS

- Generation and Regeneration of Cells of the Liver and Pancreas 1490
K. S. Zaret and M. Grompe
- Cardiogenesis and the Complex Biology of Regenerative Cardiovascular Medicine 1494
K. R. Chien et al.
- Origin of Stem Cells in Organogenesis 1498
J. M. W. Slack
- Morphogenetic Cell Movements: Diversity from Modular Mechanical Properties 1502
D. J. Montell
- Patterning Mechanisms of Branched Organs 1506
P. Lu and Z. Werb

>> News story p. 1460; for related online content, see page 1429 or go to www.sciencemag.org/organdevlopment/



NEWS OF THE WEEK

- Three Asian Nations Link Up to Form a Formidable Radio Telescope Array 1446
- Ministers Bankroll European Space Agency's Ambitions 1447
- Less Vaccine Can Be More 1449
- SCIENTESCOPE 1449
- In Rare Encounter, U.S. and Chinese Scientists Craft Nuclear Glossary 1450
- Fetal Immune System Hushes Attacks on Maternal Cells 1450
>> Report p. 1562
- Treat Everyone Now? A 'Radical' Model to Stop HIV's Spread 1453

NEWS FOCUS

- Hopping to a Better Protein 1454
>> Science Podcast
- Sanctuaries Aim to Preserve a Model Organism's Wild Type 1456
- Philippines Plans Research Revival 1459
- Coming Soon to a Knee Near You: Cartilage Like Your Very Own 1460
>> Organ Development section p. 1489

LETTERS

- Spore Show Not Gaming the Science System 1463
M. Rosenfeld
- Limiting the Impact of the Impact Factor *J. B. A. Green*
- Putting Materials and Methods in Their Place *D. Shriner*
- Artificial Intelligence Disappoints *G. Vannucci*
- ChemCam's Cost a Drop in the Mars Bucket
R. C. Wiens and S. Maurice
- An Order of Plumpy'nut, Hold the Aflatoxins
C. P. Wild and R. Montesano
- In Defense of GM Crops *N. H. Ammann*

- CORRECTIONS AND CLARIFICATIONS 1466

CONTENTS continued >>

SCIENCE EXPRESS

www.sciencexpress.org

DEVELOPMENTAL BIOLOGY

Human Fetal Hemoglobin Expression Is Regulated by the Developmental Stage-Specific Repressor *BCL11A*

V. G. Sankaran et al.

A way to reactivate a fetal form of γ -globulin in adults—by releasing it from repression by an inhibitor—may prove useful for treating certain genetic anemias.

10.1126/science.1165409

CELL BIOLOGY

Nascent RNA Sequencing Reveals Widespread Pausing and Divergent Initiation at Human Promoters

L. J. Core, J. J. Waterfall, J. T. Lis

RNA sequencing identifies antisense transcription immediately upstream of genes with transcriptionally engaged RNA polymerase.

10.1126/science.1162228

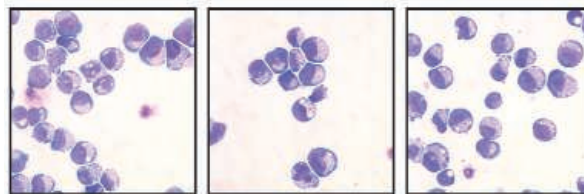
CELL BIOLOGY

Divergent Transcription from Active Promoters

A. C. Seila et al.

Active genes produce promoter-localized sense and antisense short RNAs, suggesting frequent transcription by divergently oriented RNA polymerase II complexes at mammalian promoters.

10.1126/science.1162253



CELL BIOLOGY

RNA Exosome Depletion Reveals Transcription Upstream of Active Human Promoters

P. Preker et al.

Highly unstable transcripts exist upstream of active human promoters.

10.1126/science.1164096

CELL BIOLOGY

The Antisense Transcriptomes of Human Cells

Y. He, B. Vogelstein, V. E. Velculescu, N. Papadopoulos, K. W. Kinzler

The abundance and nonrandom genomic origin of antisense transcripts in human cells suggest that these RNAs are an important feature of gene regulation.

10.1126/science.1163853

TECHNICAL COMMENT ABSTRACTS

CLIMATE CHANGE

Comment on "Phytoplankton Calcification in a High-CO₂ World"

1466

U. Riebesell et al.

[full text at www.sciencemag.org/cgi/content/full/322/5907/1466b](http://fulltextatwww.sciencemag.org/cgi/content/full/322/5907/1466b)

Response to Comment on "Phytoplankton Calcification in a High-CO₂ World"

M. D. Iglesias-Rodriguez et al.

[full text at www.sciencemag.org/cgi/content/full/322/5907/1466c](http://fulltextatwww.sciencemag.org/cgi/content/full/322/5907/1466c)

BOOKS ET AL.

Science Books for Fun and Learning—Some Recommendations from 2008

1468

BROWSINGS

1471

POLICY FORUM

The Gender Gap in NIH Grant Applications

T. J. Ley and B. H. Hamilton

1472

Science Policy in Kazakhstan

G. E. Schweitzer

1474

PERSPECTIVES

How Cold Is Cold Dark Matter?

G. Gilmore >> [Science Podcast](#)

1476

A Curious Antipathy for Water

S. Granick and S. C. Bae

1477

Crops for a Salinized World

J. Rozema and T. Flowers

1478

Controlling Cold-Atom Conductivity

L. Fallani and M. Inguscio >> [Research Article p. 1520](#)

1480

Elements and Evolution

A. D. Anbar

1481

Fat Stress and Liver Resistance

W. Ogawa and M. Kasuga >> [Report p. 1539](#)

1483

PERSPECTIVES CONTINUED...

Competitive Centromeres

1484

D. Charlesworth >> [Report p. 1559](#)

ESSAY

GE Prize Winner: Understanding a Minimal DNA-Segregating Machine

1486

E. C. Garner

BREVIA

PSYCHOLOGY

The Long-Run Benefits of Punishment

1510

S. Gächter, E. Renner, M. Sefton

In human social groups, punishment of uncooperative behaviors increases teamwork, but the benefits of cooperation only outweigh the costs of punishment after a long time.

RESEARCH ARTICLES

CELL BIOLOGY

Dynamic Proteomics of Individual Cancer Cells in Response to a Drug

1511

A. A. Cohen et al.

Cells that escape death from a chemotherapy drug express a different array of proteins than do genetically identical cells that die, which may help to inform cancer therapeutics.

MATERIALS SCIENCE

Tough, Bio-Inspired Hybrid Materials

1516

E. Munch et al.

Lamellar ice is used as a template to form an aluminum oxide scaffold that can be pressed and filled with a polymer, producing a tough layered structure reminiscent of nacre.

PHYSICS

Metallic and Insulating Phases of Repulsively Interacting Fermions in a 3D Optical Lattice

1520

U. Schneider et al.

A cold atom cloud confined to an optical lattice can be tuned from a metal to an insulator. >> [Perspective p. 1480](#)

CONTENTS continued >>

REPORTS

PHYSICS

Attosecond Ionization and Tunneling Delay Time Measurements in Helium 1525

P. Eckle et al.

A technique based on resolving the momentum of an electron escaping from a helium atom in an elliptically polarized light field clocks tunneling at less than 34 attoseconds.

GEOPHYSICS

Optical Absorption and Radiative Thermal Conductivity of Silicate Perovskite to 125 Gpa 1529

H. Keppler, L. S. Dubrovinsky, O. Narygina, I. Kantor

At high pressures, silicate perovskite, abundant in Earth's mantle, is not opaque to optical and infrared light, implying that radiative heat flow is important in the deep Earth.

PLANETARY SCIENCE

Quasi-Periodic Bedding in the Sedimentary Rock Record of Mars 1532

K. W. Lewis et al.

Stereo topographic mapping on Mars shows that some large impact craters were filled with sedimentary rock sequences made up of cyclical packages of meter-scaled beds.

MOLECULAR BIOLOGY

Photoexcited CRY2 Interacts with CIB1 to Regulate Transcription and Floral Initiation in *Arabidopsis* 1535

H. Liu, X. Yu, K. Li, J. Klejnot, H. Yang, D. Lisiero, C. Lin

Blue light triggers the association of a photoreceptor, transcription factor, and DNA site, thus inducing expression for the gene *FT* (flowering time) and initiating flowering.

CELL SIGNALING

A Stress Signaling Pathway in Adipose Tissue Regulates Hepatic Insulin Resistance 1539

G. Sabio et al.

In mice, some detrimental effects of a diet high in fat—insulin resistance, for instance—result from hormonal signals sent from fat cells to the liver. >> *Perspective p. 1483*

CELL BIOLOGY

Inhibition of Rac by the GAP Activity of Centralspindlin Is Essential for Cytokinesis 1543

J. C. Canman et al.

During cell division, a component of the spindle inhibits a small regulatory binding protein, allowing another regulator to constrict a ring between the separating daughter cells.

DEVELOPMENTAL BIOLOGY

Dynamic Analyses of *Drosophila* Gastrulation Provide Insights into Collective Cell Migration 1546

A. McMahon, W. Supatto, S. E. Fraser, A. Stathopoulos

Live fluorescence imaging of over 1500 cells within a *Drosophila* embryo during gastrulation reveals that a fibroblast growth factor coordinates cell migration.



NEUROSCIENCE

Astroglial Metabolic Networks Sustain Hippocampal Synaptic Transmission 1551

N. Rouach, A. Koulakoff, V. Abudara, K. Willecke, C. Giaume

The glial astrocytes that surround neurons supply glucose or lactate to excitatory synapses through gap junctions that open when the neurons are active.

NEUROSCIENCE

Activation of Pannexin-1 Hemichannels Augments Aberrant Bursting in the Hippocampus 1555

R. J. Thompson et al.

Activation of a glutamate receptor in hippocampal cells leads to secondary opening of a gap junction-like channel that can contribute to seizure-like bursting.

EVOLUTION

Centromere-Associated Female Meiotic Drive Entails Male Fitness Costs in Monkeyflowers 1559

L. Fishman and A. Saunders

Competition between chromosomal homologs causes non-Mendelian meiotic segregation and fitness polymorphism in a natural monkeyflower population. >> *Perspective p. 1484*

IMMUNOLOGY

Maternal Alloantigens Promote the Development of Tolerogenic Fetal Regulatory T Cells in Utero 1562

J. E. Mold et al.

Exposure of the human fetus to maternal cells during pregnancy can prompt development of regulatory T cells that prevent responses to non-inherited maternal antigens.

>> *News story p. 1450; Science Podcast*



ADVANCING SCIENCE. SERVING SOCIETY

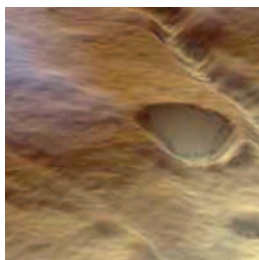
SCIENCE (ISSN 0036-8075) is published weekly on Friday, except the last week in December, by the American Association for the Advancement of Science, 1200 New York Avenue, NW, Washington, DC 20005. Periodicals Mail postage (publication No. 484460) paid at Washington, DC, and additional mailing offices. Copyright © 2008 by the American Association for the Advancement of Science. The title SCIENCE is a registered trademark of the AAAS. Domestic individual membership and subscription (51 issues): \$144 (\$74 allocated to subscription). Domestic institutional subscription (51 issues): \$770; Foreign postage extra: Mexico, Caribbean (surface mail) \$55; other countries (air assist delivery) \$85. First class, airmail, student, and emeritus rates on request. Canadian rates with GST available upon request, GST #1254 88122. Publications Mail Agreement Number 1069624. SCIENCE is printed on 30 percent post-consumer recycled paper. Printed in the U.S.A.

Change of address: Allow 4 weeks, giving old and new addresses and 8-digit account number. Postmaster: Send change of address to AAAS, P.O. Box 96178, Washington, DC 20090-6178. Single-copy sales: \$10.00 current issue, \$15.00 back issue prepaid includes surface postage; bulk rates on request. Authorization to photocopy material for internal or personal use under circumstances not falling within the fair use provisions of the Copyright Act is granted by AAAS to libraries and other users registered with the Copyright Clearance Center (CCC) Transactional Reporting Service, provided that \$20.00 per article is paid directly to CCC, 222 Rosewood Drive, Danvers, MA 01923. Science is indexed in the Reader's Guide to Periodical Literature and in several specialized indexes.



Printed on
30% post-consumer
recycled paper.

CONTENTS continued >>>



Hidden impact crater
in Canada unmasked.

SCIENCE NOW

www.sciencenow.org

HIGHLIGHTS FROM OUR DAILY NEWS COVERAGE

Lasers Uncover Craters

New technology pinpoints previously unknown meteor impacts.

The Long Road to Modernity

Archaeological dating suggests modern humans may have inherited some fancy tools.

Most Planets May Be Seeded With Life

Discovery of RNA precursor in planet-forming cloud suggests building blocks of life are common in the universe.



Ligand-binding pocket of PPAR γ .

SCIENCE SIGNALING

www.sciencesignaling.org

THE SIGNAL TRANSDUCTION KNOWLEDGE ENVIRONMENT

PERSPECTIVE: Ligand-Dependent and -Independent Regulation of PPAR γ and Orphan Nuclear Receptors

H. E. Xu and Y. Li

It is too soon to conclude that the physiological activities of PPAR γ are truly ligand-independent.

PODCAST

S. W. Lee, P. P. Ongusaha, A. M. VanHook

Sam Lee and Pat Ongusaha discuss their research on the mechanisms by which ultraviolet B radiation induces cell death.

GLOSSARY

Find out what TSC, NG2, and ASIC mean in the world of cell signaling.

PREVIEW

Get a sneak peek at articles coming up in the 9 December issue related to this week's *Science* special section on organ development.

>> *Organ Development* section p. 1489 and www.sciencemag.org/organdevlopment/



How will scientists fare in the
new administration?

SCIENCE CAREERS

www.sciencereers.org/career_development

FREE CAREER RESOURCES FOR SCIENTISTS

The Job Outlook for Physician Scientists

K. Hede

Job opportunities make a bright future for scientists with clinical degrees.

Taken for Granted: Can Scientists Believe in Change?

B. L. Benderly

Science is one of many priorities for the new presidential administration.

Beating the Odds

G. Sinha

Cinzia Casiraghi won €1.65 million for setting up her own lab in Germany.

December 2008 Funding News

J. Fernández

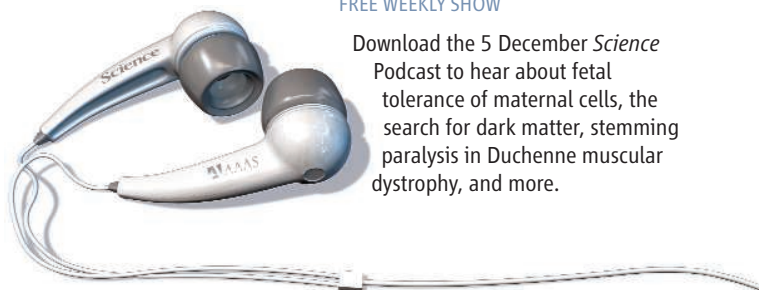
Learn about the latest in research funding, scholarships, fellowships, and internships.

SCIENCE PODCAST

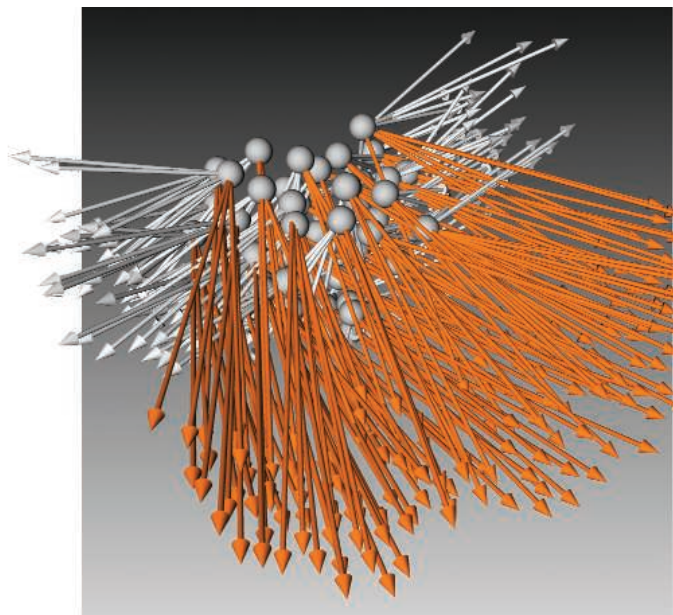
www.sciencemag.org/multimedia/podcast

FREE WEEKLY SHOW

Download the 5 December *Science* Podcast to hear about fetal tolerance of maternal cells, the search for dark matter, stemming paralysis in Duchenne muscular dystrophy, and more.



Separate individual or institutional subscriptions to these products may be required for full-text access.



<< A Closer Look

During development, the early embryo undergoes massive restructuring due to the organized migration of large numbers of cells. However, imaging complex cellular movements inside living organisms is a huge technical challenge. In species like *Drosophila*, researchers have been limited to making observations from fixed specimens. Now, as technologies have advanced, it is possible to visualize complex cellular movements as they occur in real-time. McMahon *et al.* (p. 1546) have used advances in imaging and quantitative analysis to produce a detailed description of cell behavior during *Drosophila* gastrulation. Two-photon excitation fluorescence imaging techniques were used to visualize cells inside the developing *Drosophila* embryo, while still retaining viability. The position, movement, and division of over 1500 cells from two separate germ layers could be followed, three-dimensional (3D) over the course of 2 hours, revealing the role of a fibroblast growth factor in coordinating cell migration during gastrulation.

See-Through Perovskite

Much of Earth's dynamics and plate tectonics reflect the loss of heat through its interior. Thus, understanding the nature of that heat flow and the extent to which it occurs by advection, conduction, or radiation is critical. Usually, advection and conduction have been thought to dominate, but the role of radiation at high pressures and temperatures in the mantle has also been considered. Keppler *et al.* (p. 1529) have now measured the absorption spectra of silicate perovskite, a main mineral in the lower mantle, and show that, under high pressures, it is surprisingly transparent. This would imply that the overall thermal conductivity in the deep mantle could be higher than generally assumed.

Solid State in a Cloud of Atoms

The interactions between electrons in solid-state systems can manifest a number of different electronic phases. These systems tend, however, to be fixed in terms of tunability, and complex, with the underlying physics being masked by defects and other electronic bands. Cold atoms trapped in optical lattices have offered the potential of a clean, defect free, highly tunable system in which to explore the complex interactions between interacting particles. Schneider *et al.* (p. 1520; see the Perspective by Fallani and Inguscio) demonstrate

this potential, working with potassium atoms confined to a 3D optical lattice. Tuning the depth of the trap and the interaction strength between the atoms and the physical confinement of the gas cloud allowed the system to be converted from a metallic state through a Mott-insulating state to a band-insulator. The results illustrate the possibility of using cold atoms to mimic and model complex solid state systems.

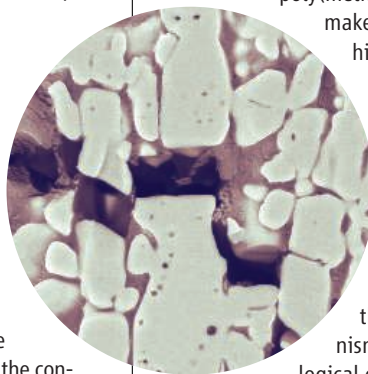
A Tunnel Clock

Among the more counterintuitive phenomena fostered by quantum mechanics at the atomic scale is the ability of particles to access spatial regions by tunneling through a barrier while lacking the energy to climb over it. Eckle *et al.* (p. 1525) have devised a technique for measuring the extremely rapid rate of this process in the context of electrons escaping from helium atoms in the presence of a strong laser field. Once free, the electrons are accelerated in whatever direction the field vector points at that instant. Applying an elliptical polarization to the laser pulse established a fixed reference point in the laboratory frame. The momentum of emergent electrons can then be resolved, and a tunneling time delay calculated, based on the known evolution of the field polarization. Intensities on the order of 10^{14} watts/square centimeter generated an upper bound of 34 attoseconds for the delay.

Bio-Inspired Materials Engineering

Nature uses many tricks to form strong composites from otherwise weak starting materials. Using an ice templating procedure, Munch *et al.* (p. 1516) combined aluminum oxide and

poly(methyl methacrylate) to make a composite with a high toughness and properties comparable to some aluminum alloys. This freeze-casting technique produces the layered materials with remarkable toughness against crack growth, similar to the toughening mechanisms found in some biological composites like nacre.



Martian Rhythmic Rocks

Mars has been known to have some layered sedimentary rocks. With the camera on the Mars Reconnaissance Orbiter, Lewis *et al.* (p. 1532) have constructed stereo images of layered rocks exposed on the floors of several large craters and are now able to measure the thicknesses of individual beds at a resolution of about 1 meter. The layering is rhythmic

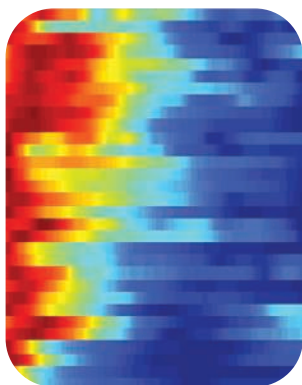
Continued on page 1433

Continued from page 1431

mic, containing several cycles over 10 meters, organized into larger units, which implies that deposition was cyclic. It is possible that variations in Mars's orbit yielded climatic variations and thereby cyclical deposition, as seen in some sedimentary rocks on Earth.

Blue-Light Response

Plants respond to light with a variety of developmental and physiological changes. The receptor for the blue-light wavelengths is cryptochrome. How blue light causes cryptochrome to alter cellular function has been a puzzle. Now, using a yeast two-hybrid screen, **Liu *et al.*** (p. 1535, published online 6 November) have identified a protein from *Arabidopsis*, CIB1, which, in the presence of blue light, interacts with the cryptochrome. CIB1 and cryptochrome colocalize in the plant cell nucleus, where CIB1 functions as a transcription factor. Together, these proteins bring the input of blue light into the signaling pathways that regulate flowering.



A Matter of Life and Death

Pooling data from a population of cells can hide physiologically important differences that can only be seen at the level of individual cells. **Cohen *et al.*** (p. 1511, published online 20 November) describe a system to observe the dynamics in space and time of about 1000 different endogenous proteins in individual living human cells at large-scale, with high temporal resolution and accuracy. A retroviral strategy was used to construct a library of 1200 cell lines, each of which had incorporated a fluorescent protein into an intron in a different gene. The cells were previously tagged for red fluorescence in the nucleus and the cytosol, making automated imaging much easier. The approach was used to identify proteins that show widely different behaviors in individual cells in response

to treatment with camptothecin, a commonly used chemotherapeutic, in a way that corresponds to outcome—cell death or survival.

A Divisive Tale

To ensure that each daughter cell receives a single genomic complement at the end of cell division, the central spindle—a set of microtubule bundles that forms between the separating chromosomes during anaphase—controls assembly and constriction of a cortical contractile actomyosin ring that bisects the separated chromosome masses. A key regulator of signaling by the central spindle is the protein complex centralspindlin. The current dominant model for signaling during cytokinesis proposes a simple positive signaling cascade in which centralspindlin tethers a Rho guanine nucleotide exchange factor (RhoGEF) to the central spindle, thereby activating the small GTPase RhoA locally at the cell equator. RhoA and its effectors, in turn, direct assembly and constriction of the contractile ring that divides the cell. Now **Canman *et al.*** (p. 1543) challenge this view by demonstrating that the critical function of centralspindlin in promoting contractile ring constriction is the negative regulation of Rac, a different Rho family GTPase. Thus centralspindlin may inactivate Rac and its effectors at the cell equator, and it is this negative regulation that promotes the RhoA-dependent constriction of the contractile ring.

How to Feed Your Neurons

The role of neuroglial interactions in brain functions has recently gained attention. Indeed, astrocytes are now viewed as integral active elements of the brain circuitry that play a crucial role in modulating synaptic activity. Astrocytes deliver metabolic substrates to neurons to face energy needs upon increased neuronal activity. However, the fine details of these processes are still unclear.

Rouach *et al.* (p. 1551) demonstrate an essential role for astroglial gap junction proteins, connexin 30 and 43, enriched in perivascular astrocyte endfeet, in the activity-dependent delivery of energetic metabolites to neurons. Glucose metabolites were delivered specifically to astrocytes via a patch pipette in wild-type or double-knockout mice for these connexins, and local neuronal activity was recorded simultaneously. The perivascular connexins allowed intercellular trafficking of glucose metabolites through astroglial networks, which were used by neurons to sustain their excitatory synaptic transmission.

CREDIT: COHEN ET AL.



Bruce Alberts is Editor-in-Chief of *Science*.

A Scientific Approach to Policy

THE FINANCIAL MELTDOWN THAT BEGAN IN THE UNITED STATES HAS NOW SPREAD AROUND THE world, providing a rare opportunity for a rethinking of priorities everywhere. We now know that a major portion of the global financial system was built on a myth—that housing prices would rise forever. This false assumption allowed a complex loan-leveraging process to create immense wealth as if by magic. The sudden collapse of this bubble is causing great hardship worldwide. Nevertheless, the new sense of reality could be beneficial, by stimulating much broader recognition of the centrality of science and engineering for successful modern societies.

Science and engineering produce a vibrant economy. Their effects are strikingly obvious in the innovative industrial clusters that have grown up and prospered near great U.S. research universities, in the Boston and San Francisco Bay areas, for example. Nations such as China have long had a clear view of the source of U.S. economic strength, and they have intensely focused on building their own scientific and technological excellence.* But in addition to the innovation that stems from research, scientific habits of mind contribute critically to a nation's success.

The first of these ways of thinking is a sense of optimism: Scientists and engineers share an assumption, based on past experience, that all problems are, in principle, solvable. Thus, they share a belief that increased fundamental knowledge about the natural world will lead to human progress, because they see this happen in their own fields. The astonishingly productive process by which new knowledge is built—combining old knowledge in unpredictable ways—was documented in the 1990s by the U.S. National Academy of Sciences in a series of 20 eight-page pamphlets that remains valuable today, called *Beyond Discovery: The Path from Research to Human Benefit* (www.beyonddiscovery.org). Every society can benefit from the “can-do” attitude of scientists and engineers.

A second valuable attitude is a focus on long-term consequences. The understandings of the natural world derived from science often allow us to predict the future; thus, we can calculate how much bladder cancer will result 30 years hence from drinking water containing trace amounts of arsenic, or the future effects of increased greenhouse gases on Earth's climate. Politicians and businesspeople too often take a short-term view when balancing costs and benefits, with disastrous effects on their societies. Organizations such as national academies of sciences and engineering can provide forceful advice to governments that highlights long-term effects, thereby mitigating this imbalance.

A third valuable characteristic of most scientists and engineers is an emphasis on discovering what works without reference to ideology. The ultimate test of ideas must come from the evidence obtained by probing the natural world, and the feedback from experiments is often surprising. Thus, success requires that we approach every problem with humility, knowing that our favorite hypotheses may be wrong.

My own field of science is cell biology. Cells are enormously complicated systems, with highly interactive molecular machinery that we are still struggling to understand. Political leaders confront equally complex societal interactions, whether they are dealing with the economy, energy policy, health care, or education. Every nation needs nonideological policy-makers who admit that they don't know all the answers; they must experiment with problem solving and expect to learn from the results, just like scientists and engineers do. In recent years, U.S. leaders have taken a very different approach, with quite unfortunate results.

When queried about how he would approach the world's economic crisis, U.S. President-elect Barack Obama responded (on 16 November 2008 on CBS's *60 Minutes*): “. . . I hope my team can . . . experiment in order to get people working again . . . I think if you talk to the average person right now that they would say, ‘. . . we do expect that if something doesn't work that they're going to try something else until they find something that does.’ And, you know, that's the kind of common-sense approach that I want to take when I take office.”

A very promising start to a hopeful new era.

— Bruce Alberts

10.1126/science.1168790

*W. Jiabao, *Science* **322**, 649 (2008).



PLANT BIOLOGY

A Question of Color

Petal color is a key morphological trait of flowers that influences reproductive success. It is controlled by the pigments produced by the plant, and by the pH at which the pigments are stored. In plants, the anthocyanins—the main class of flower pigments—reside in the vacuoles, an intracellular acidic subcompartment. Because the color of a pigment is often pH-sensitive, variations in petal color have been used to identify mutations in pH regulation. In petunias, Verweij *et al.* now identify PH5 as a P-type proton pump localized to the vacuolar membrane. Similar P-type proton ATPases have previously been found to reside on the cell surface, not on intracellular membranes, which contain their own vacuolar-type proton ATPases. In PH5 mutants, vacuolar acidification is reduced without changing the expression of the anthocyanin pigments or other coloration-related processes, leading to blue flower coloration (shown to the right of a wild-type flower), which is never observed in natural habitats. Expression of the PH5 gene is linked to the same transcription regulation involved in anthocyanin production. This coordination of pigment production and pH regulation of the pigment-containing compartment is an important aspect in maintaining flower and also seed coloration, which also requires PH5 activity during pigment accumulation. — SMH

Nat. Cell Biol. **10**, 10.1038/ncb1805 (2008).

APPLIED PHYSICS

Get IT Down on Paper

A few years ago, when you wanted to remember something, the standard thing to do was to jot it down on a piece of paper. Now you might tend to note it in some kind of electronic storage device. At the heart of these storage devices is microelectronic circuitry, with billions of transistors carved out of silicon to do the processing and memory elements that store the information either magnetically or electrically. Martins *et al.* take the process full circle by fabricating electronic transistors and storage elements using paper as the substrate and the dielectric layer within the traditional transistor design. Using multilayer compact natural cellulose fibers,

embedded in a mix of ionic resin and adhesive glue to provide mechanical stability, they fabricate transistors with respectable carrier mobilities on the order of 40 cm²/V·s. Moreover, when the transistors are switched off, they can retain their memory for more than 14,000 hours because of charge storage effects within the paper dielectric. This demonstration is encouraging for the further development of lightweight and cheap electronic technology. — ISO

Appl. Phys. Lett. **93**, 203501 (2008).

CHEMISTRY

Spinning Bases

The pH of any sample of water is easily measured nowadays and reflects in broad terms the

concentration of protons that have physically separated from charge-balancing counterions. These “free” protons are in fact still linked to water molecules, though, and the structural basis of the link—whether H₃O⁺, (H₂O)₂H⁺, or some higher cluster—remains a subject of intense research and debate. Similarly, the OH[−] ion left behind when a proton is snatched out of H₂O has its own complex interactions with the water molecules surrounding it. Thøgersen *et al.* have probed the nature of the OH[−] solvation shell using ultrafast rotational anisotropy measurements. Specifically, they excited the anion using an ultraviolet pulse resonant with a charge-transfer-to-solvent transition (cleverly chosen to select the ion from among bulk water absorptions), and then tracked its rate in tumbling out of the laser plane across a range of temperatures. Above about 17°C, the OH[−] rotates rather similarly to a water molecule, but below that temperature, the rate slows down significantly, suggesting that the ion’s motion is restricted by a more tightly bound shell of solvent. — JSY

Chem. Phys. Lett. **466**, 1 (2008).

MICROBIOLOGY

Cation Catcher

The lungs of cystic fibrosis (CF) sufferers always become colonized with antibiotic-resistant bacteria and are traumatized by inflammatory responses as they become blocked with mucus, alginate, and DNA. The DNA may originate from bacteriophage- or host-mediated disruption of bacteria but may also come from the host as infiltrated immune cells lyse. Mulcahy *et al.*

noted that DNA is highly anionic and went on to show that, whatever its source, it can act as a chelator of Mg²⁺ and Ca²⁺. At high concentrations, presumably in areas adjacent to the epithelium of the lung, DNA soaks up cations to cause gross membrane disruption and thus has a strong antimicrobial effect. It’s not all good news, though, as physicochemical gradients form deeper within the clots of mucus and the bacterial biofilm within the airways. At



Continued on page 1439

Continued from page 1437

lower concentrations, the DNA soaks up just enough cations to trigger signalling cascades that culminate in the addition of aminoarabinose to the surface lipopolysaccharide molecules of the major pathogen in CF, *Pseudomonas aeruginosa*. This change renders the bacterium resistant to small defensive peptide molecules produced by the host as well as to aminoglycoside antibiotics. — CA

PLoS Pathogens 4, e1000213 (2008).

GEOPHYSICS

Soft Vibrations

Microseisms—the continuous, low-amplitude background vibrations in the solid Earth observed between earthquakes—are generated by ocean waves. Most microseism studies have concentrated on the vibrations transmitted as surface (S) waves, and have concluded that they originate in shallow coastal regions, but relatively little is known about microseisms that propagate as body (P) waves. Gerstoft *et al.* show that body waves measured at an array of sites in southern California are generated by distant storms in



several distinct regions of the Northern and Southern Hemispheres, where the ocean is deep, and that they propagate through Earth's mantle and core. In addition to identifying source regions, these P waves can provide information about deep Earth structure along paths not usually sampled by global tomographic studies, because the earthquakes used in those analyses occur mostly along plate boundaries rather than in the open ocean. — HJS

Geophys. Res. Lett., 10.1029/2008GL036111 (2008).

CELL BIOLOGY

Roping in Rabs

The Golgi apparatus receives vesicles and other membrane-bound carriers from earlier compartments of the secretory pathway and must guide them to the correct cisternae within the Golgi stack. At the same time, it must exclude other large structures such as ribosomes. Sinka *et al.* suggest that coiled-coil domains, termed golgins, which localize to particular Golgi subdomains through their C termini, might play a role in vesicle sorting. They found that the

GRIP domain golgins in *Drosophila* bind members of the Rab family of G proteins through binding sites organized along the length of their coiled-coil domains. A single Rab showed binding to multiple GRIP domain proteins and a single golgin coiled-coil domain bound more than one Rab. They suggest that the golgins form an array that surrounds the Golgi with the coiled-coils projecting into the cytoplasm like tentacles. The tentacles might capture Rab-bearing membranes but exclude structures such as ribosomes that lack Rabs. Different binding specificities may both influence the localization of initial capture and allow iterative binding and release in order to move captured membranes to the appropriate Golgi subdomain. This scheme would be analogous to the proposal for the nuclear pore in which importins are moved through the pore by binding to a gel of phenylalanine-glycine repeats formed by nuclear porins. — VV

J. Cell. Biol. 183, 607 (2008).

BIOMEDICINE

Clues from Outside

Tumors that appear clinically related can respond quite differently to treatment and radically alter the outcome for the patient. Gene expression profiling on tumors is thus useful for detecting differences that can help to improve diagnosis and prognosis and predict patient response to treatment. It has already been used successfully in the clinic, particularly for patients with breast cancer. Hepatocellular carcinoma is often caused by hepatitis infection and liver cirrhosis. It is a major cause of cancer death worldwide, but disease recurrence has so far proven difficult to predict. Expression profiling has been limited by a requirement for frozen tissues, as many specimens have been, and are still being, formalin-fixed. Hoshida *et al.* developed a method for accurately profiling the expression of 6000 genes from formalin-fixed and paraffin-embedded samples, some of which were 24 years old. They found no association between the gene expression profiles of hepatocellular carcinoma tumors and prognosis. Instead, they found an expression signature from the surrounding non-tumoral liver tissue that could predict the late recurrence of tumors. The authors suggest that this survival signature indicates the state of the liver and how likely it is to become malignant, which may be determined by a prior event such as viral exposure. Profiling the surrounding tissue, rather than the actual tumor as is customary, may prove to be a useful tool for the treatment of other cancers. — HP*

N. Engl. J. Med. 359, 1995 (2008).

*Helen Pickersgill is a locum editor in *Science's* editorial department.

1200 New York Avenue, NW
Washington, DC 20005

Editorial: 202-326-6550, FAX 202-289-7562

News: 202-326-6581, FAX 202-371-9227

Bateman House, 82-88 Hills Road
Cambridge, UK CB2 1LQ

+44 (0) 1223 326500, FAX +44 (0) 1223 326501

SUBSCRIPTION SERVICES For change of address, missing issues, new orders and renewals, and payment questions: 866-434-AAAS (2227) or 202-326-6417, FAX 202-842-1065. Mailing addresses: AAAS, P.O. Box 96178, Washington, DC 20090-6178 or AAAS Member Services, 1200 New York Avenue, NW, Washington, DC 20005

INSTITUTIONAL SITE LICENSES please call 202-326-6755 for any questions or information

REPRINTS: Author Inquiries 800-635-7181

Commercial Inquiries 803-359-4578

202-326-7074, FAX 202-682-0816

MEMBER BENEFITS AAAS/Barnes&Noble.com bookstore www.aaas.org/bn; AAAS Online Store www.apisource.com/aaas/ code MKB6; AAAS Travels: Betchart Expeditions 800-252-4910; Apple Store www.apple/epstore/aaas; Bank of America MasterCard 1-800-833-6262 priority code FAA3YU; Cold Spring Harbor Laboratory Press Publications www.cshlpress.com/affiliates/aaas.htm; GEICO Auto Insurance www.geico.com/landingpage/go51.htm?logo=17624; Hertz 800-654-2200 CDP#343457; Office Depot www.officedepot.com/portalLogin.do; Seabury & Smith Life Insurance 800-424-9883; Subaru VIP Program 202-326-6417; VIP Moving Services www.vipmayflower.com/domestic/index.html; Other Benefits: AAAS Member Services 202-326-6417 or www.aaasmember.org.

science_editors@aaas.org (for general editorial queries)

science_letters@aaas.org (for queries about letters)

science_reviews@aaas.org (for returning manuscript reviews)

science_bookrevs@aaas.org (for book review queries)

Published by the American Association for the Advancement of Science (AAAS), *Science* serves its readers as a forum for the presentation and discussion of important issues related to the advancement of science, including the presentation of minority or conflicting points of view, rather than by publishing only material on which a consensus has been reached. Accordingly, all articles published in *Science*—including editorials, news and comment, and book reviews—are signed and reflect the individual views of the authors and not official positions of view adopted by AAAS or the institutions with which the authors are affiliated.

AAAS was founded in 1848 and incorporated in 1874. Its mission is to advance science, engineering, and innovation throughout the world for the benefit of all people. The goals of the association are to: enhance communication among scientists, engineers, and the public; promote and defend the integrity of science and its use; strengthen support for the science and technology enterprise; provide a voice for science on societal issues; promote the responsible use of science in public policy; strengthen and diversify the science and technology workforce; foster education in science and technology for everyone; increase public engagement with science and technology; and advance international cooperation in science.

INFORMATION FOR AUTHORS

See pages 634 and 635 of the 1 February 2008 issue or access www.sciencemag.org/about/authors

EDITOR-IN-CHIEF **Bruce Alberts**

EXECUTIVE EDITOR **Monica M. Bradford**

DEPUTY EDITORS

R. Brooks Hanson, Barbara R. Jasny,
Katrina L. Kelnor

NEWS EDITOR

Colin Norman

EDITORIAL SUPERVISORY SENIOR EDITOR Phillip D. Szuroni; **SENIOR EDITOR/PERSPECTIVES** Lisa D. Chong; **SENIOR EDITORS** Gilbert J. Chin, Pamela J. Hines, Paula A. Kiberstis (Boston), Marc S. Lavine (Toronto), Beverly A. Purnell, L. Bryan Ray, Guy Riddihough, H. Jesse Smith, Valda Vinson; **ASSOCIATE EDITORS** Kristen L. Mueller, Jake S. Yeston, Laura M. Zahn; **ONLINE EDITOR** Stewart Wells; **ASSOCIATE ONLINE EDITORS** Robert Frederick, Tara S. Marathe; **WEB CONTENT DEVELOPER** Martyn Green; **BOOK REVIEW EDITOR** Sherman J. Suter; **ASSOCIATE LETTERS EDITOR** Jennifer Sills; **EDITORIAL MANAGER** Cara Tate; **SENIOR COPY EDITORS** Jeffrey E. Cook, Cynthia Howe, Harry Jach, Barbara P. Ordway, Trista Wagoner; **COPY EDITORS** Chris Filiatreau, Lauren Kmeck; **EDITORIAL COORDINATORS** Carolyn Kyle, Beverly Shields; **PUBLICATIONS ASSISTANTS** Ramatoulaye Diop, Joi S. Granger, Jeffrey Hearn, Lisa Johnson, Scott Miller, Jerry Richardson, Jennifer A. Seibert, Brian White, Anita Wynn; **EDITORIAL ASSISTANTS** Carlos L. Durham, Emily Guise, Patricia M. Moore; **EXECUTIVE ASSISTANT** Sylvia S. Kihara; **ADMINISTRATIVE SUPPORT** Maryrose Madrid

NEWS DEPUTY NEWS EDITORS Robert Coontz, Elizabeth Marshall, Jeffrey Mervis, Leslie Roberts; **CONTRIBUTING EDITORS** Elizabeth Culotta, Polly Shulman; **NEWS WRITERS** Yudhijit Bhattacharjee, Adrian Cho, Jennifer Couzin, David Grimm, Constance Holden, Jocelyn Kaiser, Richard A. Kerr, Eli Kintisch, Andrew Lawler (New England), Greg Miller, Elizabeth Pennisi, Robert F. Service (Pacific NW), Erik Stokstad; **INTERN** Rachel Zerkowitz; **CONTRIBUTING CORRESPONDENTS** Jon Cohen (San Diego, CA), Daniel Ferber, Ann Gibbons, Robert Koenig, Milt Lisch, Charles C. Mann, Virginia Morell, Evelyn Strauss, Gary Taubes; **COPY EDITORS** Linda B. Felaco, Melvin Gatling, Melissa Raimondi; **ADMINISTRATIVE SUPPORT** Scherraine Mack, Fannie Groom; **BUREAU** New England: 207-549-7755, San Diego, CA: 760-942-3252, FAX 760-942-4979, Pacific Northwest: 503-963-1940

PRODUCTION DIRECTOR James Landry; **SENIOR MANAGER** Wendy K. Shank; **ASSISTANT MANAGER** Rebecca Doshi; **SENIOR SPECIALISTS** Steve Forrester, Chris Redwood; **SPECIALIST** Anthony Rosen; **PREFLIGHT DIRECTOR** David M. Tompkins; **MANAGER** Marcus Spiegler

ART DIRECTOR Yael Kats; **ASSOCIATE ART DIRECTOR** Laura Creveling; **ILLUSTRATORS** Chris Bickel, Katharine Suttiff; **SENIOR ART ASSOCIATES** Holly Bishop, Preston Huey, Nayomi Kevitiyagala; **ART ASSOCIATE** Jessica Newfield; **PHOTO EDITOR** Leslie Blizard

SCIENCE INTERNATIONAL

EUROPE (science@science-int.co.uk) **EDITORIAL: INTERNATIONAL MANAGING EDITOR** Andrew M. Sugden; **SENIOR EDITOR/PERSPECTIVES** Julia Fahrenkamp-Uppenbrink; **SENIOR EDITORS** Caroline Ash, Stella M. Hurtle, Ian S. Osborne, Peter Senior; **ASSOCIATE EDITOR** Maria Cruz; **EDITORIAL SUPPORT** Deborah Dennison, Rachel Roberts, Alice Whaley; **ADMINISTRATIVE SUPPORT** John Cannell, Janet Clements; **NEWS: EUROPE NEWS EDITOR** John Travis; **DEPUTY NEWS EDITOR** Daniel Clerly; **CONTRIBUTING CORRESPONDENTS** Michael Balter (Paris), John Bohannon (Vienna), Martin Enserink (Amsterdam and Paris), Gretchen Vogel (Berlin); **INTERN** Sara Coelho

ASIA Japan Office: Asca Corporation, Eiko Ishioka, Fusako Tamura, 1-8-13, Hirano-cho, Chuo-ku, Osaka-shi, Osaka, 541-0046 Japan; +81 (0) 6 2602 6272, FAX +81 (0) 6 2602 6271; asca@os.gulf.or.jp; **ASIA NEWS EDITOR** Richard Stone (Beijing: rstone@aaas.org); **CONTRIBUTING CORRESPONDENTS** Dennis Normile (Japan: +81 (0) 3 3391 0630, FAX +81 (0) 3 5936 3531; dnormile@gol.com); Hao Xin (China: +86 (0) 10 6307 4439 or 6307 3676, FAX +86 (0) 10 6307 4358; cindyhao@gmail.com); Pallava Bagla (South Asia: +91 (0) 11 2271 2896; pbagla@vsnl.com)

EXECUTIVE PUBLISHER **Alan I. Leshner**

PUBLISHER **Beth Rosner**

FULFILLMENT SYSTEMS AND OPERATIONS (membership@aaas.org); **DIRECTOR** Waylon Butler; **SENIOR SYSTEMS ANALYST** Jonny Blaker; **CUSTOMER SERVICE SUPERVISOR** Pat Butler; **SPECIALISTS** Latoya Casteel, LaVonda Crawford, Vicki Linton, April Marshall; **DATA ENTRY SUPERVISOR** Cynthia Johnson; **SPECIALISTS** Eintou Bowden, Tarrika Hill, William Jones

BUSINESS OPERATIONS AND ADMINISTRATION DIRECTOR Deborah Rivera-Wienhold; **ASSISTANT DIRECTOR, BUSINESS OPERATIONS** Randy Yi; **MANAGER, BUSINESS ANALYSIS** Michael LoBue; **MANAGER, BUSINESS OPERATIONS** Jessica Tierney; **FINANCIAL ANALYSTS** Priti Pamnani, Celeste Troxler; **RIGHTS AND PERMISSIONS: ADMINISTRATOR** Emilie Davis; **ASSOCIATE** Elizabeth Sandler; **MARKETING DIRECTOR** John Meyers; **MARKETING MANAGER** Allison Pritchard; **MARKETING ASSOCIATES** Aimee Aponte, Alison Chandler, Mary Ellen Crowley, Marcia Leach, Julianne Wielga, Wendy Wise; **INTERNATIONAL MARKETING MANAGER** Wendy Sturley; **MARKETING EXECUTIVE** Jennifer Reeves; **MARKETING/MEMBER SERVICES EXECUTIVE** Linda Rusk; **DIRECTOR, SITE LICENSING** Tom Ryan; **DIRECTOR, CORPORATE RELATIONS** Eileen Bernadette Moran; **PUBLISHER RELATIONS, RESOURCES SPECIALIST** Kiki Forsythe; **SENIOR PUBLISHER RELATIONS SPECIALIST** Catherine Holland; **PUBLISHER RELATIONS, EAST COAST** Phillip Smith; **PUBLISHER RELATIONS, WEST COAST** Philip Tsolakidis; **FULFILLMENT SUPERVISOR** Iquo Edim; **ELECTRONIC MEDIA: MANAGER** Lizabeth Harman; **PROJECT MANAGER** Trista Snyder; **ASSISTANT MANAGER** Lisa Stanford; **SENIOR PRODUCTION SPECIALISTS** Christopher Coleman, Walter Jones; **PRODUCTION SPECIALISTS** Nichele Johnston, Kimberly Oster

ADVERTISING DIRECTOR, WORLDWIDE AD SALES Bill Moran

PRODUCT (science_advertising@aaas.org); **MIDWEST/WEST COAST/W. CANADA** Rick Bongiovanni: 330-405-7080, FAX 330-405-7081; **EAST COAST** E. Canada Laurie Faraday: 508-747-9395, FAX 617-507-8189; **UK/EUROPE/ASIA** Roger Gonçalves: TEL/FAX +41 43 234 1358; **JAPAN** Masuyoshi Yoshikawa: +81 (0) 3 3235 5961, FAX +81 (0) 3 3235 5852; **SENIOR TRAFFIC ASSOCIATE** Deandra Simms

COMMERCIAL EDITOR Sean Sanders: 202-326-6430

PROJECT DIRECTOR, OUTREACH Brianna Blaser

CLASSIFIED (advertise@sciencemag.org); **US: RECRUITMENT SALES MANAGER** Ian King: 202-326-6528, FAX 202-289-6742; **INSIDE SALES MANAGER: MIDWEST/CANADA** Daryl Anderson: 202-326-6543; **INSIDE SALES REPRESENTATIVE** Karen Foote: 202-326-6740; **KEY ACCOUNT MANAGER** Joribah Able; **NORTHEAST** Alexis Fleming: 202-326-6578; **SOUTHEAST** Tina Burks: 202-326-6577; **WEST** Nicholas Hintzbide: 202-326-6533; **SALES COORDINATORS** Erika Foad, Rohan Edmonson, Shirley Young; **INTERNATIONAL: SALES MANAGER** Tracy Holmes: +44 (0) 1223 326525, FAX +44 (0) 1223 326532; **SALES** Sumaira Kharaz, Dan Pennington, Alex Palmer; **SALES ASSISTANT** Louise Moore; **JAPAN** Masuyoshi Yoshikawa: +81 (0) 3 3235 5961, FAX +81 (0) 3 3235 5852; **ADVERTISING PRODUCTION OPERATIONS MANAGER** Deborah Tompkins; **SENIOR PRODUCTION SPECIALIST/GRAPHIC DESIGNER** Amy Hardcastle; **SENIOR PRODUCTION SPECIALIST** Robert Buck; **SENIOR TRAFFIC ASSOCIATE** Christine Hall; **PUBLICATIONS ASSISTANT** Mary Lagnaoui

AAAS BOARD OF DIRECTORS **RETIRED PRESIDENT**, CHAIR David Baltimore; **PRESIDENT** James J. McCarthy; **PRESIDENT-ELECT** Peter C. Agre; **TREASURER** David E. Shaw; **CHIEF EXECUTIVE OFFICER** Alan I. Leshner; **BOARD** Lynn W. Enquist, Susan M. Fitzpatrick, Alice Gal, Linda P. B. Katch, Nancy Knowlton, Cherry A. Murray, Thomas D. Pollard, Thomas A. Woolsey



ADVANCING SCIENCE, SERVING SOCIETY

SENIOR EDITORIAL BOARD

John I. Brauman, Chair, Stanford Univ.
Richard Losick, Harvard Univ.
Robert May, Univ. of Oxford
Marcia McClurt, Monterey Bay Aquarium Research Inst.
Linda Partridge, Univ. College London
Vera C. Rubin, Carnegie Institution
Christopher R. Somerville, Univ. of California, Berkeley

BOARD OF REVIEWING EDITORS

Joanna Aizenberg, Harvard Univ.
R. McNeill Alexander, Leeds Univ.
David Altschuler, Broad Institute
Arturo Alvarez-Buylla, Univ. of California, San Francisco
Richard Amasino, Univ. of Wisconsin, Madison
Angelika Amon, MIT
Meinrat O. Andreae, Max Planck Inst., Mainz
Kristi S. Anseth, Univ. of Colorado
John A. Bargh, Yale Univ.
Cornelia I. Bargmann, Rockefeller Univ.
Ben Barres, Stanford Medical School
Marisa Bartolomei, Univ. of Penn. School of Med.
Ray H. Baughman, Univ. of Texas, Dallas
Stephen J. Benkovic, Penn State Univ.
Michael J. Bevan, Univ. of Washington
Ton Bisseling, Wageningen Univ.
Mina Bissell, Lawrence Berkeley National Lab
Peer Bork, EMBL
Dianna Bowles, Univ. of York
Robert W. Boyd, Univ. of Rochester
Paul M. Brakefield, Leiden Univ.
Dennis Bray, Univ. of Cambridge
Stephen Buratowski, Harvard Medical School
Joseph A. Burns, Cornell Univ.
William P. Buttz, Population Reference Bureau
Peter Carmeliet, Univ. of Leuven, VIB
Gerbrand Ceder, MIT
Milred Cho, Stanford Univ.
David Clapham, Children's Hospital, Boston
David Clary, Oxford University
J. M. Claverie, CNRS, Marseille

Jonathan D. Cohen, Princeton Univ.
Stephen M. Cohen, Temasek Life Sciences Lab, Singapore
Robert H. Crabtree, Yale Univ.
F. Fleming Crim, Univ. of Wisconsin
William Cumberland, Univ. of California, Los Angeles
George Q. Daley, Children's Hospital, Boston
Jeff L. Dangl, Univ. of North Carolina
Stanislav Dehaene, Collège de France
Edward DeLong, MIT
Emmanouil T. Dermizakis, Wellcome Trust Sanger Inst.
Robert Desimone, MIT
Dennis Discher, Univ. of Pennsylvania
Scott C. Doney, Woods Hole Oceanographic Inst.
Peter J. Donovan, Univ. of California, Irvine
W. Ford Doolittle, Dalhousie Univ.
Jennifer A. Doudna, Univ. of California, Berkeley
Julian Downward, Cancer Research UK
Denis Duboule, Univ. of Geneva/EPFL Lausanne
Christopher Dye, WHO
Richard Ellis, Cal Tech
Gerhard Ertl, Fritz-Haber-Institut, Berlin
Douglas H. Erwin, Smithsonian Institution
Mark Estelle, Indiana Univ.
Barry Everitt, Univ. of Cambridge
Paul G. Falkowski, Rutgers Univ.
Ernst Fehr, Univ. of Zurich
Ton Fenchel, Univ. of Copenhagen
Alain Fischer, INSERM
Scott E. Fraser, Cal Tech
Chris D. Frith, Univ. College London
Wulfram Gerstner, EPFL Lausanne
Charles Godfrey, Univ. of Oxford
Diane Griffin, Johns Hopkins Bloomberg School of Public Health
Christian Haas, Ludwig Maximilians Univ.
Niels Hansen, Technical Univ. of Denmark
Dennis L. Hartmann, Univ. of Washington
Chris Hawkesworth, Univ. of Bristol
Martin Heimann, Max Planck Inst., Jena
James A. Hendler, Rensselaer Polytechnic Inst.
Ray Hilborn, Univ. of Washington
Ove Hoegh-Guldberg, Univ. of Queensland
Ronald R. Hoy, Cornell Univ.
Olli Ikkala, Helsinki Univ. of Technology
Meyer B. Jackson, Univ. of Wisconsin Med. School

Stephen Jackson, Univ. of Cambridge
Steven Jacobsen, Univ. of California, Los Angeles
Peter Jonas, Universität Freiburg
Barbara B. Kahn, Harvard Medical School
Daniel Kahne, Harvard Univ.
Gerd Karsenty, Columbia Univ. College of P&S
Bernhard Keimer, Max Planck Inst., Stuttgart
Elizabeth A. Kelloff, Univ. of Missouri, St. Louis
Alan B. Krueger, Princeton Univ.
Lee Kump, Penn State Univ.
Mitchell A. Lazar, Univ. of Pennsylvania
Virginia Lee, Univ. of Pennsylvania
Norman L. Letvin, Beth Israel Deaconess Medical Center
Lois Lindvall, Univ. Hospital, Lund
John Lis, Cornell Univ.
Richard Losick, Harvard Univ.
Ke Lu, Chinese Acad. of Sciences
Andrew P. MacKenzie, Univ. of St Andrews
Raul Madariaga, Ecole Normale Supérieure, Paris
Anne Maquarrie, Univ. of St Andrews
Virginia Miller, Washington Univ.
Yasushi Miyashita, Univ. of Tokyo
Richard Morris, Univ. of Edinburgh
Edward Moser, Norwegian Univ. of Science and Technology
Naoto Nagaosa, Univ. of Tokyo
James Nelson, Stanford Univ. School of Med.
Timothy W. Nilsen, Case Western Reserve Univ.
Roeland Nolte, Univ. of Nijmegen
Heleni Nowotny, European Research Advisory Board
Eric N. Olson, Univ. of Texas, SW
Elinor O'Shea, Harvard Univ.
Elmer Ostrom, Indiana Univ.
Jonathan T. Overpeck, Univ. of Arizona
John Pendry, Imperial College
Philippe Poulin, CNRS
Molly Power, Univ. of California, Berkeley
Marty Przeworski, Univ. of Chicago
David J. Read, Univ. of Sheffield
Les Real, Emory Univ.
Colin Renfrew, Univ. of Cambridge
Trevor Robbins, Univ. of Cambridge
Barbara A. Romanowicz, Univ. of California, Berkeley
Edward M. Rubin, Lawrence Berkeley National Lab
Jürgen Sandkühler, Medical Univ. of Vienna
David S. Schimel, National Center for Atmospheric Research

David W. Schindler, Univ. of Alberta
Georg Schulz, Albert-Ludwigs-Universität
Paul Schulze-Lefert, Max Planck Inst., Cologne
Christine Seidman, Harvard Medical School
Terrence J. Sejnowski, The Salk Institute
David Sibley, Washington Univ.
Montgomery Slatkin, Univ. of California, Berkeley
George Somero, Stanford Univ.
Joan Steitz, Yale Univ.
Elisbeth Stern, ETH Zürich
Jerome Strauss, Virginia Commonwealth Univ.
Glen Telling, Univ. of Kentucky
Marc Tessier-Lavigne, Genentech
Jurg Tschopp, Univ. of Lausanne
Michiel van der Klis, Astronomical Inst. of Amsterdam
Derek van der Kooy, Univ. of Toronto
Bert Vogelstein, Johns Hopkins Univ.
Ulrich H. von Andrian, Harvard Medical School
Bruce D. Walker, Harvard Medical School
Christopher A. Walsh, Harvard Medical School
Graham Warren, Yale Univ. School of Med.
Colin Watts, Univ. of Dundee
Detlef Weigel, Max Planck Inst., Tübingen
Jonathan Weisman, Univ. of California, San Francisco
Ellen D. Williams, Univ. of Maryland
Ian A. Wilson, The Scripps Res. Inst.
Jerry Workman, Stowers Inst. for Medical Research
John R. Yates III, The Scripps Res. Inst.
Jan Zaenen, Leiden Univ.
Martin Zatz, NIMH, NIH
Huda Zoghbi, Baylor College of Medicine
Marta Zubir, MIT

BOOK REVIEW BOARD

John Aldrich, Duke Univ.
David Bloom, Harvard Univ.
Angela Creager, Princeton Univ.
Richard Sweder, Univ. of Chicago
Ed Wasserman, DuPont
Lewis Wolpert, Univ. College London

Molecular Match for Man Who Moved the Earth

Nicolaus Copernicus died in 1543, decades before his book *De Revolutionibus Orbium Coelestium* changed the world with the idea that Earth orbits the sun. He was buried in an unmarked grave.

In 2005, archaeologists from the Institute of Anthropology and Archaeology in Pultusk, Poland, used church records and ground-penetrating radar to unearth a skeleton from under a medieval cathedral in the Polish town of Frombork whose age matched the 70-year-old Copernicus. Analysis of the bones and a recon-



struction of the face supported the identification. But without DNA evidence, the team couldn't be sure—and Copernicus, a Catholic priest, left no known heirs.

He did leave hairs, however. In the archives of the University of Uppsala in Sweden, researchers found several nestled deep in the binding of Copernicus's well-thumbed copy of a standard astronomical reference, *Calendarium Romanum Magnum*. Uppsala geneticist Marie Allen extracted and amplified mitochondrial DNA from the badly degraded hairs and compared it with mtDNA from the skeleton's tooth. The results, announced last week in Warsaw, were positive.

Pultusk archaeologist Jerzy Gassowski, who led the 2005 excavation, says Copernicus's bones will be reburied in Frombork in 2010.

Soaking Up Some Rays

Fiber optics has an undersea prototype, it turns out. German marine biologists have discovered that living sponges can beam light to their innermost tissues through tubelike skeletal structures known as spicules.

Many sponges are hosts to symbiotic photo-

synthetic bacteria or algae. Scientists once thought these lived only at the surface but later discovered that even microbes deep inside were getting needed light.

But how? Franz Brümmer of the University of Stuttgart dissected the sponge *Tethya aurantium* and discovered that its silica-based spicules, which look and act a lot like optical fibers, could easily transmit light. Inserting photosensitive paper into tiny slits made in living sponges, he found that each spicule channeled light to the sun-loving microbes deep within.

Mike Taylor, a marine microbiologist with the University of Auckland, New Zealand, says the study "tells us more about how photosynthetic organisms can survive deep inside sponges" and the nature of their symbiotic relationship.

Déjà Vu: A Twitch in the Brain

An epileptic man's daily bouts of déjà vu have supplied new clues to the origins of this unsettling phenomenon.

The British man, known as MH, has temporal lobe epilepsy from a case of encephalitis. Before a seizure, he has spells lasting up to a minute in which he feels he has already experienced whatever is going on around him.

Psychologist Akira O'Connor of Washington University in St. Louis, Missouri, and colleagues say there are two prevailing interpretations of what causes déjà vu episodes. The "data-driven" theory holds that a new visual experience can seem familiar if it resembles a past memory. The "top-down" theory describes déjà vu as a twitch in the brain's circuitry that attaches a sensation of memory to anything a person sees.

After interviewing MH, the authors concluded in the November issue of *Brain and Cognition* that his experience fits the top-down theory. In fact, says O'Connor, the temporal

lobes have been previously connected to sensations of familiarity.

The "interesting and novel" report shows for the first time that déjà vu can be generated by temporal lobe misfiring—at least in people with epilepsy, says Anne Cleary, a psychologist at Colorado State University in Fort Collins. But she says it doesn't rule out external visual triggers for nonepileptics.

A cut through *Tethya aurantium* shows its light-transmitting spicules.



Artists like to push the limits of creativity. London artist Nasser Azam has gone on to push the limits of physics, creating what he calls the first-ever zero-gravity paintings.

Azam painted two triptychs labeled "Homage to Francis Bacon" during a 2-hour parabolic flight last July. To prepare for his "Life in Space" project, funded by the Russian Space Agency, Azam underwent 3 days of intensive training in Star City, the cosmonaut facility outside Moscow.

On the ground, he sketched the works in acrylic paints. Then, during 15 zero-gravity parabolic cycles at an altitude of 7000 meters, the artist, strapped to railings, finished the paintings in nondrippy oil pastels. "It was quite a harsh experience," says Azam, 45, who managed not to get sick during the flight. Still, he says, "I was quite pleased with the end result."

He might well be. Azam, former chief operating officer at Merrill Lynch in London, sold one of the triptychs for \$332,500 last month at a Phillips de Pury auction in New York City.

His next painting adventure: Antarctica.



Nonprofit World

SUSTAINABLE GOAL. Trained in the United States, Rikin Gandhi went to India in 2006 intending to help Indian farmers produce biofuels for their energy needs. But when he saw farmers struggling under crushing poverty, he decided a better use of his computer science degree would be to popularize efficient farming practices such as composting. So Gandhi (center, with camera) joined Microsoft Research India to start a project, called Digital Green, that has spread such practices by distributing demo DVDs to a dozen villages in southern and eastern India.

Within the next 3 months, Digital Green will leave the fold and become an independent nonprofit organization. Gandhi's goal is to reach 3000 villages with farming techniques that can help villagers out of poverty. "He's putting the pieces together in such a way that the direction [of the project] is not compromised, while still getting the best advice he can get," says Kentaro Toyama, who leads the Microsoft Research office in Bangalore, India.

MONEY MATTERS

CHARITABLE SCIENCE. Two former college roommates have developed a new scheme to raise and distribute money for research: Ask the public to invest in their favorite projects.

David Vitrant (below), 30, a graduate student in genetics at the University of Pittsburgh in Pennsylvania, and Mark Friedgan (bottom), 29, an entrepreneur in Chicago, launched Fund Science (www.fundscience.org) this fall.



Their goal is to raise almost \$1.5 million in the first 3 years and offer 25 grants. Donors can scroll through "public abstracts" from submitted applications, after they've been vetted by the company's board, to determine where they'd like their dollars to go.



The target recipients are young scientists. "Even if these people have ideas and they have the drive, they have no funding," says Friedgan, adding that he has been struck by how much easier it has been for him to get his business ideas funded. Even though tax dollars already support scientific research, Friedgan predicts that the public will be keen to back more—because this time, "they're going to be passionate about it." Vitrant plans to devote himself full-time to Fund Science after finishing his Ph.D.

MILESTONES

GRANDPA'S TELESCOPE.

Commissioned by astronomer George Ellery Hale, this 60-inch telescope atop Mount Wilson, California, saw first light on 13 December 1908. Hale's grandsons Sam (left) and Brack (right) peered through the instrument during a centennial celebration last month. The telescope remained the world's largest until 1917, when the 100-inch Hooker Telescope was unveiled.



THEY SAID IT

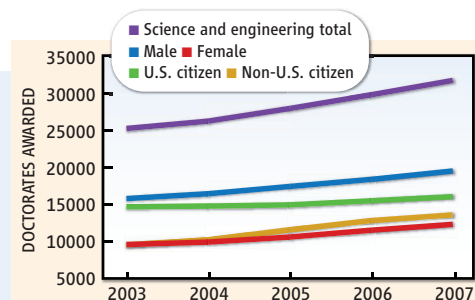
"That's an awful lot of people being pulled aside and inconvenienced. I think it's a sham. We have no evidence it works."

—Carnegie Mellon University statistician Stephen Fienberg on the U.S. Transportation Security Administration's behavioral screening program, whose primary aim is to spot suspected terrorists at airports based on suspicious behavior. Fienberg has studied the 2-year-old program and other counterterrorism efforts.

Data Point >>

CAMPUS THROING. Those who worry that the United States isn't producing enough Ph.D.s in science and engineering can take heart from the latest *Survey of Earned Doctorates* by the U.S. National Science Foundation. U.S. institutions granted a record 31,801 science and engineering doctorates in 2007, a 6.5% increase over 2006. The increase continues a steady, upward trend that began in 2003. Although driven by more non-U.S. citizens earning science and engineering doctorates (up 6%), the trend includes more U.S. citizens (up 3.6%), too.

The continuing increase in the number of foreign students earning Ph.D.s shows that "fears about the U.S. slipping as a destination for academic talent were overblown," says Daryl Chubin, director of the AAAS Center for Advancing Science & Engineering Capacity. But he cautions that rising numbers of women and minorities receiving doctorates aren't translating into a more diverse science and engineering faculty. "The achievement of the Ph.D. credential is not the end game," he says.



ASTRONOMY

Three Asian Nations Link Up to Form A Formidable Radio Telescope Array

SEOUL—The hill smack in the center of Yonsei University here gives a spectacular view of the school's gardenlike campus and, in the distance, downtown Seoul. Astronomers from South Korea and across Asia also hope this vantage point will offer an arresting view of the heavens. A 21-meter radio antenna perched on the hilltop is part of Korea's first very long baseline interferometry (VLBI) array, completed this week.

Linked to arrays in Japan and China, Korea's three instruments will fill out the densest network of its kind, says Hideyuki Kobayashi, a radio astronomer at the National Astronomical Observatory of Japan in Mitaka. The East Asia VLBI Network comprises 19 antennas scattered over 6000 kilometers, from Urumqi in northwestern China to Japan's remote Ogasawara Island, and from Hokkaido to Kunming in China's southwest. A rival to U.S. and European networks (with 10 and eight instruments, respectively), the East Asia VLBI is expected to put Asian astronomers at the vanguard of mapping stars and galaxies and studying active galactic nuclei and other exotic objects.

The three national arrays of the East Asia network were conceived independently but work well together. Japan brought its VLBI Exploration of Radio Astrometry (VERA) network of four 20-meter antennas online in 2004. Its primary objective is to construct a precise three-dimensional map of the Milky Way. For some observations, VERA's power can be augmented by eight radio telescopes in Japan. In 2006, China built a 50-meter radio telescope in Beijing and a 40-meter dish in Kunming, complementing existing 25-meter radio telescopes in Shanghai and Urumqi, to track the Chang'e-1

spacecraft now orbiting the moon. And on 2 December, Korea completed construction of the last of three 21-meter telescopes in its Korean VLBI Network (KVN). Like the dish at Yonsei, the other two are on university campuses "to make it easy to interest students in astronomy," says Hyo-Ryoung Kim, director



Tuning in. Hyo-Ryoung Kim expects South Korea's three 21-meter antennas to play a pivotal role in a new Asian array.

of radio astronomy for the Korea Astronomy and Space Science Institute in Daejeon.

The idea to link arms grew out of discussions over several years at triennial meetings of the East Asian Network of Astronomy, which brings together researchers from China, Taiwan, Korea, and Japan. (Taiwan does not have a radio antenna.) People realized that it was time to coordinate facilities "to go for some more ambitious projects," says Zhiqiang Shen, an astronomer at

Shanghai Astronomical Observatory.

One primary target of the East Asia VLBI Network will be extending and refining VERA's effort to map the Milky Way. VERA has achieved noteworthy results in locating stars, but adding KVN will double the accuracy, Kobayashi says. Their aim is to locate each star to 10% accuracy—"a unique and challenging effort that will give us very good information about the structure of the galaxy," he says. Plotting the evolution and movement of stars, he adds, will "reveal the dynamics of the galaxy very precisely."

Astronomers expect the East Asia VLBI to quickly make its mark. "The structure of the Milky Way, how massive stars form, the history and fate of local galaxies, is quite a rich field," says Mark Reid, a radio astronomer at the Harvard-Smithsonian Center for Astrophysics in Cambridge, Massachusetts. The new Asian array will "be a big player in that effort."

Achieving the target accuracy depends on a technique known as phase referencing to correct for atmospheric distortions. In this regard, the new network does not mesh seamlessly, because the Japanese and Korean telescopes use different schemes. Japan's relies on simultaneously observing two celestial objects: the target and a well-characterized reference. Data gathered from the target can be corrected based on distortion of the reference object. Korea's scopes simultaneously observe a single target at four frequencies—22, 43, 86, and 129 gigahertz—something no other telescope can do. Higher frequencies are more sensitive to atmospheric disturbances, so observations at lower frequencies are used for corrections. In principle, the two techniques can be combined, says Kobayashi. "But we have to show it can really be done." The group tried to combine observations from Yonsei and a VERA antenna for the first time in late October. "The image is still a bit dirty, but scientifically it is okay," says Kim.

A second objective is studying active galactic nuclei (AGNs), supermassive black holes surrounded by accretion disks, and jets of material ejected at relativistic speeds. AGNs are believed to lie at the center of most galaxies. "There are many theoretical predictions about the structure and the temperature and the phenomena happening around AGNs, but no one has resolved these ▶

CREDIT: D. NORMILE/SCIENCE

problems,” says Kobayashi. To try to answer the questions, the East Asia VLBI Network plans to work with VSOP 2, a radio antenna Japan plans to put in orbit in 2012.

Even before then, KVN’s observations at four frequencies, simultaneously capturing data on energy emitted at four wavelengths, could lay bare the inner workings of AGNs. According to Philip Edwards, head of scientific operations for the Australia Telescope

National Facility’s Paul Wild Observatory in Narrabri, such measurements are important for understanding transient phenomena such as bursts and flares. “If you’re going to model (the phenomena), the more simultaneous data the better,” he says.

Although the Korean network is complete, there is still much work to do. To combine data from the national arrays, Japan and Korea plan to jointly build a correlator—a

specialized computer—in Seoul. They hope to have it running by the end of next year. Meanwhile, for the next several months, the priority for China’s radio telescopes will be tracking Chang’e-1, says Shen. Full-fledged observations using the East Asia VLBI Network are expected to get under way in 2010. When that happens, the view from Yonsei’s hill campus will be all the more spectacular.

—DENNIS NORMILE

EUROPE

Ministers Bankroll European Space Agency’s Ambitions

Europe’s space scientists are breathing a collective sigh of relief because the member governments of the European Space Agency last week gave ESA more or less everything it had asked for in funding for the next few years—a total of nearly €10 billion. At a key ESA budget meeting, European politicians approved a request from the agency’s science program for modest annual increases and gave an ambitious environmental monitoring system the green light. Questions still hang over the troubled ExoMars mission slated for 2016, but researchers are now confident that it will survive. The United Kingdom also signed a deal to host an ESA facility, which will end the embarrassment of the U.K. being the only major funder of the agency without a facility on its soil. “People are very happy indeed. It seems a win, win, win situation,” says George Fraser, director of the Space Research Centre at Leicester University in the U.K.

Ministers from ESA’s 18 member governments meet every 3 years or so to agree to its budget, and there were concerns ahead of last week’s meeting in the Dutch port city of The Hague that the world financial crisis would limit governments’ generosity (*Science*, 21 November, p. 1180). Yet after more than a decade of flat budgets, ESA’s science program will now enjoy a gradual ramping up of its resources by 3.5% per year. Obtaining that funding boost was crucial, says Alan Smith, director of the Mullard Space Science Laboratory of University College London, because some of ESA’s

science missions awaiting approval, which include space telescopes, planetary missions, and an exoplanet finder, have grown overly ambitious and over budget. “To avoid collapse, we needed this uplift.”

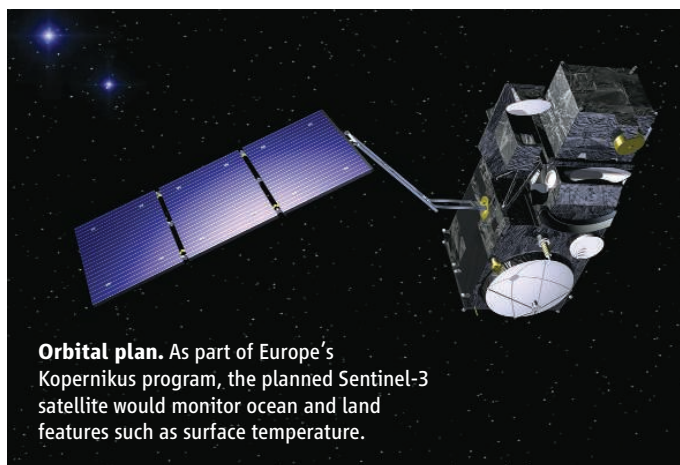
The ExoMars mission also received news that was as good as most could hope. The first part of the Aurora program of solar system exploration, ExoMars had swollen from the budget of €650 million approved 3 years ago to somewhere near €1.2 billion. Ministers balked at that sum and granted just €850 million, but the account will be left open for the next year as ESA reconfigures the mission and

fared better, winning €831 million—enough to launch the first few satellites and make the system operational. A dispute over who should pay for backup satellites, or b-units, was resolved with ESA footing the bill. “This is a very important program,” says Roger Bonnet, director of the International Space Science Institute in Bern and a former ESA science chief. “We need a [Copernicus] for the whole world, not just for Europe.”

One sour note at last week’s meeting was an apparent lack of enthusiasm among the ministers for a plan to develop ESA’s cargo vessel, the ATV, so that it can carry material back to Earth, and to conduct further studies on astronaut-carrying craft. These efforts won €62 million, less than half the amount requested. Bonnet says that Europe downplays human space flight because it does not have the “national pride” of the United States and Russia, or newcomers China and India. “Science and education are the priorities in Europe.”

The U.K. delegation at The Hague came away happy, clutching an agreement for a new ESA research center focusing on climate change modeling using space data, robotic exploration, and developing power sources for deep-space craft. It will be based at the Harwell Science and Innovation Campus in Didcot, site of the Rutherford Appleton Laboratory. “There are an awful lot of things coming together for space in the U.K.,” says Smith. “Now we’ve got to deliver to make the most of it.”

—DANIEL CLERY



Orbital plan. As part of Europe’s Copernicus program, the planned Sentinel-3 satellite would monitor ocean and land features such as surface temperature.

looks for international partners. “I hope there will be no descoping,” says astrophysicist Jean-Pierre Swings of the University of Liège in Belgium, who chairs the European Space Sciences Committee, an advisory body.

The Copernicus program, an ambitious plan to set up an environmental monitoring system for government and business users,



Scarce commodity.
People line up to receive meningitis shots in Aura, Uganda, in February 2007.

MENINGITIS

Less Vaccine Can Be More

The meningitis season has begun in Africa—and once again, it will be a tough battle. Health officials will use vaccines that act like fire brigades, squelching outbreaks where they erupt; but vaccine stocks are so tight, they have to be deployed sparingly, and there's always the danger of shortages.

In a paper this week in *PloS Neglected Tropical Diseases*, a team led by epidemiologist Philippe Guérin of Médecins Sans Frontières (MSF) shows a way to stretch those limited supplies. The team reports that just one-fifth of the standard vaccine dose triggers an immune response almost as good as that of the full dose. That means the stockpile of some 10 million doses that will be available this season might be used to vaccinate as many as 50 million people.

The idea has excited meningitis experts in and around the World Health Organization (WHO). But it has also triggered controversy. The main vaccine manufacturer, Sanofi Pasteur, worries about liability problems and wants nothing to do with the strategy. Switching doses is a logistical challenge as well and can be politically risky if it is seen as lowering the level of care. Still, WHO is laying the groundwork for a move to “fractional doses” if shortages occur, says WHO meningitis expert William Perea.

Immunity from the current generation of polysaccharide vaccines against *Neisseria meningitidis* lasts just 3 years or so, which is why the shots are used reactively to contain an outbreak rather than to prevent one. The vaccines are of little interest to companies because they are used in the poorest countries in the world—those in Africa's “Meningitis Belt”—for less than \$1 a dose. Moreover, new, more powerful “conjugated” vaccines may soon make polysaccharides obsolete (*Science*, 27 June, p. 1710). For now, WHO has struck a deal with two manufacturers—Sanofi Aventis

and Bio-Manguinhos in Brazil—to keep producing the vaccines for an emergency stockpile, managed jointly by WHO, UNICEF, MSF, and the Red Cross/Red Crescent.

Hints that fractional doses might work almost as well emerged from studies on U.S. military recruits in the 1970s and '80s. In the current study, researchers tested the same idea among 750 healthy volunteers ages 2 to 19 in Uganda, using a Sanofi Pasteur vaccine that protects against four different meningitis serotypes. One-fifth of the standard dose triggered antibodies against the A strain—by far the most prevalent in Africa—almost as well as the full dose; for two other strains, W135 and Y, one-tenth was enough.

In December 2006, Guérin presented the results to a panel of experts assembled at WHO's request to decide whether fractional doses could be used in the 2006–07 season. Yes, the panel said: During shortages, the benefit to the population as a whole would outweigh a slightly increased risk for individual vaccinees. But the operation wasn't needed that year or the following because there was enough vaccine.

A spokesperson for Sanofi Pasteur says the company can't prevent WHO or individual countries from using the vaccine however they want, but it “cannot endorse” anything except using the licensed dose. The company has warned WHO about legal risks the agency may face by recommending fractional doses, says Alejandro Costa, a scientist at WHO. (A spokesperson at Bio-Manguinhos did not respond to requests for comment.)

Perea says WHO will recommend fractional doses if necessary this winter. But expanding the vaccine supply should be the main goal, he says. Because a full dose is still the safest bet, using fractional doses “will remain the joker card that we play only when we really have to.”

—MARTIN ENSERINK

NEON Prototype Debuts

Nearly a decade after former U.S. National Science Foundation (NSF) Director Rita Colwell proposed it, the National Ecological Observatory Network (NEON) will open its first prototype site this month on Table Mountain, Colorado. When complete, the site will consist of an instrument shed, a 6-meter observation tower, and several pits for soil sampling; the plan is to monitor an area of tens of hectares. NEON has received about \$30 million from NSF since 2000 as researchers debated the best design to achieve the project's surveillance goals. The project now anticipates 60 sites like the one on Table Mountain—along with 40 mobile labs—to monitor environmental indicators such as soil pH and carbon dioxide content on a national scale. NEON officials hope to submit their final budget plan to NSF in early 2009, the first step in obtaining construction money. But just completing a prototype is very satisfying, says NEON Chief of Science Michael Keller: “We're finally seeing a lot of the ideas being put in aluminum and concrete and wires.”

—RACHEL ZELKOWITZ

Stem Cell Patent Nixed

The European Patent Office's (EPO's) highest board of appeals has rejected a controversial application covering the derivation of embryonic stem (ES) cells filed by the Wisconsin Alumni Research Foundation. The patent, which the U.S. Patent and Trademark Office granted in 1998, was initially rejected by EPO in 2004 (*Science*, 24 September 2004, p. 1887). In its 27 November decision, the Enlarged Board of Appeals upheld the original decision, citing European law that prohibits patents that involve the “use of an embryo for an industrial or commercial purpose.” The ruling does not cover human stem cells or stem cell cultures in general, however, leaving open the possibility of patents on methods using human ES cell lines that do not directly involve the destruction of embryos.

—GRETCHEN VOGEL

Become a ScienceInsider

Now there's one place to get all the breaking news and analysis from the world of science policy. It's a new blog, *ScienceInsider*, compiled by the staff of *Science* magazine.



Launched a week before Thanksgiving, the blog provides scoops as well as insights on up-to-the-minute developments from around the world. It can be accessed from the home page of our daily online news service, *ScienceNOW*, or from its own site (blogs.sciencemag.org/scienceinsider). Let us know what you think.

ARMS CONTROL

In Rare Encounter, U.S. and Chinese Scientists Craft Nuclear Glossary

BEIJING—What does nuclear deterrence mean? An active defense? Strategic defense? What constitutes a nuclear explosion? Precise definitions are critical for everything from negotiating treaties to interpreting military postures of ally and adversary alike. On 20 November, the U.S. National Academies unveiled the first Chinese-English glossary of nearly 1000 nuclear-security terms.* The compendium seeks to reduce misunderstandings between China and the United States—nuclear powers that came into conflict in the Korean War and could conceivably be in confrontation again. “Words count, and it matters how we use them,” says Raymond Jeanloz, a condensed matter physicist and national security expert at the University of California, Berkeley.

The glossary is also the first open publication of a unique forum for Chinese and

U.S. nuclear weapons experts. It’s a “successful collaboration in a rather sensitive field,” says nuclear physicist Richard L. Garwin, fellow emeritus at IBM’s Thomas J. Watson Research Center in Yorktown Heights, New York. But prospects for building on the glossary to expand such contacts in the near future appear dim.

Chinese and U.S. nuclear-weapons scientists have had few opportunities to meet in recent years, especially after a U.S. congressional panel, chaired by then-Representative Christopher Cox (R-CA), alleged in 1999 that China had been stealing U.S. nuclear secrets for years. The Chinese government flatly denied the allegations, asserting that its nuclear program is wholly indigenous. Since then, both sides have largely forbidden contact between their nuclear-weapons communities.

One permitted tête-à-tête has been a dialogue between the academies’ Committee on International Security and Arms Control



Fine point. “Active defense” has a specific meaning if applied to ballistic missiles such as the Minuteman III.

(CISAC) and the Chinese Scientists Group on Arms Control (CSGAC). Private meetings between the two sides began in 1988 and survived the post-Cox Report chill. The discussions are confidential, but it’s expected “that each side will report matters of significant interest to its government,” says Garwin, manager for the U.S. side. At a meeting in ►

* www.nap.edu/catalog/12186.html

IMMUNOLOGY

Fetal Immune System Hushes Attacks on Maternal Cells

A baby developing in the womb receives from its mother not only nutrients but also some of her cells that sneak through the placenta and survive. Such maternal crossover cells were discovered more than a decade ago, and now on page 1562, researchers provide an explanation for why they escape attack by the fetal immune system. The work also suggests a new mechanism for how the human immune system learns to spare the body’s own tissues, a tolerance that breaks down in autoimmune diseases.

The new study shows that the maternal escapees spur the baby to produce regulatory T cells, or T regs—white blood cells that can quell immune assaults. T regs are one of the hottest topics in immunology, and the authors suggest that the fetus also depends on these pacifists to become tolerant of its own cells. Immunologists Jeff Mold and Joseph “Mike” McCune of the University of California, San Francisco, and colleagues report that T regs that arise in a fetus can linger within a child for years, perhaps undermining the effectiveness of vaccines.

Other immunologists praise the study for bolstering the evidence of a robust human fetal immune system and revealing that the developing baby may have more than one way to keep it in check. “It’s a definite advance,” says immunologist J. Lee Nelson of the Fred Hutchinson Cancer Research Center in Seattle, Washington, who has been studying fetal-maternal cell exchange for years.

The paper extends a line of investigation that began with the discovery that fetal cells can persist in a mother’s blood and tissue for decades and continued with the realization that this maternal-fetal cellular traffic went both ways. Last year, for example, work by Nelson and colleagues indicated that maternal pancreatic cells that had crossed the placenta were more common in patients with type 1 diabetes.

How such maternal cells interact with a fetus’s immune system remains unclear. The human immune system is hard to study in the womb, and researchers continue to debate how quickly it matures, in part because the widely studied rodent immune system doesn’t

become functional until after birth. To gain insight into the developing human immune system, Mold and colleagues began by probing how a fetus deals with maternal wanderers. The scientists obtained lymph nodes from second-trimester fetuses and discovered that maternal cells were much more common there than previous studies indicated. In one case, cells from mom constituted nearly 1% of the cells in the lymph nodes.

So why doesn’t the fetal immune system battle the maternal interlopers? Although a baby inherits half of its DNA from mom, her cells still sport many antigens, molecules that should trigger an immune attack. And Mold’s team showed that fetal immune cells from the lymph nodes and spleen could recognize and respond to cells from unrelated adults.

The researchers suspected that intervention by fetal T regs explained the forbearance toward maternal cells, in part because that would mirror what happens in the mother. One reason that a pregnant woman’s immune system normally doesn’t destroy the fetus is that her T regs defuse such attacks. Mold and

CREDIT: JIM SUGAR/CORBIS

Vancouver, Canada, in 2006, the forum agreed to open up a bit and produce the glossary. They invited experts from outside CISAC and CSGAC to propose terms and help review the glossary before release.

Although most terminology was amenable to straightforward translation, several dozen terms have different meanings depending on the context, or various implications in each language. For example, “active defense” has three definitions. China uses the term to describe its military strategy: “gaining mastery only after the enemy has struck” and “using active military preparations and political struggle to prevent war.” To U.S. experts, the term means “the employment of limited offensive action and counterattacks to deny a contested area or position to an enemy.” A third meaning of “active defense” relates to missile defense.

For a few terms, the panelists hammered out translations but disagreed on the connotations. “There’s a big difference of opinion about what ‘deterrence’ means,” says one U.S. nuclear analyst. “The Chinese think it’s a bad word, that it means ‘coercion.’” But in the U.S. view, she says, deterrence is a virtuous principle that has kept nuclear powers from annihilating one another. The two sides

failed altogether to find common ground on a definition of limited deterrence.

Discussions were sometimes heated but always collegial, says Jeanloz, a CISAC member who served on the glossary panel. And there’s room for a more inclusive meeting of the minds. The academies asked experts from both countries for comments on the glossary over the next year. “This is the beginning of an important dialogue,” Jeanloz says.

Serious barriers impede deeper interactions between Chinese and U.S. nuclear scientists, says Li Bin, director of the arms-control program at Tsinghua University’s Institute of International Studies in Beijing. “The real obstacle is the Cox Report and its product, the new visa system in the name of antiterrorism,” he says. (U.S. security agencies submit visa applications of scientists from China and certain other countries to extra scrutiny; *Science*, 21 November, p. 1172). “That prevents scientists of the two countries from talking to each other more,” Li notes. Still, he and others say that the glossary marks a significant advance in the expansion of contacts—and trust—between two formidable communities of nuclear scientists.

—RICHARD STONE

With reporting by Rachel Zerkowitz.

colleagues were able to identify fetal T regs in the cultures of fetal lymph node cells. When they removed those T regs, cells from the lymph nodes reacted strongly to added maternal cells. These results raise “the possibility that there’s more crosstalk between mother and fetus than we’d imagined,” says McCune.

If a fetus uses T regs to squelch immune assaults on maternal cells, it likely uses the same trick to dull immune attacks on its own cells, the researchers propose. Immunologists have long recognized that the developing immune system can kill off cells threatening the fetus’s own tissues, but T regs would offer a gentler pathway to tolerance.

The new study strengthens the case that the fetal immune system is no pushover, notes immunologist Rachel Miller of Columbia University. It isn’t fully developed before birth, she cautions, but it’s certainly able to put up a fight.

Mold and McCune suggest that it’s worth investigating the long-term health effects of



Close contact. Maternal cells cross the placenta into a baby but avoid attack by the child’s immune system.

T regs generated in the womb. Their team found that regulatory T cells tuned to maternal antigens were still detectable in children as old as 17. In some people, these enduring fetal cells could blunt responses to childhood vaccinations, the researchers suggest. But the cells may be useful, too, they speculate. Physicians could in theory exploit T regs to improve the prospects for fetal organ transplants by coaxing the baby’s immune system to accept the implanted tissue. —MITCH LESLIE

Biologist’s Legal Battle Ends

The legal woes of Brazilian biologist and species hunter Marc van Roosmalen, who was sentenced last year to 14 years in prison for embezzlement and biopiracy (*Science*, 7 September 2007, p. 1303), have ended. On 25 November, an appeals court in Brasília threw out all but one charge against Van Roosmalen, says Aguinaldo Lyra, a Brazilian lawyer living in the Netherlands who has supported the Dutch-born scientist. The 2 months he spent in prison fulfill the terms of the 1-year sentence that he received, Lyra says.

Van Roosmalen—a 2000 *Time* magazine “Hero for the Planet”—has been in hiding since his release in August 2007 because of two alleged attempts to murder him and could not be reached for comment. Lyra says Van Roosmalen plans to resume his regular activities soon.

—MARTIN ENSERINK

Coral Reefs Still Reeling

As the International Year of the Reef draws to a close, a new global assessment of corals adds a few bright spots to an otherwise bleak picture of this marine ecosystem. The 304-page *Status of Coral Reefs of the World: 2008*, to be released next week by the Global Coral Reef Monitoring Network, chronicles continued problems from ocean acidification and other effects of global climate change, as well as the impact of the 2004 Indian Ocean tsunami and unusually hot weather in the Caribbean. On the positive side, several huge protected areas have been created in the Pacific, and a Coral Triangle Initiative is under way in Southeast Asia. The assessment is expected to offer lower estimates of reefs effectively lost and critically threatened since the group’s 2004 report. But network coordinator Clive Wilkinson warns that any optimism assumes that world leaders will take concerted action over the next 8 to 10 years to rein in climate change.

—ELIZABETH PENNISI

Bright Future for X-rays

The European Synchrotron Radiation Facility (ESRF), an x-ray source in Grenoble, France, will receive a €177 million upgrade over 7 years. Built for €500 million, the 14-year-old facility supports studies in materials science, structural biology, condensed matter physics, and other fields. The money will fund eight nanometer-sized x-ray beams, new instrumentation, and improvements to the accelerator. The upgrade was approved this week by representatives from all 12 countries that fund ESRF, says the lab’s director general, William Stirling.

—ADRIAN CHO

AIDS RESEARCH

Treat Everyone Now? A 'Radical' Model to Stop HIV's Spread

Confronted with the lackluster success of HIV prevention efforts, researchers are increasingly pushing treatment itself as a way to slow the spread of the AIDS epidemic. The reasoning: Antiretroviral (ARV) drugs lower the amount of HIV in infected people, likely making them less able to transmit the virus. Now the World Health Organization (WHO) has published a provocative model that explores the possibility of "eliminating" the HIV epidemic by annually testing everyone on a voluntary basis and treating all infected people, regardless of their clinical status. WHO HIV/AIDS Director Kevin De Cock, who co-authored the study that appeared online 26 November in *The Lancet*, says, "What we hope to do is stimulate discussion." And that they have.

Testing and treatment on that scale would far surpass anything done today, but the pay-offs could be huge, the authors say. According to their model, each untreated infected person infects seven others before dying. The study compares the impact of thwarting new infections when people start treatment at various stages of immune decline, and it assumes that treatment reduces a person's infectivity by 99%. Most poor countries can afford to treat only the people most in need, which is defined as anyone who has fewer than 200 CD4+ white blood cells, the critical immune warriors that HIV targets and destroys.

As an example, the study focuses on South Africa, which has an adult prevalence of 17% and offers treatment at the higher cut-off, common in wealthy countries, of 350 CD4+s. At that point, the study calculates, an HIV+ person has infected three others. But if treatment started shortly after people became infected, the model suggests, on average, the person would infect less than one person each, and the severe South African epidemic would die out in 14 years (see graph). "If we really put our mind to it, we can do things people previously didn't think were possible," says De Cock, noting that 3 million people in poor countries now receive ARVs that once were deemed impossibly expensive for them.

Geoffrey Garnett, an epidemiologist at Imperial College London, St. Mary's, co-authored an accompanying editorial that called the strategy "extremely radical" for pushing public health over individual benefits: It remains unclear that early treatment delays disease and death, and it could increase the risk of drug resistance developing. It also raises other ethical, financial, and

logistical dilemmas. And, Garnett contends, eliminating the epidemic is too ambitious a goal. But even if the strategy didn't reach all infected people, it might have a big impact on spread, he says. "It's not an idea to dismiss out of hand, but it's really challenging," says Garnett. "The *Lancet* paper throws down the gauntlet to think about it."

Other research groups received little attention—or outright derision—when they published similar models a few years ago, but now, ARVs are less toxic and cheaper

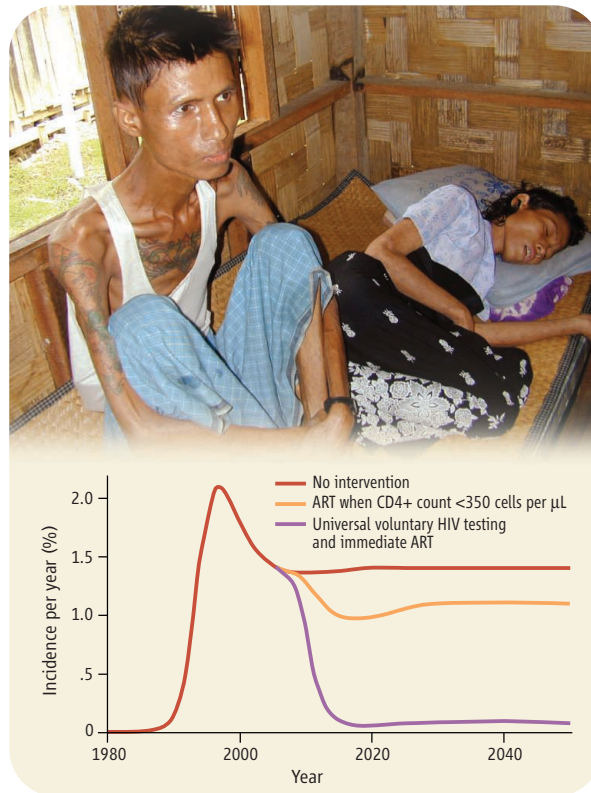
6.7 million people who badly needed the drugs were not receiving them. Poor countries also typically use ARV regimens that are below the standards of those available in wealthy countries, which means toxicity and drug resistance remain serious issues for much of the world. In these countries, there are still staggering shortages of funds and trained people to test and treat. (Estimates suggest that by 2015, it will cost at least \$41 billion annually to treat the 13.7 million HIV-infected people who then will have fewer than 200 CD4+s; wealthy countries currently donate some \$10 billion.)

De Cock and his co-authors did a preliminary cost analysis for South Africa that showed by 2015, the country would have to spend three times as much on testing and treatment as it does today. But because of declining infection rates, costs would then begin a steady decline.

HIV/AIDS researcher Julio Montaner of the University of British Columbia, Vancouver, Canada, says he got "crucified" when he published a similar paper in *The Lancet* in 2006 and is "delighted" to see that WHO's "fancier" model supports his own. The key to the strategy, he contends, is cost: In the long run, it saves money. "Front-loading the investment on ARVs is a very wise investment, even in a time of financial crisis," says Montaner. But he agrees that more data are needed to prove that starting treatment at the earliest possible point does not lead to toxicities and drug

resistance that offset the long-term benefits. "How would you like it if I say, 'You don't qualify for treatment, but I want to treat you so you don't expose anyone else?'"

De Cock says he would like researchers to launch small-scale trials of voluntary testing and immediate treatment to assess the impact on infected individuals and see whether it decreases the spread of HIV in populations, as the model predicts. WHO, he says, plans to hold a meeting early next year to discuss the strategy in more depth. —JON COHEN



All together now. Although ARVs still fail to reach many people in countries such as Myanmar (top), a model based on South Africa (bottom) shows that immediate treatment of the entire HIV-infected population could stop the epidemic there.

than ever, making the idea more realistic. Still, many question whether it could be pulled off. Today, an estimated 80% of the infected people in sub-Saharan Africa do not know their HIV status, and it's not simply a question of access to tests: In the United States, where testing is widely available, the Centers for Disease Control and Prevention says about 25% of infected people are unaware they are infected. Although the world has made much progress in delivering ARVs to poor countries, at the end of 2007,

Hopping to a Better Protein

Clinical trials are under way to test an innovative use of antisense technology to stem paralysis in Duchenne muscular dystrophy

EXON SKIPPING. IT SOUNDS LIKE A GAME, like hopscotch. But it's not child's play. A half-dozen research teams around the world are scrambling to turn exon skipping—which involves tricking a cell's protein-making machinery into skipping over defective parts of a gene—into a treatment for a devastating muscular disorder called Duchenne muscular dystrophy. "It's the best shot" for stemming the progressive paralysis that puts teenagers in wheelchairs and, in many cases, leads to premature death, says Eric Hoffman, a geneticist at Children's National Medical Center in Washington, D.C.

A concept first demonstrated in the mid-1990s, exon skipping uses short stretches of DNA-like molecules called antisense to shut down a faulty section of a gene. In the past 2 years, promising results in animals and in cell-culture tests, as well as from a safety evaluation in people, have energized the muscular dystrophy community. Clinical trials of antisense drugs that home in on defects in the gene in Duchenne muscular dystrophy are now under way to assess how much muscle function can be restored. "A lot of things are jelling," says Hoffman.

Questions still remain. It's not clear how to reach all the body's affected tissue or how effective treatments will be over the long term. There is also much uncertainty about

how these treatments would be regulated. "It's got a long way to go to determine whether it's going to be a drug or not," says C. Frank Bennett of Isis Pharmaceuticals in Carlsbad, California, a company developing antisense drugs for other diseases. But a group of experts who met in Cold Spring Harbor, New York, in October to discuss the potential of exon skipping were optimistic that the obstacles are surmountable. Researchers understand the disease and the principles of exon skipping much better and have also improved antisense technologies, says Bennett. "It's sort of a three-part stool that's come together: All this progress is really beginning to pay off."

Tough disease

Duchenne muscular dystrophy is the most common inherited childhood disorder. A sex-linked disease, it affects one in 3500 boys; without mechanical ventilation, death can occur before age 25. It is caused by mutations in the gene for dystrophin, a protein that helps stabilize the muscle cell membrane.

In severe cases, the mutations lead to an aberrant molecule of messenger RNA (mRNA), which carries the instructions for making the protein to the ribosomes, the cell's protein-making factories. The result is a highly truncated dystrophin or no protein at

all. Lacking functioning dystrophin, the muscle cell membranes leak, the muscles gradually waste away, and paralysis sets in. But some mutations result in a milder syndrome called Becker muscular dystrophy, in which the muscle cells produce dystrophin that isn't perfect but has enough activity to keep the muscle up and running.

Healthy heart. The pink latticelike staining shows that antisense restored the protein dystrophin to this diseased mouse heart.

In the early 1990s, researchers in Japan and elsewhere began to explore exon skipping. One early convert, Steve Wilton, now a molecular biologist at the University of Western Australia in Perth, discovered that in a few muscle cells of patients with Duchenne muscular dystrophy or animal models of the disease, dystrophin was restored, suggesting that the faulty sections of the dystrophin gene were being bypassed. He wondered whether it was possible to trick all the muscle cells into skipping over the mutated regions to produce a functioning protein. "I knew what I wanted to do, but I wasn't sure how," he recalls—until he heard Ryszard Kole of the University of North Carolina, Chapel Hill, describe how he had restored normal function to a mutated beta-globin gene using antisense technology in 1996. "It hit me like a brick" that the approach might work with dystrophin, says Wilton.

In a normal cell, the gene's protein-coding regions—the exons—produce stretches of RNA that are spliced together into a single mRNA molecule. But mutations in one exon can lead to faulty mRNA and make it impossible for the protein-making machinery to read the rest of the mRNA strand. The idea behind exon skipping is to target the disruptive exon, or a nearby one, with antisense drugs, so it is not transcribed into mRNA (see diagram, p. 1455). The resulting mRNA would be missing a section, and the protein produced would lack some amino acids. But it would still function, much like the dystrophin in Becker muscular dystrophy.

In a matter of months, Wilton and Kole had used antisense molecules to restore dystrophin gene function in cultured muscle cells, and a few years later, in live mice. His colleagues around the world were reporting similar successes, but Wilton had trouble getting support to follow up on the work. Antisense technology had been heavily touted in the early 1990s as a potential treatment for a variety of diseases, but it had not lived up to its promise (*Science*, 27 October 1995, p. 575). Wilton says one colleague even called exon skipping "a party trick."

Wilton and Kole had used antisense molecules to restore dystrophin gene function in cultured muscle cells, and a few years later, in live mice. His colleagues around the world were reporting similar successes, but Wilton had trouble getting support to follow up on the work. Antisense technology had been heavily touted in the early 1990s as a potential treatment for a variety of diseases, but it had not lived up to its promise (*Science*, 27 October 1995, p. 575). Wilton says one colleague even called exon skipping "a party trick."

CREDIT: QILU/CAROLINA MEDICAL CENTER

The skepticism was well-founded. The cell membrane doesn't naturally let DNA molecules in because they may belong to a pathogen, yet antisense DNA needs to infiltrate the cell to do its work. That's less of a problem in muscular dystrophy because the disease makes the cell membrane leaky, but once inside, the foreign DNA must avoid being degraded by enzymes. To make matters worse, the quantities of an antisense drug required can stimulate a strong immune response. And because mutations can occur all over the dystrophin gene, an individual patient could require an antisense molecule targeted to any one of the gene's 79 exons.

Better chemistry

None of those problems deterred Wilton and others. They began designing DNA sequences that would bind very specifically to individual exons. Wilton now has 40 that he says are ready for clinical trials. At the same time, private companies began to harness ways to disguise the antisense molecules to avoid destruction by the body. The point is to have it "look less and less like a nucleic acid," says Hoffman.

The four bases that make up DNA hang off a molecular backbone that consists of alternating sugar and phosphate molecules. Taking one approach, AVI BioPharma in Corvallis, Oregon, has replaced the pentagon-shaped sugar with a hexagon-shaped "morpholine" and substituted a linker called phosphorodiamidate for the phosphates. A Dutch biotech company, Prosensa, based in Leiden, has masked the sugar backbone by adding a methyl group.

Gert-Jan B. van Ommen of Leiden University Medical Center in the Netherlands, another pioneer in exon skipping for muscular dystrophy, has been working with Prosensa for the past 5 years testing its antisense drug candidates. "We successfully get skipping in human and mouse cells and in vivo in mouse," says Van Ommen. In 2006, he and his colleagues took the next step: They injected an antisense molecule targeted against exon 51 into the leg muscles of four patients and looked for the appearance of dystrophin at the injection sites. In each, "we got expression," says molecular biologist Gerard Platenburg, Prosensa's CEO.

The results, published in the 27 December

2007 issue of *The New England Journal of Medicine*, caused quite a stir. "After the paper came out with the beautiful pictures of dystrophin expression, the community as a whole has been excited," says Jane Larkindale, research program coordinator for the Muscular Dystrophy Association in Tucson, Arizona. "[Duchenne muscular dystrophy] patients and their families are very eager to try any therapy that has potential to work." Now Prosensa is midway through a larger study to determine the dosage requirements for effective treatment.

In the United Kingdom, another research group is testing a morpholino antisense drug. Francesco Muntoni of the University College London Institute of Child Health and colleagues have injected the feet of five of seven patients and are planning a larger study that will involve periodic injections of 16 individuals.

Qi Long Lu, a pathologist at Carolinas Medical Center in Charlotte, North Carolina, has added a peptide rich in the amino acid

Garcia, a molecular biologist at the Institut de Myologie in Paris, is pursuing exon skipping with a twist. He has come up with a minigene that codes for an antisense molecule and is developing ways to transfer the gene into the patient's own muscle stem cells to create a more permanent source of error correction with just a single injection. The approach so far has restored dystrophin in a mouse model of muscular dystrophy using patients' cells, and he's trying it out in a dog model of muscular dystrophy, he says.

Regulatory hurdles

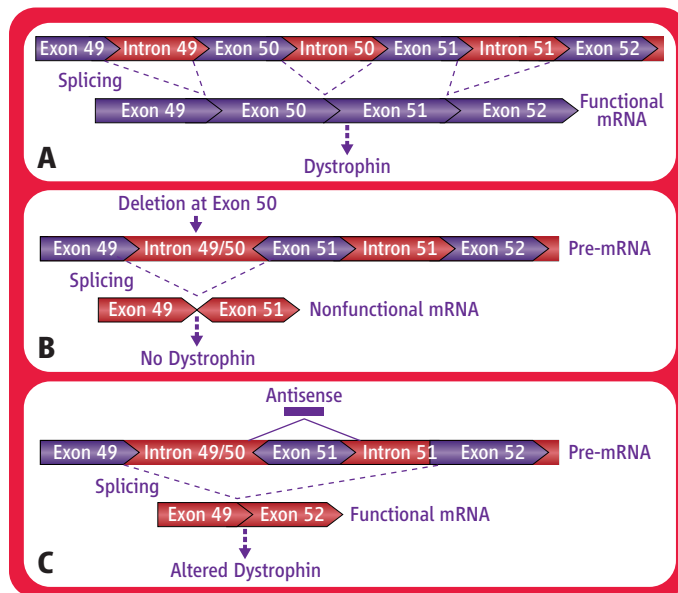
But even if antisense drugs are successful in mice, in dogs, and even in people, the nature of these small molecules is raising regulatory challenges. Because antisense drugs are a hybrid between a "biological" and a "small molecule drug," it's not completely clear which regulatory rules apply. For example, the U.S. Food and Drug Administration guidelines for

determining the correct drug dosages for humans based on animal studies might not work for these molecules, says Hoffman. Another concern is that an antisense drug might turn off an exon in another gene that has a very similar sequence to the target. Assessing that sort of toxicity will be hard to do in animals, in which such similar exons might not exist.

Furthermore, these drugs will truly be "personalized," as the antisense sequence must be tailored to the particular exon mutated in each patient. "For the rare mutations, there will not be sufficient patients to do a clinical trial," says Larkindale. And some patients may require a cocktail of antisense molecules that will coordinate the skipping of more than one exon, complicating approval procedures even further.

"There are lots of issues," says Hoffman. Nonetheless, "you have to give Wilton and others a

lot of credit for doggedly pursuing this and having it emerge as [the] winning horse." And Wilton thinks more than Duchenne muscular dystrophy is riding on their work. Others are exploring using antisense technology to treat the blood disorder thalassemia, an aging syndrome called progeria, and another degenerative disease, spinal muscular atrophy. "If exon skipping does not work for Duchenne muscular dystrophy," says Wilton, "I find it difficult to believe it could work for any other conditions." —ELIZABETH PENNISI



Exon skipping. In this section of the dystrophin gene's pre-mRNA, introns are spliced out to make functional mRNA (A). But in muscular dystrophy, a mutation in exon 50 leads to a truncated and nonfunctional mRNA (B). Antisense knocks out exon 51, such that the remaining exons stitch together nicely, and the resulting mRNA leads to an altered dystrophin protein (C).

arginine to the morpholino antisense. It readily slips into the heart muscle in a mouse model of muscular dystrophy, he and his colleagues reported in the 30 September issue of the *Proceedings of the National Academy of Sciences*. That could be a big advance because previous studies have suggested it's almost impossible to get antisense molecules into heart muscle, which would be a major potential limitation to the utility of this therapy, Lu points out.

Other approaches are in the works. Luis



◀ **Beastly beauty.** With its feathery gills and quizzical face, the axolotl is plausible as an Aztec god.

ENDANGERED SPECIES

Sanctuaries Aim to Preserve a Model Organism's Wild Type

The axolotl, a salamander that retains unique evolutionary features and is a darling of biologists because it can regenerate limbs, faces adversity on two fronts

MEXICO CITY—Leaning over the *Tragineria* flatboat's edge, Luis Zambrano surveys a canal floating with plastic bottles, Styrofoam cups, and a leafy carpet of invasive lilies. African tilapia fish ripple the brown water's surface and a Chinese carp lurks underneath, but Zambrano sees no signs of his elusive goal: the axolotl salamander.

"We've spotted only a few in 6 months," says Zambrano, a freshwater ecologist at the National Autonomous University of Mexico (UNAM) who is trying to count and preserve the feathery-gilled, 33-centimeter-long salamanders in their only natural habitat, the Xochimilco network of polluted canals and small lakes in and around Mexico City, the world's third largest metropolitan area.

Five hundred years ago, axolotls—named for an Aztec god who transformed into a water animal to avoid being sacrificed—were common in the lakes around the Aztec capital. But as the wetlands receded, so did the axolotls, to the point that Zambrano now estimates a population density of only 100 per square kilometer of wetland, compared with estimates 10 times higher in 2004 and another six times higher than that in the 1980s. The species,

Ambystoma mexicanum, is now classified as critically endangered by the International Union for Conservation of Nature.

A serious threat to axolotls could prove damaging to science, for the salamander has been used for more than a century as a model organism by developmental biologists. Even though the wild type's survival is threatened, thousands of axolotls are raised in laboratories every year for use in research projects involving regeneration, stem cells, and developmental biology. For example, more than 1000 adult and juvenile axolotls are maintained in aquariums at the University of Kentucky's *Ambystoma* Genetic Stock Center in Lexington, which distributes between 15,000 and 20,000 axolotl embryos each year to more than 100 research labs in India, Germany, Japan, Mexico, and elsewhere.

Although they are propagated as aquarium pets and are considered easy to breed, some axolotl colonies in labs are now under threat from a puzzling disease. The *Ambystoma* center's director, developmental biologist Randal Voss, is concerned about what he calls a "mysterious epidemic"—it first emerged when the center was managed at Indiana University in the 1990s and re-emerged a few years ago—that has been

killing some axolotl larvae. He says, "Very little is known about disease and pathogens of lower vertebrates."

Allowing axolotls to disappear from the wild would carry an immeasurable risk, researchers say: There's a danger that vulnerable lab populations might be wiped out by disease, and no one knows exactly how a loss of the wild type might diminish future studies of evolution and regeneration.

Axolotls in the lab

Ever since the Aztecs began using axolotls for medicine and in cultural ceremonies, the odd-looking salamanders have had a special significance outside their watery homes. The use of axolotls in modern science began in the 1860s, when a French expedition collected 34 of the amphibians and shipped them to the Natural History Museum in Paris, which gave six to French zoologist Auguste Duméril. Over the past century, various labs have bred them in colonies for research.

Among the naturalists fascinated by the axolotl's neoteny—its retention of larval characteristics such as gills into adulthood—was Stephen Jay Gould, who described the salamanders as "sexually mature tadpoles." His book *Ontogeny and Phylogeny* pictured an axolotl on its cover along with a closely related tiger salamander that had fully metamorphosed and lost its gills. "The axolotl is a fascinating case of what is known as heterochrony—that is, you evolve a brand-new life history by tinkering with the timing of developmental events," says H. Bradley Shaffer, director of the Center for Population Biology at the University of California, Davis. His research groups have worked since the 1970s on issues related to the evolution, ecology, and conservation of axolotls and tiger salamanders.

Because of their large egg and embryo size, susceptibility to tissue grafting, and ability to regrow severed limbs and tails, "axolotls have a long history as primary amphibian models, especially in research areas involving embryonic development," says Voss. He calls them a "re-emerging model organism" for scientists who study them with gene expression and other new tools. For example, cell and developmental biologist Elly Tanaka of the Center for Regenerative Therapies at the Dresden University of Technology in Germany says her lab was able to develop and breed transgenic axolotls, which "makes it easier to study the

CREDIT: JAN-PETER KASPER/EPA/CORBIS

mysterious process of regeneration on a molecular level by driving gene expression in regenerating tissues.”

When a salamander regrows its severed tail, it must regenerate a portion of the spinal cord and the neurons inside. “How these particular vertebrates have kept this ability to regenerate while others have lost or blocked it fascinated me,” says Tanaka, who describes the axolotl as “an interesting and important organism for studies on the evolution of vertebrate traits.” Her lab has analyzed signaling pathways that control regeneration, such as “proteins that tell a regenerating cell whether it should form an upper arm or lower arm cells.” In a paper last year in *Development*, her group shed light on how the axolotl’s neural progenitor cells are activated to help regenerate a segment of spinal cord.

In Kentucky, Voss’s group is studying gene expression in axolotls, including differences in how brain genes function during the larval development of axolotls in contrast to closely related tiger salamanders, which metamorphose beyond the larval stage. “The data show hundreds of stable gene-expression changes that presumably evolved between these species in the last few million years.”

Among the stem cell scientists who use axolotls in their research is Andrew Johnson of the Institute of Genetics at the University of Nottingham in the U.K., who studies the production of primordial germ cells (PGCs) in the salamander’s embryos. “Axolotls are significant in that they share a mechanism that has been conserved during the evolution of mammals, in which PGCs are produced from pluripotent stem cells,” Johnson says. His group is investigating how such stem cells ignore signals that typically trigger somatic cells to differentiate.

Salamander sanctuaries

On the flatboat, Zambrano and a local fisherman cast a gillnet every 200 meters, drag it across the canal, and then search for salamanders. They seldom find any. “The eggs and larvae do not seem to be surviving,” he says.

In a lab at UNAM, Zambrano and colleagues study about 40 juvenile and adult axolotls to find out more about their egg-laying habits, the most favorable breeding

conditions, and their vulnerability to alien fish species, especially tilapia and carp. He attributes the axolotl decline to the rapidly increasing numbers of those predatory fish as well as changes in land use that have polluted the nearby canals.

Shaffer points out, however, that the Xochimilco’s water quality has probably improved since the 1960s and 1970s, when “many thought the native axolotls were gone.” The Mexican government began cleaning up parts of the canals and, in the late 1980s, local zoologist Virginia Graue began studying axolotl population trends and tried to increase their numbers. Zambrano did not work with Graue but expanded his own research after her death in 2004.



Axolotl search. Luis Zambrano (left) and a local fisherman search for axolotls in their natural habitat, on one of Mexico City’s canals.

Noticing that the water quality varies greatly in the canal network, Zambrano has developed a model to predict where the axolotls would be able to survive. He has also outlined a plan to create sanctuaries. The first will be located in a narrow side canal in the *Chinanpera* area near Doll Island, on which superstitious local residents have left old dolls to scare away the ghost of a drowned girl. Invasive fish and plant species will be removed and kept away by wooden gates separating the canal from the main channel.

A key player in international efforts to help preserve the wild-type axolotl has been zoologist Bob Johnson, the Toronto Zoo’s

amphibian and reptile curator. He used to support Graue’s work and helped link scientists from the Mexican project with those at the Durrell Institute of Conservation and Ecology (DICE) at the University of Kent, Canterbury, in the U.K. They led a 5-year effort, supported by the Darwin Initiative, to develop a conservation program for the axolotl and the canal system. That project’s funding has ended, but Johnson has since helped Zambrano and the Chapultepec Zoo get four new grants, including \$19,000 from the Association of Zoos and Aquariums Conservation Endowment Fund, to help create canal sanctuaries.

Although everyone seems to agree that the salamander’s habitat needs to be preserved, some wonder if there are enough axolotls left to repopulate the canals. A veterinarian here has suggested releasing lab-raised axolotls into the canals, but Zambrano and others fear that the captive salamanders might introduce fungal and other diseases. “Even if you take rigorous precautions, diseases can still slip through the net,” says amphibian ecologist Richard A. Griffiths, who led DICE’s axolotl project.

Another fear is that introducing axolotls from ingrown lab colonies would reduce the genetic diversity of the wild type. Also, Zambrano says lab-raised axolotls likely would suffer the same fate in the canals as the wild type. “It is more effective to create sanctuaries in which the existing axolotls can survive and perhaps thrive,” he says.

Even scientists who see only lab colonies of the salamander worry about the wild type’s future. “We are concerned about the worldwide decline not only of axolotls but of many salamander species,” Tanaka says. “They represent a very important group to study in terms of evolution.”

Neurobiologist Alejandro Sanchez Alvarado, who studies the molecular basis of regeneration at the University of Utah School of Medicine in Salt Lake City, says losing the wild axolotls would be a tragedy. “Wild-type populations provide us with a window, a record of how biological traits evolve genetically,” he says. “Who is to say that unlocking the evolutionary mystery shrouding regenerative capacities in vertebrates will not come from studying wild axolotl gene pools?”

—ROBERT KOENIG



SCIENCE POLICY

Philippines Plans Research Revival

The Philippines government is hoping to reinvigorate its science base by improving science education, expanding scholarship programs, and raising research spending. But will it be enough to lure back expatriate scientists?

LIKE HALF OF HIS GRADUATING CLASS AT THE medical school of the University of the Philippines (UP), Manila, Edsel Salvaña grabbed his diploma and went abroad in 2001, joining an exodus that has hobbled the country's economic development. But unlike all but one other classmate who fled, Salvaña came back. After stints at the Medical College of Wisconsin in Milwaukee and at Case Western Reserve University in Cleveland, Ohio, Salvaña says, "I felt I had the skills to successfully contribute to building research efforts in the Philippines." He returned in July and is now ramping up work on HIV and methicillin-resistant *Staphylococcus aureus* at the National Institutes of Health—UP Manila.

Filipino leaders are hoping many more far-flung researchers follow in Salvaña's footsteps. After decades of neglect that resulted in a horrendous brain drain and eroding competitiveness, the Philippines government has recognized the need to reinvigorate its science base. One budding initiative is the Balik (Tagalog for "returning") Scientist Program, which helped Salvaña find a position and provided a salary and lab start-up funds. Another boost could come from a blueprint released in October by the Congressional Commission on Science and Technology and Engineering (COMSTE) to improve science education, expand Ph.D. scholarship programs, and raise research spending. "We have been trying to get policymakers to give greater support to science and technology for years," says COMSTE Executive Director Fortunato Dela Peña, an

industrial engineer at UP Diliman. "Finally, there has been some passion building regarding this advocacy [for science]."

The Philippines has a lot of ground to make up. Total R&D spending, at U.S. \$81 million in 2007, has been stagnant for a decade and is a mere 0.14% of gross domestic product—weaker than Thailand's (0.26%) and Malaysia's (0.69%). As a result, the number of scientists and engineers conducting research in the Philippines has declined 20% since 1996 to 8800, according to the Department of Science and Technology (DOST). In comparison, despite their smaller populations, Singapore has 19,377 researchers, Thailand has 92,800, and Vietnam has 41,100. During the 1990s, a tight job market led up to half of Filipino information technologists and 60% of physicians to leave the country, according to a 2002 study by Florian Alburo, an economist at UP Diliman, and Danilo Abella, a Manila-based consultant. The duo also noted that droves of high school teachers left for the United States. Perhaps as a result, a recent study found that only one of every five high school physics teachers is qualified to teach physics. Filipino eighth graders ranked 41st in math and 42nd in science among 45 nations in the 2003 Trends in International Mathematics and Science Study.



Trailblazer? Returnee Edsel Salvaña.

◀ **Uncommonly good.** This rice genetics lab in Manila is a rare hot spot of top science in the Philippines.

Filipino researchers have been bandishing such statistics at political leaders for years to make a case "that the Philippines had to start competing with other countries in the region," says Dela Peña. One outcome was COMSTE, which the legislature tasked in February 2007 with producing a road map for restoring the country's scientific respectability. The commission's preliminary recommendations call on the government to give university research more support, establish national research institutes, develop incentives for corporate R&D, and forge closer ties between public and private sector research efforts.

A key element of the plan is education. COMSTE's goal is to accrete a critical mass of researchers through a "massive science and engineering Ph.D. scholarship program." "Manpower and research output from academe is the key to Philippine competitiveness," says Reynaldo Vea, president of Mapúa Institute of Technology in Manila and head of COMSTE's education panel. COMSTE also proposes transforming several hundred secondary schools into science and math magnet schools.

After gathering public comment and sizing up the costs, COMSTE will finalize its proposals by spring. "Our approach really builds on what previous leaders have started," Dela Peña says. For example, legislation is in the

works to enhance intellectual-property protections, and the government this year doubled DOST's budget to \$110 million. The department has revamped and expanded the Balik Scientist Program, which until this year only managed to attract one or two expats a year. This year, DOST expects 50 returnees and even more in 2009. That may be a trickle of talent, but "we are confident that this program can accelerate our human resource development efforts," says DOST Secretary Estrella Alabastro. Most

returnees come on short-term visits—with transportation and per diem expenses covered by hosts—to nurture collaborations and mentor younger colleagues. A few, like Salvaña, come back full-time. Because government scholarships covered much of his education and training, he says, "I feel an obligation to give something back." As word spreads of the improving research climate, Alabastro predicts, the trickle will become a deluge.

—DENNIS NORMILE



◀ **Good as new?** NBA star Greg Oden (left) underwent surgery last year to rebuild cartilage in his knee.

TISSUE ENGINEERING

Coming Soon to a Knee Near You: Cartilage Like Your Very Own

Weaving materials science and biology together, researchers are drawing closer to the elusive goal of recreating tissues that do the body's work, such as cartilage and muscle

BASKETBALL STAR GREG ODEN HASN'T MET

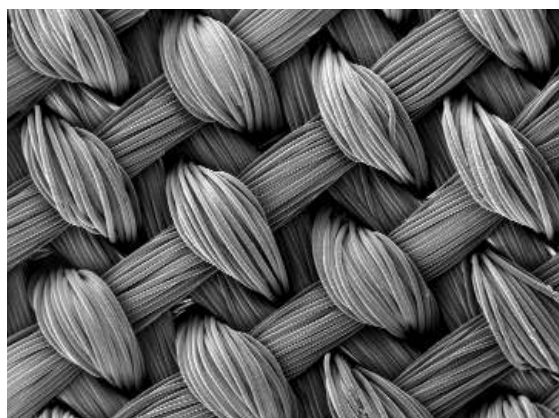
Farshid Guilak, a biomedical engineer at Duke University in Durham, North Carolina. But as an insurance policy, Oden may want to send Guilak a few tickets each time his Portland Trailblazers play in nearby Charlotte. Oden was the first player selected in the 2007 National Basketball Association draft, yet he was sidelined his entire rookie season because of a bad right knee. After cleaning out damaged cartilage in the knee, doctors performed microfracture surgery, punching several tiny holes at the tip of the surrounding bones so that the resulting influx of blood would ferry bone marrow stem cells into the region; those cells, they hoped, would later differentiate into cartilage-producing chondrocytes and repair Oden's knee.

Now, several games into this year's season, Oden's knee seems as solid as his monster dunks. But microfracture surgeries don't always help athletes recover. And they can't aid the millions of people with bad knees or hips due to more widespread cartilage problems, such as arthritis sufferers.

Guilak has a potential solution: Engineer new cartilage by seeding chondrocytes onto an ultrastrong, woven polymer matrix and implant that matrix into patients. His tissue-engineered cartilage isn't ready for human trials yet, so patients like Oden should be careful for now. Still, it's getting close,

and Guilak's strategy is a prime example of how materials scientists are teaming up with biologists to engineer tissues that perform mechanical work, such as cartilage, ligaments, and even heart muscle.

Recreating such mechanically active tissues was long thought to be easier than artificially building complex organs such as the liver and pancreas. (See special section on how organs naturally form, p. 1489.) But imitating the mechanical feats performed by natural tissue is a tall order. For example, the cartilage in your body's joints can withstand 12 megapascals of pressure—more than 10 times the amount generated if you hang from a ledge by a single fingernail. Researchers have already made significant progress in building new bone that's as strong as the natural stuff (*Science*, 1 September



Next best thing. A woven scaffold made of a biodegradable polymer helps seed cells that can produce new cartilage.

2000, p. 1498). Now, they are extending that success to softer mechanically active tissues by learning to mimic many of their key attributes. "It's a breakthrough time in this field, where we are seeing several biomimetic capabilities coming together," says Guilak.

Crunched cartilage

Off the basketball court, the most common type of cartilage damage is the widespread loss of tissue that's a hallmark of many forms of arthritis. According to the Arthritis Foundation, arthritis costs the U.S. economy alone \$128 billion per year in medical bills and indirect expenses, including lost wages and productivity. In arthritis patients, the healthy cartilage that lubricates and cushions the impact between adjoining bones breaks down over time. Bones then rub directly against one another, causing pain and loss of movement in the joint. Cartilage contains no nerves. So by the time patients feel pain, significant amounts of cartilage may already be gone.

When the loss is slight, as was the case with Oden, doctors use microfracture surgery to trigger new cartilage growth, even though replacement cartilage is typically weaker than the original. Other treatments include transplanting cartilage from elsewhere in the patient's body into the afflicted area, as well as harvesting a person's chondrocytes from a region of healthy cartilage, amplifying them in a lab, and reinjecting them into a patient's joint. But none of these efforts produce cartilage that's as strong as the original. And when cartilage loss is extensive, doctors can do little other than completely replace the joints with metal and plastic prostheses. That can offer immediate pain relief, but replacement joints often wear out after only a decade and can typically be replaced only once, due to accumulated damage to the patient's bones, says Gerard Ateshian, a biomedical engineer at Columbia University.

As an alternative, cell-free synthetic cartilage has made some progress. In select cases, doctors can inject a polymer gel into joints to help ease symptoms. But such procedures often offer only temporary relief because the gel breaks down. Prospects are a bit better for gels used to replace damaged disks between vertebrae in the spine; those gels can be injected and contained within the thin, fibrous sac that houses the cartilagelike material of a normal disk. Michele Marcolongo and colleagues at Drexel University in

CREDITS (TOP TO BOTTOM): LUCY NICHOLSON/REUTERS/LANDOV; FRANK MOUTOS AND FARSHID GUILAK

Philadelphia, Pennsylvania, for example, have made gels from a copolymer of polyvinyl alcohol and polyvinyl pyrrolidone. The gels are tough and resilient, capable of withstanding up to 10 million cycles of compression and release in lab studies. Marcolongo's technology has been picked up by the medical devices company Synthes Spine, whose pre-clinical studies on animals suggest that the treatment seems to "completely restore mechanics," Marcolongo says.

Fully synthetic gels have had less success in the knee and other less well-confined spaces. The arrangement of these joints requires that the cushioning material in the middle be able to withstand as much as 10 times a person's weight. Gels compressed with that much force typically squish out to the sides, like a spoon pressing down on a slab of Jell-O. By contrast, collagen fibers in natural cartilage make it extremely stiff so that it resists squishing outward under an applied force, Ateshian says.

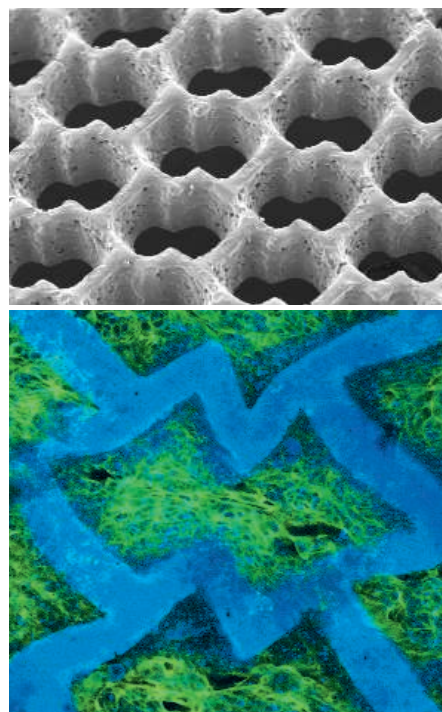
Stronger scaffolds

To craft such strong tissue, researchers have focused on coaxing the body to grow its own additional cartilage cells on a synthetic template, rather than trying to recreate cartilage from scratch. Researchers have seeded cartilage-producing chondrocytes onto synthetic scaffolds in vitro for decades in hopes that this would cause the cells to generate new cartilage with the same impressive properties as the native version. But the results have almost always been disappointing. Chondrocytes do grow and put out a mixture of collagen and charged compounds called proteoglycans. But the resulting cartilage winds up far weaker.

Ateshian has recently made tougher cartilage by applying a little force of his own. Growing cartilage can sense mechanical stress and responds by becoming stronger, akin to the way that weight training helps build strong bones. Ateshian applied this principle back in 2000, when his team reported seeding a culture of chondrocytes onto a synthetic hydrogel and compressing the gel in a chamber. The resulting new cartilage was five times stronger than that created without mechanical loading. Recently, the team has boosted that strength up to about 20% of that of native cartilage by cycling the compression on and off and adding a cocktail of growth factors.

In a variation on this theme, Rocky Tuan, a tissue engineer at the National Institute of Arthritis and Musculoskeletal and Skin Diseases in Bethesda, Maryland, is also putting weight on tissues and adding growth factors.

But Tuan and his colleagues deposit their cells atop fibers of a biodegradable polymer called poly(α -hydroxy ester). Tuan first learned to spin the fibers a decade ago with an apparatus akin to those that spin cotton candy from sugar. His lab has since perfected techniques to align the fibers to better control cartilage growth and resist compression. Tuan says his team's artificial cartilage now also has about 20% of the strength of native cartilage. "We would like to get to 40% to 50%," Tuan says. He adds that most clinicians believe that will be good enough to restore mobility for many patients. In a paper



Mending broken hearts. A polymer scaffold (top and above in blue) causes heart muscle cells (above in green) to align and contract in a preferred direction.

in press at the *Journal of Tissue Engineering and Regenerative Medicine*, Tuan and his colleagues report that after implanting their synthetic cartilage into pigs' hip joints, the material seemed to integrate well with the native cartilage; the animals appeared to walk normally as well.

Tuan's nanofiber scaffolds, however, have very small pores, making it difficult for chondrocytes to penetrate and churn out new cartilage. Guilak's team has made progress with a scaffold that leaves plenty of room for the cells. He, Franklin Moutos of Duke, and Lisa Freed of the Massachusetts Institute of Technology (MIT) in Cambridge have created a novel three-dimensional weaving technique for building high-strength scaffolds. The trio wove their scaffold

with a yarn made from a biodegradable polymer called polyglycolic acid (PGA) and seeded it with chondrocytes, they reported in *Nature Materials* last year. The woven fabric gave the scaffold compressive, tensile, and sheer strength on the same order of magnitude as native cartilage. That's a "major advance" and "an exciting opportunity for tissue engineers," Ateshian wrote in a commentary at the time.

Guilak's engineered cartilage still had some drawbacks. The PGA used to weave the scaffold degraded in about 2 weeks, too quickly for the seeded chondrocytes to churn out the collagen and proteoglycans needed to rebuild strong cartilage. Guilak's team has since turned to another polymer known as poly(ϵ -caprolactone) that degrades more slowly. Cytex Therapeutics, a biotech start-up in Durham, North Carolina, is now carrying out preclinical animal studies with the artificial cartilage and hopes to launch human trials in 2010.

Freed and her MIT colleagues have also been working to extend their success with patterned scaffolds to other tissues as well. Freed and postdoc George Engelmayer Jr. recently led a team that created artificial heart-muscle tissue from a honeycomb-shaped scaffold that flexes like an accordion. Cells in heart muscle, Freed explains, are aligned in specific directions to coordinate how the muscle flexes. Most biomaterial scaffolds, however, can't reproduce this alignment.

To do so, the team used a computer-controlled excimer laser to cut a precise pattern of holes and grooves in successive layers of a rubberlike degradable polymer scaffold. They then seeded the scaffold with neonatal rat heart cells. Not only did the cells grow in a preferred orientation, but when prompted by an electric field, they also contracted in the preferred direction, the team reports in the December issue of *Nature Materials*.

The group is working to optimize the pores in the structure and to build a microfluidic perfusion chamber to feed nutrients into the cells. Ultimately, Freed adds, the hope is that the novel scaffolds can be used to create artificial heart-muscle patches to repair small sections of diseased heart tissue. Guilak says he's impressed with Freed's team's ability to pattern cells: "You could apply this to a number of tissues, including tendons and ligaments." Tissue engineers are hoping not only that this will happen but also that the results will begin to alleviate the suffering of arthritis patients and perhaps even keep a few basketball stars on the court.

—ROBERT F. SERVICE

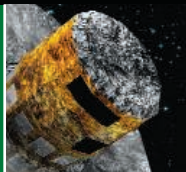
For younger readers

1468



Seeking out dark matter

1476



Life science prize essay

1486



LETTERS | BOOKS | POLICY FORUM | EDUCATION FORUM | PERSPECTIVES

LETTERS

edited by Jennifer Sills

Spore Show Not Gaming the Science System

I WAS SURPRISED TO SEE THE NEWS OF THE WEEK STORY BY J. BOHANNON ("‘SPORE’ DOCUMENTARY SPawns protest by scientists who starred in it," 24 October, p. 517) about our television documentary *How to Build a Better Being*, in which we used the video game Spore as a way to explain the latest ideas in evolutionary biology.

Contrary to the implication in Bohannon's story, any objective viewer will see a show replete with science and scientists, excitedly explaining their work and ideas. We used Spore as an entree into that scientific world as a means of informing a young audience that typically doesn't watch science programming. It was an approach designed to educate a larger audience about this dynamic field of study, and we are proud of the result.



As we said to Bohannon, our producers were transparent with all of the scientists included in the film. In many cases Spore creator Will Wright visited their labs to conduct interviews, and in no case did we attempt to disguise the premise of the show once it was developed. The reaction we have received from those who participated in the documentary has been uniformly positive.

Making complex science understandable to a mass audience is a difficult challenge. In this production, we decided to take an unconventional approach by using a vernacular familiar to millions of videogame users as a tool for exploring evolutionary biology. I deeply regret that Bohannon chose to interpret this as crass commercialism, rather than what it really is—a genuine effort to reach viewers who don't normally tune in to science.

MICHAEL ROSENFELD

President, National Geographic Television, 1145 17th Street, NW, Washington, DC 20036, USA. E-mail: mrosenfe@ngs.org

duce the results in a straightforward manner." Indeed, the principle of full disclosure is an essential element of the scientific method. Given the fundamental importance of procedural clarity, I strongly disagree that "[t]he appropriate place for most of this information is in the easily expandable Supplementary Materials that accompany each article." This information must be in the main text, not in an online supplement.

There are traditionally four main sections of a scientific article: Introduction, Materials and Methods, Results, and Discussion. Of the 24 possible permutations of these sections, only the one listed yields a logically ordered presentation. Some journals have opted for placing the Materials and Methods section after the Results and the Discussion sections. Other journals have almost completely moved the Materials and Methods section from the main text to online supplements. These journals are conveying the message, however inadvertent, that the sine qua non of the scientific method, the Materials and Methods, is the least important part of a scientific publication.

DANIEL SHRINER

13533 Aston Manor Way, Apartment K, Silver Spring, MD 20904, USA. E-mail: dshrinester@gmail.com

Artificial Intelligence Disappoints

IT IS VERY INFREQUENT THAT THE COVER OF *Science* evokes depressing thoughts. The 12 September issue's cover is one of them. It was exactly 35 years ago when, as a graduate student, I took a one-semester course in Artificial Intelligence. I had an excellent textbook: *Problem-Solving Methods in Artificial Intelligence* by Nils Nilsson. It was a fascinating subject; at the time, researchers earnestly felt that wonderful capabilities were just around the corner, if only we had somewhat more powerful computers.

I did not pursue a career in Artificial Intelligence. I regretted that for a long time, but looking at this issue's cover story, I wonder if my regrets were misplaced. After 35 years, is reCAPTCHA the state of the art in Artificial Intelligence? What happened? If I had a time machine that allowed me to go back

Limiting the Impact of the Impact Factor

K. SIMONS'S EDITORIAL "THE MISUSED IMPACT factor" (10 October, p. 165) reminded me of the Tolstoy story in which his brother tells him not to think about a white bear: When you say, "Don't think about it," it becomes hard to think of anything else. Instead, AAAS and *Science* should take the lead by defining some declarative "bibliometric postulates" that specify a code of conduct for the use of simplified indices. Postulates might include "numerical factors applied to journals should not be used to evaluate individuals" or "numerical journal factors should never be quoted without disclaimers explaining that they include falsified papers." Only an organization like *Science* with the

backing of the non-commercially beholden AAAS has the profile to defend itself and scientists from enslavement to the impact factor's absurdly one-dimensional parameterization of achievement.

JEREMY B. A. GREEN

Department of Developmental Cell Biology, King's College, London, UK. E-mail: jeremy.green@kcl.ac.uk

Putting Materials and Methods in Their Place

IN HIS EDITORIAL "SCIENTIFIC PUBLISHING standards" (5 September, p. 1271), B. Alberts wrote that scientific journals "must insist on detailed descriptions of all of the methods used, so as to allow other scientists to repro-

in time to 1973 to show today's *Science* cover story to the people working in Artificial Intelligence at that time, I wouldn't do it. Nobody would ever believe me. I find it hard to believe it myself that, in the 21st century, transcription of printed text still requires human intervention. **GIOVANNI VANNUCCI**

Milvius Research, LLC, Red Bank, NJ 07701, USA. E-mail: gv@milvius.com

ChemCam's Cost a Drop in the Mars Bucket

IN THE NEWS OF THE WEEK STORY ABOUT the ChemCam instrument on the Mars Science Laboratory (MSL) rover ("Rising costs could delay NASA's next mission to Mars and future launches," A. Lawler, 26 September, p. 1754), ChemCam, depicted in the image, contributed less than one two-hundredth of the overall overrun for the project. A collaboration between CNES and NASA, ChemCam is one of the least expensive MSL instruments from a NASA standpoint, although its role will be significant. The ChemCam mast unit, including the laser,

was provided by CNES at no charge to NASA. Contrary to your caption, the laser was not redesigned. The laser-based instrument will measure the composition of rocks some distance from the rover, even when the rocks are covered by Mars dust, a feat that could not previously be accomplished. We are proud of this innovative instrument and its future contributions to planetary science.

ROGER C. WIENS^{1*} AND SYLVESTRE MAURICE²

¹ChemCam Principal Investigator, Los Alamos, NM, USA.

²ChemCam Deputy Principal Investigator, Toulouse, France.

*To whom correspondence should be addressed. E-mail: rwiens@lanl.gov

An Order of Plumpy'nut, Hold the Aflatoxins

THE NEWS FOCUS STORY BY M. ENSERINK ("The peanut butter debate," 3 October, p. 36) discusses the value of Plumpy'nut, a peanut-containing ready-to-use food (RTUF), distributed to treat severe malnutrition. This is a complex area, particularly when extended to consider use in the prevention of malnutrition. However, we would like to sound a cau-

tionary note, a subject of much discussion that was absent from the article: the risk of contamination of the peanuts (groundnuts) with aflatoxins.

Aflatoxins are fungal metabolites ubiquitous in many staple foods, including peanuts, in sub-Saharan Africa, southeast Asia, and the southern United States (1). Regulation and testing limit human exposure in richer countries but are ineffective in many low-income countries where subsistence farming predominates. Aflatoxins are human liver carcinogens (2). More recent research also demonstrated an association between exposure and impairment of child growth (3–5). Evidence of acute toxicity and immunomodulation in people and animals has also been described (6). As a consequence, monitoring of products such as Plumpy'nut for aflatoxins is essential. It becomes particularly critical to maintain quality control as the production is franchised, as described in the article by Enserink, to numerous production sites in Africa or even adopted on a small scale at the local village [for one example, see (7)]. Representative sampling of peanuts for accurate assessment of aflatoxin is not a trivial exercise given the heterogeneity of

contamination and requires long-term commitment to training and resources.

There is a precedent for this concern. Schoolchildren in the Eastern Cape region of South Africa, through the Primary Schools Nutrition Programme, were provided with peanut butter as a nutritional supplement that allegedly contained high amounts of aflatoxin (8). Problems arose because of the lack of funding and expertise to permit adequate sampling and aflatoxin analysis. While the benefits of peanut-based RUTFs continue to be explored, this must be paralleled by emphasis on quality-control measures for possible contamination by aflatoxins.

CHRISTOPHER PAUL WILD¹*

AND RUGGERO MONTESANO²

¹Leeds Institute of Genetics, Health and Therapeutics, University of Leeds, Leeds LS2 9JT, UK. ²24 Via dei Giardini, 11013 Courmayeur, Aosta, Italy.

*To whom correspondence should be addressed. E-mail: c.p.wild@leeds.ac.uk

References

1. FAO/WHO, *WHO Food Additives Ser.* **40**, 434 (1998).
2. IARC, *Some Traditional Herbal Medicines, Some Mycotoxins, Naphthalene and Styrene* (IARC Press, Lyon, 2002).
3. Y. Y. Gong et al., *Br. Med. J.* **325**, 20 (2002).
4. Y. Y. Gong et al., *Environ. Health Perspect.* **112**, 1334 (2004).

5. P. C. Turner et al., *Int. J. Epidemiol.* **36**, 1119 (2007).
6. J. H. Williams et al., *Am. J. Clin. Nutr.* **80**, 1106 (2004).
7. R. Rosenblith, *Village Peanut Butter: Research Proposal for Local Production of Infant Formula for Chronic Malnourishment* (www.duke.edu/web/dukeglobalh/documents/VillagePeanutButter_%20Duke%20Global%20Health%20doc.pdf).
8. South African Medical Research Council, "Aflatoxin in peanut butter" (www.mrc.ac.za/promec/afloxin.htm).

In Defense of GM Crops

P. MITCHELL'S LETTER "DOUBTS ABOUT GM crops" (25 July, p. 489), referring to N. Fedoroff's Editorial (1), cannot go unanswered. Mitchell claimed that increasing yields with GM crops promoted by corporations hinders biodiversity management. Contrary to this old-fashioned framing of the issue, it is possible to combine efforts that benefit the poor as well as commercial ecological agriculture (2).

Mitchell referred to the IAASTD report (3) to degrade the importance of transgenic crops, but this report does not meet scientific review standards and comes to questionable negative conclusions about biotechnology in agriculture: "Information [about GM crops] can be anecdotal and contradictory, and uncertainty

on benefits and harms is unavoidable." Such biased judgment ignores thousands of high-quality science papers; it is not surprising that most renowned experts left the IAASTD panel before the final report was published.

Meta-analysis papers conclude that Bt crops are beneficial to nontarget insects (4). In addition, Mitchell cited Marnier's understandable call for more data (5) but ignores her previous statement that "[a] meta-analysis of 42 field experiments indicates that nontarget invertebrates are generally more abundant in Bt cotton and Bt maize fields than in non-transgenic fields managed with insecticides."

While sparing harmless (and often beneficial) insects, Bt effectively protects crops from harmful insects. Due to fewer infected insect bites and thus fewer fungal infections (6), Bt maize has been shown to contain fewer cancer-causing mycotoxins, an important benefit for human health (7). Particularly in developing countries, where storage can be problematic, regulatory offices should promote Bt maize as the healthier alternative to conventional maize.

Finally, apart from industrialized agriculture, there are positive trends associated with the adoption of GM crops by smallholders.

Public research is leading to local solutions (8) and to verifiable successes (9).

NIKLAUS H. AMMANN

Department of Biotechnology, Delft University of Technology, Delft NL-2628 BC, Netherlands. E-mail: klaus.ammann@ips.unibe.ch

References

1. N. Fedoroff, *Science* **320**, 425 (2008).
2. K. Ammann, *New Biotechnol.* **25**, 1 (2008).
3. IAASTD, www.agassessment.org/ (2007).
4. L. L. Wolfenbarger, S. E. Naranjo, J. G. Lundgren, R. J. Bitzer, L. S. Watrud, *PLoS ONE* **3**, e2118 (2008).
5. M. Marvier *et al.*, *Science* **320**, 452 (2008).
6. D. L. Kershen, *Food Drug Law J.* **61**, 197 (2006).
7. W. F. O. Marasas *et al.*, *J. Nutrition* **134**, 711 (2004).
8. J. I. Cohen, *Nat. Biotechnol.* **23**, 366 (2005).
9. R. Paarlberg, *Int. J. Technol. Globalisation* **2**, 81 (2006).

CORRECTIONS AND CLARIFICATIONS

ScienceScope: "This Jaguar's built for speed" by E. Kintisch (14 November, p. 1037). The Roadrunner supercomputer is located at the Los Alamos National Laboratory in New Mexico, not the Lawrence Livermore National Laboratory in California.

News of the Week: "Rising costs could delay NASA's next mission to Mars and future launches," by A. Lawler (26 September, p. 1754). The laser instrument mentioned in the caption was not redesigned. NASA did halt funding for the instrument in September 2007 because of a \$1.5 mil-

lion cost overrun, but reinstated that funding in 2008 after an outcry from scientists. NASA is contributing approximately \$10 million for the effort, with France's CNES contributing a larger share of the cost.

Reports: "Manipulating the metazoan mitochondrial genome with targeted restriction enzymes" by H. Xu *et al.* (25 July, p. 575). The *caa* codon in the *mt:Col^{R301L}* mutant in Fig. 1E should encode a glutamine (Q) rather than the indicated leucine (L).

TECHNICAL COMMENT ABSTRACTS

COMMENT ON "Phytoplankton Calcification in a High-CO₂ World"

Ulf Riebesell, Richard G. J. Bellerby, Anja Engel, Victoria J. Fabry, David A. Hutchins, Thorsten B. H. Reusch, Kai G. Schulz, François M. M. Morel

Iglesias-Rodriguez *et al.* (Research Articles, 18 April 2008, p. 336) reported that the coccolithophore *Emiliania huxleyi* doubles its organic matter production and calcification in response to high carbon dioxide partial pressures, contrary to previous laboratory and field studies. We argue that shortcomings in their experimental protocol compromise the interpretation of their data and the resulting conclusions.

Full text at www.sciencemag.org/cgi/content/full/322/5907/1466b

Letters to the Editor

Letters (~300 words) discuss material published in *Science* in the previous 3 months or issues of general interest. They can be submitted through the Web (www.submit2science.org) or by regular mail (1200 New York Ave., NW, Washington, DC 20005, USA). Letters are not acknowledged upon receipt, nor are authors generally consulted before publication. Whether published in full or in part, letters are subject to editing for clarity and space.

RESPONSE TO COMMENT ON "Phytoplankton Calcification in a High-CO₂ World"

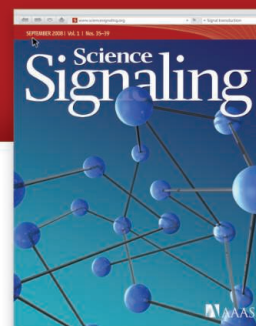
M. Debora Iglesias-Rodriguez, Erik T. Buitenhuis, John A. Raven, Oscar Schofield, Alex J. Poulton, Samantha Gibbs, Paul R. Halloran, Hein J. W. de Baar

Recently reported increasing calcification rates and primary productivity in the coccolithophore *Emiliania huxleyi* were obtained by equilibrating seawater with mixtures of carbon dioxide in air. The noted discrepancy with previously reported decreasing calcification is likely due to the previously less realistic simulation of bicarbonate due to addition of acid or base to obtain simulated future CO₂ partial pressure conditions.

Full text at www.sciencemag.org/cgi/content/full/322/5907/1466c

Call for Papers

Science Signaling



From the publishers of *Science*, *Science Signaling*, formerly known as *Science's*

STKE, now features top-notch, peer

reviewed, original research. Each week the journal will publish leading-edge findings in cellular regulation including:

- Molecular Biology
- Development
- Physiology and Medicine
- Immunology
- Neuroscience
- Microbiology
- Pharmacology
- Biochemistry
- Cell Biology
- Bioinformatics
- Systems Biology

Subscribing to *Science Signaling* ensures that you and your lab have the latest cell signaling resources. For more information visit sciencesignaling.org

Announcing Chief Scientific Editor for *Science Signaling* –

Michael B. Yaffe, M.D., Ph.D.

Associate Professor, Department of Biology
Massachusetts Institute of Technology

Now accepting original research submissions at:
sciencesignaling.org/about/help/research.dtl

Science Signaling



Comment on “Phytoplankton Calcification in a High-CO₂ World”

Ulf Riebesell,^{1*} Richard G. J. Bellerby,² Anja Engel,³ Victoria J. Fabry,⁴ David A. Hutchins,⁵ Thorsten B. H. Reusch,¹ Kai G. Schulz,¹ François M. M. Morel⁶

Iglesias-Rodriguez *et al.* (Research Articles, 18 April 2008, p. 336) reported that the coccolithophore *Emiliania huxleyi* doubles its organic matter production and calcification in response to high carbon dioxide partial pressures, contrary to previous laboratory and field studies. We argue that shortcomings in their experimental protocol compromise the interpretation of their data and the resulting conclusions.

The uptake of anthropogenic CO₂ by the ocean is projected to drive seawater pH in the course of this century to levels lower than have occurred over the past 20 million years (1). Despite much uncertainty about the resulting impacts on marine biota, there will be both winners and losers of ocean carbonation and acidification. Calcareous organisms will for the most part be on the losing side, as increasing seawater acidification (decreasing pH) incurs a greater metabolic energy requirement to precipitate calcium carbonate (2). Some photoautotrophic groups are likely to be on the winning side as increasing ocean carbonation [increasing CO₂ partial pressure (P_{CO_2})] makes it energetically less expensive to obtain the CO₂ required for photosynthesis (3). But what about organisms that perform both photosynthesis and calcification, such as the coccolithophores? Studies conducted over the past 8 years indicate marked differences in CO₂/pH sensitivities at the species level and possibly also at the strain level. In the range of P_{CO_2} changes projected for this century, calcification in *Coccolithus pelagicus* appears almost insensitive to seawater acidification, *Emiliania huxleyi* and *Calcidiscus leptoporus* show a moderate decline in calcification, and *Gephyrocapsa oceanica* shows a strong decline (4–11). In terms of photosynthesis, these species were either insensitive or responded to a doubling of present-day P_{CO_2} with a moderate increase of 5 to 15%.

In contrast, Iglesias-Rodriguez *et al.* (12) suggest that in a single strain of the most abundant coccolithophore, *E. huxleyi*, both photosynthesis and calcification increased by 100 to 150% over a CO₂ range from 280 to 750 μatm . This is an

order of magnitude larger than previously observed responses of marine phytoplankton to rising CO₂ and, in terms of the change in calcification, opposite in sign to the earlier studies, many of which manipulated the CO₂ system similar to Iglesias-Rodriguez *et al.* by bubbling with CO₂-enriched air. As discussed below, we believe that shortcomings in the experimental protocol compromise the interpretation of these data and raise doubts about the conclusions drawn from them.

First, precultures in (12) were grown to densities of up to 500,000 cells mL⁻¹, that is, 5 to 10 times as high as in the actual experiments (13). This large difference in cell concentrations can be expected to cause strong divergence in growth conditions between precultures and experimental incubations. For example, with a 6 to 13% drawdown of alkalinity in high-CO₂ experimental treatments [table 2 in (12)], a five-fold higher cell density in precultures is expected to result in an alkalinity drawdown of 30 to 65%. This would cause a severe drift in the preculture's carbonate system, including shifts in CO₂ concentration and carbonate saturation. Under these circumstances, it is questionable whether preculturing allowed true acclimatization of cells to the experimental conditions.

Second, some of the precultures used by Iglesias-Rodriguez *et al.*, particularly those in

high-CO₂ treatments, may have experienced nutrient limitation at the time of transfer to the experimental flasks. This is suggested by an estimation of nitrate drawdown based on a cell density of 500,000 cells mL⁻¹ and values from figure 1, B and E, in (12) (1.8 pmol C cell⁻¹ and cellular C:N ~7). The calculated nitrogen demand of 128.6 $\mu\text{mol N L}^{-1}$ exceeds the initial 100 $\mu\text{mol nitrate L}^{-1}$ applied in the precultures. Nitrate limitation in *E. huxleyi* is known to increase cell size and carbon quota (14) and may also explain the larger size and carbon quota of the high-CO₂-grown cells.

Third, experimental incubations lasted for only 1.5 to 3 days, allowing for about 1 to 2 cell generations. With incubation times this short, there can be little certainty that cells were actually in steady-state exponential growth, and the outcome of the experiments depended to a large extent on the cells' preconditioning. Because growth conditions in the precultures were not monitored, but likely continued to have an effect during experimental incubations, it is uncertain which growth factors have led to the observed physiological responses. Previous studies with coccolithophores have generally allowed for a minimum of 8 to 10 cell generations under experimental conditions.

Finally, cells grown at high CO₂ had a carbon quota (cellular biomass) two to three times greater than low-CO₂-grown cells [figure 1, A and B, in (12)]. As the experiments allowed for only 1 to 2 cell generations, the strong difference in biomass could not have developed during the experimental run, but could be attributable to the preculturing. Although the experiment was set out with two test variables, cellular biomass and CO₂ concentration, the former was not treated as a variable. When expressing the data on a per cell basis, as in (12), the observed trends may be related to the CO₂ treatment, or to the difference in cellular biomass between treatments, or both. Correcting for a possible biomass effect, for example, by normalizing the data to algal biomass, reverses the trends in calcification and primary production rates with P_{CO_2} reported in (12) (see Fig. 1), making their results entirely consistent

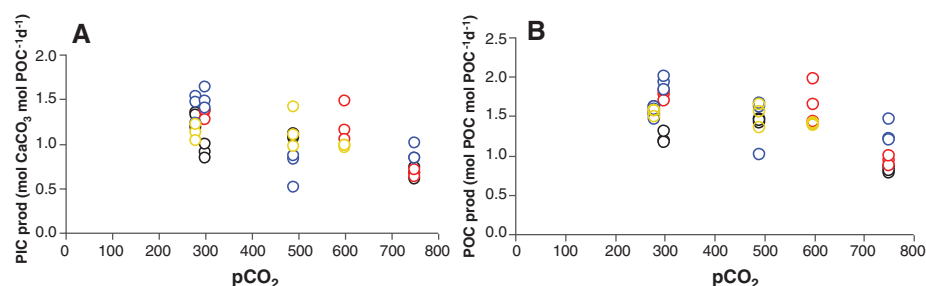


Fig. 1. Daily production of (A) particulate inorganic carbon (PIC) and (B) particulate organic carbon (POC) normalized to POC biomass for *E. huxleyi* cultures under different P_{CO_2} . Each color represents one independent experiment in (12). Calculations are based on cell numbers at the beginning and end of the experiments and cellular PIC and POC content at the time of incubation (data provided by M. D. Iglesias-Rodriguez).

¹Leibniz Institute of Marine Sciences, IFM-GEOMAR, D-24105 Kiel, Germany. ²Bjerknes Centre for Climate Research, University of Bergen, N-5020 Bergen, Norway. ³Alfred Wegener Institute of Polar and Marine Research, D-27570 Bremerhaven, Germany. ⁴Department of Biological Sciences, California State University San Marcos, San Marcos, CA 92096, USA. ⁵Department of Biological Sciences, University of Southern California, Los Angeles, CA 90089, USA. ⁶Department of Geosciences, Princeton University, Princeton, NJ 08544, USA.

*To whom correspondence should be addressed. E-mail: uriebesell@ifm-geomar.de

with previous studies on the CO₂ sensitivity of *E. huxleyi* (4–10).

Understanding what will happen to the ocean biota over the next century in response to global change is important to humanity. All efforts to augment the relatively meager experimental information on the response of marine organisms to acidification are to be encouraged, particularly if they put into question the current wisdom, but these reports must be based on sound interpretations of the available data. We contend that, to date, there is no unequivocal laboratory or field

study showing that increasing CO₂ causes an increase in coccolithophore calcification.

References

1. Royal Society, *Ocean Acidification Due to Increasing Atmospheric Carbon Dioxide* (Policy Document 12/05, Royal Society, London, 2005).
2. V. J. Fabry, B. A. Seibel, R. A. Feely, J. C. Orr, *ICES J. Mar. Sci.* **65**, 414 (2008).
3. E. Spijkerman, *Physiol. Plant.* **133**, 41 (2008).
4. U. Riebesell *et al.*, *Nature* **407**, 364 (2000).
5. I. Zondervan, R. E. Zeebe, B. Rost, U. Riebesell, *Global Biogeochem. Cycles* **15**, 507 (2001).
6. A. Sciandra *et al.*, *Mar. Ecol. Prog. Ser.* **261**, 111 (2003).
7. N. Leonardos, R. J. Geider, *J. Phycol.* **41**, 1196 (2005).
8. B. Delille *et al.*, *Global Biogeochem. Cycles* **19**, GB2023 10.1029/2004GB002318 (2005).
9. A. Engel *et al.*, *Limnol. Oceanogr.* **50**, 493 (2005).
10. Y. Feng *et al.*, *Eur. J. Phycol.* **43**, 87 (2008).
11. G. Langer *et al.*, *Geochem. Geophys. Geosyst.* **7**, Q09006 (2006).
12. M. D. Iglesias-Rodriguez *et al.*, *Science* **320**, 336 (2008).
13. M. D. Iglesias-Rodriguez, personal communication.
14. E. Paasche, *Phycologia* **40**, 503 (2001).

10.1126/science.1161096

Response to Comment on "Phytoplankton Calcification in a High-CO₂ World"

M. Debora Iglesias-Rodriguez,^{1*} Erik T. Buitenhuis,² John A. Raven,³ Oscar Schofield,⁴ Alex J. Poulton,¹ Samantha Gibbs,¹ Paul R. Halloran,⁵ Hein J. W. de Baar^{6,7}

Recently reported increasing calcification rates and primary productivity in the coccolithophore *Emiliania huxleyi* were obtained by equilibrating seawater with mixtures of carbon dioxide in air. The noted discrepancy with previously reported decreasing calcification is likely due to the previously less realistic simulation of bicarbonate due to addition of acid or base to obtain simulated future CO₂ partial pressure conditions.

Riebesell *et al.* (1) highlight our report of increased calcification and productivity of the coccolithophore *Emiliania huxleyi* at high CO₂ partial pressures (P_{CO_2}) (2), discuss discrepancies between our data (2, 3) and those of others (4, 5) and speculate on the shortcomings of our experimental protocol. However, Riebesell *et al.* ignore the problem we noted (2) in the design of previous experiments (3): adding acid or base when aiming for simulation of the future high-CO₂ ocean. Here, we address their critiques (1) and provide a further analysis of what we believe is the central issue of this debate.

The first issue raised by Riebesell *et al.* (1) concerns potential drifts in the carbonate system caused by differences in cell concentrations. The nature of these drifts is undocumented experimentally, and it is unclear how this would change the main conclusion of our work (2). We followed established semicontinuous culturing protocols and maintained cells at densities several-fold lower than those reported in recent studies specifically measuring the effect of carbonate chemistry on *E. huxleyi* physiology [e.g., (6)]. More important, the cells were not nutrient-limited and were growing exponentially (i.e., not exhibiting lag-phase), and therefore we expect a negligible effect, if any, on the observed responses.

Regarding the issue of potential nutrient limitation in precultures, nutrient stress in our cultures is not supported by our observations: Cells had high growth rates (0.53 to 0.76 d⁻¹), and the minimum ambient nutrient concentrations during

measurements (35 to 84 μM nitrate and 2 to 5 μM phosphate) (7) were at least an order of magnitude higher than reported limiting values (8). Even using the lowest N:P ratios reported for blooms (N:P <10) (9), the nitrate and phosphate availabilities (35 μM and 0.9 μM, respectively) in our cultures are well above the measured cell quotas in *E. huxleyi* under N- or P-limitation (8). When *E. huxleyi* cells were grown with ambient N:P = 1:1 (N-limited) and 300:1 (P-limited), the cellular N:P ratios varied between 12:1 and 41:1 (8). Applying the lowest cellular ratios, our experiments are nutrient-replete. A problem with Riebesell *et al.*'s argument (1) is their suggestion that the observed increase in cell size was a result of nutrient limitation. This is not supported by evidence showing that *E. huxleyi* cell size decreases under nitrate limitation (10) and increasing P_{CO_2} (11), whereas phosphate limitation induces an increase in size (10).

Riebesell *et al.* also point out the potential for non-steady-state growth in our preconditioned cells. We monitored the growth of semicontinuous cultures of exponentially growing nutrient-replete cells for nine generations, bubbled with the constant air-CO₂ mixtures, before harvesting was conducted during the final subculturing. Impacts of changes in the ocean carbon chemistry on physiology and cell size should, however, not be surprising because cell size is sensitive to many factors impacting on phytoplankton physiology, often within one or two cell divisions (12).

Riebesell *et al.* further question the value of expressing physiological rates on a per cell basis. We contend that any understanding of cellular responses requires cell-specific measurements and that this is key to understanding the ecophysiological responses of calcifying phytoplankton to increasing P_{CO_2} . It also allows our results to be compared with the rich historical primary literature [e.g., (3)]. Biogeochemically, the biomass-normalized rate is most likely more valuable, as discussed in (2), showing that the range of P_{CO_2} enhances both photosynthesis and calcification.

Experiments conducted at various dissolved inorganic carbon (DIC) conditions, that is, different relative proportions of CO₂, bicarbonate

(HCO₃⁻), and carbonate ions (CO₃²⁻) (3–5, 13) are, in principle, valid for unraveling the physiology of *E. huxleyi*. However, great care must be taken when extrapolating these results to *E. huxleyi* performance in the future high-CO₂ ocean. In these experiments, the manipulation of the carbonate system is central to the data interpretation. Because of the long residence time of alkalinity in the ocean, we can assume constant alkalinity until the end of the century (14, 15). The increasing atmospheric P_{CO_2} will yield an increase of total DIC, CO₂(aqueous), and HCO₃⁻, a decrease of CO₃²⁻ and pH: ocean acidification. Upon adding acid/base to seawater to mimic future high P_{CO_2} /past ocean, one inevitably causes a decrease/increase in alkalinity and a lesser increase/decrease of bicarbonate as compared to their predicted stability and stronger increase/decrease, respectively, in the future high-CO₂/past ocean (Fig. 1). Thus, from comparing the initial conditions (Fig. 1) of the simulation by bubbling CO₂ in air (2) with the previous acid/base perturbations (3), one realizes that CO₂ bubbling correctly mimics the constant alkalinity accompanied by major changes in bicarbonate ion of the

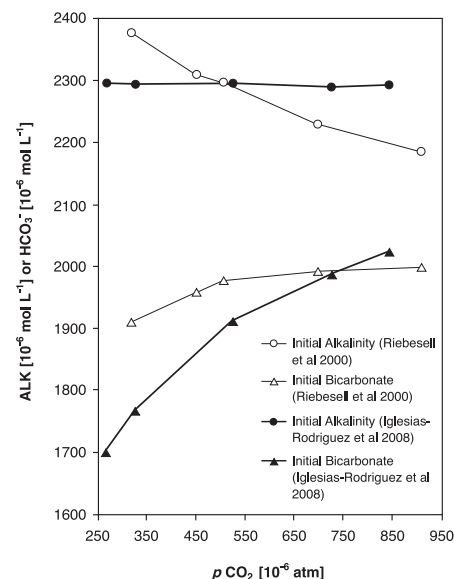


Fig. 1. Upon CO₂ in air bubbling (2) of seawater, the initial alkalinity [ALK 10⁻⁶ mol L⁻¹] (filled circles) remains constant, and the initial bicarbonate [10⁻⁶ mol L⁻¹] (filled triangles) changes strongly versus the desired P_{CO_2} [10⁻⁶ atm] to best simulate the corresponding initial conditions of a bloom of *E. huxleyi* in the future high-CO₂ ocean. In contrast, by acid/base manipulation (3), the initial alkalinity (open circles) changes strongly, whereas the initial bicarbonate has a far lesser change versus the desired P_{CO_2} than the predicted (14, 15) future high-CO₂ ocean. For latter acid/base treatments, the initial values of alkalinity and dissolved inorganic carbon were provided by U. Riebesell, from which the initial bicarbonate values were calculated. Initial conditions are for the subsequent growth experiments at light intensity of 150 10⁻⁶ mol m⁻² s⁻¹ and $T = 19^\circ\text{C}$ and $T = 15^\circ\text{C}$ after (2) and after figure 2 in (3), respectively.

¹National Oceanography Centre, Southampton, University of Southampton Waterfront Campus, European Way, Southampton SO14 3ZH, UK. ²School of Environmental Sciences, University of East Anglia, Norwich NR4 7TJ, UK. ³Division of Plant Sciences, University of Dundee at SCRI, Scottish Crop Research Institute, Invergowrie, Dundee DD2 5DA, UK. ⁴Institute of Marine and Coastal Sciences, Rutgers University, Dudley Road, New Brunswick, NJ 08901-8521, USA. ⁵Department of Earth Sciences, University of Oxford, Parks Road, Oxford OX1 3PR, UK. ⁶Ocean Ecosystems, University of Groningen, Post Office Box 14, 9750 AA Haren, Netherlands. ⁷Royal Netherlands Institute for Sea Research, Post Office Box 59, 1790 AB Den Burg, Netherlands.

*To whom correspondence should be addressed. E-mail: dir@noc.soton.ac.uk

future high-CO₂ ocean. In contrast, the acid/base treatment (3) shows major perturbation of alkalinity and too small changes of bicarbonate ions. Any conceivable relationship (2, 13, 16) between the rate of calcification and bicarbonate ions in the future high-CO₂ ocean will be obscured by the acid/base treatment (3).

Finally, Riebesell *et al.* (1) encourage efforts to better understand the response of marine organisms to ocean acidification, as do we. Contrary to their assertion of the methodological shortcomings of our study, we have justified our reasoning and approach and demonstrated that a previous report (3) has confounded the issue by using an approach (acid/base manipulation of seawater) that is not appropriate for predicting the calcification response of *E. huxleyi* in a future high-CO₂ ocean.

References and Notes

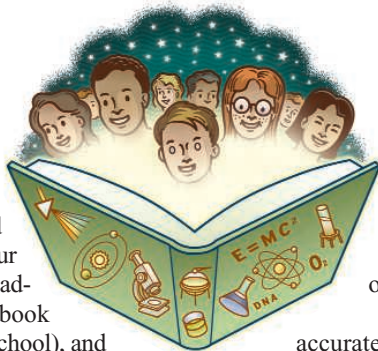
1. U. Riebesell *et al.*, *Science* **322**, 1466 (2008); www.sciencemag.org/cgi/content/full/322/5907/1466b.
2. M. D. Iglesias-Rodriguez *et al.*, *Science* **320**, 336 (2008).
3. U. Riebesell *et al.*, *Nature* **407**, 364 (2000).
4. I. Zondervan, R. E. Zeebe, B. Rost, U. Riebesell, *Global Biogeochem. Cycles* **15**, 507 (2001).
5. G. Langer *et al.*, *Geochem. Geophys. Geosyst.* **7**, Q09006 (2006).
6. N. Leonardos, R. J. Geider, *J. Phycol.* **41**, 1196 (2005).
7. We calculated the available nitrogen (N) and phosphorus (P) concentrations in the medium at the end of the preacclimation period, immediately before subculturing. N and P were calculated as follows: $N = N_0 - (C \cdot N_c)$ and $P = P_0 - (C \cdot P_c)$, where N_0 and P_0 are the initial nitrate and phosphate concentrations, respectively, in the medium at the start of growth ($N_0 = 100 \mu\text{M}$ and $P_0 = 6.24 \mu\text{M}$); C is the number of cells in the preacclimation cultures immediately before subculturing ($\sim 5 \times 10^5 \text{ cells mL}^{-1}$); and N_c and P_c are the average nitrogen and calculated phosphorus quotas using Redfield (N:P = 16:1) when cells were harvested. N_c (0.06 to 0.25 pmol N/cell) was measured and P_c ($3.93 \times 10^{-3} - 16.3 \times 10^{-3} \text{ pmol P/cell}$) was derived from it, assuming a 16:1 Redfield ratio.
8. R. Riegman *et al.*, *J. Phycol.* **36**, 87 10.1046/j.1529-8817.2000.99023.x (2000).
9. C. A. Klausmeier *et al.*, *Nature* **429**, 171 (2004).
10. M. N. Müller, A. N. Antia, J. LaRoche, *Limnol. Oceanogr.* **53**, 506 (2008).
11. R. Webster, thesis, University of Essex, United Kingdom (2009).
12. A. Sciadra *et al.*, *Mar. Ecol. Prog. Ser.* **261**, 111 (2003).
13. E. Buitenhuis, H. de Baar, M. Veldhuis, *J. Phycol.* **35**, 949 (1999).
14. Constant alkalinity (2324 mol/kg) was used in the example calculation of table 1 in (15).
15. The Royal Society, "Ocean acidification due to increasing atmospheric carbon dioxide"; <http://royalsociety.org/displaypagedoc.asp?id=13539>.
16. M. D. Iglesias-Rodriguez *et al.*, *EOS, Transactions, American Geophysical Union* **83**, 365 (2002).

10.1126/science.1161501

FOR YOUNGER READERS

Science Books for Fun and Learning— Some Recommendations from 2008

Are there children or young adults on your holiday gift list whose interest in science you are trying to encourage? If so, you may wish to consider the finalists for the 2009 *Science Books and Films* Prizes for Excellence in Science Books. These honor works that further the understanding and appreciation of science in younger readers. Sponsored by the AAAS and Subaru, they are awarded in four categories: children's science picture book (for readers in grades K to 4), middle grades science book (grades 5 to 8), young adult science book (high school), and hands-on science/activity book (any age). Again this year, the finalists for the young adult award are generally not books specifically intended for that age group—rather, they were written for the general



public. The titles considered for the 2009 prizes were published between September 2007 and August 2008.

Here, we present our short descriptions of the 19 finalists chosen by panels of librarians, educators, and scientists. Full reviews of each book have been published or will appear in *Science Books and Films*, and AAAS members can read these reviews on the Web. The four winners will be announced in January and honored at the AAAS Annual Meeting in Chicago in February.

The criteria for evaluating the books include a clear and accurate presentation of scientific concepts. But we and the judges hope that the finalists will encourage young readers to turn to science books for pleasure as well as for information.

—Heather Malcomson,¹ Barbara Jasny, and Sherman Suter

Children's Science Picture Book

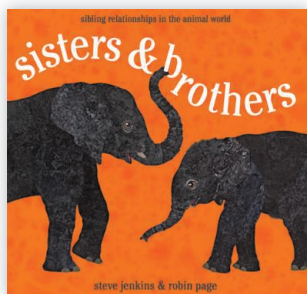
Eggs. Marilyn Singer, illustrated by Emma Stevenson. Holiday House, New York, 2008. 32 pp. \$16.95. ISBN 9780823417278.



Eggs provide a shelter in which a developing animal can breathe, be nourished with food and drink, and grow. They are laid by birds, invertebrates, fish, amphibians, reptiles, and even some mammals. Singer presents examples of their innumerable shapes, sizes, colors, and patterns. She also discusses how burial, brooding, and nests protect eggs, and she describes varieties of hatching. Stevenson's detailed gouache paintings convey the eggs' allure.

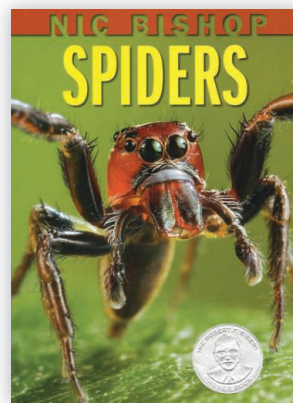
Sisters and Brothers: Sibling Relationships in the Animal World. Steve Jenkins (illustrator) and Robin Page. Houghton Mifflin, Boston, 2008. 32 pp. \$16. ISBN 9780618375967.

Animals and families always fascinate children, but the facts about siblings that fill this book will also engage adults. For example, young shrews line up holding each others' tails, with the mother leading the way. Female termites lay 30,000 eggs a day, whereas giant anteaters are always single offspring. Nile crocodiles cooperate even before they hatch, but hyena cubs can fight to the death. The authors' collages are sure to appeal to young readers.



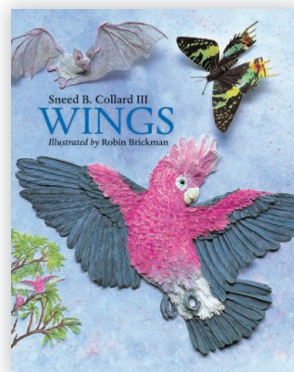
Spiders. Nic Bishop. Scholastic, New York, 2007. 48 pp. \$17.99, C\$19.99. ISBN 9780439877565.

Spider enthusiasts and arachnophobes alike will be drawn to the amazing, up-close photographs in this informative introduction to these eight-legged predators. The concise, well-written text offers numerous interesting facts about spiders. For example, they were among the earliest terrestrial predators, having arisen more than 350 million years ago. And although "silk is the secret of spider success," many of the more than 38,000 species do not use webs. Fishing spiders dart over the water's surface, and some jumping spiders can leap 20 times their body length to pounce on prey.



Wings. Sneed B. Collard III, illustrated by Robin Brickman. Charlesbridge, Watertown, MA, 2008. 32 pp. \$16.95. ISBN 9781570916113. Paper, \$7.95. ISBN 9781570916120.

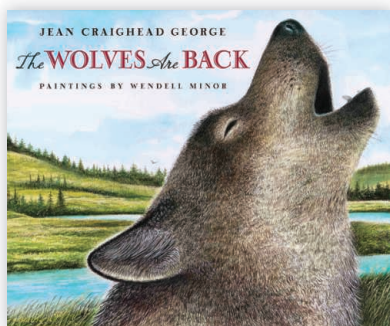
Insects, birds, and bats all move through the air on wings. Collard introduces the diversity of these appendages and their uses. Wings can be covered with scales, feathers, or bare skin. They allow peregrines to twist and turn in a dive, leaf-nosed bats to lazily flap over the ground, milkweed bugs to move short distances among patches, and Arctic terns to migrate between the polar regions. They help animals chase, catch, flee, and mate. To illustrate this variety, Brickman sculpted painted paper into colorful collages.



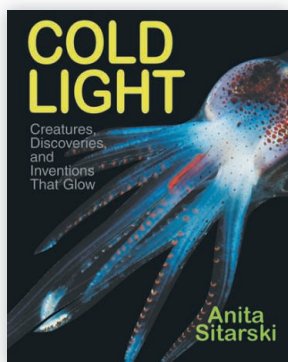
¹Science Books and Films, 1200 New York Avenue NW, Washington, DC 20005, USA. E-mail: hmalcoms@aaas.org

The Wolves Are Back. Jean Craighead George, illustrated by Wendell Minor. Dutton Children's, New York, 2008. 32 pp. \$16.99. ISBN 9780525479475.

Because "only the gentle animals should grace the beautiful wilderness," the wolves of Yellowstone were once shot until they were eliminated. However, with changed values and the yearning to again hear howls in the wild, wolves were reintroduced to the national park in 1995. As the wolves multiplied, wildflowers reappeared (wolves chased away the mountain sheep that had eaten them) and birds returned (wolves hunted bison and elk that had trampled young aspen needed for perches and grasses needed for food). By following along as a wolf pup wanders the Lamar Valley, readers learn how wolves are even important to halting river-bank erosion. George's simple text and landscape artist Minor's beautiful illustrations convey the importance of maintaining all parts of ecosystems.



Middle Grades Science Book



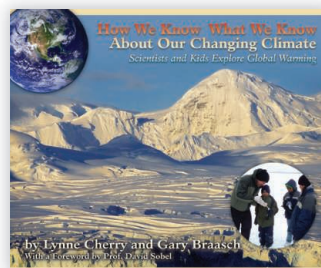
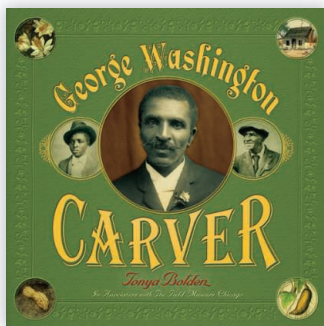
Cold Light: Creatures, Discoveries, and Inventions That Glow. Anita Sitarski. Boyd's Mills Press, Honesdale, PA, 2007. 48 pp. \$16.95. ISBN 9781590784686.

This book's theme can be described as make light, not heat. Sitarski offers an information-packed but reader-friendly account of chemical and biological sources of luminescence along with important discoveries from 1602 through to today's light-emitting diodes. Of course there are photos of fireflies and jellyfish, but the intriguing images also include a glowing chicken and art by Montana State

University students who covered the walls of a darkened gallery with dishes containing luminescent marine bacteria. Very cool indeed!

George Washington Carver. Tonya Bolden. Abrams Books for Young Readers (Abrams), New York, in association with the Field Museum, Chicago, 2008. 42 pp. \$18.95, C\$20.95, £9.95. ISBN 9780810993662.

Peanuts, sweet potatoes, and soybeans (and the products made from them) were key interests of horticulturist, educator, and inventor Carver. The ex-slave's research and teaching, which stressed scientific farming and soil conservation, helped improve agriculture in the South. Bolden's eloquent telling of Carter's life and accomplishments is enhanced with quotes from him and his contemporaries. The historical photos; evocative artifacts; and Carter's own drawings, paintings, and scientific illustrations will help captivate young readers.



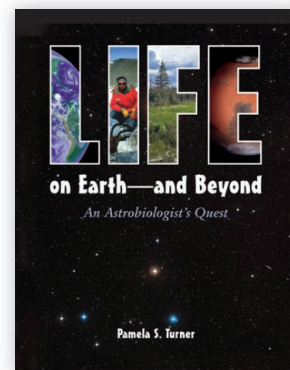
How We Know What We Know About Our Changing Climate: Scientists and Kids Explore Global Warming. Lynne Cherry and Gary Braasch. Dawn, Nevada City, CA, 2008. 66 pp. \$18.95. ISBN 9781584691037.

The title is accurate. The authors survey a wide range of indications that Earth's climate is changing. These clues include

the earlier spring arrivals of migrating birds, earlier blooming by wildflowers and Washington, DC's cherry trees, melting glaciers and icecaps, microfossils from cores of mud from the ocean floor, and bubbles of ancient air retrieved from cores of glacial ice. In his earlier *Earth Under Fire*, photojournalist Braasch visited climate researchers in the field to document their discoveries. Here he and Cherry (a seasoned author of environmental books for children) also spotlight citizen science and (especially) data that can be, and are, collected by children. They explain why data and computer models indicate that anthropogenic greenhouse gases are making our world warmer. Along the way, Cherry and Braasch remind readers of the importance of using data to test hypotheses. Reflecting the book's hopeful perspective, the authors suggest numerous things that kids and families can do to reduce their climatic footprint. An extensive list of Web sites and books offers additional "sources of information, inspiration, and action."

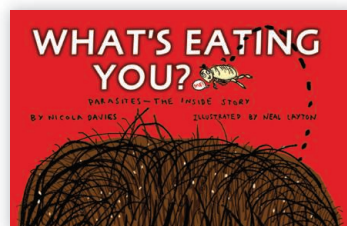
Life on Earth—And Beyond: An Astrobiologist's Quest. Pamela S. Turner. Charlesbridge, Watertown, MA, 2008. 108 pp. \$19.95. ISBN 9781580891332. Paper, \$11.95. ISBN 9781580891349.

Turner approaches astrobiology through the experiences of NASA scientist Chris McKay. Most chapters resemble a travelogue, as she describes his excursions around the world. He visits Antarctica's Dry Valleys, the Atacama and Sahara deserts, permafrost-covered tundra in Siberia, and the bottom of an Antarctic lake permanently capped by ice. Weaving the underlying science into her narrative, she explains how studying microbes from these extreme environments helps us understand whether life can exist in similar situations on Mars or another planet.

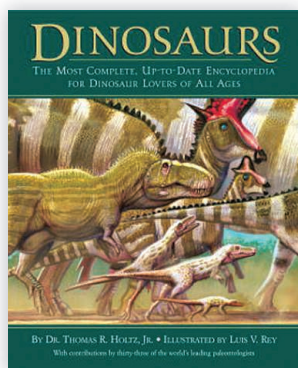


What's Eating You? Parasites—The Inside Story. Nicola Davies, illustrated by Neal Layton. Candlewick, Cambridge, MA, 2007. 60 pp. \$12.99, C\$16. ISBN 9780763634605.

This account of animals that live on or in other animals is more likely to delight than disgust. Zoologist Davies explains the advantages parasites find in being small and able to change body form during their lives. He describes the challenges they face in moving among hosts—a point reinforced in a playable "two-host tapeworm game." He also discusses parasites' amazing life cycles, their effects on hosts (including some benefits and examples of "mind control"), and some of the ways the hosts fight back. Layton's clever drawings complement the informative text.



Young Adult Science Book



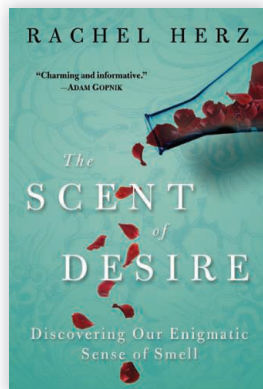
Dinosaurs: The Most Complete, Up-to-Date Encyclopedia for Dinosaur Lovers of All Ages. Thomas R. Holtz Jr., illustrated by Luis V. Rey. Random House, New York, 2007. 432 pp. \$34.99, C\$44. ISBN 9780375824197.

Anyone with even a passing interest in dinosaurs should not miss this journey into their diverse and strange world. Holtz and his colleagues fill the book with fascinating details ranging from discoveries of new species (e.g., a sauropod, *Amphicoelias*, with a mass of 18 elephants) to old favorites (e.g., *Tyrannosaurus rex*, which may have lived and hunted in

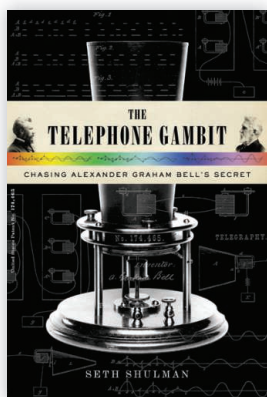
packs). They cover major and minor groups, predator-prey relations, social interactions within species, habitats and habits, and evolutionary trends. With its conversational tone and Rey's engaging illustrations, the book should appeal to young adults and a general audience alike.

The Scent of Desire: Discovering Our Enigmatic Sense of Smell. Rachel Herz. Morrow, New York, 2007. 288 pp. \$24.95. ISBN 9780060825379.

Far from a prissy survey of perfumes and odor—it starts with the suicide of a rock singer who had lost his sense of smell—this book explores how and why smell is such a central component of our lives. Explaining basic neurobiological principles in clear language, Herz intermixes them with stories and personal accounts of her research and experiences. She describes olfactory technologies, such as the development of electronic noses, that are already beginning to be used in the food industry and might even help diagnose diseases. She also dreams of a gel that would boost olfactory receptor function and restore sensation to older individuals. Her account will stimulate readers' interests in psychology and neuroscience.



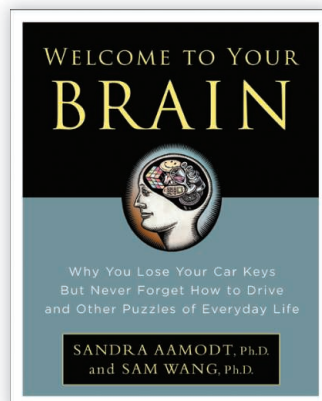
The Telephone Gambit: Chasing Alexander Graham Bell's Secret. Seth Shulman. Norton, New York, 2008. 256 pp. \$24.95, C\$27.50. ISBN 9780393062069.



Who invented the telephone? Most people would answer Alexander Graham Bell—recall “Mr. Watson, come here!” In this well-researched and well-written account, Shulman argues that Bell furtively copied crucial aspects of his device from a patent application by Elisha Gray. The author weaves science, intrigue, and romance into a fast-paced narrative. He lays his evidence out clearly while carrying readers through the steps he took to build his thought-provoking case. [For a full review, see D. L. Morton Jr., *Science* **319**, 1188 (2008).]

Welcome to Your Brain: Why You Lose Your Car Keys But Never Forget How to Drive and Other Puzzles of Everyday Life. Sandra Aamodt and Sam Wang. Bloomsbury, New York, 2008. 240 pp. \$24.95. ISBN 9781596912830.

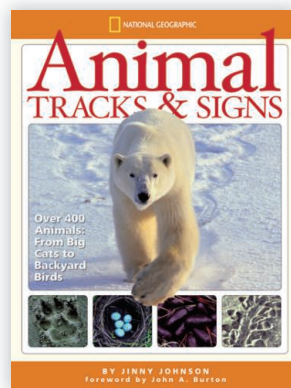
The neuroscientist authors offer a highly accessible and richly informative “user’s guide” to our brains. They cover a broad range of topics, offering up-to-date information directed to answering questions of the curious public. They supplement their narrative with frequent and quite extensive sidebars that debunk myths, focus on specific issues, and offer practical tips. Eschewing didactical lecturing, their friendly and informal writing effectively draws the reader into a comfortable, interesting, and informative dialogue.



Hands-On Science/Activity Book

Animal Tracks and Signs. Jinny Johnson. National Geographic, Washington, DC, 2008. 192 pp. \$24.95, C\$27.95. ISBN 9781426302534. Marshall (Quarto), London. £16.95. ISBN 9781845388904.

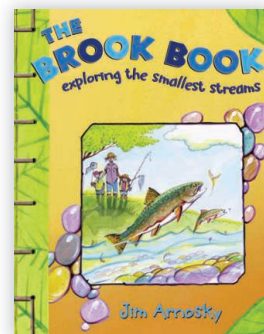
Whether they inhabit backyards, local fields or woods, or wilderness parklands, most animals can be hard to sight. But they do leave clues to their activities: tracks, nests, feeding remains, and dung. Johnson gives pointers on how to notice, record, and interpret such signs. In addition, she includes basic facts about the animals themselves. Mammals garner the most attention, while amphibians, reptiles, birds, insects, and other invertebrates are discussed in shorter sections. Although the book’s global scope limits its coverage to some 400 selected examples, the information can often also be applied to closely related species.



This appealing introduction should lead nature enthusiasts to seek additional details in field guides with a more restricted focus.

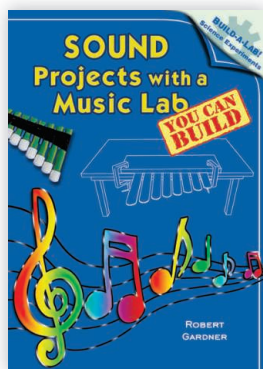
The Brook Book: Exploring the Smallest Streams. Jim Arnosky. Dutton Children's, New York, 2008. 28 pp. \$15.99, C\$19. ISBN 9780525477167.

Budding naturalists who have access to any narrow, shallow stream will find this an inviting guide to the variety of observations they can make. It begins with appropriately simple explanations of the sources and fates of the water in a brook. There are plenty of activities to satisfy young explorers, including sketching flowers, collecting smooth stones, examining aquatic insects, watching birds, and looking for animal tracks. Parents will appreciate the emphasis on safety, while children should be attracted by Arnosky's alluring text and charming illustrations (which feature flora and fauna of Vermont, where he farms).



Sound Projects with a Music Lab You Can Build. Robert Gardner. Enslow, Berkeley Heights, NJ, 2008. 128 pp. \$31.93. ISBN 9780766028098. Build-a-Lab! Science Experiments.

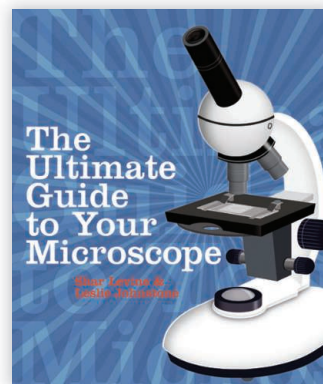
Gardner lays out hands-on experiments that explore such topics as how sounds form and travel; properties of standing waves and harmonics; and aspects of string, wind, and percussion instruments. He adroitly balances open-ended questions and necessary background information, thus enticing students to actually investigate phenomena to obtain answers. Many of the 35 experiments offer intriguing ideas for elementary or middle school science fairs. The book will reward self-motivated students who are seeking challenges in problem solving.



activities range from the obvious (use cloth bags, turn down your heat) to the creative and fun (set up a local carbon trading card system, help organize a trash-free lunch day at school). Each is described on a single page, which makes the book perfect for browsing. For those who want to do still more, the authors suggest ways to learn about jobs that will help our environment.

The Ultimate Guide to Your Microscope. Shar Levine and Leslie Johnstone. Sterling, New York, 2008. 144 pp. Paper, \$9.95, C\$11.95. ISBN 9781402743290.

Most students find their introduction to microscopes boring. They are shown a diagram of parts and given a couple of exercises that demonstrate the instruments' capabilities. The authors offer a lively alternative. After covering the basics and how to make various types of slides, they describe 41 projects involving easy-to-obtain objects such as pet hair, dead bugs, food molds, and clover. Their instructions, discussions of what is likely to be seen, and color photomicrographs should inspire readers to explore the tiny facets of our world.



10.1126/science.1167971



True Green Kids: 100 Things You Can Do to Save the Planet. Kim McKay and Jenny Bonnin. National Geographic, Washington, DC, 2008. 144 pp. \$27.90, C\$33. ISBN 9781426304439. Paper, \$15.95, C\$18. ISBN 9781426304422.

Youngsters who wish to join the green movement will enjoy this book. The 100

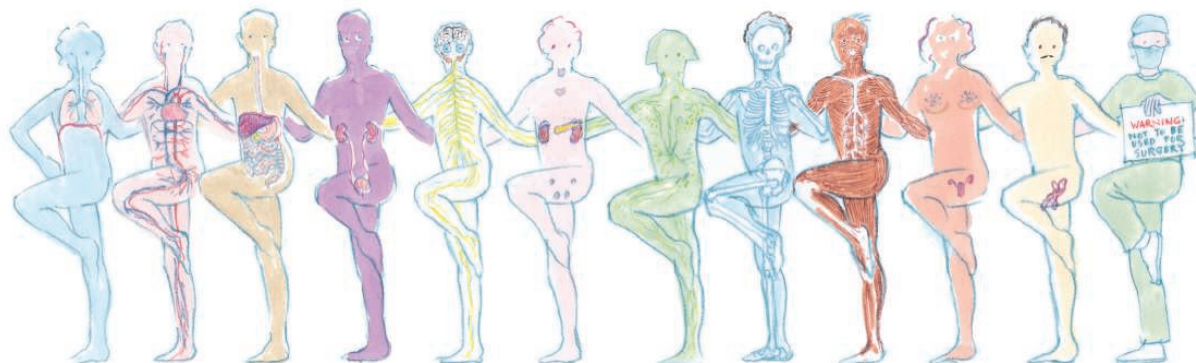
BROWSINGS

Physics: Why Matter Matters! Dan Green and Simon Basher (illustrator). Kingfisher, London, 2008. 128 pp. Paper, £6.99. ISBN 9780753416822. New York, \$8.95, C\$9.95. ISBN 9780753462140.

To introduce matter, energy, and their interactions, the authors present a cast of colorful characters. These range from classic members of our everyday world (such as force and inertia) to the flavorful quarks and the yet-to-be-found Higgs boson.

The Way We Work: Getting to Know the Amazing Human Body. David Macaulay, with Richard Walker. Houghton Mifflin, Boston, 2008. 336 pp. \$35. ISBN 9780618233786.

Renowned for his elaborately illustrated accounts of the hows and whys of buildings and machines, Macaulay here turns to human anatomy and physiology. After a brief introduction to biomolecules and cells, he leads readers from cells through organs to our body's complex, integrated systems for transporting oxygen, processing food, controlling actions, fighting infections, moving, and creating offspring. The detailed colored-pencil drawings and concise text both exhibit the authors' effective fusion of information and humor.



SOCIOLOGY

The Gender Gap in NIH Grant Applications

Timothy J. Ley^{1*} and Barton H. Hamilton²

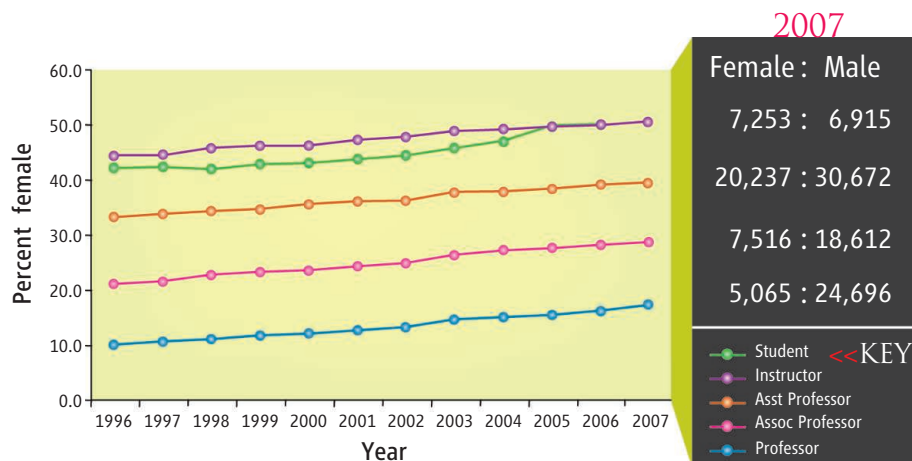
Many reports over the past two decades have drawn attention to the paucity of senior female faculty in American medical schools and universities [for recent examples, see refs. (1–5)]. As the career pipeline progresses for biomedical scientists in U.S. medical schools, there is excess attrition for women (see figure, right). However, at the beginning of the pipeline, gender parity exists for M.D.'s and Ph.D.'s. In this report, we use a data-driven approach to better understand when and why this attrition occurs.

In 2005, 49% of the 6368 Ph.D.'s awarded in the biological sciences went to women (6). Gender equity has also recently been achieved for medical school students (49% of 17,826 students admitted in 2007 were women) (7). Instructors at medical schools (51% female in 2007) reflect this gender parity, but there is a striking drop in the percentage of women who are assistant professors (39%), associate professors (25%) and full professors (17%) (8); all of these differences are statistically significant ($P < 0.001$ for each career stage to the next, by using 2007 data).

Slow improvement in the percentage of women at each of the stages in the career path is evident over the past two decades, but the rate of change is parallel to the increased proportion of female medical students. This suggests that the increase in women at later stages of the pipeline is the consequence of a slow “pull” provided by the expanding pool of women at the beginning of their medical studies—not because of an effective “push” that reduces attrition during career advancement, which would be expected to change the slope of the lines.

Many studies have recently evaluated this issue and have suggested reasons why this career attrition may be occurring (1–5, 9–14). However, gender-specific National Institutes of Health (NIH) grant application rates have thus far been examined only at a single university at different times in the career

Many qualified women scientists stop applying for NIH grants in the late postdoctoral and early faculty years.

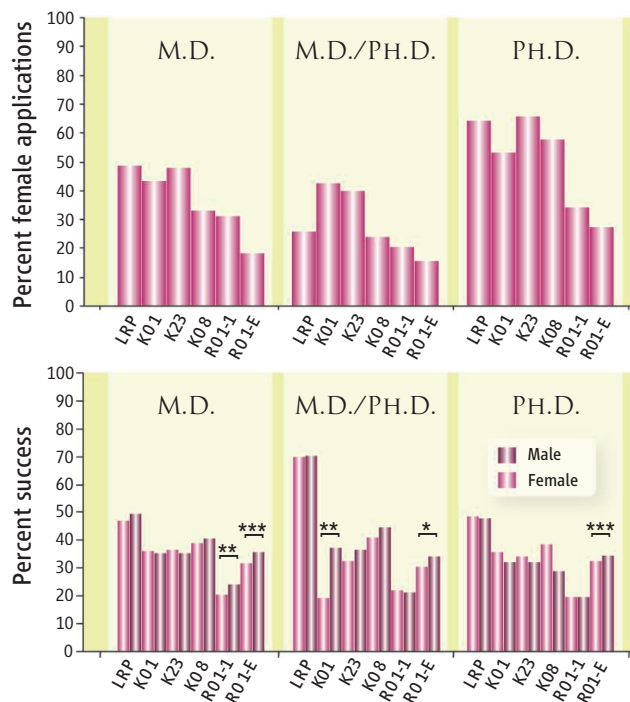


Trends in the percentages of female students and faculty in medical schools. For female medical students; female medical school instructors; and assistant, associate, and full professors. Data for each academic rank from 2007 are shown on the right.

path (14). For this reason, we obtained data from NIH to define the gender of each grant applicant and to determine the funding success rates for specific grant types that reflect different stages in the careers of biomedical scientists. Further, we have evaluated these data in the context of the degrees held by the applicants, because people with different training

backgrounds apply for different types of grants. Because recent studies have suggested that attrition might be particularly severe when female scientists are on the bridge to independence (13, 14), we specifically included several grant types that reflect this career stage, including Loan Repayment Program awards (LRPs) and mentored K series awards.

Loan Repayment Programs. LRPs are not research grants per se; they were designed to provide relief from student loans for translational and clinical investigators in their late postdoctoral or early faculty years and reflect a first attempt at NIH funding



Percentage of female applicants and success rates. (Top) Summary of pooled data from 2003 to 2007 showing the percentage of female applicants for six different NIH grant types. (Bottom) Success rates for females (red) and males (purple). * $P < 0.05$; ** $P < 0.01$; *** $P < 0.001$. R01-1 refers to first-time R01 applicants, and R01-E to experienced R01-equivalent investigators.

¹Departments of Medicine and Genetics, Washington University Medical School, St. Louis, MO 63130, USA.

²John M. Olin School of Business, Washington University, St. Louis, MO 63130, USA.

*Author for correspondence. E-mail: timley@wustl.edu

for most applicants (15). On average, applicants were in their mid- to late 30s.

Mentored Early Career Awards (K08, K01, and K23). Many LRP holders will apply for K series awards. K08 awards are predominantly applied for by M.D.'s and M.D./Ph.D.'s, and generally address basic or translational scientific questions. K01 awards are more basic in scientific scope, and nearly all applicants are Ph.D.'s. K23 awards are designed to support translational and clinical research, and most applicants are M.D.'s and M.D./Ph.D.'s. On average, applicants for these awards were in their late 30s.

Investigator-Initiated Research Project Grants (R01s). A large fraction of K award holders will apply for R series awards. We evaluated the number of first-time applicants for R01 awards (i.e., applicants who had never before received a competitive major research grant from the NIH), and also evaluated experienced R01-equivalent investigators (16) (i.e., who had been funded via a competitive major research grant). On average, applicants for first-time awards were in their early to mid-40s, and experienced investigators were in their early to mid-50s.

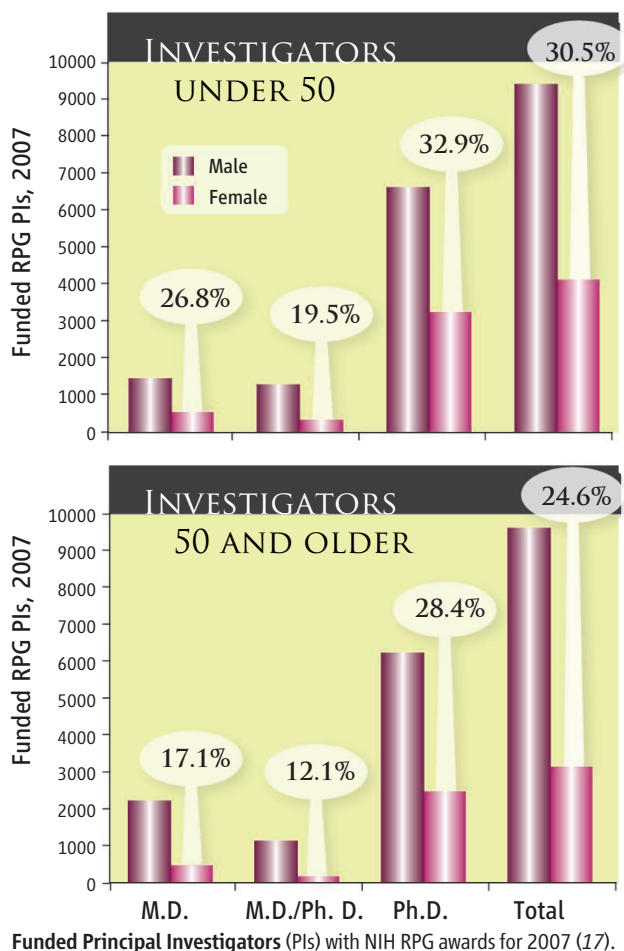
Loss of Female Applicants as Careers Progress

Applicant and award data from the past 5 years (2003–2007) are presented in supplemental online material (figs. S1 to S6 and tables S1 to S6). The data were pooled to smooth minor year-to-year variations, and are summarized here (see chart, bottom of page 1472). Statistical evaluations of this data set are presented in table S7. The trends for the past 5 years have generally been consistent, and the most current data from 2007 is very similar to that of the pooled data.

For M.D.'s, numbers of male and female applicants for LRPs and K23s have been virtually equivalent for the past 5 years (see top of chart, page 1472), mirroring the nearly equal numbers of male and female medical students. However, the number of female M.D.'s applying for K08 awards was strikingly reduced compared with males (535 versus 1077, $P <$

0.001); this trend continues for first-time R01 applicants (1596 females versus 3541 males, $P < 0.001$; change from K08, $P = 0.1101$) and is significantly lower for experienced R01 applicants (2133 versus 9620, $P < 0.001$; change from first-time R01, $P < 0.001$).

The same general patterns are evident for female M.D./Ph.D. grant applicants (see top middle of chart, page 1472), but this cohort is significantly underrepresented from the beginning of the pipeline, probably because gender parity has not yet been reached in M.D./Ph.D. programs (171 of 500 graduates in 2008 were female).



Female M.D./Ph.D. applicants were significantly underrepresented in the LRP pool (129 versus 368), the K08 pool (240 versus 763), the K01 pool (67 versus 91), and the K23 pool (108 versus 162; $P < 0.001$ for the differences between male and female applicants for all four grant types). This trend continues for first-time R01 applicants (903 females versus 3475 males, $P < 0.001$; change from K08, $P = 0.0211$) and worsens for experienced R01 applicants (1244 female versus 6741 males, $P < 0.001$; change from first-time R01, $P < 0.001$).

For Ph.D.'s, the same trends are evident (see top right of chart, page 1472), but the most dramatic decline in applicants occurred at the first R01 application. For LRPs, female applicants substantially outnumbered males from 2003 to 2007 (2345 versus 1307, $P < 0.001$). Likewise, for K23s and K01s, female applicants have significantly outnumbered males (K23, 461 versus 239, $P < 0.001$; K01, 1274 versus 1175, $P = 0.0023$). However, for first-time R01 applicants, only 9144 of 26,836 total applicants were female between 2003 and 2007 ($P < 0.001$; change from K01, $P < 0.001$); for experienced R01 applicants, the trend worsens (13,460 versus 35,427, $P < 0.001$; change from first-time R01, $P < 0.001$).

Near-Equivalent NIH Funding Success Rates for Women

Despite the oft-held perception that women do not fare as well in the NIH grantee pool as men, the data show that funding success rates for nearly all grants were essentially equal for men and women, regardless of degree (see bottom of chart, page 1472). For M.D.'s, the only significant differences in success rates for men and women were for R01 applicants: First-time women applicants had a 20% success rate, compared with 24% for men ($P = 0.006$); 32% of experienced female applicants were successful, compared with 36% of men ($P = 0.0004$). Female and male M.D./Ph.D.'s were equally successful at obtaining grants at all stages of the career path, except for K01 awards (with only 158 total applicants over 5 years, 91 males and 67 females), and experienced R01 applicants, where the difference between success rates for females (31%) and males (34%) was statistically significant ($P = 0.012$). Finally, success rates were the same for male and female Ph.D. investigators at all stages of the career path, except for experienced R01 investigators, where women had a 33% success rate, compared with men at 35% ($P < 0.0001$). When the data are pooled for all investigators and all grants studied here from 2003 to 2007, the success rates for men and women are virtually equivalent (31% success for women, and 32% for men).

To examine the consequences of these application and success rates on the current pool of funded NIH investigators, we obtained information from the NIH regarding all Principal Investigators for Research Project Grants (RPGs) (17) (see table S8 and chart, left). Women were significantly underrepresented ($P < 0.001$ for all categories). This trend is more severe for women over the age of 50, and is most severe for physician-scientists in both age groups.

Conclusions

Our data show that career paths for men and women in the biomedical sciences are different and that degree type influences career outcome. For the past several years, the numbers of female and male Ph.D. and M.D. students have been nearly equal, whereas female M.D./Ph.D. students compose about 40% of the total pool. Well into the postdoctoral years (through LRP grant applications), women and men are at least equally represented in the career path. Although female physician-scientists applying for mentored translational grants (K23 applicants) are equal in numbers to men, we estimate that nearly half of the women eligible to pursue more basic research themes (K08 applicants) are not applying. For Ph.D.'s, this trend is also clearly evident at the transition from LRP to K01, but the loss is most dramatic for first-time R01 applicants.

Although some female career attrition could be due to cohort effects (i.e., smaller numbers of female graduate students in the past, leading to smaller numbers at advanced career stages at this time) the effects that we describe here occur in a very narrow time frame and are far too large to be totally explained by this phenomenon. Instead, the data strongly suggest that a large fraction of women are choosing to leave the NIH-funded career pipeline at the transition to independence (i.e., in the late postdoctoral and early fac-

ulty years). Female physician-scientists make this decision earlier and more often, perhaps because more attractive and/or flexible career options (e.g., clinical practice) are available to them. Men and women have near-equal NIH funding success at all stages of their careers, which makes it very unlikely that female attrition is due to negative selection from NIH grant-funding decisions.

Women make up an ever-increasing fraction of the students who train to become biomedical scientists, but their career attrition is disproportionate to that of men. If these trends continue, this country will probably experience a shortage of biomedical scientists in the near future. We therefore hope that these data will provide an impetus for the NIH and academic leaders to develop more effective strategies to retain women at the critical juncture between postdoctoral training and independent careers. The attrition of women from this career path represents a critical loss of intellectual capital for all of biomedical research. Women are equally prepared for careers in the biomedical sciences, and they are successful at obtaining NIH grants at all career stages; their potential for great contributions to biomedical science cannot be wasted.

References and Notes

1. L. Nonnemaker, *N. Engl. J. Med.* **342**, 399 (2000).
2. M. B. Hamel, J. R. Ingelfinger, E. Phimister, C. G.

- Solomon, *N. Engl. J. Med.* **355**, 310 (2006).
3. N. C. Andrews, *N. Engl. J. Med.* **357**, 1887 (2007).
4. R. Jaggi, N. J. Tarbell, D. F. Weinstein, *N. Engl. J. Med.* **357**, 1889 (2007).
5. P. Leboy, *Scientist* **22**, 67 (2008); www.the-scientist.com/article/display/54076/.
6. Science Resources Statistics, National Science Foundation, *Data Tables*; www.nsf.gov/statistics/nsf07305/content.cfm?pub_id=3757&id=2
7. Association of American Medical Colleges (AAMC), *Facts—Applicants, Matriculants, Graduates, and Residency Applicants*, www.aamc.org/data/facts/.
8. AAMC, *Reports Available through Faculty Roster*, www.aamc.org/data/facultyroster/reports.
9. L. M. Buckley, K. Sanders, M. Shi, S. Kallar, C. Hampton, *Acad. Med.* **75**, 283 (2000).
10. A. J. Brown, W. Swinyard, J. Ogle, *J. Womens Health* **12**, 999 (2003).
11. E. M. Lambert, E. S. Holmboe, *Acad. Med.* **80**, 797 (2005).
12. F. M. Witte, T. D. Stratton, L. M. Nora, *Acad. Med.* **81**, 648 (2006).
13. E. D. Martinez et al., *EMBO Rep.* **8**, 977 (2007).
14. S. E. Waisbren et al., *J. Womens Health* **17**, 207 (2008).
15. T. J. Ley, L. E. Rosenberg, *JAMA* **294**, 1343 (2005).
16. R01 equivalents include R01, R23, R29, and R37 grants.
17. RPG grants include: R00, 01, 03, 15, 21, 22, 23, 29, 33, 34, 35, 36, 37, 55, 56, P01, P42, PN1, UC1, UC7, U01, U19, DP1, and DP2 awards.
18. The authors thank I. Lederhendler, R. Moore, E. Stalder, Z. Liu, S. Boehler, P. Reed, G. Garrison, J. Youngclaus, H. Alexander, C. Mikesell, and F. Slapser for providing key pieces of data. We also thank L. Rosenberg and S. Kornfeld for helpful discussions. The Alan A. and Edith L. Wolff Professorship (T.J.L.) and the Robert Brookings Smith Professorship (B.H.H.) provided support.

Supporting Online Material

www.sciencemag.org/cgi/content/full/322/5907/1472/DC1

10.1126/science.1165878

POLICY

Science Policy in Kazakhstan

Glenn E. Schweitzer

In 2006, Kazakhstan President Nursultan Nazarbayev proclaimed that Kazakhstan would advance from the world's 56th most economically competitive nation to the ranks of the top 50 within a decade (1, 2). Science and technology were to be the driving force. But now, this arid country the size of Western Europe with a population of only 15.2 million has fallen to 66th (3).

In 2006, the president announced that the nation's investment in scientific research would increase 25 times within 6 years (4), measured in the local currency, the tenge. Taking into account trends in inflation and currency exchange rates, reaching this goal

would probably result in an astounding 5- to 10-fold increase in purchasing power (5). In reality, research investment has stayed level, slipping from 0.2 to 0.15% of Gross Domestic Product (GDP), as national income from oil exports expands.

Buoyed by dramatic increases in oil revenues and abundant supplies of exportable gas, uranium and other minerals, and grains, as well as oil, the president's vision was undoubtedly sincere. He recognizes the importance of diversifying the economy beyond exports of natural resources. But there are obstacles. At the top of the list is a government bureaucracy that has not bought into the president's vision. "The president has other priorities as well" is the favorite bureaucratic rejoinder to science and technology advocates.

A robust science and technology infrastructure is an essential ingredient for devel-

Although the president of Kazakhstan advocates improving science and technology infrastructure, little has been done.

opment of middle-income economies. But even with substantial financial resources, harnessing the power of science and technology is an elusive long-term challenge, and technical wherewithal is only one element of economic progress. Only with effective fiscal, trade, industrial, natural resource, agricultural, environmental, health, and social policies will science and technology have an opportunity to achieve the much-heralded status of an engine of economic growth in Kazakhstan or other countries.

The Critical Role of Human Resources

In parallel with development of a more favorable policy environment must be an unprecedented effort to develop a much stronger human resource base. Managers, researchers, practitioners with technical skills, technicians in many fields, and science and technology

The author is the Chairman of the International Experts Council on Science and Technology established by the government of Kazakhstan. The AAAS facilitated his participation and the participation of three other American members of the Council. E-mail: gscweitzer@nas.edu

policy officials and analysts are needed throughout the country. For the past 15 years, the government has made limited progress in addressing this shortfall.

The excellent education system inherited from the USSR has decayed beyond recognition, despite the widespread national pride in Kazakhstan's achievements in space and nuclear sciences built on specialists trained in Moscow. Oil affluence has focused the attention of the entire population on a scramble for access to new streams of income with immediate financial rewards. Few talented youth are focused on long-term careers in scientific endeavors within Kazakhstan. Even the pool of well-prepared engineers, who are in high demand, in short supply, and well paid, has grown at a snail's pace. The additions to careers in business and to scientific opportunities abroad have been too great to overcome.

The government has attempted many quick fixes: Enroll more students in already overcrowded university facilities. Establish new universities with new buildings and research laboratories donated by companies that are quickly turned into testing laboratories used to help the benefactors. Establish new engineering departments at 15 unprepared provincial universities. But maintain low salaries for overloaded faculty members, continue excessive pedagogical reliance on lectures, and tolerate plagiarism and cash-for-grades that undermine the education process.

Now, there is an opportunity to demonstrate the importance of modern education. The president has decided to construct a new technological university in the capital city of Astana (4). He has allocated an initial \$100 million for the task. But the sum is woefully inadequate, even as a starter. The Saudis, for example, are investing \$8 billion in a university complex on the Red Sea (6).

In my view, the current approach in Astana of investing limited funds in facilities, while neglecting the people that are the heart of any university, will simply perpetuate mediocrity. An endowment of \$1 billion to ensure adequate faculty salaries and to support a tuition-free student body of several hundred engineering students with a policy of zero tolerance for corruption could make a real difference. The new university could be a source of urgently needed engineering leaders, while serving as a model of future approaches to education. But these goals will not be achieved without major political and financial commitments.

Even the highly publicized Bolashak Program (7), which supports 3000 Kazakhstan students studying at elite universities abroad, has failed to contribute in a discernible way to the strength of the science and technology

infrastructure. The few science participants seldom pursue research careers when they return to Kazakhstan, preferring work in business or in the ministries. However, at long last, the program will be open to many more aspiring scientists, and financial and housing incentives will be provided.

The International Experts Council

In 2007, the government commissioned assessments of science and technology in Kazakhstan by organizations in England, Ireland, Finland, and the United States (5), as well as by the Organization for Economic Cooperation and Development (OECD) (2) and the World Bank. They established an International Experts Council composed of 15 specialists from eight countries (8, 9). In July 2008, the first agenda item for the Supreme Commission for Science and Technology was the report of the International Experts Council (10). For 20 minutes, the prime minister, six ministers, and 20 other leaders of science and technology listened to a recitation of recommendations. The seven presented below were considered to be priorities in view of their potential impact on the effectiveness of the science and technology infrastructure.

1) The new Biotechnology Center should be a model institution for forefront research, in terms of leadership, facilities, student involvement, international connections, and publications record.

2) The Ministry of Energy and Natural Resources should strengthen its capabilities in the earth sciences for managing the nation's oil, gas, and mineral resources.

3) Nanotechnology research projects should be supported only if they are conducted in cooperation with specialists in industrialized countries who are working at the forefront of this new technology.

4) Evaluations should be conducted every 3 years of the impacts of each of the 77 research programs funded by the government.

5) Administration of competitive research grant programs should emphasize transparency throughout the process.

6) Salaries of educators and researchers employed in government facilities should be based on merit and levels of responsibilities.

7) Investment in research and development should reach 1% of GDP by 2011.

The prime minister and other members of the commission listened to the outsider views. He seized on the recommendation to evaluate the impacts of past investments in science and technology as guidance for the future, and the minister of Education and Science urged that the council now turn its attention to steps to

implement the recommendations, a step that the prime minister supported. The council is ready to drill deeper, but are the ministries ready to allow the necessary penetration into shortcomings in their performance?

Future Steps

Kazakhstan is truly at a crossroads. During the past 15 years, the scientific workforce has been torn asunder and has had little impact on building a robust and sustainable economy beyond exports of natural resources for imports of goods and services. The scientific leaders of the country are aging, and the small new generation of entrants into the field needs encouragement and support. A few well-prepared young science and technology advocates strategically placed within the government and in important leadership positions in the universities and research centers can invigorate the nation with important approaches. Unfortunately, there are few examples within the country to follow.

The president and prime minister seem sensitive to the opportunities. Now, they should be bold and patient; they need to give science and technology a real chance in an environment that is impatient and skeptical of new approaches that threaten current positions of authority and influence.

References and Notes

1. N. Nazarbayev, *The Kazakhstan Way* (Stacey International, London, 2008).
2. *Higher Education in Kazakhstan: Reviews of National Policies for Education* (OECD Publishing and World Bank, Paris and Washington, DC, 2007).
3. Global Competitiveness Index Rankings and 2007–2008 Comparisons, www.weforum.org/pdf/gcr/2008/rankings.pdf.
4. N. Nazarbayev, address to the 60th anniversary meeting of the National Academy of Sciences, Almaty, Kazakhstan, October 2006.
5. National Research Council, *Science and Technology in Kazakhstan: Current Status and Future Prospects* (National Academies Press, Washington, DC, 2007).
6. King Abdullah University of Science and Technology, www.kaust.edu.sa/.
7. Bolashak Program, www.bolashak.kz/.
8. Y. Suleimenov, National Center for Scientific and Technical Information, letter to each member of the International Experts council informing him/her of appointment to the council by the Supreme Scientific and Technical Commission of the Republic of Kazakhstan, N1075, from Almaty, 29 August 2007.
9. The 14 other members of the International Council on Science and Technology are from the United States, Russia, Ireland, Germany, Finland, Malaysia, Japan, and Kazakhstan.
10. Protocol of the Session of the Supreme Scientific-technical Commission of the Government of the Republic of Kazakhstan, No 04-5/1, 10 July 2008 signed by Prime Minister K. Masimov [in Russian].
11. I thank the staff of the National Center for Scientific and Technical Information, Almaty, Kazakhstan, and the 14 other members of the International Council on Science and Technology.

ASTRONOMY

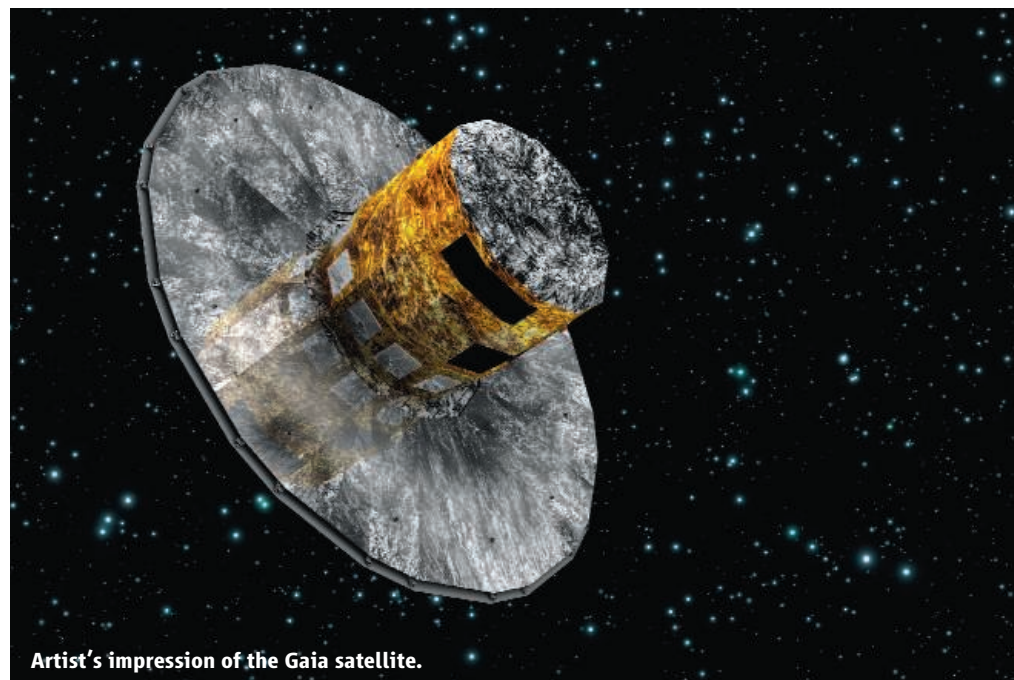
How Cold Is Cold Dark Matter?

Gerard Gilmore

Dark matter is the dominant form of mass in the Universe. Although it is nearly impervious to the weak interaction, and does not interact with the electromagnetic force, making it transparent, its presence is inferred from its direct effect on visible (baryonic) gravitating matter. Its existence, as low-mass stars, was postulated some 100 years ago, while its nonbaryonic dominant component was discovered and has been quantified on macroscopic scales over the past 70 years. Because nonbaryonic dark matter is matter, it must be described by the successor to the particle physics standard model. On microscopic scales, the several challenges facing the standard model are presumed to have a resolution that will include detection of (families of) new particles, some mix of which will turn out to be the dominant form of dark matter in the Universe. Hence, the search for dark matter is being pursued experimentally on Earth, both directly with the large hadron collider (LHC) and several elegant direct detection experiments, and indirectly through its gravitational effects on astronomical scales.

Can measurements on astronomical scales be sensitive to different types of dark matter particles? What future developments are under way? The answers lie in the dominant role played by dark matter in the growth of structure in the Universe. Solving the puzzles of galaxy and small-scale structure formation means understanding the properties of dark matter, and vice versa.

The early Universe was very smooth, as seen in extremely small fluctuations fixed in the cosmic microwave background some 300,000 years after the Big Bang. Structure grew from these fluctuations, driven largely by self-gravity in the dark matter. Fast-moving dark matter (hot and relativistic) can cluster less than slower-moving (cold) dark matter, thereby implying different scales of clustering and allowing a distinction to be made. Numerical simulations of structure growth, which reproduce superbly well the large-scale structure observed today (1), have shown that the dominant mass is cold and have allowed, for example, the neutrino mass to be quanti-



Artist's impression of the Gaia satellite.

fied. The general conclusion from such analyses is that dark matter does contain some contribution from hot matter—massive neutrinos, gravity waves, and radiation, among others—but that it is predominately some new type of matter. It is on the small scales where galaxies are formed that the simulations have proven least able to predict, or even to agree with observations of real galaxies and where we can hope to learn new physics. Disentangling the effects of baryonic astrophysics from non-baryonic dark matter is now the challenge.

Astronomy on small scales can best be studied locally, by quantifying the structure and evolution of galaxies in the Local Group, the group of nearby galaxies of which our Milky Way is part. Exploiting recent large area surveys, these studies have identified many new dwarf satellite galaxies inside and around the Milky Way (2). These galaxies show every indication of being survivors of the first gravitationally bound systems to form at high redshift, forming less than one billion years after the Big Bang, and are highly dark-matter dominated. The number of satellite galaxies found disagrees with simple prediction by large factors. More intriguingly, their luminous structures have an unanticipated minimum size of 300 light years (3). Preliminary dynamical analyses suggest that this size limit might be

Identification of the particles that constitute dark matter would revolutionize particle physics and the astrophysics of galaxy formation.

due to the clustering properties of dark matter, hinting that the imprint of the physical properties of dark matter is being seen on astronomical scales. Although considerable efforts are being made to quantify the dynamics, and hence mass distributions, of these mini-galaxies (4), disentangling particle physics from astrophysics is not going to be easy.

Most dark matter locally is associated with the Local Group galaxies, the Milky Way, and the Andromeda galaxy. Detailed mass-mapping of the Local Group, and quantification of its evolution, is clearly the key test of galaxy formation. Our appreciation that galaxy formation is a continuing process has been revolutionized over the past few years by discovery of evidence for past and continuing mergers and interactions (5–7). The ability to map, weigh, and date these events, and to determine the dark matter distributions that drive them, is the next big step, quantifying the role of dark matter in galaxy formation and evolution.

Gaia represents how this step will be taken. Gaia (8) is a European Space Agency mission, due for launch in late 2011, which will provide precision astrometric measures—absolute distances and transverse velocities—for all the one billion stars brighter than visual magnitude 20. It will deliver absolute distances, measured by trigonometric parallax using the

Institute of Astronomy, University of Cambridge,
Madingley Road, Cambridge CB3 0HA, UK. E-mail: gil@
ast.cam.ac.uk

apparent change in angular direction to a distant object as Earth orbits the Sun during a year as a fundamental distance scale (9). Gaia precision is an improvement on the best astrometry currently available by some 3 orders of magnitude, while its sensitivity provides an improvement of 4 orders of magnitude. One of Gaia's prime subjects will be galaxy evolution, including measuring the distribution of dark matter on whatever scales it is found. The technically most difficult aspect of dark matter studies in astrophysics is precision mass measurement. Usually having access only to line-of-sight velocity data and knowing little of transverse velocities means that only partial information can be modeled. Gaia will provide precision transverse kinematic data, thus giving access to reliable six-dimensional phase space measures of location and speed for large

numbers of objects, a critical precondition for accurate mass and orbit determinations.

Dark matter is the dominant gravitating mass in the Universe. It is perhaps a mix of several ingredients, with different contributions dominant on different scales, from the extremely small scale of weakly interacting massive particles to the very long scales of massive neutrinos. Disentangling this mix requires quantitative determination of the three-dimensional distribution of mass in dark matter-dominated systems on astrophysical scales to complement direct detection and creation experiments on Earth. As galaxies have been evolving for 13 billion years in real dark matter halos since they became gravitationally bound, quantification of the relevant astrophysics is also necessary. Despite the challenges, real progress is being made, while dra-

matic advances are anticipated, with the combination of the LHC and Gaia.

References and Notes

1. V. Springel, C. S. Frenck, S. D. M. White, *Nature* **440**, 1137 (2006).
2. V. Belokurov *et al.*, *Astrophys. J.* **654**, 897 (2007).
3. G. Gilmore *et al.*, *Astrophys. J.* **663**, 948 (2007).
4. M. Walker *et al.*, *Astrophys. J.* **667**, L53 (2007).
5. G. Gilmore, R. F. G. Wyse, K. Kuijken, *Annu. Rev. Astron. Astrophys.* **27**, 555 (1989).
6. S. Majewski, *Annu. Rev. Astron. Astrophys.* **31**, 575 (1993).
7. K. Freeman, J. Bland-Hawthorn, *Annu. Rev. Astron. Astrophys.* **40**, 487 (2002).
8. European Space Agency, Research and Scientific Support Department, www.rssd.esa.int/Gaia
9. Parallax distances are so fundamental in astronomy that the basic distance unit is the parsec (pc), the distance of an object that displays a parallax of one second of arc. $1 \text{ pc} = 3.26 \text{ light-years} = 3.10^{16} \text{ m}$.

10.1126/science.1165790

CHEMISTRY

A Curious Antipathy for Water

Steve Granick and Sung Chul Bae

Imagine that you are a water molecule at a hydrophobic (water-repellent) surface. Given the chance, you would bead up with other water molecules to form a droplet, just as water beads up on raincoats or leaves of plants (see the figure, left panel). But what would you do if you were inside a droplet, yet located very near the hydrophobic surface? Water molecules in this situation cannot leave the surface although they would if they could; they are frustrated. Such proximity of water to a hydrophobic surface is fundamental to the so-called hydrophobic effect. Its reasons are disputed, as is its definition.

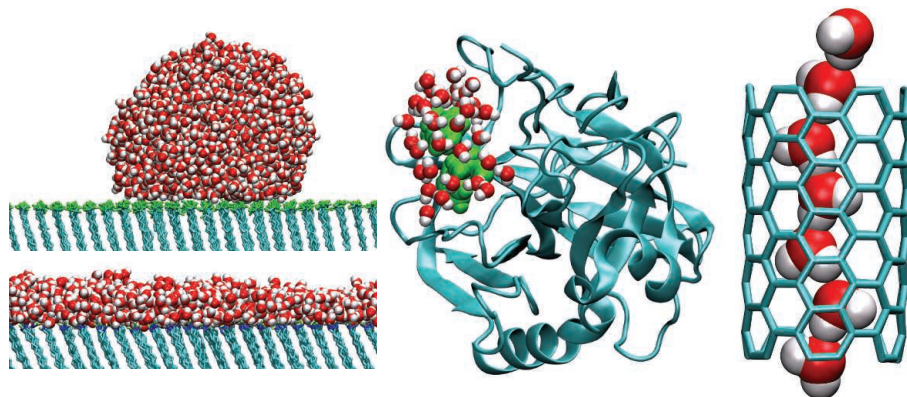
Not in dispute is its importance. For example, the side chains of roughly half the amino acids are polar, while those of the other half are hydrophobic; the nonmixing of the two is key to steering the folding of proteins and other self-assembly processes (see the figure, middle panel). As a second example, the fact that oil and water hardly mix is at the root of the self-assembly of supramolecular structures known as cell membranes (in biology) and micelles (in technology), where the self-assembling molecules contain both nonpolar and polar moieties. Furthermore, when the gap between two hydrophobic surfaces becomes critically small, water is

ejected spontaneously, whereas water films confined between symmetric hydrophilic surfaces are stable (1).

Hydrophobicity shows up differently in carbon nanotubes, within which a hydrogen-bonded chain of water molecules can form, stretching like a thread down the middle of the nanotube (see the figure, right panel) (2). The unusual hydrogen-bonding geometry and nonstick surface result in flow essentially

How does water meet a hydrophobic surface? Like great art, everyone recognizes hydrophobicity but few agree on the details.

without friction (3). Such water-filled nanotubes switch from hydrophobic at room temperature to hydrophilic when the temperature is lowered to 8°C (4), in line with predictions that a switch of this kind can happen because the free energy of a full nanotube is very close to that of an empty nanotube (2). The observation opens the possibility that temperature may one day be used as a switch to make carbon nanotubes selectively suck up chemicals



How water meets different hydrophobic elements. (Left) On flat planar self-assembled monolayers, the situation is simplest: The contact angle is high when the monolayer is terminated uniformly with CF_3 groups, and zero when it is terminated uniformly with OH groups. (Middle) The situation is more complex on the surface of a protein, α -chymotrypsin in this example. Hydrophobicity of the amino acid residues is weaker than in the left panel, the size of the hydrophobic patch is smaller, and nothing is planar. For these reasons, the tendency to dewet is less than in the left panel. Water is predicted to envelop even the hydrophobic (green) patch of amino acids, but likely with more fluctuation than at hydrophilic patches (1, 13). (Right) Water fills a carbon nanotube spontaneously, forming linear hydrogen-bonded threads of water running down the middle (2), yet the simultaneous tendency to dewet causes it to flow through the tube essentially without friction (3).

Departments of Materials Science and Engineering, Chemistry, and Physics, University of Illinois, Urbana, IL 61801, USA. E-mail: sgranick@uiuc.edu

like with a straw—not only water, but potentially other solutes also (5). It also confirms the well-known weakening of hydrophobic interactions upon cooling below room temperature (6).

Despite its obvious importance, physical insight into the origins of hydrophobicity is not easy to come by. Thermodynamic measurements are one approach, but interpreting their physical significance is extraordinarily subtle (6). Theoretical considerations and computer simulations show that a key concept is the size of the hydrophobic object (7–9). Water molecules can wrap efficiently around hydrophobic elements with a radius of curvature of 1 nm or less. When water meets hydrophobic surfaces that are flatter than this, it forms a molecularly thin cushion of depleted density between it and the hydrophobic surface.

The fly in the ointment is experiment. Putative depletion layers must fight against attraction of water to any hydrophobic surface, a ubiquitous force known as van der Waals attraction. This is probably why laboratory data have provided evidence both for [(10, 11) and references therein; (12)] and against (13) this phenomenon. Despite that controversy, there is consensus that the expected thickness of a depletion layer is less than the dimension of even one water molecule. This small thickness matters for the following reason: If water meets hydrophobic surfaces softly, because van der Waals attraction outweighs its natural reluctance to do so, the frustrated interface should fluctuate wildly—as people also do, when they are unsure about what decision to make. Experiments (1) and theory (14) support this view, which merits further investigation.

But a caution is worth emphasizing: Hydrophobicity depends on the eye of the beholder. Some of the heated discussion in this field can be traced to the simple fact that people have different ideas in mind. One common definition is that water droplets on a planar hydrophobic surface possess a contact angle larger than 90°; but given that nothing dramatic changes when the contact angle falls below this or any other point, it is just a convenient but arbitrary definition. This has special relevance when seeking to distinguish between polar and hydrophobic patches on the surface contours of proteins. Many cases of modest hydrophobicity are akin to a bald man with a few thousand hairs on his head—he is on the bald side but others are much more bald. To understand better how hydrophobicity acts in the natural and technological worlds, and to overcome controversies, the following questions are worth future investigation. First, how does it matter whether a sur-

face has the same wettability (hydrophobic or hydrophilic) everywhere, or is “patchy” from spot to spot? Answers will bring understanding in this field into closer contact with emerging issues in fields as diverse as protein folding and surface science.

Second, scientists have concentrated on systems that are subject to steady external conditions, such as a low temperature that causes proteins to denature. We do not yet have good ways to think about how aqueous systems respond to an extreme but perhaps transient change of environment. Is it realistic to expect a general theory of hydrophobic surfaces when temperature and pressure change in time and space? Empiricism shows that what matters is not just the instantaneous separation between hydrophobic surfaces but also the time (or frequency) of their contact (1); the timeline of change also matters.

Third: When does water act truly unlike other fluids? Spectroscopic studies of vibrations in water molecules are a technical tour de force but are problematic to interpret (15). Prevalent computational models use point charges and do not explicitly recognize quantum mechanics; it may be worth inquiring more critically into the assumptions made in these models. Moreover, too often the models are specific to the system under study, but common responses strongly suggest more universality. For example, when nanotubes fill with water at low temperature, one

approach is to explain this in terms of the hydrophobic effect (4), but it can also be understood on the basis of more general principles of the competition between enthalpy and entropy (16). The challenge, then, is to predict from theory, rather than from empiricism, what makes water so special.

References and Notes

1. X. Zhang, Y. Zhu, S. Granick, *Science* **295**, 663 (2002).
2. G. Hummer, J. C. Rasaiah, J. P. Noworyta, *Nature* **414**, 188 (2001).
3. A. Kalra, S. Garde, G. Hummer, *Proc. Natl. Acad. Sci. U.S.A.* **100**, 10175 (2003).
4. H.-J. Wang, X.-K. Xi, A. Kleinhammes, Y. Wu, *Science* **322**, 80 (2008).
5. A. Kalra, G. Hummer, S. Garde, *J. Phys. Chem. B* **108**, 544 (2004).
6. D. Ben-Amotz, B. Widom, *J. Phys. Chem. B* **110**, 19839 (2006).
7. F. H. Stillinger, *J. Sol. Chem.* **2**, 141 (1973).
8. K. Lum, D. Chandler, J. D. Weeks, *J. Phys. Chem. B* **103**, 4570 (1999).
9. J. Janacek, R. R. Netz, *Langmuir* **12**, 8417 (2007).
10. A. Poynor *et al.*, *Phys. Rev. Lett.* **97**, 266101 (2006).
11. A. Poynor *et al.*, *Phys. Rev. Lett.* **101**, 039602 (2008).
12. M. Mezger *et al.*, *J. Chem. Phys.* **128**, 244705 (2008).
13. K. Kashimoto *et al.*, *Phys. Rev. Lett.* **101**, 076102 (2008).
14. D. Chandler, *Nature* **437**, 640 (2005).
15. M. Sovago *et al.*, *Phys. Rev. Lett.* **100**, 173901 (2008).
16. L. Maibaum, D. Chandler, *J. Phys. Chem. B* **107**, 1189 (2003).
17. We are grateful for comments from D. Ben-Amotz, D. Chandler, and S. Garde. Supported by the Department of Energy, Basic Energy Sciences, Division of Materials Sciences, DEFG02-02ER46019.

10.1126/science.1167219

ECOLOGY

Crops for a Salinized World

Jelte Rozema¹ and Timothy Flowers²

Cultivation of salt-tolerant crops can help address the threats of irreversible global salinization of fresh water and soils.

Currently, humans use about half of the fresh water readily available to them to support a growing world population [expected to be 9.3 billion by 2050 (1)]. Agriculture has to compete with domestic and industrial uses for this fresh water. Good-quality water is rapidly becoming a limited and expensive resource. However, although only about 1% of the water on Earth is fresh,

there is an equivalent supply of brackish water (1%) and a vast quantity of seawater (98%). It is time to explore the agronomic use of these resources.

Adding to the increasing competition for fresh water is the gradual and irreversible spread of salinization. Salinity is affecting fresh water and soil, particularly in arid and semiarid climatic zones. Ironically, irrigation has resulted in the accumulation of salt to above normal concentrations in the rooting zone of arable land, as high rates of evaporation and transpiration draw soluble salts from deep layers of the soil profile. The water and salt balance has also changed in regions where dryland agriculture—growing crops without

¹Department of Systems Ecology, Vrije Universiteit, Amsterdam, Netherlands. ²School of Life Sciences, John Maynard Smith Building, University of Sussex, Falmer, Brighton BN1 9QG, UK and School of Plant Biology, Faculty of Natural and Agricultural Sciences, The University of Western Australia, Crawley, Western Australia, 6009, Australia. E-mail: jelte.rozema@falw.vu.nl; t.j.flowers@sussex.ac.uk

irrigation in areas that receive an annual rainfall of 200 to 300 mm or less—is practiced following forest clearance [this allows salts present in the groundwater to reach the surface (2)]. In addition, continuous sea-level rise in a warming world threatens increased salinity in coastal lowlands. As fertile soils become salinized (3), the yield of conventional crops decreases. For example, a survey conducted between 1993 and 1995 in the Sacramento Valley in California (4) revealed a loss of 10% as the salinity rose by 1 dS m⁻¹ (soil salinity is measured by its electrical conductivity in solution). The United Nations Food and Agri-

high concentrations of Na⁺ and Cl⁻ (about 500 mmol per liter of seawater) were effectively lost (8). Today, only about 1% of the species of land plants can grow and reproduce in coastal or inland saline sites. Among these salt-adapted halophytes are annuals and perennials, monocotyledonous and dicotyledonous species, shrubs, and some trees. There is a wide range of morphological, physiological, and biochemical adaptations in such plants, which vary widely in their degree of salt tolerance (9). Only some are tolerant to seawater salinity; more halophytes resist lower salinity concentrations. Potentially, many of these salt-adapted plants could become salt-tolerant crops in a saline agriculture in which soil salinity is less than (perhaps half) that of seawater.

Halophytes can grow at rates comparable to those of conventional forage crops (10, 11) and under saline conditions, biomass of the former is comparatively greater than that of all our major crops. For example, *Salicornia bigelovii*, a potential oil-seed crop, produces about 18.0 tons/ha of biomass and 2.00 tons/ha of seeds over a 200-day growing cycle

(10); by comparison, the average yield of sunflower across the world in 2007 was 1.2 tons/ha. Although the physiological adaptations required to tolerate salinity require energy and therefore might be predicted to reduce plant growth and yield, any decline in halophyte biomass production occurs at much higher salt concentrations than for conventional crops.

Modern agrobiotechnology might speed up the process of achieving conventional crops that are resistant to the high concentrations of Na⁺ and Cl⁻ in saline agriculture. Indeed, biotechnology has generated traditional crops that are resistant to plant pests and diseases, such as genetically modified corn and cotton. However, over the past 15 years, the bioengineering approach has not delivered salt-tolerant cultivars of conventional crops such as wheat or rice for release to farmers. So, although between 1996 and 2006 there were more than 30 reports of transformation of rice with different genes aimed at increasing salt tolerance, transgenic salt-tolerant rice is not close to release. The

likely explanation is that salt tolerance is a complex trait determined by many different genes, so that transformation of multiple genes into a plant is required (12, 13).

Because salt resistance has already evolved in halophytes, domestication of these plants is an approach that should be considered (12, 13). However, as occurred with traditional crops such as rice, wheat, corn, and potatoes, domestication of wild halophytic plant species is needed to convert them into viable crops with high yields. Such a process can begin by screening collections for the most productive genotypes. There are many uncertainties and risks: variable germination, propagation, plant diseases, scaling up, processing halophyte biomass, market demand, and economic competition with conventional bulk-produced raw materials such as potato, sugar beet, and sugar cane. The development of halophytic crops would also have to be undertaken with studies of hydrological and soil management of saline agriculture systems.

The use of saline water for irrigation is in its infancy, although experimental trials using seawater (14) and mixed saline and fresh water (15) have been conducted. A huge benefit of using saline water in agriculture is that seawater contains many of the macro- and micronutrients that are essential for plant growth and function. Seawater is a vast resource that is further supplemented by massive volumes of brackish groundwater (salt concentrations ranging from 1 to 50% of that of seawater) and waste water; all could be available for saline agriculture. Moreover, the number of halophytic crops that would produce an economically viable yield if irrigated with brackish water would be much larger than if seawater were to be used for irrigation, because there are many more halophytes and coastal plants that grow well with brackish water than grow well in seawater.

The benefits of saline agriculture encompass not only food products for human consumption and fodder crops for animals, but also renewable energy (biofuel and biodiesel) and raw materials for industrial use (16). This is particularly relevant because the traditional raw materials for energy production—oil, gas, and coal—are being depleted and are expensive. However, the relative costs of growing halophytes for bioenergy and biofuel—a process that would not compete with the growth of conventional crops and therefore not threaten the world food supply—requires evaluation. A further advantage of saline agriculture is that growing halophytes may be combined with aquaculture of sea



A salty world. The effects of salinization (and increased flooding) in the Yenying Lakes system in the Shires of Quairading and Beverley, Western Australia.

culture Organization estimates that there are currently 4 million square kilometers of salinized land, and a similar area that is affected by sodicity, a condition in which Na⁺ ions represent more than 15% of the exchangeable cations (5). Of the 230 million ha of irrigated land, 45 million are affected by an increase in salt content [figures based on data collected more than 15 years ago (6)]. Soil salinization particularly affects economically less-developed countries with large and growing populations that are located in arid climatic zones (including Pakistan, India, Egypt, Tunisia, Morocco, Peru, and Bolivia), whereas more-developed regions are much less threatened by, but not immune from, salinity (7). Soil salinization in arid regions is practically irreversible because fresh water is not available to leach any accumulated salts. Even such leaching efforts are questionable because the salt-water created has to be evaporated if it is not to cause further damage.

The evolution of plant life on Earth started 3 billion years ago in saline ocean water. With the advance of land plants about 450 million years ago, primary adaptations of plants to the

fish and shrimp. In such sustainable marine agrosystems, inorganic nutrients from fish or shrimp ponds can be used to promote the growth of halophytes (17).

Worldwide, initiatives are being undertaken to develop saline vegetable crops, as well as crops for fuel and fiber (18). And in various countries, private companies and research groups are collaborating to develop technologies that combine saline agriculture with aquaculture. The concept of a saline agriculture has been long discussed (19), but the increasing demand for agricultural products and the spread of salinity now make this concept worth serious consideration and investment.

References and Notes

1. United Nations Population Information Network; www.un.org/popin/data.html.
2. P. Rengasamy, *J. Exp. Bot.* **57**, 1017 (2006).
3. R. Munns, *New Phytol.* **167**, 645 (2005).
4. See www.plantsciences.ucdavis.edu/uccerice/WATER/salinity.htm.
5. FAO, Terrastat Database; www.fao.org/agl/agl1/terrastat.
6. FAO, Global Network on Integrated Soil Management for Sustainable Use of Salt-Affected Soils; www.fao.org/agl/agl1/spush.
7. United Nations Population Division, Charting the Progress of Populations; www.un.org/esa/population/pubsarchive/chart/3.pdf.
8. J. Rozema, in *Halophytes and Biosaline Agriculture*, R. Chouk-allah, C. V. Malcolm, A. Hamdy, Eds. (Dekker, New York, 1996), pp. 17–30.
9. T. J. Flowers, T. D. Colmer, *New Phytol.* **179**, 945 (2008).
10. E. P. Glenn, J. J. Brown, E. Blumwald, *Crit. Rev. Plant Sci.* **18**, 227 (1999).
11. B. H. Niaz, J. Rozema, R. A. Broekman, M. Salim, *J. Agr. Crop Sci.* **184**, 101 (2000).
12. T. J. Flowers, *J. Exp. Bot.* **55**, 307 (2004).
13. B. R. Stanton *et al.*, *Genes Dev.* **6**, 2235 (1992).
14. E. P. Glenn, J. W. Oleary, M. C. Watson, T. L. Thompson, R. O. Kuehl, *Science* **251**, 1065 (1991).
15. N. M. Malash, T. J. Flowers, R. Ragab, *Irrigation Science* **26**, 313 (2008).
16. T. Yamaguchi, E. Blumwald, *Trends Plant Sci.* **10**, 615 (2005).
17. J. J. Brown, E. P. Glenn, K. M. Fitzsimmons, S. E. Smith, *Aquaculture* **175**, 255 (1999).
18. R. Ahmad, K. A. Malik, *Prospects for Saline Agriculture* (Kluwer, Dordrecht, Netherlands, 2002).
19. H. W. Koyro, *Env. Exp. Bot.* **56**, 136 (2006).
20. J.R. acknowledges grant TA&G9356-R020 Zilte Landbouw Texel-BSIK-Transforum Agro&Groen-Leven met Water.

10.1126/science.1168572

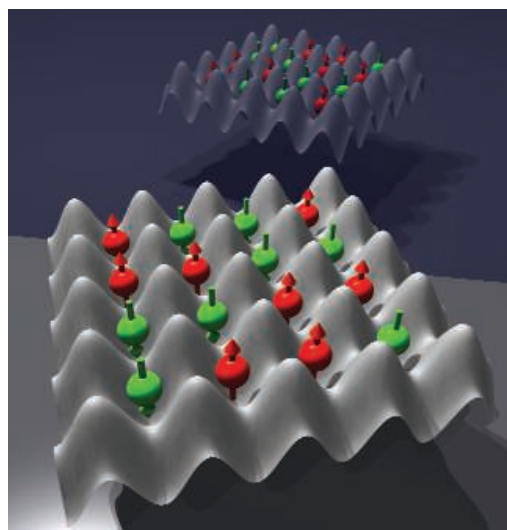
PHYSICS

Controlling Cold-Atom Conductivity

L. Fallani and M. Inguscio

Why do some solids conduct electricity like a metal, and others act like insulators? Quantum mechanics has provided some relatively simple (and quite successful) models for electron conductivity, but the underlying physics is often complex, because electrons interact with each other through Coulomb forces and because real materials are not perfectly ordered. On page 1520 of this issue, Schneider *et al.* (1) address the microscopic distinction between a conductor and an insulator by examining the conducting properties of repulsively interacting ^{40}K atoms, which, like electrons, are fermions—they have half-integer spin and obey the Pauli Exclusion Principle, which allows only one fermion to occupy a quantum state. By placing ultracold ^{40}K atoms in an artificial crystal held in place through optical fields, they can manipulate the energy scales of the system so that it varies all the way from a metallic state to different kinds of insulating phases.

In the quantum-mechanical description of electron conduction, the translational symmetry of the crystalline solid also applies to the atomic orbitals of the weakly bound electrons of the constituent atoms. The electrons interact not with a single atomic potential but with a potential that extends over the crystal lattice. The energy states of the electrons cluster so tightly that they are almost continuous and are



Quantum simulation of electronic conduction. Ultracold atoms in two different internal states (red and green) are trapped in a periodic structure generated by laser light (gray), forming a conductor or an insulator, depending on their energy and mutual interactions.

referred to as “bands.” The highest-lying bound states form what is called the valence band, and the lowest-lying set of excited states forms the conduction band.

Electrical conduction can occur if electrons in a solid can occupy states in the conduction band, where they are free to accelerate under the action of an external electric field. In a metal like copper, the valence and conduction bands overlap in energy, so that the conduction band is partially filled by electrons from the valence band. Conversely, in a

Models of electron conductivity in solids can be studied with ultracold atoms trapped in artificial crystals by lasers.

band insulator such as diamond, the valence band is completely filled, and a large energy gap separates it from the empty conduction band, which causes the material to be an insulator.

In real materials, this simple picture is complicated by additional effects, such as interactions between the electrons, which weakly repel each other, and the presence of disorder. When electron repulsion effects are sufficiently strong, the conduction electrons are forced far apart and localize in individual lattice sites, instead of having their wave function extended across the whole lattice, and a Mott insulator forms (2). When the translational symmetry of the lattice potential is broken by the presence of disorder, the electrons can move only in restricted regions of the crystal and again occupy localized states, and in this case an Anderson insulator forms (3).

The existence of these insulating phases was first predicted in the 1950s on the basis of simple theoretical models trying to capture the main mechanisms involved in electronic conduction in solids. However, a direct verification of these theories for electronic conduction has been hampered by the complexity of real materials—we cannot simply tune the potential created by the crystal lattice, nor the interactions between the electrons.

Fortunately, these theories are very general, and the ideas formulated for electrons can be verified in experiments in which clouds of neutral atoms are cooled down to temperatures

LENS European Laboratory for Nonlinear Spectroscopy, Dipartimento di Fisica, University of Florence, and INFN-CNR, Via Nello Carrara 1, I-50019 Sesto Fiorentino (FI), Italy. E-mail: fallani@lens.unifi.it (L.F.); inguscio@lens.unifi.it (M.I.)

of a few billionths of a degree above absolute zero. The ultracold atoms play the same role as the electrons; they are kept at very low densities in order not to form an ordinary solid, and the extreme cooling allows them to behave as quantum-mechanical particles. A standing wave of laser light—that is, an evenly spaced series of maxima and minima of light intensity—traps the atoms in a perfectly periodic artificial crystal (optical lattice), free from any defect or impurity (see the figure).

Unlike electrons, atoms are electrically neutral, but they can interact when they get very close and collide one with each other. A first spectacular demonstration of the possibility of using cold atoms to make quantum simulation of condensed-matter models (4) was the direct observation of the quantum phase transition from a superfluid Bose-Einstein condensate to a strongly correlated Mott insulator (5) of bosons, particles with integer spin that can multiply occupy a single quantum state. Anderson localization of matter waves was also demonstrated very recently in cold bosonic gases either with laser speckles (6) or with disordered optical lattices (7).

More insight into the physics of conduction can be obtained by using atoms that are fermions. Manipulation of ultracold fermions started with the first production of a degenerate Fermi gas of ^{40}K atoms (8) and has now become a rich and fast-developing field (9, 10). Fermionic atoms have been trapped in optical lattices (11), and the transition from a conductive state to a band-insulating state for noninteracting (noncolliding) fermions was

observed by studying their transport properties through the optical lattice (12). Very recently, a Mott insulating state for ultracold interacting fermions was reported (13).

Schneider *et al.* make an important step forward in the experimental investigation of the fermionic Hubbard model, the fundamental model describing interacting spin-1/2 fermions in a periodic potential. The fermionic gas can be switched from a metal to a band insulator to a Mott insulator “on demand,” depending on the ratio of the relevant energy scales set in the system. A decisive advance of this work is the independent control of the number of particles, the strength of interactions between them, the mobility of the particles across the lattice, and the size of the system, the latter being controlled by the application of an external trapping potential. In particular, the collisions between the neutral atoms (mimicking the electric repulsion between the electrons) are controlled by applying an external magnetic field across a Fano-Feshbach resonance (14), which allows tuning of the interaction strength between atoms.

Schneider *et al.* also present direct measurement of the compressibility of the ultracold gas, that is, its ability to change size after a variation of the trapping potential. This capability allowed them to fully characterize the different insulating phases. The experimental results are in excellent agreement with the predictions of a dynamic mean-field treatment of the Hubbard model (15).

Quantum simulation with cold atoms is becoming a mature field of research.

Experimental possibilities of control and detection have reached a level high enough to allow validity checks of different theoretical approaches. The experimental investigation of spin mixtures of fermions in optical lattices has just started, and new exciting adventures are waiting, such as the use of cold atoms as quantum simulators of high-temperature superconductors, the investigation of quantum magnetism, and the study of interacting fermions in the presence of disorder (16). There is also the possibility of using atoms of different chemical species to create ultracold dipolar molecules or to study exotic kinds of superfluid pairings.

References

1. U. Schneider *et al.*, *Science* **322**, 1520 (2008).
2. N. F. Mott, *Metal-Insulator Transitions* (Taylor & Francis, London, 1990).
3. P. W. Anderson, *Phys. Rev.* **109**, 1492 (1958).
4. I. Bloch, J. Dalibard, W. Zwerger, *Rev. Mod. Phys.* **80**, 885 (2008).
5. M. Greiner *et al.*, *Nature* **415**, 39 (2002).
6. J. Billy *et al.*, *Nature* **453**, 891 (2008).
7. G. Roati *et al.*, *Nature* **453**, 895 (2008).
8. B. DeMarco, D. S. Jin, *Science* **285**, 1703 (1999).
9. S. Giorgini, L. Pitaevskii, S. Stringari, *Rev. Mod. Phys.* **80**, 1215 (2008).
10. M. Inguscio, W. Ketterle, C. Salomon, Eds., *Ultra-Cold Fermi Gases*, International School of Physics (IOS Press, Amsterdam, 2008), vol. 164.
11. G. Modugno *et al.*, *Phys. Rev. A* **68**, 011601 (2003).
12. L. Pezzè *et al.*, *Phys. Rev. Lett.* **93**, 120401 (2004).
13. R. Jördens *et al.*, *Nature* **455**, 204 (2008).
14. D. Kleppner, *Phys. Today* **57**, 12 (2004).
15. A. Georges, G. Kotliar, W. Krauth, M. J. Rozenberg, *Rev. Mod. Phys.* **68**, 13 (1996).
16. M. Lewenstein *et al.*, *Adv. Phys.* **56**, 243 (2007).

10.1126/science.1166914

OCEANS

Elements and Evolution

Ariel D. Anbar

We think of Earth as a biologically thriving world. However, nearly half of the planet's surface is covered by ocean regions in which life is scarce. These thinly populated ecosystems do not lack water or sunshine, nor the bulk biological elements hydrogen, carbon, and oxygen. Instead, they are deficient in one or more of the other elements necessary for life. Hence, the distribution of life on Earth is captive, in part, to the distribution of the 20 or so bioessential nutrient elements—many rela-

tively rare—that are critical components of DNA, RNA, enzymes, and other biomolecules. Having substantially unraveled this relationship in today's oceans, biogeochemists are beginning to examine how it evolved over the ~4-billion-year history of life on Earth.

The distribution of bioessential elements in ancient oceans cannot be studied directly, because we cannot sample seawater from the distant past. Instead, we must draw inferences from the chemical characteristics of rocks formed from ancient seafloor sediments. Some of these characteristics varied over time in ways that are obvious to the naked eye. The best example is the abundance of iron in the geologic record (1)—in particular, massive

Changes in elemental abundances in Earth's oceans on geological time scales are intimately linked to evolutionary processes.

deposits of sedimentary iron minerals older than 1.8 billion years. These “banded iron formations” (BIFs) are the major source of industrial iron ore. Their near-disappearance from the subsequent record is equally obvious. The history of BIFs suggests that iron-rich oceans in the first half of Earth history gave way to later iron scarcity (2, 3). Today, iron is so scarce in the oceans that it is often a limiting nutrient—so much so that some propose “iron fertilization” of the oceans to stimulate marine photosynthesis, thereby drawing down atmospheric CO_2 (4).

Changes in the budgets of other bioessential elements are more subtle. They must be deduced using sophisticated analytical methods

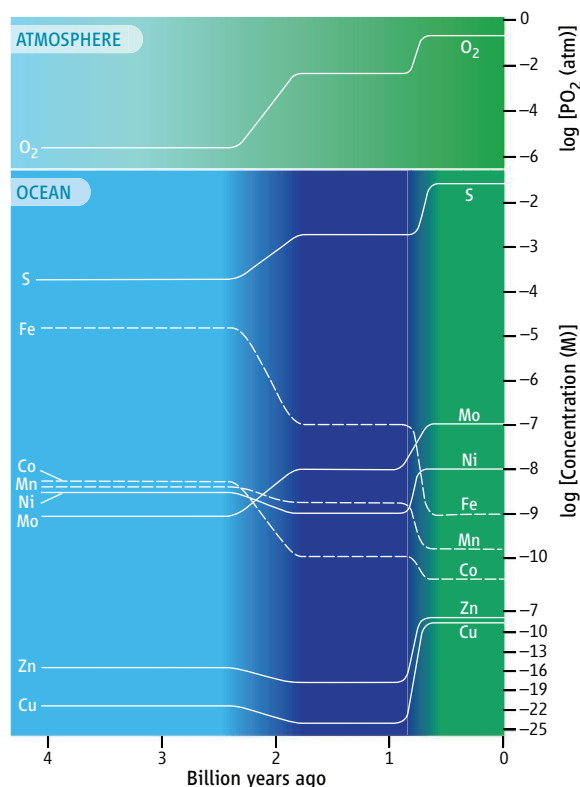
School of Earth and Space Exploration and Department of Chemistry and Biochemistry, Arizona State University, Tempe, AZ 85287, USA. E-mail: anbar@asu.edu

that measure the abundances and isotopic compositions of elements in ancient rocks. For example, mass spectrometric analyses of sulfur isotope ratios in sulfide and sulfate minerals reveal that the sulfur content of the oceans increased by as much as an order of magnitude around 2.4 billion years ago, and then again after 700 million years ago (2).

These changes in the ocean abundances of iron and sulfur were probably caused by rising amounts of O_2 in the environment (see the figure) (2, 3). In the modern, oxygenated oceans, iron is scarce because it is oxidized to Fe^{3+} , which reacts with OH^- to form insoluble iron oxyhydroxides. In contrast, sulfur accumulates in oxidized oceans as SO_4^{2-} . However, ancient oceans probably contained much less oxygen. Most researchers agree that the redox state of the environment evolved through at least three stages, with major oxygenation events occurring ~2.4 billion to 1.8 billion years ago and 800 million to 500 million years ago. During the first of these stages, the oceans were largely devoid of dissolved O_2 , and so iron was abundant in the form of dissolved Fe^{2+} complexes. Much of the sulfur at that time was in the form of insoluble sulfide minerals locked in the continental crust (2).

Ocean chemistry during the middle stage remains unclear. A counterintuitive idea gaining support posits a period of nearly a billion years, beginning ~1.8 billion years ago, during which a mildly oxygenated atmosphere overlay large ocean areas rich in H_2S (5, 6). According to this hypothesis, BIFs first disappeared because of the formation of insoluble Fe^{2+} sulfides (5).

Regardless, this redox evolution should have affected the budgets of many bioessential elements besides iron and sulfur. In particular, the ocean abundances of transition metals such as manganese, cobalt, nickel, copper, zinc, and molybdenum are sensitive to environmental redox conditions. Analyses of molybdenum concentrations and isotope abundances in ancient rocks reveal the expected three-stage trajectory (7–9). The histories of other bioessential transition metals have yet to be read from the rock record.



Changes in element abundances through time. These histories are approximate, based on simple geochemical models and inferences from ancient sediments. An expansion in H_2S -rich ocean regions after 2.4 billion years ago is assumed (2, 5). Color gradations indicate a transition from anoxic, S-poor oceans before 2.4 billion years ago (light blue) to H_2S -rich oceans between 1.8 billion and 800 million years ago (dark blue), subsequently giving way to complete ocean oxygenation (green). Different line styles are for clarity only; dashed lines are for elements with falling concentrations. [Adapted from (26), based on data from (2, 5, 9, 10)].

However, simple geochemical concepts predict that many element abundances changed markedly at least twice (see the figure) (10).

These and other changes in the chemical composition of the oceans surely affected the biosphere. There are many intriguing possibilities. First, transition metal chemistry may link atmospheric O_2 with the macronutrients nitrogen and phosphorus. For example, molybdenum and iron are important for N_2 fixation and NO_3^- assimilation by the nitrogenase and nitrate reductase enzymes. Therefore, low abundances of both elements between ~1.8 billion and 800 million years ago could have hindered the acquisition of nitrogen by the ocean biosphere (11). Before 1.8 billion years ago, coprecipitation of PO_4^{3-} with banded iron formations could have rendered phosphorus scarce (12). Although both ideas have been challenged (13, 14), they illustrate the potentially complex interplay between micronutrient budgets and wholesale changes in the nutrient status of ancient oceans.

Second, the ocean abundances of trace elements could have influenced the atmospheric budgets of biogenic greenhouse gases. For example, the abundance of N_2O may depend on the ocean availability of copper, which is essential to the enzyme that converts N_2O to N_2 during denitrification. Therefore, copper scarcity in the ocean may have resulted in an N_2O -rich “laughing gas atmosphere” between 1.8 billion and 800 million years ago (15). Similarly, atmospheric CH_4 may depend on nickel, necessary for bacterial methanogenesis. CH_4 was probably more abundant in the atmosphere before 1.8 billion years ago. At the same time, the nickel concentration in the oceans may have been surprisingly high (16). A subsequent decrease in nickel abundance may have limited the activity of methanogenic bacteria (16).

Finally, changes in the availability of bioessential elements must have shaped the evolution of life (17). For example, fossil evidence suggests that the ecological diversification of eukaryotes broadly coincided with rising redox potential of the deep oceans after ~800 million years ago (18), and hence with increases in zinc, molybdenum, and other elements and decreases in iron, manganese, and cobalt. Bioinformatic analyses of protein-metal binding motifs encoded in genomes reveal that, relative to prokaryotes, eukaryotes require more zinc, and less iron, manganese and cobalt, according to (19). Eukaryotes also require molybdenum for nitrate assimilation (11) and can use zinc in place of cobalt in the carbonic anhydrase enzyme for carbon assimilation (10). Thus, it may be that eukaryotes emerged from ecological niches as bulk ocean chemistry shifted to favor their element requirements (11, 18). Analogous logic may explain the rise of red eukaryotic phytoplankton after 250 million years ago (20).

Evaluation of such ideas requires research at the intersection of life sciences, chemistry, and geosciences. It is particularly important to quantify the element makeup of microorganisms [e.g., (21)] and their compositional “plasticity.” Changes in environmental availability of the elements create selection pressures that should alter the composition of biological macromolecules and the metals used in particular enzymatic pathways (22). While a few examples are known (23, 24), such research rarely considers the selection pressures possible in ancient oceans. In addition to shedding light on the history of life on Earth, such research will provoke us to think about alternative biochemistries unknown in living organisms (25). Someday, it may even help us to understand the distribution of life on planets other than our own.

References

1. A. E. Isley, D. H. Abbott, *J. Geophys. Res.* **104**, 15461 (1999).
2. D. E. Canfield, *Annu. Rev. Earth Planet. Sci.* **33**, 1 (2005).
3. H. D. Holland, *Philos. Trans. R. Soc. London Ser. B* **361**, 903 (2006).
4. K. O. Buesseler *et al.*, *Science* **319**, 162 (2008).
5. D. E. Canfield, *Nature* **396**, 450 (1998).
6. T. W. Lyons, *Science* **321**, 923 (2008).
7. A. D. Anbar *et al.*, *Science* **317**, 1903 (2007).
8. G. L. Arnold, A. D. Anbar, J. Barling, T. W. Lyons, *Science* **304**, 87 (2004); published online 4 March 2004 (10.1126/science.1091785).
9. C. Scott *et al.*, *Nature* **452**, 456 (2008).
10. M. A. Saito, D. M. Sigman, F. M. M. Morel, *Inorg. Chim. Acta* **356**, 308 (2003).
11. A. D. Anbar, A. H. Knoll, *Science* **297**, 1137 (2002).
12. C. J. Bjerrum, D. E. Canfield, *Nature* **417**, 159 (2002).
13. K. O. Konhauser, S. V. Lalonde, L. Amskold, H. D. Holland, *Science* **315**, 1234 (2007).
14. A. L. Zerkle, C. H. House, R. P. Cox, D. E. Canfield, *Geobiology* **4**, 285 (2006).
15. R. Buick, *Geobiology* **5**, 97 (2007).
16. E. Pecoits, S. V. Lalonde, K. O. Konhauser, *Astrobiology* **8**, 412 (2008).
17. R. J. P. Williams, J. J. R. Fraústo da Silva, *J. Theor. Biol.* **220**, 323 (2003).
18. A. H. Knoll, E. J. Javaux, D. Hewitt, P. Cohen, *Philos. Trans. R. Soc. London Ser. B* **361**, 1023 (2006).
19. C. L. Dupont, S. Yang, B. Palenik, P. E. Bourne, *Proc. Natl. Acad. Sci. U.S.A.* **103**, 17822 (2006).
20. P. G. Falkowski *et al.*, *Science* **305**, 354 (2004).
21. A. Quigg *et al.*, *Nature* **425**, 291 (2003).
22. J. Elser, *Am. Nat.* **168**, 525 (2006).
23. P. Baudouin-Cornu, Y. Surdin-Kerjan, P. Martière, D. Thomas, *Science* **293**, 297 (2001).
24. F. M. M. Morel, *Geobiology* **6**, 318 (2008).
25. F. Wolfe-Simon, P. C. W. Davies, A. D. Anbar, *Int. J. Astrobiol.*, in press.
26. A. L. Zerkle, C. H. House, S. L. Brantley, *Am. J. Sci.* **305**, 467 (2005).

10.1126/science.1163100

CELL SIGNALING

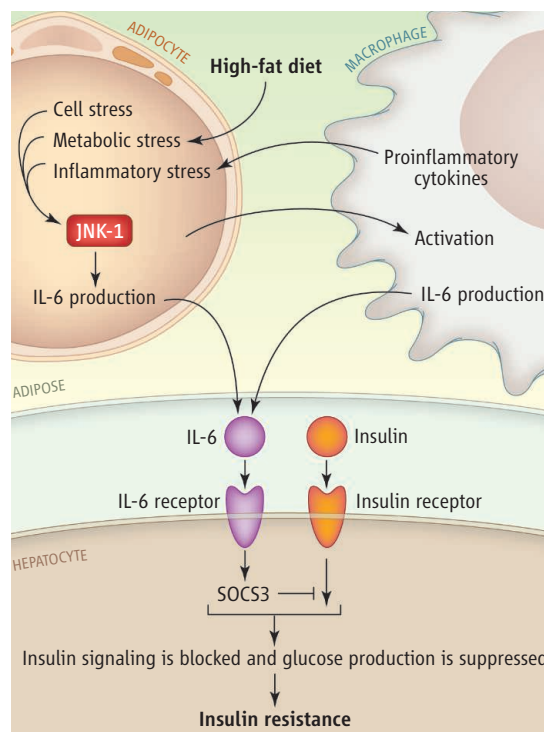
Fat Stress and Liver Resistance

Wataru Ogawa¹ and Masato Kasuga^{1,2}

Type 2 diabetes is a global health problem with about 220 million people afflicted worldwide (1). It is characterized by a defect in insulin secretion and a decrease in sensitivity to this hormone (or insulin resistance). The result is an increase in blood glucose concentration because glucose uptake by muscle cells and fat cells (adipocytes), as well as the suppression of glucose production in hepatocytes, are attenuated. Type 2 diabetes is also often associated with the condition of being overweight or obese, which is the major cause of insulin resistance. Although the mechanism by which obesity triggers insulin resistance is not fully understood, recent evidence suggests that inflammation in adipose tissue—triggered by macrophages that have infiltrated this tissue—contributes to this process (1, 2). On page 1539 of this issue, Sabio *et al.* (3) reveal that an inflammatory response within adipocytes also plays a key role in regulating insulin sensitivity in the liver.

Macrophages consist of proinflammatory (M1) and anti-inflammatory (M2) cells. M1 macrophages accumulate in adipose tissue of obese animals, probably attracted and activated by cytokines and a certain class of fatty acids produced by adipocytes (4). Once activated, M1 macrophages in adipose tissue produce proinflammatory cytokines, such as interleukin (IL)-6 and tumor necrosis factor (TNF)- α , which interfere with responses to insulin by cells, including hepatocytes. This ultimately results in insulin resistance (2, 4). This “fat inflammation” hypothesis is consistent

with clinical observations that the serum concentrations of proinflammatory cytokines correlate with adiposity or with insulin resistance (5). However, Sabio *et al.* report that the promotion of macrophage accumulation appears not to be the sole mechanism by which adipocytes contribute to the development of obesity-induced insulin resistance.



Obesity-induced insulin resistance. Cellular stress induced by a high-fat diet activates JNK1 in adipocytes, which results in an increased concentration of circulating IL-6. In the liver, IL-6 inhibits the action of insulin, likely through the induction of SOCS3 expression. JNK1 in adipocytes might contribute to activating macrophages in adipose tissue. Inflammatory cytokines secreted from activated macrophages likely augment the stress signal in adipocytes.

Communication among immune and fat cells in adipose tissue and liver hepatocytes underlies the pathogenesis of obesity-related insulin resistance.

Various stresses, including inflammation, activate the protein kinase c-Jun NH₂-terminal kinase 1 (JNK1) in different cell types. In hematopoietic cells, JNK1 induces inflammation by activating the expression of proinflammatory cytokine genes (3, 6). Moreover, it phosphorylates insulin receptor substrate, a component of the intracellular signaling pathway that is activated by insulin, thereby inhibiting the insulin signal (3, 6). Feeding mice a high-fat diet—which induces obesity and insulin resistance—activates JNK1 in various organs, including the liver, adipose tissue, and skeletal muscle (3, 6). This insulin resistance is ameliorated in mice genetically deficient in JNK1 (7), implicating this enzyme in the pathogenesis of insulin resistance.

To determine whether a specific organ is responsible for JNK1-mediated insulin resistance, Sabio *et al.* generated mice with JNK1 deficiency specifically in myeloid cells or in hematopoietic cells. Although the production of proinflammatory cytokines, including IL-6 and TNF- α , was impaired in macrophages that lack JNK1, both types of mice still developed insulin resistance when fed a high-fat diet. The authors next generated mice with JNK1 deficiency in adipocytes and found that their susceptibility to insulin resistance induced by a high-fat diet was greatly reduced. Thus, JNK1 in adipocytes—but not that in myeloid lineage cells, including macrophages—is required for obesity-induced insulin resistance.

¹Department of Internal Medicine, Division of Diabetes, Metabolism, and Endocrinology, Kobe University Graduate School of Medicine, Kobe 650-0017, Japan. ²Research Institute, International Medical Center of Japan, Tokyo 162-8655, Japan. E-mail: kasuga@med.kobe-u.ac.jp

Akt is a protein kinase that functions downstream of insulin receptor substrate in the insulin signaling cascade. Sabio *et al.* found that Akt activation was attenuated in the liver, skeletal muscle, and adipose tissue of wild-type mice fed a high-fat diet, whereas ablation of JNK1 in adipocytes restored the effect of insulin in adipose tissue (possibly by preventing JNK1-mediated phosphorylation of insulin receptor substrate). However, the authors observed that both the impairment of Akt activation in response to a high-fat diet, and impairment of the suppressive effect of insulin on glucose production in the liver, were ameliorated in mice with JNK1 deficiency in adipocytes.

Among various pro- and anti-inflammatory cytokines, as well as adipocyte-derived hormones thought to regulate insulin sensitivity, Sabio *et al.* found that only the abundance of IL-6 was substantially affected in mice with adipocyte-specific deficiency of JNK1. Increases in the serum concentration of IL-6 and in the production of this cytokine in adipose tissue that are induced by a high-fat diet were almost completely eliminated by the ablation of JNK1 in adipocytes. SOCS3, a signaling molecule that is activated by IL-6 in hepatocytes, inhibits insulin signal transduction (8). Expression of SOCS3 in the liver increased when wild-type mice were fed a high-fat diet, and this effect was prevented by JNK1 ablation in adipocytes, suggesting that increased SOCS3 expression induced by IL-6 contributes to the development of hepatic insulin resistance.

Sabio *et al.* have clearly shown that JNK1 in adipocytes of obese animals regulates the circulating concentration of IL-6, which in turn likely plays an important role in the pathogenesis of insulin resistance. Although this study uncovers the crucial role of stress signaling in adipocytes during “fat inflammation,” it does not exclude a role for macrophages in adipose tissue in obesity-induced insulin resistance. Several studies have indicated the importance of M1 macrophages in the development of obesity-induced insulin resistance (9–11). Also, the findings of Solinas *et al.* (12) contradict those of Sabio *et al.* in that ablation of JNK1 in myeloid cells ameliorated obesity-induced insulin resistance. Although the reason for this discrepancy is unclear, the results of Solinas *et al.* have also been challenged (13). Moreover, adipocytes and macrophages may influence each other's functions, with adipocytes promoting the conversion of M2 macrophages to the M1 phenotype (10, 11). Interactions between adipocytes and macrophages thus likely trigger inflammation in adipose tissue, with both cell types

contributing to the development of obesity-induced insulin resistance (see the figure).

Although Sabio *et al.* found that the extent of macrophage infiltration in adipose tissue was not altered by the ablation of JNK1 in adipocytes, it may be that the ratio of M1 to M2 macrophage cells was affected. Their study underscores the prominent role of IL-6 among cytokines in the pathogenesis of insulin resistance. Given that IL-6 exerts a glucose-lowering effect when acting in a paracrine manner in the liver (14), it is possible that a pronounced systemic increase in IL-6 abundance and a smaller local increase in the concentration of this cytokine exert opposite effects on glucose metabolism. Although the data of Sabio *et al.* indicate that adipose tissue is responsible for an increase in the circulating concentration of IL-6 in obese animals, whether adipocytes or macrophages are the source of this cytokine is not yet clear. It will thus be of interest to assess the effects of IL-6 ablation specifically in adipocytes or in myeloid cells on obesity-induced insulin resistance. Tocilizumab, a monoclonal anti-

body that inhibits the binding of IL-6 to its receptor, is currently in clinical trials for treating inflammatory diseases, including rheumatoid arthritis (15). This drug might also prove effective for the treatment or prevention of type 2 diabetes.

References

1. M. Kasuga, *J. Clin. Invest.* **116**, 1756 (2006).
2. M. Saberi, J. M. Olefsky, *J. Clin. Invest.* **118**, 2992 (2008).
3. G. Sabio *et al.*, *Science* **322**, 1539 (2008).
4. J. I. Odegaard, A. Chawla, *Nat. Clin. Pract. Endocrinol. Metab.* **4**, 619 (2008).
5. J. M. Fernandez-Real, W. Ricart, *Endocr. Rev.* **24**, 278 (2003).
6. G. S. Hotamisligil, *Nature* **444**, 860 (2006).
7. J. Hirosumi *et al.*, *Nature* **420**, 333 (2002).
8. T. Torisu *et al.*, *Genes Cells* **12**, 143 (2007).
9. D. Patsouris *et al.*, *Cell Metab.* **8**, 301 (2008).
10. J. I. Odegaard *et al.*, *Nature* **447**, 1116 (2007).
11. K. Kang *et al.*, *Cell Metab.* **7**, 485 (2008).
12. G. Solinas *et al.*, *Cell Metab.* **6**, 386 (2007).
13. S. N. Vallerie, M. Furuhashi, R. Fuchou, G. S. Hotamisligil, *PLoS ONE* **3**, e3151 (2008).
14. H. Inoue *et al.*, *Cell Metab.* **3**, 267 (2006).
15. A. Sebba, *Am. J. Health Syst. Pharm.* **65**, 1413 (2008).

10.1126/science.1167571

EVOLUTION

Competitive Centromeres

Deborah Charlesworth

Divergence in DNA sequence associated with a common chromosomal element is linked to fitness and evolution of a wild species of flower.

A case of strongly distorted genetic ratios in hybrids between two species of the monkeyflower *Mimulus* seems to be due to a competitive advantage of one version of a chromosome over its partner's homologous region during female gamete formation. On page 1559 of this issue, Fishman and Saunders (1) provide cytogenetic and genetic evidence implicating the centromere region of this chromosome. In most eukaryotes, segregation of chromosomes during cell division is controlled by the centromere regions. The new study suggests that the more competitive type of centromere spread recently in one of the species, *M. guttatus*, but not throughout the whole species, as one might have expected from its strong advantage. There may thus be some counterbalancing disadvantage. This system may advance our understanding of centromere behavior.

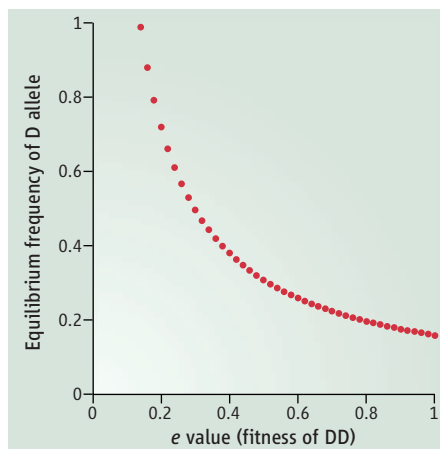
Institute of Evolutionary Biology, School of Biological Sciences, University of Edinburgh, Edinburgh EH9 3JT, UK.
E-mail: deborah.charlesworth@ed.ac.uk

In diploid eukaryotes, each parental individual contributes to a progeny one of two copies of each gene, and each progeny has a 50% chance of receiving each of the two allelic versions of the gene, giving the familiar 1:1 Mendelian ratio. But non-1:1 ratios of segregating alleles have been observed in several situations, including in offspring derived from crosses between different species. Often, this may be caused by nothing more than the presence of recessive (or nearly recessive) deleterious mutations in the parent species. Descendants (F_2) of the first generation (F_1) of offspring can thus become homozygous for two mutant alleles of such genes, leading to a deficit of this diploid genotype and of genetic markers closely linked to loci carrying such mutations (2). Such situations are helpful for studying the genetic basis of incompatibilities between different species when genes from the two species interact in ways that cause deficits of some genotypes (3). These incompatibilities are sometimes asymmetrical, differing between the reciprocal crosses—for instance,

when the diploid genome of one parent is incompatible with a maternally transmitted genome from the other; asymmetry can also appear in the first generation of offspring (4).

A completely different way in which non-Mendelian ratios can occur is when the different alleles in a heterozygous genotype, such as a hybrid, have different probabilities of forming gametes. In normal female meiosis in plants and animals, only one of the four products forms an egg nucleus while the other three are discarded into polar bodies. There might then be competition for inclusion in the egg nucleus. A successfully competing allele will be present in more than 50% of the eggs of heterozygotes, although the gametes of both kinds can function in homozygotes. An example is known in mammals, when mothers heterozygous for centric fusions between two chromosomes transmit mostly unfused chromosomes to their progeny (5). These situations with distorted segregation ratio among the gametes are called meiotic drive (6); other cases include the “selfish” preferential transmission of heterochromatic knob-bearing copies of chromosome 10 in maize, and supernumerary (B) chromosomes in many organisms (7).

Although selfish preferential transmission of centromeres and competition between centromeres have been the focus of recent interest (8–10), much of the inference is circumstantial and relies on evidence for evolutionary “arms races” between centromeres and the proteins that bind to them (perhaps to resist preferential segregation). The discovery of distorted transmission in a cross between *M. guttatus* and *M. nasutus* (11) gave promise that mechanistic details could be elucidated, because *Mimulus* species offer good opportunities for genetic and molecular studies (12). Fishman and Saunders noted that transmission ratios of some genetic markers were highly distorted when F_1 plants were pollinated by either parent species. This cannot have been attributable to pollen competition (because ratios were normal in progeny using F_1 pollen) or to mortality of zygotes (which would distort ratios regardless of whether the F_1 parent was the seed or the pollen parent). Inviability of some female gametes or segregation distortion—as seen in male *Drosophila* fruit flies (a well-studied system), in which half of the sperm of heterozygotes are defective (8)—are also unlikely because fertility was normal. A competitive effect acting in female gamete formation is therefore the most likely cause of distortion. The most distorted ratios were found at genetic map position 30 in linkage group 11, but statistically significant distortion remained for markers many



Allele frequency. The plot shows the frequency of the D allele predicted in a population that has reached equilibrium, using the equations in Fishman and Saunders (1). The plot shows the frequency values for a distortion of $d = 8\%$ and a range of male fertility disadvantages to DD homozygous plants (x axis). A disadvantage (e) greater than about 13% prevents the D allele from spreading through the whole population, and a disadvantage of around 30% is needed to produce an equilibrium population with a frequency of the D allele similar to that estimated for the *M. guttatus* population; this is remarkably good agreement between the theory and the estimated disadvantage.

centimorgans distant. This pattern suggests that this chromosome carries a distorting factor, D, that is transmitted to about 98% of the egg nuclei (11).

What is the D factor and how does it distort? The high degree of distortion suggested that the centromere might be competing for inclusion in the egg nucleus. Fishman and Saunders boldly opted for a cytogenetic approach to test this hypothesis. They searched the *M. guttatus* genome sequences for candidate centromeric repeats, on the basis of similarity to those of other plant species. In their fluorescence in situ hybridization experiments, a common repeat sequence indeed hybridized to the centromeres of the chromosomes of the *M. guttatus* parent of the hybrid, and one chromosome pair had a distinctive double-banded appearance. This chromosome corresponds to linkage group 11; when the authors tested one of the strongly distorted genetic markers on chromosome preparations, it too hybridized near the double-banded centromere region.

One hypothesis for D is that it is merely a normal allele that outcompetes a weak version that evolved in the self-fertilizing species *M. nasutus*. However, this seems unlikely, because D has clearly spread recently in the *M. guttatus* population and is still polymorphic; of nine *M. guttatus* inbred lines tested, four yielded F_1 hybrids with *M. nasutus*

showing no transmission distortion of a marker allele (at a microsatellite locus, *aat356*, in the strongly distorted chromosome region). Moreover, three of the nondistorter strains were examined cytologically and did not have the double-banded centromere.

Is this polymorphism merely a transient state, or does the D allele have disadvantages that prevent its becoming fixed in the population, thus maintaining it in a polymorphic state? To answer this, Fishman and Saunders estimated the distortion within the *M. guttatus* population. Distortion does occur, but much less than in hybrid plants (heterozygotes mated to non-D plants produce 58% D progeny). A population genetic model of a distorting allele suggests that such distortion would cause rapid spread into a population. Indeed, the authors found that chromosomes with the D allele were highly homogeneous in the alleles carried at several loci in the same region of the genetic map, just as expected if this allele has recently increased to a high frequency, whereas at the loci examined (up to 45 kb from the *aat356* locus), the non-D chromosomes included a diversity of alleles. With the rough estimates of the two governing parameters of the model (degree of distortion $d = 8\%$, fitness disadvantage $e = 20\%$), the predicted equilibrium D frequency is much higher than the estimated frequency, but higher e values rapidly lower the discrepancy (see the figure). It will be interesting to analyze the diversity in this genome region more quantitatively, using methods that can test for balancing selection (13). If balancing selection is detected, perhaps there are indeed additional disadvantages. Now that genetic resources in *Mimulus* have been developed, this wild plant system may, surprisingly, provide rich information about centromere behavior.

References

1. L. Fishman, A. Saunders, *Science* **322**, 1559 (2008).
2. D. Zamir, Y. Tadmor, *Bot. Gaz.* **147**, 355 (1986).
3. L. C. Moyle, E. B. Graham, *Mol. Biol. Evol.* **23**, 973 (2006).
4. M. Turelli, L. C. Moyle, *Genetics* **176**, 1059 (2007).
5. F. Pardo-Manuel de Villena, C. Sapienza, *Genetics* **159**, 1179 (2001).
6. L. Sandler, E. Novitski, *Am. Nat.* **91**, 105 (1957).
7. A. Burt, R. Trivers, *Genes in Conflict* (Harvard Univ. Press, Cambridge, MA, 2006).
8. S. Henikoff, K. Ahmad, H. S. Malik, *Science* **293**, 1098 (2001).
9. H. S. Malik, S. Henikoff, *Genetics* **157**, 1293 (2001).
10. P. B. Talbert, T. D. Bryson, S. Henikoff, *J. Biol.* **3**, 18 (2004).
11. L. Fishman, J. H. Willis, *Genetics* **169**, 347 (2005).
12. C. Wu et al., *Heredity* **100**, 220 (2008).
13. R. R. Hudson, K. Bailey, D. Skerckey, J. Kwiatkowski, F. J. Ayala, *Genetics* **136**, 1329 (1994).

10.1126/science.1167573

GE PRIZE ESSAY

Understanding a Minimal DNA-Segregating Machine

Ethan Clark Garner

A current challenge in biology is to bridge the gap between the parts and the whole, to reconcile the biochemical properties of individual proteins with the emergent behaviors of multipart molecular machines. In theory, if every kinetic rate constant for every interaction were measured, we could gain a complete mechanistic understanding of a biological process. Because the number of required measurements scales with the number of components, most complex biological systems present difficult challenges for this approach. However, when quantitative insight is matched with the proper system, the goal of elucidating the biochemical basis of emergent behaviors can be realized. For example, to gain a molecular-level understanding of DNA segregation, a fundamental, mesoscale process, I turned to a system that has been forced to be minimal and self-contained during its evolution: low-copy bacterial plasmids. To maintain their inheritance against the fitness costs imposed by their extra metabolic burden, these exogenous elements have evolved minimal, self-contained, DNA segregation machines.

At a minimum, a DNA-segregating system needs to accomplish three tasks. First, it must count the copies of DNA to know when to initiate segregation. Second, it must exert directional force to propel these DNA copies away from each other. Third, this system must be spatially aware of the cellular geometry so that the DNA is propelled toward each eventual daughter cell. For the *Escherichia coli* R1 drug resistance plasmid, all of these tasks are conferred by the *par* operon, which constructs a mitotic spindle out of only three components (1). The centromeric sequence *parC* contains 10 repeats that are bound by the adapter protein ParR. This ParR/*parC* complex interacts with ParM, a distant actin homolog that polymerizes into helical filaments (2). In my thesis

GE Healthcare and *Science* are pleased to present the prize-winning essay by Ethan Garner, a regional winner from North America, who is the Grand Prize winner of the GE & *Science* Prize for Young Life Scientists.



work, I determined how these three components interact to accomplish the systems-level task of DNA segregation. To elucidate this mechanism of plasmid segregation, I needed to understand the nature of ParM polymerization, how the ParR/*parC* complex affected ParM filaments, and finally, how these three components interact to push the plasmids to the poles of the cell.

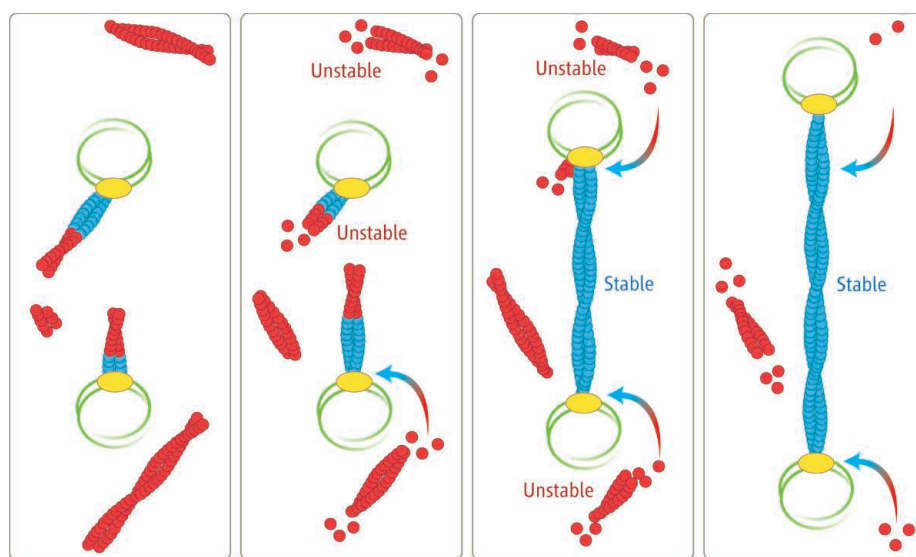
First, I conducted a complete characterization of ParM

Reconstitution of a plasmid spindle shows how three components together accomplish the task of DNA segregation.

assembly dynamics, measuring all available rate constants for this polymer (3). Although ParM is a structural homolog of eukaryotic actin, I found three distinct differences between these polymers. First, ParM nucleates filaments at a rate 300 times as fast as actin. Second, unlike any other previously observed polymer, ParM shows no polarity as it grows at equal rates at each end of the filament. The most striking difference between ParM and actin is that ParM exhibits dynamic instability, the stochastic switching between

states of growth and rapid disassembly (4). Previously, this behavior had only been observed for eukaryotic microtubules. ParM's dynamic instability is driven by ATP hydrolysis, as ADP-bound ParM filaments display a much higher dissociation rate than the ATP-bound filaments.

The combination of dynamic instability and rapid nucleation causes solutions of ParM to consist of a population of short, dynamic filaments that nucleate and turn over throughout the volume. This unstable, transient nature appears at odds with the formation of a rigid force-generating mitotic spindle, suggesting that the ParR/*parC* complex must alter ParM filament dynamics. I tested this hypothesis by reconstituting the *par* system from purified components (5), combining *parC*-conjugated beads with ParR and fluorescently labeled ParM. Isolated *parC* beads displayed short, dynamic asters of ParM emanating from their surface, as if they were searching the surrounding volume. When two *parC* beads came into close contact, stable bundles of filaments formed between the beads. These filaments then elongated at a constant rate, pushing the beads in opposite directions. Creating



Dynamic instability and bipolar stabilization drive plasmid segregation. The ParR/*parC* complex can capture cytoplasmic ParM filaments. Filament ends bound by ParR/*parC* are stabilized (blue) while unbound filaments (red) and destined to undergo catastrophe. A productive spindle is formed when both ends are bound by ParR/*parC*. Turnover of the unattached, background filaments provides the energy differential (arrows) to power spindle elongation.

Cellular and Molecular Pharmacology, University of California, San Francisco, CA 94158, USA. As of 15 December 2008: Systems Biology, Harvard Medical School, Boston, MA 02115, USA. E-mail: egarner@mullinslab2.ucsf.edu

fiducial marks on these filaments demonstrated that they elongate at equal rates at each bead surface, indicating that new monomers are added into the spindle through a process of insertional polymerization at the ParR/*parC* complex. This was the first in vitro reconstitution of a DNA-segregating system from purified components.

The fact that we observed long, stable ParM filaments only between pairs of beads indicated that the filaments are stabilized against catastrophic disassembly when bound at both ends by ParR/*parC*. When these spindles were severed with laser irradiation, these filaments would rapidly depolymerize. This bipolar stabilization provides an intrinsic counting mechanism, as productive and sustained filament elongation only occurs between *parC* pairs.

I then tested whether these spindles could locate the ends of a volume by confining them in microfabricated channels of various shapes. These spindles aligned with and elongated along the long axis of these spaces, indicating that this simple system is sufficient to

find the long axis of a cell.

In addition to demonstrating that these three components are necessary and sufficient to generate the emergent behaviors required for DNA segregation—counting, force generation, and spatial awareness—this work also elucidated the biophysical relationship between dynamic instability and force generation. By conducting spindle assembly assays at varying concentrations of ParM, I found that filaments bound at each end by ParR/*parC* behave as if the entire filament is composed of the higher-affinity, ATP-bound polymer. In essence, this stabilizes the bound filaments to a lower energetic level than the unbound filaments that turn over in solution (see the figure). This indicates that the dynamic instability of the unattached filaments provides the monomer excess that powers the elongation of the stabilized ParR/*parC* attached filaments.

These studies provide a framework for understanding the essential principles of DNA segregation. Furthermore, they demonstrate that biology can solve complex tasks

with a surprisingly small number of components. This minimal solution to DNA segregation is not an isolated case; many low-copy plasmids have independently converged on three-component systems by co-opting a variety of different polymers from their hosts (6–9). Kinetic dissection of a range of these self-contained mitotic machines may uncover the differing solutions that biology has evolved to ensure genetic inheritance and thus broaden our understanding of this fundamental biological process.

References

1. K. Gerdes, S. Molin, *J. Mol. Biol.* **190**, 269 (1986).
2. J. Möller-Jensen, R. B. Jensen, J. Löwe, K. Gerdes, *EMBO J.* **21**, 3119 (2002).
3. E. C. Garner, C. S. Campbell, R. D. Mullins, *Science* **306**, 1021 (2004).
4. T. Mitchison, M. Kirschner, *Nature* **312**, 237 (1984).
5. E. C. Garner, C. S. Campbell, D. B. Weibel, R. D. Mullins, *Science* **315**, 1270 (2007).
6. S. Austin, A. Abeles, *J. Mol. Biol.* **169**, 353 (1983).
7. T. Ogura, S. Hiraga, *Cell* **32**, 351 (1983).
8. E. Becker *et al.*, *EMBO J.* **25**, 5919 (2006).
9. R. A. Larsen *et al.*, *Genes Dev.* **21**, 1340 (2007).

10.1126/science.1168506

2008 Grand Prize Winner



Ethan Garner, the author of the prize-winning essay, was born in Richland, Washington. He received his B.S. in biochemistry from Washington State University, where he worked with Keith Dunker developing tools to predict disordered regions within proteins. He conducted his graduate work at the University of California, San Francisco, where he studied the kinetics and regulation of prokaryotic polymers with Dyche Mullins. Ethan is moving to Boston, where he will be working with Tim Mitchinson, Xiaowei Zhuang, and Alice Ting on elucidating the process of prokaryotic DNA segregation.

Regional Winners

North America: Xu Tan for his essay “Plant Hormone Auxin Functions as Novel Molecular Glue.” Dr. Tan spent his first 18 years in Changsha, China. In high school, he won a national first prize in the biology Olympiad. After earning his B.S. from the University of Science and Technology of China in Hefei, he pursued graduate studies at the University of Washington, Seattle. Under the advice of Ning Zheng, Dr. Tan did his thesis research on the structural biology of ubiquitin ligases. Looking forward to expanding his research horizons, he is starting a postdoctoral position with Steve Elledge at Brigham and Women’s Hospital, Harvard Medical School.



Europe: Sabrina Büttner for her essay “Endonuclease G Regulates Cellular Fate.” Dr. Büttner was born in Mutlangen, Germany. She studied biochemistry at the Eberhardt-Karls University, Tübingen, Germany, and received her diploma with honors in 2004. During her Ph.D. studies, conducted under the guidance of Frank Madeo at the Institute for Molecular Biosciences, University of Graz, Austria, she investigated yeast programmed cell death in the context



of aging and oxidative stress, identifying molecular mechanisms of apoptosis in *Saccharomyces cerevisiae*. After defending her doctoral thesis in 2007, Dr. Büttner continued her research in the Madeo lab as a postdoctoral fellow, focusing on the further establishment of yeast as a model for neurodegenerative diseases.

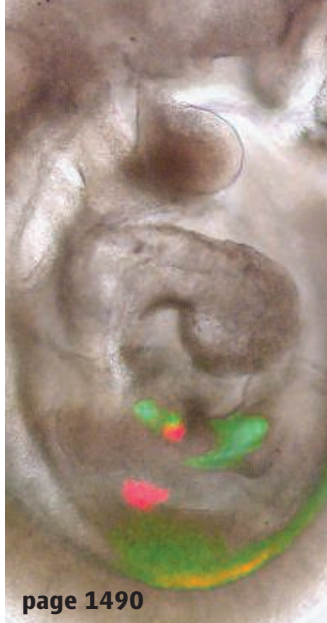
Japan: Kaori Yamada for her essay “Moving PIP₃ Regulates Cell Polarity.” Dr. Yamada grew up in Kinokawa, a beautiful town in Wakayama, Japan. She received a B.S. degree from the University of Tokyo. A strong interest in life science led her to remain there as a graduate student in Yasuhisa Fukui’s laboratory. During her Ph.D. project, she spent time in the laboratory of Athar H. Chishti, a collaborator at the University of Illinois, Chicago. There, Dr. Yamada elucidated how kinesin transports the lipid messenger PIP₃ in neurons. She completed her Ph.D. in January 2007 and is currently a postdoctoral fellow at the University of Illinois, Chicago.



All other countries: Sarel Fleishman for his essay “Modeling at the Gates of the Cell.” Dr. Fleishman received an M.Sc. in biochemistry (summa cum laude) and a Ph.D. (with distinction) from Tel-Aviv University, Israel, where he studied in the group of Nir Ben-Tal. During his graduate studies, he investigated the structure, function, and evolution of membrane proteins associated with hereditary hearing loss and neurodegenerative diseases, cancer, and bacterial drug resistance. He is currently a Human Frontier Research Postdoctoral Fellow working on computational design of protein-based inhibitors toward pathogenic molecules in David Baker’s laboratory at the University of Washington.



For the full text of essays by the regional winners and for information about applying for next year’s awards, see *Science* Online at www.sciencemag.org/feature/data/prizes/ge/index.dtl.



INTRODUCTION

New Release: *The Complete Guide to Organ Repair*

CLINICIANS AND PATIENTS WILL CLAMOR FOR A COPY WHEN PUBLISHERS SEND OUT this announcement. But how long until its release? No one knows. Fortunately, collaborations between basic research and translational medicine are providing enough information to start writing the prologue. Research is telling us that in most cases, successful organ repair will not result from simply tossing willy-nilly a few ingredients, such as stem cells, into the broken body. Instead, assembly of the repair and regeneration toolkit will require detailed knowledge of the specific cell types in an organ, efficient ways to direct cell differentiation and target cell delivery, methods to tweak cell communication, and sophisticated bioengineering innovation.

The collection of articles in this issue boasts exciting advances toward elucidating diverse organ features. A Review by Chien and colleagues (p. 1494) highlights organ complexity as exemplified in cardiogenesis. Despite a long-held view of the heart as a simple muscular pump, there is much more to it—cells of varied types and intricate collaboration with the vasculature and electrical conduction system, not to mention the involvement of biomechanical forces and three-dimensional structure. Substantial progress has been made toward understanding two other organs, the liver and pancreas, which share a common endodermal origin. Zaret and Grompe (p. 1490) detail how mechanisms of normal development are recapitulated during regeneration, or not. But where is the engine that powers organ development and regeneration? We turn to stem cells for this, at least in part. Although we've witnessed intense scientific and public interest in these valuable cells, do we really know what they are, which ones truly exist in the body, or their origin? Slack (p. 1498) gives his perspective.

To make an organ or prompt its natural regeneration, we must step back to gain an intimate understanding of basic cell movements and collaboration. As highlighted by Montell (p. 1502), single disconnected cells do not an organ make; collective cell activities are key. In a related Review, Lu and Werb (p. 1506) describe organ cell morphogenesis as it occurs in the branching systems of the vertebrate mammary gland, prostate, and lung, as well as the invertebrate tracheal system.

Related content in *Science Signaling* (9 December 2008) highlights organogenesis in plants. Root nodules develop on the roots of legumes in response to bacterial infection. These specialized organs serve as the site for nitrogen fixation. Crespi and Frugier focus on the bacterial and host-generated signals that induce and regulate nodule organogenesis. The more familiar plant organ, the leaf, is crucial for photosynthesis and respiration. Gray *et al.* discuss peptide signals that activate leucine-rich repeat receptor pathways to regulate vein versus stoma cell fate in the leaf.

Although chapters of the clinicians' and horticulturists' repair guides are in the drafting stages, the long lists of capable contributors are sure to craft a good read.

— BEVERLY PURNELL

Organ Development

CONTENTS

Reviews

- 1490 Generation and Regeneration of Cells of the Liver and Pancreas
K. S. Zaret and M. Grompe
- 1494 Cardiogenesis and the Complex Biology of Regenerative Cardiovascular Medicine
K. R. Chien et al.
- 1498 Origin of Stem Cells in Organogenesis
J. M. W. Slack
- 1502 Morphogenetic Cell Movements: Diversity from Modular Mechanical Properties
D. J. Montell
- 1506 Patterning Mechanisms of Branched Organs
P. Lu and Z. Werb

See also related online material at www.sciencemag.org/organdevelopment

Science

REVIEW

Generation and Regeneration of Cells of the Liver and Pancreas

Kenneth S. Zaret^{1*} and Markus Grompe²

Liver and pancreas progenitors develop from endoderm cells in the embryonic foregut. Shortly after their specification, liver and pancreas progenitors rapidly acquire markedly different cellular functions and regenerative capacities. These changes are elicited by inductive signals and genetic regulatory factors that are highly conserved among vertebrates. Interest in the development and regeneration of the organs has been fueled by the intense need for hepatocytes and pancreatic β cells in the therapeutic treatment of liver failure and type I diabetes. Studies in diverse model organisms have revealed evolutionarily conserved inductive signals and transcription factor networks that elicit the differentiation of liver and pancreatic cells and provide guidance for how to promote hepatocyte and β cell differentiation from diverse stem and progenitor cell types.

The liver and pancreas coordinately control body metabolism, including the modification of digested nutrients by hepatocytes in the liver and the regulation of blood glucose levels by insulin secreted from β cells in the pancreas. Liver hepatocytes are large, often polyploid cells that secrete serum proteins, express enzymes that neutralize toxicants, produce bile acids to aid in digestion, and control the bulk of intermediary metabolism. Biliary ducts of cholangiocytes, the other epithelial cell type in the liver, serve primarily as conduits of secreted bile. In contrast, the distinct pancreatic functions are partitioned into many more cell types. Pancreatic cells include insulin (β), glucagon (α), somatostatin, ghrelin, and pancreatic polypeptide-secreting endocrine types, each of which produces a single hormone. The pancreas also contains exocrine cell types, which constitute the bulk mass of the tissue and include acinar cells that produce digestive enzymes and duct cells that provide conduits to the gut for the enzymes. The greater diversity of cell types in the pancreas involves a greater array of regulatory factors and lineage decisions during organogenesis.

Clinical studies have shown that transplantation of hepatocytes can support the functions of a failed liver and correct metabolic

liver disease in the long term (1). Similarly, cadaveric islets can, for several years, support glucose homeostasis in type I diabetic individuals, in whom the β cells have been de-

programming efforts are founded on understanding how hepatocytes and β cells are normally generated in the embryo and how they arise during regeneration in adults, in response to tissue damage and disease. Here we provide an overview of the cells' development and regeneration and highlight unresolved issues in the field.

Two Progenitor Domains for Each Tissue

The liver and pancreas in terrestrial vertebrates each develop from two different spatial domains of the definitive endodermal epithelium of the embryonic foregut. Fate-mapping experiments have shown that the liver arises from lateral domains of endoderm in the developing ventral foregut (3, 4) as well as from a small group of endodermal cells tracking down the ventral midline (4) (Fig. 1A). During foregut closure, the medial and lateral domains come together (Fig. 1A, green arrows) as the hepatic endoderm is specified. The pancreas is also induced in lateral endoderm domains, adjacent and caudal to the lateral liver domains, and in cells near the dorsal midline of the foregut (5, 6) (Fig. 1A). These

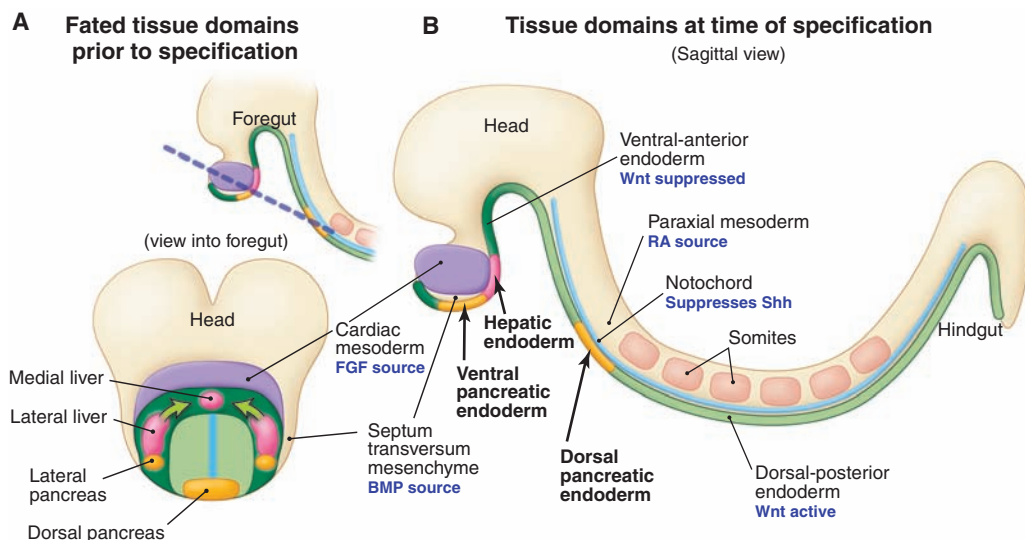


Fig. 1. Cell domains and signals for embryonic liver and pancreas specification. **(A)** Fate map of progenitor cell domains before tissue induction; view is into the foregut of an idealized mouse embryo at E8.25 (three- to four-somite stage). Green arrows indicate movement of lateral progenitor regions toward the ventral-medial region. **(B)** Sagittal view of a mouse embryo several hours later than in **(A)** showing the positions of the newly specified liver and pancreas tissue domains. Signals and cell sources that pattern the endoderm are shown. Dashed blue line indicates plane of view in **(A)**.

stroyed by an autoimmune reaction (2). In both transplantation settings, the quality and amount of donor cells are severely limiting, as is the ability to expand the terminally differentiated cell populations. These limitations have led to a search for other progenitor cell sources of hepatocytes and β cells and intense interest in how the differentiation of such progenitors can be directed, or "programmed," efficiently. The

events occur at 8.5 days of mouse gestation (E8.5), corresponding to about 3 weeks of human gestation. After the domains are specified and initiate morphogenetic budding, the dorsal and ventral pancreatic buds merge to create the gland. Despite differences in how the different progenitor domains are specified, descendants of both pancreatic progenitor domains make endocrine and exocrine cells, and descendants of both liver

¹Epigenetics and Progenitor Cells Program, Fox Chase Cancer Center, 333 Cottman Avenue, Philadelphia, PA 19111, USA.

²Oregon Stem Cell Center and Papé Family Pediatric Research Institute, Oregon Health and Science University, 3181 Southwest Sam Jackson Park Road, Portland, OR 97239, USA.

*To whom correspondence should be addressed. E-mail: zaret@fccc.edu

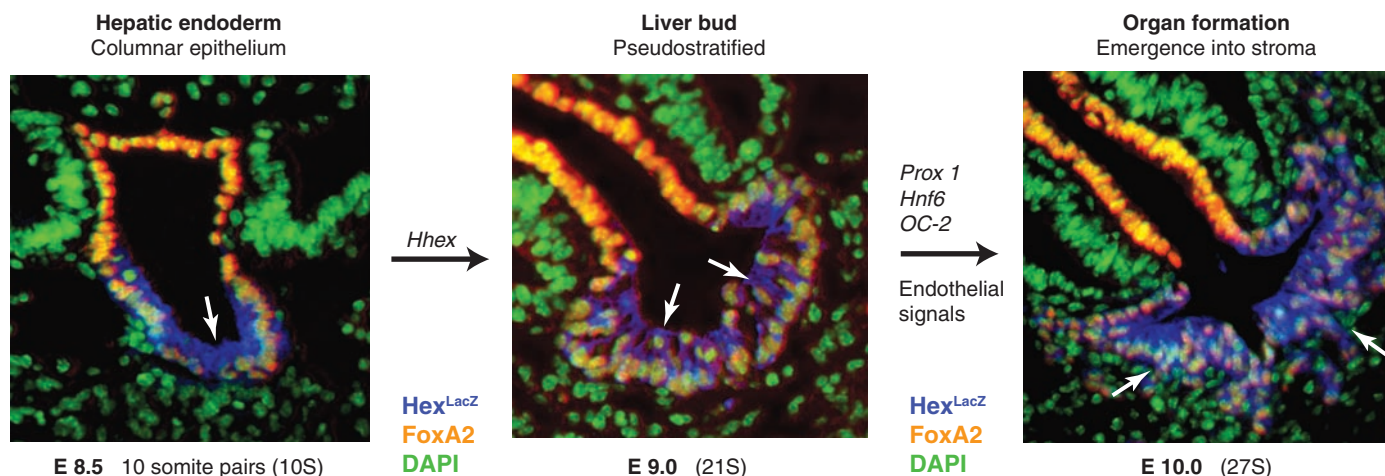


Fig. 2. Stages of liver bud organogenesis. Hepatoblasts are stained blue ($\text{Hex}^{\text{LacZ}+}$), cells with orange nuclei are gut endoderm (FoxA2^+), and all nuclei were stained green by 4',6'-diamidino-2-phenylindole. White arrows point to

the hepatic cells. Genes and signals that promote each transition are indicated. Similar morphogenetic stages occur during pancreas bud organogenesis. Images are adapted from (36). S, pair somite stage; E, embryonic day.

progenitor domains contribute to differentiating liver bud cells (3–6). Genetic lineage-marking studies are needed to determine the extent to which different descendants within each tissue may differ with regard to functionality and regenerative potential.

Signals Specifying Hepatic and Pancreatic Progenitors

Embryo tissue recombination experiments and genetic approaches in the chick, frog, mouse, and zebrafish have revealed that the liver and pancreas domains are specified within the endodermal epithelium under the influence of inductive signals from nearby mesoderm cells (7, 8). Little is known about how the signaling genes in the mesoderm are controlled, but it is remarkable how well the inductive signals are conserved across the vertebrate animal models. Initially, broad suppression of mesodermal Wnt and fibroblast growth factor 4 (FGF4) signaling in the foregut enables liver and pancreas induction, whereas active mesodermal Wnt signaling in the posterior gut suppresses these tissue fates (9, 10) (Fig. 1B). Retinoic acid signaling, apparently from paraxial mesoderm cells, helps further refine the anterior-posterior position in which the liver and pancreas can develop from the gut endoderm (11–14). Subsequently, in the ventral foregut, FGF from the cardiac mesoderm and bone morphogenetic protein (BMP) from septum transversum mesenchyme cells coordinately induce the liver program and suppress the pancreas program (15–18). Mitogen-activated protein kinase (MAPK) is activated in response to FGF in the lateral hepatic progenitors well before MAPK activation in the medial hepatic progenitors, reflecting apparent differences in patterning (19). During foregut closure, lateral ventral endoderm cells that move caudal to the cardiac domain escape the FGF and can initiate

ventral pancreatic development (20). In the dorsal foregut, signals from the notochord that include activin and FGF suppress *sonic hedgehog* (*shh*) signaling within the endoderm and allow the pancreatic program (21, 22). All of the above events occur within hours in the vertebrate embryo.

The newly specified hepatic cells in embryos are referred to as hepatoblasts. These cells express serum protein genes specific to hepatocytes, such as *albumin* (*alb1*) and *transferrin* (*ttr*), and appear to be bipotential and later give rise to hepatocytes and cholangiocytes (23); however, formal genetic lineage studies remain to be performed. The *Tbx3* gene helps expand the hepatoblast population by suppressing *p19^{ARF}* (24). The newly specified pancreatic endoderm is initially marked by the expression of the transcription factor genes *Pdx1* and then *Ptf1a* (25, 26), which are crucial for pancreatic development; *Pdx1* is also expressed in adjacent progenitors of the duodenum (27, 28).

Changes in Signal Responses as Development Proceeds

The cellular responses to inductive signals include the activation and repression of transcription factor genes that, in turn, elicit new gene expression programs required for cell differentiation. The new cell type programs can change the cellular responses to exogenous signals. Such is the case for FGFs, which are needed only transiently to help pattern the foregut endoderm (19, 29) and later promote the expansion of the newly specified progenitor cell populations (16, 30). Shh signaling initially promotes dorsal pancreatic development in the zebrafish (31, 32) and later appears to suppress it (33). Wnt signaling initially inhibits liver induction (9) but shortly afterward promotes liver bud growth and differentiation (9, 34, 35). Each

of these changes in cellular responses to inductive signals occurs in less than a day of vertebrate embryogenesis. The mechanisms underlying such changes are not known.

Organ Morphogenesis and Cell-Type Differentiation

After the hepatoblasts and pancreatic progenitors are specified, the respective endoderm cells transition from a cuboidal shape to a columnar one and then become pseudo-stratified within the epithelium (Fig. 2). This process is similar to the morphogenetic characteristics of neural epithelial development and is controlled in the foregut by the homeobox transcription factor gene *Hhex* (36). The pancreatic epithelium then branches into the stroma to create the pancreatic bud; whereas for the hepatic epithelium the basal lamina breaks down, and the cells proliferate into the surrounding stroma. These latter morphologic changes are controlled by the homeobox transcription factor genes *Prox1* (37), *Hnf6/OC-1*, and *OC-2* (38) (Fig. 2). *Hnf6* and *OC-2* regulate E-cadherin, thrombospondin-4, and *Spp1*, which control cell adhesion and migration in various contexts. The fetal liver serves as a transient site for hematopoiesis in amniotes. Hence, fetal viability is dependent on proper liver growth.

As the progenitors of both tissues bud into the stroma, they are adjacent to and receive stimulatory signals from nearby endothelial cells (39–41). Endothelial cells also promote liver regeneration after tissue damage, apparently by hepatocyte growth factor (HGF) signaling (42). The specific molecular signals produced from endothelial cells in the embryonic context have not been described, but sphingosine-1-phosphate in the circulation, delivered by the endothelium, promotes dorsal pancreatic budding (43). The emerging vascular systems in the liver and

Organ Development

pancreatic buds also provide oxygen and nutrients and ultimately allow endocrine function (44).

Neural crest cells migrate into the developing pancreas and, as they develop into neurons, affect the numbers of β cells (45). The stimulatory roles of endothelial cells and neural crest cells illustrate how crucial is the codifferentiation of the stromal environment with that of the hepatic and pancreatic progenitors.

Within the liver and pancreas buds, Notch signaling components are important for creating the proper balance in the numbers of hepatocytes and cholangiocytes from hepatoblasts (46, 47) and of endocrine and exocrine cells from pancreatic progenitor cells (48–50). Loss of Notch signaling allows the endocrine lineage, which is marked by and requires the transcription factor gene *Ngn3* (25, 48, 51).

Elegant genetic lineage studies showed that as the pancreatic bud develops into an organ, *Cpa1*-positive cells in the distal tips of the branching epithelium are multipotent progenitors that give rise to duct and endocrine descendants along the trunk of the branches, until about E14 in the

mouse (52). Afterward, the *Cpa1*-positive cells give rise to acinar cells; this corresponds to the time of the “secondary transition,” when definitive β cells are generated under the influence of the *Mafa* transcription factor (53, 54). Further genetic lineage studies, the transcription factor genes that elicit pancreatic and hepatic cell differentiation, and the parameters that affect cell growth are shown in Fig. 3 and have been reviewed extensively elsewhere (23, 55–57). There are notable differences in how the dorsal and ventral pancreatic progenitors are specified (Fig. 3), which suggests flexibility in the ways by which pancreas cells could be specified from stem cells.

Liver Regeneration

Liver regeneration after most forms of injury does not rely on stem or progenitor cells but instead involves the mitosis of mature cells (58). The regenerative capacity of hepatocytes can be assessed in animal models of liver repopulation, in which transplanted cells have a selective advantage over the host (59). By use of such models, it has been shown that mature polyploid

hepatocytes have a stem cell–like regenerative capacity rivaling that of hematopoietic stem cells and are able to divide more than 100 times without loss of function (60). Human hepatocytes are also highly regenerative (61), and this capacity for regeneration is established at the earliest embryonic stages (36). Unfortunately, it has not yet proved possible to grow and expand populations of hepatocytes in cell culture or maintain their differentiation. Even with the most sophisticated growth media, hepatocytes dedifferentiate extensively within a few hours after plating (62). Thus, the functions of adult hepatocytes, including cell division, appear to depend on complex interactions with other cells in a three-dimensional matrix. Coculture systems attempting to mimic this organization show promise in resolving these problems (63).

The adult liver also harbors facultative progenitors that can be activated in response to specific injuries (Fig. 4), usually under conditions of impaired hepatocyte replication. Progenitors give rise to an intermediary cell type, often termed “oval cells,” which are thought to differentiate into both biliary epithelium and hepatocytes (58). However, oval cells are not a homogeneous population (64), and their apparent multipotentiality has not been demonstrated by definitive lineage tracing. In the rat, oval cells resemble embryonic hepatoblasts in that they express both bile duct and hepatocyte markers as well as α -fetoprotein (58). Thus, progenitor cell activation in the adult employs some of the same genetic programs used during development (65). Details about the precise origin of adult liver progenitors and the signals that govern their activation are not clear.

Pancreas Regeneration

Whereas hepatocytes are capable of extensive regeneration, the ability of β cells to expand is more limited, especially in the adult. Some degree of regeneration can occur in young animals after physiologic stimuli such as pregnancy (66) or injury (partial pancreatectomy) (67). However, this partial growth ability is insufficient to permit recovery from cell loss in type I diabetes; yet it might, with suppression of autoimmunity (68). The restricted regenerative ability of the endocrine pancreas may be related to the defined number of pancreatic progenitors, which is not capable of compensatory growth in response to cell loss (69). In contrast, hepatoblasts can increase their proliferative rate in response to dysfunctional cells in their midst (36). The lack of regeneration in β cells has raised considerable interest in the potential of tissue repair by resident stem cells. It remains controversial whether progenitors exist in the adult pancreas. It is clear that the majority of new β cells derive from pre-existing insulin-expressing cells after surgical injury (67, 70), but recent work has shown that duct ligation can activate *Ngn3*-positive β cell

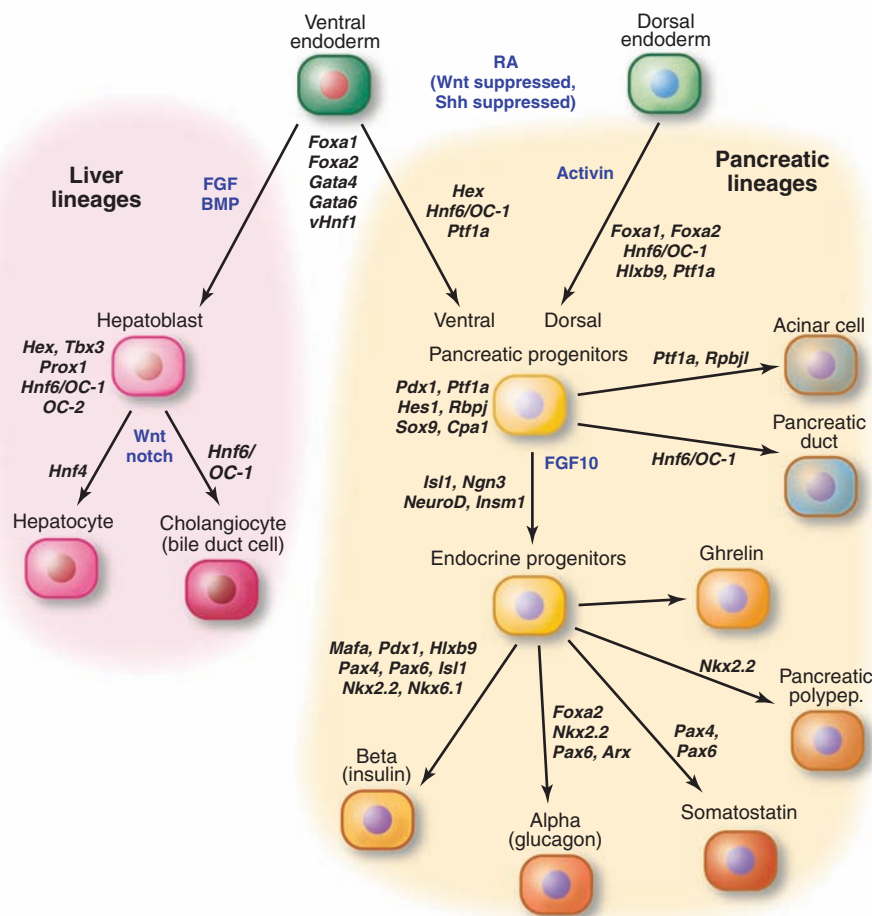


Fig. 3. Regulatory factors controlling cell type lineages within the liver and pancreas. Transcription factor genes are shown in bold; their functions have been reviewed in the text and elsewhere (23, 55–57), except for *vHnf1* in hepatic development (81). *Pdx1* initially marks duodenum and caudal stomach progenitors (not shown) as well as the pancreatic domains (28).

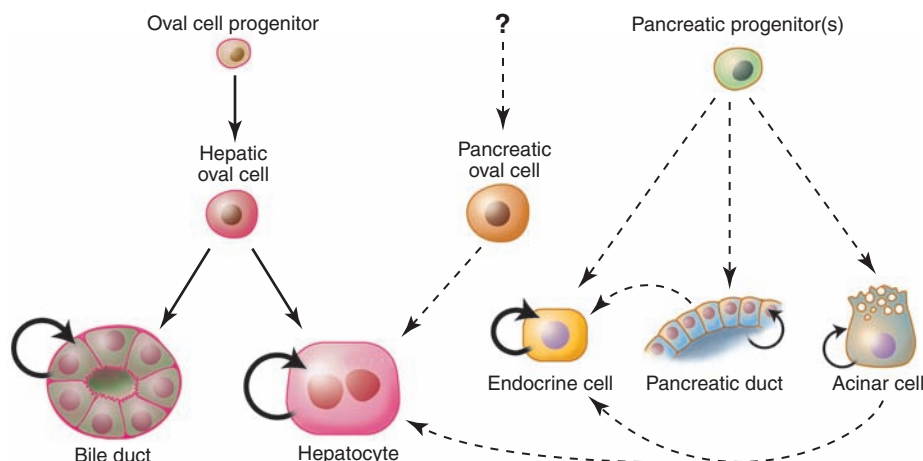


Fig. 4. Progenitor lineage relationships in adult liver and pancreas. The thickness of the arrows indicates the dominant mode of regeneration. Dashed lines delineate rare or hypothetical cell-fate transitions that occur only under specific experimental conditions.

precursors in the ductal epithelium (71). Thus, adult pancreatic progenitors exist and their activation depends on the specific injury, as does oval-cell initiation in the liver (Fig. 4).

Creating Hepatocytes and β Cells de Novo

The current inability to expand human hepatocytes in vitro is an obstacle not only for cell therapy but also for pharmaceutical drug development because of the cells' importance in assessing the metabolism of xenobiotics. Thus, the generation of hepatocytes from expandable precursors is of considerable interest. Cells with properties virtually identical to those of hepatic oval cells can also emerge in the pancreas, especially after the ablation of acinar cells (72). Upon transplantation, these pancreas-derived oval cells can differentiate into functional hepatocytes and bile ducts (73). Several reports have suggested that the reciprocal transdifferentiation is also possible; that is, the conversion of liver cells toward the pancreatic endocrine fate (74). Forced expression of pancreatic transcription factors elicit insulin expression in the liver and corrects experimental diabetes (75). Together, these findings suggest that both the adult liver and pancreas contain cells with epigenetic memory of their common embryonic origin. The existence of potential β cell precursors in the adult liver is of obvious medical interest. Because pancreatic exocrine cells greatly outnumber β cells, it is also exciting that they can be reprogrammed to make functional β cells in vivo by viral delivery of the developmental transcription factors Pdx1, Ngn3, and MafA (76).

Pluripotent stem cells, including embryonic stem cells (ESCs) and induced pluripotent stem cells (iPSCs), are a potentially abundant source of hepatocytes and β cells. Numerous groups have been developing ESC differentiation protocols that attempt to mimic normal embryonic

development. The first step of both pancreatic and hepatic development is the induction of a definitive endoderm by using activin A (77). Further treatment with BMP-4 and bFGF can then direct cells toward the hepatic lineage (78). In a protocol developed for differentiation toward endocrine pancreatic cells, definitive endoderm was treated in sequential stages with keratinocyte growth factor (KGF), retinoic acid, Noggin, and cyclopamine (79, 80). Despite remarkable progress, the resulting cells often fail to achieve complete function sufficient for regenerative therapy, remaining only, "hepatocyte- or β cell-like." It is not yet clear how precisely the known developmental signals must be orchestrated to properly program hepatic and pancreatic cells at will, but detailed studies of the activated signaling pathways and their cross-regulatory interactions during embryogenesis will be informative.

Future Prospects

Two basic opportunities for medical application of the knowledge of the developmental biology of the liver and pancreas have emerged. The first is the application of the precise conditions that exist within the embryo to differentiate pluripotent stem cells. The sequential and exactly timed use of extracellular factors and accessory cell types (such as endothelium and mesenchyme) is predicted to mimic embryogenesis and thus yield highly functional derivatives for transplantation and other applications. In this setting, competent cells respond to extrinsic signals that act on their epigenome. The second approach is to use genetic reprogramming to directly change cell fates by taking advantage of transcriptional activators, repressors, and chromatin modifiers. This method can work in vivo as well as in culture and can be applied to adult epigenetic relatives of the desired cell type. Thus, it may be possible to enhance tissue regeneration

in situ without the complications of cell engraftment and immunological rejection. However, it will be important to overcome the potential problems of insertional mutagenesis, in which stable gene integration is involved, as well as undesired transgene expression changes and physiologic responses to viral gene delivery. Emphasis is required on both approaches to use the signals and regulatory factors from developmental biology to sculpt the differentiation of progenitor and stem cells to liver and pancreas cell fates.

References and Notes

1. I. J. Fox *et al.*, *J. Med.* **338**, 1422 (1998).
2. A. M. Shapiro *et al.*, *J. Med.* **343**, 230 (2000).
3. A. D. Chalmers, J. M. Slack, *Development* **127**, 381 (2000).
4. K. D. Tremblay, K. S. Zaret, *Dev. Biol.* **280**, 87 (2005).
5. H. A. Field, P. D. Dong, D. Beis, D. Y. Stainier, *Dev. Biol.* **261**, 197 (2003).
6. J. M. W. Slack, *Development* **121**, 1569 (1995).
7. N. Le Douarin, *Bull. Biol. Fr. Belg.* **98**, 543 (1964).
8. N. K. Wessells, J. H. Cohen, *Dev. Biol.* **15**, 237 (1967).
9. V. A. McLin, S. A. Rankin, A. M. Zorn, *Development* **134**, 2207 (2007).
10. J. M. Wells, D. A. Melton, *Development* **127**, 1563 (2000).
11. Y. Chen *et al.*, *Dev. Biol.* **271**, 144 (2004).
12. M. Kumar, N. Jordan, D. Melton, A. Grapin-Botton, *Dev. Biol.* **259**, 109 (2003).
13. M. Martin *et al.*, *Dev. Biol.* **284**, 399 (2005).
14. D. Stafford *et al.*, *Development* **133**, 949 (2006).
15. G. Deutsch, J. Jung, M. Zheng, J. Lora, K. S. Zaret, *Development* **128**, 871 (2001).
16. J. Jung, M. Zheng, M. Goldfarb, K. S. Zaret, *Science* **284**, 1998 (1999).
17. J. M. Rossi, N. R. Dunn, B. L. Hogan, K. S. Zaret, *Genes Dev.* **15**, 1998 (2001).
18. D. Shin *et al.*, *Development* **134**, 2041 (2007).
19. A. Calmont *et al.*, *Dev. Cell* **11**, 339 (2006).
20. R. Bort, J. P. Martinez-Barbera, R. S. Beddington, K. S. Zaret, *Development* **131**, 797 (2004).
21. A. Apelqvist, U. Ahlgren, H. Edlund, *Curr. Biol.* **7**, 801 (1997).
22. M. Hebrok, S. K. Kim, D. A. Melton, *Genes Dev.* **12**, 1705 (1998).
23. K. S. Zaret, *Nat. Rev. Genet.* **9**, 329 (2008).
24. A. Suzuki, S. Sekiya, D. Buscher, J. C. Izpisua Belmonte, H. Taniguchi, *Development* **135**, 1589 (2008).
25. G. Gu, J. Dubauskaite, D. A. Melton, *Development* **129**, 2447 (2002).
26. Y. Kawaguchi *et al.*, *Nat. Genet.* **32**, 128 (2002).
27. U. Ahlgren, J. Jonsson, H. Edlund, *Development* **122**, 1409 (1996).
28. M. F. Offield *et al.*, *Development* **122**, 983 (1996).
29. I. Manfroid *et al.*, *Development* **134**, 4011 (2007).
30. A. Bhushan *et al.*, *Development* **128**, 5109 (2001).
31. W. S. Chung, D. Y. Stainier, *Dev. Cell* **14**, 582 (2008).
32. S. Roy, T. Qiao, C. Wolff, P. W. Ingham, *Curr. Biol.* **11**, 1358 (2001).
33. P. d'Iorio, K. Alexa, S. K. Choe, L. Etheridge, C. G. Sagerstrom, *Dev. Biol.* **304**, 221 (2007).
34. S. P. Monga *et al.*, *Gastroenterology* **124**, 202 (2003).
35. E. A. Ober, H. Verkade, H. A. Field, D. Y. Stainier, *Nature* **442**, 688 (2006).
36. R. Bort, M. Signore, K. Tremblay, J. P. Barbera, K. S. Zaret, *Dev. Biol.* **290**, 44 (2006).
37. B. Sosa-Pineda, J. T. Wigle, G. Oliver, *Nat. Genet.* **25**, 254 (2000).
38. S. Margaglioni *et al.*, *Dev. Biol.* **311**, 579 (2007).
39. E. Lammert, O. Cleaver, D. Melton, *Science* **294**, 564 (2001).
40. K. Matsumoto, H. Yoshitomi, J. Rossant, K. S. Zaret, *Science* **294**, 559 (2001).

41. H. Yoshitomi, K. S. Zaret, *Development* **131**, 807 (2004).
42. J. LeCouter *et al.*, *Science* **299**, 890 (2003).
43. J. Edsall *et al.*, *Development* **132**, 1085 (2005).
44. O. Cleaver, D. A. Melton, *Nat. Med.* **9**, 661 (2003).
45. N. Nekrep, J. Wang, T. Miyatsuka, M. S. German, *Development* **135**, 2151 (2008).
46. K. Lorent *et al.*, *Development* **131**, 5753 (2004).
47. B. McCright, J. Lozier, T. Gridley, *Development* **129**, 1075 (2002).
48. A. Apelqvist *et al.*, *Nature* **400**, 877 (1999).
49. J. Jensen *et al.*, *Nat. Genet.* **24**, 36 (2000).
50. H. Nakhai *et al.*, *Development* **135**, 2757 (2008).
51. G. Gradwohl, A. Dierich, M. LeMeur, F. Guillemot, *Proc. Natl. Acad. Sci. U.S.A.* **97**, 1607 (2000).
52. Q. Zhou *et al.*, *Dev. Cell* **13**, 103 (2007).
53. T. A. Matsuoka *et al.*, *Mol. Cell. Biol.* **23**, 6049 (2003).
54. M. Olbrot, J. Rud, L. G. Moss, A. Sharma, *Proc. Natl. Acad. Sci. U.S.A.* **99**, 6737 (2002).
55. L. C. Murtaugh, *Development* **134**, 427 (2007).
56. J. M. Oliver-Krasinski, D. A. Stoffers, *Genes Dev.* **22**, 1998 (2008).
57. M. E. Wilson, D. Scheel, M. S. German, *Mech. Dev.* **120**, 65 (2003).
58. N. Fausto, J. S. Campbell, *Mech. Dev.* **120**, 117 (2003).
59. E. P. Sandgren *et al.*, *Cell* **66**, 245 (1991).
60. K. Overturf, M. al-Dhalimy, M. Finegold, M. Grompe, *Am. J. Pathol.* **155**, 2135 (1999).
61. E. A. Kvittingen, H. Rootwelt, R. Berger, P. Brandtzaeg, *J. Clin. Invest.* **94**, 1657 (1994).
62. D. F. Clayton, J. E. Darnell Jr., *Mol. Cell. Biol.* **3**, 1552 (1983).
63. S. R. Khetani, S. N. Bhatia, *Nat. Biotechnol.* **26**, 120 (2008).
64. C. Dorrell *et al.*, *Hepatology* **48**, 1282 (2008).
65. J. M. W. Slack, *Science* **322**, 1498 (2008).
66. P. C. Butler, J. J. Meier, A. E. Butler, A. Bhushan, *Nat. Clin. Pract. Endocrinol. Metab.* **3**, 758 (2007).
67. Y. Dor, J. Brown, O. I. Martinez, D. A. Melton, *Nature* **429**, 41 (2004).
68. J. Nishio *et al.*, *Science* **311**, 1775 (2006).
69. B. Z. Stanger, A. J. Tanaka, D. A. Melton, *Nature* **445**, 886 (2007).
70. M. Teta, M. M. Rankin, S. Y. Long, G. M. Stein, J. A. Kushner, *Dev. Cell* **12**, 817 (2007).
71. X. Xu *et al.*, *Cell* **132**, 197 (2008).
72. J. K. Reddy, M. S. Rao, A. V. Yeldandi, X. D. Tan, R. S. Dwevedi, *Dig. Dis. Sci.* **36**, 502 (1991).
73. M. S. Dabeva *et al.*, *Proc. Natl. Acad. Sci. U.S.A.* **94**, 7356 (1997).
74. J. M. Slack, *Nat. Rev. Mol. Cell Biol.* **8**, 369 (2007).
75. H. Kojima *et al.*, *Nat. Med.* **9**, 596 (2003).
76. Q. Zhou, J. Brown, A. Kanarek, J. Rajagopal, D. A. Melton, *Nature* **455**, 627 (2008).
77. A. Kubo *et al.*, *Development* **131**, 1651 (2004).
78. V. Gouon-Evans *et al.*, *Nat. Biotechnol.* **24**, 1402 (2006).
79. K. A. D'Amour *et al.*, *Nat. Biotechnol.* **24**, 1392 (2006).
80. E. Kroon *et al.*, *Nat. Biotechnol.* **26**, 443 (2008).
81. L. Lokmane *et al.*, *Development* **135**, 2777 (2008).
82. We apologize to many in the field whose work we could not cite because of space constraints. We thank D. Freedman-Cass for comments and E. Pytko for help in preparing the manuscript. K.S.Z. is supported by NIH grants R37 GM36477, U01 DK072503, and P30CA06927, and M.G. by grants U01 DK072477 and RO1 DK05192 and Juvenile Diabetes Research Foundation grant 18508680-36749. The authors have patents pending related to the work in this article. M.G. is a cofounder of DNA Repair Company and the founder of Yecuris and has equities in both. K.S.Z. is on a scientific advisory board for Johnson and Johnson.

10.1126/science.1161431

REVIEW

Cardiogenesis and the Complex Biology of Regenerative Cardiovascular Medicine

Kenneth R. Chien,^{1,2*} Ibrahim J. Domian,¹ Kevin Kit Parker³

The heart is a complex organ system composed of a highly diverse set of muscle and nonmuscle cells. Understanding the pathways that drive the formation, migration, and assembly of these cells into the heart muscle tissue, the pacemaker and conduction system, and the coronary vasculature is a central problem in developmental biology. Efforts to unravel the biological complexity of in vivo cardiogenesis have identified a family of closely related multipotent cardiac progenitor cells. These progenitors must respond to non-cell-autonomous signaling cues to expand, differentiate, and ultimately integrate into the three-dimensional heart structures. Coupling tissue-engineering technologies with patient-specific cardiac progenitor biology holds great promise for the development of human cell models of human disease and may lay the foundation for novel approaches in regenerative cardiovascular medicine.

“There is always an easy solution to every human problem—neat, plausible and wrong.”
—H. L. Mencken (*1*)

The view of the heart as muscular pump has dominated cardiovascular science and medicine for over a century. However, the heart is clearly more than muscle, with a panoply of diverse cardiac and smooth muscle, valvular,

pacemaker, and endothelial cell types with discrete contractile, electrical, and vascular roles (Figs. 1 and 2). To form a fully functional heart organ system, a set of embryonic precursor cells must give rise to these distinct cell types, which must ultimately assemble and align within specific heart compartments to form ventricular chambers, coronary arteries, and the conduction system. In this regard, recent studies have identified a novel set of multipotent heart progenitors that can give rise to many of the major cell types in the heart. At the same time, a host of clinical studies in regenerative cardiovascular medicine have attempted to reverse heart muscle failure by augmenting the amount of functional human cardiac muscle via transplantation of a diverse group of adult progenitor cell types (2–8). The concept itself is relatively simple: Progenitor cells isolated from

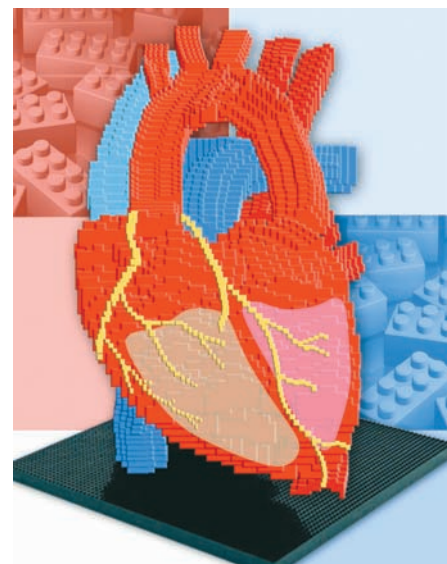


Fig. 1.

outside the heart are transplanted into the adult heart, with the hope that they will eventually expand and integrate into the intact myocardial tissue and thereby improve cardiac function. Unfortunately, to date, the results have largely been ambiguous, marginal, or negative, suggesting that simply transplanting adult nonheart progenitors and other muscle cells into a failing heart will not necessarily lead to substantial, long-term clinical improvement (9). The lessons from these clinical studies and parallel work in animal models (10–18) point to the need to account for the biological complexity of in vivo embryonic cardiogenesis. How is the diversity of heart cells generated? Is there a “master” heart progenitor that can give rise to the major muscle and non-muscle cell lineages, and, if so, how is information conveyed for the precise differentiation of daugh-

¹MGH Cardiovascular Research Center, Massachusetts General Hospital, Boston, MA 02114, USA. ²Department of Stem Cell and Regenerative Biology, Harvard University and the Harvard Stem Cell Institute, Cambridge, MA 02138, USA. ³Disease Biophysics Group, School of Engineering and Applied Sciences, Harvard University, Cambridge, MA 02138, USA.

*To whom correspondence should be addressed. E-mail: kchien@partners.org

ter cell types? What controls the expansion of progenitors and their downstream differentiated progeny into discrete tissue compartments? How are they assembled into three-dimensional structures that are required for coordination of mechanical work, electrical signal propagation, and uniform delivery of blood flow? Can we reconstruct this complexity *ex vivo* by combining recent advances in stem cell biology, developmental biology, and tissue bioengineering? This brief review will highlight how recent advances in our understanding of the biological complexity of cardiogenesis itself are beginning to point to novel approaches for regenerative cardiovascular medicine.

Generation of Diverse Heart Cell Lineages from Multipotent Progenitors

Mammalian cardiogenesis requires the generation of a highly diversified set of both muscle and nonmuscle cell types, including atrial and ventricular cardiomyocytes; conduction system and pacemaker cells; and smooth muscle, endothelial, valvular, and endocardial cells (19–21). The formation of these various cardiovascular cell lineages in distinct heart and vascular compartments has its basis in the existence of a closely related set of multipotent progenitors in the early embryonic heart field (22, 23), which can be divided into the primary heart field and secondary heart field (SHF) lineages (Fig. 2) (19, 24–26). The primary heart field arises from the anterior lateral mesoderm and forms a group of cardiovascular precursors that form a cardiac crescent in the early embryo. Later in development, these cells coalesce into the linear heart tube and ultimately give rise to the left ventricle of the mature four-chambered mammalian heart. The SHF is derived from a population of cells in the pharyngeal and splanchnic mesoderm, which migrate into the developing heart and give rise to the right ventricle, the outflow tract, and portions of the inflow tract. Recent work has now also identified a set of multipotent epicardial progenitor cells that contribute to the atrial and ventricular myocardium, coronary smooth muscle, and cardiac fibroblasts (27, 28). To date it has not been possible to isolate and characterize the developmental potential of purified populations of primary heart field progenitors because of an absence of molecular markers unique to that field. In contrast, lineage tracing experiments have demonstrated that most of the early SHF myocardial, smooth muscle, and endothelial cells can be traced to multipotent heart progenitors that express the LIM-homeodomain transcription factor *Islet1* [*Isl1* (Fig. 2)] (22, 26, 29). Clonal assays with purified *Isl1* progenitors from embryos or embryonic stem (ES) cells have also documented the ability of a single SHF progenitor to give rise to the above three cardiac lineages (22, 23, 30). In a parallel series of experiments, the cardiac-specific *Nkx2.5* enhancer has been used to isolate bipotential cardiac progenitors from

murine embryos as well as murine ES cells (20). Similarly, the mesoderm marker *Brachyury T*, in combination with the cell surface marker *Flk1*, was used to enrich for a population of multipotent cardiac progenitors from human and murine ES cells (30, 31). Unlike the *Isl1* progenitors, however, the *Nkx2.5* progenitors and the *Flk1* progenitors likely represent a heterogeneous mix of primary and secondary heart field progenitors. It is unclear whether cardiac regeneration of the left ventricle, a primary heart field–derived structure, will require purified populations of primary heart field progenitors.

Non-Cell-Autonomous Cues Control Lineage Specification and Expansion of Cardiac Progenitor Populations

Cardiac progenitor cells, which originate in the primary and secondary heart fields, are subject to a rapidly changing environment because of cell migration and changes in the three-dimensional architecture of the primitive heart. Developing cardiac progenitor populations are therefore susceptible to temporally and spatially modulated variations of non-cell-autonomous signaling molecules that originate from neighboring endothelial, endocardial, and other mesodermally derived cells in the primitive embryonic heart. These cues work in concert to control lineage commitment and expansion of the progenitor population. The

development of the SHF appears to be critically dependent on bone morphogenic protein (BMP) signaling. BMP 2, 4, 6, and 7 have overlapping patterns of expression with *Isl1*, and conditional deletion of type I BMP receptor *Bmpr1a* in *Isl1* progenitor results in multiple defects of SHF-derived structures (32). Similarly, fibroblast growth factor (FGF) signaling plays a key role in the formation and subsequent maturation of the SHF. FGF8 null mutations, for example, result in embryonic lethality at gastrulation; hypomorphic mutations result in multiple cardiovascular defects affecting primarily SHF derivatives, including the outflow tract (33). Furthermore, disruption of FGF signaling within the SHF by conditional inactivation of the FGF receptors *FGFr1* or *FGFr2* results in outflow tract defects associated with failure of extracellular matrix secretion as well as failure in BMP and transforming growth factor (TGF)- β signaling (34). Ablation of the FGF adaptor molecule *Frs2a* in outflow tract progenitor cells also inhibits their expansion and results in outflow tract hypoplasia (35).

During the later stages of cardiogenesis, the robust expansion of cardiogenic cells is critical, particularly for the ventricular chamber. The increase in muscle mass is required to generate sufficient mechanical work to maintain the demands for blood flow in the exponentially growing embryo. In the outflow tract, this expansion has to

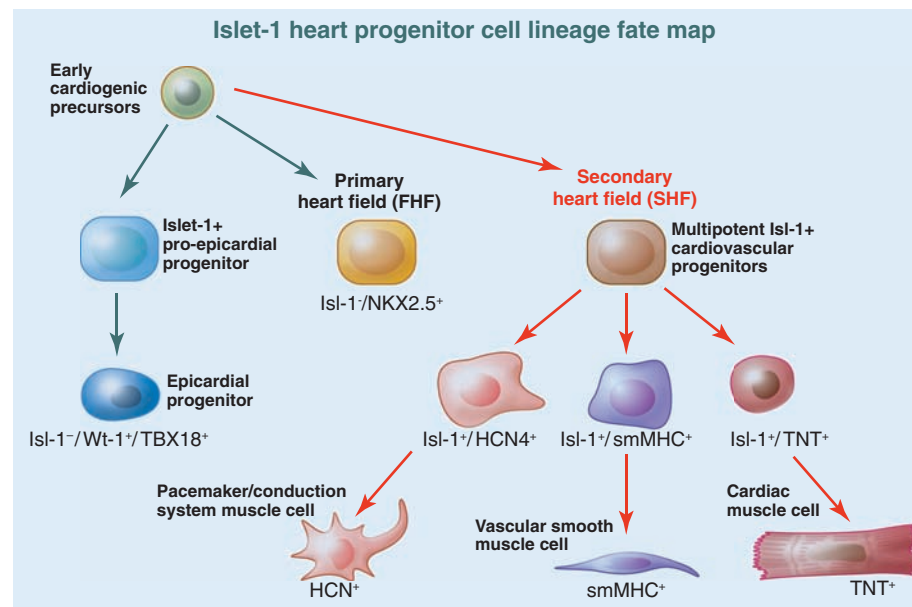


Fig. 2. Multipotent heart progenitors in the *Isl1* lineage. Early mesoderm-derived cardiac precursors give rise to progenitors in the first and second heart fields (FHF and SHF, respectively). The LIM-homeodomain transcription factor *Isl1* marks a multipotent cardiovascular progenitor that can give rise to myocardium, conduction system, smooth muscle cells, and endothelial lineages. The developmental potential of FHF progenitors is not well established because of an absence of specific molecular markers for that field and an inability to isolate purified progenitor populations of that lineage. Recent work (48) has also identified a third multipotent set of epicardial progenitors that appears to arise from a very early *Isl1* precursors and to express the transcription factors *Tbx18* or *Wt1*. TNT indicates troponin T; MHC, myosin heavy chain.

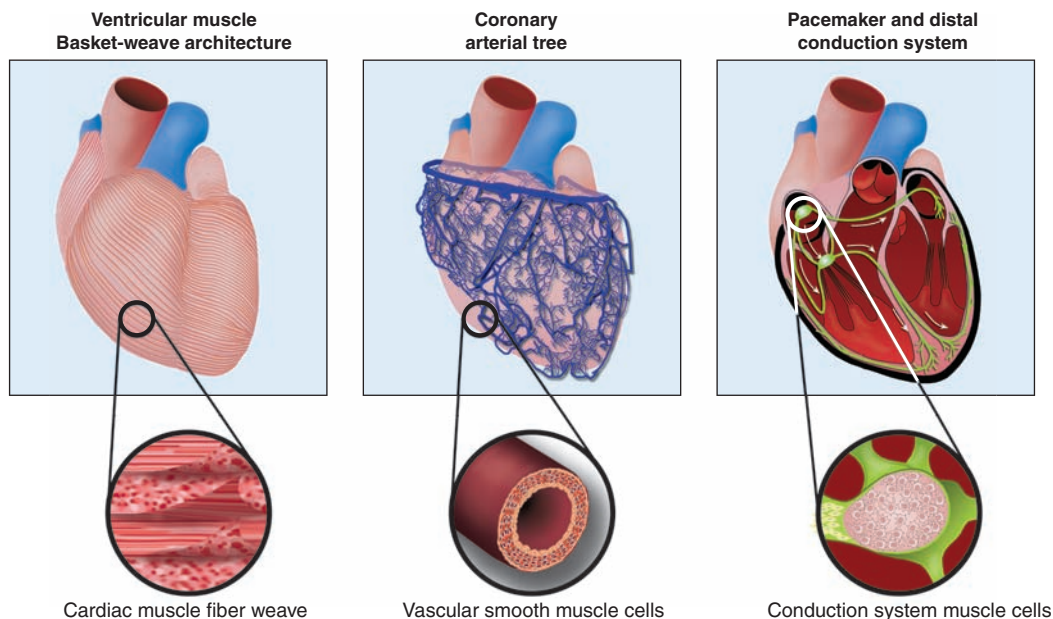


Fig. 3. Three-dimensional structure of ventricular muscle basket weave, coronary arterial tree, and pacemaker and conduction system. One of the central challenges of cell-based therapy for regenerating specific heart components is guiding transplanted cells into a functional syncytium with the existing three-dimensional architecture. Transplanted cells must make functional connections with neighboring specialized heart cells to result in a net gain of global function. Transplanted myogenic progenitors, for example, must align with and integrate into the existing ventricular muscle basket weave to allow synchronous contraction and relaxation of graft and host myocardium. Integration of pacemaker and conduction system progenitors into the appropriate tissue type is necessary to generate a biological pacemaker and avoid cardiac arrhythmia. For example, having a transplanted heart muscle progenitor integrate into the conduction system might have arrhythmogenic consequences, as would the introduction of cells with independent pacemaker potential in the heart. Similarly, cell-based therapies to promote coronary collateral formation or neo-arteriogenesis require functional integration of transplanted cells with the host coronary arterial tree.

be carefully controlled to insure the proper rotation and positioning of the aorta and pulmonary artery as they form a junction with the heart itself. The precise positioning of the aorta over the left ventricular chamber and the pulmonary artery over the right ventricular chamber is one of the most critical steps in cardiogenesis. Defects in this process are the most common cause of human congenital heart disease, and a growing body of evidence suggests that the *Isl1*-derived heart progenitors play a pivotal role. Although relatively little is known regarding how special cues control cell proliferation, recent advances from several laboratories have suggested that Wnt/ β -catenin pathways appear to play a critical role in the expansion of *Isl1* cardiac progenitors and their differentiated progeny in the right ventricle and the outflow tract. Gain-of-function mutations of β -catenin in *Isl1* progenitor lineages result in a massive expansion of the progenitor pool *in vivo* (36–38). Thus, defining the non-cell-autonomous cues that regulate *in vivo* cardiogenesis will be of critical importance to understanding normal development and generating the cell populations necessary for regenerative cardiovascular medicine. To that end, various combinations of FGF, BMP, and

Wnt signaling molecules have been used to promote cardiogenesis and expand cardiac progenitor populations in murine and human embryonic model systems (30, 31, 37).

Three-Dimensional Organizational Structure of Ventricular Muscle, Vascular Smooth Muscle, and Conduction System Muscle

Perhaps one of the most unexplored areas of cardiogenesis has been in understanding how differentiated cell types are assembled into the specific three-dimensional structures of the mature heart (Fig. 3). With regard to ventricular myocardium, a precise linear alignment of cardiac myocytes in alternating layers of muscle fibers forms a basket weave of muscle tissue and leads to a muscle fiber alignment designed to propel the blood forward through the outflow tract. This tissue alignment is evident at multiple levels, from the microscopic scale of sarcomere assembly up to the three-dimensional structure of the ventricular chamber (Fig. 4). In the failing heart, this cardiac muscle fiber linear alignment can be highly disorganized, with fibers emanating at angles within the same muscle cell layer, as well as be disrupted by tissue fibrosis. Given this loss of fiber organization, it is increasingly likely that the

transplantation of cardiac muscle progenitors or their differentiated progeny, in the absence of cues to drive their appropriate linear alignment with the native heart tissue, may not result in a substantive improvement in global heart function. Toward this goal, recent work suggests that coupling of myocytes to adjacent cells, tissues, and extracellular matrix results in external cues that shape ventricular myocytes architecture. These appear to be similar to the navigational cues that guide cell migrations and the formation of laminar layers that wrap around the ventricular cavities in the developed heart (39, 40). Whether these guidance cues are maintained in the mature heart is an important unanswered question because therapies based on the direct introduction of cardiogenic cells into the failing heart assume that transplanted cells will maintain this ability for intramyocardial pathfinding, differentiation, and functional integration into the host tissue (41).

Establishment and maintenance of blood flow through the epicardial coronary arteries and through the microcirculation, the small vessels that intercalate through the heart muscle itself, are critical for normal cardiac function and the prevention of heart failure (42, 43). The smooth muscle and endothelium of the coronary arterial tree are assembled into a labyrinth that effectively intercalates the entire myocardium, and relatively little is known about the guidance cues that drive this assembly (Fig. 3).

Similarly, the electrical conduction system has a characteristic three-dimensional structure where the heart beat is initiated in the sinoatrial node and travels through a series of modified conduction system muscle cells to carry the electrical impulse throughout the heart (Fig. 3). Understanding the pathways governing the normal development of these structures will also be critical in the application of biologically targeted approaches for cardiac regeneration.

The Road Ahead: Engineering Humanized Organ Model Systems

To unravel the biological complexity of embryonic cardiogenesis and its growing intersection with cardiovascular regenerative biology, novel model systems will be required in which the individual variables of progenitor cell type, extracellular matrix cues, two- and three-dimensional structure, and tissue function can be analyzed for their effects on the global physiological function

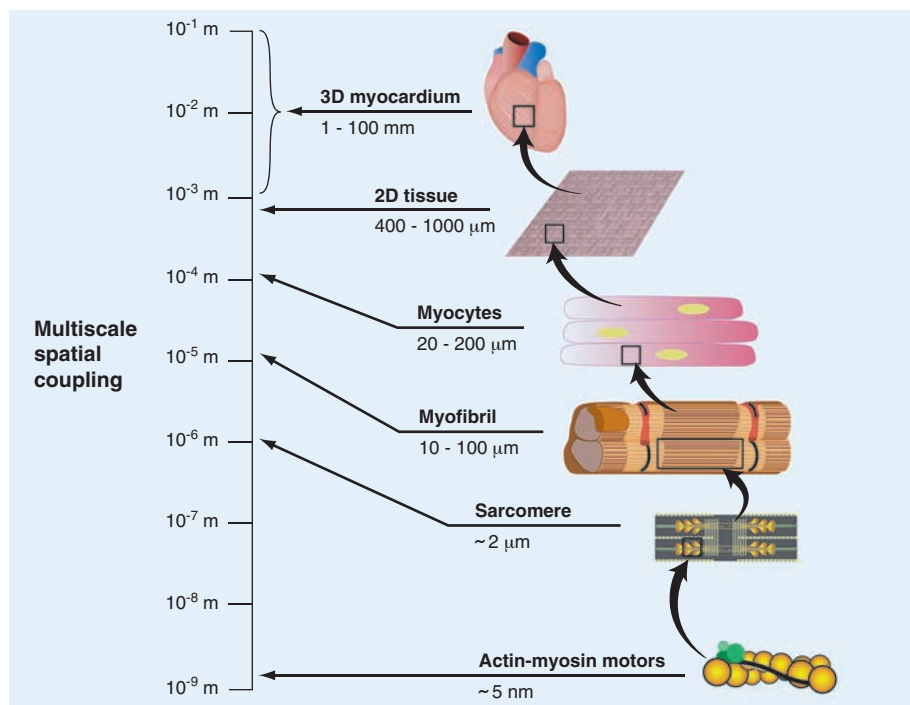


Fig. 4. Scaling of ventricular muscle. The assembly of ventricular muscle represents a scaling problem that spans several orders of spatial magnitude from the alignment of actin-myosin complexes within a sarcomere, their alignment in myofibrils, the organization of myofibrils in a myocyte, and the coupling between myocytes in anisotropic, laminar muscle. 2D and 3D indicate two- and three-dimensional, respectively.

of an intact organ. Whereas reconstructing the milieu of the entire multicellular heart will be difficult, recent advances suggest the possibility of engineering specific heart parts that correspond to the ventricular muscle, conduction and pacemaker systems, and aspects of vascular smooth muscle tissue (44–46).

To that end, one of the central challenges of cell-based therapy for the treatment of heart failure is the identification of the optimal cell type to drive robust cardiac myogenesis. The ideal cell type would be completely committed to the myogenic cell fate and yet maintain the capacity to expand in vivo or in vitro. In addition, it will be important for the cell type of interest to be able to differentiate into functional, force-generating myocardial tissue. To date, although a number of laboratories have identified multipotent cardiogenic precursors from ex vivo and in vitro sources in both mouse and human, no one has identified such a committed expandable myogenic precursor from a renewable source of cells. In addition to the identification of the appropriate cell type(s) for tissue regeneration, it will be important to define the three-dimensional structure to guide cell growth and differentiation. A complete reconstitution of cardiac muscle from a decellularized heart matrix has recently been shown, indicating that there may be specific matrix cues for the assembly of

heart progenitors and their downstream differentiated progeny (47).

Coupling tissue engineering technologies with state-of-the-art protocols for the generation of ES cell-derived heart progenitor-based systems holds great promise for a new era of cardiovascular regenerative medicine. The development of physiological assays for contractility, conduction, and mechanical work with patient-specific heart progenitors may allow the generation of heart muscle that harbors specific genetic backgrounds, facilitating the direct functional analysis of the role of specific genetic variations in human populations, as well as novel approaches for drug screening and development. In this regard, the rapid advances in the generation of inducible pluripotent stem (iPS) cells from somatic cells, such as skin cells, will clearly increase the value of having access to carefully phenotyped patient tissue. In the future, the development of patient-specific heart tissues from iPS cells might serve as prototypes for replacement parts that could be introduced in situ into diseased heart tissue components via advances in delivery device technology, ultimately offering an alternative to direct cell transplantation into the injured or disease myocardium. This may, in fact, mark a new era in which developmental biology and regenerative medicine converge to create human models of cardiovascular disease (34).

References and Notes

1. H. L. Mencken, "The divine afflatus," *A Mencken Chrestomathy* (Knopf, New York, 1949), p.443.
2. B. Assmus et al., *N. Engl. J. Med.* **355**, 1222 (2006).
3. V. Schachinger et al., *N. Engl. J. Med.* **355**, 1210 (2006).
4. J. G. Cleland, N. Freemantle, A. P. Coletta, A. L. Clark, *Eur. J. Heart Fail.* **8**, 105 (2006).
5. S. Dimmeler, A. M. Zeiher, M. D. Schneider, *J. Clin. Invest.* **115**, 572 (2005).
6. K. Lunde et al., *Scand. Cardiovasc. J.* **39**, 150 (2005).
7. S. Mansour et al., *J. Am. Coll. Cardiol.* **47**, 1727 (2006).
8. G. P. Meyer et al., *Circulation* **113**, 1287 (2006).
9. R. Passier, L. W. van Laake, C. L. Mummery, *Nature* **453**, 322 (2008).
10. P. C. Hsieh et al., *Nat. Med.* **13**, 970 (2007).
11. L. B. Balsam et al., *Nature* **428**, 668 (2004).
12. M. A. Laflamme, C. E. Murry, *Nat. Biotechnol.* **23**, 845 (2005).
13. C. E. Murry et al., *Nature* **428**, 664 (2004).
14. H. Oh et al., *Proc. Natl. Acad. Sci. U.S.A.* **100**, 12313 (2003).
15. D. Orlic et al., *Nature* **410**, 701 (2001).
16. M. Rota et al., *Proc. Natl. Acad. Sci. U.S.A.* **104**, 17783 (2007).
17. M. Rubart, L. J. Field, *Annu. Rev. Physiol.* **68**, 29 (2006).
18. R. R. Smith et al., *Circulation* **115**, 896 (2007).
19. S. Martin-Puig, Z. Wang, K. R. Chien, *Cell Stem Cell* **2**, 320 (2008).
20. S. M. Wu, K. R. Chien, C. Mummery, *Cell* **132**, 537 (2008).
21. D. J. Garry, E. N. Olson, *Cell* **127**, 1101 (2006).
22. A. Moretti et al., *Cell* **127**, 1151 (2006).
23. S. M. Wu et al., *Cell* **127**, 1137 (2006).
24. R. G. Kelly, N. A. Brown, M. E. Buckingham, *Dev. Cell* **1**, 435 (2001).
25. M. Buckingham, S. Meilhac, S. Zaffran, *Nat. Rev. Genet.* **6**, 826 (2005).
26. K. L. Laugwitz et al., *Nature* **433**, 647 (2005).
27. C. L. Cai et al., *Nature* **454**, 104 (2008).
28. B. Zhou et al., *Nature* **454**, 109 (2008).
29. C. L. Cai et al., *Dev. Cell* **5**, 877 (2003).
30. S. J. Kattman, T. L. Huber, G. M. Keller, *Dev. Cell* **11**, 723 (2006).
31. L. Yang et al., *Nature* **453**, 524 (2008).
32. L. Yang et al., *Development* **133**, 1575 (2006).
33. D. U. Frank et al., *Development* **129**, 4591 (2002).
34. E. J. Park et al., *Development* **135**, 3599 (2008).
35. J. Zhang et al., *Development* **135**, 3611 (2008).
36. C. Kwon et al., *Proc. Natl. Acad. Sci. U.S.A.* **104**, 10894 (2007).
37. Y. Qyang et al., *Cell Stem Cell* **1**, 165 (2007).
38. L. Lin et al., *Proc. Natl. Acad. Sci. U.S.A.* **104**, 9313 (2007).
39. K. K. Parker et al., *FASEB J.* **16**, 1195 (2002).
40. S. Huang, C. P. Brangwynne, K. K. Parker, D. E. Ingber, *Cell Motil. Cytoskeleton* **61**, 201 (2005).
41. L. W. van Laake, R. Passier, P. A. Doevendans, C. L. Mummery, *Circ. Res.* **102**, 1008 (2008).
42. K. Walsh, I. Shiojima, *J. Clin. Invest.* **117**, 3176 (2007).
43. S. Schiekofer et al., *Angiogenesis* **11**, 289 (2008).
44. A. W. Feinberg et al., *Science* **317**, 1366 (2007).
45. M.-A. Bray, S. Sheehy, K. Parker, *Cell Motil. Cytoskeleton* **65**, 641 (2008).
46. K. K. Parker, J. Tan, C. S. Chen, L. Tung, *Circ. Res.* **103**, 340 (2008).
47. H. C. Ott et al., *Nat. Med.* **14**, 213 (2008).
48. B. Zhou et al., *Nature* **454**, 109 (2008).
49. We thank A. Feinberg, Disease Biophysics Group, Harvard University, for help with Fig. 4.

10.1126/science.1163267

Origin of Stem Cells in Organogenesis

J. M. W. Slack

The development of individual organs in animal embryos involves the formation of tissue-specific stem cells that sustain cell renewal of their own tissue for the lifetime of the organism. Although details of their origin are not always known, tissue-specific stem cells usually share the expression of key transcription factors with cells of the embryonic rudiment from which they arise, and are probably in a similar developmental state. On the other hand, the isolation of pluripotent stem cells from the postnatal organism has encouraged the formulation of models of embryonic and postnatal development that are at variance with the conventional ones. Possible explanations for the existence of such cells, and the issue of whether they also exist *in vivo*, are discussed.

The body of an animal or human contains various populations of stem cells that sustain cell turnover in their respective tissues. Where do these stem cells come from? They must arise from the embryo—but the early embryo, before the stage of organ formation, does not contain stem cells. This apparent paradox arises from the conventional definition of a stem cell as an undifferentiated cell that can self-renew indefinitely and can give rise to at least one type of differentiated progeny. This definition was propounded nearly 30 years ago by Lajtha (1) in a theoretical paper that identified most of the key features of stem cell behavior that are considered important today. These included the distinction between stem cells (which are self-renewing) and transit-amplifying cells (which are destined to differentiate after a certain number of divisions); the occurrence of asymmetric divisions; the requirement that stem cells should self-renew for the lifetime of the organism; and the existence of stem cell niches [microenvironments formed by other cells that maintain stem cells—a concept introduced by Schofield (2)].

These properties are displayed by the adult stem cells of mammals such as those of the epidermis, the hematopoietic system, or the intestinal epithelium (3–7). However, the early embryo does not contain stem cells in this sense, because all the cells in the vertebrate embryo before the onset of organogenesis are destined to change their character as development proceeds. Embryonic stem (ES) cells grown in culture do show indefinite self-renewal, but their normal precursors within the embryo do not, as they soon turn into cells of the three germ layers: ectoderm, mesoderm, and endoderm. One particular example—the origin of hematopoietic stem cells in the mouse embryo—has been studied in detail, and it is known that cells capable of long-term repopulation of irradiated host animals are not present in the early em-

bryo and only arise after about 10.5 days of development (8).

Although the term “progenitor cell” has been less debated and less clearly defined, it carries the implication of cells in a transient state, destined eventually to become one or more differentiated types. By this definition, all mitotic cells found in the early embryo are progenitor cells, including the *in vivo* precursors of ES cells, which are located in the embryo’s inner cell mass or epiblast. The transit-amplifying cells of postnatal tissues in which there is a high level of cell turnover [“renewal tissues” (9)] are also progenitor cells. However, differentiated cells that divide slowly and simply reproduce themselves—such as pancreatic β cells or hepatocytes—might not be considered progenitor cells, as they are not progenitors to anything other than themselves. Definitions are of course arbitrary, and some authors prefer a definition of “stem cell” that is compatible with only a short-term existence. However, such a definition has the disadvantage of abolishing the

otherwise useful distinction between stem cells and progenitor cells.

Hierarchy in Development

The formation of tissue-specific stem cells is an aspect of organogenesis. So what is the relationship between the development of a specific tissue rudiment and the formation of the stem cells? Regional specification in embryonic development proceeds as a hierarchy. Starting from the blastula (or blastoderm or epiblast, depending on the species), any particular tissue rudiment or cell type is formed by a sequence of developmental decisions. This process is now understood in great detail. As an example, the progenitors of the β cells of the mammalian pancreas undergo a series of steps of developmental commitment to become definitive endoderm, foregut endoderm, dorsal or ventral pancreatic bud, endocrine precursor cell, and finally β cell (10) (Fig. 1). At each step, the production of a particular combination of transcription factors is activated or repressed in response to a particular extracellular signal, which may be composed of one or more substances (called “inducing factors” in an embryonic context). Each step leads to multiple pathways constituting a developmental “choice.” Different concentrations of the inducing factor will result in the activation or repression of genes encoding different transcription factors, and therefore the adoption of different developmental pathways. Repeated occurrence of this process enables an early embryo, consisting initially of a simple mass of similar cells, to develop autonomously into an organism with a very complex pattern of structures.

It is now clear that some tissues arise from more than one separate embryonic rudiment. This process is again exemplified by the pancreas, which

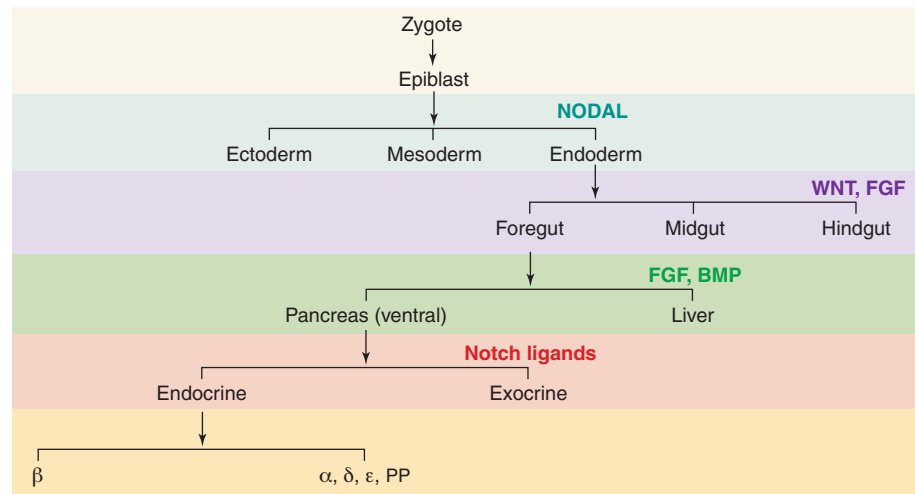


Fig. 1. The developmental hierarchy. This shows the normally accepted mode of formation of pancreatic β cells, involving six developmental steps, each controlled by one or more inducing factors. The inducing factors (NODAL, WNT, FGF, BMP, Notch ligands) are shown in color. The final step distinguishes the insulin-producing β cells from other types of endocrine cell also present in pancreatic islets (α , δ , ϵ , PP).

arises from two endodermal buds in mammals (three in birds) that have somewhat different transcription factor combinations at initial formation but become very similar once differentiated (10). This shows that there can be more than one route, in terms of intermediate developmental states, from the original progenitor cells to the final differentiated cell phenotype.

So how do stem cells fit into this hierarchical scheme? I have argued that the stem cell state arises as the final developmental decision involved in creating a particular tissue type. This implies that tissue-specific stem cells will be in a similar state of developmental commitment to the embryonic rudiment that produced them (11) (Fig. 2). This hypothesis is not yet proved. To prove or refute it will require detailed comparisons of transcriptional profiles from pure embryonic rudiments and pure populations of the corresponding tissue-specific stem cells. Collection of this material is very challenging. However, a number of studies on mice indicate that key developmental transcription factors are essential both to the formation of a specific rudiment and to the maintenance of the resulting stem cell population. For example, Sox2 is a transcription factor that determines the properties of both the embryonic neuroepithelium and the postnatal neuronal stem cells (12, 13). Runx1 is required for both the initial formation of the hematopoietic tissue in the dorsal aorta and the maintenance of adult hematopoietic stem cells (14). Cdx2 is required to specify the intestine in the embryo as well as to maintain intestinal stem cell zones in the adult (15). p63 appears when embryonic epithelia become stratified and remains critical for controlling the properties of squamous epithelia and of keratinocyte stem cells (16, 17). Sox9 has recently been shown to be expressed in a specific cell population of the epidermal placodes that form hair follicles in the embryo. It is also required for maintenance of the postnatal stem cells, which are located in the bulge region of the follicle (18). [In this case, data from cell lineage labeling experiments (18) and grafting experiments (19) indicate the distinct origin of hair follicle and interfollicular stem cells.] One recent counterexample concerns the development of the anterior pituitary gland, where a nestin-positive cell derives independently of the corresponding embryonic progenitors and has a different transcription factor profile (20). This example again illustrates that the same specific differentiated cell type may arise through more than one developmental pathway. Whether any other tissues have stem cell populations distinct from the main embryonic rudiment is an open question.

To settle the precise origin of each specific stem cell population, it will be necessary to obtain better cell lineage data by labeling specific cell populations at the tissue rudiment stage, and then determining whether the stem cells are labeled at later stages. Such studies would normally use the

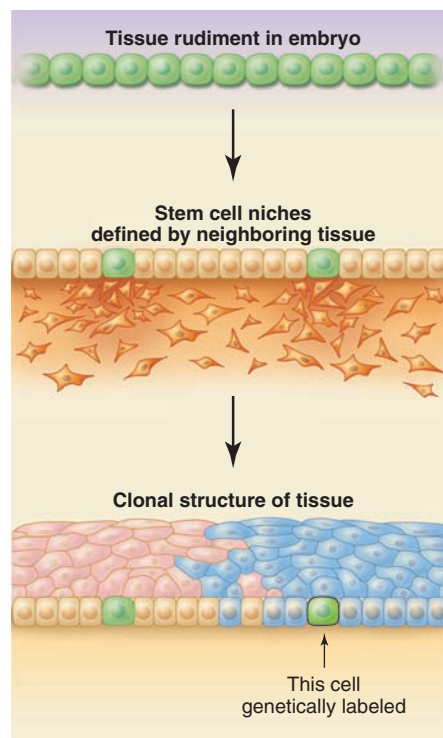


Fig. 2. Formation of stem cells in a tissue rudiment. In this hypothetical model, a few cells permanently retain their embryonic qualities because they lie in stem cell niches. Green represents cells in the embryonic tissue rudiment developmental state. Some of these are preserved as tissue-specific stem cells because of signals provided by neighboring mesenchymal cells (orange). These signals define stem cell niches. The rest differentiate to become a simple cuboidal epithelium, which later becomes a stratified epithelium maintained by production of cells from the stem cells. In such a tissue, labeling of a single stem cell (for example, by retroviral insertion) will label a domain of the tissue consisting of all the progeny of that stem cell.

CreER-lox method (21), which requires construction of transgenic mice containing two components: a gene encoding a hormone-activated DNA recombinase (CreER) driven by a tissue-specific promoter, and a reporter gene whose expression is activated by Cre-mediated excision of an inhibitory DNA segment. When the synthetic estrogen tamoxifen is given to the mice, the CreER becomes active and, in the cells where it is present, excises a segment from the reporter transgene, thereby activating production of the reporter protein and labeling the cells and all their descendants in a permanent manner (Fig. 3). The cells labeled are only those that had the tissue-specific promoter active at the time of the tamoxifen administration, rather than before or after. This is a very useful method, but it relies on high fidelity and specificity of the promoter used to drive the CreER. It is likely that some completely new method of cell lineage tracing will be needed to finally resolve such complex problems

as the origin of tissue-specific stem cells. It should also be borne in mind that some tissues (such as the heart, many glands, and connective tissue structures) show very little self-renewal in postnatal life (9), and in such cases there may not be a stem cell population at all.

The Problem of Pluripotent Adult Stem Cells

The conventional view of development as a hierarchy of decisions (Fig. 1) is generally accepted by researchers working with well-characterized tissue-specific stem cells or with ES cells. But there is another group of stem cell biologists who, explicitly or implicitly, do not accept the developmental biology consensus. Instead, they hold a view that all or most tissues in the body are continuously turning over and that the source of cells is one or more pluripotent stem cell populations—located in the bone marrow or elsewhere—that can circulate around the body and turn into multiple cell types, depending on the local environment. This view was expressed by Zipori (22), who started from the presumption that there are pluripotent adult stem cells throughout the body and preferred to define stem cell status by plasticity rather than by long-term self-renewal. Comparable models have been proposed by other authors (23, 24), who have also tended to be sympathetic to the idea that tissue-committed stem cells could “transdifferentiate” into other tissue types upon transplantation. This has now been experimentally disproved, except perhaps in very rare instances (25), although some very remarkable cell fusion events do occur after bone marrow transplantation and can involve profound respecification of gene expression by the donor cell nucleus (26, 27). Here, my intent is not to revisit the “transdifferentiation” debate but rather to consider the logically distinct proposition of whether postnatal pluripotent cells exist.

There have been numerous reports of pluripotent cells isolated from the postnatal organism. Such cells are reported to have a developmental potency much wider than that of tissue-specific stem cells and in some cases approaching that of ES cells. For example, mesenchymal adult progenitor cells (MAPCs) are described as cells isolated from the mesenchymal stem cells (MSCs) of mouse, rat, or human bone marrow that can be expanded without limit and are able to turn into most cell types of the body (28). Marrow-isolated adult multilineage inducible (MIAMI) cells are a population from human bone marrow reported to form neurons and pancreatic islet-like structures as well as the usual mesenchymal derivatives (29). Pluripotent stem cells (PSCs) can be isolated from many tissues of mice (30) and are reported to turn into muscle, adipose tissue, and neurons under suitable conditions. Tissue-committed stem cells (TCSCs) from the bone marrow of mice and humans (31) are reported to be derived from a precursor population of pluripotent cells capable

of forming most cell types. MSCs from human adipose tissue (32) are described as fibroblastic cells that adhere to plastic and have been reported to turn into a wide variety of cell types in vitro, including neurons, cardiomyocytes, hepatocytes, and pancreatic cells. Skin-derived precursors (SKPs) are isolated from dermis of rodents and humans and grow as floating spheres in neurosphere medium (33). They are described as differentiating into neurons, glia, smooth muscle, or adipocytes under appropriate culture conditions. In addition to pluripotent cells from postnatal organisms, there are also many reports of similar cells isolated from fetal sources such as placenta, umbilical cord, amniotic fluid, or fetal tissues (34–38).

Although some of these cell types have proved impossible to isolate in laboratories other than those producing the original work, the collective body of work is substantial enough to indicate that cells of wide potency can be grown in vitro from postnatal organisms. Possible in vivo precursors include the pericytes that are found on the outer surface of blood vessels (39). However, at present there is no definitive evidence that such cells exist in vivo. To prove that they do, it would be necessary to label one cell in situ and show that it formed a clone colonizing many tissue types. This could perhaps be done by means of retroviral labeling in vivo, a technique that can permanently label clones of cells at random (40, 41).

If pluripotent cells do not exist in the normal postnatal organism, then they must arise during in vitro culture. This presumably means that they spontaneously undergo changes similar to those seen during the formation of induced pluripotent stem (iPS) cells. These are cells that have been reprogrammed to a state similar to that of ES cells by the introduction of a small number of specific transcription factors (42, 43). Under the right conditions, overexpression of transcription factors known to be important in controlling the pluripotent state of ES cells (such as Oct4, Sox2, and Nanog) can reprogram differentiated cells to pluripotency in a permanent manner. However, iPS colony formation is a rare event, with a frequency between 10^{-2} and 10^{-6} depending on the starting cells and the particular genes introduced. This suggests that an unusual combination of stochastic events is necessary in addition to overexpression of the necessary genes. In the absence of overexpression of the pluripotency-

inducing transcription factors, production of a pluripotent cell would require even more events to occur spontaneously and simultaneously, which must be very rare indeed. It may well be that such cells could be isolated by using highly selective growth conditions over months of culture. However, some pluripotent cells—for example, the SKPs—can be isolated more quickly and reproducibly than this [e.g., (44)], which suggests that they do have some sort of in vivo counterpart.

Because the explicit or implicit beliefs associated with postnatal pluripotent stem cells pose a direct challenge to the orthodox models of current developmental and stem cell biology (Fig. 4), it is worth considering possible explanations for their existence. The pluripotent cells might be some type of neural crest cell, as the neural crest is an embryonic cell population that does seem to undergo a more stochastic type of differentiation than other embryonic progenitor cells. Alternatively, they might be some kind of “embryonic

remnant” comprising pluripotent cells left over from the early embryo.

The contention that some pluripotent adult stem cells are actually neural crest cells is not new. Indeed, several groups have isolated “neural crest stem cells” from various tissues: fetal sciatic nerve (45) and adult gut (46), heart (47), and skin (33, 48). Some aspects of the development of the neural crest follow the model of Fig. 1, especially its initial formation and the control of differentiation by inducing factors. However, the range of differentiated cell types that can be formed is very wide, and there seems to be an element of stochasticity in the differentiation process that is not so apparent in other parts of the embryo. The in vivo potency of individual neural crest cells has been studied by clonal labeling (49–51). This shows that there are many multipotent cells in the crest before migration. During migration, their numbers and degree of multipotency decline, although at least some degree of multipotency is retained by some cells throughout the

process. Neural crest cells become programmed to differentiate as a result of exposure to various inducing factors during their migration (52), but the stochastic nature of responses is shown by the fact that neighboring cells become committed at different times and can do different things.

There is evidence of a neural crest origin for at least two classes of relevant cell: SKPs and bone marrow MSCs. In the head of the mouse embryo, SKPs can be labeled by *wnt1-Cre*, a marker of cranial crest (53), and they also retain expression of various crest-type genes. They are at their most numerous in the late embryo, and numbers fall postnatally. The skin normally contains various neural crest derivatives, including melanocytes and Merkel cells, so it is not surprising that some precursors of these cell types may persist into the postnatal period. A labeling study that used the neural crest markers *sox1-Cre* and *P0-Cre* suggests that at least some of the MSCs found in murine bone marrow are of neural crest origin (54). Again the labeled cells declined in frequency after birth, and it seems that very few of the MSCs in bone marrow of older animals are neural crest-derived.

These labeling studies are suggestive rather than conclusive. Because Cre is expressed whenever its promoter is active, the cells would become labeled even if they had come from a non-neural crest source, so long as the

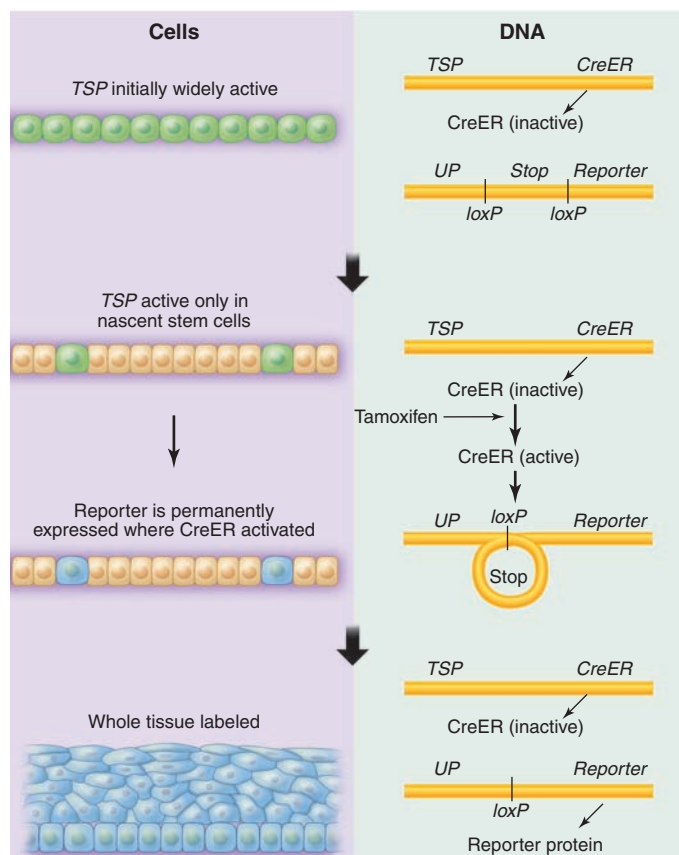


Fig. 3. The CreER labeling method (21). This requires the production of mice containing two transgenes, as shown in yellow. *TSP* represents a tissue-specific promoter, so the CreER protein is present in all cells where *TSP* is active (green). When the synthetic estrogen tamoxifen is given to the mice, the CreER becomes active and can excise DNA sequences lying between *loxP* sites. This has the effect of activating production of a reporter gene, which is driven by *UP* (a ubiquitous promoter). The reporter remains active in all progeny of the labeled cells. If stem cells are labeled, then this will result in the permanent labeling of the whole tissue that they maintain.

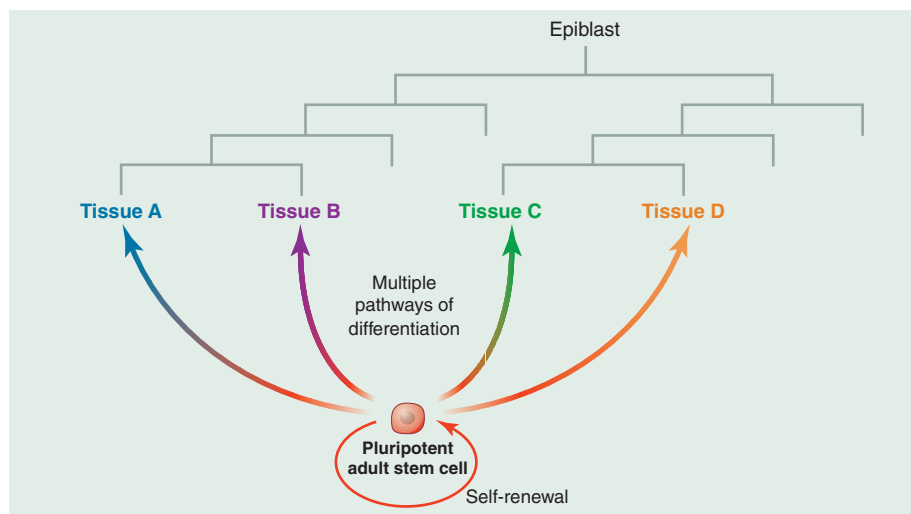


Fig. 4. The hypothetical postnatal pluripotent stem cell. The upper part represents the conventional account of development of four tissues; the lower part represents an entirely different view based on the existence of pluripotent adult stem cells. Not shown is the spatial pattern of the embryo, which is accounted for by the first model but not by the second.

appropriate promoter was activated at some stage during their formation. More definitive results could be obtained with the use of a hormone-inducible Cre, as discussed above (Fig. 3), that can confine the labeling to a specific developmental period (21).

The concept of embryonic remnants has a long history and was originally proposed as an explanation for the origin of cancer (55). There are many of types of visible embryonic vestiges that may be found in some individuals, such as remnants of Rathke's pouch, the thyroglossal duct, the urachus, the notochord, and so on (56). Smaller, and therefore less easily visible, cell clusters or persistent individual cells might be even more common and need not generate visible pathology. It is possible that some epiblast cells may lie beyond the reach of the earliest inducing signals and persist in an ES-like state. These might become incorporated into the amnion or extraembryonic endoderm, later finding their way into the bloodstream and returning to the embryo proper. They need not occur in all individuals and could be very rare when they do occur. They could be impossible to identify by conventional microscopy, yet be isolatable when a high degree of selection is imposed by tissue culture. With time, such cells would probably lose their pluripotent character or die off.

This would explain some of the less publicized properties of postnatal pluripotent stem cells: They tend to be difficult to isolate, are more common in younger animals, and show a lesser potency than ES cells. One argument against this view comes from the anatomical distribution of germ cell tumors (including teratomas). This type of tumor might be expected to arise from misplaced pluripotent cells. However, they are mostly found in the gonads and along the embryonic

migration routes of the primordial germ cells rather than elsewhere in the body (57). Having said this, there are also some germ cell-type tumors arising in the brain (pineal and neurohypophyseal regions) that cannot easily be explained as originating from primordial germ cells (58).

In summary, the well-characterized stem cells in the postnatal organism are the tissue-specific stem cells. These are believed to arise in their respective rudiments during embryonic development as the end product of a hierarchy of decisions controlled by inducing factors, and are defined by the expression of a particular combination of developmental transcription factors. But to fully understand the origin of tissue-specific stem cells, we need better cell lineage data. Pluripotent stem cells can be isolated from postnatal organisms but may not exist *in vivo*, and if they do, they are not necessarily involved in normal development or tissue turnover.

References

1. L. G. Lajtha, *Differentiation* **14**, 23 (1979).
2. R. Schofield, *Blood Cells* **4**, 7 (1978).
3. P. L. Krohn, *Proc. R. Soc. London Ser. B* **157**, 128 (1962).
4. D. E. Harrison, *Proc. Natl. Acad. Sci. U.S.A.* **70**, 3184 (1973).
5. M. Kondo et al., *Annu. Rev. Immunol.* **21**, 759 (2003).
6. C. Blanpain, E. Fuchs, *Annu. Rev. Cell Dev. Biol.* **22**, 339 (2006).
7. N. Barker, M. van de Wetering, H. Clevers, *Genes Dev.* **22**, 1856 (2008).
8. S. H. Orkin, L. I. Zon, *Cell* **132**, 631 (2008).
9. C. P. Leblond, *Natl. Cancer Inst. Monogr.* **14**, 119 (1964).
10. K. S. Zaret, M. Grompe, *Science* **322**, 1490 (2008).
11. J. M. W. Slack, *J. Theor. Biol.* **114**, 463 (1985).
12. V. Graham, J. Khudyakov, P. Ellis, L. Pevny, *Neuron* **39**, 749 (2003).
13. V. Episkopou, *Trends Neurosci.* **28**, 219 (2005).
14. T. E. North, T. Stacy, C. J. Matheny, N. A. Speck, M. F. T. R. de Bruijn, *Stem Cells* **22**, 158 (2004).

15. D. G. Silberg, G. P. Swain, E. R. Suh, P. G. Traber, *Gastroenterology* **119**, 961 (2000).
16. M. I. Koster, S. Kim, A. A. Mills, F. J. DeMayo, D. R. Roop, *Genes Dev.* **18**, 126 (2004).
17. G. Pellegrini et al., *Proc. Natl. Acad. Sci. U.S.A.* **98**, 3156 (2001).
18. J. A. Nowak, L. Polak, H. A. Pasolli, E. Fuchs, *Cell Stem Cell* **3**, 33 (2008).
19. H. Oshima, A. Rochat, C. Kedzia, K. Kobayashi, Y. Barrandon, *Cell* **104**, 233 (2001).
20. A. S. Gleiberman et al., *Proc. Natl. Acad. Sci. U.S.A.* **105**, 6332 (2008).
21. A. L. Joyner, M. Zervas, *Dev. Dyn.* **235**, 2376 (2006).
22. D. Zipori, *Stem Cells* **23**, 719 (2005).
23. H. M. Blau, T. R. Brazelton, J. M. Weimann, *Cell* **105**, 829 (2001).
24. M. Kucia et al., *Leukemia* **19**, 1118 (2005).
25. A. J. Wagers, I. L. Weissman, *Cell* **116**, 639 (2004).
26. J. M. Weimann, C. B. Johansson, A. Trejo, H. M. Blau, *Nat. Cell Biol.* **5**, 959 (2003).
27. X. Wang et al., *Nature* **422**, 897 (2003).
28. Y. Jiang et al., *Nature* **418**, 41 (2002).
29. G. D'Ippolito et al., *J. Cell Sci.* **117**, 2971 (2004).
30. J. C. Howell et al., *Ann. N.Y. Acad. Sci.* **996**, 158 (2003).
31. M. Z. Ratajczak, M. Kucia, M. Majka, R. Reca, J. Ratajczak, *Folia Histochem. Cytobiol.* **42**, 139 (2004).
32. A. Schaffler, C. Buchler, *Stem Cells* **25**, 818 (2007).
33. K. J. L. Fernandes, J. G. Toma, F. D. Miller, *Philos. Trans. R. Soc. London Ser. B* **363**, 185 (2008).
34. P. De Coppi et al., *Nat. Biotechnol.* **25**, 100 (2007).
35. A. R. Prusa, E. Marton, M. Rosner, G. Bernaschek, M. Hengstschlager, *Hum. Reprod.* **18**, 1489 (2003).
36. D. L. Troyer, M. L. Weiss, *Stem Cells* **26**, 591 (2008).
37. O. Parolini et al., *Stem Cells* **26**, 300 (2008).
38. W. A. Kues, B. Petersen, W. Mysegades, J. W. Carnwath, H. Niemann, *Biol. Reprod.* **72**, 1020 (2005).
39. L. da Silva Meirelles, A. I. Caplan, N. B. Nardi, *Stem Cells* **26**, 2287 (2008).
40. J. R. Sanes, *Trends Neurosci.* **12**, 21 (1989).
41. J. Price, D. Turner, C. Cepko, *Proc. Natl. Acad. Sci. U.S.A.* **84**, 156 (1987).
42. K. Takahashi et al., *Cell* **131**, 861 (2007).
43. J. Yu et al., *Science* **318**, 1917 (2007); published online 19 November 2007 (10.1126/science.1151526).
44. K. J. L. Fernandes et al., *Nat. Cell Biol.* **6**, 1082 (2004).
45. S. J. Morrison, P. M. White, C. Zock, D. J. Anderson, *Cell* **96**, 737 (1999).
46. G. M. Kruger et al., *Neuron* **35**, 657 (2002).
47. Y. Tomita et al., *J. Cell Biol.* **170**, 1135 (2005).
48. M. Sieber-Blum, M. Grim, Y. F. Hu, V. Szeder, *Dev. Dyn.* **231**, 258 (2004).
49. M. Bronner-Fraser, S. E. Fraser, *Nature* **335**, 161 (1988).
50. E. Frank, J. R. Sanes, *Development* **111**, 895 (1991).
51. A. Collazo, M. Bronner-Fraser, S. E. Fraser, *Development* **118**, 363 (1993).
52. N. M. Shah, A. K. Groves, D. J. Anderson, *Cell* **85**, 331 (1996).
53. Y. Chai et al., *Development* **127**, 1671 (2000).
54. Y. Takahashi et al., *Cell* **129**, 1377 (2007).
55. J. Cohnheim, in *Lectures on General Pathology: A Handbook for Practitioners and Students* (New Sydenham Society, London, 1889), section II ("The Pathology of Nutrition"), pp. 746–821.
56. R. A. Willis, *The Borderland of Embryology and Pathology* (Butterworths, London, 1962).
57. J. W. Oosterhuis, H. Stoop, F. Honecker, L. H. J. Looijenga, *Int. J. Androl.* **30**, 256 (2007).
58. P. J. Scotting, *Neuropathol. Appl. Neurobiol.* **32**, 569 (2006).

10.1126/science.1162782

Morphogenetic Cell Movements: Diversity from Modular Mechanical Properties

Denise J. Montell

Animal tissue and organ development requires the orchestration of cell movements, including those of interconnected cell groups, termed collective cell movements. Such movements are incredibly diverse. Recent work suggests that two core cellular properties, cell-cell adhesion and contractility, can largely determine geometry, packing, sorting, and rearrangement of epithelial cell layers. Two additional force-generating properties, the ability to generate cell protrusions and cell adhesion to the extracellular matrix, contribute to active motility. These mechanical properties can be regulated independently in cells, suggesting that they can be employed in a combinatorial manner. A small number of properties used in combination could, in principle, generate a diverse array of cell shapes and arrangements and thus orchestrate the varied morphogenetic events observed during metazoan organ development.

The formation of complex organs requires the concerted development of groups of cells, including coordinated regulation of their shapes and movements. Many different types of cell movements occur during normal embryonic development, including those of interconnected cell groups, known as collective cell movements. A striking feature of such movements is their diversity: Cells move in clusters, strands, sheets, and tubes, in addition to the well-studied migrations of individual cells. The variety of such movements raises the question of whether they share common cellular and molecular mechanisms, and if so, how distinct morphologies and arrangements arise.

The dominant conceptual framework over the past 15 to 20 years for the regulation of cell motility during embryonic development and tumor cell dissemination has been the epithelial-to-mesenchymal transition (EMT) and its reverse. The idea is that polarized epithelial cells exhibit a high degree of cell-cell adhesion and are not motile, whereas mesenchymal cells exhibit little cell-cell adhesion and are often highly motile (1–4). Conversion of epithelial cells into mesenchymal cells is thought to result from down-regulation of E-cadherin gene expression by the transcriptional repressor Snail and its relatives and from up-regulation of cell/matrix interactions via integrins (1, 4). The mechanisms of integrin-mediated migration of individual mesenchymal cells are well-established (5), and thus the conversion of epithelial cells to mesenchymal cells is thought to render them motile.

The EMT framework works well to explain the conversion of stationary epithelial cells, such as cells of the neural tube, into individual migratory mesenchymal cells, such as neural crest cells. However, EMT does not describe the myriad other types of morphogenetic cell movements that drive embryonic development, as discussed below. In particular, this concept does not offer insight into collective cell movements because such cells by definition retain cell-cell adhesion while moving.

A great deal of work in model organisms such as flies, frogs, and fish, has resulted in the identification of many specific molecules that participate in signaling networks and cytoskeletal dynamics and thereby contribute to different types of collective cell movements (6). However, at times the molecules seem to confound rather than clarify. For example, fibroblast growth factor signaling pathways exert virtually opposite effects on different cell types: stimulating protrusion and migration in *Drosophila* tracheal cells but causing zebrafish cells to stop moving (7). Planar cell polarity takes a lead role in cell movements of gastrulation (8, 9) but a negligible one in others (10). So how do we organize all of this information?

In his treatise *On Growth and Form*, originally published in 1917, D'Arcy Thompson articulated the view that morphogenesis should be approached as a problem of mechanics, the branch of physics concerned with forces and motion (11). This highly original concept did not reach the mainstream and fell further out of favor as the notion of genetic control of morphogenesis emerged (12). However, recent studies, reviewed here revive the contention that mechanical forces are the fundamental shapers of cells and embryos. They further suggest that,

if used in a combinatorial manner, a small number of modular mechanical (i.e., force-generating) properties—namely cell-cell adhesion, cell-matrix adhesion, protrusion, and contractility—could orchestrate morphogenesis. Interpreting the functions of specific molecules and signaling pathways within the framework of the elementary forces that shape cells and tissues may provide an opportunity to unite the mechanical view of morphogenesis with modern molecular genetics and to explain the otherwise daunting variety of cell shapes, arrangements, and movements.

Developmental Cell Movements Are Diverse

The idea that developmental cell movements are diverse and can be distinct from EMT is illustrated with a few examples from *Drosophila* development. The early fruit fly embryo consists of a single layer of epithelial cells that the process of gastrulation converts into multiple layers via numerous and complex cell motions (13–15). One of these is known as germband elongation (Fig. 1A), which doubles the length the participating cell group (the germband) and reduces its width by half (16). At the tissue level, the effect is dramatic, but at the level of each individual cell, the movements are relatively subtle: Cells exchange neighbors in a directional manner, never losing their epithelial characteristics.

After gastrulation, cells that form the branched tubular network of the *Drosophila* tracheal system begin their extraordinary movements (Fig. 1B) [see also (17)]. Initially, ~80 cells on the surface of each half-segment of the embryo invaginate (18). Specific subsets become protrusive and actively migrate. The rest do not extend obvious protrusions but instead intercalate and thus lengthen and narrow the tube. During this process, tracheal cells retain their epithelial apical/basal polarization and adhere to one another; thus, they do not undergo EMT (6).

In the adult *Drosophila* ovary (Fig. 1C), morphogenetic movements occur that are distinct from those described above. The functional unit of the ovary is the egg chamber. Each egg chamber is composed of ~650 cuboidal epithelial follicle cells surrounding 16 germline cells. The germline cells include 15 nurse cells, which are support cells, and one oocyte, which develops into the egg. As oogenesis progresses, three distinct morphogenetic changes occur within the follicle cell epithelium (19). Most of the cells assume a columnar morphology (Fig. 1C), elongating their lateral cell surfaces while shrinking their apical and basal domains. Meanwhile, cells in the anterior half of the egg chamber flatten out into a squamous morphology. This transition requires the lateral membrane to shrink while the apical and basal surfaces expand. In contrast, cells at the anterior pole of the egg chamber (the border cells) cluster together, extend protrusions in between the nurse cells,

Department of Biological Chemistry, Center for Cell Dynamics, Rangos Building, Suite 450, 855 North Wolfe Street, Baltimore, MD 21205, USA. E-mail: dmontell@jhmi.edu

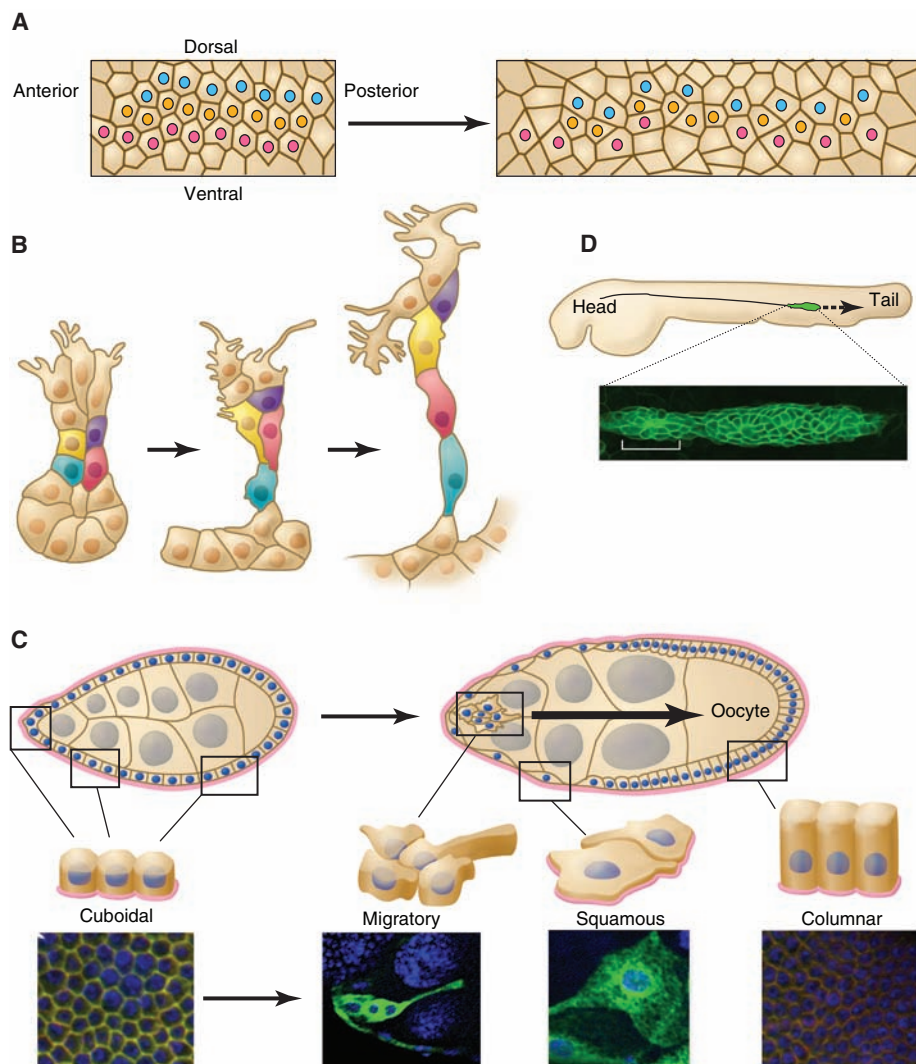


Fig. 1. Morphogenetic cell movements are diverse. **(A)** Schematic representation of germband elongation in the early *Drosophila* embryo. Three rows of cells are marked with colored dots to highlight their changes in position and shape. **(Right)** The same cells 30 min later. Individual cells intercalate, and the group lengthens and narrows. **(B)** Schematic drawing of one branch of the developing *Drosophila* tracheal tree at three time points. Cells at the tip exhibit obvious, elaborate protrusions whereas others do not. **(C)** Schematic representation of *Drosophila* follicle cell rearrangements during egg chamber development. Follicle cell nuclei, dark blue; nurse cell nuclei, gray; basement membrane, pink. At stage 7 of development (left), follicle cells are uniformly cuboidal in morphology. At stage 9 (right), follicle cells in different regions (boxed) undergo different morphological transformations. **(D)** Migration of the zebrafish lateral line primordium. **(Top)** Schematic of a fish embryo showing the overall migration path. **(Bottom)** Micrograph of migrating cells and one rosette (white bracket) being left behind.

detach from the rest of the epithelium, and then migrate as a cohesive cluster to the oocyte (20).

The morphogenetic movements described above do not resemble each other or EMT. Anterior follicle cells, for example, reduce cell-cell adhesion and expand their contact area with the basement membrane, alterations normally associated with EMT. Yet these cells do not leave the epithelium, migrate long distances, or change neighbors. Border cells, on the other hand, express a higher level of E-cadherin than do the squamous anterior follicle cells (21) and retain apical basal

polarity (22), properties usually associated with stationary epithelial cells. Yet, they invade the neighboring group of nurse cells, leave the follicle cell epithelium completely, and migrate.

Vertebrate embryos also exhibit collective cell movements that do not resemble classical EMT. One dramatic example is migration of the zebrafish lateral line. The lateral line is a group of ~100 cells that migrates down the length of the zebrafish embryo (Fig. 1D). A small group of leader cells provides direction to the followers, though most of the cells are actively motile (23).

Periodically, at the rear of the mass, a group of cells coalesces, stops moving, and is left behind to form a sensory organ. Motile cells of the lateral line exhibit some characteristics of epithelial cells, including apical/basal polarity, and other characteristics of mesenchymal cells, such as filopodial projections (7).

Some cells, such as neural crest cells and limb muscle precursors (24), undergo complete EMT, but as illustrated by the examples provided above, EMT does not provide an adequate conceptual framework for understanding collective cell movements. How then do groups of cells, some with features of both epithelial and mesenchymal cells, organize themselves in diverse and complex ways? The answer may lie in considering variations in the mechanical properties of cells.

Core Mechanical Properties Control Cell Geometry, Sorting, and Motility

To understand collective cell movements, we need to consider cell shapes, arrangement, and motility. Two cellular properties that repeatedly emerge as critical determinants of cell shape, packing geometry, and sorting are cell-cell adhesion and cell contractility (25–30). It has long been appreciated that quantitative and qualitative differences in cell-cell adhesion promote sorting of distinct cell types in vitro (31). For example, when cells expressing two different types of cell-cell adhesion molecules (such as E-cadherin and N-cadherin) are mixed together, they sort apart from one another. However, it is now becoming clear that surface tension, a property that depends on the opposing forces of both cell-cell adhesion and contractility of the cortical cytoskeleton, is likely to be a fundamental determinant of cell shape, packing, and sorting (26, 30, 32).

In a uniform, non-dividing epithelium, cells tend to form a hexagonal array that can be modeled mathematically by considering the forces of cell-cell adhesion and cortical contractility, acting in opposition (28). Whereas contractility (a constricting force exerted by myosin on the cortical F-actin cytoskeleton) acts to minimize a cell's contact surface with its neighbors, the effect of cell-cell adhesion is to increase it. An ordered hexagonal array of cells represents a ground state and an energy minimum in which these forces are balanced (28, 29). At a molecular level, cadherins contribute substantially to overall cell-cell adhesion in many embryonic cell types, and cortical F-actin and its associated myosin are major determinants of contractility. Recent atomic force measurements in zebrafish embryos provide direct evidence for this (30).

The introduction of an asymmetry in either adhesion or contractility would be expected to perturb the orderly hexagonal array of an epithelium. This is precisely the mechanism that drives directional cell intercalation during *Dro-*

Organ Development

sophila germband elongation. Cells of the early *Drosophila* embryo initially form a regular array (Fig. 2A) with symmetrical localization of myosin (33, 34), F-actin, and E-cadherin (8). However, during germband elongation, myosin becomes concentrated specifically on anterior and posterior surfaces and depleted from dorsal and ventral cell surfaces (Fig. 2B). This asymmetric myosin accumulation exerts a directional contractile force that preferentially shrinks particular sides of each cell (33) (Fig. 2C) and increases the disorder of the epithelium (8). As a result, instead of a fairly uniform hexagonal array, cells of the elongating germband exhibit a variety of polygonal shapes, some of which form clusters of four to seven cells that all meet at a vertex. These transient structures consistently resolve in a directional manner so as to promote the overall lengthening and narrowing of the cell sheet. These cell rearrangements fail if myosin activity is inhibited or remains uniformly distributed (33). Thus, enhancement of contractility in one region of a cell over another can yield directed cell rearrangement within the plane of the epithelium.

Competing forces of cell-cell adhesion and cortical contractility also determine the particular shapes of cone and pigment cells in the *Drosophila* eye. The eye is composed of repeating units of a defined number of cells. Within each unit, in a particular plane of cross section, two primary pigment cells surround four central cone cells and are in turn framed by secondary and tertiary pigment cells in a highly reproducible pattern. Beginning with random shapes, a computer simulation that allows the cells to reorganize so as to achieve an energy minimum recapitulates the precise cell shapes found in the wild-type eye (27). The simulations are based on a mathematical model that takes into account the balance of forces created by differential cell-cell adhesion and contractility of the cell cortex. This model reproduces both the beautiful regular wild-type pattern (Fig. 3) and altered shapes in a handful of mutant conditions (26). In contrast, models that account for only differential cell-cell adhesion, without considering membrane tension due to the contractility of the underlying cortical cytoskeleton, do not reproduce the proper patterns. In the future, we might hope that mathematical modeling and computer simulations will be powerful enough to account for the relative arrangements of cells in the cluster (in addition to cell shapes), starting from random values.

In early zebrafish embryos, the forces of cell-cell adhesion and cortical contractility have been measured directly for three different cell

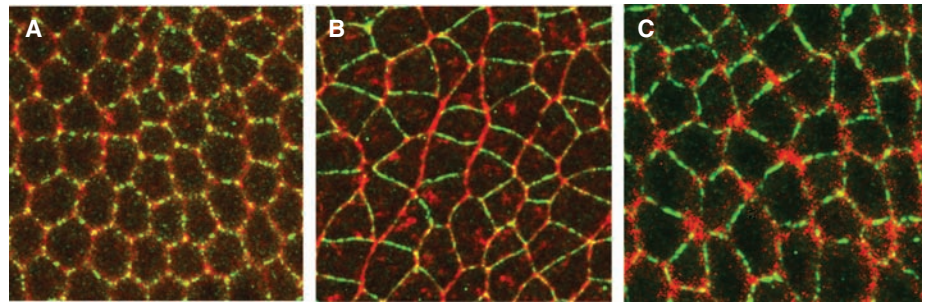


Fig. 2. Localized myosin drives cell shape changes and germband elongation. (A) At stage 6, before germband elongation, the epithelium is uniform, as are myosin (red) and bazooka (green). (B) During germband elongation, myosin II (red) accumulates specifically in anterior and posterior (vertical) membranes and is depleted from dorsal and ventral (horizontal) membranes. Bazooka localizes in a complementary pattern. (C) Membranes rich in myosin (red) shrink.

types, using atomic force microscopy (30, 35). Moreover, these measured values have been used in a mathematical model to predict cell sorting behavior. Both in vitro and in vivo tests of the model confirm that proper layering of ectoderm, mesoderm, and endoderm precursor cells can be predicted on the basis of their known adhesive and contractile properties, as long as extraembryonic cells that are normally present in the embryo are included in the simulation (30).

Whereas variation in cell-cell adhesion and cortical contractility is sufficient to determine geometry and sorting of cell types in the *Drosophila* eye and the zebrafish embryo, active cell motility requires an additional property, that of protrusion. The ability to extend and retract protrusions is an obvious feature of migrating border cells, tracheal tip cells, and the migrating lateral line, even though all of these cells retain epithelial character. In contrast, cells in the *Drosophila* germband are not protrusive, nor are cells in the developing eye. Tracheal cells that are not at the tip do not extend obvious protrusions, nor do the rosette cells that have stopped migrating at the back of the zebrafish lateral line. Border cells, tracheal tip, and mi-

grating lateral line cells migrate actively and directionally into neighboring tissues, whereas the cell types that lack protrusions do not. Therefore, although cells seem to be able to undergo local rearrangements within the plane of an epithelium in the absence of protrusions, directional migration is highly correlated with this property.

Variations in cell/matrix interactions are also apparent among different collective cell movements. In the egg chamber, for example, there is a basement membrane, produced by the follicle cells, that surrounds the whole structure (Fig. 1C). Border cells detach completely from it and discontinue production of matrix proteins such as collagen IV and laminin (36). In contrast, squamous cells increase their contact area with the basement membrane as they spread, and columnar follicle cells reduce their contact area although they remain attached.

Diversity from Combinatorial Use of Protrusion, Contractility, Cell-Cell Adhesion, and Cell-Matrix Adhesion Modules

At the molecular level, cell-cell adhesion, cell-matrix adhesion, cortical contractility, and cellular protrusions are modular properties controlled by largely different sets of molecules. Protru-

sion is driven by actin polymerization (37). Cell-cell adhesion is controlled by cadherins (38) and a variety of other molecules. Cell-matrix adhesion is regulated primarily by the interactions of integrins and their ligands (39), although other matrix components and receptors certainly contribute. Myosin and its regulators (such as Rho kinase) control contractility. There is evidence for cross talk between these modules (40, 41) through the actin cytoskeleton, which is probably important for coordinating these mechanical properties; however, it is also clear that each characteristic can vary independently among cell types (30).

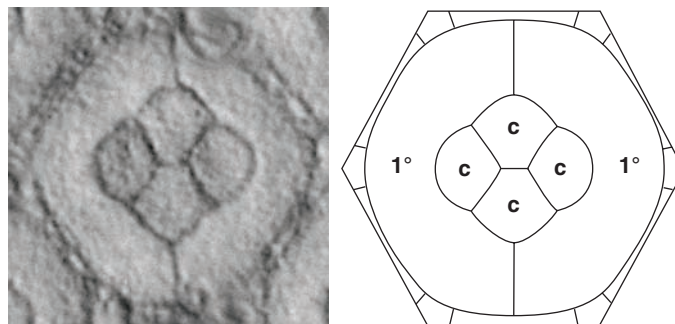


Fig. 3. Computer simulation reproduces cell shapes in the fly eye. (Left) Micrograph of a single unit in the *Drosophila* eye. (Right) Result of a computer simulation that starts with random cell shapes. Cells are allowed to change shape according to competing forces of cell-cell adhesion and cortical contractility. Four cone cells (c) are surrounded by two primary pigment cells (1°) that are, in turn, framed by secondary and tertiary pigment cells.

There are numerous examples in biology where small numbers of modular components are used in a combinatorial manner to generate complexity. In this way, four nucleotides (in combinations of three), generate 64 codons, and 20 amino acids combine together in various numbers to create hundreds of thousands of (and potentially many more) proteins. Similarly, cells may use a relatively small number of modular mechanical properties in various combinations to create diverse morphologies, arrangements, and movements. Simply varying four properties qualitatively, quantitatively, and spatially can result in hundreds of combinations, providing sufficient complexity to explain the





	Protrusiveness	Contractility	Cell-cell	Cell-matrix
 Cuboidal	–	++	++	++
 Border cells	+++	+++	+++	–
 Squamous	+/-	+/-	+/-	+++
 Columnar	–	++	++	+

Fig. 4. Distinct combinations of mechanical properties characterize follicle cells with different shapes and behaviors. The relative strengths of the indicated properties are deduced from experimental observation of the cells' interactions with each other, the distribution of cadherins, and genetic evidence. They have not been measured directly. Cell-cell and cell-matrix refer to adhesiveness.

diversity of observed cell geometries, topologies, and movements.

Different follicle cell types in the *Drosophila* ovary illustrate the concept of combinatorial use of mechanical properties to create diverse collective cell behaviors (Fig. 4). All of the cells start out in a uniform, cuboidal, hexagonal array. Border cells increase their expression of E-cadherin so as to adhere more strongly to each other (21). They extend long protrusions and require myosin activity to retract them (42, 43), and they down-regulate expression of matrix proteins (36). In contrast, squamous cells down-regulate expression of multiple cell-cell adhesion molecules, including E-cadherin, so as to adhere less well to one another, a prerequisite for their change in shape (19). These cells concomitantly expand their contact with the basement membrane, suggestive of elevated cell-matrix

adhesion. Their flat shape suggests reduced cortical tension, but this notion remains to be tested. Columnar follicle cells exhibit a distinct combination of properties: E-cadherin expression greater than that of squamous cells and less than that of border cells (19), cell-matrix contact less than that of squamous cells but greater than that of border cells, and no evidence of protrusiveness. The observed differences in expression of cadherin, cell shape, and motility are consistent with the idea that each cell type has a distinctive combination of adhesive, contractile, and protrusive mechanical properties (Fig. 3). In principle, this prediction could be tested directly, using atomic force measurements such as those obtained from cells of the early zebrafish embryo (30).

Conclusion

The great diversity of collective cell movements observed throughout development and organogenesis may result from combinatorial use of a small number of modular mechanical properties. EMTs represent a morphogenetic program that converts cells from one particular cell type (stationary columnar epithelial cells) into another cell type (individual mesenchymal cells). This particular transition involves a loss of cell-cell adhesion, up-regulation of cell-matrix adhesion, and increased protrusiveness and contractility. However, many other combinations of properties are possible, allowing cells to achieve a great diversity of individual cell shapes, as well as collective arrangements and movements. Cells with some properties of epithelial cells and some properties of mesenchymal cells may simply possess unique combinations of mechanical properties distinct from epithelial cells, mesenchymal cells, and other tissues.

Many interesting questions remain to be reviewed and investigated further. Key questions include how the myriad molecules and signaling pathways that regulate collective cell migration affect the core mechanical properties described here. It is probably generally the case that signaling pathways governing cell polarity (apical/basal, leading/lagging, and planar polarity) function to localize mechanical forces asymmetrally within cells. By definition, an asymmetry in force will cause dynamics. The mechanisms by which cell forces are coordinated in space and time represent another fascinating topic. By considering the effects of specific molecules and signaling pathways on the magnitude and direction of mechanical forces within and between cells, it may be possible to explain how individual cell shapes are achieved as well as how groups of cells sort and move, which, taken together, should go a long way toward explaining organ and tissue morphogenesis. Were he alive today, D'Arcy Thompson would probably be thrilled at the prospect of unifying molecular and cell biology with mechanics.

References and Notes

1. R. O. Hynes, A. D. Lander, *Cell* **68**, 303 (1992).
2. J. P. Thiery, *Curr. Opin. Cell Biol.* **15**, 740 (2003).
3. B. Baum, J. Settleman, M. P. Quinlan, *Semin. Cell Dev. Biol.* **19**, 294 (2008).
4. J. Yang, R. A. Weinberg, *Dev. Cell* **14**, 818 (2008).
5. E. A. Cox, A. Huttenlocher, *Microsc. Res. Tech.* **43**, 412 (1998).
6. M. Affolter, E. Caussinus, *Development* **135**, 2055 (2008).
7. V. Lecaudey, G. Cakan-Akdogan, W. H. Norton, D. Gilmour, *Development* **135**, 2695 (2008).
8. J. T. Blankenship, S. T. Backovic, J. S. Sanny, O. Weitz, J. A. Zallen, *Dev. Cell* **11**, 459 (2006).
9. C. Yin, M. Kiskowski, P. A. Pouille, E. Farge, L. Solnica-Krezel, *J. Cell Biol.* **180**, 221 (2008).
10. R. Bastock, D. Strutt, *Development* **134**, 3055 (2007).
11. D. A. W. Thompson, *On Growth and Form* (Cambridge Univ. Press, Cambridge, ed. 2, 1942), p. 1116.
12. R. C. Archibald, *Bull. Am. Math. Soc.* **24**, 403 (1944).
13. R. E. Dawes-Hoang et al., *Development* **132**, 4165 (2005).
14. P. E. Young, T. C. Pesacreta, D. P. Kiehart, *Development* **111**, 1 (1991).
15. M. Leptin, *Dev. Cell* **8**, 305 (2005).
16. K. D. Irvine, E. Wieschaus, *Development* **120**, 827 (1994).
17. P. Lu, Z. Werb, *Science* **322**, 1506 (2008).
18. R. J. Metzger, M. A. Krasnow, *Science* **284**, 1635 (1999).
19. M. Melani, K. J. Simpson, J. S. Brugge, D. Montell, *Curr. Biol.* **18**, 532 (2008).
20. D. J. Montell, P. Rørth, A. C. Spradling, *Cell* **71**, 51 (1992).
21. P. Niewiadomska, D. Godt, U. Tepass, *J. Cell Biol.* **144**, 533 (1999).
22. E. M. Pinheiro, D. J. Montell, *Development* **131**, 5243 (2004).
23. P. Haas, D. Gilmour, *Dev. Cell* **10**, 673 (2006).
24. F. Bladt, D. Riethmacher, S. Isenmann, A. Aguzzi, C. Birchmeier, *Nature* **376**, 768 (1995).
25. F. Pilot, T. Lecuit, *Dev. Dyn.* **232**, 685 (2005).
26. J. Kafer, T. Hayashi, A. F. Maree, R. W. Carthew, F. Graner, *Proc. Natl. Acad. Sci. U.S.A.* **104**, 18549 (2007).
27. S. Hilgenfeldt, S. Erksen, R. W. Carthew, *Proc. Natl. Acad. Sci. U.S.A.* **105**, 907 (2008).
28. R. Farhadifar, J. C. Roper, B. Aigouy, S. Eaton, F. Julicher, *Curr. Biol.* **17**, 2095 (2007).
29. R. Fernandez-Gonzalez, J. A. Zallen, *Curr. Biol.* **18**, R163 (2008).
30. M. Krieg et al., *Nat. Cell Biol.* **10**, 429 (2008).
31. M. S. Steinberg, *Science* **141**, 401 (1963).
32. G. W. Brodland, H. H. Chen, *J. Biomech. Eng.* **122**, 402 (2000).
33. C. Bertet, L. Sulak, T. Lecuit, *Nature* **429**, 667 (2004).
34. J. A. Zallen, E. Wieschaus, *Dev. Cell* **6**, 343 (2004).
35. A. J. Ewald, J. B. Wallingford, *Curr. Biol.* **18**, R615 (2008).
36. C. Medioni, S. Noselli, *Development* **132**, 3069 (2005).
37. T. D. Pollard, G. G. Borisy, *Cell* **112**, 453 (2003).
38. M. Takeichi, *Annu. Rev. Biochem.* **59**, 237 (1990).
39. R. O. Hynes, *Cell* **69**, 11 (1992).
40. A. Bershadsky, M. Kozlov, B. Geiger, *Curr. Opin. Cell Biol.* **18**, 472 (2006).
41. A. S. Yap, E. M. Kovacs, *J. Cell Biol.* **160**, 11 (2003).
42. M. Prasad, D. J. Montell, *Dev. Cell* **12**, 997 (2007).
43. T. A. Fulga, P. Rørth, *Nat. Cell Biol.* **4**, 715 (2002).
44. Funding was provided by NIH grants U54 GM064346 and R01GM73164. I would like to thank A. Ewald and the anonymous reviewers for their thoughtful comments. Special thanks to the reviewer who pointed me to D. A. W. Thompson's book, an inspiring work of literature, philosophy, and science. Many thanks also to D. Gilmour for the micrograph in Fig. 1D, J. Zallen for Fig. 2, and R. Carthew for Fig. 3.

Patterning Mechanisms of Branched Organs

Pengfei Lu and Zena Werb*

Branching morphogenesis is one of the earliest events essential for the success of metazoans. By branching out and forming cellular or tissue extensions, cells can maximize their surface area and overcome space constraints posed by organ size. Over the past decade, tremendous progress has been made toward understanding the branching mechanisms of various invertebrate and vertebrate organ systems. Despite their distinct origins, morphologies and functions, different cell and tissue types use a remarkably conserved set of tools to undergo branching morphogenesis. Recent studies have shed important light on the basis of molecular conservation in the formation of branched structures in diverse organs.

Branching morphogenesis is the process whereby a cell or a group of cells expands its surface area by forming cellular or tissue extensions during development. It was one of the most common processes in the emergence of organ systems as metazoans explored and adapted to previously untapped niches in nature. Various invertebrate and vertebrate organs (for example, fly trachea and mammalian salivary gland, lung, kidney, and mammary gland) (Fig. 1) undergo branching morphogenesis as an essential part of their ontogeny (1–3). Branching can occur in a single cell, such as a neuron as it forms short branches; or dendrites, to communicate with a myriad of other neurons and long branches; or axons, to relay nerve impulses to target tissues at a distance. Alternatively, branching can occur with a group of cells in the vasculature, where a network of blood vessels is formed to deliver oxygen and nutrients and remove metabolic wastes.

Historically, the mechanisms of branching and guidance of nerves and blood vessels have been well studied. Due to their structural simplicity and genetic accessibility, the *Drosophila* tracheal and air sac systems have given insight into understanding how epithelial branching occurs in the more complex organ systems of vertebrates (1, 4). With recent technical advances, including modern mouse genetics, cell fate-mapping, mosaic analysis, and live imaging of organ cultures, our understanding of vertebrate branching mechanisms has dramatically improved. One of the great surprises from

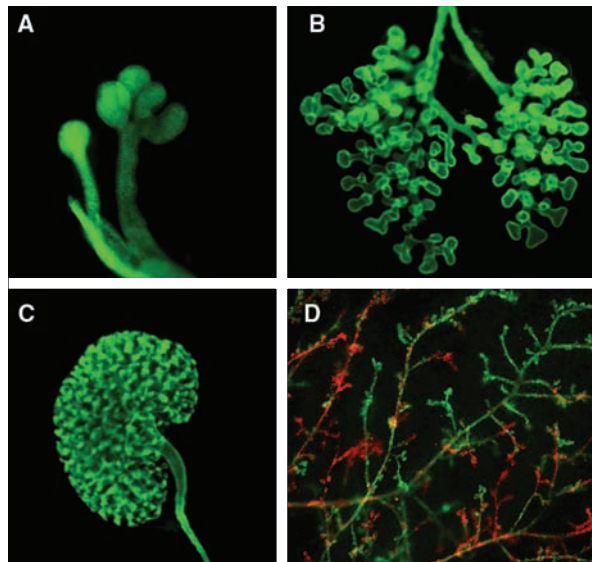


Fig. 1. Branching morphogenesis in mouse organs. (A to C) Immunofluorescent staining of E-cadherin in the branching epithelium of whole-mount salivary gland (A), lung (B) and kidney (C) from embryos at E13.5 to E15. (D) Branches of mammary epithelium derived from progenitors that were marked by expression of green and red fluorescent proteins as described previously (32).

these studies has been the realization that molecules essential for neuronal branching also play important roles in branching of invertebrate and vertebrate organs and the vasculature (3). Here, we review current understanding of the cellular and molecular mechanisms of branching morphogenesis. Comparison of the events underlying branching of different cell types has yielded insight into both emerging common themes and organ-specific mechanisms that render each of these cell and tissue types unique.

Mechanisms of Branching Morphogenesis

Different cells and tissues form branches with distinct branch patterns, defined by length, diameter, shape, and spacing. Yet, there are general themes in how branches are generated and main-

tained. It seems that there exists a branching “engine,” a special structure composed of either a single cell, a part of a cell, or a group of cells at the leading front of branch tips. This branching engine should be able to respond to an inductive signal that initiates, directs, and maintains branch outgrowth. The inductive signal must be subject to local and global regulation to achieve cell- or organ-specific branch patterns during development and remodeling processes.

Structure of the branching engine. More than a century ago, Ramón y Cajal described the growth cone, a highly specialized structure at the tip of chick neuronal axons (3). By forming actin-rich finger-like projections, or filopodia and sheet-like projections, or lamellopodia, the growth cone can respond to various guidance cues (Fig. 2A). Similarly, during vertebrate angiogenesis, migration of endothelial cells depends on tip cells, which lead trailing stalk cells as they colonize the avascular area of the embryo and form the vascular network (Fig. 2B). Likewise, in the embryonic *Drosophila* trachea, tip cells lead stalk cells as they invaginate from an epithelial sac and form the initial or primary branch (Fig. 2C). The tip cells of the primary branch are further elaborated by cellular extensions called secondary and terminal branches (5). At the late instar larval stage, the tracheal branches associated with the wing disc undergo further morphogenesis and give rise to the thoracic air sacs (1) (Fig. 2D). Again, tip cells at the migrating front send out filopodia and lamellopodia and play an important role in guiding stalk cells in a stereotypical direction (1).

In vertebrates, epithelial branching appears, at first glance, to be a relatively simple process, involving reiterative events of branch-point formation and duct elongation (also called the trunk or stalk). Branch points form through bifurcation [on rare occasions, trifurcation (6)] of the tip (also called the end bud or ampulla) or side-branching, whereby a group of cells buds out from duct epithelium. How these two modes of branch-point formation are deployed is organ-specific (6, 7) and presumably is genetically programmed. At the cellular level, vertebrate epithelial branching shows important differences from other branched systems. Unlike branch tips in the vasculature or fly trachea, those of vertebrate epithelium contain a heterogeneous and sometimes a multilayered cell population, as in the mammary gland (Fig. 2E) (8). Extensive cell proliferation is necessary for branching, especially in the tips (2, 8).

Inductive signals for branch initiation. A central event in branching morphogenesis is determining where to initiate a new branch. Remarkably, nerves, blood vessels, and epithelium all use growth factor ligands of the receptor

Department of Anatomy and Program in Developmental Biology, University of California at San Francisco, San Francisco, CA 94143–0452, USA.

*To whom correspondence should be addressed. E-mail: zena.werb@ucsf.edu

tyrosine kinase (RTK) family as inductive signals to form new branches. Neurons, for example, respond to the RTK ligand nerve growth factor (NGF), which is secreted by target tissues, for example, muscles, devoid of neuronal innervation (3) (Fig. 3). Likewise, endothelial cells are beckoned toward hypoxic tissues, which secrete the RTK ligand vascular endothelial growth factor (VEGF) during angiogenesis (3).

In the epithelium of both invertebrate and vertebrate branched organs, members of the fibroblast growth factor (FGF) family play a dominant role in branch initiation (2). In fly trachea and air sacs, for example, mesodermal cells express *Branchless* (*Bnl/Fgf*), which causes migration and branch initiation of adjacent epithelial

cells expressing the receptor *Breathless* (*Btl/Fgfr*) (4, 5). In addition to its role as a chemoattractant, *Bnl/Fgf* and its downstream events determine whether a cell becomes a tip cell or a stalk cell. Although all tracheal epithelial cells express *Btl/Fgfr* and respond to *Bnl/Fgf*, they compete for the ligand, and the cells with the highest *Bnl/Fgf* signaling activities become tip cells (9). Once tip cells have been determined, they are the only cells of the primary branch that depend on *Bnl/Fgf* signaling; the remaining stalk cells follow tip cells in a *Bnl/Fgf*-independent manner (9). Likewise, in both fly air sacs and the mammary gland, FGF signaling activity is necessary for cells to remain in the tip but not in the stalk or the duct (1, 10).

A major challenge for understanding vertebrate epithelial branching is the presence of a plethora of RTK ligands from the same or different families. These different RTK ligands can elicit collaborative, independent, or even opposing cellular behaviors, presumably depending on their specific downstream events during epithelial branching. In renal epithelium, beads soaked in either FGF (11) or glia-derived neural factor (GDNF) can induce ectopic branches (12). In addition, GDNF signaling is required for epithelial cells to remain in the tips of renal epithelium (12). These results suggest that FGF and GDNF signaling pathways may collaborate by acting in parallel or sequentially to regulate branch initiation and/or outgrowth in the kidney. On the other hand, in fly air sacs, FGF and epidermal growth factor (EGF) act independently. Thus, while FGF facilitates cell migration, EGF promotes cell proliferation of air sac cells (1). Finally, FGF7 and transforming growth factor α (TGF- α), a member of the EGF family, oppose one another during mammary epithelial branching (13).

Local and global regulation of branching patterns. The formation, maintenance, and subsequent outgrowth of a new branch are under extensive local and global regulation. Different tissues have the intrinsic ability to regulate the number of branches that form. In the fly trachea, the number of branches is regulated by mutual inhibition, whereby epithelial cells inhibit each other to take the leading position as they compete for branch-inducing factors. In both fly trachea and the vasculature, such mutual inhibition depends on Notch signaling (1, 9, 14) (Fig. 2, B and C).

Mutual inhibition also appears to be at work in the branching epithelium of vertebrates. It has long been recognized, for example, that mammary epithelial cells have self-avoidance properties. Thus, a new branch often starts off at a sharp angle and turns away or stops growing upon approaching another branch (15). In addition, when exogenous mammary epithelial cells are introduced into the mammary stroma, they can grow out and repopulate the whole gland, except in the presence of endogenous epithelium, which in-

hibits their growth. Indeed, in the mammary gland, epithelial geometry determines the potential branching sites due to self-inhibition (16). In this case, though, self-inhibition depends, at least in part, on TGF- β signaling activities (Fig. 2E). Finally, other extrinsic factors, including WNTs, hedgehogs (HHs) and bone morphogenetic proteins (BMPs), are expressed in the mesenchyme and play an important role in regulating branch initiation (2).

Because the embryonic mesenchyme and postnatal stroma are heterogeneous, it is not surprising that specific cell types participate in organ development. For example, in the mammary gland, macrophages, eosinophils, and mast cells all play a role in normal branching (17). It remains unclear, however, whether different cell populations control unique aspects of epithelial branching in vertebrate organs, for example, by secreting one or more extrinsic factors.

Finally, in many systems, including the fly trachea, the mammalian lung, large nerves, and blood vessels, branching patterns are highly conserved and stereotyped, suggesting that they are genetically programmed. Indeed, in mutant mice with reversed left-right asymmetry, the branching pattern of lung epithelium becomes the mirror image of that in the normal lung (7). For other branched organs, for example, the mammary gland and prostate, where branching is not stereotypical, branch patterns are still influenced by global physiological and/or hormonal status of the organisms. In the mammary gland, epithelial branching is regulated by growth hormone and estrogen (17), whereas in the prostate it is regulated by androgen (18).

Coordination of Branching Morphogenesis of Nerves, Blood Vessels, and the Epithelium

Branching morphogenesis of nerves, blood vessels, and the epithelium needs to be integrated, as manifested by their alignment along each other (3, 7, 19). But how is branching of different tissues coordinated during organ formation? Two effective ways of accomplishing this goal are communication between tissues and the use of common branch-regulating genes and pathways.

Communication between different tissues. It is well established that epithelial tissues attract endothelial cells and neuronal axons by secreting VEGF and NGF, respectively (Fig. 3). When *Vegf* is removed from lung epithelium, the vasculature develops abnormally (3). Likewise, disruption of NGF function or its gradient prevents neurons from innervating their target tissues (3). Conversely, endothelial cells are essential for specification and differentiation of the epithelium in the lung, pancreas, and liver (20); thus, they may play a role in epithelial branching as well. For example, lung endothelium secretes hepatic growth factor (HGF), which is essential for distal lung epithelial morphogenesis (3). Blood vessels and nerves also take advantage of one another to

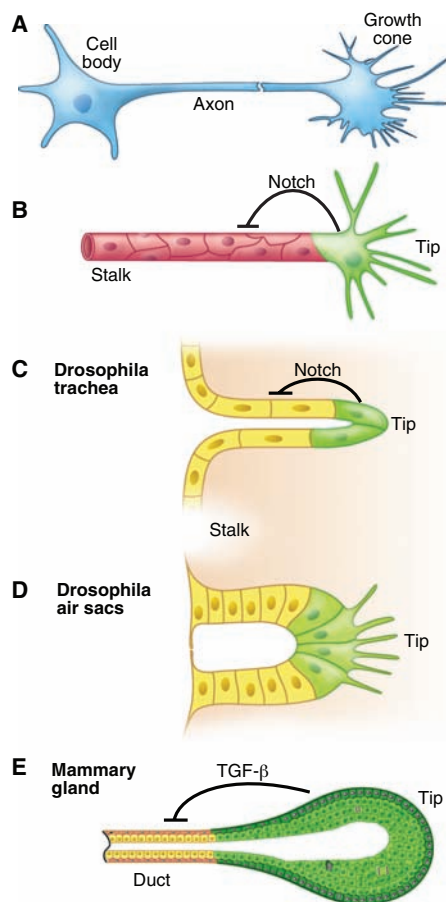


Fig. 2. Anatomy of the branching “engine.” A schematic presentation of various branched tissues: neuron (A), vasculature (B), *Drosophila* trachea (C) and air sacs (D), and mammary gland (E). Note the finger-like projections of the neuronal growth cone (A) and those of tip cells (green) of endothelium during angiogenesis (B) and *Drosophila* air sacs during larval development (D). To become tip cells, cells inhibit each other to take the leading position. In endothelium (B) and *Drosophila* trachea (C), mutual inhibition depends on Notch signaling. In the mammary gland, mutual inhibition depends on TGF- β signaling (E).

follow the same path. Endothelial cells produce molecules such as artemin and neurotrophin-3 (21) to attract axons to travel alongside the pioneer blood vessels, much like early axons guiding later axons. Likewise, nerves can produce various forms of VEGF and attract blood vessels to their side (Fig. 3).

Common genes and signaling pathways in branching tissues. Neurons rely on a small, well-conserved set of molecules to guide them toward their target tissues. Most of these guidance cues, belonging to four families, Slits, Netrins, Ephrins, and Semaphorins, can attract or repel axons (3). A major surprise is that members of all four families of axon guidance cues play roles in branching and guidance of the vasculature and invertebrate and vertebrate epithelium.

Robo4, a receptor for Slits, is expressed in the vasculature, and its activation causes repulsion of endothelial cells in vitro (21). Likewise, in the fly trachea, Slit and its receptors, Robo and Robo2, are expressed in the mesoderm and the adjacent epithelium, respectively. Interestingly, binding of Slit by Robo and Robo2, expressed in different branches, cause opposite reactions; whereas Slit attracts *Robo*-expressing epithelial cells, it repels *Robo2*-expressing ones (22). In the kidney, *Slit2* is expressed in the Wolffian duct from which the initial branch (i.e., ureteric bud) of renal epithelial network is induced. *Robo2* is expressed in the mesenchyme. Rather than directly guiding cell migration as in nerves, vessels, and fly trachea, *Slit2* regulates *Gdnf* expression and limits the number of ureteric buds that form. In the absence of *Slit2* or *Robo2*, the *Gdnf* expression domain expands and, as a result, ectopic ureteric buds form (12).

Other axon guidance cues also function in branched organs in a manner similar to or distinct from that in nerves. Like Robo4, the Netrin receptor *Unc5b* is expressed in endothelial tip cells. Its loss in mice causes aberrant extension of tip cell filopodia and excessive branching, which suggests that *Unc5b* normally represses endothelial branching in vivo (3). Consistent with these results, Netrin1 causes filopodial retraction when added to cultured endothelial cells (3). In contrast, in mammary epithelium, Netrin1 is required for cell adhesion. Thus, loss of either *Netrin1*, which is expressed in body cells of the tip, or its receptor *Neol1*, which is expressed in basal cap cells of the tip, the bilayered tip epithelium is not held together, so the tip collapses (23). Netrins and their receptors are also expressed in lung epithelium and may restrict side-branching (23).

Semaphorins signal through multimeric receptor complexes; whereas membrane-bound

semaphorins bind plexins, secreted forms bind the coreceptors neuropilins. In the vasculature, semaphorin-3a (Sema3a) represses branching by inhibiting lamellipodia formation of endothelial cells, which express various plexins and neuropilins (21). Likewise, in both the lung and kidney, *Sema3a* inhibits epithelial branching during organ formation (23, 24). However, in the salivary gland, *Sema3a* promotes branching by regulating cleft formation (25). Thus, the exact mode of *Sema3a* function in vertebrate organs remains unclear.

Ephrins and their Eph receptors are unusual in that ligand-receptor binding leads to bidirectional signaling: forward signaling in cells expressing Eph receptors and reverse signaling in those expressing the ligands. As in the nervous systems, EphrinB2 and its receptor EphB4 function as repellants in arteries and veins, respectively, and are essential for vessel maintenance by preventing intermixing of arterial and venous

must determine how these events are incorporated into branching morphogenesis. As a major source of branching regulators, mesenchyme and stroma are also essential for coordinating various aspects of vertebrate organogenesis (Fig. 4).

The instructive function of the mesenchyme during formation of several branched organs was first established by classic transplantation experiments. When combined with embryonic mammary mesenchyme, skin epithelium from mouse, or even chick or duck, embryos can be respecified to form mammary branches and milk-producing alveoli (17). The age and the differentiation state of the epithelium determine its plasticity to instructions from the mesenchyme. Thus, whereas cells of Rathke's pouch (future pituitary) epithelium from an embryonic day 8.5 (E8.5) mouse embryo can be respecified to form the salivary gland, those from an E12 embryo cannot (17). Moreover, although salivary gland mesenchyme can instruct embryonic mammary epithelium to form branches with patterns specific to the salivary gland, the grafts still retain the ability to form milk-producing alveoli (17). These results suggest that cell differentiation and branch pattern are differentially controlled by both intrinsic and extrinsic factors.

Stroma, which regulates epithelial differentiation and branching, plays an essential role in the stem cell biology of adult organs and is indispensable for organ homeostasis and regeneration in vertebrates (27, 28). The mammary gland is a nonvital organ that is readily accessible to experimental manipulations and thus is a valuable tool for understanding adult stem cell biology in vertebrates. When endogenous epithelium is surgically removed before puberty, the mammary gland

fatty stroma, which remains largely unoccupied by invading epithelium, can readily be used as a host to exogenous cells. This method has shown that a single mammary stem cell can regenerate the entire organ (29, 30). Remarkably, when testicular or neural stem cells are introduced along with mammary epithelial cells into mammary stroma, they form an epithelial branching network and differentiate as milk-producing cells (31). These results suggest the presence of a stem cell "niche" in the postnatal mammary gland, which contains essential signals that not only maintain mammary stem cells but can reprogram stem cells from other origins (Fig. 4).

Without definitive markers, it has been difficult to determine where stem cells are located in branched organs and how they are maintained throughout organ development. In the mouse mammary gland, stem cells are distributed throughout the organ and are not greatly affected

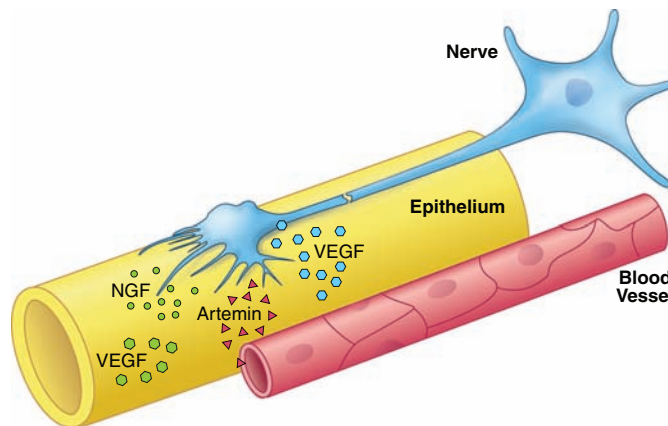


Fig. 3. Communication between epithelium, nerves, and blood vessels. Epithelium secretes NGF and VEGF (green) to attract nerves and vessels, respectively. Nerves also secrete VEGF (blue) to attract small arteries to track alongside nerve fibers. Blood vessels produce artemin and neurotrophin-3 (not shown), neurotrophic guidance signals, to guide neuronal axons.

endothelial cells (21). In the mammary gland, *EphrinB2* is expressed in luminal cells, whereas *EphB4* is expressed in basal cells (23); however, their function remains unclear. Finally, many factors, especially WNTs, BMPs, and HHs, which are known to regulate epithelial morphogenesis, also play a role in branching and guidance of nerves and blood vessels (26). By sharing these morphogens and guidance cues, branching morphogenesis of different tissues can be coordinated efficiently during organ formation.

Stromal Role in Development and Regeneration of Branched Organs

During formation of branched organs, several essential events, including organ specification, control of branch size, and cell differentiation and homeostasis, occur concomitantly or sequentially with epithelial branching. To understand development of vertebrate branched organs fully, we

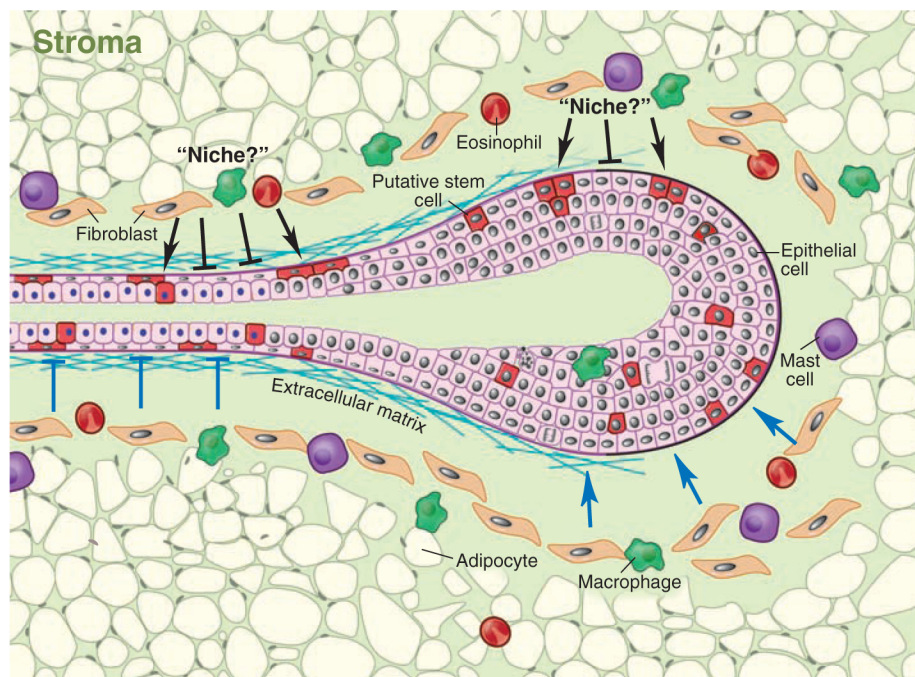


Fig. 4. Stroma role in development of vertebrate branched organs. A schematic presentation of the epithelium and stroma during mammary gland development. Stroma, which has a heterogeneous cell population, plays an important role in determining branching patterns (blue arrows and bars indicate stimulatory and inhibitory cues acting on the epithelium). Stroma also regulates biology of stem cells by contributing to a presumptive stem cell “niche.”

by the mouse's age or reproductive history (31). This distribution may have important implications for where new branches are initiated, since multiple stem cells can contribute to a single branch (32). It may also allow formation of the maximum number of alveoli, which undergo recurring cycles of cell proliferation and death during each pregnancy. In addition, “terminally” differentiated cells, for example, from the mammary gland (31) or fly trachea (33), can regain developmental potency and form various cell types under appropriate conditions. These results underscore the importance of understanding the molecular basis of stem cell differentiation and stromal role in regulating stem cell potency.

Conclusions and Future Directions

Despite their distinct origins and functions, different tissues and organs use common genes and signaling pathways for regulating branching during organ formation. One possible explanation for such molecular conservation is the existence of “branching modules,” consisting of a defined set of genes that can be activated whenever branching is needed (34). Alternatively, and perhaps more likely, branching morphogenesis, irrespective of cell and tissue types, requires a common set of cell behaviors, for example, regulation of cytoskeletal machinery that is controlled by evolutionarily conserved genes and pathways. It is thus formally possible that the genes and signaling pathways involved in neural

branching and guidance, which evolved first, were later “co-opted” by blood vessels and epithelia of various branched organs.

While continuing the quest for molecules that play conserved roles in various branched organs, we should also focus on molecules that promote organ-specific morphogenesis and functions to understand how different organs evolved. For instance, in the embryonic lung or kidney, branching of the epithelium accompanies enormous growth of the overall organ. In contrast, in the mammary gland, the epithelium primarily invades and forms branches in the stroma that have already been laid down and barely changes in size during pubertal development. Thus, in the mammary gland, unlike in most other branched organs, there is constant remodeling of the stromal compartment, extracellular matrix, and vasculature as mammary epithelium populates the fat pad. Indeed, the mammary gland may use different genes than do other organs for epithelial branching. *Shh*, which is indispensable for lung and kidney epithelial branching, is not required for mammary development (2).

Identifying stromal factors will be important for understanding essential aspects of development of vertebrate branched organs. To understand how organs are formed and maintained, and whether they can be regenerated, it will be important to determine whether a stem cell “niche” exists in vertebrates and, if so, how it regulates stem cell self-renewal and differentia-

tion. In addition, what is the nature of adult stem cells? At least in the mammary gland, the frequency and property of adult stem cells remain puzzling and do not fit current models (31, 35). Thus, it will also be important to determine the intrinsic factors that respond to the “niche” and maintain stem cells and how they can be reprogrammed upon experimental manipulations. With the emergence of the mammary gland as an amenable platform for functional testing, we can be optimistic about a better understanding of the intrinsic and extrinsic factors that regulate stem cell development in branched organs.

References and Notes

1. M. Affolter, E. Caussinus, *Development* **135**, 2055 (2008).
2. P. Lu, M. D. Sternlicht, Z. Werb, *J. Mammary Gland Biol. Neoplasia* **11**, 213 (2006).
3. P. Carmeliet, M. Tessier-Lavigne, *Nature* **436**, 193 (2005).
4. R. J. Metzger, M. A. Krasnow, *Science* **284**, 1635 (1999).
5. A. Ghabrial, S. Luschnig, M. M. Metzstein, M. A. Krasnow, *Annu. Rev. Cell Dev. Biol.* **19**, 623 (2003).
6. T. Watanabe, F. Costantini, *Dev. Biol.* **271**, 98 (2004).
7. R. J. Metzger, O. D. Klein, G. R. Martin, M. A. Krasnow, *Nature* **453**, 745 (2008).
8. A. J. Ewald, A. Brenot, M. Duong, B. S. Chan, Z. Werb, *Dev. Cell* **14**, 570 (2008).
9. A. Ghabrial, M. A. Krasnow, *Nature* **441**, 746 (2006).
10. P. Lu, A. J. Ewald, G. R. Martin, Z. Werb, *Dev. Biol.* **321**, 77 (2008).
11. L. Chi et al., *Development* **131**, 3345 (2004).
12. F. Costantini, R. Shkya, *Bioessays* **28**, 117 (2006).
13. J. E. Fata et al., *Dev. Biol.* **306**, 193 (2007).
14. C. A. Jones, D. Y. Li, *Curr. Opin. Genet. Dev.* **17**, 332 (2007).
15. G. B. Silberstein, *Microsc. Res. Tech.* **52**, 155 (2001).
16. C. M. Nelson, M. M. Vanduijn, J. L. Inman, D. A. Fletcher, M. J. Bissell, *Science* **314**, 298 (2006).
17. M. D. Sternlicht, H. Kouras-Mehr, P. Lu, Z. Werb, *Differentiation* **74**, 365 (2006).
18. G. S. Prins, O. Putz, *Differentiation* **76**, 641 (2008).
19. V. N. Patel, I. T. Rebutini, M. P. Hoffman, *Differentiation* **74**, 349 (2006).
20. N. Bahary, L. I. Zon, *Science* **294**, 530 (2001).
21. P. Carmeliet, *Nat. Rev. Genet.* **4**, 710 (2003).
22. C. Englund, P. Steneberg, L. Falileeva, N. Xylourgidis, C. Samakovlis, *Development* **129**, 4941 (2002).
23. L. Hinck, *Dev. Cell* **7**, 783 (2004).
24. A. Tufro, J. Teichman, C. Woda, G. Villegas, *Mech. Dev.* **125**, 558 (2008).
25. L. Chung et al., *Development* **134**, 2935 (2007).
26. F. Charron, M. Tessier-Lavigne, *Development* **132**, 2251 (2005).
27. J. M. W. Slack, *Science* **322**, 1498 (2008).
28. K. S. Zaret, M. Grompe, *Science* **322**, 1490 (2008).
29. M. Shackleton et al., *Nature* **439**, 84 (2006).
30. J. Stingl et al., *Nature* **439**, 993 (2006).
31. G. H. Smith, D. Medina, *Breast Cancer Res.* **10**, 203 (2008).
32. B. E. Welm, G. J. Dijkgraaf, A. S. Bledau, A. L. Welm, Z. Werb, *Cell Stem Cell* **2**, 90 (2008).
33. M. Weaver, M. A. Krasnow, *Science* **321**, 1496 (2008).
34. J. A. Davies, *Bioessays* **24**, 937 (2002).
35. K. U. Wagner, G. H. Smith, *J. Mammary Gland Biol. Neoplasia* **10**, 25 (2005).
36. We thank G. Dijkgraaf for taking the photograph of the fluorescent mammary gland and M. Chan, O. Klein, J. Phillips, and M. Zeiger for helpful discussions and insightful comments. We regret that many authors' work could not be cited because of space limitations. This work was supported by grants ES012801 and CA057621 from NIH.

10.1126/science.1162783

The Long-Run Benefits of Punishment

Simon Gächter,* Elke Renner, Martin Sefton

We investigated experimentally whether costly punishment (1, 2) to enforce socially beneficial cooperation can improve group welfare. This question is motivated by recent evolutionary (group selection) models of altruistic cooperation and punishment (2, 3). In these models, costly punishment sustains costly cooperation. Once cooperation is established, the costs of punishment are low because punishment is rarely needed. Thus, the evolutionary pressure against punishers at that stage will be weak and can be overcome by the group average benefits from cooperation (which may come from an increased likelihood of winning intergroup contests). Recent research challenged these models because in many experiments the incurred costs of punishment outweighed the gains from increased cooperation: Punishment in these experiments was detrimental, not beneficial (4–8). For instance, a recent study (6) reported cooperation experiments with and without punishment conducted in 16 participant pools around the world. With the exception of three participant pools, the average payoff in experiments with punishment opportunities was lower than the average without punishment; and in those three participant pools with higher payoffs the increase was very small.

The evidence that punishment is detrimental stems from short experiments (typically 10 periods or less), and in many of them payoffs improve over time (4–7). Thus, the time horizon of these experiments may be too short to fully reveal the effects of punishment. By contrast, the evolutionary models make predictions about ancestral groups that interacted frequently over very long periods.

We examined whether the duration of interaction affects the efficacy of punishment by running public goods experiments with punishment (the P experiments) and by varying the time horizon: The experiment either lasted 10 periods (labeled P10) or 50 periods (P50). We also ran experiments with no punishment opportunities (N10 and N50) because a long time horizon might also increase cooperation without punishment and therefore reduce the scope for punishment to be beneficial. Furthermore, in line with frequent assumptions of the group selection models, our design attempted to replicate situations in our ancestral past in which small groups had to solve public goods problems with a limited set of people who interacted over a long period of time with each other.

Participants ($n = 207$) played the public goods experiments in groups of three and knew that the group membership would stay constant for the announced duration. Participants had an endowment of 20 tokens that they could either keep or contribute to a public good. Each token kept yielded one money unit (MU) for that subject, and each token invested yielded 0.5 MUs for each group member. One unit of punishment cost the punisher one MU and reduced the punished group members' earnings by three MUs (9).

On average, cooperation was significantly higher in both P experiments than in the respective N experiment. Per-period contributions were 3.6 tokens higher in P10 than N10 ($P = 0.0343$) (10) and 9.6 tokens higher in P50 than N50 ($P = 0.0000$). Per-period contributions were substantially higher in P50 than in P10 (by 4.9 tokens, $P = 0.0027$). By contrast, per-period contributions in N50 were slightly lower than in N10 (by 0.9 tokens, $P = 0.1201$).

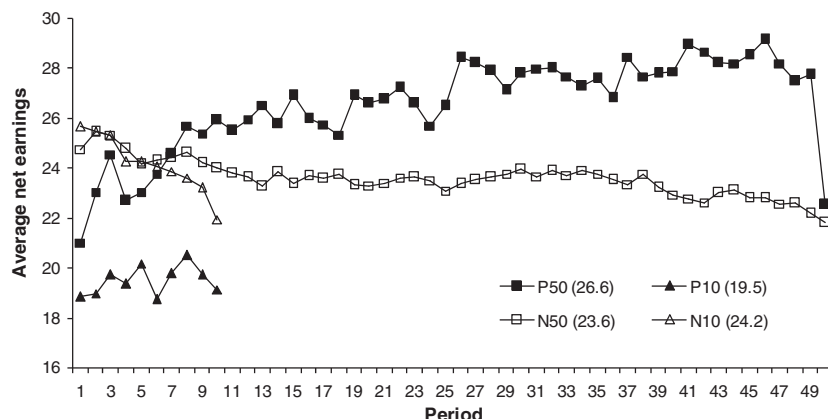


Fig. 1. Average net earnings in public goods experiments with punishment opportunities (P experiments) and with no punishment opportunities (N experiments). The experiments lasted either 10 periods (P10 and N10) or 50 periods (P50 and N50). The numbers in parentheses are the average earnings across all periods (N10 and N50, earnings from the public goods contribution stage; P10 and P50, earnings from the public goods contribution stage minus punishment expenditures minus received punishment).

The presence of a punishment option decreased the average net earnings in P10 compared with those of N10 (by 4.68 MUs per period, $P = 0.0329$). By contrast, average net earnings were significantly higher in P50 than in N50 (by 2.98 MUs per period, $P = 0.0065$) (Fig. 1). In the 10-period experiments, most groups in the N experiment did better than most groups in the P experiment, whereas in the 50-period experiments the opposite held.

The prospect of a longer duration of interaction influenced behavior already in early periods. Contributions were significantly higher, and incurred punishment costs were significantly lower, in the first 10 periods of P50 than in P10. As a result net earnings were significantly higher already in the first 10 periods of P50 compared with P10, where punishment was detrimental in all rounds. Also apparent in Fig. 1 is a prominent drop in net earnings in the last period of P50. The fixed termination period of the experiment is arguably not a feature of real interactions, and the beneficial effect of punishment would be even greater if the final period were excluded from the analysis (9).

Overall, our experiments show that punishment not only increases cooperation, it also makes groups and individuals better off in the long run because the costs of punishment become negligible and are outweighed by the increased gains from cooperation. These results support group selection models of cooperation and punishment (2, 3), which require that punishment increases not only cooperation but also group average payoffs.

References and Notes

1. K. Sigmund, *Trends Ecol. Evol.* **22**, 593 (2007).
2. R. Boyd, H. Gintis, S. Bowles, P. J. Richerson, *Proc. Natl. Acad. Sci. U.S.A.* **100**, 3531 (2003).
3. S. Bowles, *Microeconomics: Behavior, Institutions, and Evolution* (Princeton Univ. Press, Princeton, NJ, 2003).
4. E. Fehr, S. Gächter, *Nature* **415**, 137 (2002).
5. Ö. Gülerk, B. Irlenbusch, B. Rockenbach, *Science* **312**, 108 (2006).
6. B. Herrmann, C. Thöni, S. Gächter, *Science* **319**, 1362 (2008).
7. M. Eas, A. Riedl, *Proc. R. Soc. Lond. B. Biol. Sci.* **275**, 871 (2008).
8. A. Dreber, D. G. Rand, D. Fudenberg, M. A. Nowak, *Nature* **452**, 348 (2008).
9. Materials and methods are available as supporting material on Science Online.
10. All statistical tests are two-sided Mann-Whitney tests with the group averages over all periods as the independent observations.
11. This work was supported by the University of Nottingham and the British Academy.

Supporting Online Material

www.sciencemag.org/cgi/content/full/322/5907/1510/DC1

Materials and Methods

SOM Text

Fig. S1

Table S1

References and Notes

18 August 2008; accepted 16 September 2008
10.1126/science.1164744

Centre for Decision Research and Experimental Economics, University of Nottingham, School of Economics, Sir Clive Granger Building, University Park, Nottingham NG7 2RD, UK.

*To whom correspondence should be addressed. E-mail: simon.gachter@nottingham.ac.uk

Dynamic Proteomics of Individual Cancer Cells in Response to a Drug

A. A. Cohen,^{1*†} N. Geva-Zatorsky,^{1*} E. Eden,^{1*} M. Frenkel-Morgenstern,¹ I. Issaeva,¹ A. Sigal,² R. Milo,³ C. Cohen-Saidon,¹ Y. Liron,¹ Z. Kam,¹ L. Cohen,¹ T. Danon,¹ N. Perzov,¹ U. Alon¹

Why do seemingly identical cells respond differently to a drug? To address this, we studied the dynamics and variability of the protein response of human cancer cells to a chemotherapy drug, camptothecin. We present a dynamic-proteomics approach that measures the levels and locations of nearly 1000 different endogenously tagged proteins in individual living cells at high temporal resolution. All cells show rapid translocation of proteins specific to the drug mechanism, including the drug target (topoisomerase-1), and slower, wide-ranging temporal waves of protein degradation and accumulation. However, the cells differ in the behavior of a subset of proteins. We identify proteins whose dynamics differ widely between cells, in a way that corresponds to the outcomes—cell death or survival. This opens the way to understanding molecular responses to drugs in individual cells.

The state of a cell is largely determined by the levels of thousands of proteins in space and time (1–4). To affect the cell state, drugs are used (5–7), but little is known about the detailed effects of drugs on the dynamics of proteins in individual human cells. Here, we ask how a drug affects the dynamics of the proteome and how these dynamics differ for individual cells. To address this, our model system was human cancer cells responding to an anticancer drug with a well-characterized target and mechanism of action, camptothecin (CPT). This drug is a topoisomerase-1 (TOP1) poison with no other known targets. CPT locks TOP1 in a complex with the DNA, causing DNA breaks and inhibiting transcription, which eventually causes cell death (8).

To follow the response to the drug, we endeavored to accurately measure the level and localization of about 1000 proteins in individual cells over time. We found a diverse protein response to the drug, with rapid localization changes of proteins specific to the drug mechanism of action, followed by slower wide-ranging temporal changes of protein levels. Furthermore, we found that the drug target TOP1 is among the very first to respond both in protein level and localization. For most proteins, the response to the drug shows moderate cell-cell variability. Deviating from this norm is a set of proteins for which responses are widely different between individual cells. Some of these proteins are involved in cell fate decisions and at least two proteins show cell-to-cell differences that are correlated with the fate of the cell. Thus,

examining spatiotemporal proteome dynamics in individual cells offers clues about what is special about the subpopulation of cells that escapes the drug action.

Dynamic proteomics system. We used a retrovirus-based approach, called “CD tagging,” in human H1299 lung carcinoma cells (9–14). We constructed a library of over 1200 cell clones, each expressing a different fluorescently tagged, full-length protein from its endogenous chromosomal location. Time-lapse fluorescence microscopy was used to obtain movies of the proteins over several days of growth (15).

Obtaining quantitative information from time-lapse fluorescent movies is known to be challenging, because it is difficult to automatically detect the cell boundaries and track them over time (16–20). Here, we overcame this problem by a tagging strategy that made cells more easily identifiable by image-analysis software. We used two rounds of CD tagging with the red fluorescent protein mCherry to obtain a cell clone with red fluorescence in the cytoplasm and stronger red fluorescence in the nucleus (Fig. 1A). Custom software (15) used the red fluorescence pattern to automatically distinguish the cell from its background and to differentiate the nucleus from the cytoplasm (Fig. 1B). The algorithms in the software can also automatically detect morphological correlates of cell states [e.g., cell death and mitosis (15)]. We then used this clone (H1299-cherry) as a basis for our tagged protein library. We introduced an enhanced yellow fluorescent protein (eYFP or Venus) into the red-tagged cells by an additional round of CD tagging, expanded the yellow-tagged cells into clones, and identified the yellow-tagged proteins (13). Thus, the red tagging is the same in all cells of the library and is independent of the second yellow tag on the protein of interest.

The library includes over 1260 different tagged proteins, of which about 80% are characterized proteins and about 20% are not charac-

terized (for a list of tagged proteins see www.dynamicproteomics.net). We excluded the proteins whose localization did not match previous reports (about one-sixth of the proteins) and studied the remaining 1020 proteins. These include diverse functional categories and localization patterns including membrane, nuclear, nucleolar, cytoskeleton, Golgi, endoplasmic reticulum, and other cell locations (fig. S1).

The CD tagging method we used tends to preserve protein functionality (13, 21, 22). Note, however, that our use of the library does not require proteins to be functional, but merely to act as reliable reporters for the dynamics and location of the endogenous proteins. To test this, we measured the dynamics of endogenous proteins using immunoblots with specific antibodies to 20 different proteins in the parental H1299-cherry cells. In 80% of the cases (16 out of 20), the immunoblot dynamics agreed with the fluorescence dynamics from the movies (Pearson correlation $R > 0.5$, $P < 10^{-4}$) (fig. S2). Immunoblots of tagged cell clones with antibodies against green fluorescent protein (GFP) further indicated that the tagged proteins are full-length fusions (table S1). As in many high-throughput methods, we recommend that, when using the library to study specific proteins, protein functionality should be tested by other means. Most proteins named below were reannotated and tested as indicated.

Assay of proteomic response to drug. Cells were grown in 12-well optical plates in an automated fluorescence microscope with autofocus and control of temperature, CO₂, and humidity. Each well contained cells tagged for a different protein. After 24 hours of growth, the drug CPT was added (10 μ M), and cells were tracked for another 48 hours (Fig. 1C). Images in phase, red and yellow were taken every 20 min at four positions in each well. The resulting time-lapse movies had over 200 consecutive frames per protein studied, where each frame contained 10 to 40 different cells. Movies were stored and analyzed automatically (15), resulting in traces of protein level and location in each cell over time (see supporting material for sample movies).

The cells showed vigorous divisions during the 24 hours before drug addition, with a cell cycle time of ~20 hours. When the drug was added, cells showed loss of motility and growth arrest after ~10 hours and began to show cell rounding and blebbing (morphological correlates of cell death), which reached about 15% of the cells after 36 hours (fig. S3). Cell cycle stage at the time the drug was added did not seem to influence the response to the drug, as assayed by automatic identification of cell division and cell death events (detailed in SOM text and figs. S4 and S5). In experiments in which the drug was washed away after 48 hours, a small fraction of the cells (about 10⁻⁴) survived to divide and form colonies after several weeks of incubation.

Day-to-day repeats starting from frozen cells showed a mean error in the eYFP fluorescent

¹Department of Molecular Cell Biology, Weizmann Institute of Science, Rehovot 76100, Israel. ²Division of Biology, California Institute of Technology, Pasadena, CA 91125, USA. ³Department of Plant Sciences, Weizmann Institute of Science, Rehovot 76100, Israel.

*These authors contributed equally to this work.

†To whom correspondence should be addressed. E-mail: ariel.cohen@weizmann.ac.il

signals of up to 15% (fig. S6). Thus, dynamic changes as small as 20 to 30% in tagged protein intensity typically can be accurately detected by using the present assay in individual cells.

Temporal profiles of protein concentration.

We begin with an account of the average population level of the fluorescent intensity of each protein and then describe the individual cell behavior. We found that most (76%) proteins showed a significant decrease in fluorescence intensity in response to the drug, on diverse time scales. A subset of proteins (7%) showed a significant increase in intensity. The median dynamic range of this response was a 1.3-fold change in fluorescence, and the largest changes were about

fivefold. Proteins showed several classes of dynamical profiles (Fig. 2, A and B, and fig. S7) (15). The present data include dynamics of about 150 uncharacterized proteins (table S4) found throughout all profiles (Fig. 2B).

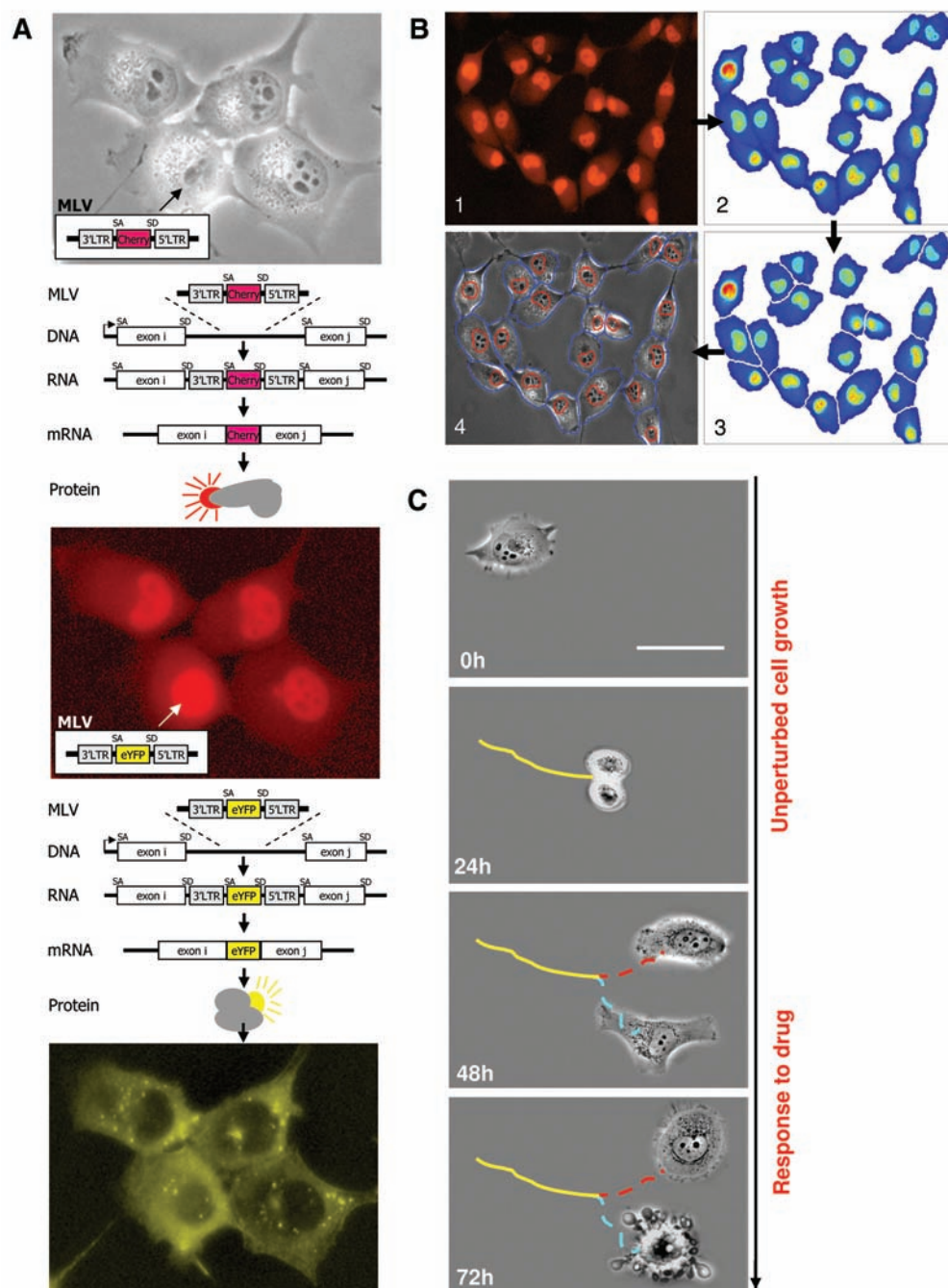
Groups of functionally related proteins tended to show similar dynamics and protein localization profiles. For example, ribosomal proteins showed rapid, highly correlated degradation (Fig. 2C), which was confirmed by immunoblots (fig. S2). Proteins with slower apparent degradation include cytoskeleton components and metabolic enzymes. The timing of degradation of most cytoskeleton-associated proteins correlated with the timing of the loss of cell motility, as measured by tracking

cell position over time (Fig. 2D). Proteins that rose late in the response include helicases implicated in DNA damage repair; apoptosis-related proteins, such as the Bcl2-associated proteins BAG2 and BAG3; and the programmed cell death protein PDCD5.

The drug target is among the first to respond.

The total cellular fluorescence levels of the tagged drug target TOP1 decreased on a time scale of <1 hour, preceding almost all other responses in the present study (TOP1 is among the first 1% of responding proteins) (Fig. 2, arrow). The rate of TOP1 fluorescence decrease was CPT dose-dependent (fig. S8, A and C). Immunoblots confirmed the rapid degradation of both eYFP-tagged

Fig. 1. Library of tagged proteins and its image analysis. (A) The cell clone library was generated in two steps: First, a red fluorescent tag (mCherry) flanked by splice signals was introduced on a retrovirus into the genome of H1299 cells, which resulted in cells that express proteins with an internal mCherry exon. After two rounds of tagging, a cell clone was selected with a red labeling pattern that is suitable for image analysis, bright in the nucleus and weaker in the cytoplasm. This clone formed the basis for an additional round of tagging, with a yellow fluorescent tag (eYFP or Venus) as an internal exon. Individual yellow-tagged cells were sorted then expanded into clones, and the tagged protein in each clone was identified. (B) Image analysis used the red fluorescent images to automatically detect cell and nuclear boundaries and to quantify the YFP intensity at each time point. (C) Cells were grown in an incubated microscope for 24 hours under normal conditions and then for an additional 48 hours in the presence of 10 μ M CPT. Cells were imaged every 20 min, and fluorescent intensity in each cell was automatically tracked. Cell divisions and morphological changes associated with cell death were automatically detected (15). Shown is a schematic of two daughter cells of the cell in the top panel. The cell labeled with the blue track shows blebbing and fragmentation typical of apoptosis. Scale bar, 45 μ m. MLV, murine leukemia virus. LTR, long terminal repeat.



and untagged TOP1 in response to CPT (fig. S8D), which was consistent with previous studies (23).

TOP1 also showed rapid localization changes. TOP1 is found in the nucleoli and nucleus of cells before drug addition (24). On CPT treatment, tagged TOP1 intensity in the nucleoli dropped in less than 2 min (Fig. 3A). Fluorescence accumulated in the cytoplasm on the time scale of 5 hours after CPT addition in a CPT dose-dependent manner (fig. S8, B and E). Immunoblot analysis of the TOP1-tagged clones indicated that as TOP1 was degraded, a fragment of ~40 kD that was detectable with GFP-specific antibody accumulated (fig. S8D). This fragment was unique to the TOP1-tagged clones (none of the other eYFP-tagged proteins tested with immunoblots in this study showed such a fragment) and may represent a degradation product of YFP-tagged TOP1. Taken together, these results suggest that, on CPT treatment, TOP1 may be proteolyzed in the nucleus (25) and that TOP1 fragments exit the nucleus after administration of the drug. Other DNA-damaging agents, such as cisplatin and the TOP-2 poison etoposide, did not show any of these effects on TOP1 (fig. S8E).

Rapid localization changes suggest nucleolar stress and DNA damage. We found that translocation events were much rarer than abundance changes (about 2% of the proteins). The trans-

locations that occurred, however, seemed highly specific to the drug mechanisms of action.

A set of 10 proteins showed rapid localization changes after CPT treatment, with timing similar to that of the drug target (table S2). Almost all of these proteins are localized to the nucleoli. Several of these nucleolar proteins showed a reduction in nucleolar fluorescence intensity (Fig. 3B); others showed an increase followed by a return to basal level (Fig. 3C). Corresponding changes in the nuclear intensity outside of the nucleoli suggested that these are translocation events. We find that these proteins demonstrated similar spatial dynamics in response to the transcriptional inhibitor actinomycin D (1 μ g/ml) (fig. S9). Similar nucleolar changes have been previously found in a mass-spectrometry study that monitored the composition of nucleoli extracted from cells responding to actinomycin D (25). These results suggest that an immediate effect of CPT on the cells used in our study is transcription inhibition, which causes nucleolar stress (26).

A slower translocation event was observed in the DNA damage repair protein RPA2. This protein moved to nuclear foci, beginning at 1.5 hours after drug addition. This is a well-characterized response to DNA breaks (27, 28), the main mechanism of cell killing by CPT. The other 14 DNA damage-related

proteins in the library did not show translocations, although some showed intensity changes (fig. S10).

Slow nuclear localization changes after drug addition include the oxidative stress response pathway. In addition to the rapid responses noted above, we found that about 1% of the proteins in this study showed substantial change in nuclear localization (a change greater than 20% in the cytoplasm/nuclear ratio), on time scales of several hours (Fig. 3D). Notably, two proteins in the stress response pathway to oxidative stress, thioredoxin and thioredoxin reductase 1, showed an increase in their nuclear/cytoplasm ratio within 8 hours after drug addition (fig. S11). As nuclear levels rise, cytoplasmic levels seem to decrease proportionally, and vice versa, which suggests that translocation occurs between these two compartments. This implies an oxidative stress response to the drug on a scale of hours, as compared with the more rapid transcription-inhibition and DNA damage responses.

We also studied the responses of 10 selected proteins to other drugs at equivalently lethal doses. A closely related derivative of CPT used clinically, Irinotecan (250 μ M), showed dynamics and localization changes that were similar to CPT's in shape, but slightly lower in amplitude (figs. S12 and S13). In contrast, unrelated drugs

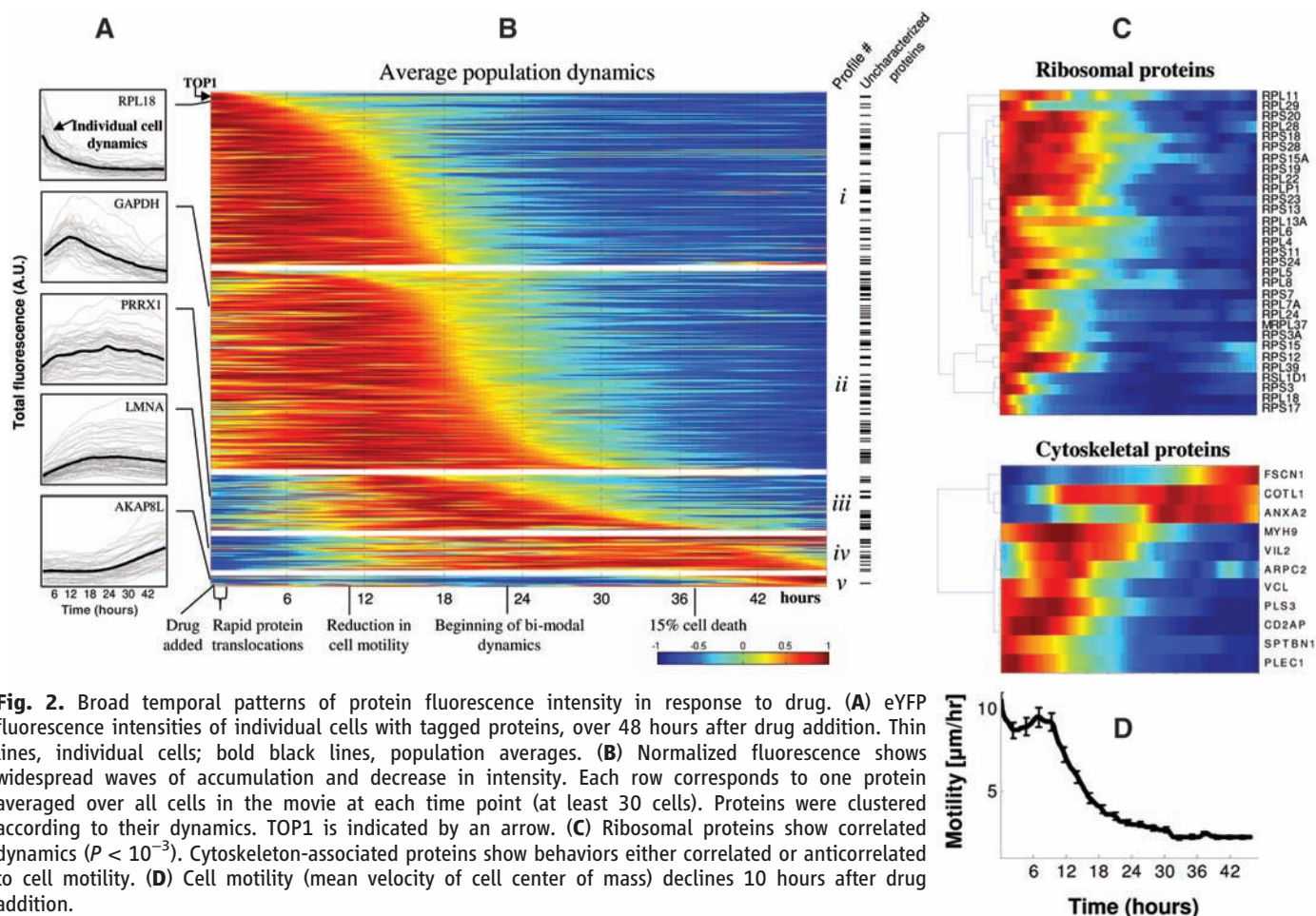


Fig. 2. Broad temporal patterns of protein fluorescence intensity in response to drug. (A) eYFP fluorescence intensities of individual cells with tagged proteins, over 48 hours after drug addition. Thin lines, individual cells; bold black lines, population averages. (B) Normalized fluorescence shows widespread waves of accumulation and decrease in intensity. Each row corresponds to one protein averaged over all cells in the movie at each time point (at least 30 cells). Proteins were clustered according to their dynamics. TOP1 is indicated by an arrow. (C) Ribosomal proteins show correlated dynamics ($P < 10^{-3}$). Cytoskeleton-associated proteins show behaviors either correlated or anticorrelated to cell motility. (D) Cell motility (mean velocity of cell center of mass) declines 10 hours after drug addition.

such as etoposide (a TOP-2 poison, 5 μ M) showed significant differences in almost every protein studied (fig. S14).

Several proteins showed behavior that differed in individual cells. The present system allows monitoring of the cell-cell variability of each protein over time. We found that, without the drug, all proteins showed moderate cell-cell variability in their fluorescence levels, with a standard deviation between cells that ranged between 10 and 60% of the mean. This variability is in accord with that previously found in microorganisms (2, 29–32) and human cells (12). Part of this variability is due to differences in the cell-cycle stage of the cells. To quantify this, we binned the cells according to the time between their last division and the time of drug addition—an *in silico* synchronization approach (13). We found that about 20% of the variability is due to cell-cycle stage difference, and the remainder is presumably due to stochastic processes.

After drug addition, cell-cell variability increased as a function of time by about 30% on average (fig. S15). Despite the variability, the dynamic profiles within a clone were similarly shaped; nearly all cells showed profiles of fluorescence dynamics that rise and fall together (Fig. 4, A and B).

Diverging from this norm were 24 proteins that displayed a special behavior (listed in table S3). At first, they showed the typical variability with similar dynamics in each cell. Then, between 20 and 30 hours after drug addition, the cell population began to show dramatic cell-cell differences in the dynamics of these proteins (Fig. 4, C to F). Some cells showed an increase in the fluorescence levels; other cells stayed constant or showed a decrease. Thus, these proteins seem to show bimodal dynamical behavior. These proteins include the BCL-2-associated proteins BAG2 and BAG3, calmodulin (CALM1), ribosomal protein RPS3, and others (see table S3) that are related to aspects of cell death.

RNA helicase DDX5 and replication factor RFC1 show cell-cell differences that correlated with cell fate. We asked whether the cell-cell variability of the bimodal proteins was correlated with differential response to the drug. Most bimodal proteins did not show behavior that was correlated with cell fate (for example fig. S17, C and D). Thus, the increase or decrease of protein levels in these clones was not an indicator of cell death or survival.

Two proteins, however, showed behavior that correlated with cell death. We find that the RNA-

helicase DDX5 increased markedly in cells that survive to the end of the movies (Fig. 5A). Its levels decreased in cells that underwent the morphological changes associated with cell death. Thus, the fluorescence dynamics of DDX5 are significantly correlated with the cell fate ($P < 10^{-13}$, Fig. 5A, inset).

We also found that the bimodality of DDX5 is drug-specific, as tagged DDX5 does not show bimodal behavior in response to other anticancer drugs, such as cisplatin (see fig. S16). A second protein, replication factor RFC1, showed bimodal behavior similar to that of DDX5, rising after 20 hours in cells that survive to the end of the experiment and decreasing in cells that die (fig. S17, A and B). This observation is in line with the role of RFC1 in DNA repair (33).

Following the observation that DDX5 dynamics correlate with cell fate, we asked whether it plays a functional role in the response to the drug. For this purpose, we knocked down DDX5 by means of RNA interference (RNAi), reducing tagged DDX5 intensity by ~80% (fig. S18). Adding CPT to DDX5-siRNA-treated cells showed a doubling in the death rate during the first 40 hours (Fig. 5B), compared with cells treated with nonspecific RNAi or no RNAi. This

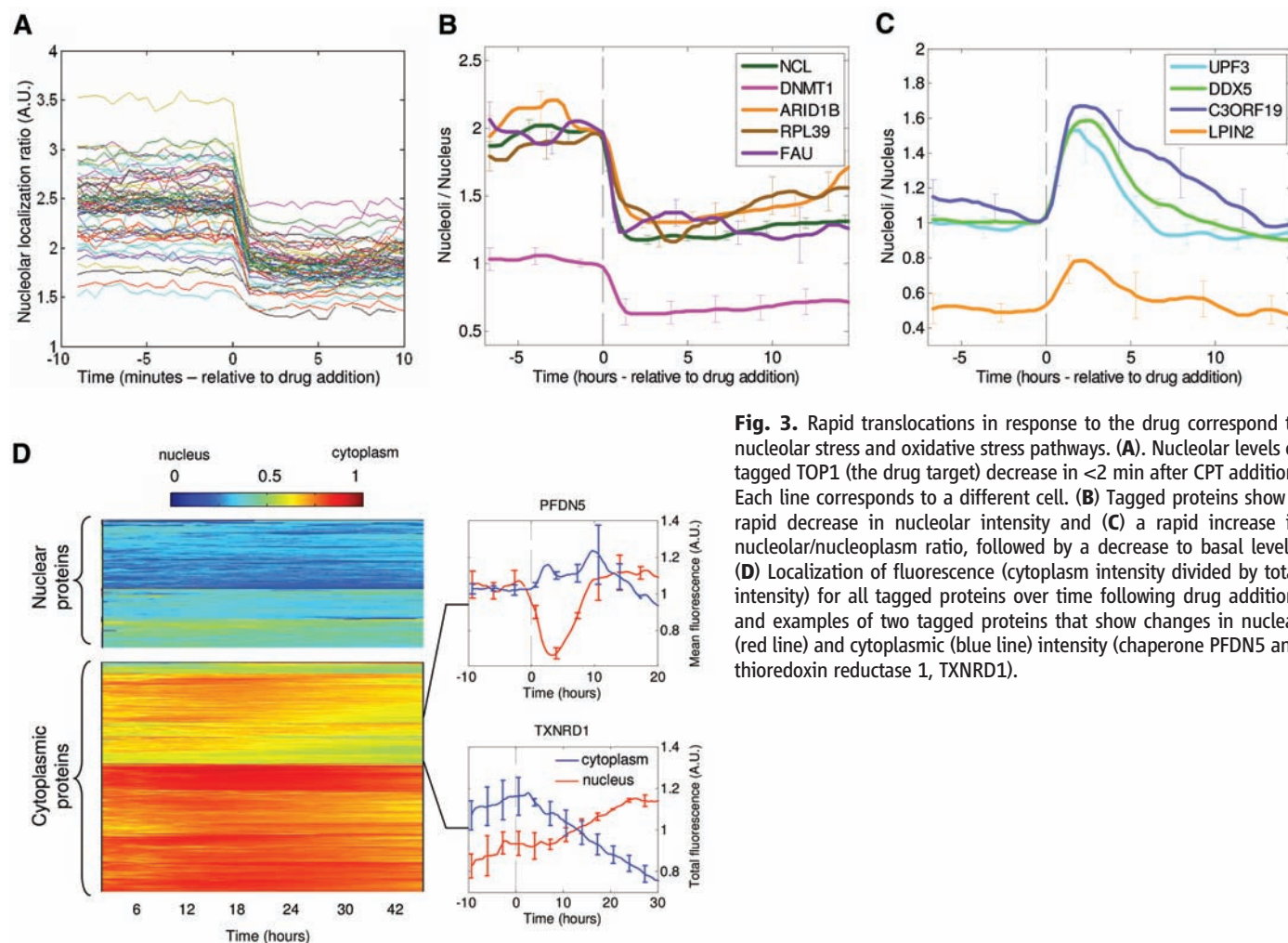


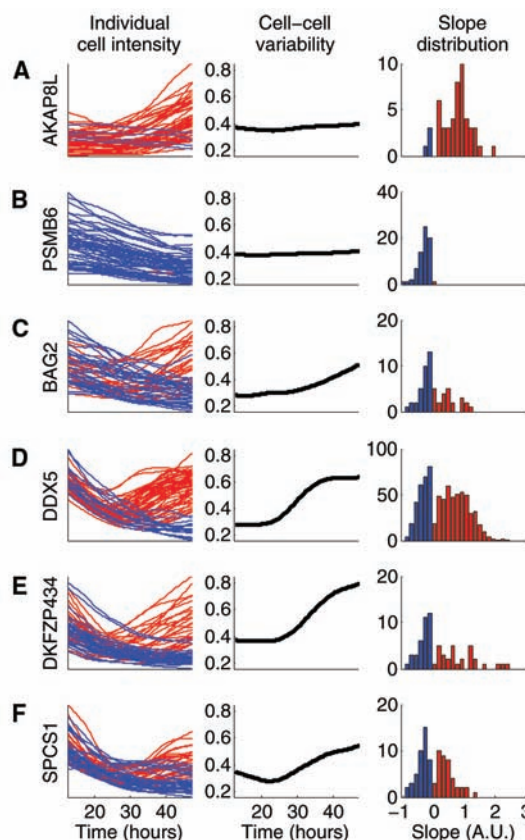
Fig. 3. Rapid translocations in response to the drug correspond to nucleolar stress and oxidative stress pathways. **(A).** Nucleolar levels of tagged TOP1 (the drug target) decrease in <2 min after CPT addition. Each line corresponds to a different cell. **(B)** Tagged proteins show a rapid decrease in nucleolar intensity and **(C)** a rapid increase in nucleolar/nucleoplasm ratio, followed by a decrease to basal levels. **(D)** Localization of fluorescence (cytoplasm intensity divided by total intensity) for all tagged proteins over time following drug addition, and examples of two tagged proteins that show changes in nuclear (red line) and cytoplasmic (blue line) intensity (chaperone PFDN5 and thioredoxin reductase 1, TXNRD1).

suggests that DDX5 plays a functional role in the fate of cells to CPT, consistent with its suggested antiapoptotic role (34).

Discussion. This study provided a view of the response to a drug in space and time for about 1000 proteins in individual cells. Whereas most proteins showed uniform behavior in different cells, a small subset showed bimodal behavior—cell-cell variability increased sharply about a day after the drug was added. The cells thus seem

to form subpopulations with distinct protein dynamics. Among these bimodal proteins, we identified an RNA helicase (DDX5) and a DNA replication factor (RFC1), whose dynamics varied widely between cells, in a way that corresponds to cell fate: They rise in cells that survive and decrease in cells that die. Knockdown of DDX5 caused accelerated cell killing by the drug. These proteins may thus play a functional role in escape of cells from the drug action.

Fig. 4. A subset of proteins displays a bimodal response at the individual cell level in response to CPT. (**A** and **B**) Examples of proteins that do not show bimodal behavior, which are representative of most proteins in the study. Profiles are similarly shaped in each individual cell. Profiles rise with time (red lines) or decrease with time (blue lines) in parallel. Cell-cell variability (CV, defined as standard deviation divided by the mean of cell-cell distribution at each time point) increases slightly over time, and the distribution of slopes of fluorescence levels shows uniform behavior. (**C** to **F**) Examples of proteins that show bimodal behavior. The dynamics after about 20 hours vary between cells: Some cells show an increase in fluorescence levels (red) and other cells show a decrease (blue). This results in bimodal distributions of fluorescent intensity slopes measured in arbitrary units (A.U.). Slopes are defined as median temporal derivative of the fluorescence levels, in the interval between 24 hours after drug addition to 48 hours (or time of cell death).



We find that the cells respond to the drug by broad waves of change in protein abundance and much fewer changes in protein localization. The localization changes occurred in a temporal sequence and seem to be indicative of the drug mechanism of action. Translocations of nucleolar proteins related to transcription inhibition occurred first, on the time scale of minutes, followed by translocation corresponding to DNA damage on the time scale of an hour, followed, after several hours, by translocations of oxidative stress-related proteins. These events help define a time course for the response to the drug. Notably, the drug target TOP1 was among the first to respond. Changes in protein intensity were generally slower than translocation events, which suggested a separation of time scales between regulation in space and abundance. The present approach might thus help to elucidate the mode of action of other drugs.

Understanding the human cell as a dynamical system will require viewing it on several levels, including mRNA and protein levels, modifications, and localizations, in individual living cells over time. The present approach is a step in this direction and can be enhanced by existing proteomic methods. For example, mass-spectrometry can provide a view of protein modifications on the level of cell averages (35, 36) that is not observable in the present approach. The present library employs tagging that preserves endogenous chromosomal context and is built to allow robust image quantification. It provides localization and dynamics for about 150 uncharacterized proteins; the library also provides a universal epitope tag (eYFP) for potential biochemical assays of these proteins (4, 37). The reproducibility, temporal resolution, and accuracy of the approach allow even small dynamical features to be reliably detected.

In summary, escape of cells from this anti-cancer drug seems to involve cell-cell variation in

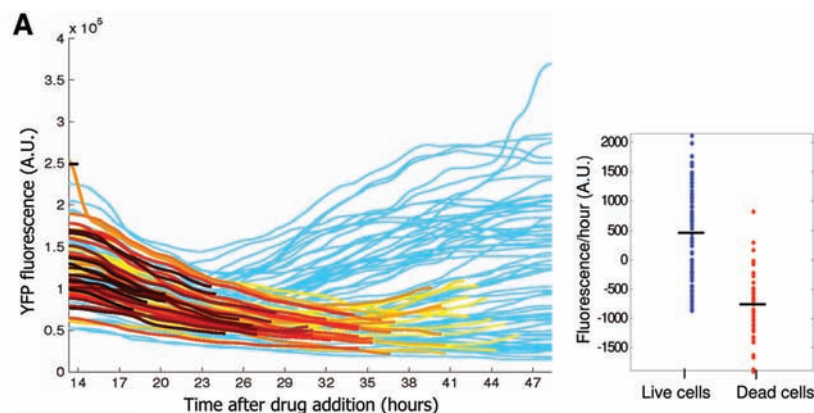
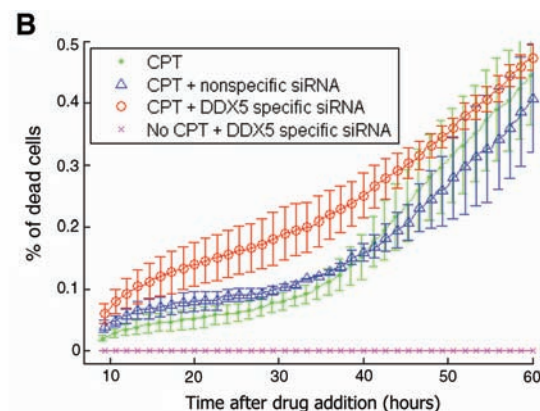


Fig. 5. DDX5 shows bimodal behavior that corresponds to the fate of individual cells. (**A**) The RNA helicase DDX5 shows an increase in intensity in cells that survive the drug after 48 hours, and a decrease in cells that show the morphological changes associated with cell death. Heavy colored lines are cells that die, with darker colors corresponding to earlier cell death. Blue lines are cells that survived to the end of the movie. (Right) Cells that show the morphological correlates of cell death



have significantly higher slopes of DDX5 fluorescence accumulation than cells that do not (*t* test, $P < 10^{-13}$). Slopes are defined as in Fig. 4. (**B**) Knockdown of DDX5 causes increased rate of cell death in the presence of CPT (red line). Controls include CPT added to cells treated with nonspecific RNAi (blue line) or no RNAi (green line). Cells treated with RNAi specific to DDX5 show no cell death in the absence of CPT (pink line).

the dynamics of specific proteins. Cells respond to the drug by highly specific translocation events that correspond to the drug mode of action. Observation of these effects was enabled by measuring the proteome dynamics in space and time in individual cells. The present approach provides a window into human cell biology and opens the way for understanding how seemingly identical cells show different responses to signals and drugs.

References and Notes

1. K. A. Janes *et al.*, *Science* **310**, 1646 (2005).
2. J. R. Newman *et al.*, *Nature* **441**, 840 (2006).
3. A. Belle, A. Tanay, L. Bitincka, R. Shamir, E. K. O'Shea, *Proc. Natl. Acad. Sci. U.S.A.* **103**, 13004 (2006).
4. W. K. Huh *et al.*, *Nature* **425**, 686 (2003).
5. Z. E. Perlman *et al.*, *Science* **306**, 1194 (2004).
6. P. Yeh, A. I. Tschumi, R. Kishony, *Nat. Genet.* **38**, 489 (2006).
7. D. W. Young *et al.*, *Nat. Chem. Biol.* **4**, 59 (2008).
8. Y. Pommier, *Nat. Rev. Cancer* **6**, 789 (2006).
9. J. W. Jarvik *et al.*, *Biotechniques* **33**, 852 (2002).
10. J. W. Jarvik, C. A. Telmer, *Annu. Rev. Genet.* **32**, 601 (1998).
11. J. W. Jarvik, S. A. Adler, C. A. Telmer, V. Subramaniam, A. J. Lopez, *Biotechniques* **20**, 896 (1996).
12. A. Sigal *et al.*, *Nature* **444**, 643 (2006).
13. A. Sigal *et al.*, *Nat. Methods* **3**, 525 (2006).
14. A. Sigal *et al.*, *Nat. Protocols* **2**, 1515 (2007).
15. Materials and methods are available as supporting material on Science Online.
16. U. S. Eggert, T. J. Mitchison, *Curr. Opin. Chem. Biol.* **10**, 232 (2006).
17. C. J. Echeverri, N. Perrimon, *Nat. Rev. Genet.* **7**, 373 (2006).
18. S. G. Megason, S. E. Fraser, *Cell* **130**, 784 (2007).
19. R. Pepperkok, J. Ellenberg, *Nat. Rev. Mol. Cell Biol.* **7**, 690 (2006).
20. L. Trinkle-Mulcahy, A. I. Lamond, *Science* **318**, 1402 (2007).
21. P. J. Clyne, J. S. Brotman, S. T. Sweeney, G. Davis, *Genetics* **165**, 1433 (2003).
22. X. Morin, R. Daneman, M. Zavortink, W. Chia, *Proc. Natl. Acad. Sci. U.S.A.* **98**, 15050 (2001).
23. S. D. Desai, L. F. Liu, D. Vazquez-Abad, P. D'Arpa, *J. Biol. Chem.* **272**, 24159 (1997).
24. M. T. Muller, W. P. Pfund, V. B. Mehta, D. K. Task, *EMBO J.* **4**, 1237 (1985).
25. J. S. Andersen *et al.*, *Nature* **433**, 77 (2005).
26. K. Kalita, D. Makonchuk, C. Gomes, J. J. Zheng, M. Hetman, *J. Neurochem.* **105**, 2286 (2008).
27. R. Sakasai *et al.*, *Genes Cells* **11**, 237 (2006).
28. V. M. Vassin, M. S. Wold, J. A. Borowiec, *Mol. Cell. Biol.* **24**, 1930 (2004).
29. M. Kaern, T. C. Elston, W. J. Blake, J. J. Collins, *Nat. Rev. Genet.* **6**, 451 (2005).
30. M. B. Elowitz, A. J. Levine, E. D. Siggia, P. S. Swain, *Science* **297**, 1183 (2002).
31. E. M. Ozbudak, M. Thattai, I. Kurtser, A. D. Grossman, A. van Oudenaarden, *Nat. Genet.* **31**, 69 (2002).
32. A. Bar-Even *et al.*, *Nat. Genet.* **38**, 636 (2006).
33. E. R. Parrilla-Castellar, S. J. Arlander, L. Karnitz, *DNA Repair (Amsterdam)* **3**, 1009 (2004).
34. L. Yang, C. Lin, S. Y. Sun, S. Zhao, Z. R. Liu, *Oncogene* **26**, 6082 (2007).
35. E. S. Witze, W. M. Old, K. A. Resing, N. G. Ahn, *Nat. Methods* **4**, 798 (2007).
36. R. Aebersold, M. Mann, *Nature* **422**, 198 (2003).
37. S. Ghaemmaghami *et al.*, *Nature* **425**, 737 (2003).
38. We thank the Kahn Family Foundation and the Israel Science Foundation for support. We thank E. Zalckvar, J. Bar, I. Glinert, T. Shlapok, and members of the Alon laboratory for discussions. The work of M.F.-M. and E.E. is supported by the Yeshaya Horowitz Association through the Center for Complexity Science.

Supporting Online Material

www.sciencemag.org/cgi/content/full/1160165/DC1

Materials and Methods

SOM Text

Figs. S1 to S20

Tables S1 to S4

References

Movies S1 to S4

7 May 2008; accepted 31 October 2008

Published online 20 November 2008;

10.1126/science.1160165

Include this information when citing this paper.

Tough, Bio-Inspired Hybrid Materials

E. Munch,¹ M. E. Launey,¹ D. H. Alsem,^{1,2} E. Saiz,¹ A. P. Tomsia,¹ R. O. Ritchie^{1,3*}

The notion of mimicking natural structures in the synthesis of new structural materials has generated enormous interest but has yielded few practical advances. Natural composites achieve strength and toughness through complex hierarchical designs that are extremely difficult to replicate synthetically. We emulate nature's toughening mechanisms by combining two ordinary compounds, aluminum oxide and polymethyl methacrylate, into ice-templated structures whose toughness can be more than 300 times (in energy terms) that of their constituents. The final product is a bulk hybrid ceramic-based material whose high yield strength and fracture toughness [~ 200 megapascals (MPa) and ~ 30 MPa \cdot m^{1/2}] represent specific properties comparable to those of aluminum alloys. These model materials can be used to identify the key microstructural features that should guide the synthesis of bio-inspired ceramic-based composites with unique strength and toughness.

The quest for more-efficient energy-related technologies necessitates the development of lightweight, high-performance structural materials with exceptional strength and toughness. Unfortunately, these two properties tend to be mutually exclusive, and attaining optimal mechanical performance is invariably a compromise often achieved through the empirical design of microstructures. Nature has long developed the ability to combine brittle minerals and organic molecules into hybrid composites with exceptional fracture resistance and structural capabilities (1–3); indeed, many natural materials

like bone, wood, and nacre (abalone shell) have highly sophisticated structures with complex hierarchical designs whose properties far exceed what could be expected from a simple mixture of their components (2, 4). Biological mineralized composites, in particular bone, dentin, and nacre (5–7), can generate fracture toughness (resistance to the initiation and growth of a crack) primarily by extrinsic toughening mechanisms (8) that “shield” any crack from the applied loads. These mechanisms—which are quite different from those that toughen metals, for example—are created over so many dimensions (nano to macro) that it makes them very difficult to replicate in a synthetic material. From a fracture mechanics perspective, the presence of these mechanisms results in characteristic crack resistance-curve (R curve) behavior such that the fracture resistance actually increases with crack extension; that is, these materials develop their toughening primarily during crack growth, not during

crack initiation. A prime example is nacre, which consists of 95 vol. % of layered aragonite (CaCO₃) platelets bonded by a thin layer of organic material, yet exhibits a toughness (in energy terms) some three orders of magnitude higher than that of calcium carbonate (2). The hard aragonite provides strength, but without a means to dissipate strain, nacre would be brittle; however, large inelastic deformation generated by interlayer shearing through the organic phase allows for such strain redistribution (9), so that toughness is achieved through viscoplastic energy dissipation in the organic layer associated with the controlled, yet limited, sliding of the aragonite layers over each other. Although there is controversy over the mechanisms that restrain sliding—resistance from the lamellae nanoroughness (10), plastic deformation of the aragonite at the nanolevel (11), the organic layer acting as a viscoelastic glue (12), or from the presence of mineral bridges (2, 13)—the resulting toughness is remarkable. Attempts have been made to simulate this in synthetic materials, such as lamellar materials fabricated with conventional processing (tape or slip casting); however, the resulting layer thicknesses are typically more than two orders of magnitude larger than the ~ 0.5 - μ m aragonite platelet spacing in nacre (14, 15). Such submicrometer layer spacings can be achieved by physical or chemical deposition, but not for bulk materials, because the techniques are restricted to the fabrication of thin films (16–19).

Processing strategy. Here, we apply this natural concept of hierarchical design to ceramic/polymer [Al₂O₃/PMMA (polymethyl methacrylate)] hybrid materials, which we fabricate in bulk form by freeze casting (20–24). Using controlled freezing of ceramic-based suspensions in wa-

¹Materials Sciences Division, Lawrence Berkeley National Laboratory, Berkeley, CA 94720, USA. ²National Center for Electron Microscopy, Lawrence Berkeley National Laboratory, Berkeley, CA 94720, USA. ³Department of Materials Science and Engineering, University of California, Berkeley, CA 94720, USA.

*To whom correspondence should be addressed. E-mail: roritchie@lbl.gov

ter, we form large porous ceramic scaffolds (fig. S1) with architectures that are templated by the ice crystals. We first use directional freezing to promote the formation of lamellar ice with prescribed dimensions; this acts as the “negative” for creation of the layered ceramic scaffolds, which are subsequently infiltrated with the polymeric second phase. In addition to making lamellar structures, we also fabricate nacre-like “brick-and-mortar” structures, with very high ceramic content, by subsequently pressing the scaffolds in the direction perpendicular to the lamellae in order to collapse them, followed by a second sintering step to promote densification and the formation of ceramic bridges between

the “bricks” (fig. S2). Using such techniques, we have made complex hierarchical architectures that allow us to refine the lamellae thickness, control their macroscopic orientation, manipulate the chemistry and roughness of the inter-lamellae interfaces, and generate a given density of inorganic bridges, all over a range of size scales.

In an attempt to replicate the microstructural design of nacre, we reduced the average lamellae thickness to 5 μm (which is still ~ 10 times thicker than the natural material) and used sucrose as an additive to the ceramic slurries (Fig. 1, A and B). Sucrose modifies the viscosity and phase diagram of the solvent,

resulting in the formation of ice crystals with a characteristic microscopic roughness and bridge density similar to that in nacre (Fig. 1, C and D). Control of the lamellae roughness provided a mechanical means to manipulate adhesion at the inorganic/organic layer interfaces. This can be complemented at the molecular level by chemically grafting a methacrylate group onto the ceramic surfaces before PMMA infiltration using in situ free-radical polymerization; the presence of the methacrylate groups then acts to promote stronger covalent bonding between the two phases (Fig. 2 and fig. S2). To achieve a macroscopic alignment of the lamellae similar to that in nacre (over millimeter

Fig. 1. Structure of ice-templated materials. (A) Al_2O_3 /PMMA lamellar composites have been fabricated by freeze casting of ceramic suspensions followed by polymer infiltration (the lighter phase is the ceramic; the dark phase is the polymer). (B) Brick-and-mortar architectures are prepared through pressing of the lamellar materials and subsequent sintering and have much larger ceramic contents (up to 80 vol. %). (C) When sucrose is used as an additive to the freeze-casting slurry, the growing ice crystals develop a characteristic surface topography that translates into a microscopic roughness in the ceramic walls. (D) The process also results in the formation of ceramic bridges between lamellae (due to the trapping of ceramic particles by the growing ice) or bricks (the bridges form during the second sintering steps). By limiting sliding, they provide very effective toughening mechanisms in natural and synthetic materials. The alumina grain size inside the lamellae or bricks is $\sim 1 \mu\text{m}$. Scale bars: 100 μm [(A) and (B)], 10 μm (C), and 600 nm (D).

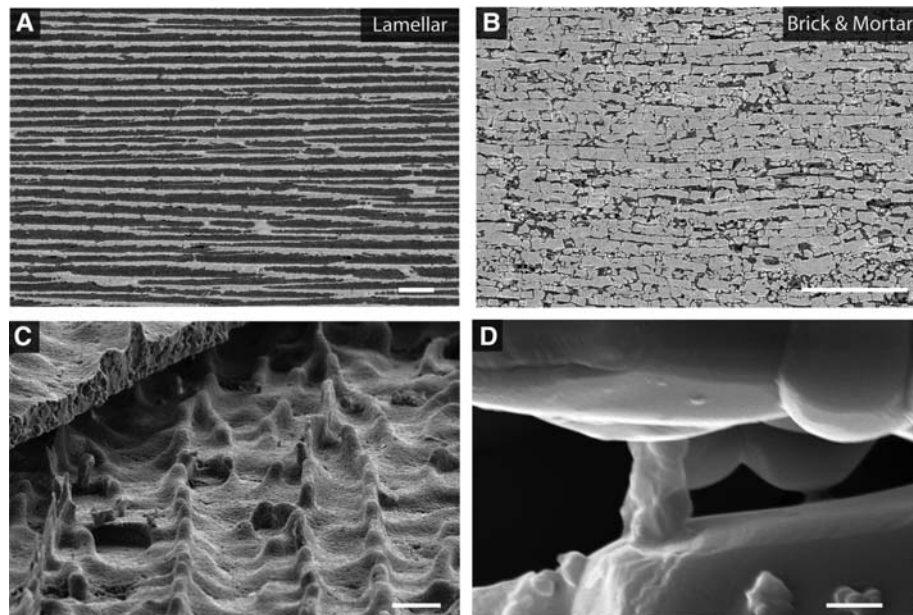
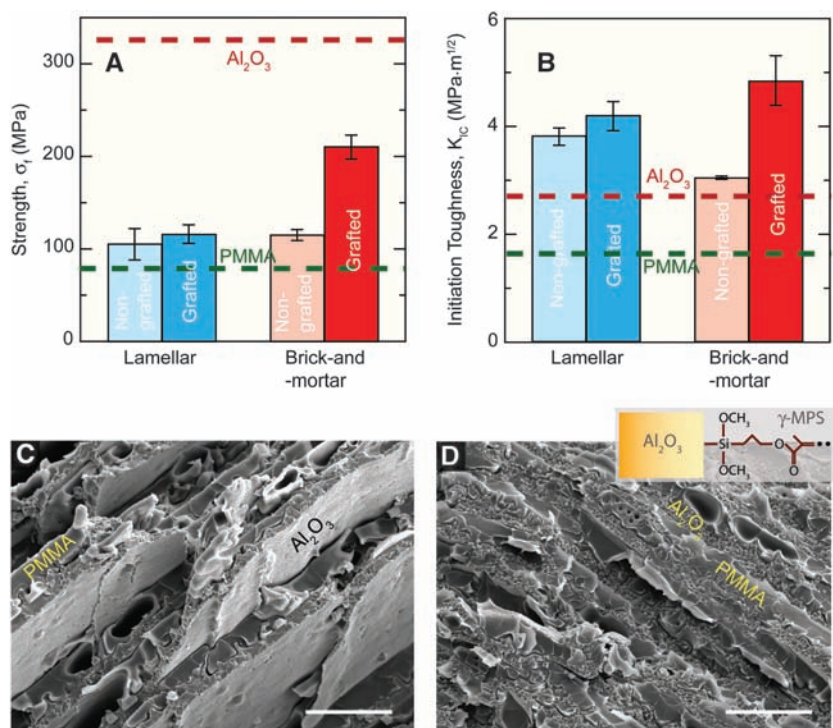


Fig. 2. Influence of interfacial chemistry on the mechanical response. (A) The strength of the hybrid composites can reach values above 200 MPa. (B) The crack-initiation fracture toughness, K_{IC} , can be up to twice that of the materials components. Chemical grafting increases the adhesion at the organic/inorganic interface and enhances both strength and initiation toughness. The error bars represent $\pm\text{SD}$. (C) The scanning electron micrograph (SEM) of the fracture surface of a lamellar material with nongrafted interfaces (which leads to weaker boundaries) shows extensive interface delamination during fracture. (D) Chemical grafting (inset) results in better adhesion (stronger boundaries) and fracture surfaces that are much flatter. Scale bars indicate 5 μm [(C) and (D)].



dimensions or more), we patterned the cold finger on which the ice nucleates using parallel, $\sim 40\ \mu\text{m}$, grooves. Brick-and-mortar architectures, prepared through pressing of the

lamellar materials and subsequent sintering, have a much larger ceramic content (up to 80 vol. %). The ceramic “bricks” are 5 to 10 μm wide and 20 to 100 μm long. Although the

polymer layers have an overall average thickness of ~ 1 to 2 μm , there are large areas in which the alumina bricks are separated by submicrometer polymer films similar to the microstructure of natural nacre (Fig. 3D). After infiltrating these porous scaffolds with the polymer, we produced a series of Al_2O_3 /PMMA hybrid composites (Fig. 1, A and B), with hierarchical structures spanning multiple length scales that exhibit distinctive structural and mechanistic features similar to those in nacre.

Replicating the mechanical response of natural structures. Matching the structural features of natural materials is not easy, but attaining their unique combinations of mechanical properties is much more difficult and has rarely been achieved. In natural and biological materials, desired properties are often achieved in a directional fashion (2, 25); indeed, certain engineering materials have also been optimized with highly anisotropic properties, as in multilayer ceramic armor materials to laminated epoxy/carbon fiber composites and directionally solidified turbine blade alloys for aerospace engineering (26–28). Similarly, the flexural strengths of our ice-templated hybrid materials are high in the direction perpendicular to the lamellae and comparable to that of alumina, with values of 120 to 210 MPa for the lamellae and brick-and-mortar structures, respectively (Fig. 2A). More importantly though, corresponding plane-strain K_{Ic} fracture toughnesses (which represent values for crack initiation) are almost double of what could be expected from the simple “rule of mixtures” of Al_2O_3 and PMMA (Fig. 2B). The reference alumina values here correspond to bulk samples prepared by slip casting in our laboratory. The suspensions for slip casting and freeze casting use the same starting powders and similar solid contents with identical sintering cycles (29). Slip casting was selected because, as for freeze casting, the ceramic sample forms through the packing of powders from a liquid suspension.

Whereas grafting to improve Al_2O_3 /PMMA interface adhesion (Fig. 2, C and D) resulted in a mildly higher strength and initiation toughness for lamellar structures, a very significant increase was seen for the brick-and-mortar structure (Fig. 2, A and B). However, the most notable feature of our synthetic composites is that they replicate the mechanical behavior of natural materials; specifically, they display large ($>1\%$) inelastic strains when loaded in tension (Fig. 3A) and develop exceptional toughness for crack growth (Fig. 3B). Like many hard mineralized biocomposites, the ice-templated materials exhibit a high degree of inelasticity, despite the brittle nature of their main ceramic constituent. Although single-value linear-elastic parameters based on crack initiation, such as K_{Ic} , have traditionally been used to quantify toughness, they cannot capture, or even represent, the multiple length-scale toughening acting in these compos-

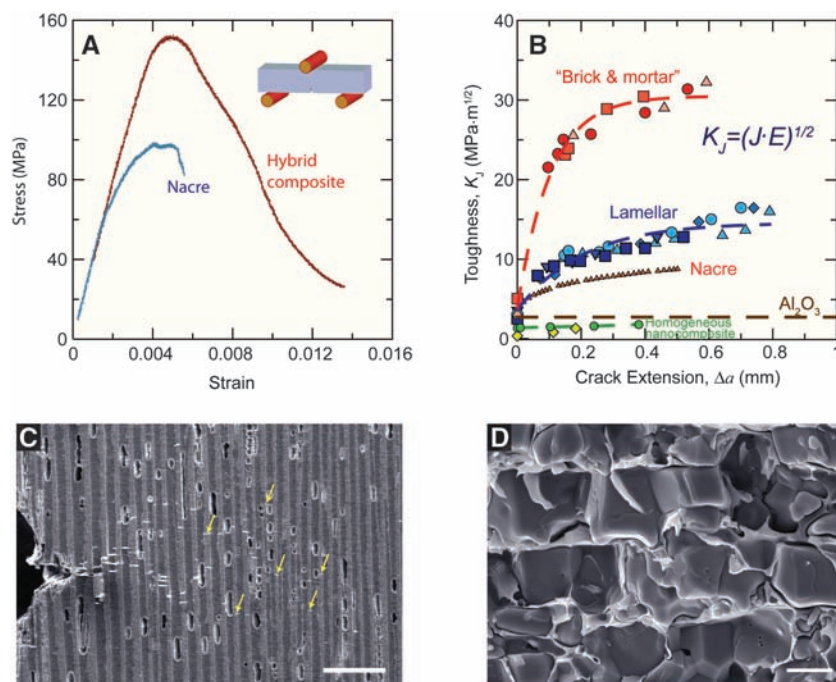


Fig. 3. Mechanical response and toughening mechanisms in the synthetic hybrid composites. **(A)** Bending stress-strain curves for the Al_2O_3 /PMMA hybrid materials mimic those of nacre and show $>1\%$ inelastic deformation before failure. The curves correspond to nongrafted lamellar hybrid composite and hydrated nacre (abalone shell). **(B)** These materials show exceptional toughness for crack growth, similar to natural composites, and display significant rising R-curve behavior. Almost negligible toughening is observed in nanocomposites consisting of 500 nm Al_2O_3 particles dispersed in PMMA. **(C)** Scanning electron micrograph taken during an in situ R-curve measurement of a lamellar structure. The image taken during crack propagation shows two of the toughening mechanisms acting at large scales: the wide distribution of damage (over millimeter dimensions) in the form of contained microcracking within the ceramic layers (yellow arrows point to some of these microcracks) and the voids in the polymer layers. **(D)** Fracture surface of a grafted brick-and-mortar structure. Controlled sliding contributes to a rise of the crack-growth toughness to values that can be >300 times higher (in energy terms) than that of Al_2O_3 . In addition to the roughness of the ceramic surfaces and the inorganic bridges between ceramic bricks, a principal reason for the controlled sliding is the presence of a submicrometer polymer film between alumina blocks. Scale bars: 250 μm (C) and 3 μm (D).

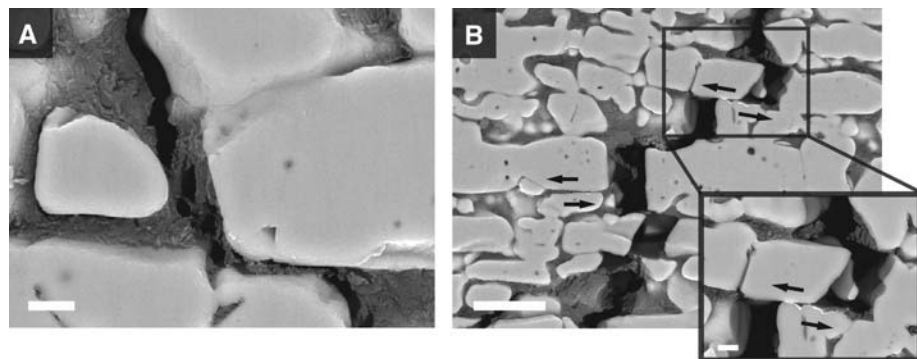


Fig. 4. Toughening mechanisms in brick-and-mortar microstructures. In situ imaging of crack propagation in brick-and-mortar structures shows clear evidence of **(A)** polymer tearing and stretching over micrometer dimensions (as have also been observed in the organic phase of nacre) and **(B)** “pull out” and frictional sliding between ceramic bricks (inset; arrows indicate the direction of sliding). The thin bright lines between the sliding grains in the inset indicate electrical charging in the SEM resulting from the deformation of the gold coating during sliding. Scale bars: 2 μm [(A) and the inset in (B)] and 10 μm (B).

of most monolithic structural ceramics with engineered grain boundaries, i.e., coarse-grained Al_2O_3 , Si_3N_4 , and SiC (35–42). However, the contribution from bridging alone does not explain why the observed toughness of the best brick-and-mortar 80% alumina structure ($J_c \sim 8000 \text{ J/m}^2$) is more than 300 times higher in terms of energy than the toughness of its main constituent, Al_2O_3 ($J_c \sim 26 \text{ J/m}^2$). We believe that of the various hybrid materials that we have fabricated, this structure best mimics nacre. Freeze casting followed by pressing and a second sintering stage results in a microstructure with high ceramic contents characterized by the submicrometer lubricating polymer interlayers between ceramic “bricks” (deformation and micrometer-scale tearing in these interlayers can be seen in Fig. 4A); combined with the roughness of the ceramic interfaces and the presence of stiff ceramic bridges between grains with micrometer and submicrometer dimensions (Fig. 1, C and D), this method promotes controlled sliding and “sliding interference” (Fig. 4) between the rough ceramic interlayers, thereby enhancing the toughness through extremely efficient energy dissipation. The result is synthetic materials that, like nacre and bone, are far tougher than what could be expected from the simple mixture of their constituents (Fig. 5A).

Concluding remarks and future challenges.

A better appreciation of the unique mechanical properties of these freeze-cast composites can be gained by comparing them to other materials. By combining two relatively ordinary phases, i.e., a hard yet brittle ceramic with a relatively soft (in comparison) polymer, we have synthesized primarily (ceramic) alumina hybrid structures with specific strength and toughness properties that match those of engineering (metallic) aluminum alloys (Fig. 5B) and moreover display a higher stiffness. This has been made possible through the development of hierarchical architectures that combine toughening mechanisms acting at multiple scales, from submicrometer dimensions (i.e., the ceramic bridges between lamellae or bricks or the inelastic polymer deformation) and higher. These results highlight the tremendous potential of the biomimetic approach and suggest promising strategies for structural optimization. In particular, a key attribute of nacre has been extremely difficult to replicate: The structure consists of 95 vol. % ceramic with very little of the organic soft phase, which is distributed as a thin (2 to 3 nm) protein film that acts like a lubricant. At present, our materials contain too much of the soft phase, and our ceramic layer thicknesses are still somewhat coarse in comparison to nacre; indeed, a reduction in the polymer content and refinement of the ceramic layers should improve strength and provide additional nanoscale toughening mechanisms similar to those acting in natural materials. In this regard, our current studies are focused on the development of these hybrid structures with

much higher inorganic content, the manipulation of the properties of the soft lubricating phase, and extending this concept to other material combinations, principally metal-infiltrated ceramics.

References and Notes

- G. Mayer, *Science* **310**, 1144 (2005).
- M. A. Meyers, P. Y. Chen, A. Y. M. Lin, Y. Seki, *Prog. Mater. Sci.* **53**, 1 (2008).
- C. Ortiz, M. C. Boyce, *Science* **319**, 1053 (2008).
- J. Aizenberg *et al.*, *Science* **309**, 275 (2005).
- F. Barthelat, H. D. Espinosa, *Exp. Mech.* **47**, 311 (2007).
- R. K. Nalla, J. H. Kinney, R. O. Ritchie, *Biomaterials* **24**, 3955 (2003).
- R. K. Nalla, J. J. Kruzic, J. H. Kinney, R. O. Ritchie, *Biomaterials* **26**, 217 (2005).
- R. O. Ritchie, *Mater. Sci. Eng. A* **103**, 15 (1988).
- R. Z. Wang, Z. Suo, A. G. Evans, N. Yao, I. A. Aksay, *J. Mater. Res.* **16**, 2485 (2001).
- A. G. Evans *et al.*, *J. Mater. Res.* **16**, 2475 (2001).
- X. D. Li, W. C. Chang, Y. J. Chao, R. Z. Wang, M. Chang, *Nano Lett.* **4**, 613 (2004).
- B. L. Smith *et al.*, *Nature* **399**, 761 (1999).
- F. Song, A. K. Soh, Y. L. Bai, *Biomaterials* **24**, 3623 (2003).
- H. M. Chan, *Annu. Rev. Mater. Sci.* **27**, 249 (1997).
- J. S. Moya, *Adv. Mater.* **7**, 185 (1995).
- A. Sellinger *et al.*, *Nature* **394**, 256 (1998).
- Z. Tang, N. A. Kotov, S. Magonov, B. Ozturk, *Nat. Mater.* **2**, 413 (2003).
- L. J. Bonderer, A. R. Studart, L. J. Gauckler, *Science* **319**, 1069 (2008).
- P. Podsiadlo *et al.*, *Science* **318**, 80 (2007).
- S. Deville, E. Saiz, R. K. Nalla, A. P. Tomsia, *Science* **311**, 515 (2006).
- S. Deville, E. Saiz, A. P. Tomsia, *Acta Mater.* **55**, 1965 (2007).
- T. Fukasawa, M. Ando, T. Ohji, S. Kanzaki, *J. Am. Ceram. Soc.* **84**, 230 (2001).
- T. Fukasawa, Z. Y. Deng, M. Ando, T. Ohji, Y. Goto, *J. Mater. Sci.* **36**, 2523 (2001).
- K. Araki, J. W. Halloran, *J. Am. Ceram. Soc.* **87**, 1859 (2004).
- K. J. Koester, J. W. Ager, R. O. Ritchie, *Nat. Mater.* **7**, 672 (2008).
- A. Tasdemirci, I. W. Hall, B. A. Gama, M. Guiden, *J. Compos. Mater.* **38**, 995 (2004).
- D. R. Johnson, X. F. Chen, B. F. Oliver, R. D. Noebe, J. D. Whittenberger, *Intermetallics* **3**, 99 (1995).
- R. M. Jones, *Mechanics of Composite Materials* (Taylor & Francis, Philadelphia, PA, ed. 2, 1999).
- Supporting online material on Science Online.
- J. K. Shang, R. O. Ritchie, *Metallurg. Trans. A* **20**, 897 (1989).
- Instead of crack extension being solely associated with the main crack tip growing forward, crack advance also can occur by microcracks (or other damage) initiated ahead of the main crack tip linking back to the tip.
- J. Cook, C. C. Evans, J. E. Gordon, D. M. Marsh, *Proc. R. Soc. Lond. A Math. Phys. Sci.* **282**, 508 (1964).
- L. S. Sigl, P. A. Mataga, B. J. Dalgleish, R. M. McMeeking, A. G. Evans, *Acta Metall.* **36**, 945 (1988).
- A. Y. M. Lin, P. Y. Chen, M. A. Meyers, *Acta Biomater.* **4**, 131 (2008).
- P. F. Becher *et al.*, *J. Am. Ceram. Soc.* **81**, 2821 (1998).
- J. J. Cao, W. J. MoberlyChan, L. C. Dejonghe, C. J. Gilbert, R. O. Ritchie, *J. Am. Ceram. Soc.* **79**, 461 (1996).
- J. J. Kruzic, R. M. Cannon, R. O. Ritchie, *J. Am. Ceram. Soc.* **87**, 93 (2004).
- J. J. Kruzic, R. M. Cannon, R. O. Ritchie, *J. Am. Ceram. Soc.* **88**, 2236 (2005).
- F. F. Lange, *J. Am. Ceram. Soc.* **56**, 518 (1973).
- Y. W. Mai, B. R. Lawn, *J. Am. Ceram. Soc.* **70**, 289 (1987).
- N. P. Padture, B. R. Lawn, *J. Am. Ceram. Soc.* **77**, 2518 (1994).
- P. L. Swanson, C. J. Fairbanks, B. R. Lawn, Y. W. Mai, B. J. Hockey, *J. Am. Ceram. Soc.* **70**, 279 (1987).
- U. G. K. Wegst, M. F. Ashby, *Philos. Mag.* **84**, 2167 (2004).
- This work was supported by the Director, Office of Science, Office of Basic Energy Sciences, Division of Materials Sciences and Engineering, of the U.S. Department of Energy under Contract No. DE-AC02-05CH11231

Supporting Online Material

www.sciencemag.org/cgi/content/full/322/5907/1516/DC1
Materials and Methods
Figs. S1 and S2
References

19 August 2008; accepted 21 October 2008
10.1126/science.1164865

Metallic and Insulating Phases of Repulsively Interacting Fermions in a 3D Optical Lattice

U. Schneider,¹ L. Hackermüller,¹ S. Will,¹ Th. Best,¹ I. Bloch,^{1,2*} T. A. Costi,³ R. W. Helmes,⁴ D. Rasch,⁴ A. Rosch⁴

The fermionic Hubbard model plays a fundamental role in the description of strongly correlated materials. We have realized this Hamiltonian in a repulsively interacting spin mixture of ultracold ^{40}K atoms in a three-dimensional (3D) optical lattice. Using in situ imaging and independent control of external confinement and lattice depth, we were able to directly measure the compressibility of the quantum gas in the trap. Together with a comparison to ab initio dynamical mean field theory calculations, we show how the system evolves for increasing confinement from a compressible dilute metal over a strongly interacting Fermi liquid into a band-insulating state. For strong interactions, we find evidence for an emergent incompressible Mott insulating phase. This demonstrates the potential to model interacting condensed-matter systems using ultracold fermionic atoms.

Interacting fermions in periodic potentials lie at the heart of condensed-matter physics, presenting some of the most challenging problems to quantum many-body theory. A prominent example is high-temperature superconductivity in cuprate compounds (1). An essential part of the physics in these systems is described by the

fermionic Hubbard Hamiltonian (2), which models interacting electrons in a periodic potential (1, 3). In a real solid, however, the effects of interest are typically complicated by, for example, multiple bands, impurities, and the long-range nature of Coulomb interactions, which becomes especially relevant close to a metal-to-insulator transition.

Probing this Hamiltonian in a controllable and clean experimental setting is therefore of great importance. Ultracold atoms in optical lattices provide such a defect-free system (4, 5), in which the relevant parameters can be independently controlled, thus allowing quantitative comparisons of the experiment with modern quantum many-body theories. For the case of bosonic particles (6, 7), the importance of ultracold quantum gases in this respect has been shown in a series of experiments on the superfluid-to-Mott insulator transition (8–10). For both bosonic and fermionic systems, the entrance into a Mott insulating state is signaled by a vanishing compressibility, which can in principle be probed experimentally by testing the response of the system to a change in external confinement. This is a straightforward way to identify the interaction-induced Mott insulator and to distinguish it, for instance, from a disorder-induced Anderson insulator (11–13). In a solid, however, the corresponding compressibility can usually not be measured directly, because a compression of the crystalline lattice by an external force does not change the number of electrons per unit cell [see supporting online material (14)].

We have studied noninteracting and repulsively interacting spin mixtures of fermionic atoms deep in the degenerate regime in a three-dimensional (3D) optical lattice, where the interaction strength, the lattice depth, and the external harmonic confinement of the quantum gas can be varied independently. By monitoring the in-trap density distribution for increasing harmonic confinement, we directly probed the compressibility of the many-body system. This measurement allows us to clearly distinguish compressible metallic phases from globally incompressible states and reveals the strong influence of interactions on the density distribution. Additionally, we measured the fraction of atoms on doubly occupied lattice sites for different experimental parameters to probe the local onsite physics of the system. In previous experiments, a suppression of the number of doubly occupied sites was demonstrated for increasing interaction strength for bosons (15) and fermions (16) at fixed harmonic confinement, signaling the entrance into a strongly interacting regime.

We compare the experimentally observed density distributions and fractions of doubly occupied sites to numerical calculations, using dynamical mean field theory (DMFT) (17–20). DMFT is a central method of solid-state theory being widely used to obtain ab initio descriptions of strongly correlated materials (18). The comparison of DMFT predictions with experimental results on ultracold fermions in optical lattices

constitutes a parameter-free experimental test of the validity of DMFT in a 3D system.

Theoretical model. Restricting our discussion to the lowest-energy band of a simple cubic 3D optical lattice, the fermionic quantum gas mixture can be modeled via the Hubbard Hamiltonian (2), with an additional term describing the underlying harmonic potential

$$\hat{H} = -J \sum_{\langle i,j \rangle, \sigma} \hat{c}_{i,\sigma}^\dagger \hat{c}_{j,\sigma} + U \sum_i \hat{n}_{i,\downarrow} \hat{n}_{i,\uparrow} + V_t \sum_i (\hat{i}_x^2 + \hat{i}_y^2 + \gamma^2 \hat{i}_z^2) (\hat{n}_{i,\downarrow} + \hat{n}_{i,\uparrow}) \quad (1)$$

Here the indices i, j denote different lattice sites in the 3D system [$i = (i_x, i_y, i_z)$], $\langle i, j \rangle$ neighboring lattice sites, $\sigma \in \{\downarrow, \uparrow\}$ the two different spin states, J the tunneling matrix element, and U the effective onsite interaction. The operators $\hat{c}_{i,\sigma}$ are the annihilation operators of a fermion in spin state σ on the i th lattice site, $\hat{c}_{i,\sigma}^\dagger$ are the creation operators, and $\hat{n}_{i,\sigma}$ measures the corresponding atom number. The strength of the harmonic confinement is parameterized by the energy offset $V_t = \frac{1}{2} m \omega_\perp^2 d^2$ between two adjacent lattice sites at the trap center, with $\omega_\perp = \omega_x = \omega_y \neq \omega_z$ being the horizontal trap frequency, d the lattice constant, and m the mass of a single atom. The constant aspect ratio of the trap is denoted by $\gamma = \omega_z/\omega_\perp$. Because of the Pauli principle, every lattice site can be occupied by at most one atom per spin state.

The quantum phases of the Hubbard model with harmonic confinement are governed by the interplay between three energy scales: kinetic en-

ergy, whose scale is given by the lattice bandwidth $12J$; interaction energy U ; and the strength of the harmonic confinement, which can conveniently be expressed by the characteristic trap energy $E_t = V_t[\gamma N_\sigma/(4\pi/3)]^{2/3}$, which denotes the Fermi energy of a noninteracting cloud in the zero-tunneling limit, with N_σ being the number of atoms per spin state ($N_\downarrow = N_\uparrow$). The characteristic trap energy depends on both atom number and trap frequency via $E_t \propto \omega_\perp^2 N_\sigma^{2/3}$ and describes the effective compression of the quantum gas, controlled by the trapping potential in the experiment.

Depending on which term in the Hamiltonian dominates, different kinds of many-body ground states can occur in the trap center (Fig. 1). For weak interactions in a shallow trap, $U \ll E_t \ll 12J$, the Fermi energy is smaller than the lattice bandwidth ($E_F < 12J$), and the atoms are delocalized in order to minimize their kinetic energy. This leads to compressible metallic states with central filling $n_{0,\sigma} < 1$, where the local filling factor $n_{i,\sigma} = \langle \hat{n}_{i,\sigma} \rangle$ denotes the average occupation per spin state of a given lattice site. A dominating repulsive interaction $U \gg 12J$ and $U \gg E_t$ suppresses the double occupation of lattice sites and can lead to Fermi liquid ($n_{0,\sigma} < 1/2$) or Mott insulating ($n_{0,\sigma} = 1/2$) states at the trap center, depending on the ratio of kinetic energy to characteristic trap energy. Stronger compressions lead to higher filling factors, ultimately ($E_t \gg 12J$, $E_t \gg U$) resulting in an incompressible band insulator with unity central filling at zero temperature ($T = 0$).

Finite temperature reduces all filling factors and enlarges the cloud size, because the system needs to accommodate the corresponding entropy. Furthermore, in the trap the filling always varies

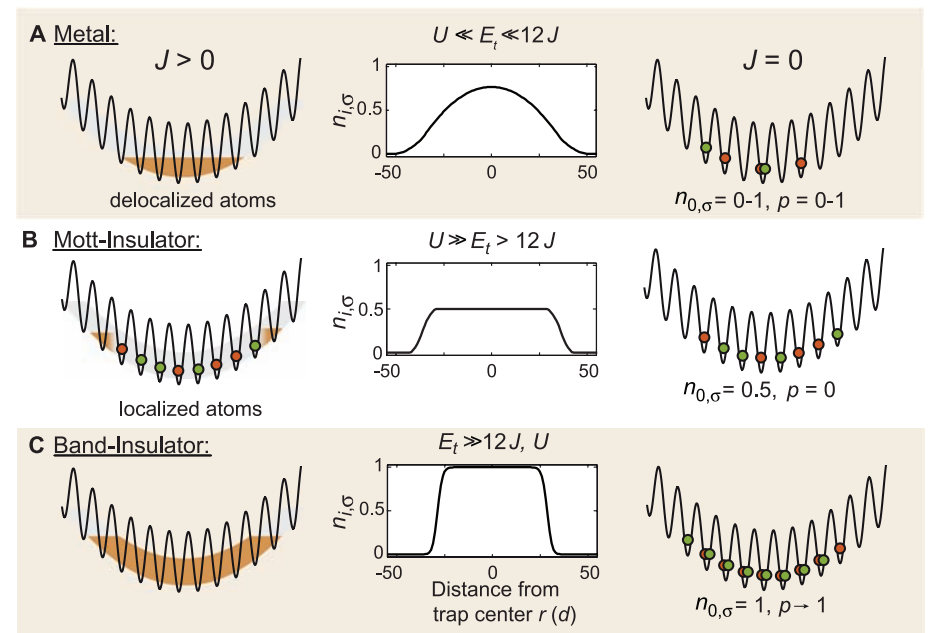


Fig. 1. (A to C) Relevant phases of the Hubbard model with an inhomogeneous trapping potential for a spin mixture at $T = 0$. A schematic is shown in the left column. The center column displays the corresponding in-trap density profiles, and the right column outlines the distribution of singly and doubly occupied lattice sites after a rapid projection into the zero tunneling limit, with p denoting the total fraction of atoms on doubly occupied lattice sites.

¹Institut für Physik, Johannes Gutenberg-Universität, 55099 Mainz, Germany. ²Max-Planck-Institut für Quantenoptik, 85748 Garching, Germany. ³Institut für Festkörperforschung und Institute for Advanced Simulation, Forschungszentrum Jülich, 52425 Jülich, Germany. ⁴Institut für Theoretische Physik, Universität zu Köln, 50937 Cologne, Germany.

*To whom correspondence should be addressed. E-mail: bloch@uni-mainz.de

smoothly from a maximum at the center to zero at the edges of the cloud. For a dominating trap and strong repulsive interaction at low temperature ($E_t > U > 12J$), the interplay between the different terms in the Hamiltonian gives rise to a wedding cake-like structure (Fig. 4, E and F) consisting of a band-insulating core ($n_{i,\sigma} \approx 1$) surrounded by a metallic shell ($1/2 < n_{i,\sigma} < 1$), a Mott insulating shell ($n_{i,\sigma} = 1/2$), and a further metallic shell ($n_{i,\sigma} < 1/2$) (19). The outermost shell always remains metallic, independent of interaction and confinement; only its thickness varies (figs. S7 and S8).

Experimental setup. We used an equal mixture of quantum degenerate fermionic ^{40}K atoms in the two hyperfine states $|F, m_F\rangle = |\frac{9}{2}, -\frac{9}{2}\rangle \equiv |\downarrow\rangle$ and $|\frac{9}{2}, -\frac{7}{2}\rangle \equiv |\uparrow\rangle$ in a pancake-shaped optical dipole trap (aspect ratio $\gamma \approx 4$), which was formed by overlapping two elliptical laser beams (wavelength $\lambda = 1030$ nm) traveling in the horizontal plane (14). Through evaporative cooling, final temperatures of $T/T_F = 0.15(3)$ with 1.5×10^5 to 2.5×10^5 potassium atoms were reached. The temperature was extracted from time-of-flight images by means of Fermi fits. A Feshbach resonance located at a magnetic field $B = 202.1$ G (21) was used to tune the scattering length a between the two spin states and thereby control the onsite interaction U . The creation of the spin mixture and the last evaporation step were performed either above the resonance (220 G), giving access to non-interacting (209.9 G) and repulsively interacting clouds with $a \leq 150 a_0$ (where a_0 denotes the Bohr radius), or below the resonance (165 G), where larger scattering lengths up to $a = 300 a_0$ (191.3 G) can be reached. A further approach to the Feshbach resonance was hindered by enhanced losses and heating in the lattice (22).

After evaporation, the magnetic field was tuned to the desired value. Subsequently, a blue-detuned 3D optical lattice ($\lambda_{\text{lat}} = 738$ nm) with simple cubic symmetry was increased to a potential depth of $V_{\text{lat}} = 1 E_r$, where $E_r = \hbar^2/(2m\lambda_{\text{lat}}^2)$ denotes the recoil energy.

The combination of a red-detuned dipole trap and a blue-detuned lattice potential allows us to vary lattice depth and external confinement independently. In this way, a wide range of horizontal trap frequencies can be accessed [$\omega_{\perp} \approx 2\pi \times (20 - 120)\text{Hz}$], especially enabling metallic states with high atom numbers. To monitor the in situ density distribution for different external confinements, we ramped the dipole trap depth in 100 ms to the desired external harmonic confinement, followed by a linear increase of the optical lattice depth to $V_{\text{lat}} = 8 E_r$ within 50 ms. An in situ image of the cloud was taken along the short (vertical) axis of the trap using phase-contrast imaging (23) at detunings of $\Delta = 2\pi \times (200 - 330)$ MHz after a hold time of 12 ms in the lattice. From this picture, the cloud size $R = \sqrt{\langle r_{\perp}^2 \rangle}$ was extracted by means of adapted 2D Fermi fits (fig. S6). Because phase-contrast imaging modifies the state of the atoms only marginally, the quasi-momentum distribution can be measured in the same experimental run with

a band-mapping technique (24–26). For this, the lattice is ramped down in 200 μs and a standard absorption image is taken after 10 ms time of flight.

All experimental data were compared to numerical calculations, in which the DMFT equations of the homogeneous model were solved for

a wide range of temperatures and chemical potentials using a numerical renormalization group approach (14) (27, 28). The trapped system can be approximated to very high accuracy by the uniform system through a local density approximation (LDA), even close to the boundary between a metal and an insulator (19, 29). For a

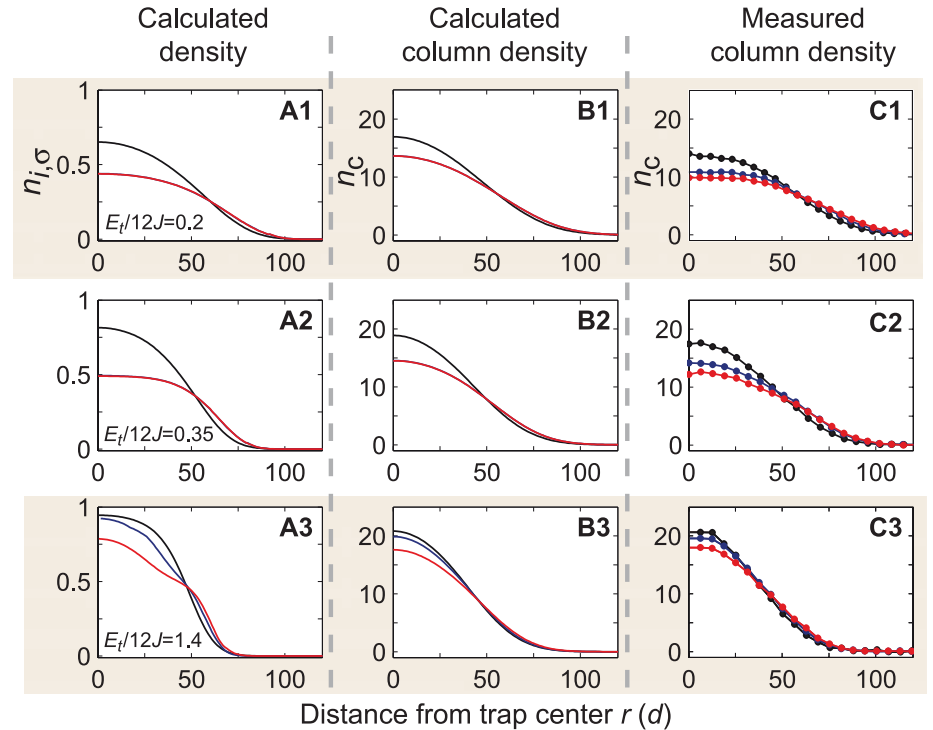


Fig. 2. Comparison of in-trap density profiles. Calculated radial density profiles for different compressions (harmonic confinements) $E_t/12J$ (left column, **A1** to **A3**), corresponding column densities obtained after integration over the z axis and convolution with the point spread function (14) of our imaging system (center column, **B1** to **B3**), and experimental results (azimuthally averaged over more than five shots) (**C1** to **C3**) for three different interaction strengths $U/12J = 0$ (black), $U/12J = 1$ (blue), and $U/12J = 1.5$ (red). At small compressions [(A) and (B)], the calculated density profiles for $U/12J = 1$ and $U/12J = 1.5$ are indistinguishable, because in both cases double occupations are almost completely suppressed for $n_{i,\sigma} < 1/2$.

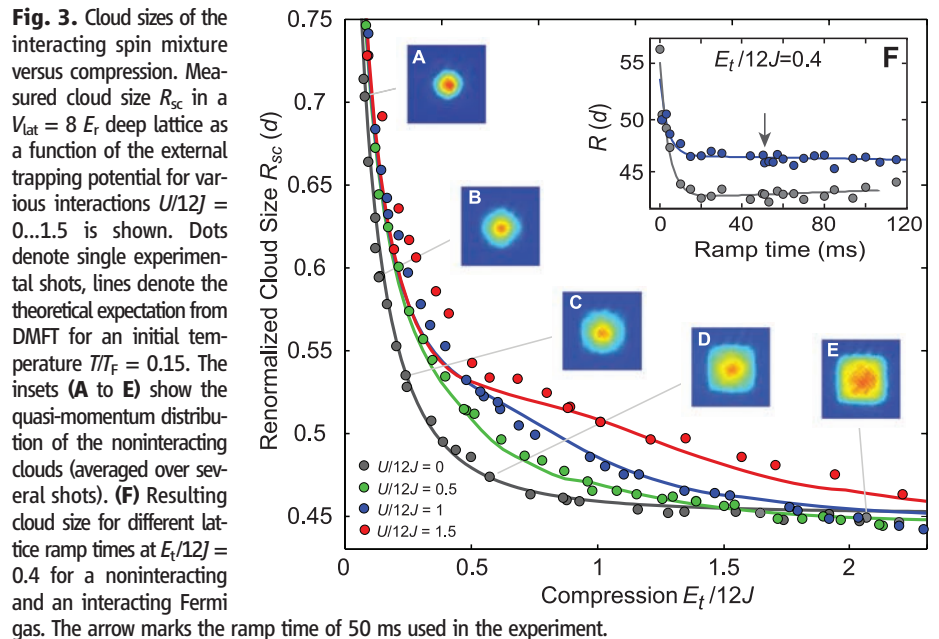


Fig. 3. Cloud sizes of the interacting spin mixture versus compression. Measured cloud size R_{sc} in a $V_{\text{lat}} = 8 E_r$ deep lattice as a function of the external trapping potential for various interactions $U/12J = 0 \dots 1.5$ is shown. Dots denote single experimental shots, lines denote the theoretical expectation from DMFT for an initial temperature $T/T_F = 0.15$. The insets (A to E) show the quasi-momentum distribution of the noninteracting clouds (averaged over several shots). (F) Resulting cloud size for different lattice ramp times at $E_t/12J = 0.4$ for a noninteracting and an interacting Fermi gas. The arrow marks the ramp time of 50 ms used in the experiment.

comparison with the experimental results, it is convenient to express the cloud size R in rescaled units $R_{sc} = R/(\gamma N_G)^{1/3}$, along with the dimensionless compression $E_t/12J$. In these units, the cloud size depends only on the interaction strength $U/12J$ and the entropy. In all calculations, we used the entropy determined from a noninteracting Fermi gas in a harmonic trap at an initial temperature T/T_F and assumed adiabatic lattice loading.

Cloud compression. The numerically calculated density distributions, the corresponding column densities, and the experimentally measured ones are presented in Fig. 2. Whereas for low compression all distributions are metallic (the first row), we find a Mott insulating core with half filling at intermediate compression and strong repulsion (the second row). For high compression, the noninteracting curve shows a band-insulating core and the repulsive curves display a metallic core. In order to compare experiment and theory quantitatively, the measured cloud size R_{sc} and the numerically calculated one are plotted in

Fig. 3 as a function of the characteristic trap energy E_t . Additionally, the global compressibility

$$\kappa_{R_{sc}} = -\frac{1}{R_{sc}} \frac{\partial R_{sc}}{\partial (E_t/12J)} \quad (\text{Fig. 4 and fig. S2})$$

of the system can be extracted from these measurements by means of linear fits to four consecutive data points to determine the derivative. In the noninteracting case, we find the cloud sizes (Fig. 3, black dots) to decrease continuously with compression until the characteristic trap energy roughly equals the lattice bandwidth ($E_t/12J \sim 1$). For stronger confinement, the compressibility approaches zero (Fig. 4A), because almost all atoms are in the band-insulating regime while the surrounding metallic shell becomes negligible. The corresponding quasi-momentum distribution (Fig. 3, A to E) changes gradually from a partially filled first Brillouin zone, characteristic for a metal, to an almost evenly filled first Brillouin zone for increasing compressions, as expected for a band insulator. However, a band-mapping technique reveals only

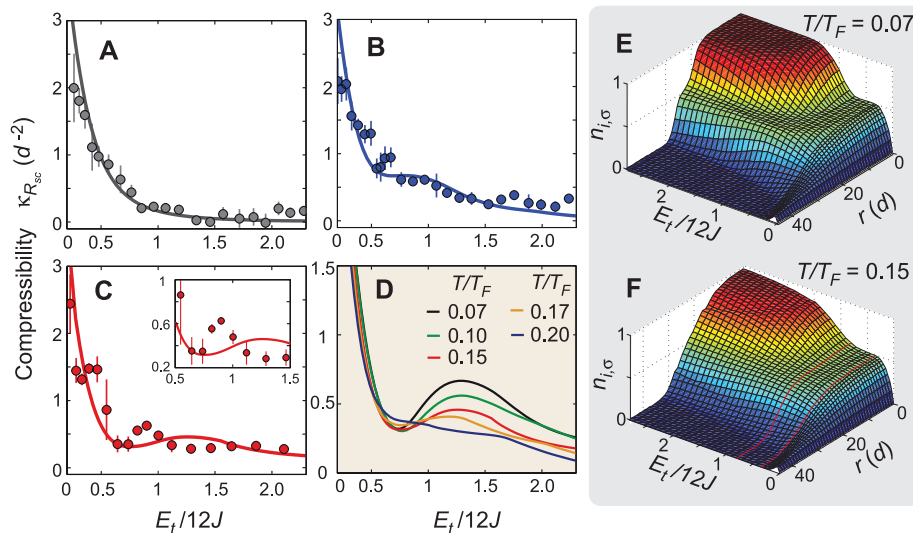
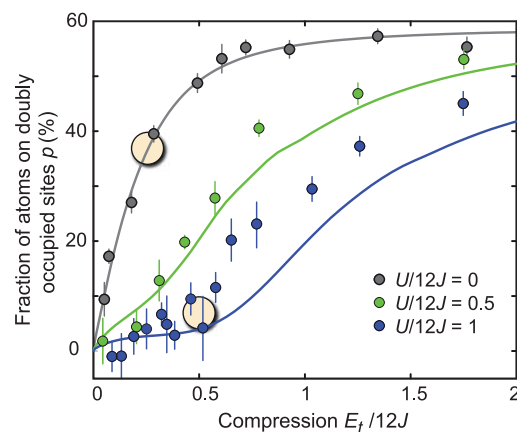


Fig. 4. Compressibility and in-trap density distribution. (A to C) Global compressibility $\kappa_{R_{sc}}$ of the atom cloud for various interactions [(A) $U/12J = 0$, (B) $U/12J = 1$, (C) $U/12J = 1.5$]. Dots denote the result of linear fits on the measured data, and the error bars represent the fit uncertainty. Solid lines display the theoretically expected results for an initial temperature $T/T_F = 0.15$. The influence of the initial temperature on the calculated compressibility is shown in (D) for $U/12J = 1.5$. The corresponding density distributions are plotted in (E) and (F), with r denoting the distance to the trap center (see also figs. S7 and S8). The red lines mark the region where a Mott insulating core has formed and the global compressibility is reduced.

Fig. 5. Fraction of atoms on doubly occupied sites versus compression for different interaction strengths $U/12J = 0 \dots 1$. The yellow circles indicate the fraction of atoms on doubly occupied sites for a constant cloud size $R_{sc} = 0.53$ (Fig. 3). The error bars denote the SD of at least four measurements.



the relative occupations of the extended Bloch states. For an inhomogeneous system, it therefore provides no information about the real-space density and especially cannot distinguish insulating from compressible states; for instance nonequilibrium states in which the atomic wavefunctions are localized to single lattice sites. In contrast, the measurements shown here directly demonstrate the incompressibility of the fermionic band insulator, in excellent agreement with the theoretical expectation for a noninteracting Fermi gas (Fig. 4A, black line).

For moderately repulsive interactions ($U/12J = 0.5, 1$) (Fig. 3, green and blue lines), the cloud size is clearly bigger than in the noninteracting case but eventually reaches the size of the band insulator. For stronger repulsive interactions ($U/12J = 1.5$) (Fig. 3B, red line), we find the onset of a region ($0.5 < E_t/12J < 0.7$) where the cloud size decreases only slightly with increasing harmonic confinement, whereas for stronger confinements the compressibility increases again. This is consistent with the formation of an incompressible Mott insulating core, surrounded by a compressible metallic shell, as can be seen in the corresponding in-trap density profiles (Fig. 4, E and F). For higher confinements, an additional metallic core ($1/2 < n_{i,\sigma} < 1$) starts to form in the center of the trap and the cloud size decreases again. A local minimum in the global compressibility is in fact a genuine characteristic of a Mott insulator, and for large U and low T , we expect the global compressibility in the middle of the Mott region to vanish as $1/U^2$ (fig. S1). The experimental data, indeed, show an indication of this behavior (Fig. 4 C) for increasing interactions. For $E_t/12J \approx 0.5$, a minimum in the compressibility is observed, followed by an increase of the compressibility around $E_t/12J \approx 0.8$, slightly earlier than predicted by theory.

When the system is compressed even further, all cloud sizes approach that of a band-insulating state and all compressibilities tend to zero. In the theory predictions, the repulsively interacting clouds can even become slightly smaller than the noninteracting ones because of Pomeranchuk cooling (30): At the same average entropy per particle, the interacting system has a considerably lower temperature in the lattice, because the spin entropy is enhanced because of interactions (fig. S4). In the experiment, this feature is barely visible, because a second effect becomes important: At very high compressions ($E_t/12J \gtrsim 2$), the second Bloch band gets slightly populated during the lattice ramp-up, which leads to smaller cloud sizes for all interactions, because a small number of atoms in a nearly empty band can carry a considerable amount of entropy.

Overall, we find the measured cloud sizes to be in very good quantitative agreement with the theoretical calculations up to $U/12J = 1.5$ ($B = 175$ G). Nevertheless, for repulsive interactions and medium compression ($E_t/12J \approx 0.5$), the cloud size is slightly bigger than the theoretical expectation. The discrepancies become more prominent for stronger interactions; that is, on further increasing the scattering length. This could be

caused by nonequilibrium dynamics in the formation of a Mott insulating state for strong interactions or may be an effect not covered by the simple single-band Hubbard model (30) or the DMFT calculations and requires further investigation.

To ensure that the lattice loading time of 50 ms was adiabatic, we measured the resulting in situ cloud size as a function of ramp time (Fig. 3F) in the regime around $E_f/12J \approx 0.5$, where the differences between experiment and theory are most pronounced. In this regime, a too-rapid loading would result in a larger cloud, and our measurement therefore indicates adiabaticity for the ramp time used. However, a second, longer time scale, which could become more relevant for stronger interactions (31), cannot be ruled out. In addition, the temperatures before loading into the lattice and after a return to the dipole trap with a reversed sequence were compared. We found a rise in temperature between $0.010(5) T/T_F$ for a non-interacting cloud and $0.05(2) T/T_F$ for a medium repulsion of $U/12J = 1$ at compressions around $E_f/12J \approx 0.5$. The good agreement between the experimental data and the numerical calculations, which assume adiabatic loading and an initial temperature of $T/T_F = 0.15$, indicates that our actual initial temperatures lie rather at the lower end of the measured temperature range $T/T_F = 0.15(3)$.

The theoretical calculations of the compressibility shown in Fig. 4D demonstrate that the minimum in the local compressibility, which signals the Mott insulating state, starts to form at initial temperatures in the range of $0.15 \leq T/T_F \leq 0.2$. At these temperatures, the entropy per particle is much higher than is possible in a Mott insulator in the homogeneous case ($< k_B \ln 2$; where k_B denotes Boltzmann's constant) and even exceeds the maximum possible entropy per particle of a half-filled homogeneous Hubbard model ($k_B \ln 4$). In the trap, however, a large fraction of the entropy is accumulated in the metallic shells at the edges of the atomic cloud where the diluted atoms have a large configurational entropy (fig. S5). Therefore, the temperature remains on the order of $k_B T_{\text{lat}} \approx J \ll U$ in the Mott insulating regime (fig. S4). This is similar to the results obtained in recent calculations and experiments on the melting of incompressible bosonic Mott insulating shells at increasing temperatures (32, 33).

Lattice occupation. In addition to the global compressibility measurements, the fraction of atoms on doubly occupied lattice sites (pair fraction p) was measured for magnetic fields above the Feshbach resonance ($U/12J = 0, 0.5, 1$) by converting all atoms on doubly occupied sites into molecules using a magnetic field ramp (0.2 ms/G) over the Feshbach resonance (16, 21). To prevent tunneling of the atoms during the field ramp, the lattice depth was further increased to $20 E_f$ in 200 μs . After the ramp, the lattice depth was linearly decreased to zero in 200 μs and the number of remaining atoms was recorded by time-of-flight absorption imaging, yielding the number of singly occupied lattice sites. The difference in atom number with and without the magnetic field ramp

normalized to the total atom number gives the desired fraction p , which is plotted in Fig. 5, including corrections for atom losses during the measurement sequence (14). The fraction of atoms on doubly occupied sites gives insight into the local onsite physics of the system. In combination with the in situ size measurements, this fraction can be compared for different interaction strengths at constant cloud size R_{sc} .

In the limit of weak confinement, the cloud is large and p tends to zero, regardless of interaction. For intermediate compressions, the fraction of doubly occupied sites depends crucially on the interaction. At a constant size $R_{\text{sc}} = 0.53$, we find a pair fraction of 40% for a noninteracting cloud and of around 5% for an intermediate repulsive interaction $U/12J = 1$ (yellow circles in Fig. 5). In this regime of repulsive interactions, it is energetically favorable to reduce the number of doubly occupied sites despite the cost in potential and kinetic energy. As a consequence, different compressions are needed to reach the same system size for different interactions (Fig. 3).

For strong compressions, the measured pair fraction becomes comparable for all interactions (Fig. 5), because all atom distributions are expected to contain a large band-insulating core (figs. S8 and S9). Ultimately, the pair fraction is limited to $< 60\%$ because of the finite entropy per particle, which reduces the filling factor in the band-insulating state. Although the noninteracting and the slightly repulsively interacting curve $U/12J = 0.5$ match the DMFT results for an initial temperature of $T/T_F = 0.15$, we see deviations for stronger repulsive interactions ($U/12J = 1$). In this case, the measured pair fraction is in general $\sim 10\%$ higher than predicted by theory; nevertheless, the qualitative behavior agrees very well. In general, a suppressed pair fraction in comparison with the noninteracting case, which was also measured in (16), occurs for all temperatures in the lattice below $k_B T_{\text{lat}} \approx U$, regardless of the formation of an incompressible Mott insulating phase in the inhomogeneous system (fig. S3). Furthermore, the pair fraction vanishes even for a compressible purely metallic phase with $n_{i,\sigma} < 1/2$ in the strongly interacting regime.

Conclusion and outlook. We have determined the global compressibility of repulsively interacting fermionic atoms in an optical lattice and have explored the different regimes from a Fermi liquid to a Mott and band-insulating state when harmonic confinements and interactions were increased. We find good agreement with the results predicted by DMFT.

Our measurements present an important step in the direction of analyzing fermionic many-body systems with repulsive interactions in a lattice. For initial entropies lower than $S/N \leq k_B \ln 2$, one expects the system to enter an antiferromagnetically ordered phase, because the temperature of the quantum gas can then drop below the superexchange coupling that mediates an effective spin-spin interaction between the particles (20, 30, 34, 35). This would open the path to the investigation of

quantum magnetism with ultracold atoms (36), being an encouraging starting point from which to ultimately determine the low-temperature phase diagram of the Hubbard model (1, 37). This includes the search for a d -wave superconducting phase (38) that is believed to emerge from within the 2D Hubbard model.

References and Notes

1. P. Lee, N. Nagaosa, X.-G. Wen, *Rev. Mod. Phys.* **78**, 17 (2006).
2. J. Hubbard, *Proc. R. Soc. London Ser. A* **276**, 238 (1963).
3. F. Gebhard, *The Mott Metal-Insulator Transition—Models and Methods* (Springer, New York, 1997).
4. D. Jaksch, P. Zoller, *Ann. Phys. (N.Y.)* **315**, 52 (2005).
5. I. Bloch, J. Dalibard, W. Zwerger, *Rev. Mod. Phys.* **80**, 885 (2008).
6. M. P. A. Fisher, P. B. Weichman, G. Grinstein, D. S. Fisher, *Phys. Rev. B* **40**, 546 (1989).
7. D. Jaksch, C. Bruder, J. I. Cirac, C. W. Gardiner, P. Zoller, *Phys. Rev. Lett.* **81**, 3108 (1998).
8. M. Greiner, M. O. Mandel, T. Esslinger, T. Hänsch, I. Bloch, *Nature* **415**, 39 (2002).
9. T. Stöferle, H. Moritz, C. Schori, M. Köhl, T. Esslinger, *Phys. Rev. Lett.* **92**, 130403 (2004).
10. I. B. Spielman, W. D. Phillips, J. V. Porto, *Phys. Rev. Lett.* **98**, 080404 (2007).
11. P. W. Anderson, *Phys. Rev.* **109**, 1492 (1958).
12. J. Billy et al., *Nature* **453**, 891 (2008).
13. G. Roati et al., *Nature* **453**, 895 (2008).
14. See supporting material on Science Online.
15. F. Gerbier, S. Fölling, A. Widera, O. Mandel, I. Bloch, *Phys. Rev. Lett.* **96**, 090401 (2006).
16. R. Jördens, N. Strohmaier, K. Günter, H. Moritz, T. Esslinger, *Nature* **455**, 204 (2008).
17. A. Georges, G. Kotliar, W. Krauth, M. J. Rozenberg, *Rev. Mod. Phys.* **68**, 13 (1996).
18. G. Kotliar, D. Vollhardt, *Phys. Today* **57**, 53 (2004).
19. R. W. Helmes, T. A. Costi, A. Rosch, *Phys. Rev. Lett.* **100**, 056403 (2008).
20. L. De Leo, C. Kollath, A. Georges, M. Ferrero, O. Parcollet, <http://arxiv.org/abs/0807.0790v1>.
21. C. A. Regal, C. Ticknor, J. L. Bohn, D. S. Jin, *Nature* **424**, 47 (2003).
22. This heating can be caused by a p -wave Feshbach resonance for $|9/2, -7/2\rangle$ atoms at 199 G. Alternatively, we have tried to use a mixture of $|9/2, -9/2\rangle$ and $|9/2, -5/2\rangle$ atoms (16). However, this mixture showed large losses due to a coupling to the same p -wave channel, for which two-body loss coefficients in excess of $10^{-12} \text{ cm}^3 \text{ s}^{-1}$ have been reported for collisional energies of $E/k_B \approx 1 \mu\text{K}$. Collisional energies in excess of $1 \mu\text{K}$ are reached on a lattice site, due to the tight confinement of two atoms and the resulting large zero-point energy.
23. M. R. Andrews et al., *Science* **273**, 84 (1996).
24. A. Kastberg, W. D. Phillips, S. L. Rolston, R. J. C. Spreeuw, P. S. Jessen, *Phys. Rev. Lett.* **74**, 1542 (1995).
25. M. Greiner, I. Bloch, M. O. Mandel, T. Hänsch, T. Esslinger, *Phys. Rev. Lett.* **87**, 160405 (2001).
26. M. Köhl, H. Moritz, T. Stöferle, K. Günter, T. Esslinger, *Phys. Rev. Lett.* **94**, 080403 (2005).
27. R. Bulla, T. A. Costi, D. Vollhardt, *Phys. Rev. B* **64**, 045103 (2001).
28. R. Bulla, T. A. Costi, T. Pruschke, *Rev. Mod. Phys.* **80**, 395 (2008).
29. R. W. Helmes, T. A. Costi, A. Rosch, *Phys. Rev. Lett.* **101**, 066802 (2008).
30. F. Werner, O. Parcollet, A. Georges, S. R. Hassan, *Phys. Rev. Lett.* **95**, 056401 (2005).
31. K. Winkler et al., *Nature* **441**, 853 (2006).
32. F. Gerbier, *Phys. Rev. Lett.* **99**, 120405 (2007).
33. S. Fölling, A. Widera, T. Müller, F. Gerbier, I. Bloch, *Phys. Rev. Lett.* **97**, 060403 (2006).
34. A. Koetsier, R. Duine, I. Bloch, H. Stoof, *Phys. Rev. A* **77**, 023623 (2008).
35. M. Snoek, I. Titvinidze, C. Toke, K. Byczuk, W. Hofstetter, *N. J. Phys.* **10**, 093008 (2008).
36. M. Lewenstein et al., *Adv. Phys.* **56**, 243 (2007).
37. W. Hofstetter, J. I. Cirac, P. Zoller, E. Demler, M. D. Lukin, *Phys. Rev. Lett.* **89**, 220407 (2002).

38. S. Trebst, U. Schollwöck, M. Troyer, P. Zoller, *Phys. Rev. Lett.* **96**, 250402 (2006).
 39. We thank E. Demler for fruitful discussions; T. Rom, D. van Oosten, and S. Braun for help during the setup of the experiment; and the Leibniz Institute of Surface Modification (IOM Leipzig) for providing the phase masks used in phase-contrast imaging. We acknowledge funding by the Deutsche Forschungsgemeinschaft

(grants FOR801, SFB608, and SFB TR 12), European Union (Scalable Quantum Computing with Light and Atoms), Air Force Office of Scientific Research, and Defense Advanced Research Projects Agency (Optical Lattice Emulator), as well as supercomputer support by the John von Neumann Institute for Computing (Jülich). S.W. acknowledges additional support by MATCOR.

Supporting Online Material

www.sciencemag.org/cgi/content/full/322/5907/1520/DC1
 SOM Text
 Figs. S1 to S8
 References

3 September 2008; accepted 20 October 2008
 10.1126/science.1165449

REPORTS

Attosecond Ionization and Tunneling Delay Time Measurements in Helium

P. Eckle,¹ A. N. Pfeiffer,¹ C. Cirelli,¹ A. Staudte,² R. Dörner,³
 H. G. Muller,⁴ M. Büttiker,⁵ U. Keller¹

It is well established that electrons can escape from atoms through tunneling under the influence of strong laser fields, but the timing of the process has been controversial and far too rapid to probe in detail. We used attosecond angular streaking to place an upper limit of 34 attoseconds and an intensity-averaged upper limit of 12 attoseconds on the tunneling delay time in strong field ionization of a helium atom. The ionization field derives from 5.5-femtosecond-long near-infrared laser pulses with peak intensities ranging from 2.3×10^{14} to 3.5×10^{14} watts per square centimeter (corresponding to a Keldysh parameter variation from 1.45 to 1.17, associated with the onset of efficient tunneling). The technique relies on establishing an absolute reference point in the laboratory frame by elliptical polarization of the laser pulse, from which field-induced momentum shifts of the emergent electron can be assigned to a temporal delay on the basis of the known oscillation of the field vector.

The tunneling process is one of the primary manifestations of quantum mechanics' departure from classical physics. However, the question of whether tunneling through an energetically forbidden region takes a finite time or is instantaneous has been subject to ongoing debate over the past 60 years (1). Recently, experimental investigations of atomic interactions with intense laser fields (2, 3) have failed to offer a definitive answer, and many different theoretical predictions seem to contradict each other (4–7).

Ionization of an atom in a strong laser field allows for addressing this question of a possible tunneling time in an experimentally and conceptually well-defined manner. The strong-field ionization process can be split in two distinct steps: First, the bound electron tunnels through the potential wall created by the superposition of the atomic Coulomb potential and the laser field. After tunnel ionization, the electron is usually treated as a free electron with zero initial kinetic energy at the exit of the tunnel. In the second step, the now-free electron is accelerated by the laser field and receives a linear drift momentum that only depends on the laser field strength at the time of

tunneling. This is in strong analogy to the three-step model in high harmonic generation (8) using linearly polarized light.

In our experiment, we used close-to-circular polarization, thereby ensuring a unique relationship between the time at which the electron exits the tunnel and the direction of its momentum after the laser pulse. The measured momentum vector of the electron hence serves as the hand of a clock, indicating the time when the electron appeared from the tunnel in the laser field. The clock face is determined by the rotating electric field of the close-to-circularly polarized laser pulse. Thus, if we know the direction of laser field at time zero, $t_{0,\text{field}}$, when the tunneling process is initiated, we can determine the time the electron has spent in the tunnel in the classically forbidden region inside the potential wall. This difference or delay we refer to as the tunneling delay time, Δt_D .

The high-field ionization process exhibits different regimes that are distinguished by the Keldysh parameter, γ , which is given for circularly polarized light by (9)

$$\gamma = \frac{\omega_0 \sqrt{2I_p}}{E_0} \text{ (atomic units)} \cong 0.327 \sqrt{\frac{I_p \text{ (eV)}}{I_0 (10^{14} \text{ W/cm}^2) [\lambda (\mu\text{m})]^2}} \quad (1)$$

where I_p is the ionization potential, ω_0 the center laser angular frequency, E_0 the electric field amplitude of the intense infrared (IR) laser pulse, I_0 the peak intensity of the pulse, and λ the laser

wavelength. For example, for the helium ionization potential of 24.59 eV, a peak intensity of 10^{14} W/cm², and a center wavelength of 725 nm, we obtain $\gamma = 2.24$ for circular polarization (Eq. 1). For the same peak intensity, γ is a factor of $\sqrt{2}$ larger for circularly polarized light than for linearly polarized light. For $\gamma \gg 1$, that is, for short wavelength and low intensity, the ionization is most properly described by the simultaneous absorption of many discrete photons. On the other hand, if $\gamma \ll 1$, tunneling of the bound electron through a classical potential barrier provides the appropriate physical picture of the ionization process. The two regimes are not expected to be separated by a sharp transition, and both tunneling and multiphoton ionization contribute in the intermediate regime with $\gamma \approx 1$. Recently this intermediate regime was referred to as the regime of nonadiabatic tunneling (12). So far, all high laser field experiments have confirmed that, in this intermediate regime, the tunnel ionization is the dominant process, fully explaining, for example, high harmonic generation (8), quantum path interferences (10), and laser-induced electron tunneling and diffraction (11). A simple tunneling time was introduced by Keldysh (9) and more recently extended to the nonadiabatic tunneling regime (12), which formally agrees with the Büttiker-Landauer traversal time for tunneling, Δt_T (9, 13):

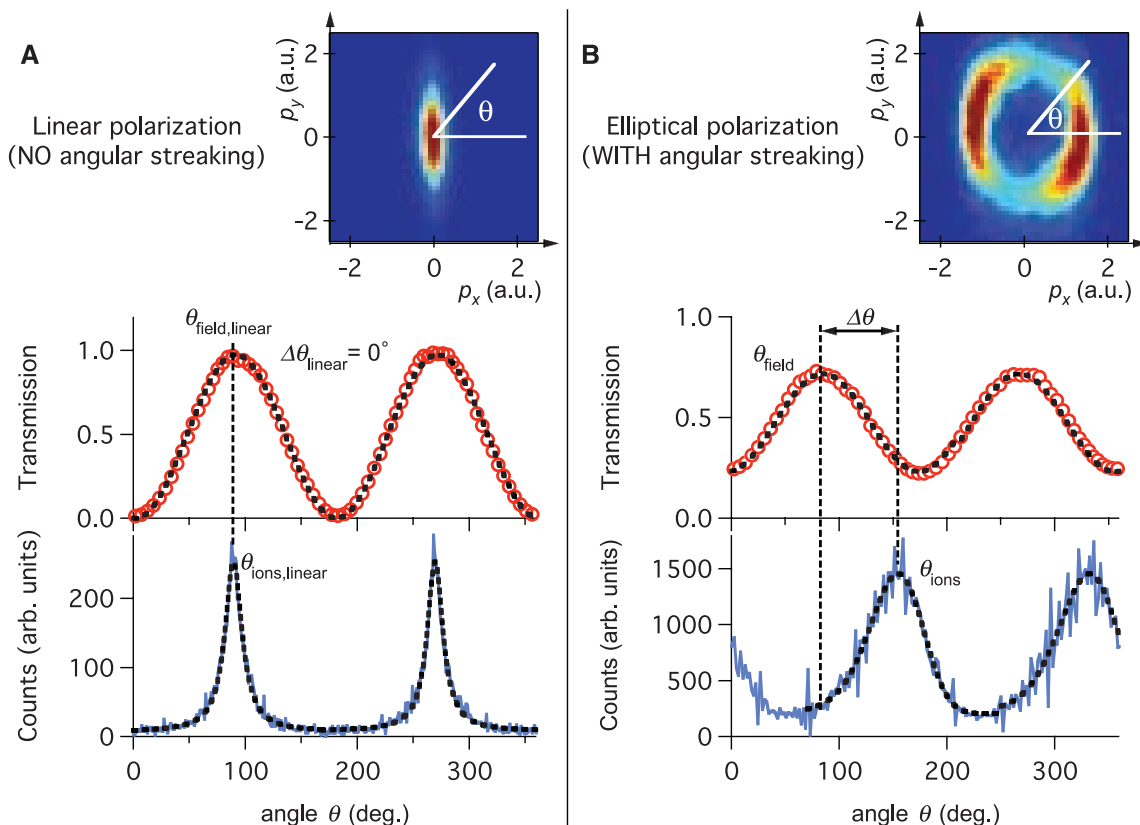
$$\gamma = \omega_0 \Delta t_T \Rightarrow \Delta t_T \text{ (as)} = 0.531 \cdot \gamma \cdot \lambda (\mu\text{m}) = 0.174 \times \sqrt{\frac{I_p \text{ (eV)}}{I_0 (10^{14} \text{ W/cm}^2)}} \quad (2)$$

We have experimentally explored the nonadiabatic tunneling regime in helium atoms exposed to laser fields with γ ranging from 1.45 to 1.17 corresponding to a peak intensity ranging from 2.3×10^{14} to 3.5×10^{14} W/cm² (Eq. 1), which in turn corresponds to a Δt_T between 450 to 560 as. At these intensities, over-the-barrier ionization (14) is negligible because for helium the critical intensity is $\approx 1 \times 10^{15}$ W/cm² (i.e., $\gamma = 0.71$ for circular polarization and $\lambda = 725$ nm).

Close-to-circularly polarized pulses with a duration in the two optical cycle regime (5.5 fs) and a center wavelength of 725 nm, which were produced by a Ti:Sapphire based laser system and a two-stage filament compressor (15), were focused onto helium atoms inside a COLTRIMS apparatus (16). Instead of measuring the electron momentum distributions directly, we recorded helium ion distributions. Momentum conservation

¹Physics Department, Eidgenössische Technische Hochschule (ETH) Zürich, CH-8093 Zürich, Switzerland. ²Steele Institute for Molecular Sciences, National Research Council of Canada, 100 Sussex Drive, Ottawa, Ontario K1A 0R6, Canada. ³Institut für Kernphysik, Johann Wolfgang Goethe Universität, Max-von-Laue-Straße 1, 60438 Frankfurt am Main, Germany. ⁴Stichting voor Fundamenteel Onderzoek der Materie—Institute for Atomic and Molecular Physics, Kruislaan 407, 1098 SJ Amsterdam, Netherlands. ⁵Physics Department, University of Geneva, CH-1211 Geneva, Switzerland.

Fig. 1. Angular calibration. p_x and p_y are the ion momentum components integrated over p_z along the laser propagation direction for both linearly (A) and elliptically (B) polarized light measured with the COLTRIMS. For both polarizations we measured the optical transmission through a rotating polarizer (red data points): Adjusting the wave plate for linear polarization we measured a 100% modulation depth in the transmission signal. For elliptical polarization, this modulation depth is reduced and so determines the amount of ellipticity introduced by the rotated wave plate. In addition, we measured for both polarizations also the ion momentum distribution (blue data below) where the angle is now determined by the streaking angle θ in the x - y plane. Because there is no angular streaking for linearly polarized light we obtained a direct calibration between the rotating polarizer angle and the streaking angle, and we set the difference to zero, that is, $\Delta\theta_{\text{linear}} = 0^\circ$. a.u. indicates atomic units.



guarantees that the electron momentum is reflected in the parent ion. The explored Keldysh parameter range was limited in the current experimental setup at high intensities (i.e., small γ) by detector saturation and at low intensities (i.e., high γ) by acquisition time. In high laser field physics, this is a typical range of operation.

We discovered a technically very simple method for achieving absolute time zero calibration. By applying a close-to-circular and well-characterized ellipticity to the polarization of the pulse, we introduced small subcycle oscillations on the time-dependent electric field amplitude that became strongly enhanced in the angular ion momentum distribution (17). The main axis of the E-field ellipse provides a fixed reference point in time. The comparison of the major axis of the ellipse to the oscillations in the momentum distribution of the ionized helium atoms then directly yields the tunneling delay time Δt_D , as illustrated in Figs. 1 and 2. This method removes the need to stabilize or measure the laser pulse's carrier envelope offset phase (CEP) (18–20).

We used linearly polarized light to obtain an absolute angular reference that compares the angles extracted from the peak positions in the ion data with the angles obtained from the polarization measurement (Fig. 1A). In ionization by linearly polarized light, no angular streaking takes place; that is, the streaking angle offset has to be $\Delta\theta_{\text{linear}} = 0^\circ$. Thus, field transmission and ion distribution are aligned in space independent of

any potential tunneling delay time. We measured the polarization direction with a polarizer and a power meter, obtaining a sinusoidal intensity modulation with a 100% contrast ratio (Fig. 1A, transmission through the polarizer versus polarizer angle). The angular direction, θ_{field} , of the polarization in the x - y plane is then determined by the maximum transmission and the maximum ion count measured in the COLTRIMS apparatus (Fig. 1A, counts versus angle).

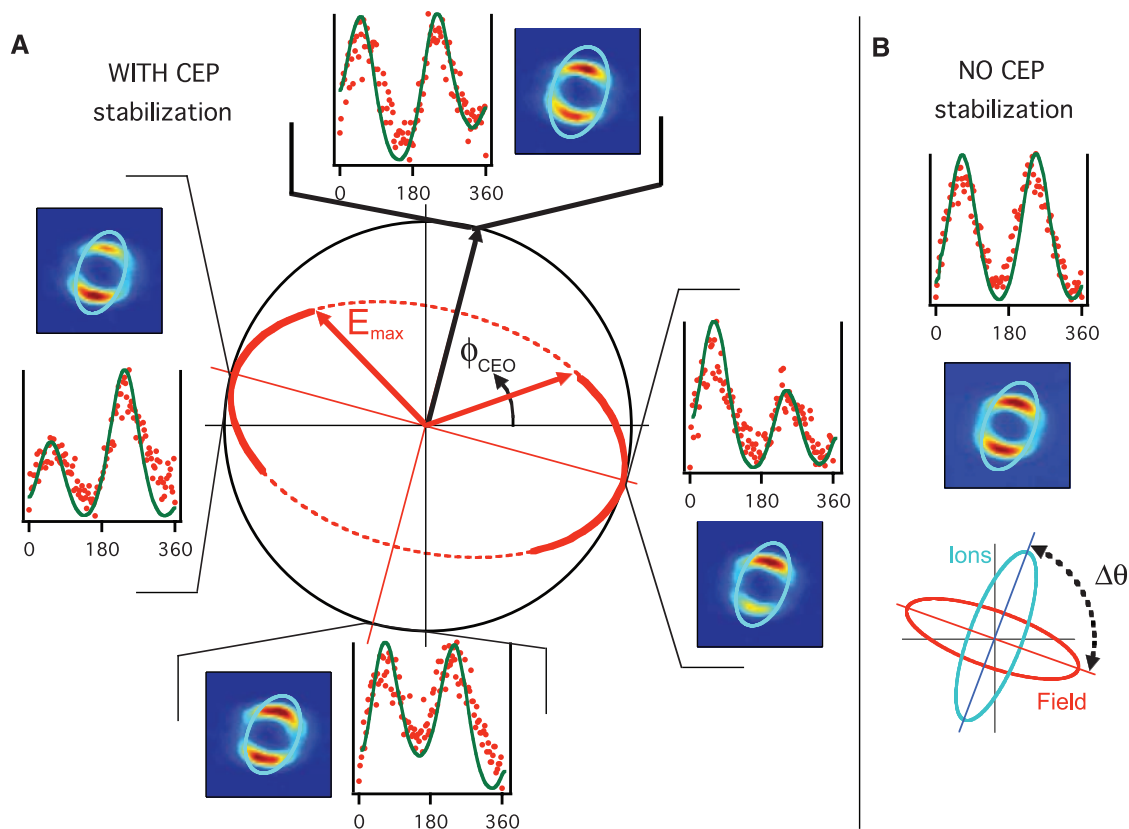
The measurements with elliptically polarized pulses are shown in Fig. 1B. From the angle calibration obtained with linearly polarized light as described above, we know the angular orientation of the polarization ellipse in the x - y plane. Because the polarization measurement temporally integrates over the entire pulse field, it is independent of the CEP. In addition, the measured modulation contrast (Fig. 1B, transmission versus angle) determines the ellipticity of the incident pulse. In contrast to ionization under linear polarization, an electron that tunnels in a close-to-circularly polarized field will receive a drift momentum that points about 90° ahead of the laser field direction at the time of the exit of the tunnel, $t_{0,\text{ion}}$. Hence, the peaks in the observed ion momentum distribution resulting from the ellipticity are rotated about 90° from their angle at $t_{0,\text{ion}}$ (i.e., at the instant of ionization). This rotation of the streaking angle depends on the ellipticity and can be calculated with a semi-classical simulation (17, 21). Δt_D results from the angular

offset between the maximum of the electric field, $t_{0,\text{field}}$, which is given by the orientation of the polarization ellipse and the instant of ionization, $t_{0,\text{ion}}$, that is, $\Delta t_D = t_{0,\text{ion}} - t_{0,\text{field}}$. Such a tunneling delay time is then determined from the difference between the measured streaking angle, $\Delta\theta$ (Fig. 1B), and the calculated streaking angle assuming instantaneous tunneling.

With the help of Fig. 2, we explain why we can perform the tunneling delay time measurements without CEP stabilization. Figure 2A shows the measured two-dimensional He^+ ion momentum distributions and the corresponding one-dimensional radially integrated angular momentum distributions for four different CEP values. The two peaks change in relative intensity but are only weakly shifted in angle with changing CEP because the spatial orientation of the electric field ellipse (in red) is not CEP-dependent (17). The CEP vector (black) is rotating over a full cycle of 360° , whereas the direction of the maximum electric field vector (red) is defined by the ellipse and covers a much smaller angular span. Therefore CEP-dependent angular shifts become negligible, and the double peak ion structure is very well resolved even without CEP stabilization, as shown in Fig. 2B. This means that even without CEP stabilization the double peak oscillations do not smear out in space, which enables CEP-independent measurements.

The measured streaking angle, $\Delta\theta$, as a function of ellipticity is shown in Fig. 3. The elliptic-

Fig. 2. Determination of time zero using an elliptically polarized intense streaking field. No CEP stabilization is needed. **(A)** The polarization ellipse (red) and four helium momentum distributions in the polarization plane and the corresponding radially integrated distributions are shown for four different carrier envelope offset phases (CEPs). Whereas the CEP vector rotates over a full 360° cycle (black circle), the maximum electric field is moving only along a smaller angular span (red solid line) defined by the ellipse. The resulting ion distributions show the characteristic two peaks, whose angular position is only weakly changed upon a variation of the CEP. When the CEP vector points in the direction of the minor axis of the polarization ellipse (as sketched in the figure), the two peaks have similar intensity. A dominant peak in the ion distribution is obtained when the CEP vector points in the direction of the major axis of the ellipse. **(B)** The momentum distributions are accumulated over all CEP values in the calculation as well as in the data. The ellipticity peaks are clearly resolved also in the CEP-averaged case and can be used to determine $t_{0,\text{ion}}$.



ity was adjusted by rotating a broadband quarter wave plate, which tunes the polarization between linear and circular extremes. The measured contrast ratio as described in Fig. 1 then gives a calibration between the wave plate angle and the ellipticity of the pulse. $\Delta\theta$ is shown for a constant intensity of $2.3 \times 10^{14} \text{ W/cm}^2$, where the error bars result from the individual errors in the curve-fitting procedures for the polarization and helium ion momentum data (21). The error is highest for polarizations closer to circular because the peak-to-peak modulation decreases in the ion data as well as in the polarization measurement. These measurements are compared with a very simple semi-classical simulation without (dashed line in Fig. 3) and with (solid line in Fig. 3) Coulomb correction in the streaking assuming instantaneous tunneling. Therefore, $\Delta\theta$ gives access to Δt_D once the simulated zero-time-delay streaking angle is subtracted.

The simple semi-classical simulation (Fig. 3 dashed line) has its basis in the ADK (Ammosov, Delone, and Krainov) ionization rates, assuming instantaneous tunneling (21, 22) and classical propagation in the measured electric field of the pulse. We calculated angular momentum distributions averaged over all CEP values and obtained very good agreement with our measurements. This semi-classical simulation shows an average deviation of $\approx 6.5^\circ$ with respect to the data. However, in this simulation we neglected the effect of the Coulomb potential between the electron and the

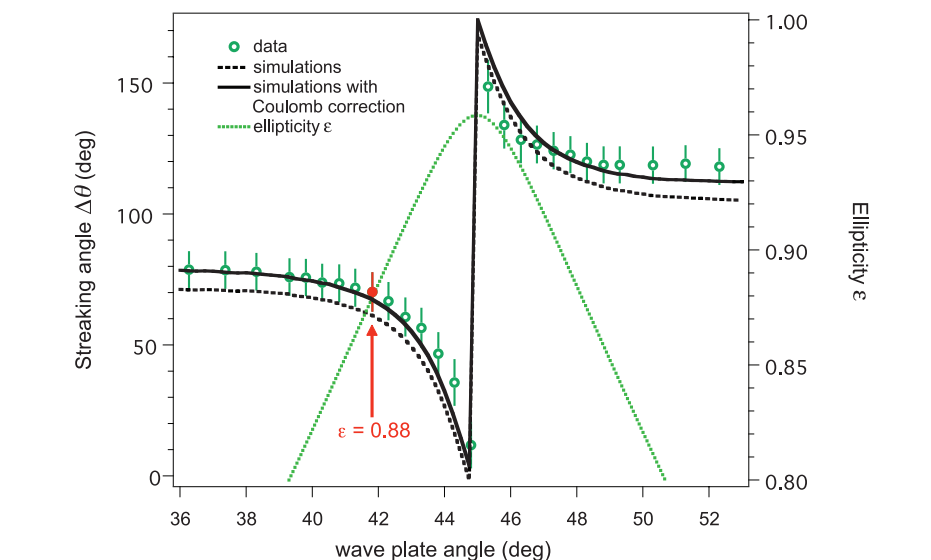


Fig. 3. Measured streaking angle (data points) as a function of $\lambda/4$ -wave plate angle (i.e., ellipticity) for a fixed peak intensity of $\approx 2.3 \times 10^{14} \text{ W/cm}^2$. The semi-classical simulation assuming instantaneous tunneling with Coulomb correction in the streaking (solid line) gives a very good agreement with the measurement. In red, marked with an arrow, the value of ellipticity (0.88) at which the intensity dependent curve of Fig. 4 was measured.

parent ion during the streaking process. This Coulomb potential was incorporated into an additional simulation as a function of ellipticity varying from 0.7 to 1.00 at a fixed peak intensity of $2.3 \times 10^{14} \text{ W/cm}^2$. The Coulomb potential was found

to account for an additional 8.6° at an ellipticity of 0.7 to 5.5° at an ellipticity of 1.0 in the streaking angle, shifting the theoretical curve upward to higher angles (solid line in Fig. 3) as compared with the dashed curve in Fig. 3.

To determine the intensity dependence of a possible Δt_D , we then fixed the ellipticity to 0.88 (marked in red in Fig. 3) and varied the peak intensity from 2.3 to 3.5×10^{14} W/cm² (corresponding to a γ variation of 1.45 to 1.17, Eq. 1). The Coulomb correction in the streaking angle for an ellipticity of 0.88 gives 6.46° at 2.3×10^{14} W/cm² and 6.54° at 3.5×10^{14} W/cm². Thus, the Coulomb correction shows no significant intensity dependence of the streaking angle over the intensity range of our experiment. Figure 4 shows the measured Δt_D (data points) as a function of peak intensity and Keldysh parameter. This tunneling time delay is the difference between the measured streaking angle and the calculated propagation streaking angle, taking into account the 6.5° offset resulting from the Coulomb potential (solid line set to zero in Fig. 4). We measure a weighted intensity-averaged offset of 6.0 as with a standard deviation of 5.6 as, taking into account the individual data errors ranging between 14 and 20 as (21). This results in an intensity-averaged upper limit for the tunneling time delay of 12 as. The accuracy in this measurement is higher compared with the ellipticity-dependent streaking angle measurement presented in Fig. 3 for two reasons: First, at an ellipticity of 0.88, the modulation amplitudes in the ellipticity peaks for both the polarization measurement and the ion data are high enough to allow for more reliable peak fitting (Fig. 4); second, in this measurement, larger data sets were available because the measurement duration was extended. For a more conservative upper limit estimate of 34 as, we use the data point at the lowest intensity, which also has the largest de-

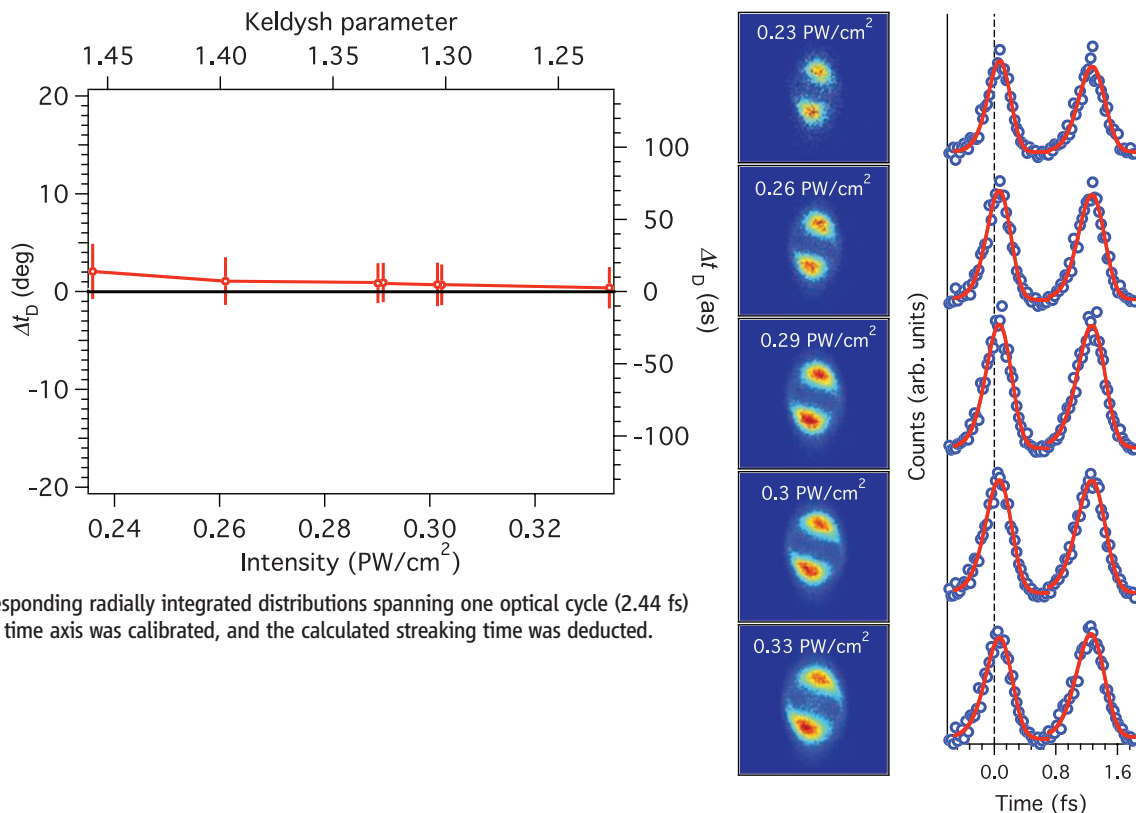
viation from zero and the largest error. At that intensity, the tunneling delay time was measured to be 13.9 as with an error of 19.7 (Fig. 4). We then obtain 34 as by adding 13.9 as and 19.7 as (21). Thus, we can conclude that we have measured a tunneling delay time with an upper limit of 34 as without any significant intensity dependence from 2.3×10^{14} to 3.5×10^{14} W/cm². In comparison, the traversal time for tunneling (Eq. 2) would vary between 450 to 560 as.

A numerical simulation based on the time-dependent Schrödinger equation of the ionization process reproduced the experimental observations: A few-optical-cycle pulse with close-to-circular polarization, with CEP chosen to simultaneously reach the maximum electric field strength of carrier and envelope at the center of the pulse, caused a single burst of ionization peaking in the direction 95° from that of the major polarization axis, with a full width at half maximum of 80° (21). Thus, the numerical simulations, like the experiment, lead to a momentum distribution that is consistent with a zero delay time for tunneling.

Among the numerous theoretical approaches toward addressing the tunneling time question, two principal frameworks are the Wigner-Eisenbud-Smith time delay (23) and the Buttiker-Landauer traversal time for tunneling (13). The Wigner-Eisenbud approach considers a wave packet and follows its peak. Such motion in the classically allowed region is characterized by the familiar group velocity. In the tunneling regime, the Wigner-Eisenbud time can be much shorter than the time necessary for propagation of light over the same distance and, if taken at face value, gives super-

luminal tunneling times. This concept is rather similar to superluminal group velocities discussed in the context of photon propagation through media with anomalous dispersion. Several objections are possible against the Wigner-Eisenbud approach: First, there is no conservation law in physics for peaks of wave packets; and, second, superluminal velocities cannot characterize a causal process. The answer of Sommerfeld and Brillouin to superluminal velocities in regions of anomalous dispersion was to characterize pulse propagation by a signal velocity, which is always limited by the velocity of light (24–26). The Buttiker-Landauer traversal time for tunneling is similarly an effort to obtain a more obviously physical answer for the speed of the tunneling process. In the Buttiker-Landauer approach, the height of the tunneling barrier is modulated in time, acting as a clock against which the tunneling time can be measured. This model leads to the distinction of an adiabatic regime, where the tunneling barrier oscillates slowly compared with the tunneling process, and a nonadiabatic regime, where the oscillation is fast. A traversal time for tunneling is obtained by considering the crossover between these two regimes. For linearly polarized light, the Buttiker-Landauer time is directly related to the adiabaticity parameter of Keldysh (9). In our experiment, a helium atom is ionized by an intense laser field, and we define a tunneling delay time, Δt_D , as the time delay between the lowering of the barrier and the time at which the escaping electron first experiences acceleration by the external field of the laser. This means that these two tunneling times consider entirely different aspects of the tunneling process.

Fig. 4. Measured tunneling time delay, Δt_D (data points), for a fixed ellipticity (i.e., $\varepsilon = 0.88$) as a function of peak intensity and Keldysh parameter (Eq. 1). The tunneling time delay is the difference between the measured and the calculated propagation streaking angle assuming instantaneous tunneling. In the calculated streaking angle, we also took into account the Coulomb potential (solid line set to zero). We measured an intensity-averaged offset of 6.0 as with a standard deviation of 5.6 as. The two-dimensional helium momentum distributions measured at different intensities and the corresponding radially integrated distributions spanning one optical cycle (2.44 fs) are shown on the right. The time axis was calibrated, and the calculated streaking time was deducted.



We conclude that with our measurement we can put an upper limit of 34 as on a Δt_D in the nonadiabatic tunneling regime with a γ ranging from 1.45 to 1.17. Quantum mechanical simulations using the time-dependent Schrödinger equation predict instantaneous ionization with no angular delay. We measured a weighted intensity-averaged tunneling delay time of 6.0 as with a standard deviation of the weighted mean of 5.6 as, which would result in an intensity-averaged upper limit of 12 as (21). Our experiments access a tunneling delay time in a conceptually well-defined manner that is closely related to the successful three-step model in high harmonic generation (8). We can clearly distinguish between the tunneling process and the consecutive acceleration of the free electron in the close-to-circular polarized laser field. This has given us direct experimental access to the tunneling delay time with a time accuracy of a few tens of attoseconds using attosecond angular streaking (17). The measured upper limit of the tunneling delay time is much shorter than the Buttiker-Landauer traversal time, Δt_T , which for the present conditions is predicted to range be-

tween 450 and 560 as. We reiterate that the Buttiker-Landauer traversal time, Δt_T , considers an entirely different aspect of the tunneling process. Our experimental results give a strong indication that there is no real tunneling delay time, and we expect that this conclusion will shed some light on the ongoing theoretical discussion on tunneling time.

References and Notes

1. L. A. MacColl, *Phys. Rev.* **40**, 621 (1932).
2. G. G. Paulus *et al.*, *Phys. Rev. Lett.* **80**, 484 (1998).
3. M. Uiberacker *et al.*, *Nature* **446**, 627 (2007).
4. R. Landauer, T. Martin, *Rev. Mod. Phys.* **66**, 217 (1994).
5. J. Ruseckas, *Phys. Rev. A* **63**, 052107 (2001).
6. H. G. Winful, *N. J. Phys.* **8**, 101 (2006).
7. J. G. Muga, R. S. Mayato, I. L. Egusquiza, in *Time in Quantum Mechanics*, J. G. Muga, R. S. Mayato, I. L. Egusquiza, Eds., vol. 734 of *Lecture Notes in Physics* (Springer, Berlin, ed. 2, 2008).
8. P. B. Corkum, *Phys. Rev. Lett.* **71**, 1994 (1993).
9. L. V. Keldysh, *Sov. Phys. JETP* **20**, 1307 (1965).
10. A. Zair *et al.*, *Phys. Rev. Lett.* **100**, 143902 (2008).
11. M. Meckel *et al.*, *Science* **320**, 1478 (2008).
12. G. L. Yudin, M. Y. Ivanov, *Phys. Rev. A* **63**, 033404 (2001).
13. M. Büttiker, R. Landauer, *Phys. Rev. Lett.* **49**, 1739 (1982).
14. M. Protopapas, C. H. Keitel, P. L. Knight, *Rep. Prog. Phys.* **60**, 389 (1997).
15. C. P. Hauri *et al.*, *Appl. Phys. B* **79**, 673 (2004).
16. J. Ullrich *et al.*, *Rep. Prog. Phys.* **66**, 1463 (2003).
17. P. Eckle *et al.*, *Nat. Phys.* **4**, 565 (2008).
18. H. R. Telle *et al.*, *Appl. Phys. B* **69**, 327 (1999).
19. D. J. Jones *et al.*, *Science* **288**, 635 (2000).
20. A. Apolonski *et al.*, *Phys. Rev. Lett.* **85**, 740 (2000).
21. Computational methods and error estimates are detailed on *Science Online*.
22. M. V. Ammosov, N. B. Delone, V. P. Krainov, *Sov. Phys. JETP* **64**, 1191 (1986).
23. E. P. Wigner, *Phys. Rev.* **98**, 145 (1955).
24. A. Sommerfeld, *Phys. Z.* **8**, 841 (1907).
25. L. Brillouin, *Ann. Phys.* **349**, 203 (1914).
26. M. Büttiker, H. Thomas, *Ann. Phys.* **7**, 602 (1998).
27. This work was supported by Natural Center of Competence in Research Quantum Photonics (NCCR QP), research instrument of the Swiss National Science Foundation, the Alexander-von-Humboldt Stiftung, and the Deutsche Forschungsgemeinschaft. H.G.M. was supported by FOM (Fundamental Research on Matter), which is subsidized by NWO (Netherlands Organization for the Advancement of Research).

Supporting Online Material

www.sciencemag.org/cgi/content/full/322/5907/1525/DC1

Materials and Methods

References

18 July 2008; accepted 22 October 2008

10.1126/science.1163439

Optical Absorption and Radiative Thermal Conductivity of Silicate Perovskite to 125 Gigapascals

Hans Keppler,^{1*} Leonid S. Dubrovinsky,¹ Olga Narygina,¹ Innokenty Kantor^{1,2}

Mantle convection and plate tectonics are driven by the heat flow from Earth's core to the surface. The radiative contribution to heat transport is usually assumed to be negligible. Here, we report the near-infrared and optical absorption spectra of silicate perovskite, the main constituent of the lower mantle, to 125 gigapascals. Silicate perovskite remains quite transparent up to the pressures at the core-mantle boundary. Estimates of radiative thermal conductivity derived from these spectra approach 10 watts meter⁻¹ kelvin⁻¹ at lowermost mantle conditions, implying that heat conduction is dominated by radiation. However, the increase in radiative conductivity with temperature (*T*) is less pronounced than expected from a *T*³ dependency.

Temperatures near Earth's core-mantle boundary are believed to be between 3300 and 4300 K (1). At these temperatures, one would expect heat transfer by radiation to be important because radiative thermal conductivity should increase with the third power of temperature (2–5). However, early experimental work appeared to imply that iron-bearing minerals generally become optically opaque already at moderately high pressures (6). Therefore, it has been thought that the minerals in Earth's lower mantle absorb radiation so strongly that the contribution of radiation to heat transport is negligible (1). Recently, the discovery of spin-pairing in

mantle minerals under high pressure (7) has led to a renewed interest in radiative conductivity, because spin-pairing could potentially change optical absorption spectra drastically and it may therefore have a strong effect on radiative heat transport (8, 9). At the same time, recent optical absorption measurements at high pressures suggested that iron-bearing mantle minerals do not necessarily become opaque at high pressures (10, 11). Rather, the changes in optical absorption with pressure strongly depend on the content and particularly on the oxidation state of iron in the sample. For example, ferroperricite, (Mg,Fe)O, synthesized at low pressures becomes optically opaque at high pressure because of its high Fe³⁺ content (9). However, samples annealed at 25 GPa have much lower concentrations of Fe³⁺ and remain optically transparent to deep lower mantle pressures (11). We therefore studied the optical absorption spectrum of aluminous silicate

perovskite, the main constituent of Earth's lower mantle, to 125 GPa, corresponding to the pressure near the core-mantle boundary. Perovskite is expected to be stable in the hot areas above the core-mantle boundary, which are the roots of mantle plumes, whereas it probably transforms to post-perovskite in cooler areas (1).

A sample of aluminous silicate perovskite with composition (Mg_{0.892}Fe_{0.059}Fe_{0.042})₂(Si_{0.972}Al_{0.028})O₃ according to electron microprobe and Mössbauer data was synthesized from glass powder at 25 GPa and 2000°C in a multi-anvil press using a Re capsule. A doubly polished, optically clear piece of a crystal with 30-μm thickness was loaded into a modified Merrill Bassett diamond anvil cell. Pressure medium was neon; pressure was measured by ruby fluorescence. Near-infrared and optical absorption spectra were collected with use of a Bruker IFS 125 (Bruker Optics, Karlsruhe, Germany) Fourier transform spectrometer together with an all-reflecting microscope (12).

The measured absorption spectra from 1 bar to 125 GPa is shown in Fig. 1. The main feature seen is a broad band located between about 15,000 cm⁻¹ and 20,000 cm⁻¹, depending on pressure. Position and width of this band are characteristic for a Fe²⁺-Fe³⁺ intervalence charge transfer band; that is, light absorption is caused by the transfer of electrons from Fe²⁺ ions to neighboring Fe³⁺ ions (13, 14). The increasing absorption at high wave numbers is probably related to O²⁻-Fe³⁺ ligand-to-metal charge transfer. The crystal field bands of Fe²⁺ are not visible in these spectra, although they can be found around 7000 cm⁻¹ in the absorption spectrum of aluminum-free (Mg,Fe)SiO₃ perovskite (15). The invisibility of these bands is probably a combined result of their generally low intensity and the overlap with the intervalence charge transfer bands

¹Bayerisches Geoinstitut, Universität Bayreuth, 95440 Bayreuth, Germany. ²Advanced Photon Source, Argonne National Laboratory, Argonne, IL 60439, USA.

*To whom correspondence should be addressed. E-mail: hans.keppler@uni-bayreuth.de

and because only about half of the iron in the sample is in the Fe^{2+} state. The high concentration of Fe^{3+} even under reducing conditions is characteristic of Al-bearing silicate perovskites.

The spectra in Fig. 1 were deconvoluted into a linear baseline, a Gaussian peak describing the intervalence charge transfer band, and a Lorentz peak describing the high-frequency slope. The intensity of the intervalence charge transfer band increased between 1 bar and 47 GPa. From 47 to 125 GPa, it shifted continuously in frequency from $15,060\text{ cm}^{-1}$ to $19,377\text{ cm}^{-1}$, whereas both absorbance (0.312 ± 0.065) and width ($14,732\text{ cm}^{-1} \pm 1342\text{ cm}^{-1}$) remained unchanged within the error limits of the deconvolution. The frequency shift of the intervalence charge transfer band can be approximately described by the equation $\tilde{\nu} = 9382.9 + 161.69P - 0.6681P^2$, where $\tilde{\nu}$ is wave number in cm^{-1} and P is pressure in GPa. There is no obvious evidence in the spectra for spin-pairing of either Fe^{3+} or Fe^{2+} . If spin-pairing or partial spin-pairing does indeed occur in silicate perovskite over the pressure range studied, its effects on optical absorbance are negligible.

The spectra in Fig. 1 show that the changes in optical absorption up to 125 GPa are subtle and that the sample does not become opaque at high pressure. A visual inspection of the sample in the diamond cell (Fig. 2) also shows that silicate perovskite is still quite transparent at 125 GPa, and the color is not very different from the color at ambient pressure. A similar observation can be made for ferropericlase (11), the second most abundant phase in the lower mantle (Fig. 2).

From optical absorption spectra, the radiative thermal conductivity can be calculated (2–5). The radiative thermal conductivity, k_R , is given by

$$k_R = \frac{16n^2\sigma T^3}{3\alpha_R} \quad (1)$$

where n is the refractive index of the medium, σ is the Stefan-Boltzmann constant, T is temperature in K, and α_R is the Rosseland mean absorption coefficient, which is defined by

$$\frac{1}{\alpha_R} = \frac{\int_0^\infty \frac{1}{\alpha(\nu)} \frac{de(\nu, T)}{dT} d\nu}{\int_0^\infty \frac{de(\nu, T)}{dT} d\nu} \quad (2)$$

where $e(\nu, T)$ is the Planck blackbody emission function. The Rosseland mean absorption coefficient is essentially a weighed average of the measured absorption coefficient $\alpha(\nu)$. The weighing function is the temperature derivative of the Planck emission function. As a result, the Rosseland mean absorption coefficient is dominated by the absorption coefficient measured close to the frequencies of maximum blackbody emission. The absorption coefficient used in the calculation of radiative conductivity has its basis in the natural logarithm of light intensity, whereas the absorption coefficient used in spectroscopy is usually defined on the basis of the decadic logarithm.

Radiative heat transport can be accurately described by the formalism outlined above if the medium is optically thick, that is, if the average photon path length is much smaller than the dimension of the medium. From the spectra in Fig. 1, one can estimate a typical photon path length on the order of 100 to 200 μm . This means that, for a grain size of several millimeters or more, the radiative contribution to heat conduction should be properly described. Considering the high temperatures in the lower mantle and that recrystallization of grains is thermally activated, it is plausible to assume that the grains in the lower mantle will be this size or larger.

To calculate the radiative thermal conductivity of silicate perovskite as a function of temperature (Fig. 3) from the 1-bar and the 125-GPa spectra, we first corrected the measured spectra for reflection losses on the sample surface by using a frequency-independent refractive index of 1.8 (12, 16). At the highest temperatures expected near the core mantle boundary, the radiative thermal conductivity approaches $10\text{ W m}^{-1}\text{ K}^{-1}$. However, the increase of radiative thermal conductivity is weaker than expected from a T^3 dependency because with increasing temperature the maximum of the blackbody radiation moves toward higher frequencies, where perovskite absorbs more strongly. For example, the Rosseland mean absorption coefficient calculated from the 125 GPa spectrum increases from 4.07 mm^{-1} for 1500 K to 12.3 mm^{-1} for 4500 K. Therefore, over the same temperature range, radiative conductivity increases only from $0.815\text{ W m}^{-1}\text{ K}^{-1}$ to $7.27\text{ W m}^{-1}\text{ K}^{-1}$, whereas from a T^3 dependency

an increase to $22.0\text{ W m}^{-1}\text{ K}^{-1}$ would have been expected.

Absorption spectra may change with temperature, and therefore a calculation of the actual mantle radiative thermal conductivity requires measurements of optical absorption at combined lower mantle pressures and temperatures. Such measurements are currently not feasible. However, it is possible to predict how the absorption spectra may change with temperature. Crystal field bands at low frequencies and the intervalence charge transfer band in the visible range interact with most of the blackbody emission. Crystal field bands are strictly symmetry forbidden. They can be activated by either static or dynamic distortions in the environment that remove the center of symmetry of the involved d orbitals. Fe^{2+} in the perovskite structure is located on a distorted dodecahedral site with site symmetry m (17), that is, without a center of symmetry. In this case, coupling with vibrations is not required to lift the Laporte selection rule, and accordingly the intensity of these bands is expected to be nearly independent of temperature, as has been verified for Fe in the acentric M2 site of olivine (18). Also, the extinction coefficients of transition metals in acentric sites in silicate melts vary little up to 1400°C (19). On the other hand, many intervalence charge transfer bands, such as the one observed in the perovskite spectra, are known to decrease in intensity with temperature (20). This trend implies that, at high pressures and temperatures, the actual absorption spectrum of perovskite may resemble the spectrum measured at 1 bar, where the intervalence

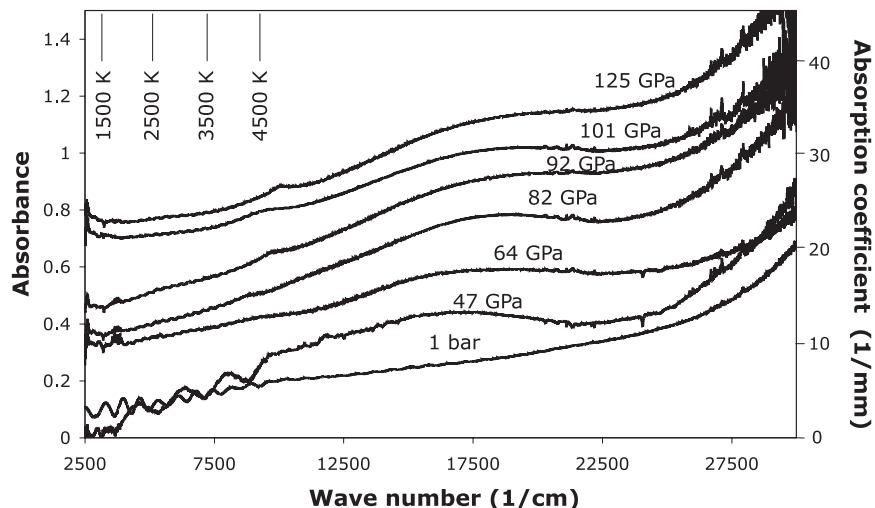


Fig. 1. Near-infrared and optical absorption spectra of silicate perovskite to 125 GPa. The 1-bar spectrum is shown as measured; the other spectra are offset vertically for clarity. Without offset, the low-frequency parts of the spectra below 7500 cm^{-1} would nearly coincide. Sample thickness at ambient pressure is $30\text{ }\mu\text{m}$. On the right-hand side of the diagram, absorption coefficients based on the decadic logarithm and normalized to this sample thickness are given. Because of the compression of the sample, the absorption coefficients increase by about 9% relative to these values at 125 GPa. To obtain absorption coefficients based on the natural logarithm, which are used in Eq. 2, the absorption coefficients shown in this figure have to be multiplied with $\ln 10 = 2.30$. The position of the maxima of thermal blackbody radiation at different temperatures is also shown for reference. The slight oscillations at low frequency in some spectra are artifacts (interference fringes). The small peak seen in some spectra close to $10,000\text{ cm}^{-1}$ is probably not real; it is likely related to the change in detector close to this frequency.

Fig. 2. Optical images of silicate perovskite at 125 GPa (**top**, thickness of 30 μm) and of ferropericlase at 84 GPa (**bottom**, thickness of 21 μm) in the diamond cell. Pressure medium is neon. The width of both images is about 100 μm .

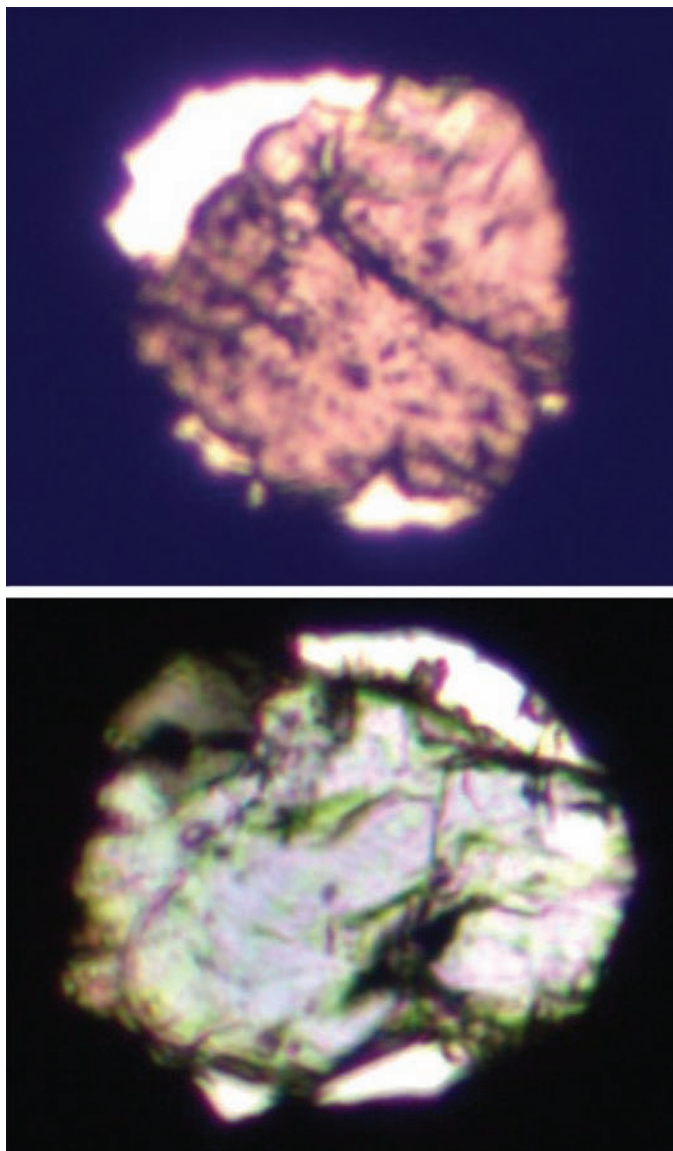
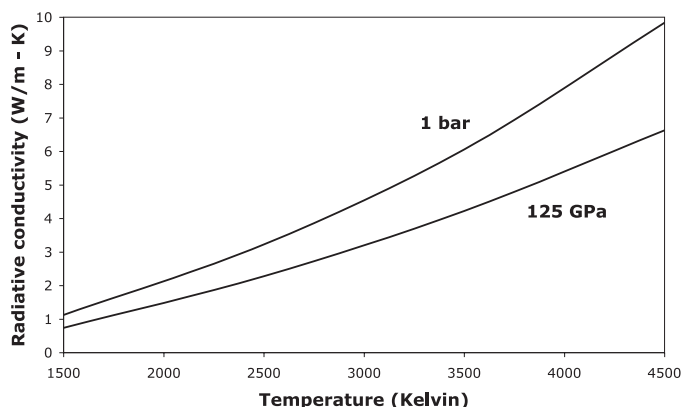


Fig. 3. Estimated radiative thermal conductivity of silicate perovskite as a function of temperature. Calculations have their bases in the 125-GPa spectrum and the 1-bar spectrum in Fig. 1. The 125-GPa data contain a correction for the increase of the optical absorption coefficient that results from the reduction of sample thickness by about 9% upon compression, calculated with $K = 261$ GPa and $K' = 4.1$ (25). At high temperatures, the intervalence charge transfer band seen in the 125-GPa spectrum may disappear, and therefore the calculation based on the 1-bar spectrum may actually give more accurate values for the radiative thermal conductivity in the lower mantle. Whereas temperatures at the core mantle boundary are between 3300 and 4300 K, mantle temperatures at 125 GPa (2770 km depth) may reach 3000 to 3500 K (26).



At high temperatures, the intervalence charge transfer band seen in the 125-GPa spectrum may disappear, and therefore the calculation based on the 1-bar spectrum may actually give more accurate values for the radiative thermal conductivity in the lower mantle. Whereas temperatures at the core mantle boundary are between 3300 and 4300 K, mantle temperatures at 125 GPa (2770 km depth) may reach 3000 to 3500 K (26).

charge transfer band is not detectable. Accordingly, we suggest that the range of radiative thermal conductivities calculated from the 1-bar and 125-GPa spectra in Fig. 3 gives a robust estimate of the actual radiative thermal conductivity in the lower mantle. The presence of ferropericlase in the lower mantle will not change the radiative conductivity substantially, because its abundance is low and because ferropericlase with a Fe^{3+} content realistic for the lower mantle does not become opaque at high pressures either (11). For the possible effect of grain boundaries, see (12).

The thermal conductivity in the deep lower mantle affects Earth's heat flow and thermal evolution and the mode of mantle convection. A high radiative contribution to heat flow should help to stabilize large plume structures (21–23) because in the presence of a strong radiative component heat flow will increase with temperature, whereas the phonon part of thermal conductivity decreases with temperature. But, this benefit may be less than previously assumed because the conductivity increase with temperature is lower than that expected from a T^3 dependence. Our value for the radiative thermal conductivity in the lowermost mantle is comparable to the usually assumed bulk thermal conductivity at the core mantle boundary of $10 \text{ W m}^{-1} \text{ K}^{-1}$ (1), which is the sum of phonon (lattice) conductivity and the radiative conductivity. Allowing for a reasonable contribution from phonon conductivity consistent with recent measurements on high-pressure phases (24) suggests that the widely accepted value of $10 \text{ W m}^{-1} \text{ K}^{-1}$ is a large underestimate of the actual thermal conductivity in the lowermost mantle. Because the phonon contribution of thermal conductivity decreases with temperature (24), heat conduction in the lowermost mantle is certainly dominated by radiation. On the other hand, our measurements rule out the possibility that radiative heat transport in the lower mantle could increase the thermal conductivity by orders of magnitude (21).

References and Notes

1. T. Lay, J. Hernlund, B. A. Buffett, *Nat. Geosci.* **1**, 25 (2008).
2. S. Rosseland, *Theoretical Astrophysics: Atomic Theory and the Analysis of Stellar Atmospheres and Envelopes* (Clarendon, Oxford, 1936).
3. R. Siegel, J. R. Howell, *Thermal Radiation Heat Transfer* (McGraw Hill, New York, 1972).
4. M. Q. Brewster, *Thermal Radiative Transfer and Properties* (Wiley, New York, 1992).
5. M. F. Modest, *Radiative Heat Transfer* (Academic Press, Amsterdam, 2003).
6. H. K. Mao, P. M. Bell, *Science* **176**, 403 (1972).
7. J. Badro *et al.*, *Science* **300**, 789 (2003).
8. J. Li *et al.*, *Proc. Natl. Acad. Sci. U.S.A.* **101**, 14027 (2004).
9. A. F. Goncharov, V. V. Struzhkin, S. D. Jacobsen, *Science* **312**, 1205 (2006).
10. H. Keppler, J. R. Smyth, *Am. Mineral.* **90**, 1209 (2005).
11. H. Keppler, I. Kantor, L. S. Dubrovinsky, *Am. Mineral.* **92**, 433 (2007).
12. Materials and methods are available as supporting material on Science Online.
13. S. M. Mattson, G. R. Rossman, *Phys. Chem. Miner.* **14**, 94 (1987).
14. R. G. Burns, *Mineralogical Applications of Crystal Field Theory* (Cambridge Univ. Press, Cambridge, ed. 3, 1993).

15. H. Keppler, C. A. McCammon, D. C. Rubie, *Am. Mineral.* **79**, 1215 (1994).
16. A. Wall, G. D. Price, S. C. Parker, *Mineral. Mag.* **50**, 693 (1986).
17. Y. Kudoh, C. T. Prewitt, L. W. Finger, *Geophys. Res. Lett.* **17**, 1481 (1990).
18. K. Ullrich, K. Langer, K. D. Becker, *Phys. Chem. Miner.* **29**, 409 (2002).
19. H. Keppler, N. Bagdassarov, *Chem. Geol.* **158**, 105 (1999).
20. M. N. Taran, K. Langer, *Neues Jahrb. Mineral. Abh.* **172**, 325 (1998).
21. A. P. van den Berg, D. A. Yuen, V. Steinbach, *Geophys. Res. Lett.* **28**, 875 (2001).
22. C. Matyska, J. Moser, D. A. Yuen, *Earth Planet. Sci. Lett.* **125**, 255 (1994).
23. C. Matyska, D. A. Yuen, *Earth Planet. Sci. Lett.* **234**, 71 (2005).
24. Y. Xu et al., *Phys. Earth Planet. Inter.* **143-144**, 321 (2004).
25. S. Lundin et al., *Phys. Earth Planet. Inter.* **168**, 97 (2008).
26. F. Deschamps, J. Trampert, *Earth Planet. Sci. Lett.* **222**, 161 (2004).
27. This work was supported by German Science Foundation (DFG; Leibniz award to H.K.). A. Audétat took the photographs of the samples at high pressure.

Supporting Online Material

www.sciencemag.org/cgi/content/full/322/5907/1529/DC1
Materials and Methods
References and Notes

13 August 2008; accepted 23 October 2008
10.1126/science.1164609

Quasi-Periodic Bedding in the Sedimentary Rock Record of Mars

Kevin W. Lewis,^{1*} Oded Aharonson,¹ John P. Grotzinger,¹ Randolph L. Kirk,² Alfred S. McEwen,³ Terry-Ann Suer¹

Widespread sedimentary rocks on Mars preserve evidence of surface conditions different from the modern cold and dry environment, although it is unknown how long conditions favorable to deposition persisted. We used 1-meter stereo topographic maps to demonstrate the presence of rhythmic bedding at several outcrops in the Arabia Terra region. Repeating beds are ~10 meters thick, and one site contains hundreds of meters of strata bundled into larger units at a ~10:1 thickness ratio. This repetition likely points to cyclicity in environmental conditions, possibly as a result of astronomical forcing. If deposition were forced by orbital variation, the rocks may have been deposited over tens of millions of years.

Sedimentary rocks record surface and environmental conditions throughout the history of Mars (1, 2). Landed missions have studied a few locations in detail, but most deposits remain accessible only from orbital data. The High Resolution Imaging Science Experiment (HiRISE) (3) has revealed meter-scale bedding in the rocks at many locations. Stereo observations allow the three-dimensional structure of these stratified outcrops to be determined, from which bedding orientations and true thicknesses can be calculated. Here, we report on the measurement of several stratified deposits in the Arabia Terra region that contain highly rhythmic bedding and may record a history of orbitally forced variations in surface conditions. Previous attempts have been made to correlate layers within the north polar ice cap of Mars to the most recent orbital history (4, 5). In contrast, the rocks of Arabia Terra record ancient surface conditions.

The intracrater layered deposits of Arabia Terra are thick sequences of sedimentary rocks distributed widely across Mars from 350°E to 30°E and from the equator up to 25°N (6). Although the deposits are separated by large distances, the region in which they occur is greater than 500 km by 1000 km in area. Most sequences are several hundred meters thick and have eroded back to remnant mounds on the floors of large craters, natural locations for both deposition and preser-

vation. Many deposits have a stair-stepped morphology, with the differential resistance of the outcrops highlighting their stratified internal structure (1). The origin of these sedimentary rocks is uncertain, although there is a general lack of valley incision in western Arabia Terra (7, 8), and there is no observed evidence for fluvial channels within these deposits. Although erosion may have removed overlying strata (8), the craters we studied do not have breached or heavily incised rims and show little evidence for lacustrine processes.

Among the craters containing light-toned layered deposits in Arabia Terra, four have adequate stereo coverage to make quantitative measurements of the stratigraphy. These sedimentary sequences contain tens to hundreds of beds of similar morphology with planar and parallel bedding. Faults offset the stratigraphy in places, but we have avoided these areas in our analysis. Extensive aeolian erosion has revealed the thick sections and also provides a clue to the depositional origin of the rocks. Few craters are observed on the light-toned deposits, and little talus is observed at the

base of steep slopes, which suggests that the deposits are weakly lithified and consist of grains fine enough to be transported away by modern aeolian activity. The striking differential resistance to erosion seen across each bed points to a repeated change in the depositional environment as the strata were formed.

To assess the structure of layered deposits, we created digital terrain models (DTMs) with 1-m grid spacing from HiRISE stereo images, using the techniques of (9). These products were controlled to the Mars Orbiter Laser Altimeter (MOLA) data set as part of the generation process; they have a vertical accuracy of <1 m, allowing analysis of meter-scale bedding (table S1). Figure 1 shows a cross section along one outcrop, demonstrating that 10-m-scale layers are well resolved in the stereo DTM. Although the apparent thicknesses are variable in plan view, the true bed thicknesses are highly regular when the erosional topography and southward dip are accounted for. Accordingly, bedding orientations were calculated via linear regression and were typically derived from hundreds of individual topographic data points, resulting in a precision of <0.5° on the dip of a bed. We made measurements throughout each section to ensure that the orientation was consistent. At the Becquerel crater site, a slight change in bedding orientation was observed and accounted for within the upper 80 m of section. We then identified bed boundaries in plan view and projected each to a common reference frame using the measured orientation of the outcrop.

For each of the Arabia sites, the bed thicknesses are tightly clustered around a mean value (Table 1 and tables S2 to S6). The thinnest beds are still above the resolution limits of both the images and the DTMs, which have a pixel scale of 1 m but typically sample the stratigraphic col-

Table 1. Bed thicknesses measured from HiRISE stereo topographic data at four outcrops in the Arabia Terra region of Mars. Each location shows regularly cyclic sequences, possibly indicative of depositional control by an external climate cycle. The characteristic thicknesses vary between sites, which suggests that the deposits formed in isolation rather than as a widespread regional geologic unit.

Crater	Location	Number of beds measured	Mean thickness ± SD (m)
Becquerel (beds)	22°N, 352°E	66	3.6 ± 1.0
Becquerel (bundles)	22°N, 352°E	10	35.5 ± 9.2
Crommelin	5°N, 350°E	8	19.6 ± 4.0
Unnamed	8°N, 353°E	14	9.7 ± 1.5
Unnamed	9°N, 359°E	10	12.6 ± 2.6

¹Division of Geological and Planetary Sciences, California Institute of Technology, 150-21, Pasadena, CA 91125, USA. ²U.S. Geological Survey, 2255 N. Gemini Drive, Flagstaff, AZ 86004, USA. ³Lunar and Planetary Laboratory, University of Arizona, Tucson, AZ 85721, USA.

*To whom correspondence should be addressed. E-mail: klewis@gps.caltech.edu

umn at even finer intervals (~ 0.1 m) because of the slope of the outcrops. Although the scale of the bedding varies from site to site, it is consistent among outcrops at the same location. Within the two unnamed craters at 8°N , 353°E and 9°N , 359°E , the characteristic thicknesses are about 10 and 13 m, respectively. At Crommelin crater (5°N , 350°E), beds are 20 m thick, whereas Becquerel (22°N , 352°E) shows two scales of stratification at 3.6 and 36 m. The distribution of bed thicknesses at each location is consistent with a normal distribution via the Kolmogorov-Smirnov test. Alternative hypotheses that the data are distributed either exponentially or according to a power law can be rejected (10). We consider possible interpretations of these observed distributions below.

We used spectral analysis of the stratigraphic records to further assess the periodicity of the bedding at these locations. Image grayscale values and DTM slope profiles both provide a continuous record of the stratigraphy. In three of the four locations, we analyzed the image brightness record, whereas at the 9°N , 359°E site, slope values provided a better record because of unfavorable lighting conditions. The data were sampled from the orthorectified images or DTM and were then corrected for the structural dip and topography. To obtain a uniformly spaced record, we resampled the record in the stratigraphic reference frame to the mean spacing of the data (~ 0.1 m in all four cases). We derived spectral estimates via the multitaper method of (11), which were then assessed relative to a first-order autoregressive (red noise) background. We used the robust estimation technique of (11) to model the red noise component of the data and derive corresponding confidence levels. Spectral peaks exceeding these thresholds indicate that a quasi-

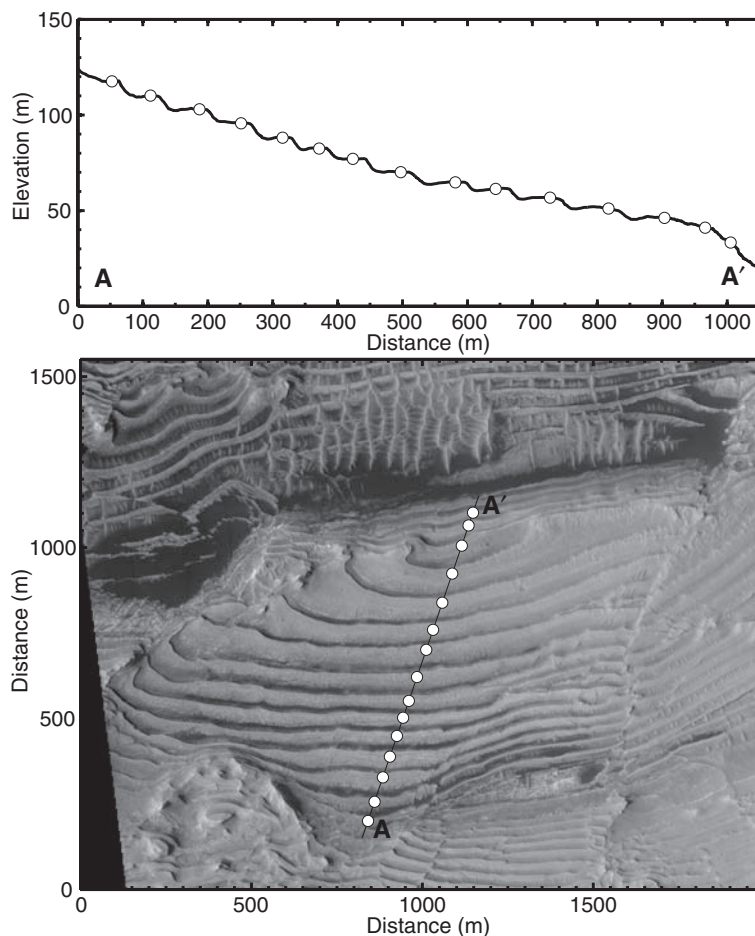


Fig. 1. Topographic profile across one rhythmically bedded outcrop, showing that strata are well resolved in the stereo DTM. Although the beds have varying apparent thicknesses in the original images, the true thicknesses are quasi-periodic when the erosional topography and southward dip is properly accounted for. The lower panel is an orthogonal projection of HiRISE image PSP_002733_1880 and shows the location of profile A-A' along with the corresponding bed positions.

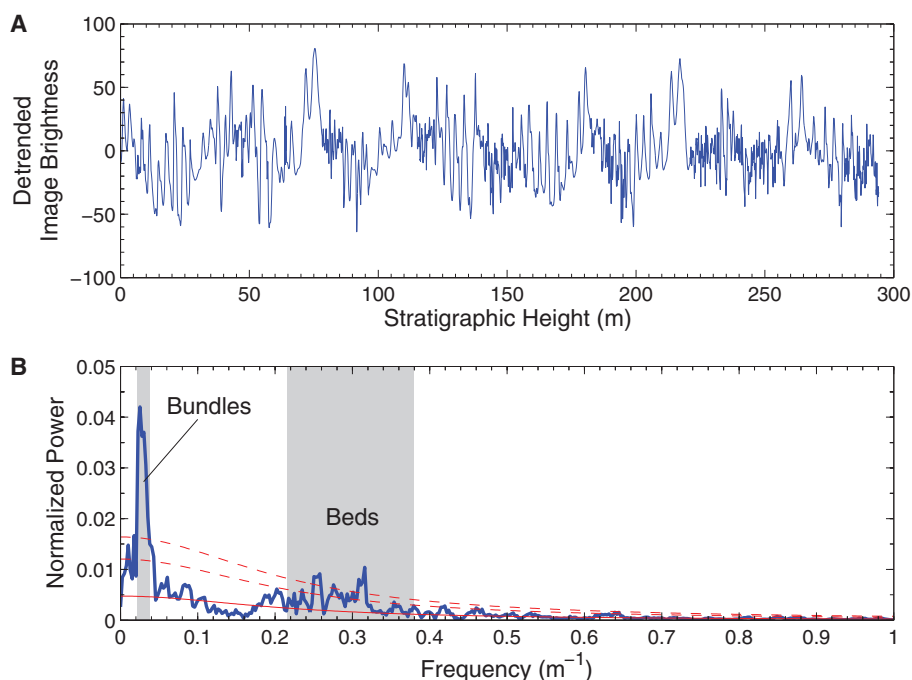


Fig. 2. (A) Detrended image grayscale levels of the Becquerel crater outcrop, topographically corrected and resampled at a uniform interval of 0.1 m in the stratigraphic column. (B) Power spectrum of the Becquerel crater stratigraphy. Estimated red noise background (red solid line) and 95% and 99% confidence levels (red dashed lines) are indicated. Shaded regions indicate the 1σ range of bed and bundle thickness measurements, which correspond well to the two regions where power exceeds the 99% confidence level, indicating quasi-periodicity at both scales.

periodic component is nonrandom with the specified confidence. The spectra showed peaks that exceeded the 99% confidence levels at the measured bedding scales for all sites except Crommelin crater, where the excess power only surpassed the 95% threshold. In the Becquerel spectrum, power exceeded the 99% confidence level relative to the estimated background at both 3 to 4 m and 30 to 40 m, demonstrating statistically significant quasi-periodicity in the Becquerel stratigraphy at both scales (Fig. 2).

The observation of rhythmic layering on Mars at multiple locations across the Arabia region constitutes evidence of cyclic variation in ancient surface conditions. The different scales measured, along with the varying morphologies observed between sites and the dearth of similar deposits on the intervening plains in Arabia (12), suggest that these deposits formed in isolation rather than as part of a regionally extensive

sedimentary unit. Still, the presence of several regularly cyclic sequences within this region of Mars hints at a common external driver, with the local conditions of each sedimentary basin influencing the expression of climate cycles in the stratigraphy.

From orbit, it is difficult to determine the nature of the prominent bed boundaries that give rise to the alternating pattern of erosional resistance. Each erosional step may record discrete or continuous changes in the bulk composition or lithification history of the sediments, overlain on a steady background sedimentation rate. Alternatively, the deposition rate may have varied over each cycle, with episodes of relatively low accumulation leading to more complete induration of the sediment. In either case, quasi-periodic bedding will result when the sediment accumulation rate is roughly constant when averaged over each cycle. With either model, the observed periodic-

ity in stratigraphic position represents a record of cyclicity in time.

An alternative depositional model is that each bed was laid down by discrete, aperiodic events of similar magnitude. This is seen, for example, on Earth in the flood deposits of glacial Lake Missoula, where outbursts of comparable magnitude created repeating beds of similar thickness (13). Two observations argue against this possibility in Arabia Terra. First, the bundling of strata into repeating packages seen in Becquerel crater would require an unlikely additional level of incidental cyclicity. Second, the apparent lack of coarse sediment, channel incision, or erosional unconformities argues against fluvial emplacement of these several-meter-thick beds. Emplacement of a bed in this scenario must occur in a single depositional event to be time scale-independent. This requirement likely rules out formation by individual dust storms, for instance, as current dust deposition rates are on the order of only micrometers per year (14). It is impossible to rule out any scenario without knowing the precise relationship between time and depth. However, we find this case improbable given the bundling seen at Becquerel crater, the volumes of sediment required, and the lack of evidence for aqueous deposition.

The nature of the sedimentation process that deposited the Arabia layers remains uncertain. However, the observation of regularly cyclic bedding rules out processes that occur in a purely stochastic manner, including volcanism and impact cratering. Such events recorded at random intervals within a stratigraphic column are expected to result in an exponential distribution of intervals (15). Further, the size-frequency distributions of many stochastic depositional processes are skewed toward smaller events and can be described in many cases by a power law. Such processes include turbidites, flood events, landslides, volcanic eruptions, and impacts [(16, 17) and references therein]. As both power-law and exponential distributions can be statistically rejected for several of the Arabia sites, a stochastic process of this nature is unlikely without forcing by environmental cyclicity.

On Earth, periodic stratification in the rock record is often associated with cyclic driving mechanisms, which influence the deposition and preservation of sediments. Tidal, seasonal, solar, and orbital cycles have all been documented in sedimentary records (18–20). Quasi-periodic climate cycles on Earth can also arise from internal atmospheric, ocean, and ice sheet dynamics, without an obvious external forcing function (20). On Mars, the likelihood of such internally generated cycles is diminished in the absence of oceans, wet-based ice sheets, and biological feedbacks (21). Martian global dust storms may be quasi-periodic, although at shorter, interannual time scales (22).

In analogy to Earth, the strongest periodic signals on Mars arise at diurnal, annual, and orbital frequencies, all of which cause large variations in local surface conditions. As on Earth,

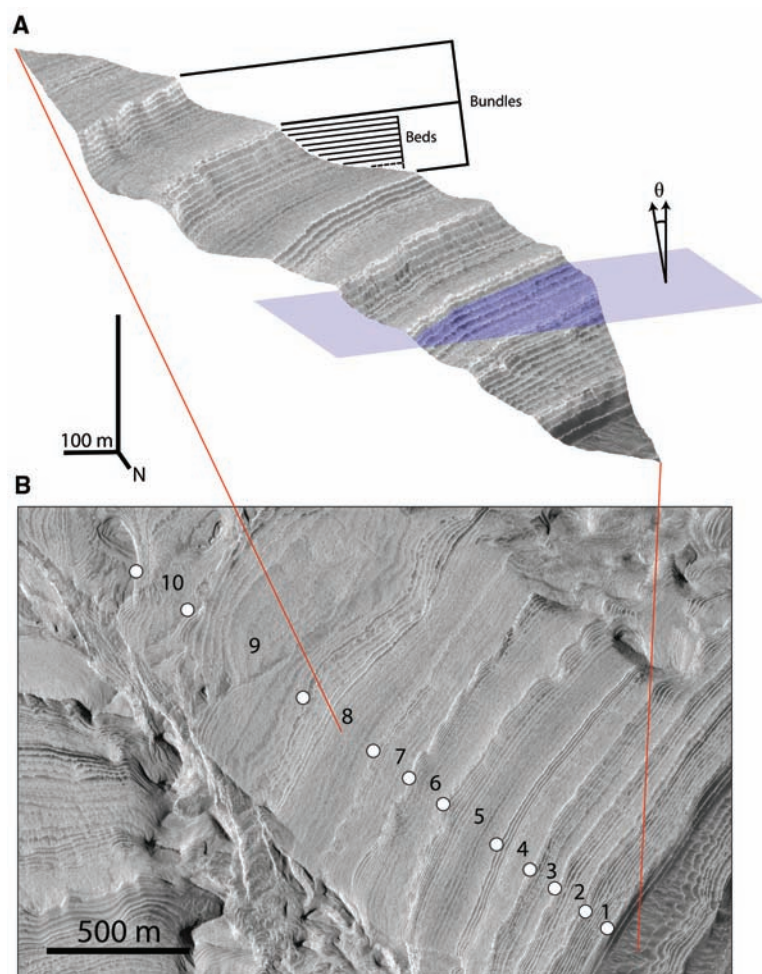


Fig. 3. (A) Three-dimensional view of the stratified deposit within Becquerel crater. This location shows two scales of quasi-periodic bedding, marked as beds and bundles. The ratio of these characteristic thicknesses is a potential clue to the forcing mechanisms responsible for the cyclicity seen in the rocks. The blue plane indicates the best-fit orientation of the bedding, which has a dip of $\sim 3^\circ$. To obtain true thicknesses, it is necessary to account for both the erosional morphology and the tilt of the bedding from horizontal (indicated by θ). HiRISE image PSP_001546_2015 is shown draped over digital stereo topography. Scale bars, 100 m (both horizontal and vertical). (B) Plan view of HiRISE image PSP_001546_2015, showing context for (A); north is down. Numbers mark the boundaries between successive bundles as revealed in the topography.

these cyclic forcing mechanisms are dominant at periods shorter than ~10 years and longer than a few tens of thousands of years (19). The thickness of the beds in Arabia argues against deposition on diurnal or annual time scales. Annual accumulation of more than 10 m of sediment would represent an extremely high deposition rate and would imply that the kilometer-thick deposits accumulated in as little as tens of years. In contrast, deposition at orbital frequencies (~100,000 years) assumes a modest average accumulation rate of ~100 μm per year. This value allows for alternating accumulation and erosion of sediment on shorter time scales, requiring only that the net deposition is roughly constant over long time scales.

Bundling within rhythmic sequences has been a useful indicator of Milankovitch forcing on Earth. In particular, the 5:1 frequency ratio of the precession cycle to the eccentricity cycle for Earth has been observed in the rock record (19, 23). A hierarchy of this type can be used not only to confirm the influence of a periodic forcing mechanism, but also to translate stratigraphic cycles to relative time scales (24). At Becquerel crater (Fig. 3), we observed a roughly 10:1 ratio of frequencies over several hundred meters of section, for a total of at least 10 bundles. Individual beds here have a mean thickness of 3.6 ± 1 m, and the bundles are 36 ± 9 m thick. Strata are less distinct near the bottom of each bundle, making it difficult to obtain a precise count for each cycle.

The obliquity of Mars has the largest effect on the global climate, and is one of the most frequently invoked mechanisms for climate change (2, 21, 25, 26). The tilt of the planet's spin axis ranges over tens of degrees and can have a strong effect on climate, changing the mean annual insolation even at low latitudes by 10% or more, and affecting the global distribution of volatiles. Among the leading effects, polar condensation of carbon dioxide is expected to reduce atmospheric pressure at low obliquity (27). For an aeolian depositional scenario, reduced pressure limits the capacity of the atmosphere to transport sediment (28). The obliquity of Mars oscillates with a period of ~120,000 years and is modulated on a time scale of ~1.2 and ~2.4 million years (29, 30). Orbital calculations show that this modulation is expressed more strongly at 2.4 million years for the recent history of Mars, although the ancient history is unknown because of the chaotic nature of the obliquity over long time scales (31). As the absolute frequencies of these orbital cycles will not vary greatly over geologic time scales (30), this 10:1 ratio in the obliquity cycle is a potential candidate for orbital forcing of the cyclic stratigraphy measured at Becquerel crater. This would imply a formation of one bed per 120,000-year obliquity cycle, one bundle per 1.2-million-year modulation cycle, and deposition of the entire measured section over roughly 12 million years.

The identification of quasi-periodic signals within these layered terrains provides a possible relative chronometer within the martian rock re-

cord. Orbital variations stand out as a possible driver of the observed quasi-periodicity, although definitive identification of the cycles involved will require additional information. Likewise, whereas an aeolian scenario provides a clear link to orbital forcing, the specific formation model remains uncertain. Determination of formation time scales ultimately provides a calibration for interpreting the geological history of Mars. With the tentative but reasonable assumption that some water was required to lithify the Arabia deposits, the suggestion of orbital cyclicity implies that a hydrologic cycle may have been active at least intermittently over millions of years. In contrast to the catastrophic surface conditions inferred from impact craters and outflow channels, this strong cyclicity observed in the martian rock record depicts a fundamentally more predictable and regular environment in the ancient past.

References and Notes

1. M. C. Malin, K. S. Edgett, *Science* **290**, 1927 (2000).
2. P. R. Christensen, H. J. Moore, in *Mars*, H. H. Kieffer, B. M. Jakosky, C. W. Snyder, M. S. Matthews, Eds. (Univ. of Arizona Press, Tucson, AZ, 1992), pp. 686–729.
3. A. S. McEwen *et al.*, *J. Geophys. Res.* **112**, E05502 (2007).
4. J. Laskar, B. Levrard, J. F. Mustard, *Nature* **419**, 375 (2002).
5. S. M. Milkovich, J. W. Head, *J. Geophys. Res.* **110**, E01005 (2005).
6. K. Edgett, *J. Geophys. Res.* **107**, 5038 (2002).
7. M. H. Carr, F. C. Chuang, *J. Geophys. Res.* **102**, 9145 (1997).
8. B. M. Hynek, R. J. Phillips, *Geology* **31**, 757 (2003).
9. R. L. Kirk *et al.*, *J. Geophys. Res.* **113**, E00A24 (2008).
10. By comparing the data to ideal distributions via the Kolmogorov-Smirnov test, the hypothesis that the bed thicknesses were drawn from an exponential distribution can be rejected for four out of five data sets at a 95% confidence level. For a power-law distribution, the null hypothesis can be similarly rejected for all of the data sets. In contrast, a normal distribution is consistent with all of the data sets using this test.
11. M. E. Mann, J. M. Lees, *Clim. Change* **33**, 409 (1996).
12. K. S. Edgett, M. C. Malin, *Geophys. Res. Lett.* **29**, 2179 (2002).
13. J. Waitt, R. B. J. *Geol.* **88**, 653 (1980).
14. G. A. Landis, P. P. Jenkins, *J. Geophys. Res.* **105**, 1855 (2000).
15. B. H. Wilkinson, N. W. Diedrich, C. N. Drummond, E. D. Rothman, *Bull. Geol. Soc. Am.* **110**, 1075 (1998).
16. J. Carlson, J. Grotzinger, *Sedimentology* **48**, 1331 (2001).
17. B. D. Malamud, D. L. Turcotte, *J. Hydrol.* **322**, 168 (2006).
18. A. G. Fischer, *Annu. Rev. Earth Planet. Sci.* **14**, 351 (1986).
19. M. R. House, in *Orbital Forcing Timescales and Cyclostratigraphy*, M. R. House, A. S. Gale, Eds. (Geological Society of London, London, 1995), pp. 1–18.
20. G. Weedon, *Time-Series Analysis and Cyclostratigraphy: Examining Stratigraphic Records of Environmental Cycles* (Cambridge Univ. Press, Cambridge, 2003).
21. H. H. Kieffer, A. P. Zent, in *Mars*, H. H. Kieffer, B. M. Jakosky, C. W. Snyder, M. S. Matthews, Eds. (Univ. of Arizona Press, Tucson, AZ, 1992), pp. 1180–1218.
22. R. Kahn, T. Martin, R. Zurek, S. Lee, in *Mars*, H. H. Kieffer, B. M. Jakosky, C. W. Snyder, M. S. Matthews, Eds. (Univ. of Arizona Press, Tucson, AZ, 1992), p. 1017–1053.
23. W. Schwarzacher, *Earth Sci. Rev.* **50**, 51 (2000).
24. L. A. Hinnov, *Annu. Rev. Earth Planet. Sci.* **28**, 419 (2000).
25. W. R. Ward, B. C. Murray, M. C. Malin, *J. Geophys. Res.* **79**, 3387 (1974).
26. J. W. Head, J. F. Mustard, M. A. Kreslavsky, R. E. Milliken, D. R. Marchant, *Nature* **426**, 797 (2003).
27. F. P. Fanale, J. R. Salvail, *Icarus* **111**, 305 (1994).
28. J. A. Cutts, B. H. Lewis, *Icarus* **50**, 216 (1982).
29. W. R. Ward, in *Mars*, H. H. Kieffer, B. M. Jakosky, C. W. Snyder, M. S. Matthews, Eds. (Univ. of Arizona Press, Tucson, AZ, 1992), pp. 298–320.
30. J. Laskar *et al.*, *Icarus* **170**, 343 (2004).
31. J. Touma, J. Wisdom, *Science* **259**, 1294 (1993).
32. Supported by NASA's Mars Data Analysis Program and by the NASA Earth and Space Science Fellowship program. We thank two anonymous reviewers for helpful comments and suggestions.

Supporting Online Material

www.sciencemag.org/cgi/content/full/322/5907/PAGE/DC1
Tables S1 to S6

16 June 2008; accepted 10 November 2008
10.1126/science.1161870

Photoexcited CRY2 Interacts with CIB1 to Regulate Transcription and Floral Initiation in *Arabidopsis*

Hongtao Liu, Xuhong Yu, Kunwu Li, John Klejnot, Hongyun Yang, Dominique Lisiero, Chentao Lin*

Cryptochromes (CRY) are photolyase-like blue-light receptors that mediate light responses in plants and animals. How plant cryptochromes act in response to blue light is not well understood. We report here the identification and characterization of the *Arabidopsis* CIB1 (cryptochrome-interacting basic-helix-loop-helix) protein. CIB1 interacts with CRY2 (cryptochrome 2) in a blue light–specific manner in yeast and *Arabidopsis* cells, and it acts together with additional CIB1-related proteins to promote CRY2-dependent floral initiation. CIB1 binds to G box (CACGTG) in vitro with a higher affinity than its interaction with other E-box elements (CANNTG). However, CIB1 stimulates *FT* messenger RNA expression, and it interacts with chromatin DNA of the *FT* gene that possesses various E-box elements except G box. We propose that the blue light–dependent interaction of cryptochrome(s) with CIB1 and CIB1-related proteins represents an early photoreceptor signaling mechanism in plants.

Arabidopsis cryptochromes (CRY) mediate light regulation of cell elongation and photoperiodic flowering (1, 2), but the photoactivation mechanism of cryptochrome re-

mains unclear. It has been hypothesized that, similar to other photoreceptors, photoexcited cryptochromes may interact with target proteins to regulate gene expression and physiological

responses (3–7). However, no light-dependent cryptochrome target protein has been reported in plants, impeding a direct test of this hypothesis. We used a yeast two-hybrid assay to screen for proteins that interacted with *Arabidopsis* CRY2 in a blue light-specific manner (8). Because cryptochromes contain the same chromophores—flavin adenine dinucleotide (FAD) and methyltetrahydrofolate (MTHF)—as that of yeast DNA photolyase (9–11), we reasoned that an *Arabidopsis* cryptochrome expressed in yeast cells should bind the native chromophores to undergo light-dependent protein-protein interactions. Four clones identified in our screen encode various lengths of a basic helix-loop-helix (bHLH) protein (At4g34530), which was referred to as cryptochrome-interacting bHLH or CIB1 (fig. S1). CIB1 is a bHLH protein, for which the function has not been reported, but the mRNA expression is known to be moderately responsive to light (12). In yeast cells, the full-length CIB1 and the N-terminal domain of CIB1 interacted with CRY2 in blue light but not in red light or darkness, as shown by two different reporter assays (Fig. 1A and fig. S2). For example, yeast cells irradiated with blue light at the fluence rate of

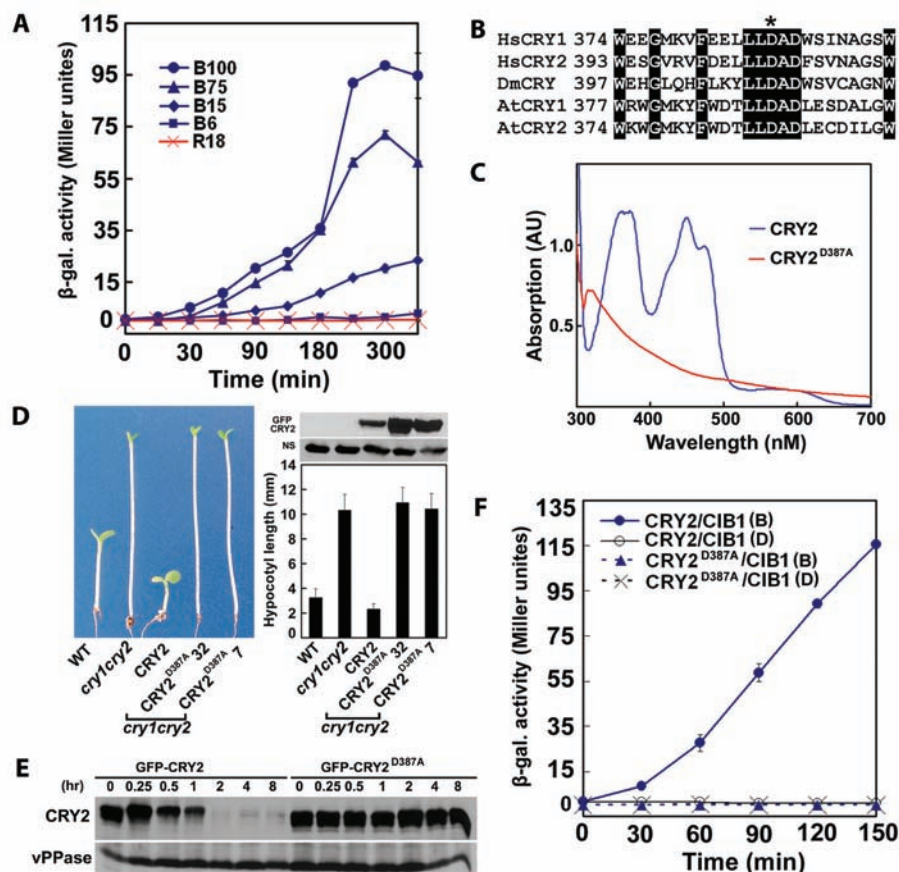
15 $\mu\text{mol m}^{-2} \text{s}^{-1}$ showed appreciable reporter [β -galactosidase (β -Gal)] activity after 60 min of irradiation (Fig. 1A, B15), but no β -Gal activity was detected in cells irradiated with red light of 18 $\mu\text{mol m}^{-2} \text{s}^{-1}$ for up to 360 min (Fig. 1A, R18). The CRY2-CIB1 interaction requires relatively high fluence rates. For instance, cells irradiated with 100 $\mu\text{mol m}^{-2} \text{s}^{-1}$ blue light showed a CRY2-CIB1 interaction stronger than that in cells irradiated with 15 $\mu\text{mol m}^{-2} \text{s}^{-1}$ blue light (Fig. 1A, comparing B100 to B15), whereas little CRY2-CIB1 interaction was detected in cells exposed to 6 $\mu\text{mol m}^{-2} \text{s}^{-1}$ blue light for the time tested (Fig. 1A, B6).

We next examined whether the CRY2-CIB1 interaction was dependent on the chromophores of the CRY2 photoreceptor. Because none of the previously isolated *cry2* mutant is known to specifically affect chromophore binding (2, 13), we prepared a site-specific *cry2* mutant, CRY2^{D387A}, in which the residue aspartic acid at position 387 was changed to alanine. The residue D387 of *Arabidopsis* CRY2 is part of the FAD-binding pocket conserved in cryptochromes from *Arabidopsis* to human (Fig. 1B and fig. S3) (14). In contrast to the wild-type (WT) CRY2 protein, the CRY2^{D387A} mutant protein expressed and purified from insect cells does not contain flavin (Fig. 1C). The flavin-deficient CRY2^{D387A} fusion protein expressed in *Arabidopsis* is “blind” in two blue-light responses: It failed to mediate blue-

light inhibition of hypocotyl elongation (Fig. 1D), and it showed no blue light-induced degradation (Fig. 1E). The CRY2^{D387A} mutant protein did not interact with CIB1 in yeast cells (Fig. 1F and fig. S2A). The lack of interaction between CRY2^{D387A} and CIB1 is unlikely due to denaturation of the CRY2^{D387A} mutant protein, because CRY2^{D387A} interacted with constitutive photomorphogenic protein 1 (COP1) in a light-independent manner similar to that shown by the WT CRY2 protein (15) (fig. S2E). In addition to flavin, cryptochromes are also known to associate with a folate, MTHF, which acts as the second chromophore (10, 16). However, folate usually disassociates from the apoprotein during purification, and recombinant plant cryptochromes purified from insect cells contain little folate (Fig. 1C) (11, 17, 18). The folate-deficient CRY2 interacted with CIB1 regardless of light in the *in vitro* pull-down assays (fig. S2C). It remains unclear whether the lack of light responsiveness of the CRY2-CIB1 interaction *in vitro* was due to the experimental conditions used or the lack of folate of the purified CRY2.

CIB1 is a nuclear protein that colocalized with CRY2 in the nucleus (fig. S4), and it interacted with CRY2 in plant cells in the BiFC (bimolecular fluorescence complementation) assay (fig. S5). Strong fluorescence was detected in the nuclei of cells cotransfected with C-terminal cyan fluorescent protein (cCFP)-CRY2 and N-

Fig. 1. CRY2 interacts with CIB1 in a blue light-specific and FAD-dependent manner. **(A)** β -Gal assays of yeast cells expressing indicated proteins irradiated with red light (R18, 18 $\mu\text{mol m}^{-2} \text{s}^{-1}$) or blue light (B6 to B100, 6 to 100 $\mu\text{mol m}^{-2} \text{s}^{-1}$) for the durations indicated. **(B)** The FAD-binding pocket of human (Hs), *Drosophila* (Dm), and *Arabidopsis* (At) cryptochromes. Asterisk indicates D387 of CRY2 and equivalent residues in other CRYs (34). **(C)** Absorption spectrum of CRY2 and CRY2^{D387A} mutant proteins. **(D)** A hypocotyl inhibition assay showing the lack of photoreceptor activity of CRY2^{D387A}. (Left) Five-day-old seedlings of indicated genotypes grown in blue light (20 $\mu\text{mol m}^{-2} \text{s}^{-1}$). (Upper right) An immunoblot probed with antibody to CRY2 (NS is a loading control). (Lower right) Means of hypocotyl lengths ($n \geq 20$). **(E)** Immunoblot of samples prepared from 5-day-old etiolated seedlings exposed to blue light for the indicated time and probed with antibody to CRY2 and antibody to vacuolar pyrophosphatase (vPPase, the loading control). **(F)** β -Gal assays of yeast cells grown in the dark (D) or irradiated with blue light (B, 30 $\mu\text{mol m}^{-2} \text{s}^{-1}$) for the time indicated.



terminal yellow fluorescent protein (nYFP)–CIB1 plasmids (fig. S5), suggesting reconstitution of the fluorophore upon cCFP-CRY2–nYFP–CIB1

interaction. In contrast, no fluorescence was detected in cells transfected separately with the cCFP-CRY2 or nYFP–CIB1 plasmid (fig. S5).

Because of technical difficulties using the BiFC method to study light effects, we examined the CRY2–CIB1 complex formation in plants ex-

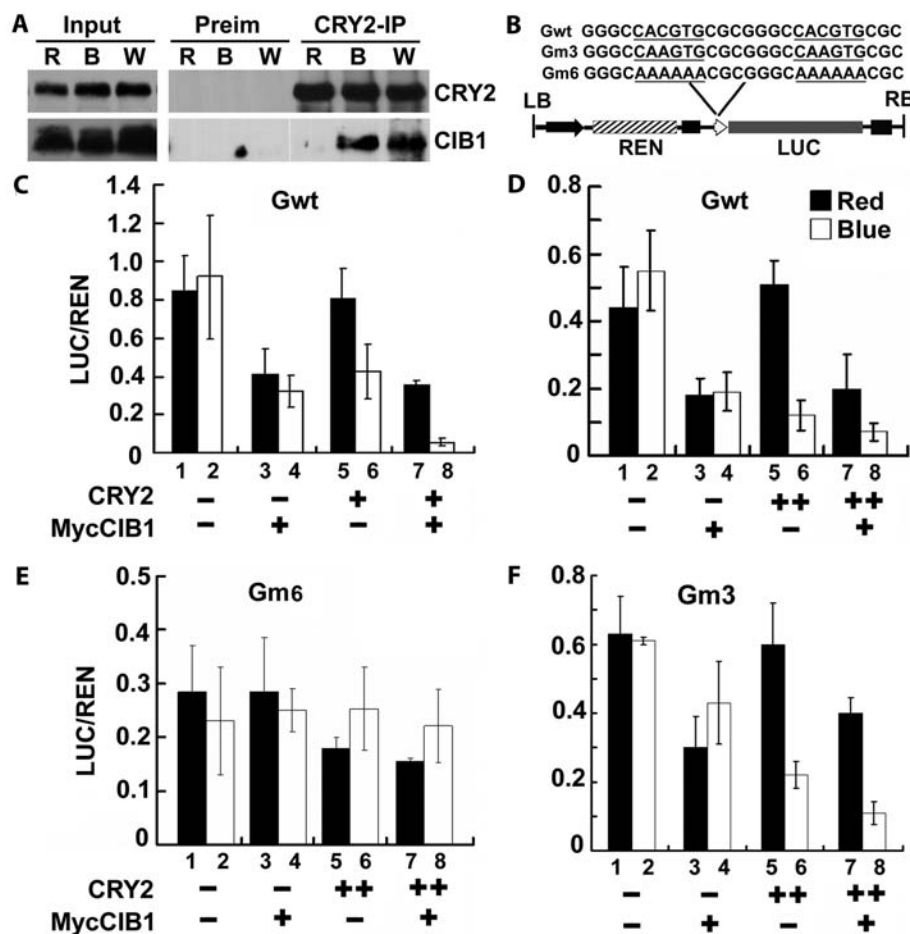


Fig. 2. CIB1 interacts with CRY2 and regulates transcription in plant cells. **(A)** Co-IP assays of samples prepared from 12-day-old *35S::MycCIB1* seedlings grown in continuous red light, pretreated in MG132, then exposed to white light (W), or red light (R), or blue light (B, $20 \mu\text{mol m}^{-2} \text{s}^{-1}$, 20 min). Total proteins (Input) or IP product of antibody to CRY2 (CRY2-IP) or preimmune serum (Preim) were probed, in immunoblots, by the antibody to CRY2, stripped, and reprobed by the antibody to Myc (MycCIB1). **(B)** Structure of the G-box-driven dual-Luc reporter gene and DNA sequences of the recombinant G-box (Gwt) or mutant promoters (Gm6 and Gm3). 35S promoter (black arrow), 35S minimum promoter (white arrow head), *Renilla* luciferase (REN), firefly luciferase (LUC), and T-DNA (left border (LB) and right border (RB)) are indicated. **(C to F)** Relative reporter activity (LUC/REN) in plants of the indicated genotypes, light condition, and effector (MycCIB1) expression. MycCIB1+, transiently expressed MycCIB1; CRY2+, WT; CRY2-, *cry1cry2* mutant; CRY2++, CRY2 overexpressing in the WT background. Leaves were transfected with the reporter and the effector (MycCIB1), kept in white light for 3 days, transferred to red light for 1 day (Red), and irradiated with blue light ($20 \mu\text{mol m}^{-2} \text{s}^{-1}$) for 2 hours (Blue). The relative LUC activities normalized to the REN activity are shown (LUC/REN, $n = 3$).

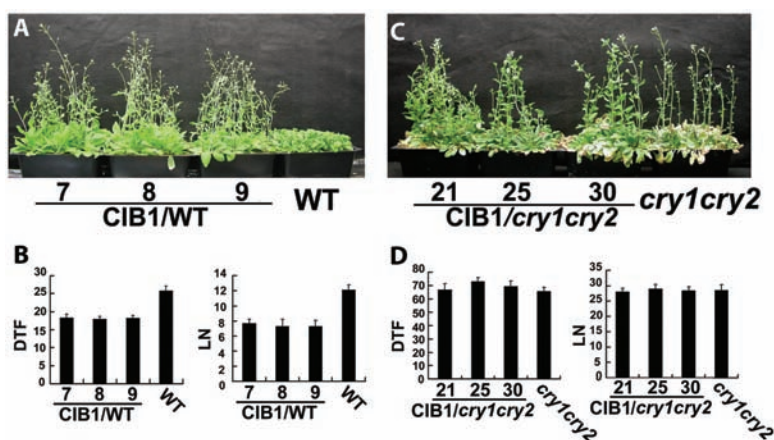


Fig. 3. CIB1 promotes floral initiation in a CRY2-dependent manner by stimulating the *FT* mRNA expression. **(A and C)** 23-day-old (A) or 78-day-old (C) plants of indicated genotypes grown in long-day (LD) photoperiods (16 hours light, 8 hours dark). **(B and D)** The time to flowering and the number of rosette leaves at the time of flowering of the indicated genotypes shown in A [for (B)] and C [for (D)]. **(E)** Quantitative PCR (qPCR) results showing mRNA expression of the indicated genes in the WT (black diamonds) and transgenic plants overexpressing CIB1 in the WT background (CIB1/WT, blue circles). Plants grown for 6 days under LD photoperiod (light phase, white; dark phase, black) were transferred to continuous white light for 2 days (subjective dark phase, striped). Samples were collected every 3 hours for 1 day in photoperiod and 2 days in continuous light, and the representative results of qPCR are shown.

pressing Myc-tagged CIB1 (MycCIB1/WT), using a coimmunoprecipitation (co-IP) assay designed to detect unstable protein complexes (8, 19). In this experiment, seedlings were pretreated with the proteasome inhibitor MG132 to block blue light-dependent CRY2 degradation (20). Samples were then exposed to red light, white light, or blue light ($20 \mu\text{mol m}^{-2} \text{s}^{-1}$) and subjected to co-IP analyses. CIB1 was coprecipitated with CRY2 in samples irradiated with white light (Fig. 2A, W) or blue light (Fig. 2A, B). In contrast, little CIB1 was coprecipitated with CRY2 in samples irradiated with red light (Fig. 2A, R). These results argue strongly that blue light stimulates accumulation of the CRY2-CIB1 complex in plant cells. Taken together, we concluded that CRY2 increases its affinity to CIB1 and CIB1-related proteins in response to blue light.

Like many bHLH proteins, CIB1 interacted in vitro with the highest affinity to an E-box (CACGTG) DNA sequence, which is also known as G box (21) (fig. S6). To determine whether CIB1 may act as a transcriptional regulator in vivo, we developed a transient transcription assay in *Arabidopsis* plants (8), using a dual luciferase assay (Fig. 2B) (22). We examined the effects of Myc-tagged CIB1 (MycCIB1) transiently expressed in plants of different genotypes on the activity of the recombinant G-box promoter under different light conditions (Fig. 2, C to F, and fig. S7). As shown in fig. S7A, both the endogenous CRY2 and transiently expressed MycCIB1 acted as the suppressor of the recombinant G-box promoter in this assay

system. The G-box reporter showed MycCIB1- and cryptochrome-independent activities, and MycCIB1 exhibited blue light- and cryptochrome-independent activities (Fig. 2, C and D, and fig. S7A). These observations may be explained by the fact that the activity of the recombinant G-box promoter was affected by multiple photoreceptors and transcription factors in vivo and that CIB1 may have a blue light/cryptochrome-independent effect on transcription. On the other hand, our results also demonstrate that (i) cryptochromes mediate blue-light suppression of the recombinant G-box promoter (Fig. 2, C and D, and fig. S7B, comparing 1/2 to 5/6); (ii) CIB1 possess a blue light- and cryptochrome-dependent activity suppressing the G-box promoter (Fig. 2C and fig. S7B, comparing 3/4 to 7/8, and 5/6 to 7/8); and (iii) the activities of cryptochrome and CIB1 are detected on the reporter promoter containing G box but not on the reporter promoter lacking G box (Fig. 2, comparing 2D and 2E). We concluded that CIB1 is a transcriptional regulator and that the transcriptional regulatory activity of CIB1 is at least partially dependent on blue light and cryptochromes.

The *cib1* loss-of-function mutant showed no apparent phenotype (fig. S8), which suggests that the function of CIB1 may be redundant to that of other bHLH proteins. To test this hypothesis, we examined seven bHLH proteins related to CIB1, including CIB5, which interacts with both CRY2 and CIB1 (figs. S1 and S8). The *cib1cib5* double mutant showed a mild but statistically significant delay of flowering under the photoperiodic induction condition (23, 24) (fig. S8), which sug-

gests that CIB1 may act to promote floral initiation and that multiple CIB1-related proteins may act redundantly. Consistent with this hypothesis, transgenic plants overexpressing CIB1 in the WT background flowered significantly earlier than the parents in two different light conditions tested (Fig. 3, A and B, and fig. S9). We reasoned that if the function of CIB1 in promoting floral initiation is directly related to its physical interaction with CRY2, this activity of CIB1 should be dependent on CRY2. Indeed, transgenic plants overexpressing CIB1 in the *cry1cry2* mutant background (*CIB1/cry1cry2*) flowered at the same time as the *cry1cry2* parent in both light conditions tested (Fig. 3, C and D, and fig. S9), demonstrating that the function of CIB1 in promoting floral initiation is dependent on CRY2. The different effects of CIB1 overexpression in the two different genetic backgrounds is not due to different levels of CIB1 expression, because CIB1 protein level in none of the three independent *CIB1/cry1cry2* lines tested was lower than that in any of the three independent *CIB1/WT* lines tested (fig. S9B).

Transgenic plants overexpressing CIB1 exhibited elevated mRNA expression of the flowering-time gene *FT* (Fig. 3E and fig. S10). CIB1 appeared to affect primarily the amplitude, but not the period, of the circadian rhythm of the *FT* mRNA expression (Fig. 3E and fig. S10). CIB1 did not seem to affect mRNA expression of other genes tested, including *CCA1* or *LHY*, which are the clock genes possessing the G-box promoter elements (7) (Fig. 3E and fig. S10A). These results indicate that CIB1 may not necessarily tar-

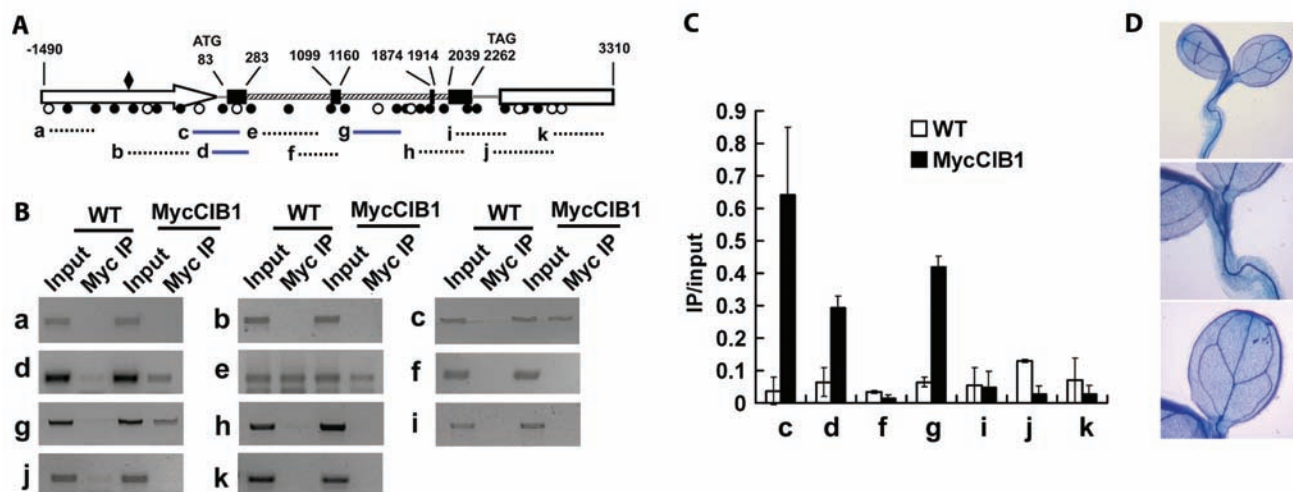


Fig. 4. ChIP-PCR showing interaction of CIB1 and chromatin regions of the *FT* gene. (A) A diagram depicting the putative promoter (arrow), 5'UTR (untranslated region) (gray line), exons (black boxes), introns (striped boxes), 3'UTR (gray line), and the putative terminator (white box) of the *FT* gene. Black and white circles indicate positions of E boxes (CANNTG) and 4-nucleotide core of G box (ACGT), respectively. The diamond symbol indicates the position of a CCAAT box. Blue solid lines or black dashed lines depict the DNA regions that were amplified or not amplified by ChIP-PCR using the indicated primer sets, respectively. (B) Representative results of the ChIP-PCR assays. Chromatin

fragments (~500 base pairs) were prepared from 7-day-old WT seedlings or transgenic seedlings expressing MycCIB1 (MycCIB1/WT), immunoprecipitated by the antibody to Myc, and the precipitated DNA PCR-amplified using the primer pairs indicated. Input, PCR reactions using the samples before immunoprecipitation. (C) ChIP-PCR results for the primer pairs that were repeated at least three times were quantified by normalization of the Myc-IP signal with the corresponding input signal (IP/input). The standard deviations ($n \geq 3$) are shown. (D) GUS staining of a seedling expressing the CIB1::GUS transgene; different magnifications of the same sample are shown.

get the G-box elements *in vivo*, although it has the highest affinity to the G-box DNA *in vitro*. Consistent with this notion, CRY2 and CIB1 exhibited similar effects on a recombinant E-box reporter (Gm3, CAAGTG) as they did on the recombinant G-box reporter *in vivo* (Fig. 2, comparing D to F), although this E box interacted with CIB1 poorly *in vitro* (fig. S7). This result suggests that CIB1 may heterodimerize with other proteins, such as CIB5, to interact with E boxes *in vivo*. We therefore examined whether CIB1 might interact with the *FT* gene that contains various E-box elements, except G box, throughout the genomic DNA (Fig. 4A), using the ChIP-PCR (chromatin immunoprecipitation–polymerase chain reaction) assay. Figure 4, B and C, shows that CIB1 indeed interacted with chromatin fragments associated with the *FT* genomic DNA *in vivo*. Given that CRY2 control of *FT* transcription took place primarily in the vascular bundle cells (25), we also tested whether CIB1 was expressed in those cells. Analyses of the GUS (β -glucuronidase) reporter expression in transgenic plants expressing GUS under control of the CIB1 promoter demonstrated that CIB1 promoter was active in the vascular bundle cells (Fig. 4C). These results support a hypothesis that CIB1 interacts with the E-box regulatory elements of the *FT* gene, whereas CRY2 interacts with CIB1 in response to blue light to affect *FT* transcription and floral initiation.

It has been previously shown that cryptochromes mediate blue-light activation of *FT* mRNA expression by suppressing CO proteolysis (23, 24). The effect of CRY2 on CO protein can be explained by interaction between cryptochromes and the COP1 complex (15, 26, 27) (fig. S2E), because COP1 acts as an E3 ubiquitin ligase partially responsible for the CO ubiquitination and degradation (15, 26, 27). On the other hand, our study indicates that CRY2 also functions by

interacting with CIB1 to directly affect *FT* transcription. Therefore, cryptochromes may mediate photoperiodic control of floral initiation by at least three different mechanisms: suppression of CO protein degradation (23), regulation of light entrainment of the circadian clock (28), and direct modulation of *FT* transcription (fig. S11).

Cryptochrome is the only photoreceptor found in all three major evolutionary lineages, from bacteria to plants and animals, although its role as a photoreceptor in mammals remains controversial (29–31). It has been previously shown that mouse cryptochromes physically interact with two bHLH proteins, CLOCK and BMAL, to suppress their activity on the E-box–dependent transcription (32). Given the current hypothesis that cryptochromes evolved independently in different lineages (29–31, 33), it remains to be explained how the three-party molecular interaction of CRY, bHLH transcription factors, and E-box DNA elements have evolved in organisms as remotely related as mouse and *Arabidopsis*.

References and Notes

- M. Ahmad, A. R. Cashmore, *Nature* **366**, 162 (1993).
- H. Guo, H. Yang, T. C. Mockler, C. Lin, *Science* **279**, 1360 (1998).
- H.-Q. Yang *et al.*, *Cell* **103**, 815 (2000).
- X. Yu *et al.*, *Proc. Natl. Acad. Sci. U.S.A.* **104**, 7289 (2007).
- M. F. Ceriani *et al.*, *Science* **285**, 553 (1999).
- M. Ni, J. M. Tepperman, P. H. Quail, *Cell* **95**, 657 (1998).
- J. F. Martinez-Garcia, E. Huq, P. H. Quail, *Science* **288**, 859 (2000).
- Materials and methods are available as supporting material on Science Online.
- J. L. Johnson *et al.*, *Proc. Natl. Acad. Sci. U.S.A.* **85**, 2046 (1988).
- K. Malhotra, S. T. Kim, A. Batschauer, L. Dawut, A. Sancar, *Biochemistry* **34**, 6892 (1995).
- C. Lin *et al.*, *Science* **269**, 968 (1995).
- L. Ma *et al.*, *Plant Cell* **13**, 2589 (2001).
- S. El-Din El-Assal, C. Alonso-Blanco, A. J. Peeters, V. Raz, M. Koornneef, *Nat. Genet.* **29**, 435 (2001).

- C. A. Brautigam *et al.*, *Proc. Natl. Acad. Sci. U.S.A.* **101**, 12142 (2004).
- H. Wang, L. G. Ma, J. M. Li, H. Y. Zhao, X. W. Deng, *Science* **294**, 154 (2001).
- S. Ozgur, A. Sancar, *Biochemistry* **42**, 2926 (2003).
- R. Banerjee *et al.*, *J. Biol. Chem.* **282**, 14916 (2007).
- J. P. Bouly *et al.*, *J. Biol. Chem.* **282**, 9383 (2007).
- S. S. Gampala *et al.*, *Dev. Cell* **13**, 177 (2007).
- X. Yu *et al.*, *Plant Cell* **19**, 3146 (2007).
- G. Toledo-Ortiz, E. Huq, P. H. Quail, *Plant Cell* **15**, 1749 (2003).
- R. P. Hellens *et al.*, *Plant Methods* **1**, 13 (2005).
- F. Valverde *et al.*, *Science* **303**, 1003 (2004).
- M. J. Yanovsky, S. A. Kay, *Nature* **419**, 308 (2002).
- M. Endo, N. Mochizuki, T. Suzuki, A. Nagatani, *Plant Cell* **19**, 84 (2007).
- L. J. Liu *et al.*, *Plant Cell* **20**, 292 (2008).
- S. Jang *et al.*, *EMBO J.* **27**, 1277 (2008).
- D. E. Somers, P. F. Devlin, S. A. Kay, *Science* **282**, 1488 (1998).
- A. R. Cashmore, *Cell* **114**, 537 (2003).
- C. Lin, D. Shalitin, *Annu. Rev. Plant Biol.* **54**, 469 (2003).
- A. Sancar, *Chem. Rev.* **103**, 2203 (2003).
- E. A. Griffin Jr., D. Staknis, C. J. Weitz, *Science* **286**, 768 (1999).
- T. Todo, *Mutat. Res.* **434**, 89 (1999).
- Single-letter abbreviations for the amino acid residues are as follows: A, Ala; C, Cys; D, Asp; E, Glu; F, Phe; G, Gly; H, His; I, Ile; K, Lys; L, Leu; M, Met; N, Asn; P, Pro; Q, Gln; R, Arg; S, Ser; T, Thr; V, Val; W, Trp; and Y, Tyr.
- The authors thank J. Ecker, Z. Wang, W. Laing, S. Poethig, G. Chen, L. Johnson, S. Jacobsen, S. Knowles, E. Tobin, and R. Goldberg for materials and technical assistance. This work is supported in part by NIH (GM56265 to C.L.), University of California–Los Angeles faculty research, and Sol Leshin UCLA-BGU Academic Cooperation programs.

Supporting Online Material

www.sciencemag.org/cgi/content/full/1163927/DC1

Materials and Methods

Figs. S1 to S11

Table S1

References

29 July 2008; accepted 28 October 2008

Published online 6 November 2008

10.1126/science.1163927

A Stress Signaling Pathway in Adipose Tissue Regulates Hepatic Insulin Resistance

Guadalupe Sabio,^{1,2} Madhumita Das,² Alfonso Mora,² Zhiyou Zhang,³ John Y. Jun,^{3,4} Hwi Jin Ko,³ Tamera Barrett,² Jason K. Kim,³ Roger J. Davis^{1,2*}

A high-fat diet causes activation of the regulatory protein c-Jun NH₂-terminal kinase 1 (JNK1) and triggers development of insulin resistance. JNK1 is therefore a potential target for therapeutic treatment of metabolic syndrome. We explored the mechanism of JNK1 signaling by engineering mice in which the *Jnk1* gene was ablated selectively in adipose tissue. JNK1 deficiency in adipose tissue suppressed high-fat diet–induced insulin resistance in the liver. JNK1-dependent secretion of the inflammatory cytokine interleukin-6 by adipose tissue caused increased expression of liver SOCS3, a protein that induces hepatic insulin resistance. Thus, JNK1 activation in adipose tissue can cause insulin resistance in the liver.

Metabolic stress caused by a high-fat diet (HFD) results in activation of the regulatory protein JNK1 (1). JNK1 is ac-

tivated, in part, by increased serum-free fatty acids that induce a stress signaling pathway in target tissues (2). JNK1 phosphorylates the adapter

protein insulin receptor substrate 1 (IRS1) at an inhibitory site that can block signal transduction by the insulin receptor (3). JNK1 may therefore directly induce insulin resistance (4). However, JNK1 may also influence insulin sensitivity indirectly. Thus, JNK1 may act in hematopoietic cells to regulate the expression of cytokines that can influence insulin sensitivity (5). Indeed, myeloid cells, including macrophages, may be critical (5).

To examine the role of JNK1 in myeloid cells during the development of diet-induced insulin resistance, we examined the phenotype of mice with JNK1 deficiency in myeloid cells (figs. S1 and S2) and hematopoietic cells (fig. S3). No significant difference in the response of these JNK1-deficient HFD-fed mice, compared with control HFD-fed mice, was detected in glucose and insulin tolerance tests (figs. S2 and S3). These data indicate that, although JNK1 in hematopoietic cells may contribute to HFD-induced insulin resistance, other cell types must also participate in the development of insulin resistance. Adiposity is known

to influence insulin responsiveness (6) through a mechanism that involves adipose-derived fatty acids and hormones/cytokines (collectively termed “adipokines”) that can modulate insulin sensitivity (7). We examined the role of JNK1 in adipocytes on the regulation of insulin sensitivity.

Mice lacking JNK1 in adipose tissue (F^{KO}) were generated using animals with conditional (floxed) *Jnk1* and adipose tissue-specific expression of *Cre* recombinase (*Fabp4-Cre⁺ Jnk1^{f/f}*). Littermates without conditional *Jnk1* (*Fabp4-Cre⁺ Jnk1^{f/+}*) were used as control mice (F^{WT}). The *Jnk1⁺*, *Jnk1^f*, and deleted *Jnk1* ($\Delta Jnk1$) alleles were detected by polymerase chain reaction (PCR) amplification of genomic DNA (fig. S1A). Efficient deletion of *Jnk1^f* was detected in the adipose tissue of F^{KO} mice (fig. S1B). In contrast, *Jnk1^f* was not deleted in other tissues of F^{KO} mice, including macrophages (fig. S1C). Quantitative PCR analysis demonstrated that *Jnk1* mRNA was markedly reduced in epididymal fat and brown fat of F^{KO} animals (Fig. 1A). Immunoblot analysis confirmed the reduction of JNK1 protein in fat depots from F^{KO} mice, whereas JNK1 was preserved in liver, muscle, and macrophages (Fig. 1B). JNK1 is activated in mice after exposure to metabolic stress (4). Indeed, we found that JNK1 was activated

in the adipose tissue, striated muscle, and liver of HFD-fed F^{WT} mice (Fig. 1C). In contrast, HFD-fed F^{KO} mice exhibited JNK activation in muscle and liver but not adipose tissue (Fig. 1C). Together, these data indicate that F^{KO} mice are useful for studies of the role of JNK1 in adipose tissue.

Comparison of HFD-fed F^{WT} and F^{KO} mice demonstrated that these animals gained similar body mass (fig. S4) and blood lipids (fig. S5), became glucose intolerant (Fig. 2A) with reduced glucose-induced insulin secretion (Fig. 2C), and developed mild fasting hyperglycemia (Fig. 2L). In contrast, when compared with HFD-fed F^{WT} mice, the HFD-fed F^{KO} mice showed improved insulin sensitivity during an insulin tolerance test (Fig. 2B) and reduced hyperinsulinemia (Fig. 2K). We performed a 2-hour hyperinsulinemic-euglycemic clamp study to assess organ-specific glucose metabolism in awake F^{WT} and F^{KO} mice. After 3 weeks of HFD, both groups of mice developed whole-body insulin resistance, as indicated by significant reductions in glucose infusion rate and whole-body glucose turnover during the clamp (Fig. 2, D and E). HFD-fed F^{WT} mice developed insulin resistance in liver, as indicated by increased hepatic glucose production (HGP) during the clamp, but HFD-fed F^{KO} mice remained insulin sensitive in liver (Fig. 2, H and I). Basal HGP was not affected by feeding a HFD or by JNK1 deletion in adipose tissue (Fig. 2G). Studies of hepatic gluconeogenesis demonstrated that increased blood glucose caused by pyruvate administration was suppressed in HFD-fed F^{WT} mice but not HFD-fed F^{KO} mice (fig. S6). No differences in whole-body glycolysis or glycogen synthesis were detected between HFD-fed F^{WT} and F^{KO} mice (Fig. 2, F

and J). Together, these data demonstrate that adipose-specific disruption of the *Jnk1* gene prevents diet-induced hepatic insulin resistance.

To confirm the effect of adipose JNK1 deficiency on insulin sensitivity, we tested insulin-stimulated Ser/Thr phosphorylation and activation of AKT. HFD-fed F^{WT} mice exhibited reduced insulin-stimulated AKT activation in adipose tissue (Fig. 3B), liver (Fig. 4B), and muscle (fig. S7). In contrast, F^{KO} mice exhibited HFD-induced inhibition of insulin-stimulated AKT activation in muscle but not in adipose tissue or liver (Figs. 3B and 4B). This effect of adipose-specific JNK1 deficiency on hepatic AKT activation (Fig. 4B) is consistent with the observation that HFD-fed F^{KO} mice showed improved hepatic insulin sensitivity compared with HFD-fed F^{WT} mice (Fig. 2I). Interestingly, HFD-fed F^{KO} mice also exhibited reduced hepatic steatosis compared with HFD-fed F^{WT} mice (Fig. 4A). These data confirm that JNK1 in adipose tissue is, at least in part, required for HFD-induced insulin resistance in both adipose tissue and liver.

The total fat mass, weight of the epididymal fat pads, and the size of adipocytes were not significantly different between HFD-fed F^{WT} and F^{KO} mice (fig. S4). The HFD increased *Tnfa* and *Il6* mRNA expression in adipose tissue of F^{WT} mice, but only increased *Tnfa* mRNA expression was detected in F^{KO} mice (Fig. 3A). Moreover, the HFD caused a similar increase in the serum concentration of tumor necrosis factor- α (TNF- α) in F^{WT} and F^{KO} mice, but increased serum interleukin-6 (IL-6) was only detected in F^{WT} mice (Fig. 3C). Thus, JNK1 deficiency in adipocytes prevented the HFD-induced increase in the expression of the

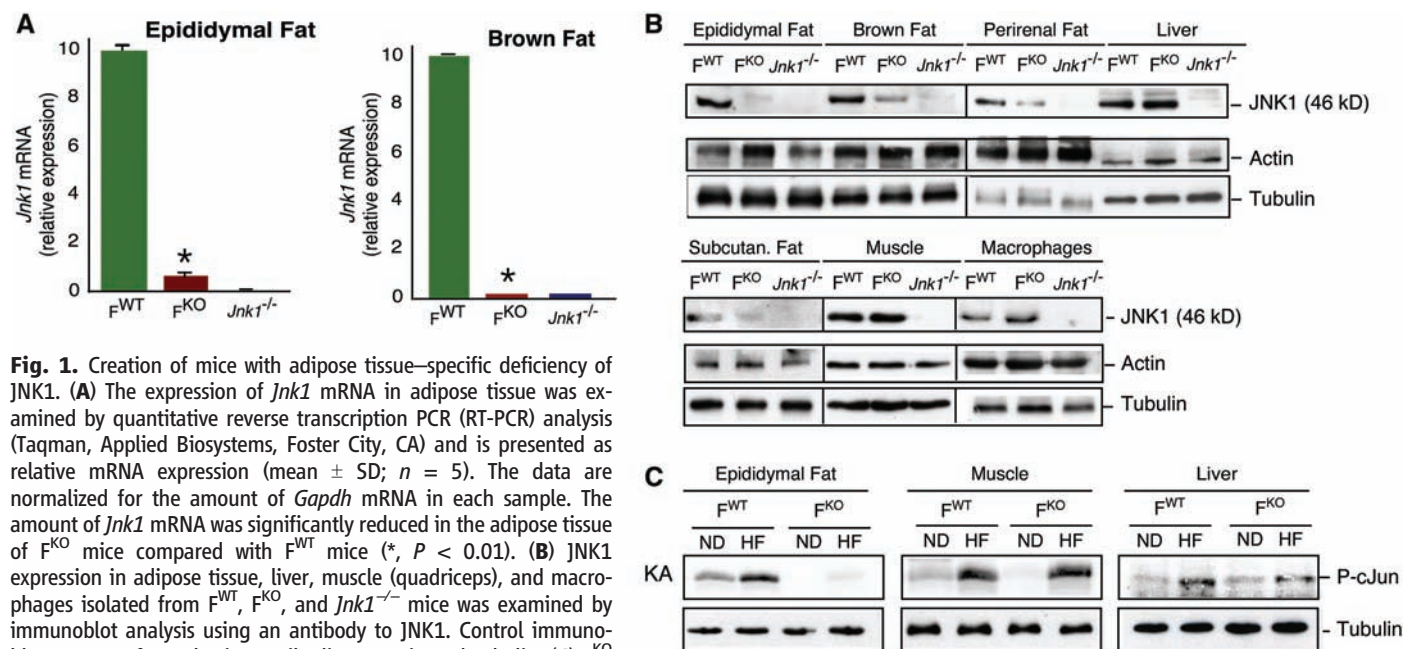


Fig. 1. Creation of mice with adipose tissue-specific deficiency of JNK1. (A) The expression of *Jnk1* mRNA in adipose tissue was examined by quantitative reverse transcription PCR (RT-PCR) analysis (Taqman, Applied Biosystems, Foster City, CA) and is presented as relative mRNA expression (mean \pm SD; $n = 5$). The data are normalized for the amount of *Gapdh* mRNA in each sample. The amount of *Jnk1* mRNA was significantly reduced in the adipose tissue of F^{KO} mice compared with F^{WT} mice (*, $P < 0.01$). (B) JNK1 expression in adipose tissue, liver, muscle (quadriceps), and macrophages isolated from F^{WT} , F^{KO} , and $Jnk1^{-/-}$ mice was examined by immunoblot analysis using an antibody to JNK1. Control immunoblots were performed using antibodies to Actin and Tubulin. (C) F^{KO} and F^{WT} mice were maintained on a standard chow diet (ND) or on a high-fat diet (HF) for 16 weeks. Protein extracts were prepared from epididymal fat, muscle (quadriceps), and liver. Equal amounts of cell extract prepared from F^{WT} and F^{KO} mice, confirmed by immunoblot analysis using an antibody to Tubulin, were used to measure JNK activity in a kinase assay (KA) using adenosine 5'-triphosphate (ATP)- γ - 32 P and cJun as substrates.

inflammatory cytokine IL-6. This effect on IL-6 expression was selective because no significant differences in circulating leptin or resistin concentrations were detected between F^{WT} and F^{KO} mice (Fig. 3C). Furthermore, no significant differences in the serum concentration of other interleukins and adipokines were detected between F^{WT} and F^{KO} mice (figs. S8 to S10). The inflammatory cytokines TNF- α and IL-6 can cause insulin resistance (8, 9), and JNK can regulate the expression of both cytokines (4). However, JNK1-deficiency in adipose tissue selectively prevented HFD-induced IL-6 expression (Fig. 3, A and C). This finding suggests

that adipocytes play a primary role in obesity-induced IL-6 expression (10). In contrast, macrophages may represent the major source of TNF- α expression (11). No differences in macrophage infiltration of the liver and adipose tissue were detected between HFD-fed F^{WT} and F^{KO} mice (figs. S6E, S9D, and S11). Moreover, no defects in IL-6 or TNF- α expression by macrophages isolated from F^{KO} mice were detected (fig. S12).

IL-6 can induce hepatic insulin resistance (12, 13), and loss of IL-6 selectively improves hepatic insulin action in obese mice (14). IL-6-induced hepatic insulin resistance is mediated, in

part, by increased expression of SOCS3 (15, 16), a protein that binds and inhibits the insulin receptor (17, 18) and also targets IRS proteins for proteosomal degradation (19). Expression of SOCS3 was increased and IRS1 was decreased in the liver of HFD-fed F^{WT} mice, but not HFD-fed F^{KO} mice (Fig. 4, C and D). Dysregulated expression of SOCS3 and IRS1 in the liver of HFD-fed F^{KO} mice is consistent with the observation that HFD-fed F^{KO} mice exhibit a low circulating concentration of IL-6 (Fig. 3C) and improved hepatic insulin sensitivity (Fig. 2I) compared with HFD-fed F^{WT} mice.

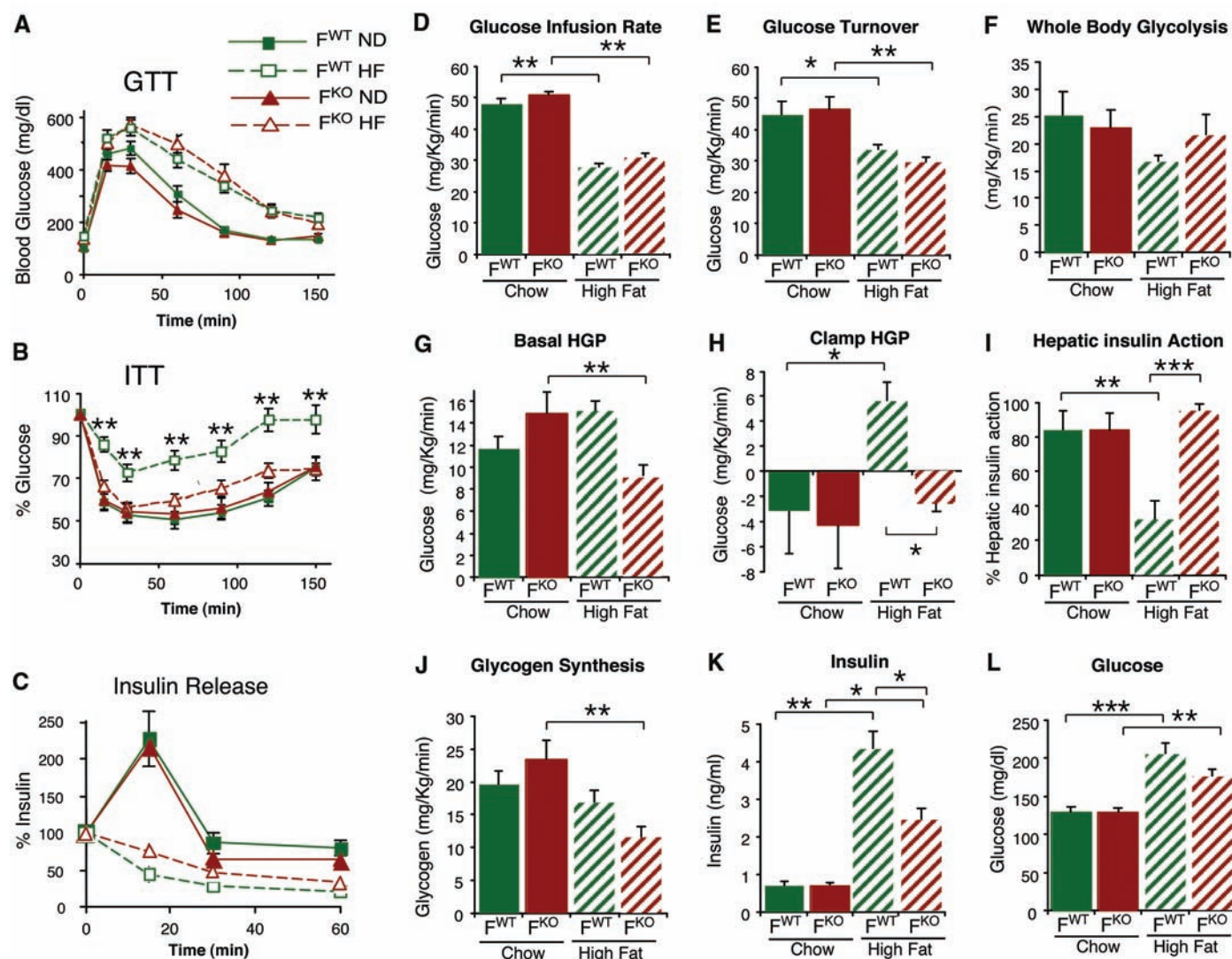


Fig. 2. JNK1-deficient adipose tissue prevents diet-induced insulin resistance. (A to C) F^{KO} and F^{WT} mice were maintained on a standard chow diet (ND) or on a high-fat diet (HF) for 16 weeks. (A) Glucose tolerance test (GTT). Mice fasted overnight were injected intraperitoneally with glucose (1 mg per gram of body mass). Blood glucose concentration was measured at the indicated times (mean \pm SD; $n = 14$). (B) Insulin tolerance test (ITT). Mice fasted overnight were injected intraperitoneally with insulin (0.75 mU/g). Blood glucose concentration was measured at the indicated times (mean \pm SD; $n = 14$). (C) Glucose-induced insulin release. Mice fasted overnight were injected intraperitoneally with glucose (2 mg/g). Blood insulin concentration was measured at the indicated times (mean \pm SD; $n = 14$). No statistically significant differences between F^{KO} and F^{WT} mice were detected ($P > 0.05$).

(D to J) F^{KO} and F^{WT} mice were maintained on an ND or HF diet for 3 weeks. (D) Steady-state glucose infusion rates to maintain euglycemia during the hyperinsulinemic-euglycemic clamps. (E) Insulin-stimulated whole-body glucose turnover. (F) Whole-body glycolysis. (G) Basal hepatic glucose production (HGP). (H) Insulin-stimulated rates of HGP during clamps. (I) Hepatic insulin action, expressed as insulin-mediated percent suppression of basal HGP. (J) Glycogen synthesis. The data presented are the mean \pm SE for six to eight experiments. Statistically significant differences are indicated (*, $P < 0.05$; **, $P < 0.01$; ***, $P < 0.001$). (K and L) Resting blood insulin and glucose were examined in mice that were fasted overnight (mean \pm SD, $n = 10$). Statistically significant differences between F^{KO} mice and F^{WT} mice are indicated (*, $P < 0.01$).

To determine whether the defect in adipose tissue expression of IL-6 contributes to the improved hepatic insulin sensitivity of HFD-fed F^{KO}

mice, we examined whether administration of IL-6 would restore HFD-induced insulin resistance phenotypes in F^{KO} mice. Acute IL-6 treatment

increased hepatic SOCS3 expression in HFD-fed F^{KO} mice to the same amount that was detected in HFD-fed F^{WT} mice (Fig. 4E). Insulin tolerance tests demonstrated that IL-6-treated HFD-fed F^{KO} mice became equally insulin resistant as HFD-fed F^{WT} mice (Fig. 4F). Moreover, IL-6 treatment reduced insulin-stimulated AKT activation in the liver of HFD-fed F^{KO} mice (Fig. 4G). In contrast, only a moderate effect of IL-6 on AKT in the adipose tissue of HFD-fed F^{KO} mice was detected (Fig. 4H). These data demonstrate that the effect of JNK1 deficiency in adipose tissue on hepatic insulin sensitivity is, at least in part, mediated by a requirement of JNK1 for HFD-induced expression of IL-6.

Adipose tissue plays a critical role in glucose homeostasis by releasing adipokines that regulate insulin sensitivity in other organs (8, 20). One of these, IL-6, is elevated in obese, diabetic subjects (9) and regulates glucose metabolism in multiple cell types (21–23). However, the role of IL-6 in whole-body insulin resistance has been debated because IL-6 alters insulin signaling differently in individual tissues (24, 25). Furthermore, IL-6 regulates the hypothalamic-pituitary-adrenal axis (26), and the IL-6/Stat3 pathway is required for the action of insulin signaling in the brain on hepatic gluconeogenesis (27). Thus, IL-6 has both central and peripheral roles on metabolism, and its effects on systemic insulin resistance are complex. Nevertheless, neutralization of IL-6 selectively im-

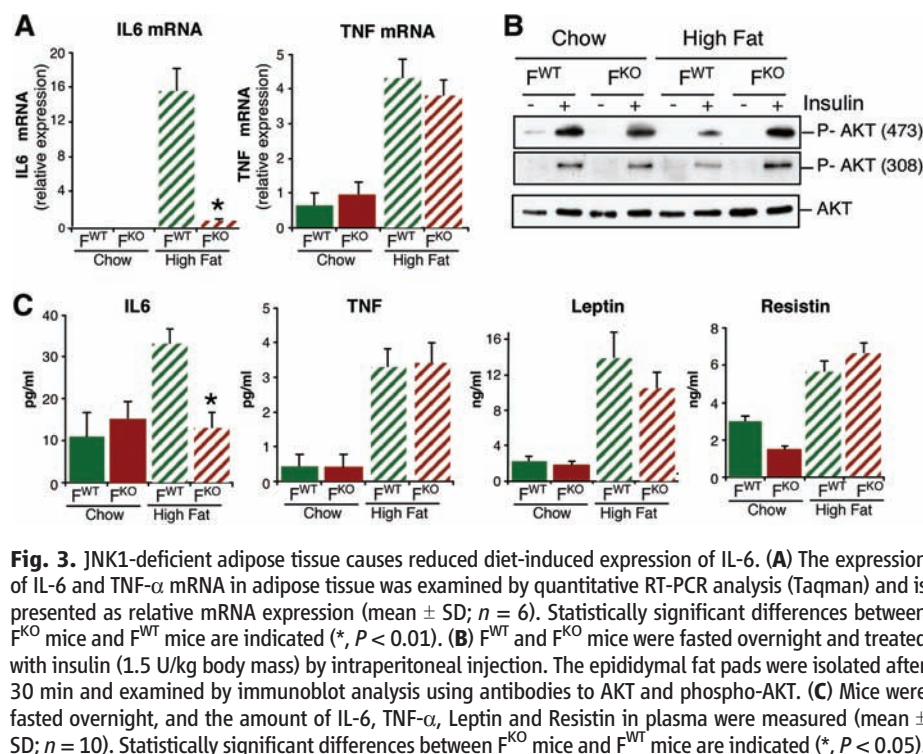


Fig. 3. JNK1-deficient adipose tissue causes reduced diet-induced expression of IL-6. **(A)** The expression of IL-6 and TNF- α mRNA in adipose tissue was examined by quantitative RT-PCR analysis (Taqman) and is presented as relative mRNA expression (mean \pm SD; $n = 6$). Statistically significant differences between F^{KO} mice and F^{WT} mice are indicated (*, $P < 0.01$). **(B)** F^{WT} and F^{KO} mice were fasted overnight and treated with insulin (1.5 U/kg body mass) by intraperitoneal injection. The epididymal fat pads were isolated after 30 min and examined by immunoblot analysis using antibodies to AKT and phospho-AKT. **(C)** Mice were fasted overnight, and the amount of IL-6, TNF- α , Leptin and Resistin in plasma were measured (mean \pm SD; $n = 10$). Statistically significant differences between F^{KO} mice and F^{WT} mice are indicated (*, $P < 0.05$).

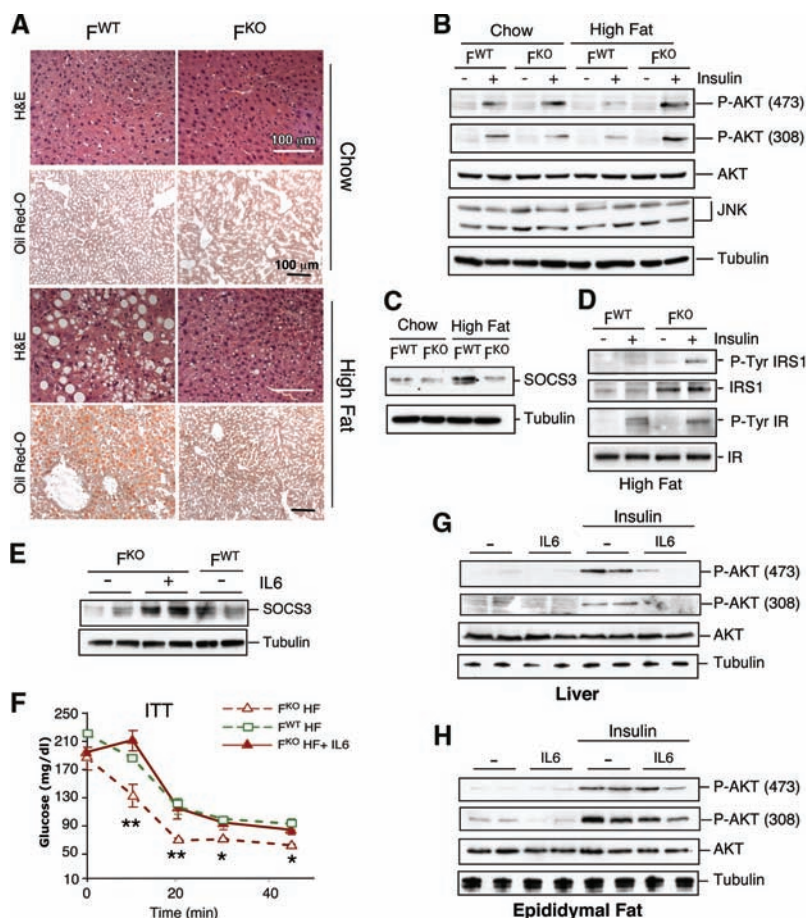


Fig. 4. JNK1 deficiency in adipose tissue causes increased hepatic insulin sensitivity. **(A)** F^{WT} and F^{KO} mice were fed a standard chow diet or a high fat diet for 16 wk. Representative histological sections of liver stained with hematoxylin and eosin or Oil Red O are presented. **(B)** Mice were fasted overnight and treated with insulin (1.5 U/kg) by intraperitoneal injection. Livers were isolated after 30 min and examined by immunoblot analysis to detect AKT, phospho-AKT, JNK1/2, and Tubulin. **(C)** The expression of SOCS3 in the liver was examined by immunoblot analysis. Control immunoblots were performed using an antibody to Tubulin. **(D)** The tyrosine phosphorylation and expression of the insulin receptor (IR) and IRS1 in the liver were examined by immunoblot analysis. **(E)** F^{WT} and F^{KO} mice were fed a HFD (16 weeks). F^{KO} mice were treated with IL-6 (1 μ g/kg) by subcutaneous injection. At 90 min after injection, the blood concentration was 44 ± 9.1 pg/ml (mean \pm SD; $n = 8$). The liver was isolated (90 min after injection), and the expression of SOCS3 and Tubulin were examined by immunoblot analysis. **(F)** Insulin tolerance test. Mice were treated by subcutaneous injection with IL-6 (1 μ g/kg) and then treated (after 90 min) with insulin (0.75 mU/g) by intraperitoneal injection. Blood glucose concentration was measured at the indicated times. Statistically significant differences between F^{KO} and F^{WT} mice are indicated (*, $P < 0.05$; **, $P < 0.01$). **(G and H)** HFD-fed F^{KO} mice were treated by subcutaneous injection with IL-6 (1 μ g/kg) and then treated (after 90 min) with insulin (0.3 mU/g) by intravenous injection. The liver (G) and epididymal fat pads (H) were isolated after 5 min and examined by immunoblot analysis to detect AKT, phospho-AKT, and Tubulin.

proves obesity-induced hepatic insulin resistance, and treatment with IL-6 can increase hepatic insulin resistance (12–15). Moreover, ablation of the IL-6 target gene *Socs3* in the liver of young mice causes improved hepatic insulin sensitivity (16). Together, these data and our study demonstrate that adipose tissue-derived IL-6 is an important mediator of hepatic insulin resistance and that JNK1 is a component of a metabolic stress signaling pathway that regulates IL-6 expression in adipose tissue. The serum concentration of IL-6 represents a possible biomarker for the evaluation of the efficacy of drugs that target JNK1 and may be useful for the treatment of metabolic diseases.

References and Notes

1. J. Hirosumi *et al.*, *Nature* **420**, 333 (2002).
2. A. Jaeschke, R. J. Davis, *Mol. Cell* **27**, 498 (2007).
3. V. Aguirre, T. Uchida, L. Yenush, R. J. Davis, M. F. White, *J. Biol. Chem.* **275**, 9047 (2000).
4. C. R. Weston, R. J. Davis, *Curr. Opin. Cell Biol.* **19**, 142 (2007).
5. G. Solinas *et al.*, *Cell Metab.* **6**, 386 (2007).
6. D. G. Carey, A. B. Jenkins, L. V. Campbell, J. Freund, D. J. Chisholm, *Diabetes* **45**, 633 (1996).
7. H. Waki, P. Tontonoz, *Annu. Rev. Pathol.* **2**, 31 (2007).
8. B. M. Spiegelman, J. S. Flier, *Cell* **87**, 377 (1996).
9. J. P. Bastard *et al.*, *Eur. Cytokine Netw.* **17**, 4 (2006).
10. V. Mohamed-Ali *et al.*, *J. Clin. Endocrinol. Metab.* **82**, 4196 (1997).
11. S. P. Weisberg *et al.*, *J. Clin. Invest.* **112**, 1796 (2003).
12. P. J. Klover, T. A. Zimmers, L. G. Koniaris, R. A. Mooney, *Diabetes* **52**, 2784 (2003).
13. H. J. Kim *et al.*, *Diabetes* **53**, 1060 (2004).
14. P. J. Klover, A. H. Clementi, R. A. Mooney, *Endocrinology* **146**, 3417 (2005).
15. J. J. Senn *et al.*, *J. Biol. Chem.* **278**, 13740 (2003).
16. T. Torisu *et al.*, *Genes Cells* **12**, 143 (2007).
17. B. Emanuelli *et al.*, *J. Biol. Chem.* **276**, 47944 (2001).
18. B. Emanuelli *et al.*, *J. Biol. Chem.* **275**, 15985 (2000).
19. L. Rui, M. Yuan, D. Frantz, S. Shoelson, M. F. White, *J. Biol. Chem.* **277**, 42394 (2002).
20. F. Mauvais-Jarvis, R. N. Kulkarni, C. R. Kahn, *Clin. Endocrinol. (Oxf.)* **57**, 1 (2002).
21. T. Kishimoto, *Blood* **74**, 1 (1989).
22. J. J. Senn, P. J. Klover, I. A. Nowak, R. A. Mooney, *Diabetes* **51**, 3391 (2002).
23. B. K. Pedersen, A. Steensberg, P. Schjerling, *Curr. Opin. Hematol.* **8**, 137 (2001).
24. R. A. Mooney, *J. Appl. Physiol.* **102**, 816 (2007).
25. B. K. Pedersen, M. A. Febbraio, *J. Appl. Physiol.* **102**, 814 (2007).
26. V. Wallenius *et al.*, *Nat. Med.* **8**, 75 (2002).
27. H. Inoue *et al.*, *Cell Metab.* **3**, 267 (2006).
28. We thank V. Benoit, J. Cavanagh-Kyros, K. Gemme, N. Kennedy, J. Liu, and J. Reilly for expert assistance. These studies were supported by grants from NIH (to R.J.D.), the American Diabetes Association (1-04-RA-47 to J.K.K.), and the Pennsylvania State Department of Health (to J.K.K.). Core facilities at the University of Massachusetts used by these studies were supported by the National Institute of Diabetes and Digestive and Kidney Diseases, Diabetes and Endocrinology Research Center (DK52530). R.J.D. is an Investigator of the Howard Hughes Medical Institute.

Supporting Online Material

www.sciencemag.org/cgi/content/full/322/5907/1539/DC1
Materials and Methods
Figs. S1 to S12
References

21 May 2008; accepted 9 October 2008
10.1126/science.1160794

Inhibition of Rac by the GAP Activity of Centralspindlin Is Essential for Cytokinesis

Julie C. Canman,^{1,2*} Lindsay Lewellyn,² Kimberley Laband,² Stephen J. Smerdon,³ Arshad Desai,² Bruce Bowerman,^{1†} Karen Oegema^{2**†}

During cytokinesis, the guanosine triphosphatase (GTPase) RhoA orchestrates contractile ring assembly and constriction. RhoA signaling is controlled by the central spindle, a set of microtubule bundles that forms between the separating chromosomes. Centralspindlin, a protein complex consisting of the kinesin-6 ZEN-4 and the Rho family GTPase activating protein (GAP) CYK-4, is required for central spindle assembly and cytokinesis in *Caenorhabditis elegans*. However, the importance of the CYK-4 GAP activity and whether it regulates RhoA remain unclear. We found that two separation-of-function mutations in the GAP domain of CYK-4 lead to cytokinesis defects that mimic centralspindlin loss of function. These defects could be rescued by depletion of the GTPase Rac or its effectors, but not by depletion of RhoA. Thus, inactivation of Rac by centralspindlin functions in parallel with RhoA activation to drive contractile ring constriction during cytokinesis.

Cytokinesis completes mitosis, partitioning a single cell into two. To coordinate cell division with chromosome segregation, the mitotic apparatus directs the assembly and constriction of a contractile ring composed of filamentous actin and myosin II that physically divides the cell (1). Understanding how the mitotic apparatus communicates with the cell cortex during cytokinesis is a major challenge. One critical mediator of this signaling is the small guanosine triphosphatase (GTPase) RhoA (1, 2).

RhoA signaling is thought to be controlled by an array of antiparallel microtubule bundles, called the central spindle, that forms between the separating chromosomes during anaphase (1). Consistent with a central role in cytokinesis, RhoA and its activating guanine nucleotide exchange factor (GEF) ECT-2 are essential for contractile ring assembly and constriction (3–5).

Centralspindlin, a conserved heterotetrameric complex consisting of two molecules of kinesin-6 (ZEN-4 in *C. elegans*) and two molecules of a protein containing a GTPase activating protein (GAP) domain (CYK-4 in *C. elegans*), is critical for central spindle assembly and cytokinesis (1, 6). The current dominant model proposes that centralspindlin targets the ECT-2 GEF to the central spindle, thereby contributing to the equatorial activation of RhoA (3, 4, 7). Formation of the heterotetrameric centralspindlin complex

requires an interaction between the N-terminal region of CYK-4 and the central region of ZEN-4 (Fig. 1A) (6, 8). Mutant forms of CYK-4 and ZEN-4 that disrupt centralspindlin assembly lead to a phenotype similar to that resulting from depletion of centralspindlin subunits by RNA interference (RNAi) (Fig. 1, C and D): failure to form a central spindle, accompanied by a defect in contractile ring constriction (9–12).

The conserved GAP domain in the CYK-4 C terminus is predicted to inactivate Rho family GTPases (Fig. 1A) (11). However, the role of the CYK-4 GAP domain in cytokinesis and the identity of the Rho family GTPase that it targets are unknown (11, 13–15). In vitro, the GAP domains of CYK-4 and its homologs are active toward all three subclasses of Rho family GTPases: RhoA, Rac, and CDC-42 (11, 16, 17). It has been assumed that the CYK-4 GAP activity acts on RhoA because it is the only Rho family member essential for cytokinesis (11). CYK-4 has been proposed to promote RhoA cycling (18) or to inactivate RhoA after cytokinesis during contractile ring disassembly (1). It is also possible that RhoA is not the critical target of the CYK-4 GAP domain. In support of this hypothesis, haploinsufficiency of Rac can suppress the rough-eye phenotype induced by RNAi of the *Drosophila* CYK-4 homolog (14). Although cytokinesis was not examined, this result indicates that in some contexts CYK-4 may oppose Rac activation.

To study the role of the CYK-4 GAP domain in cytokinesis (19), we characterized two conditional *C. elegans* alleles (20) that lead to residue substitutions within the GAP domain—a Glu → Lys change at residue 448 (CYK-4^{GAP(E448K)}) and a Thr → Ile change at residue 546 (CYK-4^{GAP(T546I)}), respectively (Fig. 1, A and B). On the basis of the x-ray structure of the human CYK-4 homolog (PDB ID: 2OVJ), the charge reversal resulting from the Glu → Lys substitution would disrupt a network of salt-bridge and

¹Institute for Molecular Biology, University of Oregon, Eugene, OR 97403, USA. ²Ludwig Institute for Cancer Research, University of California, San Diego, La Jolla, CA 92093, USA. ³National Institute for Medical Research, The Ridgeway, Mill Hill, London NW7 1AA, UK.

*To whom correspondence should be addressed. E-mail: jcanman@ucsd.edu (J.C.C.); koegema@ucsd.edu (K.O.)

†These authors contributed equally to this work.

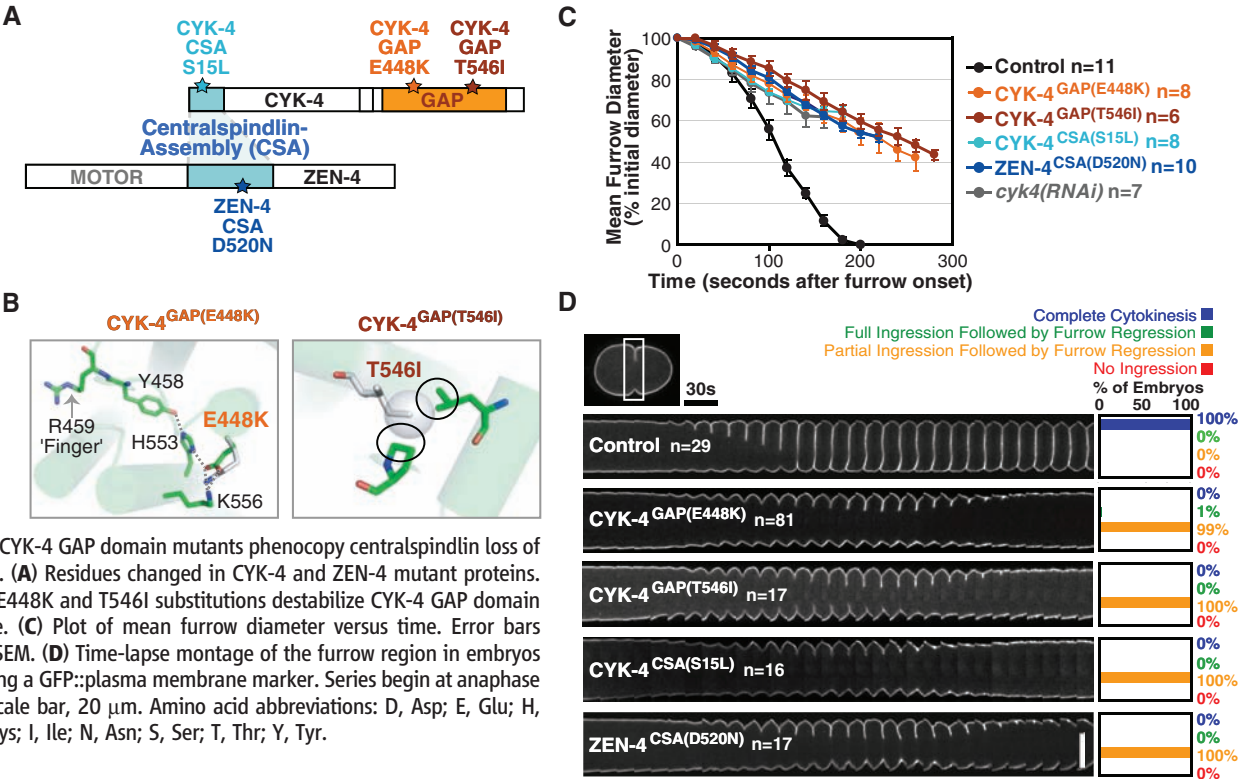


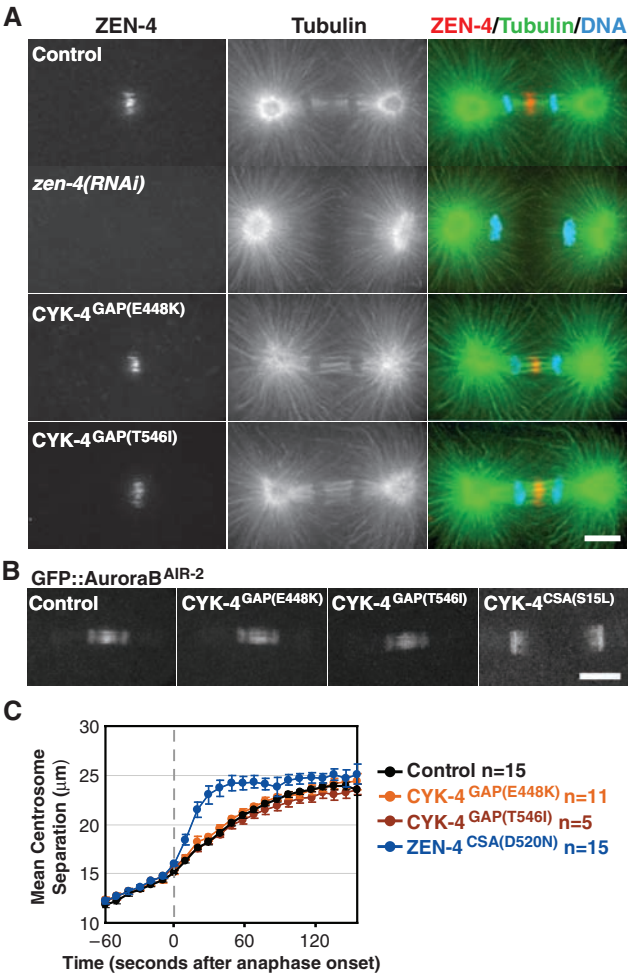
Fig. 1. CYK-4 GAP domain mutants phenocopy centralspindlin loss of function. **(A)** Residues changed in CYK-4 and ZEN-4 mutant proteins. **(B)** The E448K and T546I substitutions destabilize CYK-4 GAP domain structure. **(C)** Plot of mean furrow diameter versus time. Error bars denote SEM. **(D)** Time-lapse montage of the furrow region in embryos expressing a GFP::plasma membrane marker. Series begin at anaphase onset. Scale bar, 20 μ m. Amino acid abbreviations: D, Asp; E, Glu; H, His; K, Lys; I, Ile; N, Asn; S, Ser; T, Thr; Y, Tyr.

hydrogen-bond interactions that positions the arginine finger (Arg⁴⁵⁹), a conserved residue essential for GAP activity (Fig. 1B) (17, 21, 22). Although the effects of the Thr \rightarrow Ile substitution are less clear, the larger isoleucine side chain may clash with surrounding residues and also interfere with arginine finger positioning. Both alleles are strictly recessive (fig. S1), temperature-sensitive, and fast-inactivating, showing a fully penetrant cytokinesis defect within 1 min of shifting to the restrictive temperature. Thus, these are loss-of-function alleles affecting the CYK-4 GAP domain.

We used quantitative live-imaging assays to characterize cytokinesis in the CYK-4 GAP mutant embryos. Although no obvious defects were evident during the initial stages of contractile ring assembly (fig. S2, B and C), the GAP mutants exhibited a severe defect in contractile ring constriction. The constriction rate was slower than in control embryos by a factor of ~ 3 , and cleavage furrows only ingressed to $\sim 50\%$ of the initial cell diameter before regressing. This ingression defect mimicked that in the centralspindlin-assembly mutants and in embryos depleted of CYK-4 by RNAi (12) (Fig. 1, C and D, fig. S3, and movie S1). Thus, the CYK-4 GAP domain is fundamental to the role of centralspindlin in promoting contractile ring constriction.

Because centralspindlin is also required for assembly of the central spindle (9–11), we next examined central spindle structure in the GAP mutant embryos. In contrast to the absence of a central spindle after depletion of the kinesin-6 ZEN-4, there were no clear defects in central

Fig. 2. Central spindle assembly is not disrupted in the GAP mutants. **(A)** Immunofluorescence staining for ZEN-4, tubulin, and DNA. **(B)** Images of GFP::AuroraB^{AIR-2} 40 s after anaphase onset. **(C)** Plot of mean centrosome separation versus time. Error bars denote SEM. Scale bars, 10 μ m.



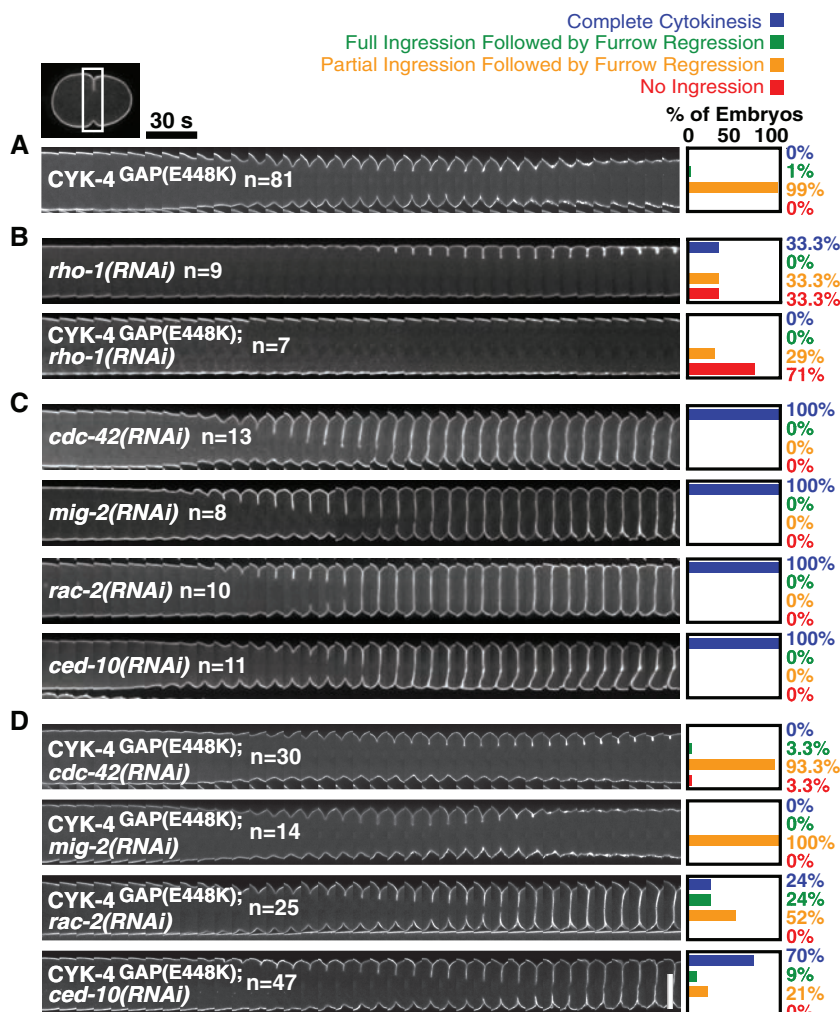


Fig. 3. Rac depletion suppresses the cytokinesis defect in CYK-4^{GAP(E448K)} embryos, as shown by time-lapse montages of the furrow region in embryos expressing a GFP::plasma membrane marker. Series begin at anaphase onset. (A) CYK-4^{GAP(E448K)} embryos exhibit partial furrow ingression followed by regression. (B) Partial depletion of RhoA^{RHO-1} enhances the CYK-4^{GAP(E448K)} cytokinesis defect. (C) RNAi of other Rho family members does not disrupt cytokinesis. (D) RNAi of Rac^{CED-10} or Rac^{RAC-2} rescues cytokinesis success in CYK-4^{GAP(E448K)} embryos. Scale bar, 20 μ m.

spindle organization or ZEN-4 targeting in the GAP mutants (Fig. 2A). The recruitment of a green fluorescent protein (GFP) fusion with AuroraB^{AIR-2} kinase (the enzymatic component of the chromosomal passenger complex) to the central spindle was also not affected in the GAP mutants (Fig. 2B and movie S2). Disrupting central spindle structure in *C. elegans* embryos leads to abrupt centrosome separation after anaphase onset (23). This phenotype was not observed in the CYK-4 GAP mutants, thereby confirming a mechanically intact central spindle (Fig. 2C). Thus, CYK-4^{GAP(E448K)} and CYK-4^{GAP(T546I)} are separation-of-function mutants that uncouple the role of CYK-4 in contractile ring constriction from its role in central spindle assembly.

CYK-4 GAP activity is expected to down-regulate a Rho family GTPase; therefore, RNAi-mediated depletion of the target GTPase should rescue the cytokinesis defect in CYK-4 GAP

mutant embryos. There are five Rho family members in *C. elegans*: RhoA^{RHO-1}, Rac^{CED-10}, Rac^{RAC-2}, RhoG^{MIG-2}, and CDC-42 (24). Because RhoA^{RHO-1} depletion results in a cytokinesis defect on its own (11, 16, 17), we tested whether partial depletion of RhoA^{RHO-1} or its activating ECT-2 GEF could suppress the GAP mutant phenotype. Instead of suppressing, partial depletion of either RhoA^{RHO-1} or ECT-2 enhanced the CYK-4^{GAP(E448K)} cytokinesis defect, which suggests that RhoA^{RHO-1} is not the main target of CYK-4 GAP activity (Fig. 3, A and B, and fig. S4A).

Unlike depletion of RhoA^{RHO-1}, RNAi of the other Rho family members does not affect cytokinesis in control embryos (Fig. 3C). RNAi of CDC-42 or RhoG^{MIG-2} also did not ameliorate the CYK-4^{GAP(E448K)} cytokinesis phenotype (Fig. 3D). However, RNAi of Rac^{CED-10} or Rac^{RAC-2} led to substantial rescue, allowing 70% and 24%,

respectively, of CYK-4^{GAP(E448K)} embryos to successfully complete the first cytokinesis (Fig. 3, A and D). Simultaneous RNAi of Rac^{CED-10} and Rac^{RAC-2} did not increase the efficiency of rescue over RNAi of Rac^{CED-10} alone (fig. S4D). These results indicate that CYK-4 GAP activity promotes furrow ingression by down-regulating Rac. Consistent with a role for CYK-4 in Rac inactivation, the overexpression of a GAP-dead CYK-4 mutant in dividing mammalian cells was previously found to increase the level of active Rac at the cell equator (25).

If CYK-4 GAP activity is critical for the role of centralspindlin in contractile ring constriction, Rac^{CED-10} depletion should also rescue the furrow ingression defect resulting from inhibiting centralspindlin assembly. Indeed, 85% of furrows in ZEN-4^{CSA(D520N)} embryos ingressed fully when Rac^{CED-10} was depleted (fig. S4B). However, Rac^{CED-10} depletion was less efficient in rescuing cytokinesis completion in the ZEN-4^{CSA(D520N)} mutant relative to the CYK-4 GAP mutant (fig. S4B). This result suggests an additional role for either centralspindlin or the central spindle in the completion of cytokinesis that is independent of CYK-4 GAP activity. Rac^{CED-10} depletion had no effect on furrow ingression in AuroraB^{AIR-2(P265L)} embryos, which have a spectrum of defects in central spindle assembly and furrow ingression similar to that resulting from centralspindlin disruption (12) (fig. S4C); this result confirmed the specificity of the rescue.

Why is inhibition of Rac signaling important for contractile ring constriction? Rac promotes activation of the Arp2/3 complex via its effectors WASP^{WSP-1} and WAVE^{WVE-1}, resulting in the formation of a branched meshwork of short cross-linked actin filaments (26). Possibly, these Rac effectors interfere with actin filaments nucleated by the cytokinesis formin, CYK-1, which functions with myosin II to drive cytokinesis. To test this idea, we determined whether depletion of WASP^{WSP-1}/WAVE^{WVE-1} or the Arp2/3 complex could also rescue the CYK-4^{GAP(E448K)} cytokinesis defect (27, 28) (Fig. 4, A and B). Although their individual depletions did not markedly suppress the CYK-4^{GAP(E448K)} cytokinesis defect, co-depletion of WASP^{WSP-1} and WAVE^{WVE-1} led to substantial rescue: 69% of furrows ingressed fully and 38% of embryos successfully completed cytokinesis (Fig. 4A). RNAi of Arp2^{ARX-2} also suppressed the CYK-4^{GAP(E448K)} cytokinesis defect, with 74% of furrows ingressing fully and 52% of embryos completing division (Fig. 4B). Thus, cytokinesis depends on CYK-4 GAP to inactivate Rac, thereby reducing activation of the Arp2/3 complex via WASP and WAVE. Active Arp2/3 complex in the furrow region may disrupt contractile ring constriction by branching formin-nucleated actin filaments. Alternatively, active Arp2/3 complex could nucleate the formation of an independent branched actin network that competes for essential contractile ring components or presents a structural barrier to furrow ingression.

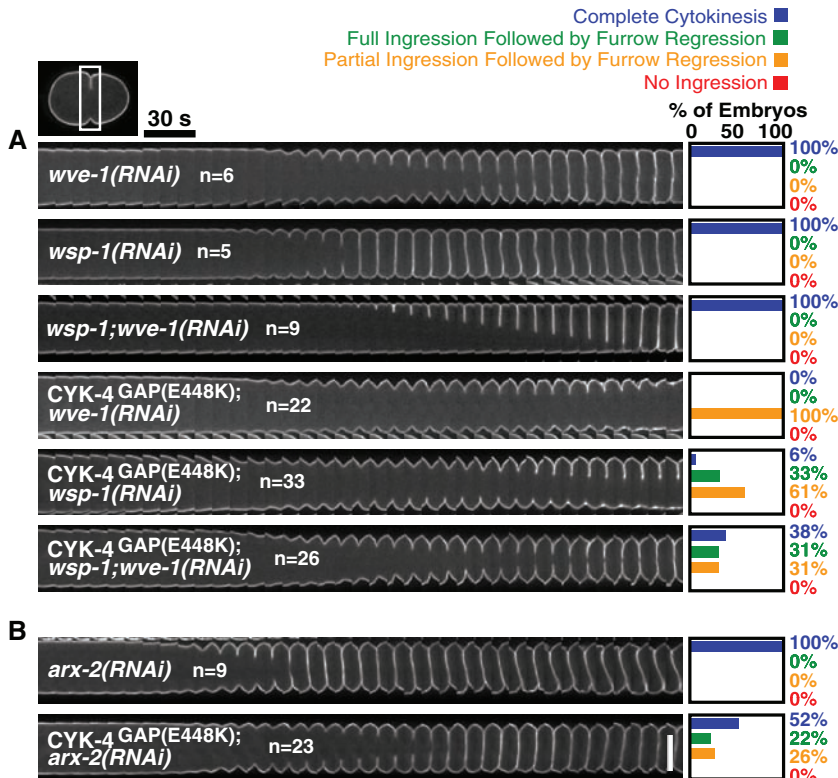


Fig. 4. CYK-4 GAP inactivates Rac and its effectors, WASp/WAVE and the Arp2/3 complex, to promote cytokinesis. Cytokinesis in CYK-4^{GAP(E448K)} embryos is rescued by (A) co-depletion of WASp^{WSP-1} and WAVE^{WVE-1} or (B) depletion of Arp2^{ARX-2}. Scale bar, 20 μ m.

We have uncovered a negative regulation cascade that is essential for successful cytokinesis. Although negative regulation has been proposed to be important during cytokinesis, previous models have emphasized inhibition of cortical contractility by astral microtubules that contact the polar regions of the cell (29, 30). A requirement for negative regulation of an inhibitory pathway at the cell equator has not been widely considered. Our findings lead to a model in which inactivation of Rac by CYK-4 GAP functions in parallel with activation of RhoA to drive contractile ring constriction during cytokinesis (fig. S7).

References and Notes

1. M. Glotzer, *Science* **307**, 1735 (2005).
2. W. M. Bement, H. A. Benink, G. von Dassow, *J. Cell Biol.* **170**, 91 (2005).
3. Y. Nishimura, S. Yonemura, *J. Cell Sci.* **119**, 104 (2006).
4. O. Yuce, A. Piekny, M. Glotzer, *J. Cell Biol.* **170**, 571 (2005).
5. K. Kamijo et al., *Mol. Biol. Cell* **17**, 43 (2006).
6. M. Mishima, S. Kaitna, M. Glotzer, *Dev. Cell* **2**, 41 (2002).
7. W. G. Somers, R. Saint, *Dev. Cell* **4**, 29 (2003).
8. V. Pavicic-Kaltenbrunner, M. Mishima, M. Glotzer, *Mol. Biol. Cell* **18**, 4992 (2007).
9. W. B. Raich, A. N. Moran, J. R. Rothman, J. Hardin, *Mol. Biol. Cell* **9**, 2037 (1998).
10. J. Powers, O. Bossinger, D. Rose, S. Strome, W. Saxton, *Curr. Biol.* **8**, 1133 (1998).
11. V. Jantsch-Plunger et al., *J. Cell Biol.* **149**, 1391 (2000).
12. A. F. Severson, D. R. Hamill, J. C. Carter, J. Schumacher, B. Bowerman, *Curr. Biol.* **10**, 1162 (2000).
13. Y. Minoshima et al., *Dev. Cell* **4**, 549 (2003).
14. P. D'Avino, M. S. Savoian, D. M. Glover, *J. Cell Biol.* **166**, 61 (2004).

15. T. Yamada, M. Hikida, T. Kurosaki, *Exp. Cell Res.* **312**, 3517 (2006).
16. A. Toure et al., *J. Biol. Chem.* **273**, 6019 (1998).

17. T. Kawashima et al., *Blood* **96**, 2116 (2000).
18. W. M. Bement, A. L. Miller, G. von Dassow, *Bioessays* **28**, 983 (2006).
19. See supporting material on Science Online.
20. S. E. Encalada et al., *Dev. Biol.* **228**, 225 (2000).
21. S. Ahmed et al., *J. Biol. Chem.* **269**, 17642 (1994).
22. K. Rittinger, P. A. Walker, J. F. Eccleston, S. J. Smerdon, S. J. Gamblin, *Nature* **389**, 758 (1997).
23. K. Oegema, A. Desai, S. Rybina, M. Kirkham, A. A. Hyman, *J. Cell Biol.* **153**, 1209 (2001).
24. E. A. Lundquist, in *WormBook* (www.wormbook.org/chapters/www_smallGTPases/smallGTPases.pdf).
25. H. Yoshizaki et al., *J. Biol. Chem.* **279**, 44756 (2004).
26. T. D. Pollard, *Annu. Rev. Biophys. Biomol. Struct.* **36**, 451 (2007).
27. A. F. Severson, D. L. Baillie, B. Bowerman, *Curr. Biol.* **12**, 2066 (2002).
28. J. Withee, B. Galligan, N. Hawkins, G. Garriga, *Genetics* **167**, 1165 (2004).
29. R. Rappaport, *Cytokinesis in Animal Cells* (Cambridge Univ. Press, Cambridge, 1997).
30. R. Dechant, M. Glotzer, *Dev. Cell* **4**, 333 (2003).
31. We thank all members of the Oegema, Desai, and Bowerman labs; A. Maddox, J. Dumont, and R. Green for reading this manuscript; J. Dumont for making double-stranded RNAs; Y. Kohara for cDNA clones; and the *Caenorhabditis* Genetics Center for strains. Supported by the Jane Coffin Childs Memorial Fund for Medical Research and the Leukemia and Lymphoma Society (J.C.C.), National Institute of General Medical Sciences grant T32 GM008666 and National Cancer Institute grant T32 CA067754 (L.L.), the Ludwig Institute for Cancer Research (K.O. and A.D.), and NIH grant GM058017 (B.B.).

Supporting Online Material

www.sciencemag.org/cgi/content/full/322/5907/1543/DC1

Materials and Methods

Figs. S1 to S7

Movies S1 and S2

References

10 July 2008; accepted 24 October 2008
10.1126/science.1163086

Dynamic Analyses of *Drosophila* Gastrulation Provide Insights into Collective Cell Migration

Amy McMahon,^{1*} Willy Supatto,^{2*} Scott E. Fraser,² Angelike Stathopoulos^{1†}

The concerted movement of cells from different germ layers contributes to morphogenesis during early embryonic development. Using an optimized imaging approach and quantitative methods, we analyzed the trajectories of hundreds of ectodermal cells and internalized mesodermal cells within *Drosophila* embryos over 2 hours during gastrulation. We found a high level of cellular organization, with mesoderm cell movements correlating with some but not all ectoderm movements. During migration, the mesoderm population underwent two ordered waves of cell division and synchronous cell intercalation, and cells at the leading edge stably maintained position. Fibroblast growth factor (FGF) signaling guides mesodermal cell migration; however, we found some directed dorsal migration in an FGF receptor mutant, which suggests that additional signals are involved. Thus, decomposing complex cellular movements can provide detailed insights into collective cell migration.

An embryo is shaped by a complex combination of collective cell movements that result in cell diversification and tissue formation (1–4). The majority of these morphogenetic events are dynamic and involve the simultaneous execution of different movements, with large pop-

ulations of cells moving in three-dimensional (3D) space deep inside the embryo (4, 5). Gastrulation is the earliest morphogenetic event involving massive cellular movements of the germ layers (6). Because it is technically challenging to image individual cell movements inside an embryo without

compromising its viability, studies of mesoderm cell migration during gastrulation in *Drosophila* have relied on the extrapolation of dynamical events from observations of fixed embryos (Fig. 1, A and B) or from in vivo descriptions of small numbers of cells (7–9).

We used optimized two-photon excited fluorescence (2PEF) (10, 11) to image large domains of *Drosophila* embryos ubiquitously expressing nuclear green fluorescent protein (GFP) (Fig. 1, C and D) (12) with sufficient spatial and temporal resolution to examine mesoderm spreading non-invasively over 2 hours (Fig. 1E and movie S1) (13). We extracted the complex cell movements of the mesoderm and ectoderm cells from each large imaging data set (~3 billion voxels) by using 3D segmentation of cell positions and 3D tracking over time (Fig. 1, F to H, and movie S2). This involved the analysis of over 100,000 cell positions per embryo (movie S3) (13). We used computational analysis to capture the three main morphogenetic events of the mesoderm (Fig. 1F) and confirmed

that the ectoderm cell layer, upon which mesoderm cells are migrating, undergoes germ-band elongation by means of convergent extension movements (Fig. 1, I and J) (14, 15).

We developed custom software tools to extract quantitative information from the cell trajectories and to describe the dynamic behavior in detail (movie S3) (13). First, we redefined the positions of cells in accordance with a cylindrical coordinate system [radial (r), angular (θ), and longitudinal (L)] by fitting a cylinder on the average position of ectoderm cells. This coordinate system, unlike the standard Cartesian system (x , y , and z), is more appropriate for the body plan of *Drosophila* embryos and the geometry of their morphogenetic events (Fig. 2, A to E, fig. S1, and movie S4) (14, 15).

We determined the influence of ectoderm cell movements on the migratory path of the overlying mesoderm by investigating the coupling between the motions of these two cell populations. The ectoderm is in close physical contact with the mesoderm: The mesoderm invaginates from the ectoderm, and the ectoderm serves as the substratum on which the mesoderm cells spread during germ-band elongation (15, 16). Previous qualitative studies suggested a coupling of their movements; in mutants that fail to form ectoderm, mesoderm cells are specified but fail to move

(14). Statistical analysis of our data revealed that the trajectories of mesoderm and ectoderm cells correlate highly in the anterior-posterior (AP) direction (the L axis) (Fig. 2H). However, in the other directions (the r and θ axes), little to no correlation was found (Fig. 2, F and G). Subtracting axial motions of the local ectoderm cells from the motion of each mesoderm cell resulted in no residual movement of the mesoderm in the L direction (Fig. 2I and movies S5 and S6), which suggests that the mesoderm cells are carried by the strong movement of the ectoderm during germ-band elongation in this direction. The lack of correlation in the radial and angular directions suggests that mesoderm cells undergo active movement, distinct from that of the ectoderm.

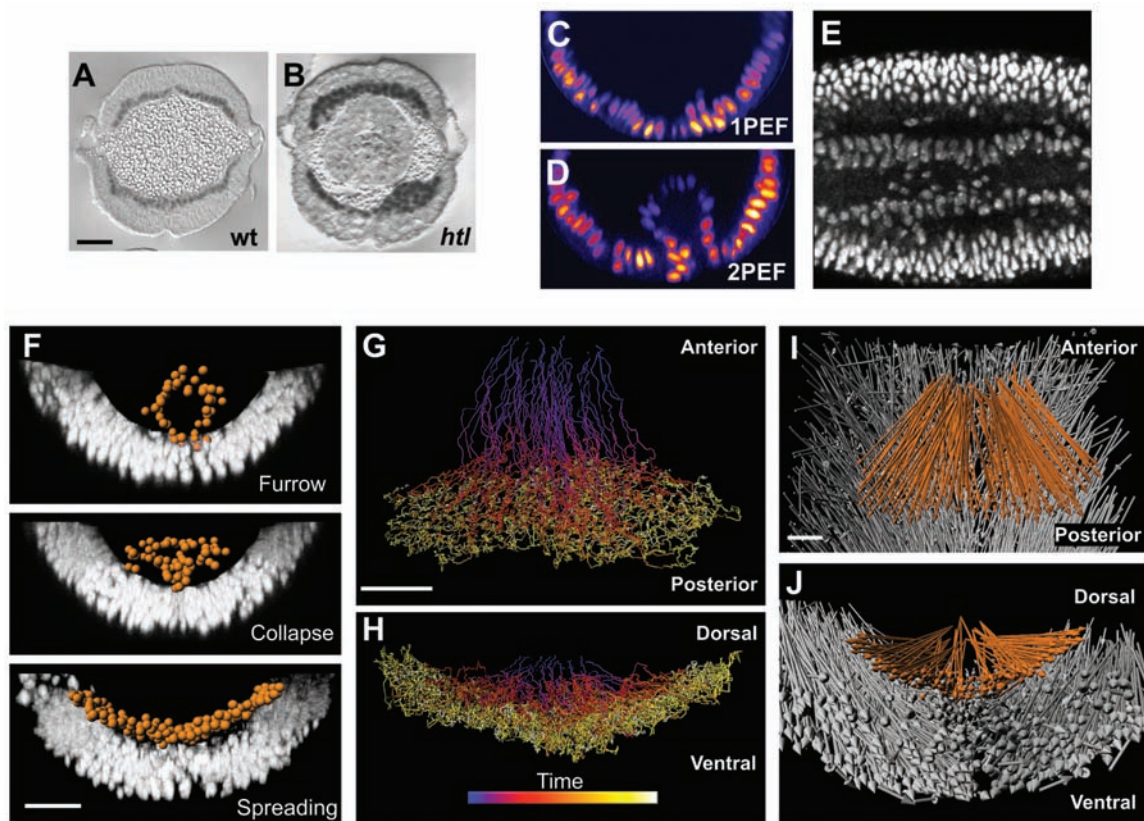
In the angular direction (θ), mesoderm cell movement was symmetrical with respect to the ventral midline of the embryo, as demonstrated by a θ mean value of 0 (Fig. 2D). Using a color code to identify each cell track by its position of origin in the furrow (Fig. 3A), we revealed a stable chromatic pattern of the trajectories in the θ direction, highlighting the fact that the spatial organization of cells in this direction is preserved over time. The straightness of the trajectories and the limited intermixing of cells support the view that cell movements are directed. The cell trajectories revealed that a group of cells originating

¹Division of Biology, California Institute of Technology, 1200 East California Boulevard, Pasadena, CA 91125, USA. ²Beckman Institute, California Institute of Technology, 1200 East California Boulevard, Pasadena, CA 91125, USA.

*These authors contributed equally to this work.

†To whom correspondence should be addressed. E-mail: angelike@caltech.edu

Fig. 1. Two-photon microscopy and analysis of histone2A (H2A)-GFP expressing embryos captures key events in gastrulation. (A and B) Cross-sections of wild-type (A) and *htl* mutant (B) embryos stained with antibody to Twist. (C and D) Confocal 1PEF (C) fails to image internalized mesoderm cells, whereas 2PEF (D) captures the positions of the internalized cells. (E) A 50- μ m-deep and 10- μ m-thick lateral slice through an H2A-GFP embryo demonstrates the signal-to-noise ratio (anterior, left). (F) Segmentation of mesoderm nuclei (orange spheres) by the use of Imaris software (Bitplane AG, Zurich, Switzerland). Each sphere was defined by the fluorescent intensity of H2A-GFP. Furrow formation, furrow collapse as a result of an EMT, and spreading of the mesoderm to form a monolayer are illustrated from top to bottom, respectively. (G to J) Tracking cell positions in three dimensions over time. Shown are dorsal (G) and posterior (H) views of mesoderm tracks (blue and yellow indicate early



and late time points, respectively) and dorsal (I) and posterior (J) views of mesoderm (orange) and ectoderm (gray) net displacement vectors. Scale bars, 20 μ m.

from the upper lateral parts of the furrow (Fig. 3A) becomes positioned at each leading edge of the mesoderm cell population, which was maintained for the entire course of their migration (movie S7). These leading cells were neither the first nor the last to invaginate; instead, their location within the furrow positioned them to land in the leading position as the furrow collapsed after the epithelial-to-mesenchymal transition (EMT).

We explored other morphogenetic events that might contribute to mesoderm spreading, such as cell division pattern and cell intercalation, based on our cell-tracking data. Each mesoderm cell divided twice (7, 8, 17, 18), and these divisions were ordered in space and time (Fig. 3B). Cells nearest the ectoderm divided first, followed by cells nearer to the top of the ventral furrow. This order was maintained during the second division cycle. Analysis of the cell division mutants did not uncover any of the characteristic mesoderm migration defects observable in fixed sections (fig. S6) (18). Our tracking data revealed that the orientation of cell divisions within the mesoderm is random and that altering the organization of cell divisions had no effect on mesoderm spreading or embryo viability (fig. S7, A to C). Thus, it is unlikely that these organized cell divisions play a role in mesoderm spreading. The radial cell intercalation events (19) were synchronous with the second wave of cell division (Fig. 3, C and D), but the orientation of the cell divisions did not seem to play a causal role in the intercalation motions. Mesoderm cell intercalation contributes to monolayer formation and spreading (Fig. 3, C and D).

To facilitate comparisons between embryos, we developed a statistical analysis characterizing the spreading behavior of the mesoderm cells. As suggested by the spatial organization of the spreading (Fig. 3A), the angular positions of each cell at the onset (θ_{start}) and at the end (θ_{end}) of the process were highly correlated. A plot of starting and ending positions revealed a linear relationship (fig. S4, A to C). Given this, linear regressions that were applied to the $\theta_{\text{end}}(\theta_{\text{start}})$ values provided a measure of both the strength of the spreading (as the slope of the line, A) (fig. S4, D and E) and a quantitative measure of collective behavior (the degree of correlation, R) (13). Wild-type cells followed an ordered spreading behavior [$\theta_{\text{end}} \approx 2(\theta_{\text{start}})$], which is shared by the majority of cells ($R > 0.9$) (fig. S5). Comparison of the regression analysis from five wild-type embryos showed the consistency of cell behaviors ($n = 5$ embryos and $n = 596$ cells) (fig. S5).

Previous studies of fixed embryos (8, 9, 20, 21) have suggested that fibroblast growth factor (FGF) signaling is involved in regulating mesoderm cell migration, but its exact function has remained elusive. We used our methodology to study the function of the FGF signaling pathway on the regulation of gastrulation by analyzing embryos of the FGF receptor mutant *heartless* (*hlt*) in the same way as wild-type embryos (figs. S2 and S3 and movie S9). We decomposed the cell move-

ments within *hlt* mutant embryos into their components in r , θ , and L (fig. S3, A to C), permitting direct comparisons with wild-type embryos (Fig. 2,

C to E). The ectoderm-coupled movements of mesoderm cells in the L direction were unaffected in *hlt* mutants (fig. S3F), and we obtained no evi-

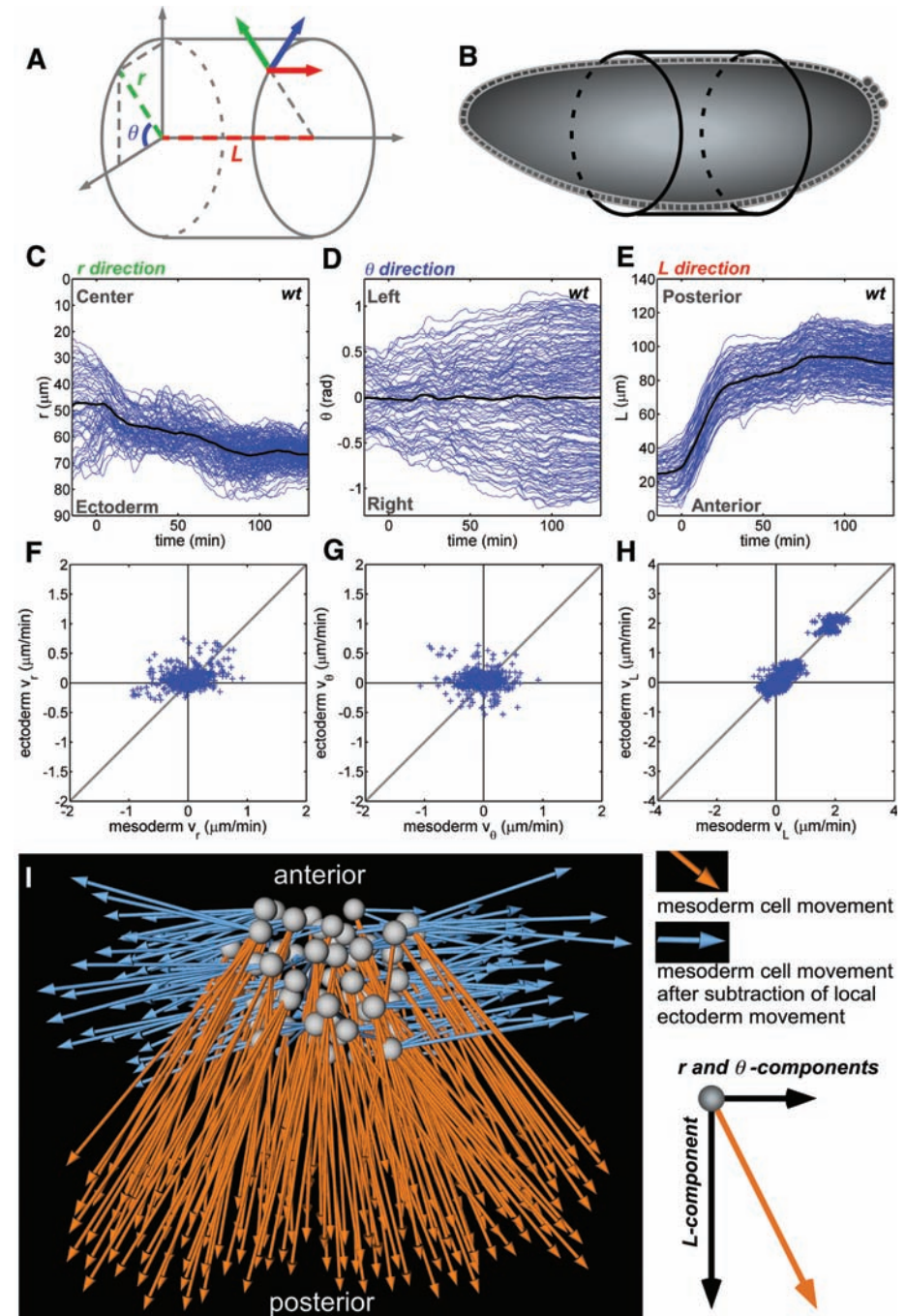


Fig. 2. Decomposition and correlative analysis of cell movements with the use of cylindrical coordinates. (A and B) The use of cylindrical coordinates allows the positioning of cells according to the body plan of the embryo at stage 6. (C to E) Cell trajectories (blue lines) reveal that each axis corresponds to a morphogenetic movement. (C) r is the radial position over time (for example, furrow collapse and intercalation; 0 indicates the center of the embryo). (D) θ is the angular movement (for example, mesoderm spreading and ectoderm convergence; 0 indicates the position of the ventral midline). (E) L corresponds to the movement of cells along the length of the embryo (for example, germ-band elongation). In (C) to (E), time ($t = 0$) is set as the point when AP movement begins. (F to H) Correlation of the velocity (v) of each mesoderm cell with its six nearest ectodermal neighbors along the (F) radial, (G) angular, and (H) AP axes, with correlation values of 0.21 ± 0.43 , 0.08 ± 0.18 , and 0.90 ± 0.06 , respectively ($n = 3$ embryos). (I) Dorsal view of mesoderm cell displacement before (orange) and after (blue) subtraction of local ectoderm cell movements.

dence for defects in cell-division events (fig. S7D). However, *htl* mutant embryos displayed mesoderm cell defects that affected both collapse of the furrow (r axis) and spreading in the angular direction (θ axis) (fig. S3, A and B). A statistical analysis of cell movement conducted on *htl* mutant-tracking data showed a scattered distribution of $\theta_{\text{end}}(\theta_{\text{start}})$ values (figs. S4I and S5), resulting in low spreading and correlation values ($A < 1$ and

$R < 0.5$ to 0.7 , respectively) (fig. S5C). Values obtained with analysis of individual *htl* embryos or by pooling the cells from multiple *htl* embryos ($n = 3$ embryos and $n = 284$ cells) (fig. S5, B and C) quantitatively demonstrated that a similar disruption of spreading is present in all *htl* embryos.

Cell tracking analysis revealed that loss of FGF signaling affected the mesoderm cells non-homogeneously (movie S10). In the radial direc-

tion, cells originating from the upper half of the furrow ("upper-furrow" cells) in general did not collapse, remaining far from the ectoderm during the entire acquisition time (Fig. 4A, fig. 3SA, and movies S11 and S8). The angular movement of upper-furrow cells was strongly affected in *htl* mutants (Fig. 4, B to G). In contrast, the last cells to invaginate in *htl* mutants, which make up the lower furrow, behaved in a manner similar to wild-type mesoderm cells and could achieve the same dorsal position as the wild type (Fig. 4G). Our statistical analysis of cell movements of upper- and lower-furrow cells confirmed the presence of two distinct cell behaviors in *htl* embryos (fig. S5, D and E). Other cell labeling approaches, such as photoactivatable GFP, can be used to characterize mutant phenotypes, but the limited number of cells they can follow (7) make interpretation difficult, especially when there are multiple behaviors, such as in *htl* mutant embryos.

Some cells from the upper furrow in *htl* mutants displayed normal positions in the $\theta_{\text{end}}(\theta_{\text{start}})$ graph, similar to those of wild-type embryos. These cells were positioned close to the ectoderm at the end of spreading (Fig. 4, I and J, and fig. S4J). This suggested that the distance from the ectoderm might have a major influence on spreading behavior. Indeed, the distinction between the two migratory behaviors observed was more clear when analyzing cells that were close to or far from the ectoderm (Fig. S5, D and E). We confirmed this by plotting a $\theta_{\text{end}}(\theta_{\text{start}})$ graph using a color code for the radial position of the cells at the end of the spreading process (Fig. 4, H and I): The *htl* cells that followed wild-type behavior [$\theta_{\text{end}} \approx 2(\theta_{\text{start}})$ such that $A = 2$] ended up close to the ectoderm (Fig. 4I, green), whereas the cells that stayed far from the ectoderm (Fig. 4I, red) had clearly disrupted behaviors, with several cells crossing the midline and migrating in the wrong direction ($A < 0$). All wild-type cells ended up close to the ectoderm (Fig. 4H).

Our analysis provides several insights into the *htl* mutant phenotype. First, the primary function of FGF signaling must be to help all cells within the furrow to collapse, directing them toward the ectoderm (Fig. 4K). Second, another as-yet unidentified signal must guide the migration of the cells in the angular direction toward the dorsal ectoderm, because movement is observed even in the absence of FGF signaling. Third, contact with the ectoderm is key for the mesoderm to respond to this guidance cue, because the distance of the mesoderm cells from the ectoderm defines their migratory competence. Any cell that encounters the ectoderm is capable of directed movement in the angular direction in response to a cue that cannot be solely FGF-dependent. Movement of the mesoderm cells might require contact with the ectoderm to make them competent to respond to a directional signal, as evidenced in other systems (22–24).

This study demonstrates that stereotypical morphogenetic events during embryo development can be systematically quantified, analyzed, and compared between wild-type and mutant em-

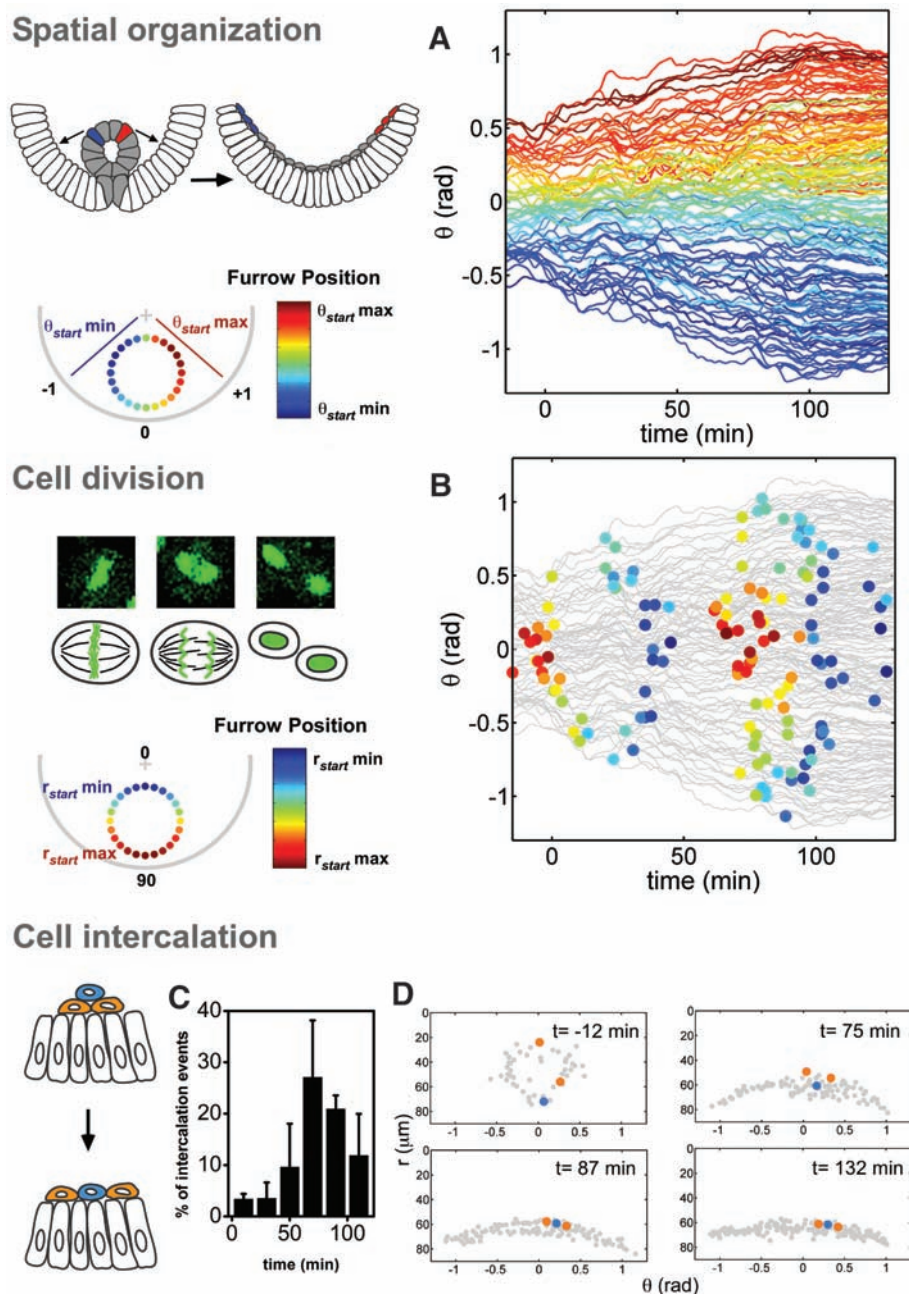


Fig. 3. Quantitative analysis of morphogenetic events reveals a high level of organization in wild-type embryos. **(A)** A color code marks the angular position of cells in the furrow at stage 7 and shows the spatial organization as cells move over time. rad, radians. Each line represents the trajectory of one cell. **(B)** Position and timing of each cell division (colored circle). The color code represents the radial position in the furrow at stage 7. DNA morphology during cell division in H2A-GFP embryos is shown (top left). **(C)** Analysis of intercalation events within the mesoderm over time shown as a percentage of mesoderm cells intercalating ($n = 3$ embryos). **(D)** The position of mesoderm cells before and after intercalation events.

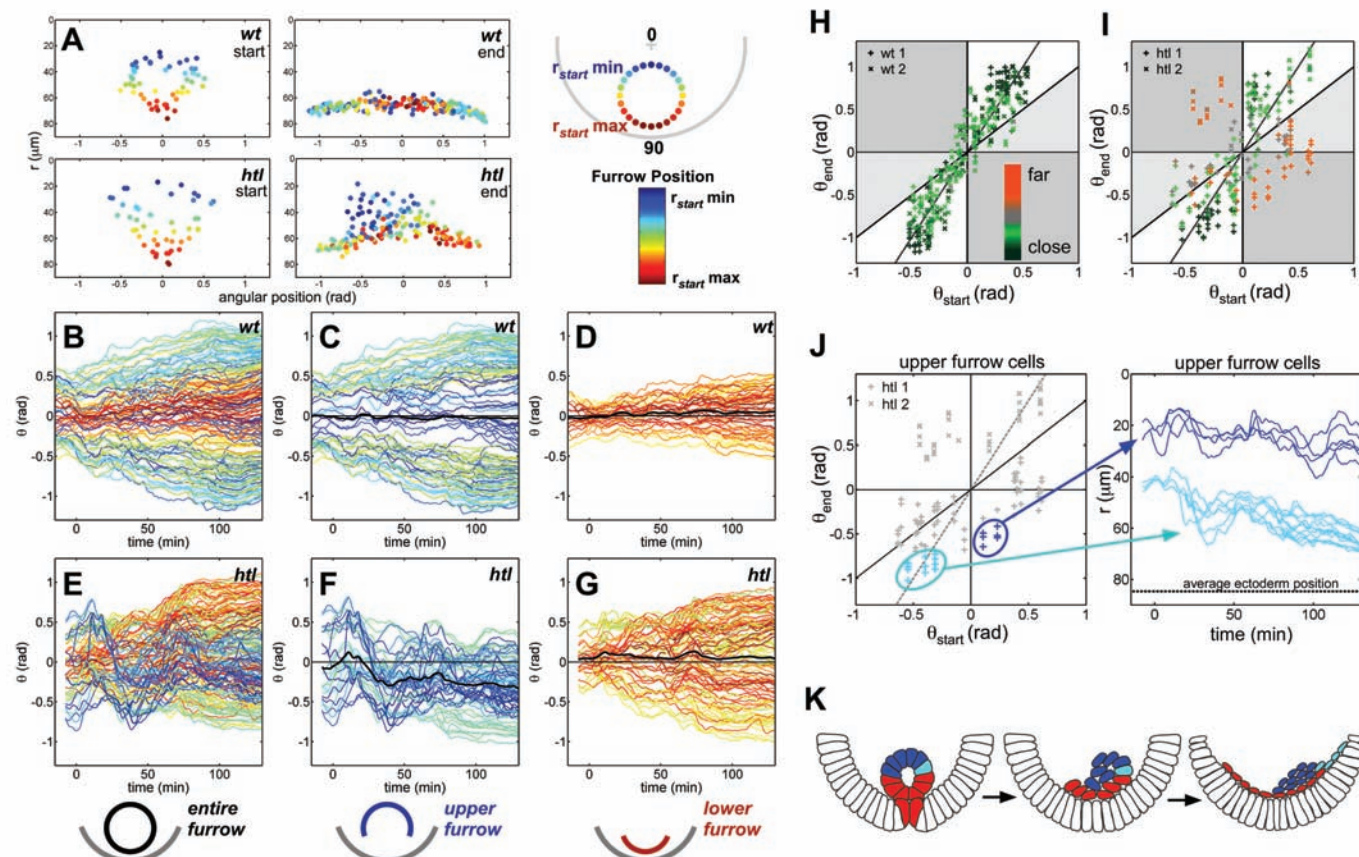


Fig. 4. Furrow collapse and spreading of mesoderm cells are disrupted in *htl* mutants. **(A)** Position of mesoderm cells (circles) at stage 7 and stage 10 in wild-type and *htl* embryos shown with a radial color code. **(B to G)** Angular movement of cells over time analyzed in wild-type **(B to D)** and *htl* mutant **(E to G)** embryos within the entire **(B and E)**, upper **(C and F)**, and lower **(D and G)** furrow (black line indicates the average mesoderm displacement with respect to the midline). **(H and I)** Spreading profile of wild-type **(H)** and *htl* **(I)** embryos. The color code represents the distance from the ectoderm at the end of spreading (red indicates far from ectoderm and green indicates close to ectoderm). The gray line represents a spreading coefficient of $A = 2$, where $\theta_{\text{end}} = A(\theta_{\text{start}}) + B$, constant (13). Cells that do not spread within the collective are represented within gray regions of the graph (13). In general, cells located close to the ectoderm fall along the gray line. **(J)** The radial position (r) of two particular groups of mesoderm cells from the upper furrow of *htl* mutants is depicted over time. One group exhibits normal spreading behavior (light blue), and the other group exhibits aberrant spreading behavior (dark blue). **(K)** The furrow collapse in *htl* mutants is disrupted, resulting in cells falling randomly to one side of the embryo. Upper-furrow cells that reach the ectoderm (light blue) undergo normal spreading, whereas cells that remain far from the ectoderm spread abnormally (dark blue). Red cells are Red indicates lower-furrow cells.

constant (13)]. Cells that do not spread within the collective are represented within gray regions of the graph (13). In general, cells located close to the ectoderm fall along the gray line. **(J)** The radial position (r) of two particular groups of mesoderm cells from the upper furrow of *htl* mutants is depicted over time. One group exhibits normal spreading behavior (light blue), and the other group exhibits aberrant spreading behavior (dark blue). **(K)** The furrow collapse in *htl* mutants is disrupted, resulting in cells falling randomly to one side of the embryo. Upper-furrow cells that reach the ectoderm (light blue) undergo normal spreading, whereas cells that remain far from the ectoderm spread abnormally (dark blue). Red cells are Red indicates lower-furrow cells.

bryos by means of the live imaging of large groups of cells. Complex cell movements are decomposed into particular cell behaviors, revealing a high level of organization and permitting the interpretation of subtle mutant phenotypes in *Drosophila*. Future developments in imaging and cell tracking will facilitate this quantitative approach, enabling its application at a larger scale and in other model systems, to expand the understanding of collective cell migration and embryonic development from the molecular level to that of the entire organism (25).

References and Notes

- P. Rorth, *Trends Cell Biol.* **17**, 575 (2007).
- D. J. Montell, *Curr. Opin. Genet. Dev.* **16**, 374 (2006).
- C. D. Stern, *Gastrulation: From Cells to Embryo*. (Cold Spring Harbor Laboratory Press, Cold Spring Harbor, NY, 2004).
- V. Lecaudey, D. Gilmour, *Curr. Opin. Cell Biol.* **18**, 102 (2006).
- L. A. Rohde, C. P. Heisenberg, *Int. Rev. Cytol.* **261**, 159 (2007).
- M. Leptin, *Dev. Cell* **8**, 305 (2005).
- M. J. Murray, R. Saint, *Development* **134**, 3975 (2007).
- R. Wilson, E. Vogelsang, M. Leptin, *Development* **132**, 491 (2005).
- S. Schumacher, T. Gryzik, S. Tannebaum, H. A. Muller, *Development* **131**, 2631 (2004).
- F. Helmchen, W. Denk, *Nat. Methods* **2**, 932 (2005).
- W. Supatto et al., *Proc. Natl. Acad. Sci. U.S.A.* **102**, 1047 (2005).
- M. Clarkson, R. Saint, *DNA Cell Biol.* **18**, 457 (1999).
- Materials and methods are available as supporting material on Science Online.
- K. D. Irvine, E. Wieschaus, *Development* **120**, 827 (1994).
- J. A. Zallen, J. T. Blankenship, *Semin. Cell Dev. Biol.* **19**, 263 (2008).
- R. Wilson, M. Leptin, *Philos. Trans. R. Soc. London Ser. B* **355**, 891 (2000).
- T. C. Seher, M. Leptin, *Curr. Biol.* **10**, 623 (2000).
- J. Grosshans, E. Wieschaus, *Cell* **101**, 523 (2000).
- O. Voiculescu, F. Bertocchini, L. Wolpert, R. E. Keller, C. D. Stern, *Nature* **449**, 1049 (2007).
- S. Gisselbrecht, J. B. Skeath, C. Q. Doe, A. M. Michelson, *Genes Dev.* **10**, 3003 (1996).
- M. Beiman, B. Z. Shilo, T. Volk, *Genes Dev.* **10**, 2993 (1996).
- M. Krieg et al., *Nat. Cell Biol.* **10**, 429 (2008).
- M. Sato, T. B. Kornberg, *Dev. Cell* **3**, 195 (2002).
- X. Yang, D. Dormann, A. E. Munsterberg, C. J. Weijer, *Dev. Cell* **3**, 425 (2002).
- S. G. Megason, S. E. Fraser, *Cell* **130**, 784 (2007).
- We thank M. Levine and E. Meyerowitz for comments on the manuscript, M. Liebling for advice on Imaris and Matlab, and the Caltech Biological Imaging Center for sharing equipment. This work was supported by grants to A.S. from NIH (R01 GM078542), the Searle Scholars Program, and the March of Dimes (Basil O'Connor Starter Scholar Award, 5-FY06-12), and grants to S.F. from the Caltech Beckman Institute and NIH (Center for Excellence in Genomic Science grant P50 HG004071).

Supporting Online Material

www.sciencemag.org/cgi/content/full/322/5907/[page]/DC1
Materials and Methods
Figs. S1 to S7
Movie S1 to S11
References

16 May 2008; accepted 12 November 2008
10.1126/science.1167094

Astroglial Metabolic Networks Sustain Hippocampal Synaptic Transmission

Nathalie Rouach,^{1*} Annette Koulakoff,¹ Veronica Abudara,^{1,2} Klaus Willecke,³ Christian Giaume¹

Astrocytes provide metabolic substrates to neurons in an activity-dependent manner. However, the molecular mechanisms involved in this function, as well as its role in synaptic transmission, remain unclear. Here, we show that the gap-junction subunit proteins connexin 43 and 30 allow intercellular trafficking of glucose and its metabolites through astroglial networks. This trafficking is regulated by glutamatergic synaptic activity mediated by AMPA receptors. In the absence of extracellular glucose, the delivery of glucose or lactate to astrocytes sustains glutamatergic synaptic transmission and epileptiform activity only when they are connected by gap junctions. These results indicate that astroglial gap junctions provide an activity-dependent intercellular pathway for the delivery of energetic metabolites from blood vessels to distal neurons.

Glucose, transported by the blood, is the major source of energy used by the brain for neuronal activity (1). It has been proposed that neurons obtain most of their energy from extracellular lactate, a glucose metabolite

produced by astrocytes (2). Indeed, astrocytes provide by their perivascular endfeet (3, 4) and processes a physical link between the vasculature and the synaptic terminals, supporting the concept of metabolic coupling between glia and neurons (2).

Moreover, a typical feature of astrocytes is their network organization resulting from extensive intercellular communication through gap-junction channels formed by connexins (Cx) (5). Thus, the aim of this work was to determine whether and how the connectivity of local perivascular astroglial networks contributes to their metabolic supportive function to neurons.

The expression of Cx43 and Cx30, the main astroglial gap-junction proteins (6), is enriched in perivascular endfeet of astrocytes and delineates blood vessel walls in mouse hippocampus (Fig. 1A and fig. S1), as previously described in the cortex for Cx43 (4) and Cx30 (7). Around blood vessels, Cx immunoreactive puncta are larger than those in the parenchyma and form honeycomb patterns,

¹INSERM U840, Collège de France, 11 place Marcelin Berthelot, 75005 Paris, France. ²Facultad de Medicina, Universidad de la Republica, Montevideo, Uruguay. ³Institute of Genetics, University of Bonn, Roemerstraße 164, 53117 Bonn, Germany.

*To whom correspondence should be addressed. E-mail: nathalie.rouach@college-de-france.fr

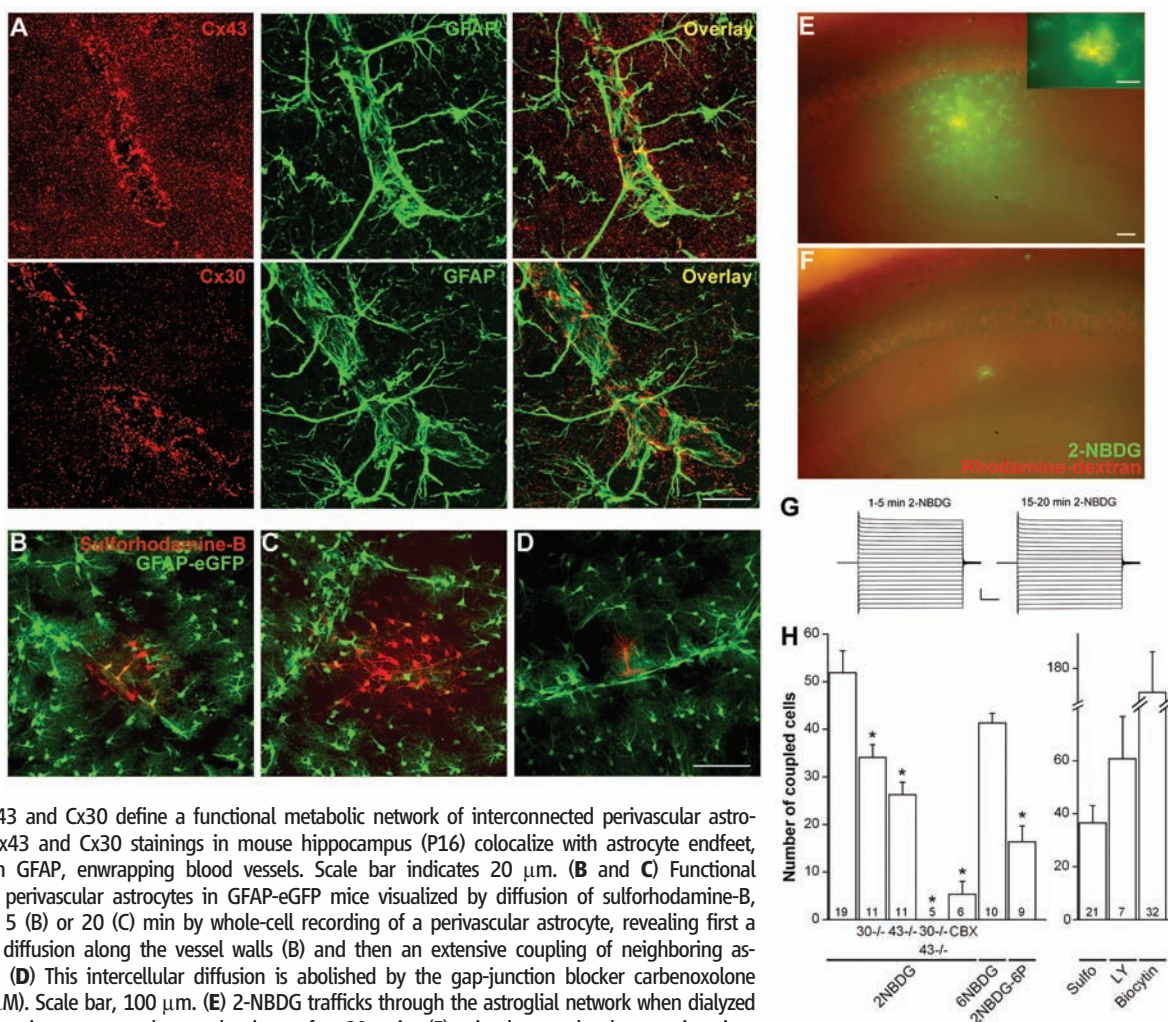


Fig. 1. Cx43 and Cx30 define a functional metabolic network of interconnected perivascular astrocytes. (A) Cx43 and Cx30 stainings in mouse hippocampus (P16) colocalize with astrocyte endfeet, labeled with GFAP, enwrapping blood vessels. Scale bar indicates 20 μ m. (B and C) Functional coupling of perivascular astrocytes in GFAP-eGFP mice visualized by diffusion of sulforhodamine-B, dialyzed for 5 (B) or 20 (C) min by whole-cell recording of a perivascular astrocyte, revealing first a preferential diffusion along the vessel walls (B) and then an extensive coupling of neighboring astrocytes (C). (D) This intercellular diffusion is abolished by the gap-junction blocker carbenoxolone (CBX, 150 μ M). Scale bar, 100 μ m. (E) 2-NBDG trafficks through the astroglial network when dialyzed in a perivascular astrocyte by patch clamp for 20 min (E); simultaneously the gap-junction-impermeable dye (dextran tetramethylrhodamine, molecular weight = 10,000) was dialyzed to localize the recorded astrocyte (inset). Scale bars, 50 μ m. (F) 2-NBDG interastrocytic trafficking is mediated by gap junctions because it is abolished by CBX. (G) 2-NBDG does not modify within 20 min current/voltage (*I/V*) curve of the recorded astrocyte illustrated in (E). (H) Graph summarizing the extent of astrocytic coupling for several fluorescent glucose metabolites (2-NBDG, 6-NBDG, and 2-NBDG-6P) and tracers (Sulfo, sulforhodamine; LY, Lucifer yellow; biocytin) in wild-type and knockout mice for Cxs [30-/-, Cx30-/-; 43-/-, Cx43(f/f):GFAP-cre; and 30-/-43-/-, double-knockout Cx30-/-Cx43(f/f):GFAP-cre]. Asterisks indicate statistical significance ($P < 0.01$); error bars indicate standard error of mean (SEM).

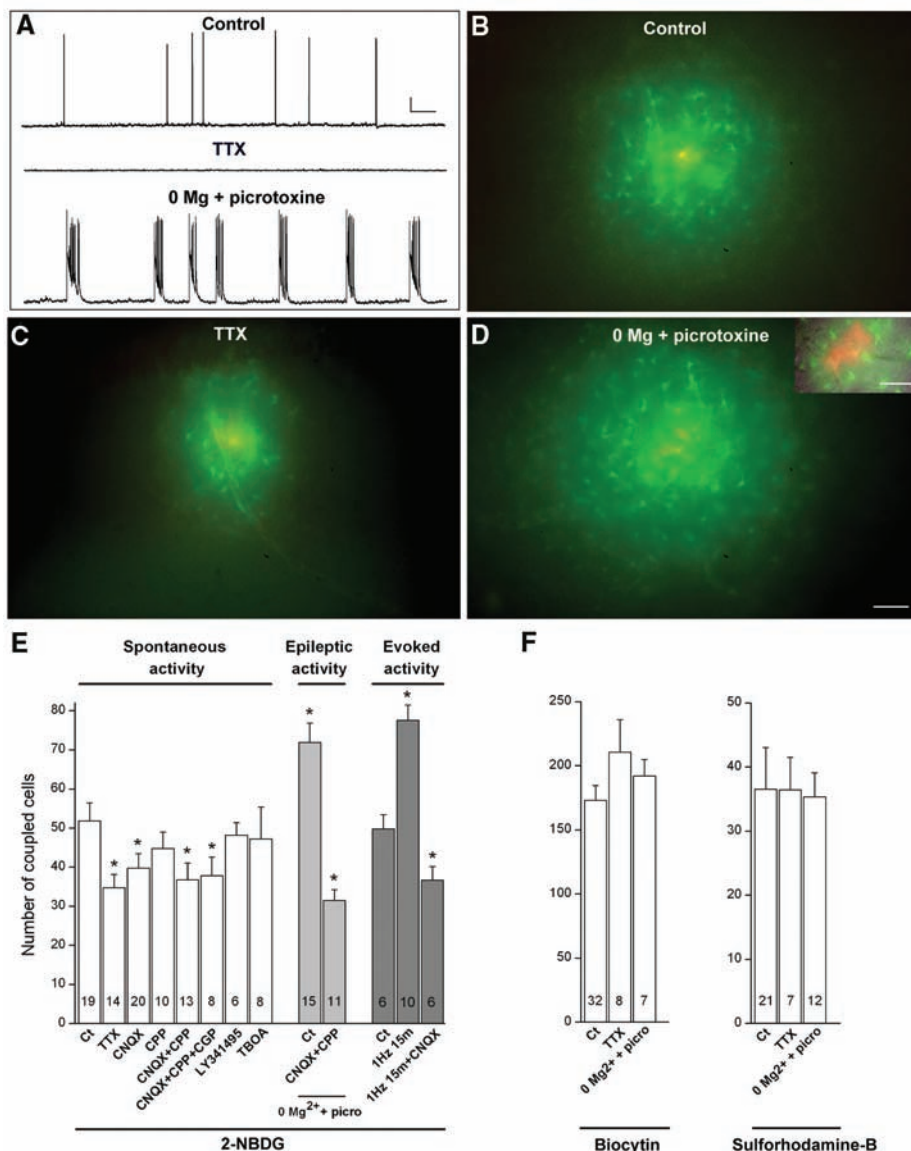


Fig. 2. Activity-dependent glucose trafficking in the astroglia network. **(A)** Spontaneous activity of hippocampal CA1 pyramidal cells recorded in current clamp in control, TTX (0.5 μ M, 1 to 4 hours), and 0 Mg^{2+} -picrotoxin (100 μ M, 1 to 4 hours) conditions. Scale bar, 20 mV, 6.7 s. **(B to D)** Sample pictures showing that 2-NBDG trafficking in astrocytes is decreased in TTX (C) and increased in 0 Mg^{2+} -picrotoxin (D), as compared with control conditions (B). **(D Inset)** The recorded perivascular astrocyte labeled with dextran tetramethylrhodamine (red) and 2-NBDG (green). Scale bars, 50 μ m. **(E)** Graph summarizing the extent of astrocytic coupling for 2-NBDG during spontaneous, epileptic (0 Mg^{2+} -picrotoxin) and evoked activity (1 Hz, 15 min). In all cases, glutamate increases the trafficking of 2-NBDG in astrocytic networks by activating AMPA receptors (AMPA). All drugs were applied for 1 to 4 hours: CNQX (AMPA antagonist, 10 μ M); 3-(2-carboxypiperazin-4-yl)-propyl-1-phosphonic acid (CPP) (NMDAR antagonist, 10 μ M), (2S)-3-[[1(1S)-1-(3,4-Dichlorophenyl)ethyl]amino-2-hydroxypropyl](phenylmethyl)phosphonic acid (CGP55845) (GABA_BR antagonist, CGP, 2 μ M), LY143495 (mGluR antagonist, 20 μ M), and threo- β -benzyloxyaspartic acid (TBOA) (glutamate transporter inhibitor, 100 μ M). Asterisks indicate statistical significance ($P < 0.01$). **(F)** Biocytin or sulforhodamine-B trafficking in astrocytic networks is not regulated by neuronal activity. Error bars indicate SEM.

outlining the areas of contact between endfeet. Outside blood vessels, Cx43 staining is abundant, whereas Cx30 immunoreactivity is much weaker.

To determine whether gap junctions between perivascular astrocytes are functional, we analyzed the diffusion of gap-junction channel-permeable dyes (sulforhodamine-B, Lucifer yellow) or tracer

(biocytin), dialyzed by whole-cell recording of a perivascular astrocyte. A preferential diffusion along the vessel wall was revealed by a 5-min dialysis of sulforhodamine-B (Fig. 1B), whereas a 20-min dialysis resulted in extensive intercellular diffusion into neighboring astrocytes (58 ± 10 cells, $n = 11$) (Fig. 1, C and H). This diffusion

was mediated by gap junctions because it was abolished by the gap-junction blocker carbenoxolone (CBX) (Fig. 1D). Most of the coupled cells (133 ± 12 cells for biocytin, $n = 36$) were identified as astrocytes by immunohistochemical staining (fig. S2).

Perivascular astrocytes take up glucose from the blood by the glucose transporter-1 located in their endfeet (3). Therefore we investigated whether glucose, once taken up, can traffic through astroglial networks. Glucose trafficking was examined in hippocampal slices by using the fluorescent glucose derivatives 2-[N-(7-nitrobenz-2-oxa-1,3-diazol-4-yl)amino]-2-deoxyglucose (2-NBDG) and the nonhydrolyzable 6-[N-(7-nitrobenz-2-oxa-1,3-diazol-4-yl)amino]-6-deoxyglucose (6-NBDG) (8). When injected for 20 min by whole-cell recordings of astrocytes lining blood vessels in stratum radiatum, 2-NBDG diffused through the astroglial network (52 ± 5 cells, $n = 19$) (Fig. 1E) mediated by Cx30 and Cx43 channels. Indeed, its trafficking was reduced by $\sim 35\%$ in Cx30^{-/-} mice ($n = 11$) and by $\sim 50\%$ in Cx43(f/f):glial fibrillary acidic protein (GFAP)-cre mice ($n = 11$) and was totally abolished in the double-knockout mice Cx30^{-/-}Cx43(f/f):GFAP-cre ($n = 5$) (Fig. 1H). Interestingly, the trafficking of 2-NBDG-6P, the first phosphorylated metabolite of 2-NBDG, was decreased by $\sim 70\%$ compared with 2-NBDG (Fig. 1H), whereas gap-junction permeability was not affected as indicated by the unchanged cell membrane resistance. This suggests a selectivity of gap-junction channels for energetic metabolites according to their phosphorylation, implying that glucose, rather than glucose-6-phosphate, is a preferred metabolite for gap-junction trafficking. When 2-NBDG was dialyzed into CA1 pyramidal cells and interneurons, it never diffused to neighboring cells (fig. S3, A and D). Moreover, neuronal (fig. S3) and astroglial (Fig. 1G) electrophysiological properties were not altered by the intrapipette 2-NBDG.

Because astrocytes provide energetic substrates to neurons in an activity-dependent manner (9), we investigated whether 2-NBDG interastrocytic trafficking was regulated by various regimes of neuronal activity. First, inhibition of spontaneous activity by tetrodotoxin (TTX) (Fig. 2A) decreased 2-NBDG diffusion by $\sim 35\%$ ($n = 14$) (Fig. 2, C and E). In this condition, the basal glutamatergic activity exerts a tonic effect because CNQX reduced by $\sim 25\%$ the number of 2-NBDG-coupled astrocytes (Fig. 2E). In contrast, NMDA (N-methyl-D-aspartate), GABA_B (γ -aminobutyric acid type B), metabotropic glutamate receptors, and glutamate transporters were not involved in such regulation (Fig. 2E). Then, intense neuronal activity generated by epileptiform bursts (Fig. 2A) increased by $\sim 40\%$ ($n = 15$) 2-NBDG diffusion in the astroglial network (Fig. 2D), an effect also due to glutamatergic activity because it was abolished by AMPA and NMDA receptor antagonists (Fig. 2E). Lastly, evoked activity by repetitive stimulation of the Schaffer collaterals (1 Hz, 15 min) increased 2-NBDG trafficking in the astroglial network

(+50%, $n = 10$), an effect also mediated by AMPA receptors (Fig. 2E). Therefore glutamate, released by spontaneous, epileptiform, or evoked activity, increases glucose trafficking in astroglial networks by activating AMPA receptors. Because hippocampal astrocytes connected by gap junctions lack AMPA receptors (10, 11), these effects were presumably the consequence of neuronal AMPA receptor activation.

These activity-dependent regulations were specific to glucose. They were not observed when gap-junction-permeable tracers were used (Fig. 2F), suggesting that glutamatergic synaptic activity does not regulate gap-junction channel permeability but may trigger an energetic demand that generates a diffusion gradient for glucose directly linked to the level of neuronal activity. To address this issue,

we delivered 2-NBDG in a perivascular astrocyte patched in stratum oriens at an average distance of $30 \pm 4 \mu\text{m}$ ($n = 12$) above the pyramidal cell body layer, whereas a local increase in neuronal demand was induced in stratum radiatum by Schaffer collaterals stimulation (1 Hz, 20 min) (Fig. 3A). Dual extracellular recordings of field excitatory postsynaptic potentials (fEPSPs) revealed that such stimulation evokes a larger glutamatergic synaptic activity in stratum radiatum than in stratum oriens (+392%, $n = 8$) (Fig. 3, B and E), although both recording pipettes were equally distant from the stimulation electrode ($279 \pm 6 \mu\text{m}$ versus $264 \pm 6 \mu\text{m}$, $n = 8$) and from stratum pyramidale ($74 \pm 5 \mu\text{m}$ versus $75 \pm 5 \mu\text{m}$, $n = 8$). In control conditions, 2-NBDG diffusion in astrocytes was largely confined to stratum oriens (75% of the coupled

cells, $n = 6$) and occasionally crossed the pyramidal cell body layer to reach stratum radiatum (25% of the coupled cells, $n = 6$) (Fig. 3C). When the Schaffer collaterals were stimulated, the extent of glucose diffusion into stratum pyramidale and radiatum astrocytes almost doubled compared with control conditions ($n = 8$), whereas the number of 2-NBDG positive astrocytes was similar (Fig. 3, D and E). These data suggest that glutamatergic synaptic activity in stratum radiatum signals a local energetic demand that induces the diffusion of 2-NBDG to these sites, resulting in an activity-dependent shape change of astroglial metabolic networks.

What might be the role of this glucose trafficking through astroglial networks? To test whether it contributes to glutamatergic synaptic activity, we performed extracellular recordings of fEPSPs evoked by Schaffer collaterals stimulation during exogenous glucose deprivation (EGD), while selectively delivering and increasing intracellular glucose in a single astrocyte via the recording pipette (supporting online text and fig. S4). We hypothesized that glucose can spread into the astroglial network because the number of coupled astrocytes after 1 hour of dialysis with sulforhodamine-B, also included in the patch pipette, reached 87 ± 7 astrocytes ($n = 12$) in wild-type mice (Fig. 4A). To detect local neuroglial interactions involving a group of connected astrocytes, we located the astrocyte recording pipette at $77 \pm 5 \mu\text{m}$ ($n = 19$) from the neuronal extracellular recording pipette. EGD (30 min) induced a slow and reversible depression of synaptic transmission in hippocampal slices (~50%) (Fig. 4, C, E, and G). Such depression of fEPSPs during EGD was not observed when glucose (20 mM) was administered to the astroglial network (Fig. 4, C, E, and G). This effect was suppressed when lactate transport inhibitor α -cyano-4-hydroxycinnamic acid (4-CIN) was applied 10 min before and during EGD (Fig. 4G). This demonstrates that glucose, initially delivered to one astrocyte, is metabolized into lactate, which is then released extracellularly by astrocytes of the metabolic network and taken up by neurons to sustain their synaptic activity. When lactate (20 mM) instead of glucose was provided directly to the astroglial network, the depression of fEPSPs was also inhibited (Fig. 4G). Lactate can thus traffic through astrocytic gap junctions and be used by neurons as an energetic substrate to sustain their excitatory synaptic transmission. When the same experiment was performed in double-knockout mice for Cx43 and Cx30, fEPSPs depression after EGD persisted with a similar kinetic to control conditions, in which intracellular glucose was not provided to the patched astrocyte (Fig. 4, D, F, and G). This suggests that gap-junction-mediated astroglial networks are involved in energetic metabolites trafficking from astrocytes to neurons sustaining their activity and that, in wild-type mice, inhibition of fEPSPs depression by astrocytic glucose is not due to leakage of glucose from the patch pipette. The magnitude and kinetic of fEPSPs depression induced by EGD in control conditions

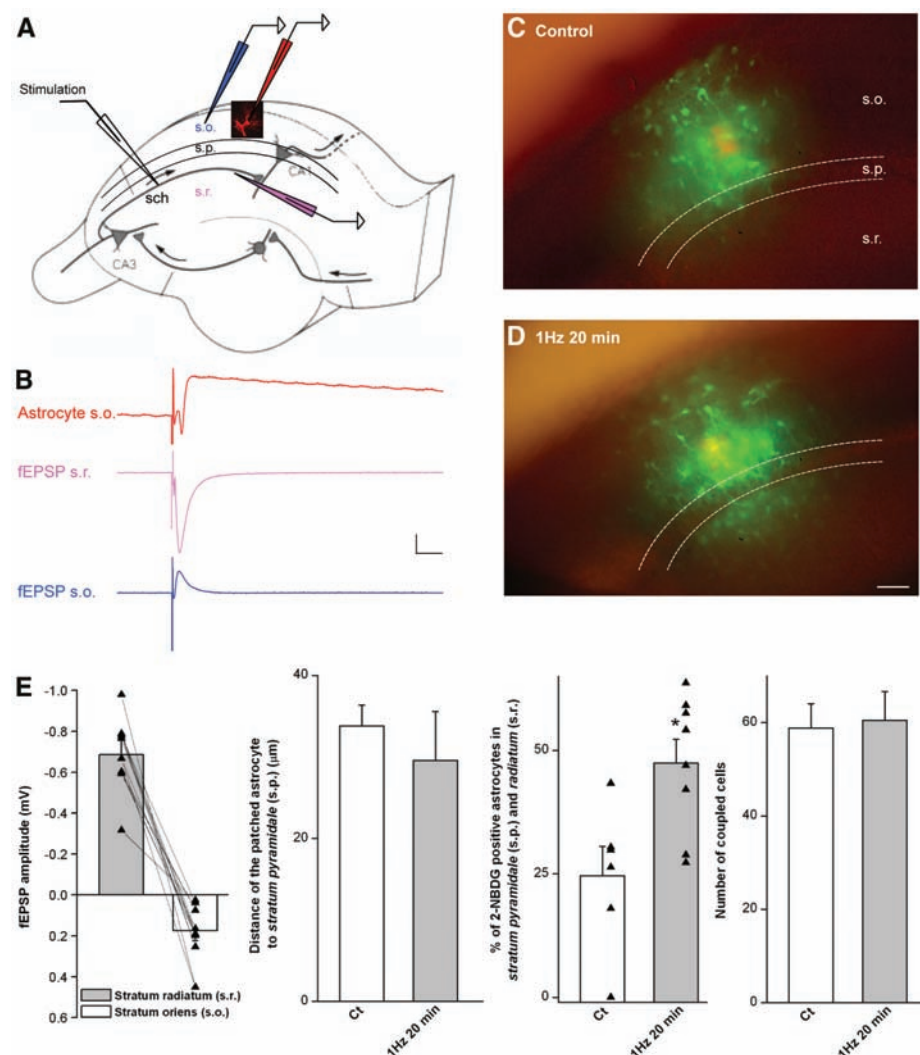


Fig. 3. Activity-dependent change in the shape of astroglial metabolic networks by local energetic demand. (A) Schematic drawing depicting recordings of an astrocyte located in stratum oriens (s.o.) at $<50 \mu\text{m}$ from stratum pyramidale (s.p.) with a patch pipette containing both 2-NBDG and tetramethylrhodamine-dextran, during stimulation of the Schaffer collaterals (sch) in stratum radiatum (s.r.). Extracellular pipettes for simultaneous recordings of evoked fEPSPs in s.o. (blue) and s.r. (pink) are also represented. (B) Sample traces of the evoked depolarization in s.o. astrocytes (scale bar, 0.5 mV and 12.5 ms) and paired s.o. and s.r. fEPSPs (scale bar, 0.15 mV and 12.5 ms) during stimulation of the sch. (C to E) Sample pictures and graphs showing that sch stimulation (1 Hz, 20 min, $n = 8$) extends 2-NBDG diffusion to s.r. astrocytes (Ct, control without stimulation, $n = 6$). Scale bar, $50 \mu\text{m}$. Error bars indicate SEM.

was similar in wild-type and double-knockout mice for Cx43 and Cx30 (Fig. 4, E and F), suggesting that astroglial glycogen stores and downstream energetic metabolism steps are comparable in both genotypes.

We further investigated the involvement of gap-junction full channels versus Cx hemichannels in providing a pathway for glucose delivery

from astrocytes to neurons during EGD. EGD (30 to 60 min) had no effect on astrocytic coupling for sulforhodamine-B (fig. S5, A and B), whereas it slightly decreased (~25%) 2-NBDG coupling (fig. S5, C and D), suggesting again that the activity-dependent regulation of glucose trafficking is selective (Fig. 2). Indeed, EGD (30 to 60 min) decreased glutamatergic synaptic activity

by 50 to 80% (fig. S5). Because Cxs also act as hemichannels mediating the release or uptake of molecules in physiopathological conditions (12), they could release glucose or lactate, administered to the astrocytic network. However, their involvement was discarded because ethidium bromide uptake by GFAP-enhanced green fluorescent protein (eGFP) astrocytes showed no difference between control and EGD-treated slices (fig. S5, E and F).

Recent work proposed an involvement of astrocytes (13) and energetic metabolism (14) in epilepsy. Indeed, ketogenic diets and antiglycolytic compounds such as 2-deoxy-D-glucose have anti-epileptic properties (14). Therefore, we investigated whether glucose from astroglial networks could also sustain epileptiform activity. Epileptiform activity was recorded extracellularly by fEPSPs and consisted of bursts occurring at a frequency of 1.9 ± 0.6 per minute ($n = 6$) (Fig. 2A). EGD (30 min) almost totally abolished the bursting activity (fig. S6, A and C), whereas intracellular glucose delivery to astroglial networks during EGD maintained 31% of the bursts (fig. S6, B and C). Hence, glucose trafficking through astroglial networks can partially sustain epileptiform activity. This suggests that energy metabolism of astroglial networks may be a promising target for novel antiepileptic drugs.

Our findings identify a previously unknown role for Cx43 and Cx30 gap-junction channels in hippocampal astrocytes. The Cxs constitute the molecular basis for perivascular astroglial metabolic networks, allowing activity-dependent intercellular trafficking of energetic metabolites used to sustain glutamatergic synaptic activity. Importantly, lactate is the final metabolite released by astrocytes and used by neurons to maintain their activity in physiopathological conditions. These data extend the classical model of astroglial energy metabolism in brain function, in which up to now astrocytes were generally considered as single entities. By including gap-junction-mediated metabolic networks of astrocytes, we propose that supply of energetic metabolites involves groups of connected astrocytes to reach more efficiently and distally the sites of high neuronal demand. Gap junctions are directly involved in the metabolic supportive function of astrocytes by providing an activity-dependent intercellular pathway for glucose delivery from blood vessels to distal neurons. Such a pathway may be important to sustain neuronal activity and survival in pathological conditions that alter energy production, such as hypoglycemia or anoxia/ischemia, in which gap-junction channels are still functional (15).

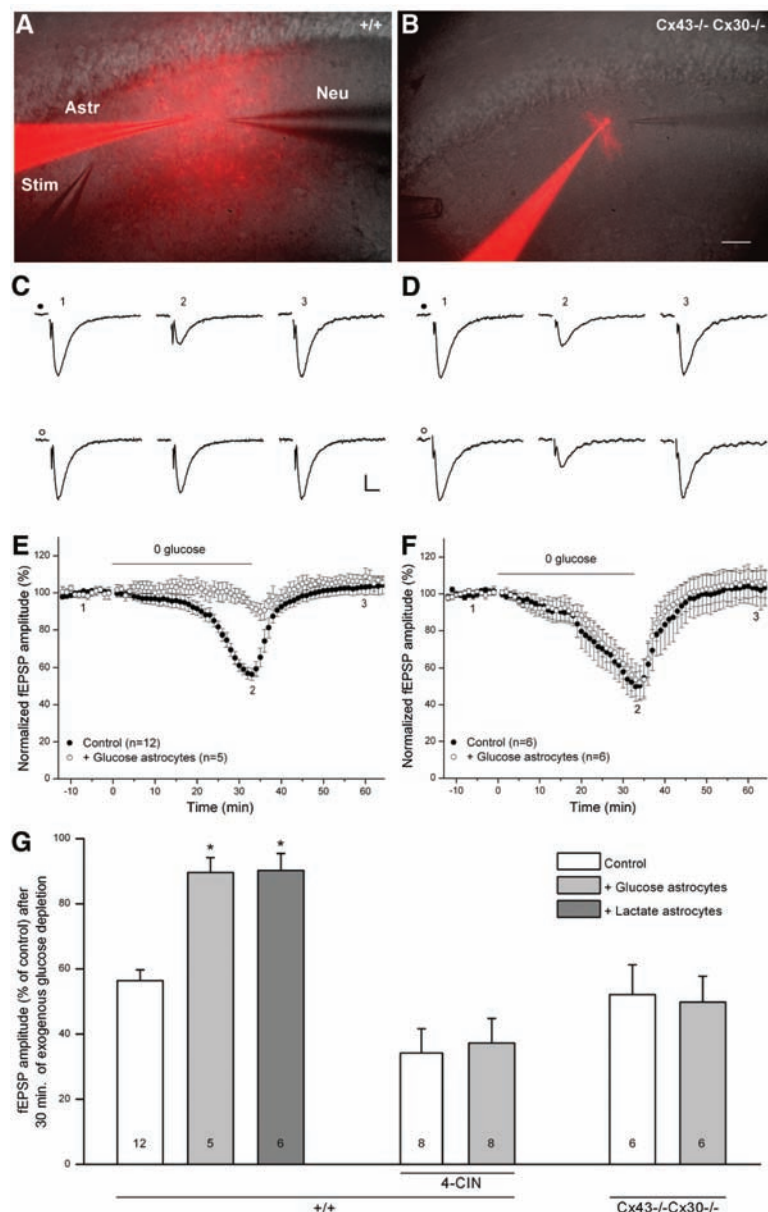


Fig. 4. Metabolic supply through astrocytic networks sustains synaptic transmission during exogenous glucose deprivation. (A and B) Sample pictures depicting paired recordings of fEPSPs (Neu), evoked by Schaffer collaterals stimulation (Stim), and one astrocyte (Astr) with a pipette containing glucose or lactate (20 mM) and sulforhodamine-B (red, 0.1%). Sulforhodamine-B diffuses extensively in astrocytes from wild-type (+/+) but not from Cx43^{-/-}Cx30^{-/-} mice. Scale bar, 50 μ m. (C to G) Intracellular glucose delivery to astrocytic networks (+ Glucose astrocytes) through the patch pipette inhibits fEPSPs amplitude depression induced by EGD (0 glucose, 32 min) in wild-type [(C) and (E)] but not in Cx43^{-/-}Cx30^{-/-} [(D) and (F)] mice. [(C) and (D)] Sample fEPSPs recorded before (trace 1), during (trace 2), and after EGD (trace 3), as indicated by the numbers in (E) and (F), are shown above the curves. Scale bar, 0.2 mV, 5 ms. (G) Graph summarizing fEPSPs amplitude after 30 min of EGD in different conditions [intra-astroglial delivery of glucose (20 mM, + Glucose astrocytes) or lactate (20 mM, + Lactate astrocytes)], lactate transport inhibition by 4-CIN (200 μ M) in wild-type (+/+) and Cx43^{-/-}Cx30^{-/-} mice.

References and Notes

1. D. D. Clarke, L. Sokoloff, in *Basic Neurochemistry*, G. J. Siegle, B. W. Agranoff, R. W. Albers, P. B. Molinoff, Eds. (Raven, New York, 1994), pp. 645–680.
2. M. Tsacopoulos, P. J. Magistretti, *J. Neurosci.* **16**, 877 (1996).
3. K. Kacem, P. Lacombe, J. Seylaz, G. Bonvento, *Glia* **23**, 1 (1998).
4. M. Simard, G. Arcuino, T. Takano, Q. S. Liu, M. Nedergaard, *J. Neurosci.* **23**, 9254 (2003).

5. C. Giaume, K. D. McCarthy, *Trends Neurosci.* **19**, 319 (1996).
6. J. I. Nagy, J. E. Rash, *Brain Res. Brain Res. Rev.* **32**, 29 (2000).
7. J. I. Nagy, D. Patel, P. A. Y. Ochalski, G. L. Stelmack, *Neuroscience* **88**, 447 (1999).
8. Materials and methods are available as supporting material on Science Online.
9. L. Pellerin, P. Magistretti, *Proc. Natl. Acad. Sci. U.S.A.* **91**, 10625 (1994).
10. K. Matthias et al., *J. Neurosci.* **23**, 1750 (2003).
11. A. Wallraff, B. Odermatt, K. Willecke, C. Steinhäuser, *Glia* **48**, 36 (2004).
12. D. C. Spray, Z. C. Ye, B. R. Ransom, *Glia* **54**, 758 (2006).
13. G. F. Tian et al., *Nat. Med.* **11**, 973 (2005).
14. M. Garriga-Canut et al., *Nat. Neurosci.* **9**, 1382 (2006).
15. M. L. Cotrina et al., *J. Neurosci.* **18**, 2520 (1998).
16. We thank P. Ezan for technical assistance and R. Nicoll, G. Bonvento, J. Deitmer, and P. Magistretti for helpful discussions. This work was supported by grants from the Human Frontier Science Program Organization (Career Development Award) and Agence Nationale de la Recherche (Programme Jeunes chercheurs) to N.R.; from INSERM to N.R., A.K., and C.G.; from the German

Research Association (SFB 645, B3) to K.W.; and from International Brain Research Organization to V.A. N.R. dedicates this work to her daughter Angela.

Supporting Online Material

www.sciencemag.org/cgi/content/full/322/5907/1551/DC1

Materials and Methods

SOM Text

Figs. S1 to S6

References

31 July 2008; accepted 29 October 2008

10.1126/science.1164022

Activation of Pannexin-1 Hemichannels Augments Aberrant Bursting in the Hippocampus

Roger J. Thompson,^{1,†} Michael F. Jackson,² Michelle E. Olah,² Ravi L. Rungta,¹ Dustin J. Hines,¹ Michael A. Beazely,² John F. MacDonald,² Brian A. MacVicar^{1†}

Pannexin-1 (Px1) is expressed at postsynaptic sites in pyramidal neurons, suggesting that these hemichannels contribute to dendritic signals associated with synaptic function. We found that, in pyramidal neurons, *N*-methyl-D-aspartate receptor (NMDAR) activation induced a secondary prolonged current and dye flux that were blocked with a specific inhibitory peptide against Px1 hemichannels; knockdown of Px1 by RNA interference blocked the current in cultured neurons. Enhancing endogenous NMDAR activation in brain slices by removing external magnesium ions (Mg^{2+}) triggered epileptiform activity, which had decreased spike amplitude and prolonged interburst interval during application of the Px1 hemichannel blocking peptide. We conclude that Px1 hemichannel opening is triggered by NMDAR stimulation and can contribute to epileptiform seizure activity.

Hemichannels are formed by pannexin or connexin proteins and mediate large ionic currents and the passage of small molecules (<1 kD) across plasma membranes. Pannexin-1 (Px1) forms hemichannels in a number of cell types and can be opened by ischemic-like conditions in pyramidal neurons (1) or purinergic receptor stimulation in red blood cells (2). Px1 has been observed at the postsynaptic density by electron microscopy and colocalization with postsynaptic density protein 95 (PSD95) (3); therefore, we hypothesized that Px1 hemichannels may have an undiscovered function at postsynaptic sites. Glutamate mediates excitatory synaptic communication via activation of fast AMPA/kainate and slower *N*-methyl-D-aspartate receptors (NMDARs). We investigated the possibility that NMDAR activation opens Px1 hemichannels because of reports that NMDARs lead to a prolonged but unidentified secondary inward current (4–6).

Under conditions in which voltage-dependent ion channels were blocked, we recorded NMDAR secondary currents (I_{2nd}) from acutely isolated hippocampal neurons with whole-cell patch clamp and activated them by either repeated (10-s duration at 1-min intervals) (Fig. 1A) or continuous (5 to 15 min) 100 μ M NMDA with concomitant voltage commands from -80 to $+80$ mV (Figs. 1D and 2) (7). I_{2nd} was evident as an increase in holding current (Fig. 1A, downward shift in middle trace) and was secondary to the NMDAR because it persisted after washout of the agonist (Fig. 1A). Furthermore, I_{2nd} was blocked by 50 μ M carbenoxolone (Cbx) (Fig. 1, A to C), an inhibitor of gap junctions and hemichannels (8). We tested a selective small peptide inhibitor of Px1, $^{10}panx$ (100 μ M; WRQAAFVDSY) (9, 10), that blocked I_{2nd} [Fig. 1, B and C; $P < 0.05$, analysis of variance (ANOVA)], whereas a scrambled version, $^{sc}panx$ (FSVYWAQADR), was ineffective (Fig. 1C; Px1 group, $P > 0.05$, ANOVA). Block of the NMDAR ligand-gated currents with 1 mM kynurenic acid prevented activation of I_{2nd} (Fig. S1). Furthermore, the NMDAR currents were not directly affected by Cbx or $^{10}panx$ as determined by applying these blockers before activation of I_{2nd} (Fig. 1C; $P > 0.05$, ANOVA). Similar to Px1 activation by ischemia (1), I_{2nd} had a linear current-voltage relation (Fig. 1B). Although this differs from some Px1 expression systems (8, 9, 11), it is

similar to the “large-conductance” mode of P2X7 in human embryonic kidney cells (12), which may be mediated by Px1 (9).

The pores of hemichannels are large enough to permit flux of large molecules (13), making dye flux a powerful tool for identifying the involvement of Px1. If Px1 mediates I_{2nd} , then NMDAR activation should evoke efflux of calcein (a non-reactive fluorescent indicator) from hippocampal neurons. We loaded acutely isolated hippocampal neurons with calcein red/orange and with a calcium indicator (Fluo-4 or Fluo-4FF) to monitor activation of the NMDAR. NMDA (100 μ M), applied for 5 to 10 min to acutely isolated hippocampal neurons in 0 Mg^{2+} solution to enhance NMDA currents without requiring simultaneous membrane depolarization, evoked rapid rises in intracellular calcium concentration ($[Ca]_i$) that persisted after washout of the agonist. Calcein red/orange efflux from single neurons occurred with a delay (average 7.9 ± 1.6 min; $n = 7$ number of cells) after the NMDA-induced $[Ca]_i$ rise, (Fig. 1, D to F). Dye efflux was blocked when 100 μ M $^{10}panx$ was present (Fig. 1, E and F) (1, 14).

By using RNA interference of Px1 in cultured hippocampal neurons, we next confirmed that the NMDAR-evoked I_{2nd} was due to Px1 hemichannels. We first demonstrated that short hairpin RNA (shRNA) delivered to cultured hippocampal neurons via lentivirus (see supporting online material) reduced Px1 levels. Infection of cultured neurons with green fluorescent protein (GFP) and the shRNA vector was achieved at >80% efficiency and with minimal infection of non-neuronal cells. This resulted in knockdown of the Px1 protein in the total culture to $43 \pm 10\%$ of control ($P < 0.05$; ANOVA; $n = 4$), as determined by Western blot analysis with an antibody against a C-terminal region of Px1 (Fig. 2A) (15). The remaining 43% may be due to expression of Px1 in other cell types in the culture, such as astrocytes (16), and incomplete efficacy of the shRNA. We then used sister cultures to test whether the NMDAR I_{2nd} was reduced after shRNA knockdown of Px1. Intensely GFP-positive (that is, shRNA-expressing) neurons were patch-clamped, and NMDA (100 μ M) was applied for 2 to 10 min, which activated I_{2nd} (Fig. 2, B and D). Maximal activation was achieved after 5 min of agonist application (Fig. 2, B and D). The Px1 inhibitor, $^{10}panx$ (100 μ M) blocked activation of I_{2nd} (Fig. 2, C and D), and shRNA-expressing neurons had significantly reduced I_{2nd} (by >70%),

¹Department of Psychiatry and Brain Research Centre, University of British Columbia, 2211 Wesbrook Mall, Vancouver, BC V6T 2B5, Canada. ²Robarts Research Institute, University of Western Ontario, London, ON N6A 5K8, Canada.

*Present address: Department of Cell Biology and Anatomy and Hotchkiss Brain Institute, University of Calgary, 3330 Hospital Drive Northwest, Calgary, AB T2N 4N1, Canada.

†To whom correspondence should be addressed. E-mail: rj.thompson@ucalgary.ca (R.J.T.); bmacvicar@brain.ubc.ca (B.A.M.)

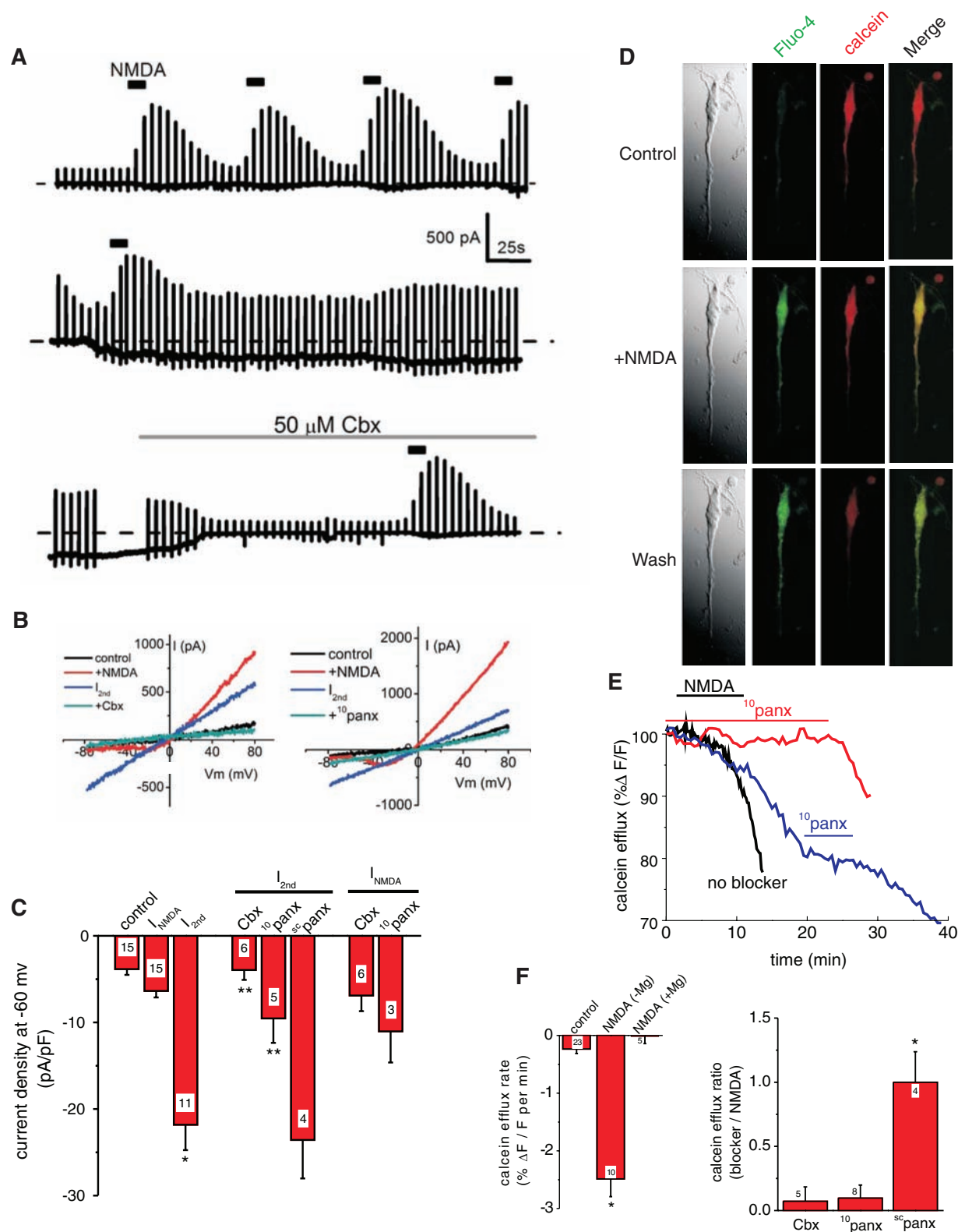


Fig. 1. NMDAR activation opens Px1 hemichannels in hippocampal neurons. **(A)** Continuous voltage-clamp recording ($V_m = -60$ mV) from a neuron exposed to repetitive 10 s applications of 100 μ M NMDA (bars). I_{2nd} (downward shift in middle trace) was blocked by carbenoxolone (Cbx). Each spike is an applied voltage ramp from -80 to $+80$ mV. **(B)** Current-voltage plots of applied voltage ramps. I_{2nd} was inhibited by Cbx and a peptide inhibitor of Px1, 10 panx. **(C)** Quantification of NMDAR current (I_{NMDA}) and I_{2nd} recorded from isolated hippocampal neurons. Activation of I_{2nd} was significantly (asterisk) larger than

control and blocked (two asterisks) by Cbx or 10 panx, but not scrambled 10 panx (sc panx). I_{NMDA} (before I_{2nd} activation) was not affected by Cbx or 10 panx. Error bars indicate SEM. **(D)** Acutely isolated hippocampal neuron loaded with Fluo-4 and calcein red/orange. Calcium remained elevated and calcein red/orange efflux occurred after NMDA exposure. **(E)** Efflux was blocked by 10 panx when applied concomitantly with NMDA (red) or once dye loss had begun (blue), as quantified in **(F)**. Cbx, 10 panx, and Mg^{2+} prevented efflux. In the right graph of **(F)**, a value of 1.0 indicated no effect of the blocker.

but those infected with a scrambled shRNA were not different from control (Fig. 2, A, C, and D). The residual currents that remained (<30% of control) in the shRNA-infected individual neurons (Fig. 2, C and D) were probably due to incomplete block of Px1 expression by shRNA vectors, but the possibility that other cation channels make a minor contribution cannot be excluded.

The activation of Px1 hemichannels by NMDAR stimulation and the reported expression of these hemichannels at postsynaptic sites (3) raised the interesting possibility that Px1 can be opened by synaptically released glutamate. Hippocampal slices were thus exposed to low Mg^{2+}

concentrations plus 5 mM KCl to potentiate NMDAR currents in intact tissue. These slices displayed a pattern of rhythmic epileptiform-like bursting called interictal spiking—a correlate to repetitive bursting electroencephalography rhythms observed in epilepsy patients (17). We confirmed that the initiation of interictal bursts in brain slices was triggered by synaptic NMDAR activation, as previously reported (18), by blocking the induction of bursting with NMDAR antagonists. We tested whether Px1 hemichannels are opened by synaptic activity (during 0 Mg^{2+} triggered bursting) via measuring dye uptake by neurons through Px1 and the electrophysiological contribution of Px1 to interictal discharges.

Exposure of 400- μ m-thick rodent brain slices to nominally Mg^{2+} -free solutions induced uptake of a fluorescent dye, sulforhodamine 101 (SR101), into neurons in the CA1 region of the hippocampus (Fig. 3). SR101 is normally a selective marker of astrocytes and is excluded from neurons (Fig. 3A) (19). However, in our previous work, SR101 influx into cortical neurons occurred during ischemia and was indicative of Px1 opening (1). In 0 Mg^{2+} exposed hippocampal slices, SR101 influx into CA1 hippocampal neurons was observed (Fig. 3A), and dye influx was blocked by 10 panx or pre-treatment with 50 μ M APV [(2R)-amino-5-phosphonovaleric acid], an NMDAR antagonist (Fig. 3).

Fig. 2. NMDAR I_{2nd} block by RNA interference of Px1. (A) Cultured hippocampal neurons infected with GFP and shRNA against Px1 had significant ($P < 0.05$, ANOVA) knockdown of the hemichannel, as assayed by Western blot. siRNA, small interfering RNA. Error bars indicate SEM. (B) Time-dependent activation of the I_{2nd} on exposure of cultures to NMDA (arrow) for the time indicated. (C) 10 panx blocked the I_{2nd} activated by 5-min NMDA. Knockdown of Px1 with shRNA, but not a scrambled shRNA (sc), blocked the I_{2nd} recorded from GFP-positive neurons. (D) Quantification of I_{2nd} (at -60 mV) of cultured hippocampal neurons exposed to NMDA. All statistical comparisons were made to the current amplitude for a 5-min exposure to NMDA (ANOVA; $P < 0.05$). The asterisk indicates a significant difference from the 5-min NMDA application.

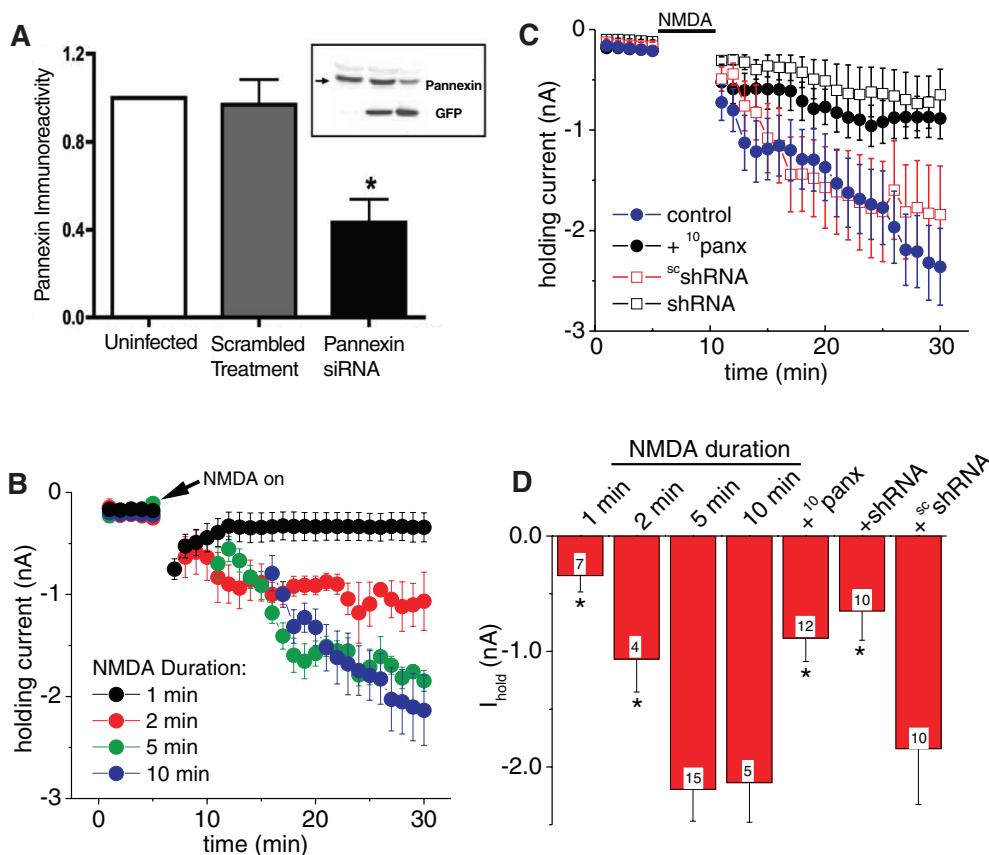
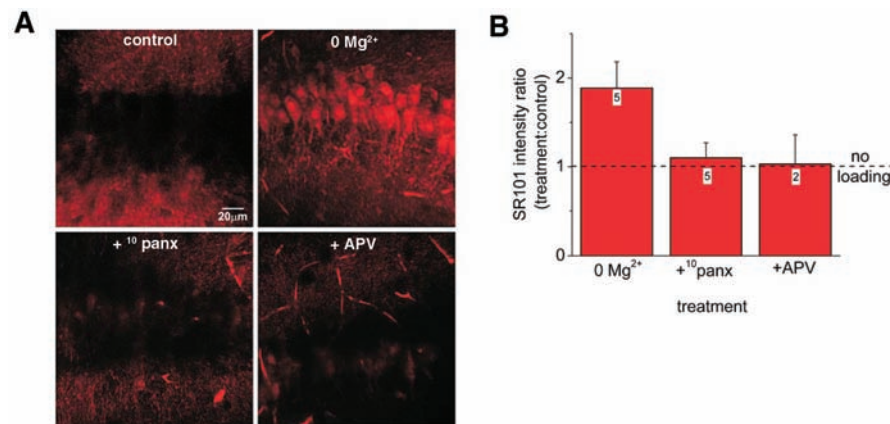


Fig. 3. NMDAR potentiation in hippocampal brain slices opens Px1. (A) CA1 region of the hippocampus is shown 75 μ m deep into 400- μ m slices. The red fluorescent dye SR101 is excluded from neurons (control). A 1-hour exposure to Mg^{2+} -free (+5 mM KCl) bathing solution evoked dye uptake that was blocked by 10 panx or APV. (B) Dye uptake, expressed as fluorescence intensity after treatment with 0 Mg^{2+} , 0 Mg^{2+} + 10 panx, or 0 Mg^{2+} + APV as the ratio of SR101 intensity to that in control slices. Error bars indicate SEM.



To further test the involvement of Px1 in hippocampal synaptic function, we recorded the extracellular field potentials that spontaneously occur after a ~1-hr exposure of hippocampal slices to 0 Mg^{2+} plus 5 mM KCl bathing solutions. These interictal bursts (Fig. 4A) in the CA1 region occurred at 0.6 ± 0.2 Hz ($n = 5$ slices), and the addition of $^{10}panx$ reduced the interburst frequency by $24 \pm 6\%$, which recovered to $103 \pm 8\%$ of control upon washout of the blocking peptide (Fig. 4, A, B, and D). Block of Px1 during interictal bursting also decreased the mean amplitude of spikes within a burst by $34 \pm 6\%$ ($P < 0.05$ by ANOVA), with recovery to $73 \pm 12\%$ of control ($n = 5$) (Fig. 4, A to C). When $^{10}panx$ was coapplied initially with the 0 Mg^{2+} solutions, interictal bursting still occurred, but the amplitude and frequency increased after

washout of the peptide (fig. S2). The effect of Px1 block on spike properties and bursting in the epileptic-like hippocampus was not attributable to nonspecific inhibition of fast (AMPA receptor-mediated) synaptic transmission because $^{10}panx$ did not affect field potentials evoked by stimulation of the Schaeffer collateral pathway in the presence of 2 mM extracellular Mg^{2+} (Fig. 4D).

The data presented here demonstrate that Px1 hemichannels are activated by NMDARs and contribute to postsynaptic responses in the hippocampus during seizure-like activity. This result is consistent with Px1 providing a tonic depolarizing current in dendrites during intense NMDAR activity. This could be initiated either synaptically or extra-synaptically, but the presence of Px1 in the postsynaptic density suggests that synaptic

activation of Px1 is probably involved. We have determined that Px1 hemichannels constitute a major portion of the NMDAR-evoked I_{2nd} which can lead to Ca^{2+} deregulation in hippocampal pyramidal neurons and possibly to the establishment of acquired epilepsy (4–6, 20). It has been suggested that interneuronal gap junctions contribute to epileptogenesis in the hippocampus (21). It will be interesting to determine the relation between these junctions and Px1 hemichannel activation during seizures.

What is the mechanism that links NMDAR to Px1 activation? Surprisingly, it does not appear to involve increased intracellular Ca^{2+} , because altering neuronal Ca^{2+} buffering did not affect Px1 opening (fig. S3). The mechanism may, however, involve intracellular adenosine triphosphate (ATP) depletion during NMDAR activation (22), be-

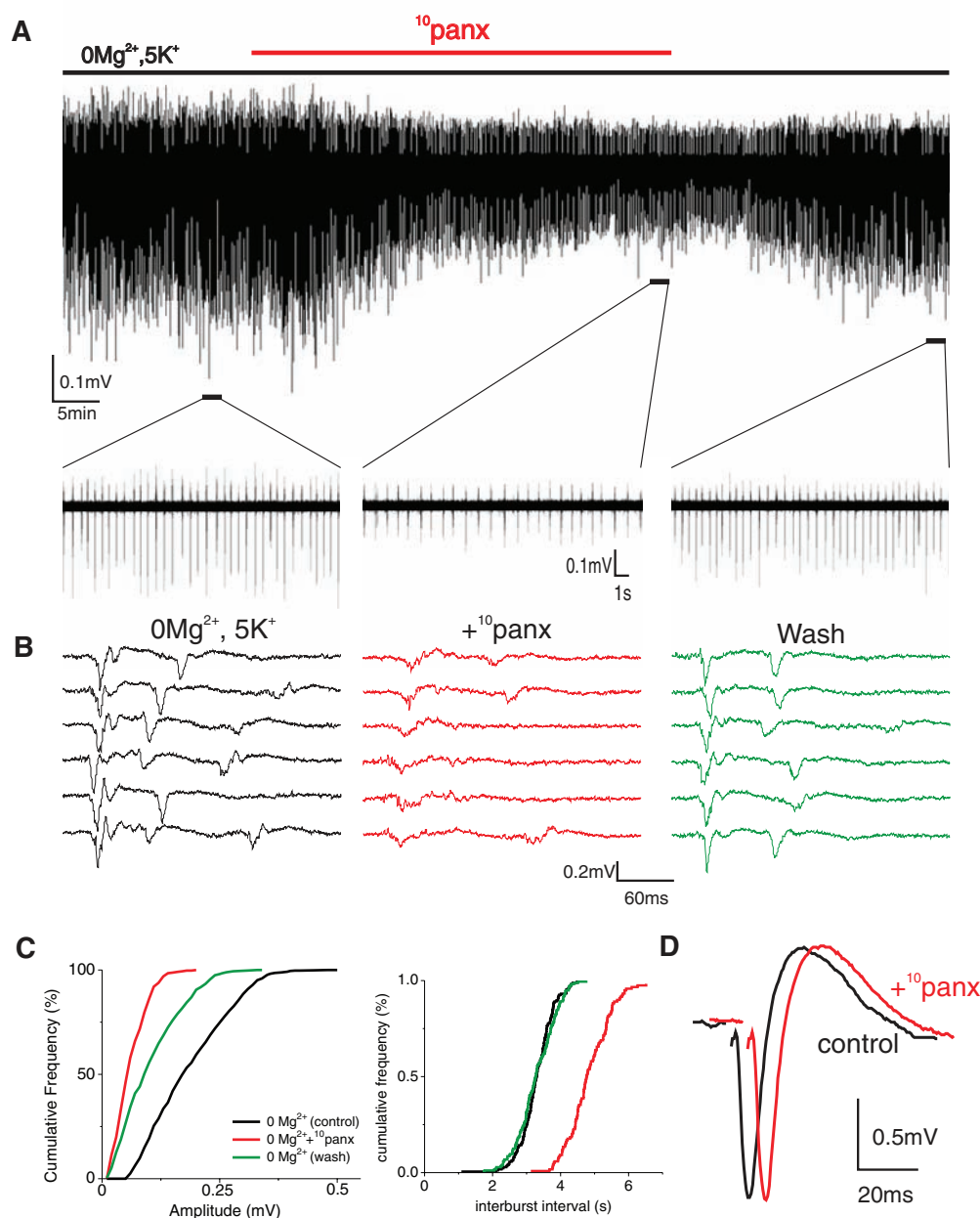


Fig. 4. Px1 block alters bursting properties of hippocampal neurons during seizure-like events. **(A)** Interictal spiking, induced by low Mg^{2+} concentration plus 5 mM KCl, was affected by $^{10}panx$. Decreases in burst frequency and amplitude are evident. **(B)** Expanded bursts demonstrated significant (ANOVA; $P < 0.05$) alteration of electrophysiological properties by Px1 inhibition. **(C)** Cumulative frequency plots of spike amplitude and interburst interval showing decreased spike amplitude and a longer interval between bursts when Px1 was blocked. **(D)** Evoked potentials by stimulation of Schaeffer collaterals in the presence of 2 mM extracellular Mg^{2+} to block NMDARs, demonstrating that $^{10}panx$ did not directly block fast synaptic transmission via AMPA receptors.

cause intracellular perfusion with 4 mM MgATP significantly protected against Px1 activation; current density was -30.2 ± 8.6 pA/pF ($n = 3$) with 1 mM MgATP and -9.4 ± 3.7 pA/pF ($n = 5$) with 4 mM MgATP. We recently reported that Px1 is opened by ischemia (1) and that the timing of this opening appears to follow the anoxic depolarization (23) in a manner analogous to Px1 activation after NMDAR stimulation. Therefore, Px1 not only appears to be involved in neuronal dysfunction during ischemia but also plays a role in the potentiation of seizure-like activity. These unique ion channels should therefore be considered important targets for the treatment of neurological disorders such as epilepsy and stroke.

References and Notes

- R. J. Thompson, N. Zhou, B. A. MacVicar, *Science* **312**, 924 (2006).
- S. Locovei, L. Bao, G. Dahl, *Proc. Natl. Acad. Sci. U.S.A.* **103**, 7655 (2006).
- G. Zoidl et al., *Neuroscience* **146**, 9 (2007).
- Q. X. Chen, K. L. Perkins, D. W. Choi, R. K. S. Wong, *J. Neurosci.* **17**, 4032 (1997).
- J. A. Connor, R. J. Cormier, *J. Neurophysiol.* **83**, 90 (2000).
- M. Tymianski, M. P. Charlton, P. L. Carlen, C. H. Tator, *J. Neurosci.* **13**, 2085 (1993).
- Materials and methods are available as supporting material on Science Online.
- R. Bruzzone, S. G. Hormuzdi, M. T. Barbe, A. Herb, H. Monyer, *Proc. Natl. Acad. Sci. U.S.A.* **100**, 13644 (2003).
- P. Pelegri, A. Surprenant, *EMBO J.* **25**, 5071 (2006).
- Single-letter abbreviations for the amino acid residues are as follows: A, Ala; C, Cys; D, Asp; E, Glu; F, Phe; G, Gly; H, His; I, Ile; K, Lys; L, Leu; M, Met; N, Asn; P, Pro; Q, Gln; R, Arg; S, Ser; T, Thr; V, Val; W, Trp; and Y, Tyr.
- L. Bao, S. Locovei, G. Dahl, *FEBS Lett.* **572**, 65 (2004).
- C. Virginio, A. MacKenzie, R. A. North, A. Surprenant, *J. Physiol.* **519**, 335 (1999).
- D. C. Spray, Z.-C. Ye, B. R. Ransom, *Glia* **54**, 758 (2006).
- P. Pelegri, A. M. Surprenant, *EMBO J.* **25**, 5071 (2007).
- S. Penuela et al., *J. Cell Sci.* **120**, 3772 (2006).
- Y. Huang, J. B. Grinspan, C. K. Abrams, K. S. Scherer, *Glia* **55**, 46 (2007).
- H. Walther, J. D. C. Lambert, R. S. G. Jones, U. Heinemann, B. Hamon, *Neurosci. Lett.* **69**, 156 (1986).
- J. P. Dreier, U. Heinemann, *Neurosci. Lett.* **119**, 68 (1990).
- A. Nimmerjahn, F. Kirchhoff, J. N. D. Kerr, F. Helmchen, *Nat. Methods* **1**, 31 (2004).
- E. A. Waxman, D. R. Lynch, *Neuroscientist* **11**, 37 (2005).
- M. V. L. Bennett, A. Pereda, *Brain Cell Biol.* **35**, 5 (2007).
- T. A. Vander Jagt, J. A. Connor, C. W. Shuttleworth, *J. Neurosci.* **28**, 5029 (2008).
- T. H. Murphy, P. Li, K. Betts, R. Liu, *J. Neurosci.* **28**, 1756 (2008).
- This work was supported by grants to B.A.M. from the Heart and Stroke Foundation of British Columbia, to B.A.M. or J.F.M. (15514) from the Canadian Institutes of Health Research, and by a grant from the Canadian Stroke Network to B.A.M., J.F.M., and R.J.T. B.A.M. holds a Canada Research Chair (Tier 1) in Neuroscience. The authors kindly acknowledge Y. T. Wang for critical reading of the manuscript and S. Panuela and D. Laird for generously providing the anti-Px1 antibody.

Supporting Online Material

www.sciencemag.org/cgi/content/full/322/5907/1555/DC1
Materials and Methods

Figs. S1 to S3
References

27 August 2008; accepted 29 October 2008
10.1126/science.1165209

Centromere-Associated Female Meiotic Drive Entails Male Fitness Costs in Monkeyflowers

Lila Fishman* and Arpiar Saunders†

Female meiotic drive, in which paired chromosomes compete for access to the egg, is a potentially powerful but rarely documented evolutionary force. In interspecific monkeyflower (*Mimulus*) hybrids, a driving *M. guttatus* allele (*D*) exhibits a 98:2 transmission advantage via female meiosis. We show that extreme interspecific drive is most likely caused by divergence in centromere-associated repeat domains and document cytogenetic and functional polymorphism for drive within a population of *M. guttatus*. In conspecific crosses, *D* had a 58:42 transmission advantage over nondriving alternative alleles. However, individuals homozygous for the driving allele suffered reduced pollen viability. These fitness effects and molecular population genetic data suggest that balancing selection prevents the fixation or loss of *D* and that selfish chromosomal transmission may affect both individual fitness and population genetic load.

In the female meioses of both plants and animals, all but one of the meiotic products generally degenerate (1). This asymmetry of cell fate can allow homologous chromosomes to compete for inclusion in the single surviving egg or megaspore, a process termed “female meiotic drive” (1–4). Female meiotic drive may explain the rapid diversification of centromeres, the DNA-protein complexes that mediate chromosomal segregation (5), and may promote speciation through the evolution of hybrid incompatibilities (5) and karyotypic rearrangements (6). Because nondisjunction during chromosomal competition can cause infertility (2, 5), female meiotic drive may also contribute to genetic variation for reproduc-

tive fitness within populations (7), a central issue in evolutionary biology (8–12) and human health. Despite its potential importance as an evolutionary force, little is known about female meiotic drive in natural populations.

The female meiotic-drive locus in *Mimulus* (*D*) exhibits extreme non-Mendelian segregation through female meiosis in hybrids between *M. guttatus* (IM62 inbred line) and its close relative *M. nasutus* (SF inbred line), which is predominantly self-fertilizing (13, 14). As seed parents, interspecific heterozygotes transmit >98% *M. guttatus* (IM62) alleles at markers tightly linked to *D*, and there is no evidence of postmeiotic mechanisms of transmission ratio distortion (13). Near-complete transmission bias via female meiosis suggests that *D* is the functional centromere of the chromosome corresponding to the linkage group [linkage group 11 (LG11)] on which it is located (13), because only the centromere (and linked loci) can attain >83.3% transmission via

female drive (15). To test this inference, we cytogenetically mapped *D* in *M. guttatus*, *M. nasutus*, and interspecific hybrids (Fig. 1) (SOM text). Because plant centromeres generally consist of megabases of tandemly repetitive DNA with individual repeats 150 to 1000 base pairs (bp) in length (16, 17), we searched the *M. guttatus* (IM62 line) 6× draft whole-genome sequence [Mimulus Genome Project, U.S. Department of Energy (DOE) Joint Genome Institute] for repeats with those features. A probe for the most common class of repeat found, 728 bp in length (Cent728; fig. S1), hybridized to a single narrow band near the center of each IM62 metaphase chromosome (Fig. 1A and fig. S2A). However, a single pair of homologous chromosomes exhibited two unusually large regions of hybridization (arrows; Fig. 1A and fig. S2A). A probe for the *CycA* genetic marker tightly linked to *D* (13) localized between the large Cent728 arrays on this chromosome (Fig. 1B and fig. S2B), demonstrating that this distinctive chromosomal structure (henceforth, C11.2) corresponds to the driving region of IM62 LG11. The region of Cent728 hybridization on each non-C11.2 chromosome was flanked by arrays of typically pericentromeric retrotransposons (Fig. 1C and fig. S2C) (18). This pattern suggests that Cent728 is, if not the centromere-specifying DNA repeat, a marker for centromeric chromosomal regions. Although we cannot yet determine whether the molecular mechanism of *Mimulus* drive is strictly centromeric (5) and whether the duplication and expansion of Cent728 arrays is causal, this association is consistent with the genetic evidence for centromeric drive (13, 15).

We examined metaphase chromosomes from nearly isogenic lines (NILs) containing heterozygous introgressions of *M. guttatus* *D* in a largely *M. nasutus* genetic background (13). Both strong Cent728 arrays from IM62 C11.2 appear present in the NILs (Fig. 1D and fig. S2D), which

Division of Biological Sciences, University of Montana, Missoula, MT 59812, USA.

*To whom correspondence should be addressed. E-mail: lila.fishman@mso.umt.edu

†Present address: Program in Neuroscience, Harvard Medical School, Boston, MA 02115, USA.

indicates that they were transmitted as a single genetic unit over five generations of recombination (there is a single weak Cent728 array on LG11 in the SF *M. nasutus* parent; fig. S3). Thus, the two IM62 C11.2 arrays are inherited as a single genetic locus. The large physical size of the D locus is similar to that of the best-known female meiotic drive system, Ab10-knob in maize (19), but in that case the drive elements are DNA arrays (knobs) that segregate as genetic loci unlinked from the centromeric regions (20). In contrast, our data suggest that female meiotic drive in *Mimulus* results from competition between chromosomal homologs divergent in centromere-associated repetitive DNA arrays. Regardless of its molecular mechanism, *Mimulus* drive differs from maize drive in its genomic location relative to centromeres (19–21) and thus provides a comparative model for understanding selfish chromosomal evolution.

To investigate drive within *M. guttatus*, we examined Cent728 hybridization to chromosomes from inbred lines from the Iron Mountain *M. guttatus* population (10). Some lines completely lacked the distinct C11.2 found in IM62 (Fig. 1E and fig. S2E), suggesting that the driving chromosome is structurally divergent from homologs within the same species. The Iron Mountain *M. guttatus* population is also polymorphic for heterospecific female meiotic drive, exhibiting discrete variation in segregation patterns at drive-linked markers (Fig. 2). Of the eight independently derived inbred lines test-crossed to *M. nasutus*, four exhibited strongly distorted segregation (*M. guttatus* allele transmitted at ~95% via F₁ female meiosis) similar to SF × IM62 hybrids (13, 14) and four exhibited Mendelian segregation. Thus, the driving allele (*D*) is at intermediate frequency in this *M. guttatus* population, along with nondriving alternative alleles (henceforth, *D*[−]). In addition, all three nondriving lines that we examined cytogenetically (including IM767; Fig. 1E and fig. S2E) lack the C11.2 arrays, supporting the inference that drive is associated with chromosomal divergence. This analysis also revealed that allelic variation at the microsatellite marker *aat356* (13, 14) was diagnostic for the drive genotype, because all five *D* lines shared the most common 180-bp allele [overall frequency = 37 out of 113 lines tested (33%)], whereas the four *D*[−] lines were diverse and carried other alleles (*P* < 0.008; Fisher’s exact test).

Because the driving *D* allele shows a near-complete transmission advantage over *M. nasutus* alleles via female meiosis (13), we tested whether it exhibits female drive against alternative conspecific genotypes by examining segregation in within-population test-crosses (SOM text). On average, *D* displayed a 58:42 conspecific transmission advantage via female meiosis ($\chi^2 = 4.45$, *P* = 0.035), but was transmitted in a Mendelian fashion via male meiosis ($\chi^2 = 0.51$, *P* = 0.475), resulting in 16% excess transmission of *D* via female function. Thus, although weaker than heterospecific drive, chromosomal competition appears to be a potent selective force within this

Fig. 1. Fluorescence in situ hybridization to *M. guttatus* lines and *M. nasutus* × *M. guttatus* hybrids (2*N* = 28). (A) IM62 *M. guttatus* metaphase karyotype showing a single band of Cent728 hybridization (green) on each chromosome and two large regions of Cent728 hybridization on one pair of chromosomes (arrows). (B) Colocalization of a genetic marker for drive (*Cycl*; red; above) with C11.2 Cent728 arrays (merged; below). (C) Pachytene IM62 chromosomes with Cent728 (green; above) and flanking *Mg_Copia69.2* retrotransposon arrays (red; overlay with Cent728 below). (D) C11.2 (arrow) from IM62 introgressed into *M. nasutus* genetic background. (E) IM767, an independent inbred line derived from the Iron Mountain *M. guttatus* population. Each image includes merged false-colored images of DNA-bound DAPI (4′,6-diamidino-2-phenylindole) (blue) with images of additional probes labeled in Alexa-Fluor (green) and/or Texas Red (red); component images are in fig. S2. Scale bar: 2 μ m.

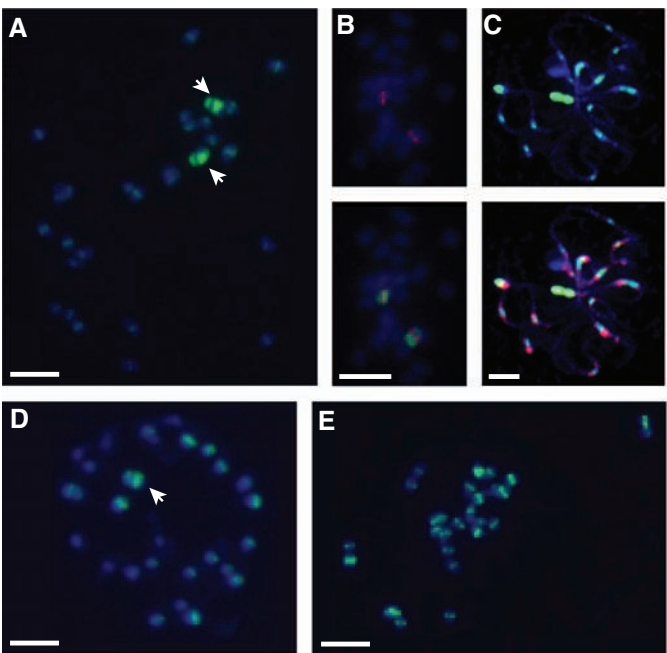


Fig. 2. Cumulative frequencies of *M. nasutus* homozygotes (NN; black), *M. guttatus* homozygotes (GG; white), and heterozygotes (NG; gray) for eight F₂ testcross families. By χ^2 tests (df = 2), four families (*D*) differed significantly (all *P* < 0.0001) from Mendelian segregation (1:2:1; NN:NG:GG), but not from the IM62 heterospecific drive expectation of 2:49:49 (*P* range: 0.12 to 0.40), whereas four families (*D*[−]) did not differ from Mendelian (*P* range: 0.34 to 0.97).

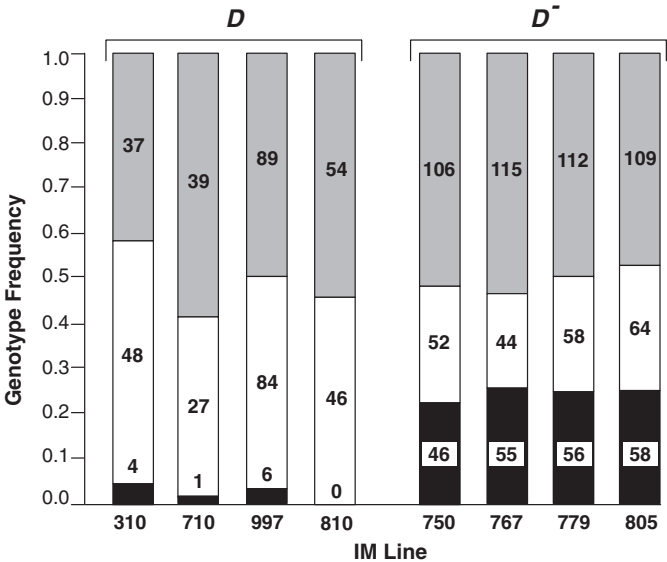
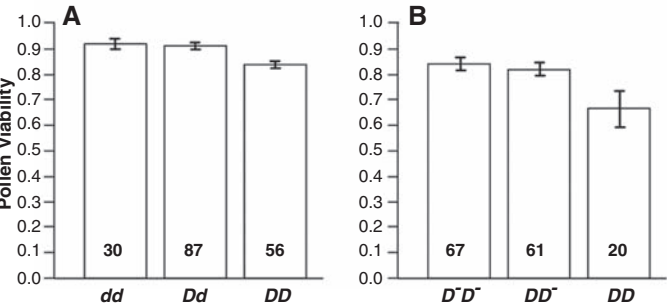


Fig. 3. Mean pollen viability (\pm SEM) of drive genotypes in (A) controlled heterospecific genetic background and environment and (B) wild *M. guttatus* plants. In both cases, the overall effect of *D* genotype was highly significant (one-way analysis of variance: *P* < 0.007) and *DD* homozygotes had significantly lower pollen viability than the other genotypes, which did not differ from each other. (A) Least squares means (LSMs) contrasts. *DD* versus other: *P* = 0.0003; *dd* versus *Dd*: *P* = 0.82. (B) LSMs contrasts. *DD* versus other: *P* = 0.0018; *D[−]D[−]* versus *DD[−]*: *P* = 0.59.



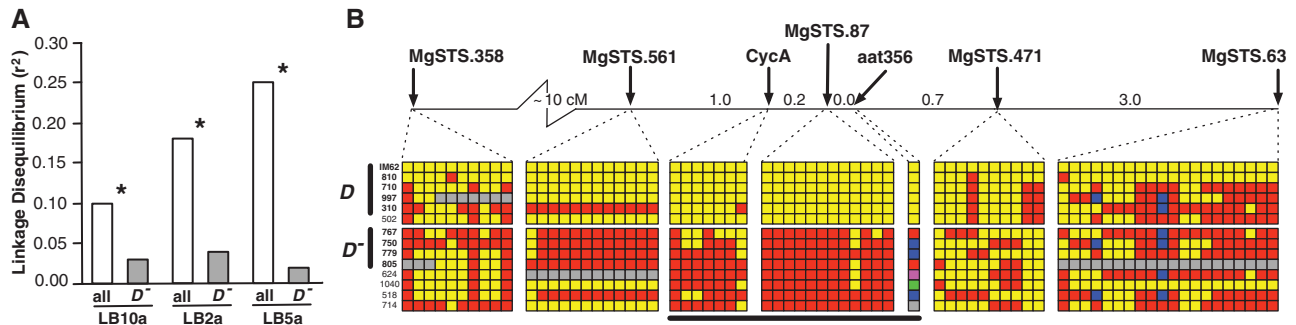


Fig. 4. (A) LD between *CycA* BAC microsatellites and *aat356* for all *D* and *D⁻* lines ($N = 74$) and *D⁻* lines only ($N = 45$). Asterisks indicate significant LD ($P < 0.05$). (B) Haplotype structure in the region flanking *D* (map location underlined) (13). Polymorphic sites (singletons excluded) are

shown (IM62 reference sequence: yellow; alternative alleles: blue, pink, green, and red; missing data: gray). The nine lines of known heterospecific drive phenotype (*D* and *D⁻*, respectively) are linked by vertical lines. See SOM text for methods. Full alignments are in fig. S4.

interbreeding population. The difference in strength between heterospecific and conspecific drive suggests that suppression of drive has evolved within *M. guttatus* or that genomic divergence between *M. guttatus* and *M. nasutus* intensifies chromosomal competition.

In the absence of countervailing selection, we would expect conspecific female drive to rapidly fix the driving *D* allele. Therefore, the observed polymorphism within the Iron Mountain *M. guttatus* population predicts that female meiotic drive has deleterious effects on individual fitness. We characterized the male fitness effects of heterospecific drive in the segregating progeny of a NIL with a heterozygous introgression at *D* (*Dd*, where *d* is the nondriving *M. nasutus* allele) (13). *DD* homozygotes had significantly reduced pollen viability relative to *Dd* heterozygotes and *dd* homozygotes (Fig. 3A). Because female meiotic drive in heterospecific (*Dd*) heterozygotes was near 100%, this suggests that even strongly biased chromosomal segregation may impose little direct cost via nondisjunction. This result supports the assumption of costs in the female meiotic drive model of centromere evolution (5), but rejects non-random chromosomal segregation in heterozygotes as the mechanism of drive costs in this system.

We assessed the effects of *D* on male fertility in wild *M. guttatus* plants at the Iron Mountain population (SOM text). The inferred genotype at the *D* locus strongly affected pollen viability in the field (Fig. 3B). *DD* homozygotes suffered a 20% reduction in pollen viability relative to other genotypic classes. Thus, deleterious recessive effects of *D* contribute to male fitness variation under natural conditions. Pollen inviability may be a pleiotropic effect of meiotic interactions between paired C11.2 homologs that cause nondisjunction or may reflect hitchhiking at a locus linked to *D*, because the C11.2 region contains expressed genes (SOM text).

The opposition of female meiotic drive and associated male fertility costs may produce a true balanced polymorphism in *M. guttatus*. In a random mating population, selection against a female meiotic drive allele in homozygous males must be approximately greater than twice its advantage in heterozygous females to prevent its fixation (Eq.

S1). Given the measured male fertility cost of ~0.20 to *D* homozygotes, any female-specific transmission ratio distortion below 60:40 should result in a protected polymorphism. Our observation of a 58:42 transmission advantage for *D* is within this range, indicating that *D* cannot be lost and is unlikely to fix under current conditions.

Patterns of molecular polymorphism and linkage disequilibrium (LD) also suggest short-term balancing selection or an ongoing selective sweep by *D* (22). We estimated LD between the drive-diagnostic marker *aat356* and three highly polymorphic microsatellites (6 to 19 alleles each; table S2A) that are physically associated with *CycA* and located at least 45 kb from *aat356* (SOM text). Like *aat356*, these markers each had one or two alleles only found in *D* lines, leading to high pairwise LD with *aat356* across all lines analyzed ($N = 74$; Fig. 4A). This was due to the low polymorphism of the inferred *D* lines, because inferred *D⁻* lines ($N = 45$) were diverse and exhibited no significant LD when analyzed separately. Sequencing of the nine lines of known drive phenotype confirmed the uniqueness of the driving haplotype and revealed that drive-specific LD extends up to 2 cM (Fig. 4B and fig. S4). Thus, the driving allele *D* is a single physically and genetically extensive haplotype associated with the C11.2 chromosomal structure. As in maize (21), structural differences between driving and nondriving haplotypes (which may cause variation in recombination rate) complicate the interpretation of molecular population genetic data. However, the extent and uniformity of the *D* haplotype are consistent with recent selfish spread via female meiotic drive.

We have shown that selfish chromosomal drive has brought an allele with unconditionally deleterious effects on individual fitness to high frequency in a primarily outcrossing wildflower population. This high frequency contrasts with the generally low frequency of male drive elements (23, 24), which generally achieve excess transmission via the postmeiotic disabling of gametes with alternative genotypes, often entailing high fitness costs in heterozygotes. Female meiotic drivers such as *D*, which take advantage of the intrinsic asymmetry of female meiosis and

may have primarily recessive costs, may spread to high frequency despite biologically significant effects. Biometric tests (10) have found more standing variation for pollen viability at Iron Mountain than predicted under mutation-selection balance models, and female meiotic drive by *D* may account for this unexpectedly high genetic load. By contributing to inbreeding depression for male fertility, *D* may play an important role in mating system and floral trait evolution in monkeyflowers.

Untangling the molecular mechanism and evolutionary origins of *Mimulus* drive remains a challenge, as we do not yet know whether *D* biases transmission by using the machinery of normal centromere function or via an alternative mechanism. Regardless of mechanism, however, it is clear that selfish chromosomal drive can be an important determinant of fitness variation within natural populations.

References and Notes

1. F. Pardo-Manuel de Villena, C. Sapienza, *Mamm. Genome* **12**, 331 (2001).
2. M. E. Zwick, J. L. Salstrom, C. H. Langley, *Genetics* **152**, 1605 (1999).
3. R. K. Dawe, E. N. Hiatt, *Chromosome Res.* **12**, 655 (2004).
4. G. Wu et al., *Genetics* **170**, 327 (2005).
5. S. Henikoff, K. Ahmad, H. S. Malik, *Science* **293**, 1098 (2001).
6. F. Pardo-Manuel de Villena, C. Sapienza, *Genetics* **159**, 1179 (2001).
7. A. Daniel, *Am. J. Med. Genet.* **111**, 450 (2002).
8. R. C. Lewontin, *The Genetic Basis of Evolutionary Change* (Columbia Univ. Press, New York, 1974).
9. N. H. Barton, P. D. Keightley, *Nat. Rev. Genet.* **3**, 11 (2002).
10. J. K. Kelly, *Genetics* **164**, 1071 (2003).
11. T. Johnson, N. Barton, *Philos. Trans. R. Soc. London B* **360**, 1411 (2005).
12. B. Charlesworth, T. Miyo, H. Borthwick, *Genet. Res.* **89**, 85 (2007).
13. L. Fishman, J. H. Willis, *Genetics* **169**, 347 (2005).
14. L. Fishman, A. Kelly, E. Morgan, J. H. Willis, *Genetics* **159**, 1701 (2001).
15. H. S. Malik, *Trends Ecol. Evol.* **20**, 151 (2005).
16. J. Jiang, J. A. Birchler, W. A. Parrott, R. K. Dawe, *Trends Plant Sci.* **8**, 570 (2003).
17. J. C. Lamb, W. Yu, F. Han, J. A. Birchler, *Curr. Opin. Plant Biol.* **10**, 116 (2007).
18. A. Kumar, J. L. Bennetzen, *Annu. Rev. Genet.* **33**, 479 (1999).
19. J. A. Birchler, R. K. Dawe, J. F. Doebley, *Genetics* **164**, 835 (2003).
20. E. S. Buckler IV et al., *Genetics* **153**, 415 (1999).
21. R. J. Mroczek, J. R. Melo, A. C. Luce, E. N. Hiatt, R. K. Dawe, *Genetics* **174**, 145 (2006).

22. D. Charlesworth, *PLoS Genet.* **2**, e64 (2006).

23. K. G. Ardlie, *Trends Genet.* **14**, 189 (1998).

24. K. A. Dyer, B. Charlesworth, J. Jaenike, *Proc. Natl. Acad. Sci. U.S.A.* **104**, 1587 (2007).

25. We thank J. H. Willis, J. K. Kelly, J. Birchler, D. Charlesworth, H. Malik, C. Barr, V. Ezenwa, D. Emlen, and S. Miller for critical comments; J. H. Willis, C. Wu, T. J. Vision, E. Ganko, L. Bridges, and J. K. Kelly for materials and communicating unpublished results; and D. Pedersen, D. Carvey, T. Huggins, E. Peters, and B. Utgaard for lab, greenhouse, and field assistance. D. Rokhsar and J. Schmutz of DOE Joint Genome Institute provided the *M. guttatus* draft whole-genome sequence. Supported by NSF grants DEB-0316786 (L.F.) and BIO-0328326 (J. H. Willis, L.F., et al.). Sequences have been deposited in GenBank, with the accession numbers FJ147360 to FJ147465.

Supporting Online Material

www.sciencemag.org/cgi/content/full/322/5907/1559/DC1

Materials and Methods

Figs. S1 to S4

Tables S1 and S2

Equation S1

References

5 June 2008; accepted 26 September 2008

10.1126/science.1161406

Maternal Alloantigens Promote the Development of Tolerogenic Fetal Regulatory T Cells in Utero

Jeff E. Mold,^{1,2} Jakob Michaëlsson,³ Trevor D. Burt,^{1,4} Marcus O. Muench,⁵ Karen P. Beckerman,^{6*} Michael P. Busch,⁵ Tzong-Hae Lee,⁵ Douglas F. Nixon,¹ Joseph M. McCune^{1†}

As the immune system develops, T cells are selected or regulated to become tolerant of self antigens and reactive against foreign antigens. In mice, the induction of such tolerance is thought to be attributable to the deletion of self-reactive cells. Here, we show that the human fetal immune system takes advantage of an additional mechanism: the generation of regulatory T cells (T_{regs}) that suppress fetal immune responses. We find that substantial numbers of maternal cells cross the placenta to reside in fetal lymph nodes, inducing the development of CD4+CD25^{high}FoxP3+ T_{regs} that suppress fetal antimaternal immunity and persist at least until early adulthood. These findings reveal a form of antigen-specific tolerance in humans, induced in utero and probably active in regulating immune responses after birth.

Fifty years ago, Billingham, Brent, and Medawar first advanced the concept that “actively acquired immunologic tolerance” in the mouse occurs as a result of fetal exposure to foreign antigens (1). There have since been numerous reports suggesting that the transfer of foreign antigens (including proteins, parasites, and even cells) from the mother to the fetus is a common occurrence (2–4); however, the mechanism by which the fetal immune system recognizes and responds to such antigens is unclear.

Temporal differences in the development of the adaptive immune system vary substantially between species (5). Newborn mice show few signs of peripheral T cell colonization (6), whereas in the human fetus, peripheral lymphoid tissues are populated by T cells as early as 10 gestational weeks (g.w.) (7). Therefore, it is not

clear whether in utero tolerance induction would occur upon fetal exposure to foreign antigens in the human as it does in the mouse (8). In fact, not

much is known about the functional properties of the human fetal immune system: Some reports suggest that it is functionally deficient, whereas others indicate that fetal immune responses to pathogens and vaccines are intact (9–12). In two independent clinical studies (13, 14), specific tolerance toward noninherited maternal alloantigens (NIMAs) was observed in organ transplant recipients, consistent with the possibility that fetal exposure to NIMAs may promote lasting tolerance in humans.

In certain circumstances [for example, severe combined immunodeficiency disease (15)], maternal cells cross the placenta and engraft into human fetal tissues in utero, resulting in “maternal microchimerism” (4). Because the human fetal immune system may be functionally responsive against NIMAs in utero, we wished to understand whether such microchimerism was the exception or the norm. Lymph nodes (LNs) were isolated from the mesentery of 18 fetal products of conception at 18 to 22 g.w. and analyzed for the presence of maternal DNA (16). Maternal microchimerism was observed in 15 out of 18 LN samples (Table 1 and fig. S1), with a

Table 1. Maternal microchimerism in fetal LNs. We analyzed fetal mesenteric lymph nodes (18 to 22 g.w.) for levels of maternal microchimerism with the use of two separate assays (16). Informative HLA types and/or insertion/deletion (in/del) polymorphisms are listed for each donor. “None” refers to situations where no informative HLA type or polymorphisms were identified; “Neg.” refers to samples where no microchimerism was detected; N.A., not applicable.

Sample number	HLA type/ (in/del) marker	% Microchimerism (HLA type)	% Microchimerism (in/del)
1	DR13/SO10	0.3860%	0.3080%
2	None/SO3	N.A.	0.1640%
3	DR11/None	0.8260%	N.A.
4	DR4/None	0.0035%	N.A.
5	None/None	N.A.	N.A.
6	DR9/SO7B	0.0370%	0.0906%
7	DR1/SO6	0.0650%	0.0190%
8	DR13/None	Neg.	N.A.
9	DR7/SO8	0.1780%	0.4934%
10	SO6/None	0.0062%	N.A.
11	None/SO9	N.A.	0.0070%
	SO10		0.0039%
12	DR1/SO4B	0.0312%	0.0234%
13	None/SO9	N.A.	0.4869%
	SO11		0.1933%
14	DR1/None	0.3663%	N.A.
15	DR15/SO3	Neg.	Neg.
16	DR11/None	0.0114%	N.A.
17	DR15/SO3	0.0161%	0.006%
18	DR15/None	0.1158%	N.A.

¹Division of Experimental Medicine, Department of Medicine, University of California at San Francisco (UCSF), San Francisco, CA 94110, USA. ²Biomedical Sciences Graduate Program, UCSF, San Francisco, CA 94143, USA. ³Center for Infectious Medicine, Department of Medicine, Karolinska University Hospital, Karolinska Institutet, 141 86, Stockholm, Sweden. ⁴Department of Pediatrics, Division of Neonatology, UCSF, San Francisco, CA 94143, USA. ⁵Blood Systems Research Institute and Department of Laboratory Medicine, UCSF, San Francisco, CA 94118, USA. ⁶Department of Obstetrics, Gynecology, and Reproductive Sciences, UCSF, San Francisco, CA 94143, USA.

*Present address: Albert Einstein College of Medicine, Bronx, NY 10461, USA.

†To whom correspondence should be addressed. E-mail: mike.mccune@ucsf.edu

frequency (0.0035 to 0.83%) comparable to that reported in nonlymphoid organs from human fetal specimens, neonates, and healthy adults (17, 18). Our analysis of the cellular composition of maternal cells in neonatal cord blood revealed a predominance of hematopoietic cells (fig. S2). To determine whether human fetal T cells are responsive against foreign human leukocyte antigens (HLAs) (alloantigens), fetal (~20 g.w.) lymphocytes from the spleen or LNs (Fig. 1A and fig. S3) were labeled with the dye carboxy-fluorescein diacetate succinimidyl ester and cocultured with irradiated antigen-presenting cells (APCs) from the peripheral blood of a single healthy, unrelated adult donor (19). After 5 days in this mixed leukocyte reaction (MLR), substantial proliferative responses were observed for both CD4⁺ and CD8⁺ fetal T cells (Fig. 1A), prompting the following question: If fetal T cells respond so vigorously against alloantigens in vitro, would they not also respond against NIMAs expressed by ma-

ternal cells that have moved into fetal LNs in utero?

We recently reported that, compared to adults, elevated frequencies of regulatory T cells (T_{regs}) are found in human secondary fetal lymphoid tissues (20). Because T_{regs} are known to regulate maternal immunity to fetal alloantigens (21), we reasoned that fetal T_{regs} may suppress fetal immune responses against invading maternal cells. Depletion of T_{regs} (CD25⁺ T cells) resulted in a highly significant increase in proliferation of fetal T cells against maternal APCs but only a slight increase against unrelated APCs (Fig. 1, B to D). We also noted an increase in proliferation when autologous APCs were used as stimulators, suggesting that T cell responses to self antigens are suppressed by fetal T_{regs} . These data indicate that fetal T cells are not inherently deficient at responding to maternal alloantigens; rather, their function is actively suppressed by a large pool of fetal T_{regs} .

Natural T_{regs} originate in the thymus and are specific for self antigens presented by thymic

epithelial cells (22). We found no difference in the frequency of CD4⁺ FoxP3⁺ T_{regs} between the fetal and infant thymus (fig. S4). In contrast, the frequency of T_{regs} in peripheral lymphoid organs changes markedly during the course of gestation, falling from ~15 to 20% of total CD4⁺ T cells at 12 to 20 g.w. to ~3 to 7% at birth (23). We reasoned that this change in frequency might reflect a greater propensity of naïve fetal T cells to differentiate into T_{regs} in response to stimulation. To test this, we depleted fetal LNs (and spleen) (fig. S5A) of CD25⁺ T_{regs} and stimulated the remaining cells with irradiated APCs from an unrelated donor. After a 5-day culture period, many of the dividing fetal T cells had up-regulated the transcription factor FoxP3, which is directly involved in promoting T_{regs} development and function (24) (Fig. 2A). To further characterize the kinetics of this response, we performed a parallel analysis of FoxP3 up-regulation after stimulation of fetal or adult T cells (depleted of T_{regs}) with a single unrelated donor (Fig. 2B and figs. S5 and S6).

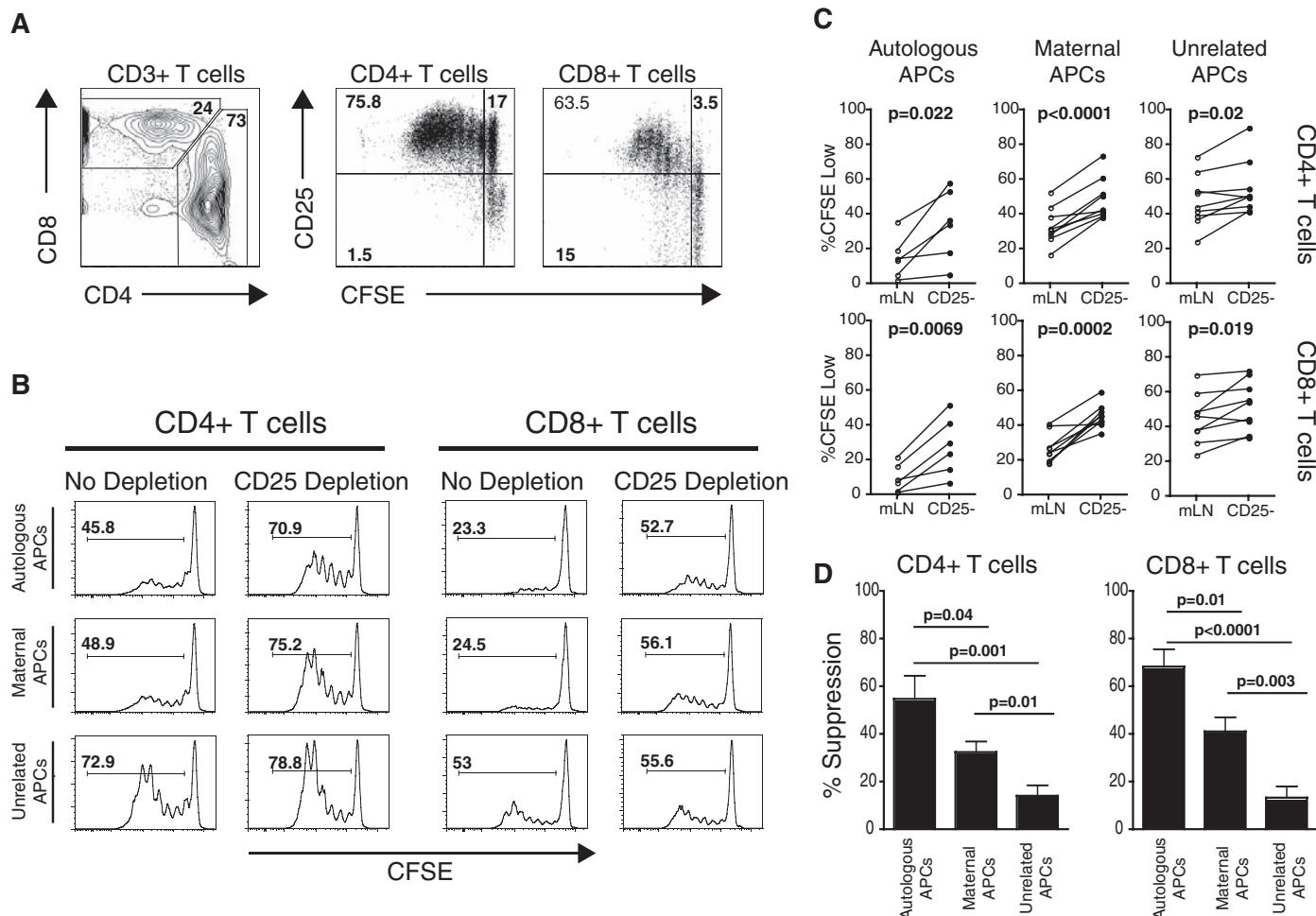


Fig. 1. Fetal T_{regs} suppress fetal T cell responses to maternal alloantigens. **(A)** Fetal T cell proliferation after stimulation with allogeneic APCs from an unrelated donor for 5 days (3:1 ratio of fetal lymphocytes:allogeneic APCs). **(B)** Proliferative responses to autologous, maternal, or unrelated APCs after a 5-day MLR. Histograms depict proliferation in the presence (no depletion) or absence (CD25 depletion) of fetal T_{regs} . CFSE, carboxy-fluorescein di-

acetate succinimidyl ester. **(C)** Summary of all experiments addressing fetal T cell proliferative responses to autologous ($n = 6$), maternal ($n = 9$), or unrelated ($n = 9$) APCs in the presence or absence of fetal T_{regs} . Statistical significance was determined by paired Student's t test. mLN, mesenteric lymph nodes. **(D)** Comparison of T_{regs} suppression against autologous, maternal, or unrelated APCs.

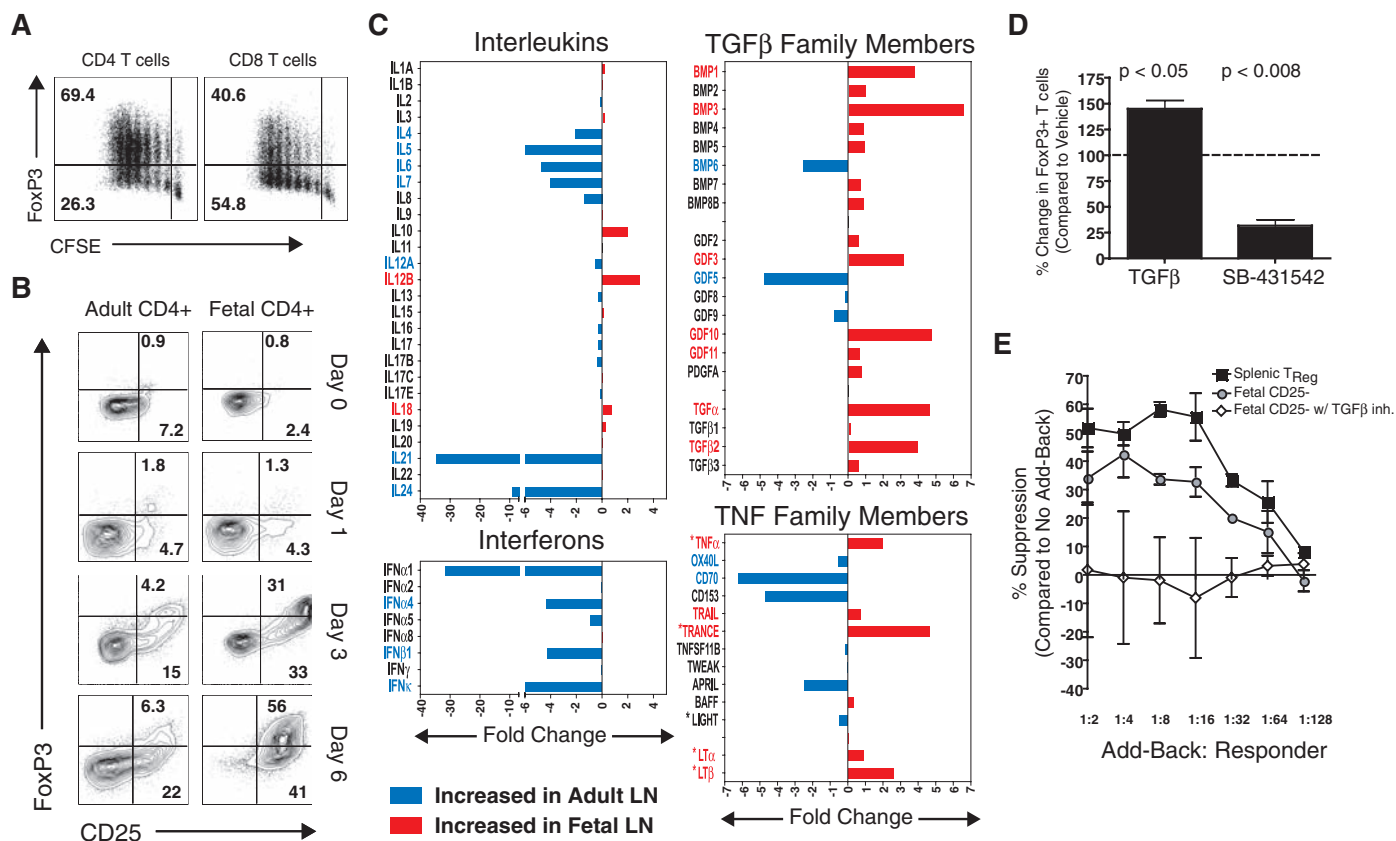


Fig. 2. Fetal T cells differentiate into T_{regs} upon stimulation with alloantigens. **(A)** Fetal T cells depleted of CD25+FoxP3+ cells were stimulated for 5 days with unrelated APCs, and FoxP3 expression was measured in proliferating T cells. **(B)** Kinetic analysis of CD25 and FoxP3 up-regulation by adult and fetal CD4+ T cells after stimulation with alloantigens. **(C)** Fold difference in cytokine mRNA expression in normal adult ($n = 4$) and fetal ($n = 5$) LNs. Genes found to be significantly different are

labeled in red (fetal) or blue (adult) ($P < 0.05$, unpaired Student's t test). Asterisks denote TNF family members involved in organogenesis. **(D)** Inhibition of TGFβ signaling by addition of the activin receptor-like kinase inhibitor, SB-431542 (1 uM), which blocks FoxP3 up-regulation by fetal T cells stimulated with unrelated APCs. **(E)** TGFβ-dependent acquisition of suppressive function after stimulation of fetal T cells with alloantigens. Error bars indicate SD observed in three separate experiments.

Whereas both fetal and adult T cells displayed similar patterns of activation during the first 2 days of stimulation (figs. S5 and S6), fetal T cells showed greater signs of activation thereafter (Fig. 2B and figs. S5 and S6). Sustained expression of FoxP3 is a necessary feature of T_{regs} in both mice and humans. Whereas adult T cells can express FoxP3 after stimulation (22), we found that most activated adult T cells were CD25+FoxP3- after 6 days of stimulation. Expression of FoxP3 by fetal T cells was maintained over the course of the stimulation period, with ~50% of fetal CD4+ T cells expressing both CD25 and FoxP3 by day 6 (Fig. 2B).

Environmental cues play a central role in determining T cell differentiation pathways during an immune response. To address whether fetal lymphoid tissues are enriched for cytokines that might favor T_{regs} differentiation during T cell activation, cytokine gene expression patterns were evaluated in fetal ($n = 5$) and adult ($n = 4$) LNs (Fig. 2C). As anticipated, adult LNs had elevated levels of interleukins and interferons as compared with fetal LNs. Analysis of tumor necrosis factor (TNF) family members revealed more variable expression patterns, with transcripts

for some genes (e.g., OX40L, CD70, and APRIL) being higher in adult LNs, whereas others (e.g., LTα, LTβ, TRANCE) were more highly expressed in fetal LNs. TNF family members more highly expressed by fetal LNs were predominantly those important for LN organogenesis in mice (e.g., LTα, LTβ, TRANCE, and TNFα) (25). Many transforming growth factor-β (TGFβ) family members were more highly expressed in fetal LNs, including bone morphogenic proteins 1 to 5, 7, and 8B; growth and differentiation factors 2, 3, 10, and 11; as well as TGFα and TGFβs. High expression of various TGFβ family members in developing LNs is consistent with the role that members of this family play in embryonic developmental pathways (26). TGFβ signaling is known to induce FoxP3 up-regulation during T cell activation and to be critical for the differentiation of T_{regs} during an immune response. To test whether TGFβ signaling was required for FoxP3 up-regulation during fetal T cell responses, we measured FoxP3 expression in a 5-day MLR in the presence or absence of a TGFβ inhibitor (SB 431542) and found that inhibition of TGFβ signaling resulted in a large reduction in FoxP3 up-regulation by fetal T cells (Fig. 2D).

Because FoxP3 can be induced in some activated T cells that are not functionally suppressive (22), we determined whether FoxP3 expression after fetal T cell activation was associated with the acquisition of suppressive function. Primary MLRs were performed with fetal CD25-depleted LN cells, with or without TGFβ inhibition; endogenous splenic T_{regs} served as a positive control. After a 7-day culture period, fetal CD25-depleted LN cells and splenic T_{regs} were tested for function in a conventional add-back assay. Fetal LN cells that had up-regulated FoxP3 after stimulation with adult allogeneic APCs were functionally suppressive, whereas those activated in the presence of the TGFβ inhibitor lacked the ability to suppress T cell proliferation (Fig. 2E and fig. S7). Although the endogenous pool of fetal splenic T_{regs} appeared to have increased suppressive function (Fig. 2E), this may reflect a greater percentage of FoxP3+ cells within this population: ~30 to 50% of CD4+ T cells from fetal LNs had up-regulated FoxP3+ after 7 days of stimulation in vitro, whereas ~50 to 80% of splenic endogenous T_{regs} were FoxP3+ after 7 days in culture (fig. S7B).

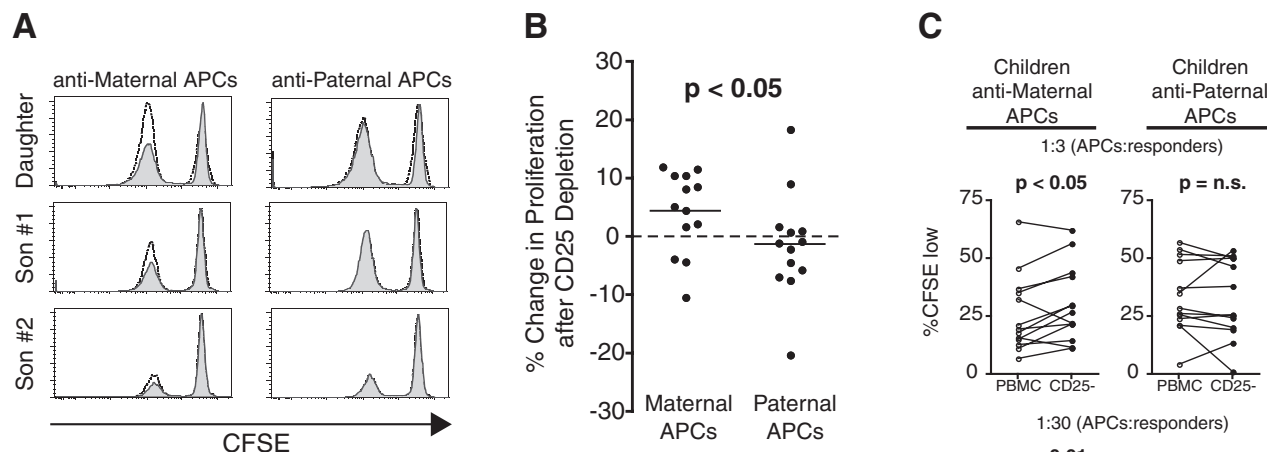


Fig. 3. T_{regs} specific for non-inherited maternal alloantigens persist long after birth. **(A)** CD8 $^{+}$ T cell proliferation in mock-depleted (gray histograms) and CD25-depleted (unshaded histograms) T cells after an 8-day MLR with maternal (left) and paternal (right) APCs. Three children from a single family are represented. **(B)** Summary of all children tested, comparing the relative increase in proliferation after depletion of CD25 $^{+}$ cells from MLRs against maternal (left) or paternal (right) APCs (1:3 ratio of APCs: responders). Statistical analysis calculated by Mann-Whitney U rank sum test. **(C)** Summary of individual responses of all children tested, showing proliferation of mock-depleted (PBMC) or CD25-depleted (CD25 $^{-}$) T cells in response to maternal or paternal APCs. Two different dilutions of APCs:responders (1:3, top; 1:30, bottom) are depicted. Statistical significance was determined by paired Student's t test.

The above studies indicate that suppressive T_{regs} are generated against NIMAs in utero. Given previous reports indicating that NIMAs are better tolerated than non-inherited paternal alloantigens in the setting of adult solid organ transplantation (13, 14), we tested the possibility that T_{regs} generated against NIMAs in utero might persist after birth. We performed MLRs using lymphocytes of children (ages 7 to 17 years old) to measure T cell proliferation in response to maternal or paternal alloantigens, with or without prior depletion of T_{regs} (Fig. 3, A to C). Some children demonstrated T_{regs} suppression against maternal alloantigens but not against paternal alloantigens (Fig. 3, B and C) or autologous APCs (fig. S8). A parallel analysis of maternal and paternal T cell responses directed against their children's alloantigens revealed that maternal T_{regs} with specificity for their children's alloantigens persist long after birth as well (fig. S8H). These preliminary findings indicate that T cell tolerance to alloantigens perceived in utero may, in some cases, be maintained after birth through the establishment of long-lived T_{regs} , as has been reported for B cell tolerance (13).

It has long been recognized that central deletion of autoreactive T cell clones is an important mechanism for generating immunological tolerance. Here, we demonstrate that the fetal peripheral adaptive immune system can rapidly generate functionally suppressive T_{regs} , providing another mechanism by which the fetus can establish tolerance to foreign and self antigen present during development in utero. Although this study has focused on fetal tolerance to maternal alloantigens, there is no reason to believe a priori that the fetal immune system would respond differently to other antigens encoun-

tered in utero, including self antigens, food antigens, and antigens associated with infectious agents carried by the mother. Further investigation into these areas is likely to provide important insights about the treatment of fetal disease, the development of tolerance to self and foreign antigens in humans, the establishment of strategies to induce antigen-specific tolerance during fetal development, and the pathogenesis of mother-to-child transmission of pathogens, such as HIV, in utero.

References and Notes

- R. E. Billingham, L. Brent, P. B. Medawar, *Nature* **172**, 603 (1953).
- D. Gittlin, J. Kumate, J. Urrusti, C. Morales, *J. Clin. Invest.* **43**, 1938 (1964).
- J. S. Remington, J. O. Klein, C. B. Wilson, Carol J. Baker, *Infectious Diseases of the Fetus and Newborn Infant* (Elsevier Saunders, Philadelphia, PA, ed. 6, 2006), pp. 11–16.
- K. M. Adams, J. L. Nelson, *JAMA* **291**, 1127 (2004).
- A. M. Silverstein, *Science* **144**, 1423 (1964).
- S. H. Friedberg, I. L. Weissman, *J. Immunol.* **113**, 1477 (1974).
- B. F. Haynes, C. S. Heinly, *J. Exp. Med.* **181**, 1445 (1995).
- L. J. West, *Hum. Exp. Toxicol.* **21**, 499 (2002).
- L. S. Rayfield, L. Brent, C. H. Rodeck, *Clin. Exp. Immunol.* **42**, 561 (1980).
- C. Granberg, T. Hirvonen, *Cell. Immunol.* **51**, 13 (1980).
- A. Marchant *et al.*, *J. Clin. Invest.* **111**, 1747 (2003).
- D. Rastogi *et al.*, *J. Clin. Invest.* **117**, 1637 (2007).
- F. H. Claas, Y. Gijbels, J. van der Velden-de Munck, J. J. van Rood, *Science* **241**, 1815 (1988).
- W. J. Burlingham *et al.*, *N. Engl. J. Med.* **339**, 1657 (1998).
- S. M. Muller *et al.*, *Blood* **98**, 1847 (2001).
- T. H. Lee *et al.*, *Transfusion* **46**, 1870 (2006).
- A. M. Jonsson, M. Uzunel, C. Götherström, N. Papadogiannakis, M. Westgren, *Am. J. Obstet. Gynecol.* **198**, 325.e1 (2008).
- L. S. Loubière *et al.*, *Lab. Invest.* **86**, 1185 (2006).
- Materials and methods are available as supporting material on Science Online.
- J. Michaëlsson, J. E. Mold, J. M. McCune, D. F. Nixon, *J. Immunol.* **176**, 5741 (2006).
- V. R. Aluvihare, M. Kallikourdis, A. G. Betz, *Nat. Immunol.* **5**, 266 (2004).
- D. A. A. Vignali, L. W. Collison, C. J. Workman, *Nat. Rev. Immunol.* **8**, 523 (2008).
- Y. Takahata *et al.*, *Exp. Hematol.* **32**, 622 (2004).
- S. Hori, T. Nomura, S. Sakaguchi, *Science* **299**, 1057 (2003); published online 9 January 2003 (10.1126/science.1079490).
- R. E. Mebius, *Nat. Rev. Immunol.* **3**, 292 (2003).
- K. Kitisin *et al.*, *Sci. STKE* **2007**, cm1 (2007).
- We would like to thank the families who donated blood for the studies shown in Fig. 3. We also thank B. Kanwar, D. Favre, E. Trachtenberg, R. Derynck, and S. Fisher for technical assistance and valuable discussions. Support for this work was provided by grants from NIH to J.M.M. (OD000329 and AI40312) and D.F.N. (AI68498) and from the AIDS Biology Program of the AIDS Research Institute at UCSF. J.M. is supported by the Swedish Research Council. T.D.B. is a National Institute of Child Health and Development fellow (HD00850) and was also funded by the American Academy of Pediatrics and the American Pediatric Society. M.O.M. was supported by grants from the Broad Medical Research Program of The Eli and Edythe L. Broad Foundation, National Blood Foundation, and Blood Systems, Inc. K.P.B. was supported by grants from the UCSF Clinical and Translational Institute Clinical Research Center (RR024131) and the Elizabeth Glaser Pediatric AIDS Foundation (PG-50804). M.P.B. and T.-H.L. were both supported by grants from the National Heart Lung and Blood Institute (HL083388). J.M.M. is a recipient of the NIH Director's Pioneer Award Program.

Supporting Online Material

www.sciencemag.org/cgi/content/full/322/5907/1562/DC1
Materials and Methods

Figs. S1 to S9
References

11 August 2008; accepted 6 November 2008
10.1126/science.1164511

CELL SIGNALING: ChIPping Away at Gene Expression

Chromatin immunoprecipitation reveals where proteins interact with DNA, and advances in this technology—including simplified applications, improved sensitivity, and higher throughput—allow scientists to track increasingly complex details of gene regulation in normal development and disease conditions.

by Mike May

A microscopic voyage would turn truly fantastic if scientists could watch the molecular pathways that regulate gene expression. Chromatin immunoprecipitation (ChIP) brings researchers closer to that capability. “You can detect protein on DNA sites in the native chromatin context,” says Jim Bone, strategic marketing manager at **Active Motif** of Carlsbad, California. “It’s not like in vitro experiments with naked DNA in a reaction tube using purified protein to see if it binds.”

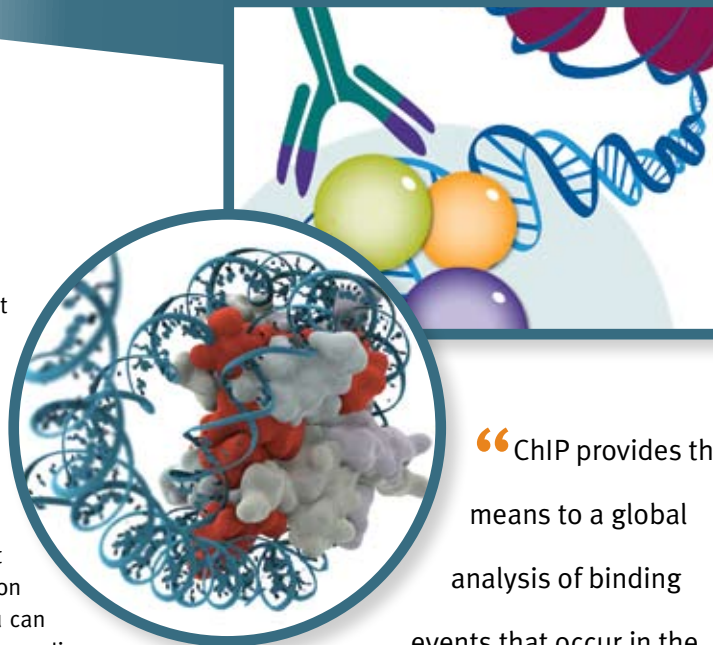
So researchers can use ChIP to see which proteins bind to a specific DNA site in its natural environment. Then, experimental manipulations can show how cellular conditions change the protein’s binding behavior. ChIP can also be used to study histone modifications. “These are very dynamic,” says Bone. “They change with cell type, stage of development, and different extracellular signals.”

This technology can even deliver a broad perspective. “ChIP provides the means to a global analysis of binding events that occur in the living cells, leading to better understanding of regulation of chromatin structure and gene expression,” says Marjeta Urh, leader of the protein analysis group at **Promega** in Madison, Wisconsin.

In typical approaches to ChIP, scientists use formaldehyde to fix cells, which keeps proteins sequestered where they were interacting with DNA. Then, enzymes snip the DNA into pieces, and antibodies are used to bind specific proteins, which remain bound to the DNA. To collect the entire complex created during a ChIP reaction, the antibody-protein-DNA is bound by beads coated with protein A or protein G. The bead makes it easier to collect the complexes from the solution. In some forms of ChIP, known as ChIP-Seq, the DNA can then be sequenced and mapped to its spot in the genome.

Although the first commercial kits for ChIP came out about a decade ago, many new ones add features to this technology. In general, new kits for ChIP work faster and with smaller samples. In the past, for example, it took several days to run a ChIP assay, but the latest kits provide results in just one day. Moreover, today’s kits can usually perform ChIP with as few as one million cells, when it used to take 10 million.

Today’s ChIP antibodies also provide more specificity. “Recently, what’s become powerful is the ability to use antibodies against specific posttranslational modification states of histones and other nuclear proteins to perform global chromatin location analysis,” says John Rosenfeld, manager of the R&D chromatin biology group at **Millipore** in Temecula, California. In addition, ChIP keeps getting easier to use. “ChIP is challenging,” says Sallie Cassel, director of marketing at Millipore. “It used to be the focus of only histone **continued** >



“ChIP provides the means to a global analysis of binding events that occur in the living cells, leading to better

understanding of regulation of chromatin structure and gene expression.”

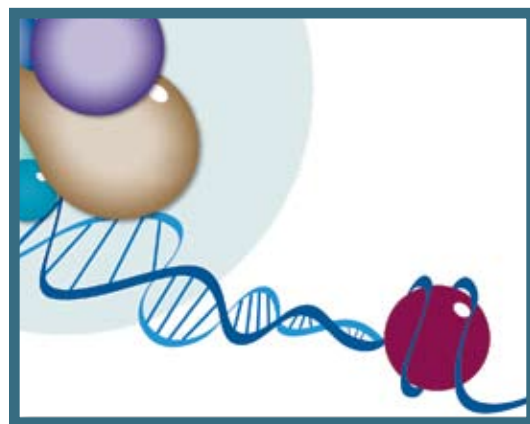


IMAGE COURTESY OF CELL SIGNALING TECHNOLOGY

Look for these Upcoming Articles

Proteomics:

MS Purification/Separation — February 20

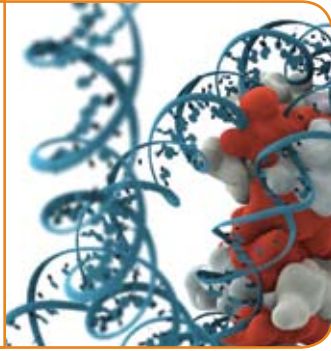
In Vivo Imaging — March 6

Genomics: Next Gen Sequencing — April 10

Inclusion of companies in this article does not indicate endorsement by either AAAS or Science, nor is it meant to imply that their products or services are superior to those of other companies.

Cell Signaling

“When you can reprogram
a somatic cell into a
cell that can generate
an entire organism,
that is pretty profound.”



and chromatin researchers. However, because today's kits have so simplified the procedure, the technique has evolved into a general application.”

Building Broader ChIPs

To expand studies, tool developers are taking a broader view of chromosomes. “We’re moving toward a higher density microarray platform to accomplish this,” says Renee Zuckerman, genomics marketing manager at **Agilent** in Santa Clara, California. She cites growing interest in DNA methylation analysis using ChIP on a microarray platform. “As researchers seek to understand how gene regulation works on a global scale, these higher density arrays let them look at more areas of interest, and do so more cost effectively,” says Rini Saxena, senior product manager for methylation and ChIP-on-chip at Agilent. In fact, Agilent’s newest ChIP-on-chip arrays will provide one million features—up from 244,000. Saxena adds, “All of our probes are empirically validated, making them highly specific and sensitive. The result is a very high signal-to-noise level, which provides high-quality data.” This system includes Agilent’s newest DNA Microarray Scanner, which provides a resolution down to 2 microns.

Although scientists want large numbers of features on a ChIP or DNA-methylation microarray, many require custom features. “We provide web-based customization tools,” says Saxena. “When looking at regulatory networks, for instance, somebody might want to study transcription-factor networks in a specific set of chromosomes.” This researcher can turn to Agilent’s online tools to create a custom array. Agilent then prints these in just a few weeks.

To help drive advances in ChIP, companies often collaborate. As one example, Agilent and Millipore agreed to combine their microarrays and antibodies, respectively. “We found that researchers were buying these antibodies for ChIP,” says Saxena. “So now they get an end-to-end solution.”

Moreover, academic and industrial collaborations show what ChIP-on-chip can unveil. For example, Richard Young, member of the **Whitehead Institute for Biomedical Research** and professor of biology at the **Massachusetts Institute of Technology**, consults with Agilent. Young used ChIP-on-chip, with Agilent microarrays, to show that, as he explains, “most signaling pathways in *Saccharomyces* have terminal kinases that associate with the signaling pathway’s target genes.” In addition, Young recently used ChIP-on-chip data to design experiments that show that the Wnt signaling pathway can enhance reprogramming of somatic cells into embryonic stem cells. “When you can reprogram a somatic

cell into a cell that can generate an entire organism, that is pretty profound,” Young says.

Other companies also focus on improving ChIP through specialized kits. For instance, **Sigma-Aldrich** in St. Louis, Missouri, developed its ChIP1 Imprint kit. “It is one of the fastest ChIP kits, running a reaction in about six to seven hours,” says Savita Bagga, product manager for epigenetics at Sigma-Aldrich. “It comes in eight-well strips, enabling high throughput screening of 96 samples simultaneously,” Bagga says. Each well should contain about 100,000 cells, but this kit can work with as few as 10,000 cells per well, according to Bagga. Moreover, the reactions run completely on the plate. “You don’t need columns except for DNA purification, and these come with the kit,” Bagga explains.

Some companies even specialize in ChIP antibodies. For example, Ricardo de Medeiros, scientist in the department of antibody applications at **R&D Systems** in Minneapolis, Minnesota, says, “We have kits that contain ChIP-validated antibodies plus all of the buffers necessary to perform this assay.” These kits also include positive and negative controls. So far, R&D Systems offers about 25 antibody kits for ChIP with optimized antibody-buffer combinations.

Adding Magnetism

Some vendors have modified traditional ChIP to use magnetic beads. For example, Active Motif’s Chip-IT Express HT Kit combines magnetic beads with a 96-well plate. “I’ve done hundreds of ChIP reactions,” says Bone of Active Motif, “but I could never do more than two or three dozen in a day, and those were extremely long days. Now, you can do 96 reactions at one time.” In general, says Bone, the magnetic bead approach speeds up ChIP. “You don’t need to clean samples as much,” he says, “because using these beads reduces non-specific binding of chromatin relative to agarose beads.”

Traditional ChIP was also more technically challenging, according to Bone. “You needed to be very consistent,” he says. “In pipetting by hand, for example, you had to be careful to avoid accidentally pulling up agarose beads.” He adds, “You weren’t guaranteed success your first time out.” With the magnetic bead approach, the beads are pulled to the side of the tube, allowing the liquid to be removed more cleanly and easily.

Other companies, such as Millipore, also take the magnetic bead approach. Cassel says, “Our Magna ChIP kits are easy to use and experiments can actually be performed in a single day, unlike the traditional ChIP methods which can often take up to three days.” And thanks to its acquisition of Upstate, Millipore now provides a wide range of antibodies that are specifically designed for use with ChIP assays.

Invitrogen in Carlsbad, California, uses its magnetic Dynabeads in ChIP applications. “We offer Dynabeads Protein A and Dynabeads Protein G,” says Amy Cuneo, product manager for epigenetics at Invitrogen. “These magnetic beads make handling easier, protocols faster, and there is less background.” Invitrogen’s wide collection of antibodies can also be used with ChIP to capture a range of transcription factors.

Invitrogen looks at ChIP as one step in bigger experiments. Kristin Wiederholt, R&D manager for epigenetics and the RNAi group at Invitrogen, says, “We have a broad portfolio of products around downstream applications that are compatible with ChIP.” As examples, she mentions qRT-PCR reagents and array- **continued** ➤

labeling kits. In addition, Wiederholt points out that Invitrogen's RNAi reagents could be used to knock down specific genes and researchers can then use ChIP to see what happens to transcription factor binding at that gene location.

Covering All Angles

Like many technologies that gain popularity, ChIP entices companies to develop complete product lines that cover many experimental angles. At **Illumina** in San Diego, California, for example, Chris Streck, gene expression and regulation product manager, says, "We provide all the necessary reagents, consumables, and sequencing technology coupled with software analysis tools for genomewide ChIP-Seq analysis."

ChIP-sequencing, often called ChIP-Seq, combines traditional ChIP with high throughput DNA sequencing. In ChIP-Seq, enriched DNA fragments isolated from protein-DNA complexes are sequenced and the frequency of each unique sequence is calculated. The resulting counts are aligned to the genome to identify specific DNA-binding sites. In particular, Illumina focuses on providing improved resolution for protein-binding site location in addition to decreasing input requirements to 10 nanograms of DNA for genomewide analyses.

For researchers who want to take advantage of ChIP without gearing up to run this assay themselves, Illumina and **Genpathway** in San Diego, California, teamed up to offer a beginning-to-end service for ChIP-Seq. A researcher provides cells or tissue and receives analyzed data in 8–10 weeks or less. This service uses Genpathway's ChIP processes—including sample processing, antibody selection and library preparation, and quality control—and Illumina's Genome Analyzer to sequence the resulting libraries.

Beyond wanting to know which protein binds to a specific spot on DNA, researchers might also want to know if two proteins bind to the

same spot. Likewise, they may want to determine if a protein binds at a spot where there's a specific histone modification. This can be deciphered with Active Motif's Re-Chip-IT Kit. This process—called ChIP-ChIP—runs two sequential ChIP reactions. The first uses an antibody for one protein, and the second ChIP uses an antibody for another protein. "In other words, you start the second ChIP with the results of the first," says Active Motif's Bone.

Getting Away from Antibodies

Nearly all ChIP processes use antibodies to grab the protein-DNA complexes, but Promega takes a different approach with its HaloCHIP System, which uses HaloTag technology. Here a DNA-binding protein that a researcher wants to study is expressed as a HaloTag fusion protein and—as in the traditional ChIP approach—the binding of the fusion protein to DNA is preserved by cross-linking with formaldehyde. Then, the protein-DNA complexes are captured directly onto HaloLink Resin without the need for an antibody.

"This approach works faster than traditional homebrew methods," says Paula Phenix, Promega's global product manager in the proteomics group. Urh adds that the HaloCHIP requires fewer cells than traditional ChIP techniques. She says, "Some ChIP techniques require 10 million cells, but HaloCHIP needs a million or fewer." In addition, if a reliable antibody does not exist for a target protein, a researcher can still study protein-DNA interactions with the HaloCHIP.

HaloCHIP System belong to a family of HaloTag applications, each allowing analysis of a different aspect of protein function. As Urh explains, "A researcher can use the same sample containing HaloTag fusion proteins not only to analyze protein-DNA interactions but also protein-protein interactions, and to observe movement of proteins within the cell. Ultimately, these data together lead to better understanding of protein function and cell physiology."

Automation Ahead

In the future, ChIP should get even simpler. "I'd like to see it automated," says Bone. "Then, you could do true high throughput ChIP. When we get to 1,536 ChIPs in a day, that's high throughput—provided you don't need 50 graduate students and postdocs to accomplish it."

Moreover, at the Whitehead Institute, Young would like to see ChIP reveal the entire population of proteins that play a role in regulating a gene. "If we can develop a method that isolates individual promotor regions and then discovers all of the factors that occur there, that would be extremely valuable," he says. In addition, Young wants to see ChIP techniques that require fewer cells, down to hundreds or even dozens. "That would help us to explore more human disease states," he says.

Advances in ChIP continue to bring researchers closer to observing the steps behind the signaling pathways in gene regulation. ChIP's perspective also keeps expanding. As the technology improves, scientists will be better equipped to obtain a clearer picture of the inner working of cells in both broader perspective and finer detail.

Mike May is a publishing consultant for science and technology.

Featured Participants

Active Motif

www.activemotif.com

Millipore

www.millipore.com

Agilent

www.agilent.com

Promega

www.promega.com

Genpathway

www.genpathway.com

R&D Systems

www.rndsystems.com

Illumina

www.illumina.com

Sigma-Aldrich

www.sigma-aldrich.com

Invitrogen

www.invitrogen.com

Whitehead Institute for

Biomedical Research

www.wi.mit.edu

Massachusetts Institute of Technology

www.mit.edu

New Products



Electrophysiological Microscope

The Axio Examiner Fixed Stage Microscope for electrophysiological experiments is particularly well suited for patch clamp experiments on nerve cells, examinations of brain cells, and for measuring electrical signals on cells. With the new Zeiss LSM 710 NLO laser scanning microscope, it is integrated into a sensitive, multiphoton system. The connection of one or two AxioCam cameras and the use of the AxioVision 4.7 software with a special physiology module make the quantitative evaluation of typical experiments comfortable and convenient, including the ability to visualize infrared differential interference contrast and fluorescence in individual and merged live windows. Axio Examiner is designed so that complex experiments are easy to set up and safe to use. To configure a specific system, the user has a choice of four upper parts, two lower parts, and a large number of different components and motorization options.

Zeiss

For information 800-233-2343

www.zeiss.com/micro

Cell Signaling Computational Platform

Cellucitate is a new computational platform for cell signaling researchers. The Cellucitate collaborative workspace features an intuitive visual language for describing protein interactions coupled with advanced computational techniques to enable researchers to discover, model, and analyze signaling pathways and run virtual experiments. With this web-based platform, biologists can publish their work and access a repository of evolving data, knowledge, and models to facilitate collaboration and build on prior research. The dynamic webs of protein interactions involved in cell signaling processes tend to overwhelm traditional static or statistical techniques. This technology is designed to give researchers the tools to quickly and easily identify new knowledge, assess its impact on prior work, and decide whether to incorporate it into their work.

Plectix BioSystems

For information 617-591-2400

www.plectix.com

Highly Validated Antibodies

Sigma-Aldrich announced the addition of over two thousand antibodies to its line of Prestige Antibodies. These antibodies were developed by the Human Proteome Resource and are commercially available through an exclusive partnership with Sigma-Aldrich and Atlas Antibodies. Prestige Antibodies are highly validated for specificity and are designed to have low cross-reactivity to other human proteins. These reagents are available online, where customers can search or browse for available antibodies by specific gene name and ID, or by keywords.

Sigma-Aldrich

For information 800-521-8956

www.sigma.com/prestige

Universal Prokaryotic Arrays

The Universal Prokaryotic high-density oligonucleotide arrays are suitable for use in gene expression and comparative genomics research. The microarrays feature multiple arrays per slide, allowing researchers to carry out versatile, integrated experiments in more than one application area, even on the same array, which saves

time and money. The Universal Prokaryotic arrays make use of long oligonucleotides that are synthesized using advanced printing technology, resulting in more consistent data. They were designed in collaboration with the prokaryotic community to be targeted to real research needs. They are available for many popular research targets, including *E. coli*, *S. typhimurium*, *Streptomyces coelicolor*, and *Mycobacterium tuberculosis*.

Oxford Gene Technology

For information +44-(0)-1234-210555

www.ogt.co.uk

Stem Cell Analysis Kits

Six new flow cytometry kits are designed to make stem cell research faster, easier, and more accurate. With these robust, three-parameter FlowCelect kits, scientists can easily assess embryonic and neural stem cell phenotypes at various stages of differentiation. Designed to eliminate the need for researchers to spend time on assay development, the kits help characterization by analyzing stem cell phenotypes and tracking the progress of differentiation along various lineages. The kits are optimized for use on the Guava EasyCyte Plus system.

Millipore

For information 800-548-7853

www.millipore.com

Confocal Imaging System

The VT-Infinity3SL confocal imaging system integrates a single solid-state laser with VisiTech's patented two-dimensional Array Scanning Technology. The new instrument eliminates the need for an external laser subsystem, thus reducing the system footprint to a minimum, while providing all the advantages of the VT-Infinity product family. Advantages include selectable confocal pinhole sizes, low photobleaching, and high-speed scanning (up to a thousand scans per second), making it suitable for live-cell imaging experiments. It can be expanded to incorporate additional laser lines.

VisiTech International

For information +44-(0)-191-5166255

www.visitech.co.uk

Electronically submit your new product description or product literature information! Go to www.sciencemag.org/products/newproducts.dtl for more information.

Newly offered instrumentation, apparatus, and laboratory materials of interest to researchers in all disciplines in academic, industrial, and governmental organizations are featured in this space. Emphasis is given to purpose, chief characteristics, and availability of products and materials. Endorsement by *Science* or AAAS of any products or materials mentioned is not implied. Additional information may be obtained from the manufacturer or supplier.

Science Careers Classified Advertising



We've got **Careers** down to a **Science**.

For full advertising details, go to
www.sciencecareers.org and click on
For Advertisers, or call one of our representatives.

United States & Canada

E-mail: advertise@sciencecareers.org
Fax: 202-289-6742

IAN KING

Associate Director, *Science Careers*
Phone: 202-326-6528

JORIBAH ABLE

Industry - US & Canada
Phone: 202-326-6572

ALEXIS FLEMING

Northeast Academic
Phone: 202-326-6578

TINA BURKS

Southeast Academic
Phone: 202-326-6577

DARYL ANDERSON

Midwest/Canada Academic
Phone: 202-326-6543

NICHOLAS HINTIBIDZE

West Academic
Phone: 202-326-6533

Europe & International

E-mail: ads@science-int.co.uk
Fax: +44 (0) 1223 326532

TRACY HOLMES

Associate Director, *Science Careers*
Phone: +44 (0) 1223 326525

ALEX PALMER

Phone: +44 (0) 1223 326527

DAN PENNINGTON

Phone: +44 (0) 1223 326517

SUSANNE KHARRAZ TAVAKOL

Phone: +44 (0) 1223 326529

LOUISE MOORE

Phone: +44 (0) 1223 326528

Japan

MASHY YOSHIKAWA

Phone: +81 (0) 3 3235 5961
E-mail: myoshiyawa@aaas.org

To subscribe to *Science*:

In US/Canada call 202-326-6417 or 1-800-731-4939
In the rest of the world call +44 (0) 1223-326-515

Science makes every effort to screen its ads for offensive and/or discriminatory language in accordance with US and non-US law. Since we are an international journal, you may see ads from non-US countries that request applications from specific demographic groups. Since US law does not apply to other countries we try to accommodate recruiting practices of other countries. However, we encourage our readers to alert us to any ads that they feel are discriminatory or offensive.

Science Careers

From the journal *Science*



POSITIONS OPEN

EPIDEMIOLOGIST

University of California, Davis

ASSISTANT PROFESSOR in the Department of Plant Pathology, University of California, Davis. The successful candidate will be expected to develop effective teaching and research programs, and to participate in outreach activities that contribute to the success of the University. The applicant should have a Ph.D. degree in plant pathology, plant biology, microbiology, microbial ecology, ecology, genetics, bio-statistics, or other closely related field. Postdoctoral experience is desirable. A strong commitment to teaching at undergraduate and graduate levels is expected. The appointee is expected to develop an extramurally funded research program emphasizing modern approaches to the quantitative ecology of plant-associated microbes and the epidemiology of plant diseases in agricultural and/or natural ecosystems. The successful candidate should have the interest and ability to develop and utilize sophisticated computational methodologies to model the behavior of complex systems. The candidate would be expected to employ an integrated approach that takes advantage, perhaps through collaborations, of advanced methodologies for acquisition and processing of data on environmental parameters and/or genome level studies to investigate ecological relationships between pathogens and their hosts. Teaching will be at both the undergraduate and graduate levels in the area of the candidate's expertise, and will include contributions to a new curriculum in agricultural sustainability. Supervision of graduate students, student advising, participation in outreach programs, curricular development, and performance of University service are expected. Research, teaching, and outreach efforts are expected to contribute to the mission of plant pathology in the Agricultural Experiment Station.

This will be a nine-month, tenure-track position. Fiscal year (11 months) term employment to be offered and continued based on academic personnel review.

The position is available on or about July 1, 2009. This position will be located in the Plant Pathology Department. Applicants should submit curriculum vitae including publication list, a statement of research and a separate statement describing teaching interests and background, a summary or abstract of the Ph.D. dissertation; and the names, addresses including e-mail, and telephone numbers of four references online at [website: http://plantpathology.ucdavis.edu](http://plantpathology.ucdavis.edu). Inquiries should be directed to **Dr. David Rizzo, Search Committee Chair, Department of Plant Pathology, University of California, One Shields Avenue, Davis, CA 95616; telephone: 530-754-9255; e-mail: dmrizzo@ucdavis.edu**. Open until filled, but to ensure consideration, applications should be received by February 1, 2009. A more detailed job description can be obtained at [website: http://plantpathology.ucdavis.edu](http://plantpathology.ucdavis.edu).

UC Davis is an Affirmative Action/Equal Employment Opportunity Employer and is dedicated to recruiting a diverse faculty community. We welcome all qualified applicants to apply, including women, minorities, veterans, and individuals with disabilities.

Two **POSTDOCTORAL POSITIONS**, in molecular endocrinology and cancer therapeutics. Seeking recent Ph.D. graduates for funded openings to study: (1) growth hormone action and Janus activated kinase-signal transducer and activator of transcription signaling, using genome-wide technologies combined with computational analysis and traditional molecular approaches to elucidate sexually dimorphic liver gene expression (*Molecular Endocrinology* 20:2613-29, 2006); (2) cytochrome P450-based cancer chemotherapeutics in combination with anti-angiogenesis (*Molecular Cancer Therapeutics* 7:79-89, 2008; 6:2879-90, 2007). Expertise in cell and molecular biology, genomics/computational biology, gene therapy and/or pharmacology, and animal models highly desirable. Flexible start date.

Send curriculum vitae, summary of research experience and interests, and names of three references to: **Dr. David Waxman, Department of Biology, Boston University, 5 Cunningham Street, Boston, MA 02215; e-mail: djw5@bu.edu**.

POSITIONS OPEN

STAFF SCIENTIST: MOUSE SPECIALIST Position Available

A position is available for a highly motivated individual to manage mouse projects in a neuroscience research laboratory. A minimum of two years of experience in mouse genetics, molecular biology, mouse colony management, genotyping, mouse phenotyping, and behavior is required. Honed experimental skills, familiarity with mouse databases, organizational abilities, and effective communication and interpersonal skills are essential. Competitive salary commensurate with experience. Interested candidates should send resumes and three references to: **Dr. Michael Ehlers, M.D., Ph.D., Howard Hughes Medical Institute, Department of Neurobiology, Duke University Medical Center, P.O. Box 3209, Durham, NC 27710 U.S.A. Fax: 919-668-0631. E-mail: ehlers@neuro.duke.edu**.

TENURE-TRACK FACULTY POSITIONS Biological Sciences

The Department of Biological Sciences at Mississippi State University invites applications for two tenure-track **ASSISTANT PROFESSOR** positions to begin August 16, 2009. Successful candidates will be expected to develop externally funded research programs that complement the existing strengths of the Department. Desired areas of expertise include, but are not limited to: molecular, cellular, and evolutionary genetics; ecological, environmental, and industrial microbiology; molecular ecology; and infectious diseases and pathogenesis. Additionally, successful candidates will be those who can direct graduate students and contribute to both the undergraduate and graduate teaching missions of the Department. Minimum requirements for consideration include a Ph.D. in a related biological sciences field or equivalent field. Postdoctoral experience is preferred.

Scientific infrastructure at Mississippi State University supports focus areas in proteomics, genomics, and computational sciences. University Centers that house these facilities include the Life Sciences and Biotechnology Institute, the Electron Microscopy Center, the Geosystems Research Institute, and the Center for Computational Sciences. For more information on the department or these entities, please visit the Department of Biological Sciences [website: http://www.msstate.edu/dept/biosciences](http://www.msstate.edu/dept/biosciences).

Applicants should submit curriculum vitae, reprints of three representative publications, a concise statement of current and future research interests (one page), and a brief statement of teaching philosophy including relevant areas of teaching competence. Also, arrange for at least three letters of reference to be sent to the address below. Send applications (hard copy or electronic) to: **Dr. Nancy Reichert, Professor and Head, Department of Biological Sciences, P.O. Box GY, Mississippi State University, Mississippi State, MS 39762; e-mail: narl@msstate.edu**. Screening will begin January 15, 2009, and will continue until the positions are filled.

Mississippi State University is an Affirmative Action/Equal Opportunity Employer.

SHULL FELLOWSHIP at the Oak Ridge National Laboratory (ORNL): the Neutron Sciences Directorate of the ORNL invites applications for the Clifford G. Shull Fellowship. The Shull Fellowship provides an exciting opportunity to pursue research applying neutron scattering methods to forefront problems in physics, chemistry, biology, or materials science and engineering. Applications for Shull Fellowships commencing in 2009 are now being accepted. To receive full consideration applications must be submitted by December 12, 2008. For more information, and to apply, go to [website: http://jobs.ornl.gov/index.cfm](http://jobs.ornl.gov/index.cfm). ORNL is an Equal Opportunity Employer, committed to work force diversity. Applicants need not be U.S. citizens.

VCU

Virginia Commonwealth University

CHAIR OF BIOMEDICAL ENGINEERING

School of Engineering

Virginia Commonwealth University (VCU) seeks a highly qualified individual for the position of Chair in the Department of Biomedical Engineering. The Department has maintained a strong graduate program for over twenty years and has close ties with faculty in the VCU Medical Center, including the Schools of Medicine, Dentistry, Allied Health, Pharmacy, and Nursing. The VCU School of Engineering, founded in 1996, is a remarkable example of a public-private partnership. The School comprises five departments and has state-of-the-art facilities, including a new building that will be devoted to interdisciplinary research. The Biomedical Engineering undergraduate program was established in 1998 and is fully ABET-accredited. Current faculty research areas include biomechanics, tissue engineering, signal processing, human machine interface, rehabilitation engineering, and medical instrumentation.

The successful candidate will be expected to have a proven record of excellence in teaching and externally-funded research, as well as demonstrated leadership skills. He/she will be expected to support a vibrant research program, to teach at the undergraduate and graduate levels, to continue the expansion of student enrollment, and to increase sponsored research within the department, in particular by further promoting interdisciplinary research collaborations with the VCU Medical Center. An earned doctorate in Biomedical or Bioengineering or other closely related discipline is required, as well as experience with the ABET process.

Candidates should submit a statement of interest including their vision and a curriculum vitae detailing their research, teaching and leadership experience along with a list of four references to: **Dr. Alison Baski, Chair of Search Committee, Virginia Commonwealth University, 701 West Grace St. -Room 2401, Richmond, VA 23284-2000.** Electronic submissions with attached PDF files are also accepted and can be sent to: aabaski@vcu.edu. Candidates must be eligible for employment in the United States. Applications will be reviewed until the position is filled.

Virginia Commonwealth University (VCU) is the largest university in the state of Virginia and is ranked internationally and nationally as a prominent research institution. Located in Richmond on two downtown campuses, VCU enrolls nearly 32,000 students in 205 certificate and degree programs in the arts, sciences, humanities, engineering and medicine. Sixty-five of the programs are unique in Virginia, with many crossing disciplines among 15 schools and one college. The VCU Medical School and Hospitals comprise the VCU Medical Center, a comprehensive health care system.

Virginia Commonwealth University is an equal opportunity/affirmative action employer. Women, minorities and persons with disabilities are encouraged to apply.



FACULTY POSITIONS

Lupus and Autoimmunity Research

Hospital for Special Surgery and Weill Cornell Medical College



Tenure-track faculty positions at the Assistant Professor, Associate Professor and Professor level are available for established M.D./Ph.D., Ph.D., or M.D. immunologists, cell or molecular biologists with an interest in research relevant to systemic lupus erythematosus or other autoimmune and inflammatory rheumatic diseases. Applicants should have demonstrated high productivity and an outstanding record of funded research. Physician scientists are especially encouraged to apply.

Successful applicants will develop an independent research program focused on basic cellular, molecular or genetic mechanisms relevant to systemic autoimmune and inflammatory rheumatic diseases and will have joint appointments and participate in the academic programs of HSS and WCMC. Desired targeted areas of investigation include functional implications of disease-associated genetic variants; environment-host interactions in induction of disease, including the role of microbial, non-specific adjuvant, or other triggers of immune activation; mechanisms of lymphocyte activation and regulation; and mechanisms of target organ inflammation and damage. An extensive start up package and competitive compensation will be offered to successful applicants.

HSS is a unique institution, providing a multidisciplinary approach to research, patient care, and education focused on the autoimmune rheumatic and musculoskeletal diseases. Located in the York Avenue complex of biomedical institutions on Manhattan's Upper East Side, including WCMC, Sloan-Kettering Institute, and Rockefeller University, HSS is renowned for outstanding research in the pathogenesis of systemic autoimmune disorders and is rich in resources for translational research, including extensive clinical registries and sample repositories. Opportunities for participation in the clinical and academic activities of the Division of Rheumatology are available for physician applicants.

Please address inquiries, including CV and a two page summary of research accomplishments and plans, to:

Peggy Crow, MD
Chair, Lupus and Autoimmunity Research Search Committee
Hospital for Special Surgery
535 East 70th Street, R-200
New York, NY 10021
crowm@hss.edu

The Hospital for Special Surgery is an Equal Opportunity, Affirmative Action Employer. Women and minorities are strongly encouraged to apply.



Université Laval is North America's first French-language university and one of Canada's largest. With a strong commitment to the local community, it boasts first-class study and research facilities in the heart of Québec City, a UNESCO-designated world heritage site.

FACULTY MEMBER

IMMUNOLOGY (INFLAMMATION / ARTHRITIS / HOST-PATHOGEN INTERACTIONS)

THE FACULTY OF MEDICINE AT LAVAL UNIVERSITY

The Faculty of Medicine at Laval University (Québec city, Québec, Canada) is considering applications to fulfill a Senior (Tier 1) Canada Research Chair in immunology, inflammation, autoimmune diseases, or host-pathogen interactions. Excellence is our main criterion. A full professor tenured position is associated with the research chair. Innovative research in all aspects of Immunology will be considered. We seek an energetic scientist whose research synergizes with research areas of current members of the Immunology-Infectiology Team. The candidate will conduct his/her research in the Research Center of the Centre Hospitalier Universitaire de Québec. The candidate will be exposed to a highly interactive scientific environment that offers excellent laboratory and animal facilities along with state-of-the-art newly built and fully equipped genomic and proteomic platform. The applicant must have a proven track record of independence with demonstrated abilities to obtain peer-reviewed funding from recognized funding agencies (e.g. CIHR, NIH, NCIC, etc) and to supervise graduate students and postdoctoral fellows.

The successful applicant will be expected to maintain a highly productive scholarly agenda including the development of research relationships with researchers across Canada and internationally, to demonstrate effective teaching and mentoring of undergraduate and graduate students, and to take on a leadership role in the Faculty's initiatives.

The Canada Research Chair (CRC) program was established by the Government of Canada to enable Canadian Universities to achieve the highest levels of research excellence in the global, knowledge-based economy (<http://www.chairs.gc.ca>). Tier 1 Chairs are for outstanding researchers acknowledged by their peers as world leaders in their fields. The successful applicant will work with the staff of the Faculty of Medicine to submit a CRC application by April 2009, and the academic appointment is contingent on the success of this application.

We invite all qualified investigators to apply by sending a curriculum vitae, the name of three referees, and a brief description of the applicant's teaching and research accomplishments to:

Dr. Michel J. Tremblay
 Directeur, Axe de recherche en Infectiologie et Immunologie
 Centre de Recherche en Infectiologie, RC709
 Centre Hospitalier Universitaire de Québec
 2705 boul. Laurier, Québec (QC), Canada, G1V 4G2
 Tel: 1-418-654-2202; Fax: 1-418-654-2212; Email: michel.j.tremblay@crchu.ulaval.ca

Closing date for applications is January 15, 2009.

Université Laval is an equal opportunity employer that values diversity in its workforce and encourages applications from all qualified candidates, in particular, women, members of visible and ethnic minorities, and people with disabilities. However, Canadians and permanent residents of Canada are given first priority.



**National Institute of Neurological Disorders and Stroke;
Radiology and Imaging Sciences Program, Clinical Center**

**Tenure-Track/Tenure-eligible Investigator
Neuroimaging of Multiple Sclerosis (Clinical)
Division of Intramural Research**

The Division of Intramural Research of the National Institute of Neurological Disorders and Stroke and the Radiology and Imaging Sciences Program of the Clinical Center, NIH are recruiting an individual for a tenure-track/tenure eligible position in the area of neuroimaging with a focus on clinical research in multiple sclerosis. The individual will develop and direct an independent research program on imaging diseases of the nervous system and especially multiple sclerosis. The program will conduct its work in conjunction with the Neuroimmunology Branch (NIB) which was established to study the cause and treatment of immunological mediated diseases of the central nervous system. The successful candidate will be able to develop strong interactions with an active neuroradiology program and an active neuroimaging program at the NIH. The individual should have a demonstrated background and knowledge in research focused on neuroimaging diseases of the nervous system. In addition to imaging expertise, the individual should have experience in neurology and/or radiology and the application of clinical trial methodology to the study of disease mechanisms and testing new therapies. The candidate will have earned a M.D. or Ph.D. degree and will have excellent scientific skills in structuring an original and productive research program using outstanding communication and collaborative abilities. Preference will be given to individuals who have a medical license in the United States, who have completed training in an accredited training program in radiology or neurology, and is either board eligible or board certified in one of these disciplines. In rare cases outstanding senior candidates will be considered for a tenured position if there is a demonstrated international reputation and well-documented evidence of ongoing independent accomplishments. An individual selected for a tenure-track position is expected to build a dynamic and productive research group. Laboratory facilities, state-of-the-art neuroimaging facilities, research funds and salary are competitive with premier academic institutions. Applicants should send curriculum vitae, bibliography, statement of research interests, and have three letters of reference sent to: **Alan Koretsky, Ph.D., c/o Peggy Rollins, Office of the Scientific Director, Division of Intramural Research, National Institute of Neurological Disorders and Stroke, NIH, Building 35, Room GA908, NIH, Bethesda, MD 20892** or to Peggy.Rollins@nih.gov. Applications will be reviewed upon receipt.



Tenure-Track Investigator Position Available

The National Institute on Alcohol Abuse and Alcoholism (NIAAA), a major research component of the National Institutes of Health (NIH) and the Department of Health and Human Services (HHS), is recruiting for a tenure-track Investigator to establish and direct an independent research program in the area of comparative behavioral genomics in the Laboratory of Neurogenetics (LNG), Division of Intramural Clinical and Biological Research (DICBR), NIAAA.

The selected candidate will be expected to establish an independent research program that examines how genetic and environmental factors relate to intra- and inter-specific variation in traits that, in humans, are known risk factors for alcohol use disorders (e.g., stress reactivity, behavioral dyscontrol, reward seeking/sensitivity). Candidates must hold a Ph.D., M.D. or equivalent degree. Criteria for selection will include: a strong publication record in the field of genetics/genomics, demonstrated experience using animal models of human psychiatric disorders or addictions, demonstrated success in establishing and maintaining collaborations and demonstrated success in leading and mentoring research staff at various levels (e.g., postdoctoral fellows, research associates, and/or technicians).

Resources provided to the selected candidate include laboratory and core laboratory facilities, office space, personnel and an operating budget sufficient to develop this independent research program.

Interested candidates wishing to be considered for this position may submit a curriculum vitae, bibliography, the names and addresses of three references, and a brief proposal that reflects the applicant's research interests/goals and an approach for establishing an independent research program, by the closing date to Ms. Patricia Scullion at address below. *Note – we encourage you to submit your complete application electronically so that we may confirm receipt of your materials. **Chair, Search Committee, c/o Ms. Patricia Scullion, National Institute on Alcohol Abuse & Alcoholism (NIAAA), NIH, c/o Ms. Patricia Scullion, 5635 Fishers Lane, Room 2023, Bethesda, MD 20892, **For Federal Express delivery, Rockville, MD 20852. OR Submit Via Secure Email to: LNGRecruit@mail.nih.gov. The closing date for receipt of applications is **January 28, 2009**.**



NATIONAL CANCER INSTITUTE (NCI)

**Metabolism Branch
Center for Cancer Research
Tenured or Tenure Track Researcher**

The Metabolism Branch, NCI, is searching for a tenure-track or tenured investigator engaged in laboratory-based research in the biology of normal or malignant lymphocytes. The research program should be in any area of basic or patient oriented investigation that complements the existing focus of the Branch on the pathogenesis, diagnosis or treatment of lymphomas and multiple myeloma. The Metabolism Branch is located on the Bethesda campus of the NIH. Current areas of research include the molecular diagnosis of lymphomas, the use of genome-wide RNA interference screens to uncover molecular targets in cancer, the analysis of signal transduction and transcription factor networks in normal and malignant B cells, the biochemistry of transcriptional regulation, the development of monoclonal and cytokine-based therapies for lymphomas, and the clinical evaluation of novel chemotherapeutic strategies and molecularly-targeted therapies for lymphoma. Candidates for the position should have an M.D./Ph.D., Ph.D., or M.D. and strong research credentials. Applicants for this position should submit a curriculum vitae including bibliography, a statement of research interests, a two-page outline of the proposed research program, and three letters of recommendation to **Drs. Thomas A. Waldmann and Louis M. Staudt, Attention: Jean Decker, Bldg 10, Rm 4N115, 10 Center Drive, M.S.C. 1374, Bethesda, MD, 20892-1374**. You may also e-mail your application to: deckerj@mail.nih.gov.



ENDOWED CHAIR IN STEM CELL AGING

The EWING HALSELL FOUNDATION DISTINGUISHED CHAIR IN AGING RESEARCH is available for an eminent **stem cell biologist** with an interest in aging research to **lead the development** of a new initiative in stem cell biology. The primary academic appointment will be held in the Department of Cellular and Structural Biology as an **Associate Professor or Professor**, with membership in the Barshop Institute for Longevity and Aging Studies. Applicants should have demonstrated academic scholarship in terms of publications in major peer-reviewed journals, a strong record of sustained extramural research support and the ability and willingness to build multidisciplinary research programs. The successful applicant will be expected to establish and maintain a premier multidisciplinary program in **aging stem cell biology**. Opportunities are available to interact with established and emerging researchers and to mentor predoctoral PhD, MD/PhD, and DDS/Ph.D. students. The Department is highly active in research, teaching and service throughout the UT Health Science Center at San Antonio and is the primary academic home to over 30 tenured or tenure-track faculty.

Departmental faculty oversee three research core facilities: an optical imaging facility, a genomics core and a bone core. In efforts to support and enhance research activities in stem cell biology and regenerative medicine, a stem cell core is under development. Access to institutional core facilities (<http://cores.uthscsa.edu/>) is readily available. The Department of Laboratory Animal Resources, and a number of other service departments are available to support research activities. Investigators seeking to promote collaborative multidisciplinary opportunities and to lead in the development of stem cell research at the UT Health Science Center at San Antonio are encouraged to apply. The UT Health Science Center at San Antonio is home to one of five Nathan Shock Centers for Excellence in Biology of Aging, an NCI-designated Cancer Center, an NIH-funded Clinical Translational Science Award, and the Greehey Children's Cancer Research Institute. An attractive startup package will be offered to the successful candidate. A highly competitive candidate may be eligible for additional startup funds from the UT System STARS program (http://www.utsystem.edu/Aca/initiatives/STARS_Program.htm).

Interested applicants should submit a curriculum vitae, a summary of research accomplishments, future goals (2-3 pages) and contact information for five references to (ENDCHCSB@UTHSCSA.EDU) directed to the attention of **Christi A. Walter, Ph.D., Professor and Chair, Department of Cellular and Structural Biology, The University of Texas Health Science Center at San Antonio, 7703 Floyd Curl Drive, San Antonio, TX 78229-3900**.

The University of Texas Health Science Center at San Antonio is an Equal Employment Opportunity/Affirmative Action Employer. All faculty appointments are designated as security sensitive positions.

Faculty Positions at Barley Genetic Resource Center Research Institute for Bioresources (RIB) Okayama University (Japan)

RIB is seeking candidates for two contracted positions, one FULL PROFESSOR, and the other either ASSOCIATE PROFESSOR or ASSISTANT PROFESSOR. Both positions are available on April 1, 2009.

1. The successful candidate for FULL PROFESSOR should have outstanding records in Plant Genomics and Breeding. The candidate will be responsible for maintaining the barley genetic resources and for studying genetic diversity in barley germplasm through genomics. Responsibility includes teaching and supervision at the graduate school of Okayama University.
2. The candidate for ASSOCIATE or ASSISTANT PROFESSOR is expected to perform molecular biological research on important traits of Triticeae, particularly barley, utilizing the genetic resources. Teaching at the graduate school will be required.

Both successful candidates should have a Ph.D. degree. Application should be made on the form provided at <http://www.rib.okayama-u.ac.jp/index.html>. All application materials should be sent to Dr. Minoru Murata, Director, Research Institute for Bioresources, Okayama University, 2-20-1 Chuo, Kurashiki 710-0046, Japan, by December 26, 2008. Application by e-mail is not acceptable.



Marine Biogeochemistry Position Duke University

Duke University's Division of Earth and Ocean Sciences in the Nicholas School of the Environment invites applicants for a tenure-track faculty position in marine biogeochemistry, with the appointment at the assistant professor level. We are interested in individuals who conduct research in biogeochemical cycling in the context of ocean ecosystems, particularly those who study the ocean's response to climate change. We seek an interdisciplinary scientist who will develop a strong, externally funded research program and participate in undergraduate, graduate and professional teaching and mentoring within the Nicholas School. This search is part of our ongoing efforts to expand the Earth and Ocean Sciences faculty and strengthen research and teaching in the areas of climate, water resources, and energy.

The Nicholas School focuses on leadership in education, research, and service to understand basic earth and environmental processes, to understand human behavior related to the environment, and to inform society about the conservation and enhancement of the environment and its natural resources. Research interests within Earth and Ocean Sciences and the Nicholas School that will complement this position include oceanic ecosystem dynamics, physical oceanography, terrestrial and aquatic biogeochemistry, climate dynamics, paleoclimatology, oceanic biodiversity and marine geospatial analysis. Additional interactions in marine conservation and policy are possible with social scientists within the School and the Nicholas Institute. Duke University is a member of the Duke/University of North Carolina Oceanographic Consortium that operates and supports the regional oceanographic vessel R/V *Cape Hatteras*.

Letters of interest should include a curriculum vitae and names of three references and be sent to: **Marine Biogeochemist Search Committee, Division of Earth and Ocean Sciences, Nicholas School of the Environment, Box 90227, Duke University, Durham, NC 27708**. The search committee will begin to review applications on **December 15, 2008**, with an anticipated start date of September 1, 2009.

Duke University is an Affirmative Action/ Equal Opportunity Employer.



Eidgenössische Technische Hochschule Zürich
Swiss Federal Institute of Technology Zurich

Assistant Professor of Physical-Organic Chemistry

The Department of Chemistry and Applied Biosciences (www.chab.ethz.ch) at ETH Zurich invites applications for an Assistant Professor of Physical-organic Chemistry.

The research program of the candidates should focus on the discovery and development of novel methods and strategies to investigate organic advanced materials. A combination of experimental and theoretical approaches is highly desirable. The successful candidate will be expected to teach organic undergraduate level courses (German or English) and graduate level courses (English).

Requirements for candidacy are the commitment to build a successful, internationally recognized research program, excellence in teaching, and a willingness to collaborate within and outside ETH Zurich.

Assistant professorships have been established to promote the careers of younger scientists. The initial appointment is for four years with the possibility of renewal for an additional two-year period.

Please submit your application together with a curriculum vitae and list of publications to the **President of ETH Zurich, Prof. Dr. Ralph Eichler, Raemistrasse 101, 8092 Zurich, Switzerland, no later than February 28, 2009**. With a view toward increasing the number of female professors, ETH Zurich specifically encourages female candidates to apply.

Programme and Research Leader Posts

The Institute of Food Research is launching an international search for senior research leader positions in the following areas.

A Programme Leader to lead our Strategic Programme in "Biology and Complexity of Foodborne Bacterial Pathogens".

New Research Leaders posts in "Molecular Microbiology of the GI Tract" and in "Bioactive Carbohydrates".

IFR is the UK's only integrated basic science provider focused on food and is a world leading contributor to harnessing food for health and controlling food-related disease. The outcomes of its work feed into national and international strategies and deliver advice and solutions for UK Government, public sector bodies, regulatory authorities, industry and consumers.

IFR is situated on the Norwich Research Park, alongside the University of East Anglia, the John Innes Centre and the Norfolk and Norwich University Hospital. These Institutions are working in partnership to a common set of goals – the Norwich Science and Innovation Vision.

In addition to integration with in-house programmes, IFR would particularly wishes to encourage the development of new links with researchers across the NRP.

Research Leader in 'Bioactive Carbohydrates'

The Institute of Food Research (IFR) is seeking to attract a new project leader to develop research into understanding the molecular and cellular mechanisms by which dietary carbohydrates promote health through the prevention of long-term chronic disease.

IFR is a multidisciplinary organisation with relevant research expertise in:

- The physical chemistry of bioactive plant carbohydrates and the use of plant polysaccharides in the development of encapsulation and release systems
- The immunology, colloid science and cell biology associated with uptake through the gut and functional roles of natural carbohydrates
- The role of carbohydrates in bacteria-host interactions (commensals and human pathogens) in the gut

In addition to creating their own research programme there are opportunities for collaborations with researchers at IFR in the above areas and with other researchers on the NRP interested in glycobiology.

As part of the ongoing development of the IFR research portfolio, we are now looking to recruit an ambitious and talented individual with research interests that complement and extend current activities. This is a non-teaching position, with core staff and running budgets, and with limited administration over the first few years.

Informal enquiries from those wishing to discuss potential research topics may be directed to Dr ENC Mills (clare.mills@bbsrc.ac.uk). Further information on current carbohydrate research at IFR can be obtained from Prof. VJ Morris (vic.morris@bbsrc.ac.uk) and at the JIC from Prof R Field (rob.field@bbsrc.ac.uk).

Salary on appointment will be within the range £41,930 to £46,589 per annum depending on qualifications and experience. This is an indefinite term contract. **Job reference 0128.**

Programme Leader in Foodborne Bacterial Pathogens

We seek to appoint an internationally-recognised senior molecular microbiologist to lead the IFR Institute Strategic Programme (ISP) on bacterial foodborne pathogens, and also to lead their own high profile research on the physiology and molecular biology of a foodborne pathogen.

The Programme Leader will be directly responsible for the management of the ISP, direct management of four other theme leaders, for finance and administration of the programme, contributing to the strategy and scientific management of IFR, and will play a role in the development of IFR science in the context of the exciting Norwich Science Vision. In addition, the Programme Leader will direct one of the research themes on foodborne bacterial pathogens, to complement the existing themes focused upon *Clostridium botulinum*, *Campylobacter*, and microbial complexity.

Suitable candidates will have an international reputation for their work on the physiology/molecular biology of bacterial foodborne pathogens, and experience in senior management of science. The candidates should have an outstanding publication record and will have attracted significant levels of external income.

Salary on appointment will be within the range £53,495 to £59,438 per annum depending on qualifications and experience. This is an indefinite term contract. **Job reference 0341.**

Research Leader in Molecular Microbiology of the GI Tract

The Gastrointestinal Tract Strategic Programme is one of four newly established strategic research programmes established at IFR and collaborating with the University of East Anglia. The GI-tract to be led by Professor Simon Carding, aims to explore the tract as a complex series of interconnected biological systems. The overarching question to be addressed is how intestinal health is established and maintained. This includes analysis of the complex GI tract micro biota, the mucosal epithelium and the immune system. The programme aims to characterise these components and understand how they interact with each other and with the broader host physiology with the ultimate objective of providing new insights into the maintenance of health and prevention / curing of acute and chronic disease.

We seek candidates with outstanding research and publication records with a background in microbial genetics and physiology. Applicants with a more general microbiology background who have the enthusiasm and dedication to make a difference to gut microbial ecology, and have a strong willingness to adopt a cross-and multi-disciplinary approach to this area of research are encouraged to apply. The successful candidate will be expected to establish an internationally high profile independent research programme, and be responsible for developing and seeking funding for collaborative projects with other members of the Gastrointestinal Tract SP and with research groups within the Norwich Research Park.

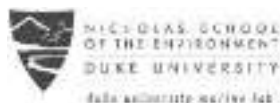
Salary on appointment will be within the range £41,930 to £46,589 per annum depending on qualifications and experience. This is an indefinite term contract. **Job reference 1001728.**

For further information and details of how to apply, please visit our website <http://jobs.ifr.ac.uk> or contact Human Resources, The Operations Centre, Norwich Bioscience Institutes, Norwich, NR4 7UH, UK. Tel: (01603) 450462. Please quote the relevant job reference number. Closing date for all posts: 25th January 2009.



The Institute of Food Research is a registered charity (No 1058499) grant-aided by the Biotechnology and Biological Sciences Research Council and is an Equal Opportunities Employer.





**Mary Derrickson McCurdy Visiting Scholar in
Conservation Genetics
at the Marine Laboratory, Beaufort NC**

The Nicholas School of the Environment at Duke University invites applications for the Mary Derrickson McCurdy Visiting Scholar at the Marine Laboratory in Beaufort, North Carolina. The Nicholas School focuses on leadership in research, education, and service to understand basic Earth and environmental processes, to understand human behavior related to the environment, and to inform society about the conservation and enhancement of the environment and its natural resources for future generations. We seek a young scientist of outstanding promise in the field of Conservation Genetics, which we define broadly as the use of molecular approaches to assess, protect, restore, or maintain species, communities, habitats, or ecosystems, particularly those that are threatened or endangered. We are especially interested in the application of novel molecular approaches to the conservation of marine organisms and ecosystems; in support of this research, the Marine Laboratory maintains the Marine Conservation Molecular Facility (<http://www.nicholas.duke.edu/marinelab/molecular.html>). The McCurdy Scholar carries an appointment as Visiting Assistant Research Professor. The successful candidate is expected to engage fully in the intellectual life of the Marine Laboratory, including research, teaching, and mentoring. The term of the appointment is for one year, with potential for renewal in years 2 and 3.

Interested individuals should send curriculum vitae, summary of research interests and accomplishments, reprints of three recent papers and names of three references to the search chair. Electronic submission is strongly encouraged, but if necessary, please submit hard copy materials to the search chair:

Dr. Douglas Nowacek
Chair, Search Committee, Conservation Genetics
135 Duke Marine Lab Road
Beaufort, NC 28516-9721
dnp3@duke.edu

The search committee will begin reviewing applications on **January 15, 2009**. The search will remain open until the position is filled.

Duke University is an Affirmative Action/ Equal Opportunity Employer.

**Dean of the School of
Graduate Studies/Vice Dean
of Basic Science Research for
the College of Medicine**

The State University of New York Downstate Medical Center, located in Brooklyn, New York, seeks a dynamic leader to serve as Dean of the School of Graduate Studies and Vice Dean of Basic Science Research for the College of Medicine. The Dean of the School of Graduate Studies will provide leadership and support to approximately 100 faculty and 85 students who participate in three Ph.D. and MD/Ph.D. programs: Molecular and Cellular Biology, Neural and Behavioral Science, and Biomedical Engineering. The Dean will work closely with the faculty to ensure an outstanding education for our students, will spearhead efforts to obtain extramural funding to supplement state support of the graduate school, and will direct the recruitment of students. As Vice Dean for Basic Science Research, he/she will provide support and oversight of the Center's basic research programs, promote basic science and translational research interactions within the institution, and assist faculty in identifying and securing additional extramural funding. Candidates should have a strong track record of sponsored biomedical research and experience training graduate students. Send CV and statement of educational philosophy by February 15 to: GradSearch@downstate.edu



**SUNY
DOWNSTATE**
Medical Center
SUNY Downstate is an EOE

FELLOWSHIPS



**Office of the Science and
Technology Adviser to the
Secretary of State**

Jefferson Science Fellowship

The National Academies is pleased to announce a call for nominations and applications for the 2009 Jefferson Science Fellows program. This program establishes a new model for engaging the American academic science, technology and engineering communities in the formulation and implementation of U.S. foreign policy.

Jefferson Science Fellows will spend one year at the U.S. Department of State in Washington, D.C. and may periodically travel to U.S. foreign embassies and/or missions.

Jefferson Science Fellow awards are open to tenured academic scientists, technologists and engineers from U.S. institutions of higher learning. Nominees/applicants must be U.S. citizens and will be required to obtain a security clearance.

Detailed information on the Jefferson Science Fellows program is available on the web:

www.national-academies.org/jsf

The deadline for nominations and applications for the 2009 program year is **January 15, 2009**.

The Jefferson Science Fellows program is sponsored by the U.S. Department of State.

THE NATIONAL ACADEMIES
Advisers to the Nation on Science, Engineering, and Medicine



Weill Cornell Medical College

**Faculty Position
Director
Appel Institute for Alzheimer's Research**

Weill Cornell Medical College is currently undergoing a major expansion of its research program including the construction of a new research building. As part of this expansion we are seeking a Director to establish a new institute; The Appel Institute for Alzheimer's Research. The goal of the Institute, consistent with the donor's wishes, is to better understand the mechanisms behind this disease and to develop treatments leading to a cure.

Candidates should have an outstanding record of productivity in basic or clinical research with a major program likely to impact Alzheimer's research. The recruited faculty will be provided with generous support and space as part of this initiative. In addition to medical student teaching, candidates will participate in the Graduate School of Medical Sciences Program which includes faculty from the Weill Cornell Medical College and the Sloan-Kettering Institute, and in the Tri-Institutional MD-PhD Program and the Training Program in Chemical Biology, which also include faculty from The Rockefeller University. Applications should include a curriculum vitae and a statement of research interests. Applications should be sent electronically to: hmlander@med.cornell.edu (**Dr. Harry Lander, Associate Dean for Research Administration, Weill Cornell Medical College, 1300 York Avenue, New York, NY 10021**). All applications will be treated confidentially.

EEO/AA/M/F/D/V

PICTURE YOURSELF AS A AAAS SCIENCE & TECHNOLOGY POLICY FELLOW

Make a Difference.

Help give science a greater voice in Washington, DC! Since 1973, AAAS Fellows have applied their skills to federal decision-making processes that affect people in the U.S. and around the world, while learning first-hand about the government and policymaking.

Join the Network.

Year-long fellowships are available in the U.S. Congress and federal agencies. Applicants must hold a PhD or equivalent doctoral-level degree in any behavioral/social, biological, medical/health, or physical science, or any engineering discipline. Individuals with a master's degree in engineering and three years of post-degree professional experience also may apply. Federal employees are not eligible and U.S. citizenship is required.

Apply.

The application deadline for the 2009-2010 AAAS Fellowships is 15 December 2008. Fellowships are awarded in the spring and begin in September. Stipends range from \$70,000 to \$92,000.

Note: Additional fellowships are available through approximately 30 scientific society partners. Individuals are encouraged to apply with AAAS as well as with any scientific societies for which they qualify.

Full details at: **fellowships.aaas.org**



*Enhancing Public Policy,
Advancing Science Careers*

Kathy Kahn, PhD

Interdisciplinary Biological
Sciences, University of
Missouri

2004-2006 AAAS Fellow
at the U.S. Department of
Agriculture, Biotechnology
Group in the Foreign
Agricultural Service

Currently at the Bill and
Melinda Gates Foundation
as a program officer in
global development



ADVANCING SCIENCE. SERVING SOCIETY



FACULTY RECRUITING

The Jackson Laboratory, a mammalian genetics research institution, has launched a major research expansion. Faculty members, **especially those with a focus on using mouse models to understand human biology and disease processes**, will be recruited in the following areas:

- **Computational Biology/Bioinformatics/Genomics**
- **Cancer Biology**
- **Immunology/Inflammation/Hematology**
- **Metabolic Disease/Aging Research**
- **Neurobiology**
- **Reproductive and Developmental Biology/Stem Cells**

We seek applicants at the Assistant, Associate and Full Professor levels. Candidates should have a Ph.D., M.D., or D.V.M., and have completed postdoctoral training with a record of research excellence. They must have the ability to develop a competitive, independently funded research program.

The Jackson Laboratory offers a unique scientific research environment characterized by excellent collaboration among our faculty, unparalleled mouse and genomic resources, outstanding scientific support services, postdoctoral and pre-doctoral training programs, and numerous courses and conferences centered on the mouse as a genetic model for human biology and disease.

For more information go to: www.jax.org

Applicants should send a curriculum vitae and a concise statement of research interests and plans, and arrange to have three letters of reference sent to: facultyjobs@jax.org.

Review of applications will begin in **January, 2009**.

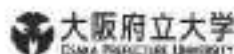
The Jackson Laboratory is an EOE/AA Employer.

FACULTY POSITIONS DEPARTMENT OF PHYSICS THE UNIVERSITY OF TEXAS AT AUSTIN

The Department of Physics at The University of Texas at Austin is seeking candidates for tenure-track assistant professorship positions in physics starting in September 2009. In special cases, appointments at more senior levels will be considered. Successful candidates will assume full teaching responsibilities for undergraduate and graduate courses in the Department of Physics and are also expected to conduct vigorous research programs. Research areas of current highest priority for the Department are Biophysics Experiment and Fundamental Theory/Cosmology. Outstanding candidates in other areas of departmental focus will also be considered. Excellent English language communication skills are required. Applicants must have a Ph.D. (or equivalent) and a demonstrated potential for excellence in teaching and research.

Interested applicants should send a curriculum vitae, a list of publications, a statement of research interests, a research plan, and should arrange for at least five letters of recommendation to be sent to: **Prof. John T. Markert, Chair, Department of Physics, The University of Texas at Austin, 1 University Station C1600, Austin, TX 78712-0264**. Review of completed applications began in **October, 2008** and is ongoing.

The University of Texas at Austin is an Equal Opportunity/Affirmative Action Employer.



Tenure Track Positions (2nd Term) Nanoscience and Nanotechnology Research Center Osaka Prefecture University, Osaka, Japan

Osaka Prefecture University is seeking to appoint suitable candidates for tenure track positions as second-term special lecturers at the Nanoscience and Nanotechnology Research Center. This recruitment is held under the "Leading University in the Region as a Base for Human Resource Development in Nanoscience and Nanotechnology" program. Applicants should hold a PhD degree acquired within the past 10 years; a track record of three or more years as an assistant professor, postdoctoral fellow or an equivalent title as of April 1, 2009; and excellent research achievements in the fields of nanoscience or nanotechnology.

- **Number of tenure track positions available:** Three special lecturers.
- **Research areas:** A wide range of research areas related to nanoscience and nanotechnology.
- **Appointment duration:** From April 1, 2009 to March 31, 2014.
- **Annual salary:** Approximately 8,000,000 yen.
- **Research fund:** During the first fiscal year, 10,000,000 yen will be provided as a start-up fund, and from the second year onward, 5,000,000 yen per annum will be ensured.
- **Promotion to tenured associate professors:** Tenure track lecturers hired through this recruitment program will be promoted to tenured associate professors of Osaka Prefecture University—or tenured full professors if they have shown an excellent record of accomplishment—starting from April, 2014 after successfully passing the final evaluation. In such cases, those who have been promoted may be positioned to their preferred department and faculty at the university.
- **Submission deadline:** December 25, 2008, 5 p.m. Japan Standard Time. All documents must be submitted online through our website by the deadline, with hard-copy documents to follow.
- Please refer to our official website below for a complete description of the position and application information.

<http://www.nanosq.21c.osakafu-u.ac.jp/>
<http://www.nanosq.21c.osakafu-u.ac.jp/en/>



The Centre Director Heart and Stroke Foundation Centre for Stroke Recovery

..... a cutting edge leadership position

The Heart and Stroke Foundation Centre for Stroke Recovery (HSFCSR) is a unique organization created in 2002 in response to a bold new vision to transform research in Stroke Recovery. A virtual organization, the HSFCSR is based in Ontario and is comprised of three sites, four academic institutions, and five partners. Collectively, these three sites, each with a core research specialty cover the critical research components and create an entity much bigger than the constituent parts.

Success in the first five years has led to larger funding commitments and a bigger and more ambitious vision going forward. The new vision prompts the creation of this exciting and challenging new position.

The Centre Director will manage the Centre, provide leadership, and support to the Site Leaders and their scientific teams. The focus is on strategic direction and charting the course ahead; providing direction and inspiration to the research teams; communicating status and progress to stakeholders; fund raising; and representing the HSFCSR as required.

Applications will be accepted until **January 30, 2009**. Interested applicants should send their CV and contact information to:

Chris Nelson
Executive Director
Heart and Stroke Foundation Centre for Stroke Recovery
601 Golden Avenue
Ottawa, ON
K2A 2E8
Office - 613-729-6618
E-Mail - chris_nelson@sympatico.ca

The HSFCSR Board welcomes applications from visible minority group members, women, Aboriginal persons and persons with disabilities. All qualified candidates are encouraged to apply; however, Canadians and permanent residents will be given priority.



THE CHINESE UNIVERSITY OF HONG KONG



Applications are invited for:-

Director and Professor, School of Life Sciences

(Ref. 08/227(665)/2)

The Chinese University of Hong Kong, founded in 1963, aspires to be acknowledged regionally and internationally as a first-class comprehensive research university. The University offers a broad spectrum of programmes up to PhD level in various disciplines organized under eight Faculties (viz. Arts, Business Administration, Education, Engineering, Law, Medicine, Science and Social Science), with a team of over 2,000 full-time teaching and research staff. In 2008-09, undergraduate and postgraduate enrolment in publicly-funded programmes stands close to 11,000 and 3,200 respectively (<http://www.cuhk.edu.hk>).

The Faculty of Science comprises six Departments: Biochemistry, Biology, Chemistry, Mathematics, Physics and Statistics, and one School: Chinese Medicine, and also offers a number of multidisciplinary programmes: Cell and Molecular Biology, Environmental Science, Food and Nutritional Sciences, Molecular Biotechnology, Mathematics and Information Engineering (double degree), Quantitative Finance and Risk Management Science (double major), and Risk Management Science. The Faculty has 300 full-time teaching and research staff, 1,600 undergraduate and 500 postgraduate research students. Detailed information on the Faculty is available at <http://www.cuhk.edu.hk/sci/>.

A new School of Life Sciences will be established within the Faculty of Science through re-organization of teaching and research programmes in the existing Departments of Biochemistry (Science) and Biology. The School will ultimately have more than 40 academic staff, about 900 undergraduate and 300 postgraduate students. World-class research facilities are available. The School will create synergies in research and scholarship, and provide the institutional framework for taking advantage of exciting new opportunities in modern life sciences, both within the Faculty of Science and also in collaboration with the Faculty of Medicine.

The School will offer six undergraduate major programmes and corresponding research postgraduate programmes in Cell and Molecular Biology, Biochemistry, Biology, Environmental Science, Food and Nutritional Sciences, and Molecular Biotechnology; and also two taught MSc programmes: Biochemical and Biomedical Sciences, and Nutrition, Food Science and Technology. The School will enter a period of expansion with the introduction of the Cell and Molecular Biology programme in 2009-10 and the change of the normative undergraduate curriculum from 3 years to 4 years in 2012-13.

Applicants should be academics with (i) an outstanding record of scholarship appropriate for senior appointment at professor level in a discipline of life sciences; (ii) an appreciation of the breadth and depth of research and educational activities in life sciences, in particular the opportunities ahead for cutting-edge research; (iii) experience in leading well-funded, internationally-recognized, and preferably multi-disciplinary collaborative research programmes; (iv) demonstrated leadership and management ability at an appropriate level in higher education institutions; (v) long-term vision for the development of the School into a centre of research excellence; and (vi) excellent interpersonal and communication skills.

As the academic and executive head of the School reporting to the Dean of the Faculty of Science, the appointee will (a) be responsible for the vision and stewardship of the School; (b) undertake overall responsibility for academic, financial, staff and student matters; and (c) provide strong leadership in the re-organization process particularly in planning and leading research directions of the School. Appointment will initially be made on contract basis for up to five years commencing as soon as possible, leading to longer-term appointment or substantiation later subject to mutual agreement. The selected candidate will also be offered a full professorship appointment in a subject related to his/her own speciality area of scholarly interests, to be held concomitantly with the Directorship of the School.

Consideration of applications/nominations will begin in February 2009 and will continue until the post is filled. The University reserves the right to fill the post by invitation.

Salary and Fringe Benefits

Salary will be highly competitive, commensurate with qualifications and experience. The University offers a comprehensive fringe benefit package, including medical care, a contract-end gratuity for an appointment of two years or longer, and housing benefits for eligible appointees.

Further information about the University and the general terms of service for appointments is available at <http://www.cuhk.edu.hk/personnel>. The terms mentioned herein are for reference only and are subject to revision by the University.

Application Procedure

Please send full resume, copies of academic credentials, a publication list and/or abstracts of selected published papers, together with names, addresses and fax numbers/e-mail addresses of three referees to whom the applicants' consent has been given for their providing references (unless otherwise specified), to the Personnel Office, The Chinese University of Hong Kong, Shatin, N.T., Hong Kong (Fax: (852) 2603 6852). The Personal Information Collection Statement will be provided upon request. Please quote the reference number and mark 'Application - Confidential' on cover.

Wyeth Leading the way in making a difference in the world.

Vaccines from Wyeth are making a difference in the quality of people's lives around the world. For over 100 years, Wyeth has been a leader in vaccines research and innovation, developing products to combat significant public health threats. Our award-winning pneumococcal vaccine, Prevnar, has prevented millions of cases of pneumococcal disease and saved thousands of lives worldwide. At Wyeth, scientists are focused on developing innovative products like Prevnar to address unmet health needs throughout the world.

We're helping people around the globe by building one of the industry's strongest R&D pipelines, responsible for some of today's most important R&D in Vaccines. Current areas of research include:

- PEDIATRIC AND ADULT INFECTIOUS DISEASES
- NEUROLOGICAL DISORDERS
- NOSOCOMIAL INFECTIONS

We currently have the following opportunities for experienced scientific professionals at our Research facility located in the Metropolitan New York area of Pearl River, NY:

- FORMULATION SCIENTISTS
- ANALYTICAL & PROCESS DEVELOPMENT PROFESSIONALS
- DISCOVERY RESEARCH
- CLINICAL RESEARCH, PHYSICIAN LEADS

Ideal candidates will have experience in candidate discovery, analytical, formulations, bio-process development and assay development to contribute to our expanding vaccine pipeline. B.Sc., M.Sc., or Ph.D. in Bacteriology, Molecular Biology, Immunology, or Biochemistry required. Pharmaceutical or biotech industry experience preferred. M.D. with infectious disease focus for clinical medical monitor and other leadership roles essential.

We offer extensive training and mentoring, a competitive compensation package including comprehensive benefits, child-care subsidies, educational assistance and professional development programs. For more information on these and other available opportunities, please visit: www.wyeth.com/careers

Wyeth

www.wyeth.com/careers

Wyeth is an equal opportunity employer that shares the vision of a diverse workplace.

Leading the way to a healthier world



Affiliated with the University of Southern California

Scientist Positions: (all levels) Division of Cell Biology and Genetics

As part of a major expansion of its research enterprise, the House Ear Institute is launching a search to fill 3 - 4 Laboratory Head positions over the next three years in the newly reorganized Division of Cell Biology and Genetics. The House Ear Institute is a private, non-profit research organization affiliated with the University of Southern California (USC) in Los Angeles.

Candidates with expertise in developmental biology, regeneration/stem cell biology, systems biology, and human and mouse genetics are particularly encouraged to apply. Candidates should have an excellent publication record, and are expected to have or to develop an externally funded research program in their field of expertise.

Appointees will receive a generous startup package, including competitive salary and benefits, recently built or renovated lab space, subsidized core facilities, and generous animal care subsidies. HEI scientists hold appointments in appropriate basic science departments at USC's Keck School of Medicine, and are expected to take part in graduate student and postdoctoral training.

Current interests in the Division of Cell Biology and Genetics include: developmental biology and regeneration; stem/progenitor cell biology; genetics and pathology of auditory system disorders in model systems and humans; cancer of the nervous system; otitis media/bacterial pathogenesis; structure and function of the inner ear.

Consideration of candidates begins **January 1, 2009**. Interested candidates should forward their curriculum vitae, a brief statement of research accomplishments and future goals, and the names of three references to: **Cell Biology and Genetics Search Committee, The House Ear Institute, 2100 West Third Street, Los Angeles, CA 90057; CBGsearch@hei.org**.

HEI is an Equal Opportunity Employer.



IN 2009

CNRS IS RECRUITING FOR 300 TENURED RESEARCHER POSITIONS IN ALL FIELDS OF SCIENCE

- MATHEMATICS • PHYSICS
- NUCLEAR AND HIGH-ENERGY PHYSICS
- CHEMISTRY
- SCIENCE AND TECHNOLOGY OF INFORMATION AND ENGINEERING
- UNIVERSE AND EARTH SCIENCE
- ENVIRONMENT AND SUSTAINABLE DEVELOPMENT
- LIFE SCIENCES • HUMANITIES AND SOCIAL SCIENCES

CNRS encourages junior and senior scientists from around the world to apply for its tenured researcher positions.

CNRS provides an enriching scientific environment:

- numerous large-scale facilities
- highly skilled technical support
- multiple international and interdisciplinary networks
- access to university research and teaching
- lab-to-lab and international mobility

Application deadline: January 6th, 2009

www.cnrs.fr



Department of Health and Human Services Office of Public Health and Science Office of Research Integrity Health Scientist Administrator Position



The Division of Investigative Oversight (DIO) within The Office of Research Integrity (ORI) is seeking two experienced scientists or physicians with research/clinical experience to serve under the Director, DIO, as an Investigator/Scientist. DIO's primary task is to conduct oversight reviews of institutional investigations of research misconduct. Applicants should be experienced in running a research program, supervising students and postdoctoral fellows, successfully competing for Federal extramural or intramural funds, and preparing peer reviewing manuscripts and grant applications. Applications with a broad range of experience and scientific interests are preferable because of the wide range of topics that ORI deals with. Good oral and written communication skills are essential.

Please apply online at <http://usajobs.opm.gov/> and go to job announcement **HHS-OS-2009-0034**. Applications must be received by approximately **December 24, 2008**. If you need assistance, contact the **Rockville, MD, HelpDesk at 888-478-4340 (7:30 am - 4:00pm M-F) or quickquestions@psc.gov (TTY/TDD: 800-877-8339)**. The position is at the GS-13/14 level (\$98,033-\$127,442), with the actual salary commensurate with experience. You may also reach **John Dahlberg, Director of DIO at 240-453-8800/John.Dahlberg@hhs.gov** for more information. This position offers full benefits including retirement, health insurance, life and long-term health care insurance, and thrift-saving plan participation (matched up to 5% of your salary).

Selection will be based on merit and without consideration for race, color, religion, sex, national origin, politics, marital status, sexual orientation, physical handicap, or membership or non-membership in an employee organization.



Director of the Institut Pasteur

The Search Committee for Director of the Institut Pasteur invites expression of interest from potential candidates for the position of Director of the Institute.

Since its creation in 1887, the Institut Pasteur has been a world leader in fundamental biology and biomedical research as well as a renowned teaching center. The Institut Pasteur is an independent private non-profit foundation for research into biomedicine and public health. In addition to its history of excellence into research on infectious diseases and major discoveries in microbiology, virology, immunology and vaccines, it also has a major commitment to cross-disciplinary approaches, and has extended its focus to other biomedical fields. The Director will join an exciting and innovative academic environment of over 2500 people, in the Campus in the heart of Paris.

The Director will provide the executive leadership for the Institute. He/She will develop an ambitious and strategic vision for the scientific activities to take the Institut Pasteur into the 21st century. He/She will be responsible for the successful translation of basic science into improvement of human health, and will forge industrial partnerships and the fundraising efforts of the Institute. The Director's responsibilities include catalysis of a cooperative research network between the 30 Institutes making up its outstanding international network.

The Search Committee for Director of the Institut Pasteur welcomes letters of interest which should be sent to Professor Jean-Claude Lehmann, Chair of the Search Committee, 26, rue Erlanger F75016 Paris, France, or by e-mail at jc.lehmann@free.fr, before January 31st, 2009.

The committee encourages expression of interest from scientists of the highest international standing/stature, irrespective of their nationality or their experience of working in France.

Inserm scientists work towards improving human health



Inserm is the only French public research body entirely dedicated to human health. Its researchers are committed to studying all diseases, whether common or rare, through their research in the fields of biology, medicine and public health. Through its diversity of approaches, richness of internal expertises, interdisciplinary as well as geographical mobility, Inserm provides a unique environment for researchers.

15000 researchers, engineers and technicians work in the 300 Inserm laboratories housed in hospitals, universities and research campuses, all over France. The positions of Research Associates and of Research Directors are open to PhD (or equivalent title) holders, without nationality restriction.

orc.fr

More than 100 tenure positions available for
scientists m/f
dedicated to biomedical research

Application modalities : visit our website : <http://www.eva2.inserm.fr>

Application deadline : January 9th, 2009 - 4.00.pm (GMT+1)

GRADUATE PROGRAM



Discover the formula
for **business success**

Master in Biotechnology Management

Recent advances in life sciences have brought about a revolution in the biotechnology industry. To face these challenges and meet the business opportunities, IE Business School offers an innovative and challenging Master's program in Biotechnology Management, which combines essential business knowledge with specialized industry know-how.

The program is aimed at professionals from either a scientific or management background looking to jump-start or further their careers within the biotech industry.

Our online program methodology reflects today's international business environment, where cross-cultural teams work on global projects regardless of their geographic location. You will not have to leave your residence or work place for extended periods of time to pursue this career-advancing degree.

For details of this program, please visit: www.ie.edu/biotech

For admissions, contact: biotech@ie.edu



State University of New York State College of Optometry

VISION SCIENCE, OPTOMETRY AND/OR CLINICAL SCIENCES

The State University of New York, State College of Optometry, located in New York City, invites applications for two open rank faculty positions. A strategic priority of SUNY Optometry is to expand its clinical and basic research programs building on its team of leading ocular and vision researchers. Priority will be given to applicants with significant research accomplishment in visual function and/or eye care and demonstrated ability/potential to attract substantial extramural funding. The area of vision research is open, but individuals involved in clinical applications and translational research are especially encouraged to apply, and we aim to fill at least one position with an individual engaged in patient-based research. A capability to interact with the College's clinical faculty is desirable.

Applications (in pdf format) and inquiries should be sent by email to: **Dr. Benjamin Backus, Search Committee Chair, facsearch@sunopty.edu** (receipt will be confirmed). Please include a cover letter, a statement summarizing research interests, a curriculum vitae including a complete list of publications, three sample reprints of published research, and evidence of ability to teach at the graduate/Ph.D. or professional/O.D. level (if available). Applicants at the level of Assistant Professor should also provide three letters of reference (sent by email to facsearch@sunopty.edu, or by regular mail to **Ms. Debra Berger, Faculty Search Committee, SUNY Optometry, 33 W. 42nd St., New York, NY 10036**). Complete applications that are received by Friday, January 30, 2009 will be given priority; applications received after that will be considered until the position is filled.

For further information visit www.sunopty.edu.

*The State University of New York State College of Optometry
is an Affirmative Action, Equal Opportunity Employer.*

SENIOR FACULTY POSITION IN SOFT CONDENSED MATTER PHYSICS

Department of Physics ARTS AND SCIENCE

The Center for Soft Matter Research and the Department of Physics at New York University solicits applications for a senior-level faculty position in experimental soft condensed matter physics to begin September 1, 2009, pending administrative and budgetary approval. The successful candidate must have an internationally-recognized distinguished record of research and a strong commitment to teaching. This appointment is part of an ongoing multi-year program that NYU has embarked on to develop an international center for research at the interface between physics, chemistry, biology, and engineering.

Applicants should send a letter describing current and planned research and teaching activities, a curriculum vitae and list of publications to the **Soft Condensed Matter Search Committee, Department of Physics, New York University, 4 Washington Place, New York, NY 10003**. Applications received by **January 31st, 2009** will get first consideration.



NEW YORK UNIVERSITY

NYU is an Equal Opportunity/Affirmative Action Employer.



Ontario Institute for Cancer Research Director, Transformative Pathology

The Ontario Institute for Cancer Research (OICR) is seeking a Director of Transformative Pathology to develop an innovative research program in molecular pathology and cytopathology. The Director will join OICR's senior management team which oversees OICR's research plan.

OICR is a new research institute, created by the Government of Ontario to enhance cancer research, particularly translation of new discoveries into effective interventions that impact cancer and promote knowledge-based industries in Ontario.

Qualifications:

- An MD with a proven track record in molecular pathology or related discipline(s);
- A relevant international reputation and strong publication record;
- Proven leadership, management experience and communications skills;
- Previous experience in leading multidisciplinary, multi-institutional teams;
- Proven ability to recruit outstanding clinical and basic scientists;
- Excellent and broad understanding of the field of molecular diagnostics and/or therapeutics, genomics, biomarkers, informatics and imaging in oncology;
- Eligible to hold the rank of associate or full professor at an Ontario university.

Conditions of Employment: The Director will devote at least 80 per cent of time to research and may devote up to 20 per cent of time to clinical duties. Academic and clinical appointments may be obtained at the University of Toronto and its affiliated hospitals. The initial appointment is for five years, renewable pending satisfactory review. A competitive salary and benefits package will be negotiated.

Application Process: Candidates are invited to submit a curriculum vitae, a vision statement on the opportunities for OICR to play a lead role in transforming pathology in the health care system and names of three references, electronically to search@oicr.on.ca. For more information about OICR please visit the website at www.oicr.on.ca.

The position will remain open until a suitable candidate is found, however applications are preferred by **January 31, 2009**.

DIRECTOR CENTER FOR NEUROSCIENCE UNIVERSITY OF CALIFORNIA, DAVIS

The University of California, Davis, invites applications and nominations for the position of Director of the Center for Neuroscience, an interdisciplinary unit involving faculty from two different Colleges and the School of Medicine at UC Davis. The integrative and interactive core faculty of the Center for Neuroscience are housed in three research buildings devoted to neuroscience research. Research interests of the current faculty are broad, including molecular, cellular, systems, cognitive, and translational research. The Center provides research space, a variety of shared research facilities, seminar programs, and administrative support for faculty members, graduate students, postdoctoral associates, and distinguished visitors. The Davis campus has made a major commitment to the development of neuroscience through the Center, and will continue this commitment into the future.

We seek as Director an outstanding individual with interests and abilities that are sufficiently broad to provide intellectual and administrative leadership for all neuroscientists at UC Davis. This person should have the ability to work collegially within a diverse environment. In addition to recruiting new faculty, we envision a Director who will be an integral part of facility and building expansion and who will foster bridges between the existing faculty and the School of Medicine, the Center for Mind and Brain, and the M.I.N.D. institute. The Director's research could be in any area of neuroscience ranging from molecular to cognitive neuroscience.

The new Director will have a faculty appointment at the professorial level in an academic department in one of the colleges and schools with programs in neuroscience. The appointment carries an administrative stipend.

All applicants should send a letter of interest or nomination, curriculum vitae, and the names of at least five references by **February 1, 2009** to: **Leo M. Chalupa, CNS Director Search Committee, Neurobiology, Physiology, and Behavior, UC Davis, One Shields Ave., Davis, CA 95616**.

The University of California, Davis, is an Equal Opportunity/Affirmative Action Employer with a strong institutional commitment to the development of a climate that supports equality of opportunity and respect for differences.



STANFORD CANCER CENTER

The Stanford University School of Medicine, the Stanford Institute for Stem Cell Biology and Regenerative Medicine (ISCBRM), and the Stanford Cancer Center are holding open searches for two tenure-line faculty in the areas of cancer gene discovery, cancer stem cell biology and cancer immunology with research centered around basic cancer cell biology, the use of new immune therapies, or the development and use of new targeted agents. Positions are open at the assistant, associate or full professor level.

The overriding requirement for faculty appointment, reappointment and promotion within the UTL must be distinguished performance, or (in the case of junior faculty) the promise of distinguished performance. There should be a major commitment to research and teaching. There must be outstanding accomplishments in research and excellent overall performance in teaching, as well as in clinical care and institutional service appropriate to the programmatic need the individual is expected to fulfill.

Successful candidates will have an outstanding record of research and a strong interest in translating these discoveries into pre-clinical and clinical research. All appointments to the Institute for Stem Cell Biology and Regenerative Medicine or in the Stanford Cancer Center will be in departments at Stanford University. Interested candidates should indicate preferences for department affiliation. Appointees will work on location in the Institutes for Medicine laboratories or in the Cancer Center, and will participate in their research and teaching activities. While excellence in teaching is an important criterion, the appointments will be based primarily on research accomplishments and the promise of future research and translational medicine advances. Salary will be commensurate with the level of employment, relevant experience, and accomplishments. Physician scientists are especially encouraged to apply.

Please address and mail letters of interest, along with full curriculum vitae and the names and addresses of three references to the address below by **January 15, 2009**:

Beverly S. Mitchell, MD
Director, Stanford Cancer Center
Stanford University
800 Welch Road, MC 5796
Palo Alto, CA 94305-5796

Stanford University is an Equal Opportunity Employer and is committed to increasing the diversity of its faculty. It welcomes applications from, and nominations of, women and members of minority groups, as well as others who would bring additional dimensions to the university's research, teaching, and clinical missions.

GRADUATE PROGRAM

biological design

graduate program

Are you interested in learning how to conduct interdisciplinary research that focuses on:

- eradicating cancer
- presymptomatic diagnosis of disease
- sustainable energy sources
- outpacing infectious diseases

Our new Ph.D. program offers unique interdisciplinary training that focuses on large scale, use-inspired research.

Experience a new dimension of scientific exploration...

biologicaldesign.asu.edu/bd

graduate.asu.edu



Department of Health and Human Services National Institutes of Health National Institute on Aging Intramural Research Program



Staff Scientist - Animal Program Director

The National Institute on Aging (NIA), a major research component of the National Institutes of Health (NIH) and Department of Health and Human Services (DHHS), is recruiting for a Staff Scientist-Facility Head who will serve as the Animal Program Director for the NIA Intramural Research Program (IRP), as well as Section Chief of the Comparative Medicine Section (CMS) of the Research Resources Branch (RRB). The incumbent will be responsible for an AAALAC accredited animal care and use program and for support of the animal research programs in the Institute, studying animal models of development and aging, and interventions to prevent or alleviate aging-related deficits. The supervisory and regulatory responsibilities of this position require the applicant to hold a veterinary degree (D.V.M., V.M.D., or equivalent degree) with certification or eligibility for board certification in laboratory animal medicine or veterinary pathology.

Applicants must have a proven record of management of an animal research program. The expertise and experience should include, but not be limited to interaction and cooperation with scientific staff in a manner that promotes and facilitates their scientific programs. Duties will include cost-effective breeding and maintaining numerous transgenic and knockout lines (currently in excess of 600) including "difficult" lines, collaboration with scientific staff in effective production and import of new genetically manipulated lines, and, especially, in maintaining a current and accurate database on the colony status. The incumbent will oversee animal health surveillance and maintain both a barrier facility and a quarantine area. The incumbent will perform animal surgery and teach appropriate procedures to animal care and technical staff.

Salary is commensurate with experience and accomplishments. The salary range for Staff Scientists is \$82,961 - \$166,430. A full Civil Service package of benefits (including retirement, health, life and long term care insurance, Thrift Savings Plan, etc.) is available. Additional information regarding the NIA, IRP and the RRB is available at the following websites: <http://www.grc.nia.nih.gov> and <http://grc.nia.nih.gov/branches/rrb/rrb.htm>. To apply: Please send a cover letter, curriculum vitae, bibliography, statement of research interests, and three letters of recommendation to: Peggy Grothe, Intramural Program Specialist; Office of the Scientific Director; National Institute on Aging, 251 Bayview Boulevard, Suite 100- Room 04C232, Baltimore, MD 21224-6825. Advertisement is open until the position is filled. Please include the following vacancy number in all correspondence: Vacancy # **NIA-IRP-08-09**. If additional information is needed, please call 410-558-8012 or email: grothep@mail.nih.gov.



DHHS and NIH are Equal Opportunity Employers





CANADA RESEARCH CHAIR (TIER 2) BONE and JOINT IMAGING

Applications are invited for a Canada Research Chair Tier 2 position (applicant must be less than 10 years from MD or PhD) in bone and joint imaging leading to work with Synchrotron Light. This position will capitalize and strengthen existing research collaborations within the University of Saskatchewan (www.usask.ca) in regards to both basic science and clinical aspects of bone and joint health. The University is world renowned for its longitudinal studies of pediatric bone health and more recently for growing expertise in bone imaging with micro- and peripheral quantitative computed tomography (QCT). The position of Chair will consolidate this expertise and mesh both clinical and basic science research leading to synchrotron-based investigations. The University of Saskatchewan is home to the Canadian Light Source (CLS), a world-class synchrotron facility that will feature a newly constructed Biomedical Imaging and Therapy (BMIT) beamline (www.lightsource.ca).

This proposed CRC Chair position will expand and maximize the research potential of imaging modalities at the CLS for better diagnosis of bone disorders, joint and inflammatory pain and other related diseases using relatively non-invasive techniques. This Chair position will create opportunities to form research links between the Colleges of Kinesiology, Engineering, Medicine, Veterinary Medicine, and the Saskatoon Health Region, along with the Canadian Light Source and will access the extensive resources of these various units. The candidate will contribute to graduate and undergraduate teaching and knowledge exchange activities relating to bone and/or joint research.

We are seeking applications from basic or clinical research scientists (MD, PhD or MD/PhD) with a demonstrated track record in the field of bone and/or joint research and the potential to achieve international recognition. Expertise in image analysis, synchrotron imaging, or 3-D imaging techniques, including QCT and micro-computed tomography, is highly desirable. Candidates should have outstanding communication and leadership skills for the facilitation and growth of the research program and the desire to work in a multi-disciplinary environment. The candidate's research program should complement existing University strengths and link with current clinical and basic science expertise. The successful candidate will hold a tenure-track position at appropriate rank within a department of the College of Medicine at the University of Saskatchewan (www.medicine.usask.ca).

Interested candidates should send an updated CV and three letters of reference (other examples of publications or scholarly work and a teaching dossier may be included) to: **Dr. Jim Thornhill, Associate Dean of Research and Graduate Studies, College of Medicine, University of Saskatchewan, B103 Health Sciences Building, Saskatoon, SK, CANADA S7N 5E5.** For more information, e-mail jim.thornhill@usask.ca or call 1-306-966-8119.

Applications will be accepted until **January 31, 2009.**

The University is committed to Employment Equity. Members of Designated Groups (women, aboriginal people, people with disabilities and visible minorities) are encouraged to self-identify on their applications. All qualified candidates are encouraged to apply; however, Canadians and permanent residents will be given priority.



VISION RESEARCH Tenure-Track Faculty Position

The Eye Research Institute (ERI), an independent academic unit of Oakland University, invites applications for a tenure-track faculty position at the **ASSISTANT or ASSOCIATE PROFESSOR** level. The successful candidate must have a Ph.D. and post doctoral experience, and will establish (or bring) a vigorous, NIH-funded program in the broad area of vision research. Academic rank and salary will be commensurate with experience.

Oakland University is a growing public institution, situated on an attractive 1400-acre campus in southeastern Michigan, and is scheduled to launch a new private Medical School with nearby William Beaumont Hospital in 2010. ERI faculty members conduct research on the biochemistry, physiology, cell and molecular biology of eye tissues, with emphasis on the retina. A variety of clinical research studies are performed in conjunction with investigators at the Beaumont Hospital Department of Ophthalmology. Additional information is available on the ERI website: <http://www2.oakland.edu/eri>.

Applicants should submit via email (PDF or Word files): (1) C.V., (2) statement of research interests and accomplishments, (3) contact information for three references, and (4) three significant publications, to **Dr. Andrew Goldberg, ERI Search Committee Chair**, at: pmrealy@oakland.edu. The review process will begin **January 15, 2008** and continue until the position is filled.

Oakland University is an Equal Opportunity Employer and encourages applications from women and minorities.



Evolutionary and Environmental Genomics

The Department of Ecology and Evolutionary Biology at the University of Arizona seeks to hire at the Assistant, Associate or Full Professor level in the areas of evolutionary and environmental genomics. Candidates' research should show evidence of originality and address significant evolutionary or ecological questions. Approaches can include population genetics, functional and comparative genomics, bioinformatics, field and experimental studies, and can focus on any group of organisms, including microbes. Multidisciplinary research and potential links to other UA programs, such as the initiatives at Biosphere 2 and the BIO5 Institute, are particularly welcomed.

To apply, please submit statements of research and teaching interests, complete CV, and up to five reprints of published work, and arrange for three letters of recommendation to be sent to: **Evolutionary and Environmental Genomics Search Committee, Department of Ecology and Evolutionary Biology, 1041 E. Lowell Street, University of Arizona, Tucson AZ 85721.**

The University of Arizona is an EEO/AA - M/W/D/V Employer.

Fellowships for Postdoctoral Scholars at Woods Hole Oceanographic Institution

New or recent doctoral recipients with research interests associated with the following are encouraged to submit scholarship applications prior to January 15, 2009.

Departments - Awards related to the following areas are anticipated: **Applied Ocean Physics & Engineering; Biology; Marine Chemistry & Geochemistry; Geology & Geophysics; Physical Oceanography**

Institutes - Each of the following Institutes, which foster interdisciplinary research addressing critical issues, will award a scholarship to support related research: **Coastal Ocean Institute; Deep Ocean Exploration Institute; Ocean and Climate Change Institute; Ocean Life Institute**

Awards are competitive, with primary emphasis placed on research promise. Scholarships are for 18 months with an annual stipend of \$55,000, a modest research budget and eligibility for group health and dental insurance. Recipients are encouraged to pursue their own research interest in association with Resident Scientific and Senior Technical Staff. Communication with potential WHOI advisors prior to submitting an application is encouraged.

Further information, application forms, and links to the individual departments and institutes and their research themes may be obtained at: <http://www.whoi.edu/apo/postdoctoral> or by contacting the Postdoctoral Fellowship Committee at: (508) 289-2219, or postdoc@whoi.edu.

An Equal Opportunity/Affirmative Action Employer



Faculty Positions In Biomedical Sciences

The University of Texas Health Science Center at San Antonio (UTHSCSA) and the Regional Academic Health Center (RAHC) Campus in Edinburg invites applications from highly qualified individuals for several faculty positions with the academic rank commensurate with experience and qualifications. The successful candidates should have a PhD and/or MD and appropriate postdoctoral training in chronic disease prevention with an emphasis on diabetes, obesity, and cancer. A strong research background with existing or the potential for NIH funding in cellular and molecular aspects of chronic inflammation and immune dysfunction is desirable. Attractive startup and benefit packages are offered.

Submit a letter of application, curriculum vitae, statement of research interests, and the name, address and email address of three references to: **Thomas J. Slaga PhD, Director, The University of Texas Health Science Center at San Antonio, Edinburg-Regional Academic Health Center, 1214 W. Schunior, Edinburg, TX 78541.** All faculty appointments are designated as security sensitive positions.

More information about the Edinburg RAHC Research Facility can be found on our website at www.rahc.uthscsa.edu.

The University of Texas Health Science Center at San Antonio is an Equal Employment Opportunity/Affirmative Action Employer.



UNIVERSITY OF
CALGARY

DIRECTOR, McCAIG INSTITUTE OF BONE & JOINT HEALTH

The McCaig Institute of Bone & Joint Health represents a partnership between the Alberta Health Services Calgary Health Region and the University of Calgary, Faculty of Medicine. The Institute was created to facilitate the coordination and integration of bone and joint health promotion, health care innovation, research, and education in southern Alberta. Linkages with other health regions and Faculties, as well as with aligned community-based services, are essential to the Institute's success. Institute membership is interdisciplinary and is comprised of bone and joint researchers, educators, clinicians, and allied health professionals.

The Institute and its founding partners are searching for an outstanding individual to assume the role of Director, McCaig Institute of Bone & Joint Health. The Director is responsible for realizing the Institute's vision of bone & joint health, internationally recognized and funded research, and multidisciplinary educational programs that attract quality learners. The Director will attract and manage financial resources so that the Institute's goals are achieved. Communicating and reporting to the Institute's partners, community, and members about the Institute's programs and performance will be important aspects of the Director's role.

The selected candidate must have a strong academic background with demonstrated research and educational achievements, as well as proven leadership strengths and experience. The candidate must possess either a PhD and/or an MD. If the successful candidate wishes to practice clinically, he/she must be eligible for medical licensure in the Province of Alberta.

Applications and nominations, including a curriculum vitae, a statement of research interests, leadership philosophy, academic goals, and the names of three referees should be forwarded by **January 31, 2009** to:

Dr. T.E. Feasby
Dean, Faculty of Medicine
3280 Hospital Drive N.W.
Calgary, AB, Canada T2N 4Z6

In accordance with Canadian immigration requirements, priority will be given to Canadian citizens and permanent residents of Canada. The University of Calgary respects, appreciates and encourages diversity.

www.ucalgary.ca

Professor of Medical Bioinformatics

School of Medicine, Dentistry & Biomedical Sciences,
Centre for Cancer Research and Cell Biology Ref: 08/100714

Applications are invited for a Professorial level appointment in Medical Bioinformatics in the Centre for Cancer Research and Cell Biology (CCRCB) at Queen's University Belfast. The successful candidate will join a dynamic research environment at an exciting time for Medical Bioinformatics within Northern Ireland. Applicants must hold a PhD in Bioinformatics, Computer Science, Computational Biology or a closely related subject. Preference may be given to applicants who have proven ability to collaborate with industry and to commercialise their research.

The successful individual will play a leading role in promoting the profile of the CCRCB, Queen's University in Bioinformatics and the All Ireland Institute for Biomedical Informatics (IBI). Based at the new Centre for Cancer Research and Cell Biology (CCRCB) on the Belfast City Hospital campus, the successful candidate will enhance academic development in Medical Bioinformatics within the new £22 million Centre for Cancer Research and Cell Biology

(<http://www.qub.ac.uk/research-centres/CentreforCancerResearchCellBiology/>). The successful individual will develop his/her own academic research programmes and be encouraged to collaborate with other investigators in the Centre.

Informal enquiries may be directed to Dr Frank Emmert-Streib, Centre for Cancer Research and Cell Biology, e-mail: f.emmertstreib@qub.ac.uk, telephone: 028 9097 2792.

Candidates who have not yet achieved the requisite criteria in research or leadership for a Chair position may be considered for appointment at a reader/senior lecturer level.

Salary will be determined in accordance with the appropriate non-clinical Professorial ranges as applied within the University.

Closing date: 4.00 pm, Friday 16 January 2009

Please visit our website for further information and to apply online -

www.qub.ac.uk/jobs or alternatively contact the address below.

The University is committed to equality of opportunity and to selection on merit. It therefore welcomes applications from all sections of society and particularly welcomes applications from people with a disability.

Personnel Department
Queen's University Belfast

Belfast, BT7 1NN.
Tel (028) 90973044
Fax (028) 90971040
E-mail on personnel@qub.ac.uk



Queen's University Belfast is a member of the Russell Group of universities.
One of the United Kingdom's top 20 research-intensive universities.



Department of Health and Human Services
National Institutes of Health
National Institute on Aging



Statistical Genetics Director

The National Institute on Aging (NIA), a major research component of the National Institutes of Health (NIH) and Department of Health and Human Services (DHHS), is recruiting for a Staff Scientist (Facility Head) who will serve as the Statistical Genetics Director of the Laboratory of Genetics (LG), Intramural Research Program (IRP), in Baltimore, MD. The incumbent will be responsible for collaborating in and coordinating statistical genetic and epidemiological analyses of aging-related human conditions and diseases. The collaborative research includes the adaptation or development of new analytic programs with participation in an interactive group studying genetic and epidemiological data for selected aging-related phenotypes in the Baltimore Longitudinal Study of Aging; in other outbred populations; and in the Sardinian "founder population".

Accordingly, the duties of this position require the applicant to hold a Ph.D. and have at least 2 years of additional postdoctoral experience in statistical genetics or comparable epidemiological statistics. Applicants must have a record of scientific accomplishments, including excellence in statistical analyses and qualifications to develop, update, and manage statistical staff and analysis software.

Salary is commensurate with experience and accomplishments. The salary range for Staff Scientists is \$82,961 - \$166,430. A full Civil Service package of benefits (including retirement, health, life and long term care insurance, Thrift Savings Plan, etc.) is available. Applicants must send curriculum vitae, bibliography, and three letters of recommendation to: Chair, LG Staff Scientist - Statistical Genetics Search Committee; Vacancy #NIA-IRP-09-02; c/o Peggy Grothe, Intramural Program Specialist; Office of the Scientific Director, National Institute on Aging, 251 Bayview Blvd, Suite 100, Room 04C221 Baltimore, MD 21224. Position will remain open until filled; however, the application review process will begin **February 28, 2009**. If additional information is needed, please call 410-558-8012 or email: grothep@grc.nia.nih.gov.

DHHS and NIH are Equal Opportunity Employers

POSITIONS OPEN



FACULTY POSITION Vermont Immunobiology/ Infectious Diseases Center University of Vermont

The Vermont Immunobiology/Infectious Diseases Center is undergoing significant expansion and is seeking an outstanding tenure-track faculty member at the **ASSISTANT, ASSOCIATE, or FULL PROFESSOR** level to contribute to the Center's research and teaching programs. Candidates appointed at the level of Assistant Professor may be eligible for research funding from a recently awarded NIH Center of Biomedical Research Excellence (COBRE) Award. We are seeking a scientist with a demonstrated research track record and an innovative research program in the areas of microbial/viral pathogenesis or immune response to infectious agents. Extensive opportunities for collaborative research exist within and outside the Center in cell, molecular, and structural biology. Primary appointment will be in the Department of Microbiology and Molecular Genetics. Details about the Center, the Department, the University, and the Burlington area may be accessed at **websites:** <http://www.med.uvm.edu/vci> and http://www.uvm.edu/microbiology/mmg_home.php. Curriculum vitae, a summary of research interests, and three letters of reference should be sent electronically (if possible) to: **Search Committee Chair, c/o Ms. Debra Stern (e-mail: debra.stern@uvm.edu), 201 Stafford Hall, University of Vermont, 95 Carrigan Drive, Burlington, VT 05405, or apply online at website: <https://www.uvmjobs.com/applicants/jsp/shared/frameset/frameset.jsp?time=1170944834156>.** Review of applications will begin immediately and continue until a suitable candidate is identified. *The University of Vermont is an Equal Opportunity, Affirmative Action Employer. Women and underrepresented minorities are encouraged to apply.*

FACULTY POSITION, BIOLOGY Broad Institute/ Massachusetts Institute of Technology

The Broad Institute and the MIT Department of Biology seek applications for a tenure-track faculty position. The individual would serve as a Core Faculty Member at the Broad Institute and an **ASSISTANT or ASSOCIATE PROFESSOR** at MIT.

We seek outstanding scientists whose research explores comprehensive approaches to biology, as well as potential applications to disease. Relevant fields include genomics, medical genetics, cancer biology, cell biology, systems biology, molecular physiology, stem cell biology, neurobiology, chemical biology, computational biology, or biological engineering. The candidate's independent research program would benefit from and contribute to a highly interdisciplinary and collaborative research environment at the Broad Institute and MIT.

We require that applicants submit curriculum vitae, summary of current and proposed research programs, and three letters of recommendation online at **websites:** <https://www.academicjobsonline.org> (<https://academicjobsonline.org/ajob/mit/biology/91>).

We request that your letters of reference be submitted by the reviewers online via **website:** <http://academicjobsonline.org>. Alternatively, they may be submitted as PDF attachments e-mailed to **e-mail:** lucasm@mit.edu or as paper copies mailed to: **Biology Search Committee, Attn.: Prof. Eric Lander, MIT Room 68-132, 77 Massachusetts Avenue, Cambridge, MA 02139-4307.**

Consideration of completed applications will begin on December 1, 2008.

MIT and the Broad Institute are Affirmative Action Employers and we encourage applications from women and underrepresented minorities.

POSITIONS OPEN

CELL BIOLOGIST, ASSISTANT PROFESSOR Tenure Track, Academic Year 100 Percent HUMAN PHYSIOLOGIST, ASSISTANT PROFESSOR

Tenure Track, Academic Year 100 Percent PLANT BIOLOGIST, ASSISTANT PROFESSOR Tenure Track, Academic Year 100 Percent

The Department of Biology in the College of Science and Health at the University of Wisconsin, La Crosse is expanding and invites applications for three new academic year, tenure-track positions at the level of Assistant Professor. The Cell Biologist will teach cell biology and develop a course in an area of expertise or participate in teaching our biology core curriculum. Research and teaching interests in signal transduction or other areas of cell biology is preferred. The Human Physiologist will teach human anatomy and physiology and develop a course in their area of expertise or participate in teaching in our biology core curriculum. Research and teaching interests in endocrinology or human physiology is preferred. The Plant Biologist will teach plant biology, part of organismal biology, and a course in an area of expertise or other courses. Training and research interests in seedless plants/algae, classical plant pathology, or plant anatomy and physiology is preferred. For each position, a Ph.D. in a biological science is required. We seek engaging teachers and scholars with a strong commitment to undergraduate education to serve as inspirational mentors and role models for students with diverse career goals and backgrounds. Previous teaching and experience with diversity issues is desirable. Successful candidates will be expected to develop an externally funded research program and direct undergraduate and graduate (M.S.) research. Academic year salary is competitive and commensurate with experience. Start August 31, 2009. UW-L is nationally renowned as a comprehensive university with demonstrated excellence in undergraduate and graduate education and research. Coupled with the beautiful surroundings of the region, UW-L offers a stellar environment for professional and personal achievement. Applicants should submit letter of application, indicating the position of interest, Plant Biologist (10BIO01), Human Physiologist (10BIO02), or Cell Biologist (10BIO03); curriculum vitae; statements of teaching philosophy and research interests; graduate and undergraduate transcripts; and three letters of recommendation to: **Dr. Mark Sandheinrich, Department of Biology, University of Wisconsin-La Crosse, La Crosse, WI 54601.** Electronic applications cannot be accepted, and applications must be received by February 1, 2009. *As an Affirmative Action Equal Opportunity Employer, UW-La Crosse is engaged in an effort to be a leader in Wisconsin's movement towards increased diversity and inclusiveness. Women, persons of color, and individuals with a disability are encouraged to apply. If you have a special need/accommodation to aid your participation in our hiring process, please contact Mark Sandheinrich to make appropriate arrangements. Employment will require a criminal background check. A pending criminal charge or conviction will not necessarily disqualify an applicant. In compliance with the Wisconsin Fair Employment Act, UW-La Crosse does not discriminate on the basis of arrest or conviction record.*

ANIMAL or COMPARATIVE PHYSIOLOGIST Minnesota State University, Mankato

The Department of Biological Sciences invites applications for a tenure-track **ASSISTANT PROFESSOR** position. Candidates must have a Ph.D. related to animal/comparative physiology. Duties include teaching undergraduate and graduate courses, developing a research program that involves both undergraduate and graduate students, and serving on departmental committees. Position begins on August 17, 2009. Priority consideration will be given to applications received by January 16, 2009. Complete position description, qualifications, and application procedures can be obtained at **website:** <http://www.mnsu.edu> (link to employment at MSU), or by contacting the **Department of Biological Sciences at telephone: 507-389-5736.** *Affirmative Action/Equal Opportunity Employer and a member of the Minnesota State Colleges and Universities System.*

POSITIONS OPEN

TENURE-TRACK FACULTY POSITION (ASSISTANT PROFESSOR) Molecular Genetics Oakland University Department of Biological Sciences

The Department of Biological Sciences at Oakland University invites applications for a tenure-track Assistant Professor position to be filled by August 2009. We seek a candidate whose biomedical research is focused on the identification of genes that contribute to complex disorders and/or the analysis of genetic variation in the human population. A Ph.D. and postdoctoral experience are required as well as a strong research track record evidenced by publications. Laboratory space and competitive startup package will be provided. The successful candidate is expected to develop a vigorous, extramurally funded research program, to teach effectively at the undergraduate and graduate levels, and to mentor graduate students in doctoral programs.

The Department of Biological Sciences (**website:** <http://www2.oakland.edu/biology/>) is a modern, well-equipped, and research-oriented department. The Department has active graduate programs at the Master's and Ph.D. level. Oakland University is a state-supported institution of 18,000 students situated on a beautiful 1,500-acre campus 25 miles north of Detroit. Opportunities exist for clinical collaborations through the recently established Oakland University William Beaumont School of Medicine.

Applicants should mail their curriculum vitae, statement of research plans and teaching philosophy, copies of key reprints, and a list of three references with contact information by January 16, 2009, to: **Douglas Wendell, Molecular Genetics Search Chair, Department of Biological Sciences, Oakland University, Rochester, MI 48309-4401.**

Oakland University is an Equal Opportunity Employer.

TENURE-TRACK FACULTY POSITION Departments of Biology and Chemistry and Physics

The University of North Carolina at Pembroke (UNCP) seeks an experienced scientist and educator to fill an **ENDOWED CHAIR** position, the **WILLIAM C. FRIDAY DISTINGUISHED PROFESSORSHIP** in molecular biology and biochemistry. The appointment will be made at the rank of **FULL PROFESSOR**, though qualified candidates currently employed at the **ASSOCIATE or ASSISTANT** level are encouraged to apply. The successful candidate will have a Ph.D. in molecular biology, biochemistry, or a related field, and a record of externally funded research and resultant publication. Additional qualifications include a demonstrable potential for outstanding teaching, and a desire to promote interactions across the life sciences and to work with a talented, underrepresented undergraduate population in emerging programs that have seen substantial recent growth. Laboratory space and startup funds for research will be provided. Duties will include: leading research efforts at the newly established Biotechnology Facility; conducting a vigorous externally funded research program that engages undergraduate students; and developing and teaching upper-level undergraduate courses. UNCP is a member of the University of North Carolina system with uniquely diverse enrollment of approximately 6,300 students: 50 percent Caucasian, 21 percent Native American, 23 percent African American, and 3 percent Hispanic. For more information, visit **website:** <http://www.uncp.edu/fridayprofessor> or contact: **Dr. Robert Poage (e-mail: bob.poage@unp.edu), Department of Biology, P.O. Box 1510, Pembroke, NC 28372-1510.**

Review of applications will begin immediately and will continue until the position is filled. *UNC Pembroke is an Equal Opportunity, Affirmative Action Employer and has a strong commitment to diversity.*



Drexel University, a private, nationally ranked academic research institution in Philadelphia seeks a new Department Head for Biology. The College of Arts and Sciences wants an innovative research scientist, educator, and mentor to lead one of the largest departments in the University. The Department boasts 25 faculty members and over 700 undergraduate and 100 graduate students. It offers a broad range of studies in the life sciences leading to Baccalaureate, Master's, and Doctoral degrees. Ground has been broken on the new 130,000 sq. ft. building, which is slated for completion the Fall of 2010. Drexel will be the first university in the U.S. to include a Bio-Wall and is striving for LEED certification.

Candidates must:

- Qualify for the rank of Professor.
- Have a Ph.D. in a relevant discipline.
- Have a track record of ongoing extramural Federal research funding
- Possess commitment to excellence in teaching at the undergraduate and graduate levels
- Possess administrative experience.
- Desire the opportunity to work in a highly collaborative environment across the University

Questions, inquiries, applications, and nominations (including a cover letter, curriculum vitae and the names of five references) should be electronically directed in confidence to: **Andrew Wheeler, Managing Director or Khalilah Lawson, Associate, Diversified Search/Ray and Berndtson, One Commerce Square, 2005 Market Street, Suite 3300, Philadelphia, PA 19103; Drexel-10430@DivSearch.com; Tel: 215-656-3555.**

For further information about Drexel University, please consult its website at www.drexel.edu.

Drexel University is an Equal Opportunity, Affirmative Action Employer.



**Ontario Institute
for Cancer Research**

Deputy Director

The Ontario Institute for Cancer Research (OICR) is seeking a Deputy Director to work closely with the President on the Institute's Strategic Plan, including the allocation of an \$80 million annual budget.

The Deputy Director will share responsibility for the Institute's programs and platforms with the President and will oversee scientific review of OICR's programs, promotion of inter-program partnerships, and operations and communications.

OICR is a new research institute, created by the Government of Ontario to enhance cancer research, particularly translation of new discoveries into effective interventions that impact cancer and promote knowledge-based industries in Ontario.

Qualifications: The successful candidate should have:

- An MD and/or PhD with a visionary approach for building partnerships for the translation of innovative research discoveries into clinical applications;
- Proven track record in research administration in academia or industry;
- Proven leadership and management experience including the building of strong research teams and excellent communications skills;
- Excellent understanding of cancer research - knowledge of the Canadian cancer system would be an advantage.

Conditions of Employment: Based in the MaRS Centre in Toronto, the Deputy Director will devote at least 80 per cent of time to the responsibilities of the position. Up to 20 per cent of time may be used for clinical or research activities. Academic and clinical appointments may be obtained at the University of Toronto and its affiliated hospitals.

The initial appointment is for five years, renewable pending satisfactory review. A competitive package of salary and benefits will be negotiated.

Application Process: Candidates are invited to submit a curriculum vitae, vision statement and names of three references electronically to search@oicr.on.ca. For more information about OICR, please visit the website at www.oicr.on.ca.

The position will remain open until a suitable candidate is found, however applications are preferred by **January 31, 2009.**

**Chair, Department of Biochemistry and
Biophysics**



**UNIVERSITY OF
PENNSYLVANIA
SCHOOL OF MEDICINE**

The University of Pennsylvania School of Medicine invites applications for the position of Chair of the Department of Biochemistry and Biophysics as professor with tenure. The Search Committee seeks candidates with a distinguished and internationally recognized record in a relevant research area who can build on the established strengths of the Department and provide leadership to the larger biochemistry and biophysics community at Penn, which includes faculty in the School of Medicine, Children's Hospital of Philadelphia, the Wistar Institute and multiple schools and departments across campus. A commitment to graduate education and mentoring is required. Applicants must hold a Ph.D. or equivalent degree.

Information about the department can be found at:
<http://www.uphs.upenn.edu/biobiop/>

Please submit your curriculum vitae by February 1, 2009, to:

Robert W. Doms, M.D., Ph.D.
Chair, Biochemistry and Biophysics Search Committee
c/o Margaret M. Lizotte
Administrative Liaison to Search Committee
290 John Morgan Building
3620 Hamilton Walk
Philadelphia, PA 19104-6055

Or lizotte@exchange.upenn.edu

The University of Pennsylvania is an equal opportunity affirmative action employer, and women and minorities are strongly encouraged to apply.

COURSE



DREW UNIVERSITY

**RESIDENTIAL SCHOOL ON MEDICINAL CHEMISTRY:
CHEMISTRY AND BIOLOGY IN DRUG DISCOVERY**
Madison, New Jersey - June 8-12, 2009

The Residential School on Medicinal Chemistry is a week-long graduate level course organized to provide an accelerated program for medicinal chemists, biologists and other industrial and academic scientists who wish to broaden their knowledge of small molecule drug discovery and development. The School's aim is to concentrate on the fundamentals that are useful in drug discovery spanning initial target validation through clinical development. Several case histories of recent successful drug development programs will also be presented.

The five-day program consists of lectures, seminars, case histories and discussions covering the following topics:

Target validation	Structure-based drug design
Receptor binding	Drug-like properties
Enzyme inhibition	Patents
Kinases	Plasma protein binding
Ion channels	Cheminformatics
High throughput screening	PK & drug metabolism
Hit-to-lead progression	Preclinical toxicology
Lead discovery & modification	Clinical development

*William Greenlee, Vincent Gullo and Kenneth Thomas,
Co-organizers*

More information and application forms can be obtained at
www.drew.edu/depts/resmed.aspx or by contacting the
School's office at Drew University, Phone: 973/408-3787;
Fax: 973/408-3504 or email: resmed@drew.edu

POSITIONS OPEN

The Department of Biological Sciences invites applications for two faculty positions in systematics and evolution with an appointment date starting in September 2009. The first is the **ROBERT GRIGGS PROFESSOR**, a tenure-track **ASSISTANT or ASSOCIATE PROFESSORSHIP** in phylogenetic biogeography/co-evolution. For this position we seek a **PHYLOGENETICIST** who uses comparative data to study historical biogeography or interactions among species (for example, parasites and their hosts or herbivores and their host plants). The second position is the **LOUIS WEINTRAUB PROFESSOR**, a tenure-track **ASSISTANT or ASSOCIATE PROFESSORSHIP** in molecular systematics. For this position we seek a Phylogeneticist who uses molecular data to address questions in phylogeny, systematics, and evolution. Successful candidates will have teaching and research interests which will expand and strengthen our Department and the Weintraub Program in Systematics and Evolution (see [website: http://www.gwu.edu/~clade](http://www.gwu.edu/~clade)) and be expected to develop an externally funded research program and participate in graduate and undergraduate education. Basic qualifications: a completed Ph.D. in a relevant field and commitment to scholarly research as evidenced by publications in scholarly journals and scholarly works in progress is required. Postdoctoral experience is preferred. To be considered at the Associate Professor level, the candidate must already be at that rank or have seven years or more equivalent experience. Review of applications begins January 2, 2009, and will be ongoing until the position is filled.

Application procedure: Interested candidates should e-mail a letter of application, indicating the position they are applying for, curriculum vitae, a statement of research and teaching interests, electronic copies of up to three publications, and have three letters of recommendation sent (Assistant Professor applicants) or provide a list of references (Associate Professor applicants) to:

Weintraub Search Committee Chair
Department of Biological Sciences
340 Lisner Hall, 2023 G Street NW
The George Washington University
Washington, DC 20052
E-mail: wssearch@gwu.edu
Telephone: 202-994-6090

Only complete applications will be considered.

The George Washington University is an Equal Opportunity/Affirmative Action Employer. The University Search Committee seeks to attract an active, culturally and academically diverse faculty of the highest caliber.

FACULTY POSITION, CANCER GENETICS Northwestern University Feinberg School of Medicine

Northwestern University Feinberg School of Medicine and the Robert H. Lurie Comprehensive Cancer Center are recruiting an outstanding individual for full-time, tenure-track, faculty position at the level of **ASSOCIATE or FULL PROFESSOR** depending upon prior experience and research accomplishments. This position will be filled by a senior researcher in the broad area of cancer genetics. The successful candidate will be also appointed as the co-leader of the Cancer Genomics Program at Robert H. Lurie Comprehensive Cancer Center.

Candidates should have a Ph.D. and/or M.D. degree and exceptional research potential, with significant prior accomplishments. Applications must include curriculum vitae, and a brief statement of their research interests. To ensure consideration, completed applications must be received by November 30, 2008. Submissions to (e-mail preferred):

Leonidas Platanius, M.D., Ph.D.
Deputy Director
Robert H. Lurie Comprehensive Cancer Center
303 E. Chicago Avenue
Lurie 3-125
Chicago, IL 60611
E-mail: c-alexan@northwestern.edu

Reference faculty position # P-155-04.

Northwestern University is an Affirmative Action/Equal Opportunity Employer; hiring is contingent upon eligibility to work in the United States.

POSITIONS OPEN



FACULTY POSITION Department of Bioengineering Bourns College of Engineering

The Bioengineering Department at the University of California at Riverside invites applications for a **JUNIOR or SENIOR** faculty position in the area(s) of: cellular bioengineering, tissue engineering, systems physiology, and regenerative medicine. Applicants should have a doctoral degree in the relevant engineering discipline or a related field. Details and application materials can be found at [website: http://www.engr.ucr.edu/facultysearch](http://www.engr.ucr.edu/facultysearch). For more information please visit [website: http://www.bioeng.ucr.edu](http://www.bioeng.ucr.edu). The Search Committee will review applications beginning on January 15, 2009, and will continue to receive applications until the positions are filled. *The University of California, Riverside is an Equal Opportunity/Affirmative Action Employer.*

PHYSIOLOGICAL GENOMICS Biological Sciences Department

California State Polytechnic University, Pomona

The Biological Sciences Department at California State Polytechnic University, Pomona (Cal Poly Pomona) invites applications for a tenure-track **ASSISTANT PROFESSOR** position in physiological genomics, beginning September 2009. This position is intended to integrate with and contribute to our strong and growing Biotechnology Program. Candidates who use molecular, genomic, and/or proteomic techniques to address physiological questions at the organ-system level are encouraged to apply. A Ph.D. in physiology or related field is required. Postdoctoral experience is preferred. The successful candidate will have the potential for excellence in undergraduate teaching, and for developing an externally funded research program that will involve undergraduate and Master's students. Teaching responsibilities will include human physiology and specialty courses in the candidate's area of expertise, and may also involve participation in human anatomy and introductory biology courses. Cal Poly Pomona is a comprehensive Master's-level university with a diverse student body. The successful candidate will have demonstrated ability to be responsive to the educational equity goals of the University and its increasing ethnic diversity and international character. Applicants should forward (1) curriculum vitae, (2) statement of teaching philosophy, (3) proposed plan of research, (4) representative publication reprints, and (5) the names and contact information of five references to: **Chair, Physiological Genomics Search Committee, Biological Sciences Department, California State Polytechnic University, 3801 West Temple Avenue, Pomona, CA 91768-4132**. Review of applications begins on January 15, 2009. Official transcripts will be required for final appointment. For further information, visit the Department [website: http://www.csupomona.edu/~biology/](http://www.csupomona.edu/~biology/).

California State Polytechnic University, Pomona is an Equal Opportunity, Affirmative Action Employer. Cal Poly Pomona subscribes to all state and federal regulations and prohibits discrimination based on gender, race, sexual orientation, national origin, disability, marital status, age, religion, or covered veteran's status.

ASSISTANT PROFESSOR of biology, position number 84204, University of Hawai'i at Hilo, nine-month, tenure-track appointment. Teach in areas related to biochemistry, physical chemistry for the life sciences, or cell and molecular genetics. Advise students, publish in peer-reviewed journals, maintain active research program, and participate in community and University service activities. Complete application description available at [website: http://www.uhh.hawaii.edu/uhh/hr/jobs.php](http://www.uhh.hawaii.edu/uhh/hr/jobs.php). *University of Hawai'i at Hilo is an Equal Employment Opportunity/Affirmative Action Employer. Persons with Disabilities, Minorities, Veterans, Women.*

POSITIONS OPEN

SENIOR POSTDOCTORAL ASSOCIATE

Stony Brook University's Institute for Ocean Conservation Science is seeking a candidate with skills in quantitative ecosystem modeling and management strategy evaluation for major investigation into marine forage fish management. The Associate will provide technical assistance to a blue ribbon task force, develop and examine in-depth case studies, and generate models for ecosystems with dominant forage fish populations. For a full position description, or to view the application procedures, or to apply online, visit [website: http://www.stonybrook.edu/jobs](http://www.stonybrook.edu/jobs) (reference #WC-R-5414-08-11-S).

Equal Opportunity/Affirmative Action Employer.

POSTDOCTORAL POSITION

University of Louisville School of Medicine

A position is available to study breast cancer susceptibility with research involving genetics and genotype-environment interactions. Experience in molecular biology, flow cytometry, and rodent work is desired. Strong communication and organizational skills are necessary. Send curriculum vitae, summary of research experience, and contact information of three references to: **David Samuelson, Ph.D., Department of Biochemistry and Molecular Biology, University of Louisville; e-mail: david.samuelson@louisville.edu**.

Coe College invites applications for an **ASSISTANT PROFESSOR**, tenure track in biology with specialty in cell biology, to begin August 2009. Ph.D. required. For more detailed job description and application information see [website: http://www.coe.edu/aboutcoe/employment](http://www.coe.edu/aboutcoe/employment). *Coe College is an Affirmative Action/Equal Opportunity Employer and especially encourages applications from women and minority candidates.*

MARKETPLACE



Promab Biotechnologies Inc. Custom Monoclonal Antibody \$4,200

>3,000 CLONES WILL BE SCREENED

1-866-339-0871

www.promab.com info@promab.com

For COLLAGEN Detection... Connect with Cosmo Bio

ELISAs to measure COLLAGENS: Type 1 (hu); Type 2 (hu, ms, rt, +). **ELISAs to measure ANTI-COLLAGEN ANTIBODIES:** Type 1 (hu); Type 2 (hu, ms, rt, +). **SPECIFIC ANTIBODIES:** Types 1, 2, 3, 4, 5, 6, 7, 8, 9, 10, 11, 12, 14.

Research Products from Japan
www.cosmobio.com

COSMO BIO CO., LTD.
Research Products from Japan

Oligo Synthesis Columns

↳ Columns For All Synthesizers

↳ Bulk Column Pricing Available

↳ Call for Free Column Samples

**BIOSEARCH
TECHNOLOGIES**
Advancing Nucleic Acid Technology™

+1.800.GENOME.1
www.btcicolumns.com